

**NUMERICAL MODELLING OF COMPLEX SLOPE  
DEFORMATIONS**

A Thesis Submitted to the College of  
Graduate Studies and Research  
in Partial Fulfillment of the Requirements  
for the Degree of Doctor of Philosophy  
in the Department of Geological Sciences  
University of Saskatchewan  
Saskatoon

By  
**Boris Benko**  
March 1997



National Library  
of Canada

Acquisitions and  
Bibliographic Services

395 Wellington Street  
Ottawa ON K1A 0N4  
Canada

Bibliothèque nationale  
du Canada

Acquisitions et  
services bibliographiques

395, rue Wellington  
Ottawa ON K1A 0N4  
Canada

*Your file Votre référence*

*Our file Notre référence*

The author has granted a non-exclusive licence allowing the National Library of Canada to reproduce, loan, distribute or sell copies of this thesis in microform, paper or electronic formats.

The author retains ownership of the copyright in this thesis. Neither the thesis nor substantial extracts from it may be printed or otherwise reproduced without the author's permission.

L'auteur a accordé une licence non exclusive permettant à la Bibliothèque nationale du Canada de reproduire, prêter, distribuer ou vendre des copies de cette thèse sous la forme de microfiche/film, de reproduction sur papier ou sur format électronique.

L'auteur conserve la propriété du droit d'auteur qui protège cette thèse. Ni la thèse ni des extraits substantiels de celle-ci ne doivent être imprimés ou autrement reproduits sans son autorisation.

0-612-24004-5

**UNIVERSITY OF SASKATCHEWAN**

College of Graduate Studies and Research

**SUMMARY OF DISSERTATION**

Submitted in partial fulfillment

of the requirements for the

**DEGREE OF DOCTOR OF PHILOSOPHY**

by

**BORIS BENKO**

**Department of Geological Sciences  
University of Saskatchewan**

**Spring 1997**

**Examining Committee:**

Dr. W. Barr

~~Dean/Associate Dean~~ Dean's Designate, Chair  
College of Graduate Studies and Research

Dr. M.J. Reeves

Department of Geological Sciences

Dr. D. Stead

Supervisor, Department of Geological Sciences

Dr. B. Pratt

Department of Geological Sciences

Dr. R. Renaut

Department of Geological Sciences

Dr. E.K. Sauer

Department of Civil Engineering

**External Examiner:**

Dr. Malcolm Scoble

Department of Mining & Metallurgical Engineering

McGill University

3450 University Street

Montreal, Quebec

H3A 2A7

## **NUMERICAL MODELLING OF COMPLEX SLOPE DEFORMATIONS AND LANDSLIDES**

This study presents the application of numerical modelling techniques to the analysis of complex slope deformations and landslides. Complex slope deformations and landslides, in this thesis, include cases where the use of more conventional analytical tools such as limit equilibrium techniques or the use of empirical criteria are not readily applicable. Such a scenario often results from adverse geological and environmental conditions or from human activity.

Two numerical modelling programs FLAC (Fast Lagrangian Analysis of Continua) and UDEC (Universal Distinct Element Code) were used in the research work. Three main groups of problems were investigated:

- The analysis of block-type movements, associated with the deformations of rigid jointed rocks overlying relatively weak, low shear strength layers. Components of deformation due to the translational sliding along basal surfaces, sliding along subvertical discontinuities, rotation and vertical subsidence movements as well as their interaction, are all involved in this type of instability. The mechanism of the slow creep deformation taking place in the foundation of the Spis castle in Slovakia as well as analysis of several hypothetical slopes were investigated.
- The analysis of toppling deformation in a weak rock slope comprising several lithostratigraphic units. The presence of thinly bedded strata and pervasive bedding plane discontinuities with cross joints daylighting from the slope face, as well as the presence of weak shales in most parts of the slope, create a complex slope instability problem. The distinct element method was utilized in the present analysis, providing further insight on the failure mechanism and an improved understanding about the failure development.



- The analysis of interaction between underground mining and slope instability. This situation is quite common when underground mining takes place in mountainous or hilly topography or where a certain inter-relationship exists between underground and surface mining. The deformation induced by underground mining may contribute significantly to the destabilization of existing slopes. The Frank Slide in southwestern Alberta was analyzed to illustrate this. It is shown that underground mining at the foot of the Turtle Mountain acted as a trigger to the final slope failure.

The advantages of numerical modelling approaches to slope stability over more conventional methods such as limit equilibrium methods are highlighted and critically discussed. New interpretations of existing failure mechanisms are presented as is the case of the Frank slide and more understanding on the failure and slope deformation is illustrated as in the cases of Luscar Mine and Spis castle. Furthermore, hypothetical situations, as in the case of underground mining and its influence on slope stability are presented.

## **BIOGRAPHICAL**

- 1965**            Born in Bratislava, Czechoslovakia
- 1988**            Diploma (5-year), Hydrogeology, Engineering Geology & Applied Geophysics, Comenius University
- 1989**            RNDr., Hydrogeology, Engineering Geology & Applied Geophysics, Comenius University

## **PERMISSION TO USE**

In presenting this thesis in partial fulfillment of the requirements for a Doctor of Philosophy degree from the University of Saskatchewan, I agree that the libraries of this university may make it freely available for inspection. I further agree that permission for copying of this thesis in any manner, in whole or in part, for scholarly purposes may be granted by my supervisor Dr. D. Stead or, in his absence, by the head of the Department of Geological Sciences or Dean of Arts and Science. It is understood that any copying of this thesis, or parts thereof, shall not be allowed without my written permission. It is also understood that due recognition shall be given to me and the University of Saskatchewan in any scholarly use which may be made of any material in this thesis.

Request for permission to copy or make other use of material in this thesis, in whole or in part, should be addressed to:

Head of the Department of Geological Sciences  
114 Science Place, University of Saskatchewan  
Saskatoon, Saskatchewan, S7N 5E2.

## **ABSTRACT**

This thesis presents the analysis of complex slope deformations through the application of numerical modelling techniques. Complex slope deformations, in this thesis, include cases where the use of more conventional analytical tools such as limit equilibrium techniques or the use of empirical criteria are not readily applicable. Such a scenario often results from adverse geological and environmental conditions or from human activity. Examples of complex slope deformations are the influence of underground mining on a slope, or situations where rigid jointed rocks overly relatively weak layers.

The use of numerical modelling techniques, both continuum and discontinuum, in the analysis of slope stability problems has increased rapidly in the last decade and proved valuable in the analysis of complex geomechanical problems. Two numerical modelling programs FLAC (Fast Lagrangian Analysis of Continua) and UDEC (Universal Distinct Element Code) were used in this thesis.

Three main groups of problems were investigated:

1. The analysis of deformation associated with rigid jointed rocks overlying relatively weak layers including a case study involving deformation taking place in the foundation of the Spis Castle in Slovakia. It was demonstrated that the type of deformation in such cases depends on the strength, deformability and thickness of the weak layer as well as the jointing pattern of the overlying rocks. It was shown, that the deformations at Spis castle are governed primarily by the presence of a weak, plastic “creep zone” under the base of the travertine blocks on which the castle is founded.
2. The analysis of toppling deformation in a weak rock slope comprising several lithostratigraphic units at the Luscar Mine, Alberta. It was found that the instability mechanism in the initial phase was flexural toppling, confined to a distinct quasi-linear failure surface which provided the shear plane for subsequent sliding

movement. A prediction of slope stability for a planned mine extension in the same pit was made, thereby determining “safe excavation limits”.

3. The analysis of interaction between underground mining and slope instability. The analyses of various slope deformation mechanisms that can be induced by underground mining are presented. The analysis of the Frank Slide in southwestern Alberta illustrated the critical role of underground mining at the base of the Turtle Mountain on triggering the final slope failure.

The analyses present within this thesis demonstrate the application of numerical modelling techniques in the characterization of complex slope deformations. New interpretations of existing failure mechanisms were presented in the case of the Frank Slide, and improved understanding of the failure mechanism and slope deformation were gained in the Luscar Mine and Spis Castle case studies. Furthermore, hypothetical modelling studies relevant to underground mining and block-type deformations allow an increased understanding of complex slope deformations.

## **ACKNOWLEDGEMENTS**

I would like to acknowledge many people who directly or indirectly helped in the successful completion of this thesis.

First of all the guidance, help, advise and friendship of the thesis supervisor Professor Doug Stead is highly appreciated. His support in freedom of research thinking and good spirits when climbing either the Canadian Rockies, Italian Alps, Slovak Carpathians or quarries in Portugal are unparalleled.

I am grateful to my research co-supervisor Professor Malcolm J. Reeves, especially when trying to understand the “mysterious computer world” over the past 5 years. I am highly indebted to Professors J. Malgot and F. Baliak from the Slovak Technical University who were the first people who showed me what landslides look like and taught me how to find, map, analyze and prevent them. The superb teaching of Geological Engineering and Hydrogeology by R. Ondrasik and K. Hyankova from the Comenius University is highly acknowledged and was probably the main reason for my further research in this field.

This work has only been possible through the scholarship provided by the University of Saskatchewan and partly by the NSERC grant to Professor Doug Stead. I would like to acknowledge both with appreciation. I would like to thank also P. Machibroda for his support in the final year of my thesis.

The assistance and advice of members of the examination committee - J. Basinger, B. Pratt, R. Renaut, E.K. Sauer and the late H. Hendry is acknowledged with appreciation.

There were many friends during the graduate studies who made my life in Saskatoon pleasant and inspiring - Eric Eberhardt and Darren Kennard from the Geological Engineering/Rock Mechanics Group, S. Gill, S. Bezdán, W. Gaskin, B. Rostron, P.

Redly, B. Nemeth, C. Funk, B. Assmus, L. Ruo, M. Kotyk, C. Lawby, B. Janser, C. Hooge, J. Long, J. Nyman, F. Hrды, D. Schultz, A. Benn, Z. Szczepanik as well as the players from CAMECO and University of Saskatchewan “Huskies” soccer teams.

I would like to thank my wife Catherine Elizabeth Dimmock for her continuous support, patience, encouragement and understanding.

Finally I would like to thank my parents Ivan and Elena Benko for everything they taught me in life and without whom I would never have been able to reach so far.

## TABLE OF CONTENTS

PERMISSION TO USE .....	i
ABSTRACT .....	ii
ACKNOWLEDGMENTS .....	iv
TABLE OF CONTENTS .....	vi
LIST OF TABLES .....	xii
LIST OF FIGURES .....	xiii
1. INTRODUCTION .....	1
1.1 Background .....	1
1.2 Objectives .....	2
1.3 Research Procedure and Thesis Structure .....	3
2. LANDSLIDE MECHANISMS AND ANALYSES .....	6
2.1 Definition and Classification of Landslides .....	6
2.2 Stability Investigation .....	10
2.3 Methods of Analysis .....	16
2.3.1 Empirical and Analogue Approach .....	18
2.3.2 Kinematic Methods .....	19
2.3.3 Slope Stability Charts .....	19
2.3.4 Limit Equilibrium Methods .....	20
2.3.5 Fracture Mechanics .....	23
2.3.6 Probabilistic Analyses .....	23
2.3.7 Physical Modelling .....	25
2.3.8 Numerical Modelling .....	26
2.3.8.1 Numerical Modelling Techniques .....	30
2.3.8.2 Continuum and Discontinuum .....	32
2.3.8.3 Finite Difference Method and the FLAC Program	35
2.3.8.4 Distinct Element Method and the UDEC Program	40

3.	<b>BLOCK-TYPE DEFORMATIONS OF RIGID JOINTED ROCK MASSES OVERLYING WEAK LAYERS .....</b>	<b>45</b>
3.1	Introduction .....	45
3.2	Literature Review .....	48
3.2.1	Physical Modelling .....	52
3.2.2	Numerical Modelling Studies on Block-Type Slope Deformations .....	53
3.3	Block-Type Movements .....	56
3.4	Application of Distinct Element Method to the Analysis of Block-Type Slope Deformations .....	60
3.5	Gravitational deformations at the Spis Castle .....	71
3.5.1	Geological Structure .....	72
3.5.2	Previous Investigations .....	74
3.5.3	The Rock Mass Structure of the Spis Castle Foundation	75
3.5.4	Rock Material Properties .....	78
3.5.5	Landslide Types and Slope Deformations at the Site ..	80
3.5.6	Groundwater .....	81
3.5.7	Numerical Analysis of Block-Type Deformations in the Spis Castle Foundation .....	82
3.5.7.1	Numerical Modelling Results .....	85
3.6	Conclusions .....	89
4.	<b>TOPPLING WITH EMPHASIS ON SLOPE DEFORMATION AT THE LUSCAR MINE, ALBERTA .....</b>	<b>91</b>
4.1	Introduction .....	91
4.2	Literature Review .....	95
4.2.1	Methods of Analysis .....	99
4.2.1.1	Physical Modelling .....	99
4.2.1.2	Kinematic Analysis .....	99
4.2.1.3	Limit Equilibrium Analysis .....	101



	4.2.1.4 Numerical Modelling of Toppling Instability ..	103
4.3	Toppling Instability at the Cardinal River Mine, Luscar, Alberta .....	106
4.3.1	Introduction .....	106
4.3.2	Geology and Rock Mass Structure .....	108
4.3.3	Rock Mass Properties .....	112
4.3.4	Highwall Failure 50-A-5 Pit; Section C20+00 .....	113
4.3.5	Numerical Modelling .....	116
	4.3.5.1 Previous Work .....	117
	4.3.5.2 Geometry .....	118
	4.3.5.3 Rock and Discontinuity Strength .....	120
	4.3.5.4 Initial Stress Field .....	122
	4.3.5.5 Modelling Procedure .....	122
	4.3.5.6 Results - Section C20+00 .....	123
	4.3.5.7 Prediction of Slope Deformation in the C25+00 Section .....	137
	4.3.6 Conclusions .....	141
5.	THE INFLUENCE OF UNDERGROUND MINING ON COMPLEX SLOPE DEFORMATION MECHANISM .....	146
5.1	Introduction .....	146
5.2	Previous Work .....	147
	5.2.1 Previous Analyses of the Influence of Underground Mining on Slope Instability .....	157
5.3	Factors Affecting Mining Induced Slope Deformation and Instability .....	163
	5.3.1 Longwall Mining .....	165
	5.3.1.1 Longwall Mining within the Slope .....	165
	5.3.2 Room and Pillar Mining .....	169
	5.3.3 Stopes, Shafts, Adits, Bell-pits, Solution Mining and	

	Sublevel Caving .....	175
5.3.4	Workings on the Dip or Rise Side, Directly Underneath the Slope or Transient Position .....	176
5.3.5	Influence of Timing Between Slope Excavation and Underground Workings .....	178
5.3.6	Influence of Slope Angle on the Type of Deformation	178
5.3.7	Analysis of Slope Stability with Respect to Conditions Generated by Underground Mining Activity .....	179
5.4	Application of Numerical Modelling to Slope Stability Analysis Influenced by Underground Mining .....	180
5.4.1	Longwall Mining with Backfill under a Level and Sloping Topography - Continuum Approach .....	180
	5.4.1.1 Geometry and Discretization of the Rock Mass	181
	5.4.1.2 Rock Mass Properties and Initial Stress Condition	182
	5.4.1.3 Modelling Procedure .....	184
	5.4.1.4 Level Topography - 60 m Overburden .....	185
	5.4.1.5 Level Topography - 100 m Overburden .....	186
	5.4.1.6 Slope Topography - Longwall Mining Approaching from the Toe and Crest Side ...	188
5.4.2	Influence of Longwall Panel Location on Slope Deformation - Mining Parallel to Slope Strike - Discontinuum Approach .....	196
	5.4.2.1 MODEL 1 - Level Topography .....	199
	5.4.2.2 MODEL 2 - 40 m High, 45° Angle Slope .....	206
	5.4.2.3 MODEL 3 - 40 m High, 45° Angle Slope with Different Discontinuity Geometry in the Slope	214
	5.4.2.3.1 Fault Daylighting in the Slope Face	215
	5.4.2.3.2 Bedding Planes Daylighting in the Slope Face .....	217
	5.4.2.3.3 Bedding Planes Dipping into the Slope	220

5.5	Conclusions and Recommendation for Future Work .....	222
6.	<b>THE FRANK SLIDE: A RE-EXAMINATION OF THE FAILURE MECHANISM .....</b>	<b>225</b>
6.1	Introduction .....	225
6.2	History of Investigation .....	226
6.3	Geology and Stratigraphy .....	231
6.4	Failure Mechanism .....	234
6.5	Influence of Mining on the Stability of Turtle Mountain .....	236
6.6	Previous Analyses of the Frank Slide .....	238
6.7	Numerical Modelling of the Frank Slide .....	240
6.7.1	Continuum Approach .....	242
6.7.1.1	Location of Failure Surface .....	247
6.7.1.2	Influence of Mining on Slope Failure Development - Continuum Model .....	252
6.7.2	Discontinuum Approach .....	254
6.7.2.1	Modelling Procedure .....	256
6.7.2.2	Elastic Isotropic Model with Slip Allowed on Discontinuities .....	257
6.7.2.3	Elasto-Plastic Model .....	260
6.8	Conclusions .....	265
6.9	Suggestions for Future Research .....	267
7.	<b>DISCUSSION AND CONCLUSIONS .....</b>	<b>268</b>
7.1	Summary of Results and Recommendation for Future Work .....	269
7.1.1	Block-Type Deformations of Rigid Joint Bounded Rocks Overlying Weak Base .....	269
7.1.2	Toppling with Emphasis on Slope Deformations at the Luscar Mine, Alberta .....	270

7.1.3	The Influence of Underground Mining on the Slope Instability Mechanisms .....	271
7.1.4	The Frank Slide: A Re-examination of the Failure Mechanism .....	272
7.2	Discussion .....	273
8.	REFERENCES .....	278

## APPENDIX A

## LIST OF TABLES

<b>Table 2.1.</b>	Classification of landslides (after Varnes, 1978) .....	6
<b>Table 2.2.</b>	Spectrum of modelling situations (after Coetzee et al., 1978)	28
<b>Table 2.3.</b>	Set of guidelines in modelling of geomechanical problems (after Starfield and Cundall, 1988) .....	29
<b>Table 2.4.</b>	Material models and input parameters commonly used in geomechanical analysis using FLAC and UDEC (after Itasca, 1992) .....	39
<b>Table 3.1.</b>	Input properties for numerical model .....	63
<b>Table 3.2.</b>	Input properties for numerical model .....	84
<b>Table 4.1.</b>	Secondary toppling mechanisms (after Hoek and Bray, 1981)	95
<b>Table 5.1.</b>	Material properties for continuum analysis .....	183
<b>Table 5.2.</b>	Properties for backfill .....	184
<b>Table 5.3.</b>	Initial material properties for blocks and discontinuities.....	201
<b>Table 5.4.</b>	Summary of results for mining subsidence with overburden\ thickness of 100m and 60m .....	204
<b>Table 6.1.</b>	Summary of main contributions to investigation of Frank Slide stability .....	227
<b>Table 6.2.</b>	Summary of factors influencing the stability of Turtle Mountain	235
<b>Table 6.3.</b>	Summary of test results of the main discontinuities (after Cruden and Krahn, 1978) .....	238
<b>Table 6.4.</b>	Results of stability analysis (after Cruden and Krahn, 1978) .	238
<b>Table 6.5.</b>	Rock mass properties for the numerical modelling of the Frank Slide .....	244

## LIST OF FIGURES

<b>Figure 1.1.</b>	Research overview. ....	4
<b>Figure 2.1.</b>	Examples of the main types of landslide mechanisms. ....	7
<b>Figure 2.2.</b>	General analytical procedure for slope stability investigation. ....	12
<b>Figure 2.3.</b>	Examples of landslide mitigation method (modified from VanDine, 1996). ....	14
<b>Figure 2.4.</b>	Categories of rock slope stabilization measures (after Wyllie and Norrish, 1996). ....	15
<b>Figure 2.5.</b>	Approaches to potential slope stability problems (after Holtz and Schuster, 1996). ....	16
<b>Figure 2.6.</b>	Commonly used approaches to slope stability analysis. ....	17
<b>Figure 2.7.</b>	Forces acting in and on slope considered in a limit equilibrium analysis for a circular failure surface (a) and a failure surface confined to pre-existing discontinuities (b) (based on Fredlund, 1992 and Wyllie and Norrish, 1996). ....	21
<b>Figure 2.8.</b>	Factor of safety (a) and capacity and demand (b) probability distributions (after Pine, 1992). ....	24
<b>Figure 2.9.</b>	Relationship between data and understanding (after Holling, 1978). ....	27
<b>Figure 2.10.</b>	Development of a finite-element model of a continuum (after Brady and Brown, 1993). ....	30
<b>Figure 2.11.</b>	Diagrammatic representation of scale effects (modified after Cunha, 1990). ....	33
<b>Figure 2.12.</b>	Various elements of a FLAC model (after Itasca, 1992). ....	36
<b>Figure 2.13.</b>	The basic explicit calculation cycle (after Coetzee et al., 1993). ....	36
<b>Figure 2.14.</b>	Example of numerical modelling analysis of slope stability using FLAC; (a) finite difference grid, (b) displacement vectors and ground surface boundary. ....	38
<b>Figure 2.15.</b>	Principles of UDEC - (a) rock slope in orthogona-jointed	

	strata, (b) rigid or deformable blocks, (c) spring-slider elements for joint representation. ....	41
<b>Figure 2.16.</b>	UDEC application to slope stability (toppling) analysis; (a) toppling of rigid (non-deformable) blocks on an inclined base, (b) flexural toppling of deformable blocks (magnified 10x). ..	43
<b>Figure 2.17.</b>	General solution procedure in FLAC and UDEC (based on Itasca, 1993). ....	44
<b>Figure 3.1.</b>	Two examples of block-type movement (after Cruden and Varnes, 1996). ....	46
<b>Figure 3.2.</b>	Various secondary landslide mechanisms associated with block-type movements. ....	47
<b>Figure 3.3.</b>	View of landslide topography in the Chasm area. ....	50
<b>Figure 3.4.</b>	Different block-type-type deformations on various types of soft base, (a) - Viscous, (b) - Viscoplastic -brittle, (c) - Viscoplastic-ductile, (after Kostak, 1977). ....	52
<b>Figure 3.5.</b>	Deformation and instability of rigid joint bounded rock overlying soft base; studied at the Technical University of Vienna, (a) finite element simulation of syncline development, (b) three different modes of instability for "tower shaped blocks, (c) rotational failure and toppling of blocks as simulated with the finite element method (after Poisel et al, 1991). ....	54
<b>Figure 3.6.</b>	Types of block-type movements over plastic substratum. ....	57
<b>Figure 3.7.</b>	Sketch of geological structure analyzed, using distinct element method. ....	61
<b>Figure 3.8.</b>	Examples of distinct element models with simulation of (a) single block (b) multiple blocks used in the analysis. ....	62
<b>Figure 3.9.</b>	Displacement of a single joint bounded block on a 50 m weak base. ....	65
<b>Figure 3.10.</b>	Record of horizontal and vertical displacement for a point	

	on top of the joint separated rock block and 50 m thick weak base. ....	65
<b>Figure 3.11.</b>	Displacement of a single joint bounded block on a 5 m weak base. ....	67
<b>Figure 3.12.</b>	Record of horizontal and vertical displacement for a point on top of the joint separated rock block and 5 m thick weak base. ....	67
<b>Figure 3.13.</b>	Deformation of an orthogonal-jointed block on a 50 m weak base. ....	68
<b>Figure 3.14.</b>	Deformations in model assuming vertical jointing of the rigid rock. ....	69
<b>Figure 3.15.</b>	Deformations in model assuming various joint direction in the rigid rock. ....	70
<b>Figure 3.16.</b>	General view of the Spis castle looking north-west. ....	71
<b>Figure 3.17.</b>	Cross-section through the Spis castle hill. ....	73
<b>Figure 3.18.</b>	Plan view of the Spis castle (after Malgot et al., 1992). 1-Romanesque Palace, 2-Chapell, 3-Late Gothic Palace, 4-Storage, 5-Water Reservoir, 6-1 <sup>st</sup> Romanesque Courtyard, 7-2 <sup>nd</sup> Romanesque Courtyard, 8-Lower Courtyard, 9-Entrance, 10-Main discontinuities, 11-Separated travertine blocks, 12-Cross-section lines, 13-Debris. ....	76
<b>Figure 3.19.</b>	Orientation of main discontinuities at the Spis castle. ....	78
<b>Figure 3.20.</b>	Contact zone of travertines and underlying shales. ....	79
<b>Figure 3.21.</b>	Geometry of distinct element models used for the analysis. Only central part of N-S cross-section is shown. ....	83
<b>Figure 3.22.</b>	Discretization of blocks used for the analysis. ....	84
<b>Figure 3.23.</b>	Differential settlement of travertine blocks in the central part of model. ....	86
<b>Figure 3.24.</b>	Displacement in the northern part of N-S cross section and tensile failure in the simulated castle wall. ....	87



<b>Figure 3.25.</b>	Displacement of travertine blocks for the eastern part of the E-W cross- section. ....	88
<b>Figure 3.26.</b>	Displacement vectors in the creep zone and travertine blocks for the eastern part of E-W cross-section. ....	88
<b>Figure 3.27.</b>	Deformation of simulated castle wall. ....	89
<b>Figure 4.1.</b>	Primary Toppling Modes (after Goodman and Bray, 1976).	92
<b>Figure 4.2.</b>	Secondary toppling mechanisms (after Hoek and Bray, 1981). ....	94
<b>Figure 4.3.</b>	Examples of multiple block (a) and block-flexure (b) toppling on “underdip” slopes (after Cruden and Hu, 1994).	98
<b>Figure 4.4.</b>	Example of large scale toppling deformation at the Chabenec Ridge in Slovakia (after Nemcok, 1982). 1 - Gneiss, 2 - Granodiorite, 3 - Rockfall debris, 4 - Fluvial deposits, 5 - Shear planes, 6 - Direction of block movement.	98
<b>Figure 4.5.</b>	Kinematic analysis for toppling failure (after Norrish and Wyllie, 1996). ....	100
<b>Figure 4.6.</b>	Principle of Limit Equilibrium Method for Toppling Analysis (after Hoek and Bray, 1981). ....	102
<b>Figure 4.7.</b>	Distinct element model of toppling in Brenda mine, B.C., (a) grid point velocity vectors, (b) horizontal displacement contours in meters, (c.) area of failed nodes (after Pritchard and Savigny, 1990). ....	104
<b>Figure 4.8.</b>	Sketch map showing the location of Luscar Mine near Hinton, Alberta. ....	107
<b>Figure 4.9.</b>	Schematic plan view of the “A-pits”, location of cross sections C20+00 and C25+00 and location of monitoring points on the slope. ....	107
<b>Figure 4.10.</b>	View of the 50-A-5 pit and surrounding area looking northeast.	108
<b>Figure 4.11.</b>	The general stratigraphy at the mine site. ....	109
<b>Figure 4.12.</b>	Simplified geological structure, pit geometry and estimated	

	failure plane in the 50-A-5-2 pit, section C20+00.	
	1 - Nikanassin formation, 2 - Cadomin conglomerate,	
	3 - Gladstone Member, 4 - Moosebar Member, 5 - Torrens	
	Member (interbedded siltstones and sandstones, 6 - Torrens	
	Member (sandstone), 7 - Jewel seam, Member "D". .....	110
<b>Figure 4.13.</b>	Summary of main discontinuity data (after Hebil, 1993). .....	111
<b>Figure 4.14.</b>	Simplified geological structure and pit geometry in the	
	50-A-5-2 pit, section C25+00. 1 - Nikanassin formation,	
	2 - Cadomin conglomerate, 3 - Gladstone member,	
	4 - Moosebar Member, 5 - Torrens Member (interbedded	
	siltstones and sandstones, 6 - Torrens Member (sandstone),	
	7 - Jewel seam, Member "D". .....	112
<b>Figure 4.15.</b>	Tension crack at the top of the hillside defining the	
	southern limit of failure. ....	114
<b>Figure 4.16.</b>	Displacement history for selected prisms on the open pit	
	slope. Location of prisms shown in figure 4.9. ....	115
<b>Figure 4.17.</b>	Schematic illustration of discontinuum method for	
	geomechanical representation of jointed rock masses. ....	117
<b>Figure 4.18.</b>	Failure extent in section C20+00 at mining elevation	
	1804 m and 1768 m, (after Bucek and Barron, 1994). ....	118
<b>Figure 4.19.</b>	Distinct element model for 50-A-5-2 pit, section C20+00	
	at the Cardinal River mine. ....	119
<b>Figure 4.20.</b>	Distinct element model for 50-A-5-2 pit, section C25+00	
	at the Cardinal River mine. ....	119
<b>Figure 4.21.</b>	Summary of the initial input properties for numerical	
	modelling analysis assuming dry conditions and	
	Mohr-Coulomb constitutive criterion. ....	121
<b>Figure 4.22.</b>	Initial ground stress conditions after the excavation of	
	1840 m level. ....	124
<b>Figure 4.23.</b>	Velocity vectors in the upper two benches and slope	

	above the pit crest after the excavation of 1840 m level. ....	125
<b>Figure 4.24.</b>	Tensile failure in the Cadomin conglomerate and yielding in the Gladstone member after the excavation of the 1840 m level. ....	126
<b>Figure 4.25.</b>	Magnified displacements (25x) in model after the excavation of the 1840 m level. ....	127
<b>Figure 4.26a.</b>	Zone limiting the toppling after excavation of the 1840 m level. ....	129
<b>Figure 4.26b.</b>	Zone limiting the toppling after excavation of the 1828 m level. ....	129
<b>Figure 4.26c.</b>	Zone limiting the toppling after excavation of the 1816 m level. ....	130
<b>Figure 4.26d.</b>	Zone limiting the toppling after excavation of the 1804 m level. ....	130
<b>Figure 4.26e.</b>	Zone limiting the toppling after excavation of the 1792 m level. ....	131
<b>Figure 4.26f.</b>	Zone limiting the toppling after excavation of the 1768 m level. ....	131
<b>Figure 4.27.</b>	Plasticity indicators (yield and tension) after excavation of the 1768 m level. ....	132
<b>Figure 4.28.</b>	Detail view of flexural toppling in the lower part of hillslope (Moosebar and Gladstone members) after excavation of the 1768 m level. ....	132
<b>Figure 4.29.</b>	Displacement vectors in benches and the lower part of slope after the excavation of the 1868 m level. ....	133
<b>Figure 4.30.</b>	Shear displacement on discontinuities after the excavation of the 1868 m level. ....	133
<b>Figure 4.31.</b>	Model with assumed groundwater table - Section C20+00. ...	134
<b>Figure 4.32.</b>	Domain pore pressures in the model with groundwater assumption - Section C20+00. ....	135

<b>Figure 4.33.</b>	Zone limiting the toppling after excavation of the 1840 m level with assumed groundwater in model. ....	135
<b>Figure 4.34.</b>	Velocity vectors in the upper two benches and slope above the pit crest after the excavation of 1840 m level and assumed ubiquitous constitutive criterion. ....	137
<b>Figure 4.35.</b>	Model with assumed groundwater table and bench reference numbers in Section C25+00. This model shows the excavation of the upper six benches and the position of present mining level. ....	138
<b>Figure 4.36.</b>	Failure location in model after the excavation of the seventh bench - section C25+00. ....	139
<b>Figure 4.37.</b>	Shear displacement on discontinuities after the excavation of the seventh bench. ....	140
<b>Figure 4.38.</b>	Location of failure plane at the maximum planned deepening of pit in Section C25+00. ....	140
<b>Figure 5.1.</b>	Spoil failure involving translational movement along a weak layer with room and pillar workings underneath (after Stead and Singh, 1989). ....	151
<b>Figure 5.2.</b>	Underground coal mining in the Vtacnik Mountains, Slovak Republic (after Malgot et al., 1986). 1 - Tuffites, 2 - Coal seam, 3 - Mined-out coal seam, 4 - Clays, 6 - Andesites, 7 - Landslide debris, 8 - Failure surfaces in pre-volcanic sediments (gravitational tectonics), 9 - Creep zones, 10 - Failure of recent landslides, 11 - Failure of recent landslides activated by underground mining, 12 - Boreholes, 13 - Mine shaft, 14 - Village. ....	152
<b>Figure 5.3.</b>	One of the damaged houses in the village of Podhradie (Slovak Republic), resulting from a landslide triggered by underground mining. ....	153
<b>Figure 5.4.</b>	Schematic illustration of slope classification based on the	

	type of instability, (after Sassa et al., 1979). .....	157
<b>Figure 5.5.</b>	Relationship and factors of influence between slope stability and underground mining. ....	163
<b>Figure 5.6.</b>	Factors to be considered when analyzing the relationship between slope stability and underground mining. ....	164
<b>Figure 5.7.</b>	Subsidence, strain and displacement above longwall extraction with a surface ground slope of 15° (after Whittaker and Reddish, 1989). ....	166
<b>Figure 5.8.</b>	Subsidence, strain and displacement above longwall extraction with a surface ground slope of 45° (after Whittaker and Reddish, 1989). ....	166
<b>Figure 5.9.</b>	Initiation of subsidence and trough development with increasing depth of overburden. A case with and without a supporting pillar at the outcrop is presented. ....	168
<b>Figure 5.10.</b>	Tension zone above excavation with simulated void migration (after Stead and Benko, 1993). ....	170
<b>Figure 5.11.</b>	Slope face collapse due to advance of mine slope towards old workings (after Stead and Benko, 1993). ....	170
<b>Figure 5.12.</b>	Modes of failure of shallow mine workings (after Walton and Taylor, 1977). ....	172
<b>Figure 5.13.</b>	Sliding, buckling and ploughing instability due to void migration. ....	173
<b>Figure 5.14.</b>	Relatively safe (a) and unsafe (b) direction of surface mining layout in an area of previous room and pillar mining. ....	175
<b>Figure 5.15.</b>	Three different positions of the underground mining and slope. ....	176
<b>Figure 5.16.</b>	Investigating of the influence of mining direction on slope instability and deformation (sketch not to scale). ....	181
<b>Figure 5.17.</b>	Finite difference grid and geometry of model for continuum analysis of the influence of underground	

	mining on slope stability. ....	182
<b>Figure 5.18.</b>	Location of shear strain in model with level ground surface, overburden of 60 m after mining advance of 300 m. ....	185
<b>Figure 5.19.</b>	Location of shear strain in model with level ground surface, overburden of 100 m after mining advance of 300 m. ....	187
<b>Figure 5.20.</b>	Location of shear strain concentration in model with slope after mining advance of 300 m, (a) mining approaching from the toe side, (b) mining approaching from the crest side. ....	188
<b>Figure 5.21.</b>	Displacement vectors in slope area for mining approaching and undergoing slope from the crest side. Mining 30 m right from crest (a), mining 30 m left from toe (b). ....	190
<b>Figure 5.22.</b>	Displacement vectors in slope area for mining approaching and undergoing slope from the crest side. Mining 30 m right from crest (a), mining 30 m left from toe (b). ....	191
<b>Figure 5.23.</b>	Principal stresses in slope area for mining approaching and undergoing slope from the toe side. Mining 30m left from toe (a), mining 30 m right from crest (b). ....	192
<b>Figure 5.24.</b>	Principal stresses in slope area for mining approaching and undergoing slope from the crest side. Mining 30 m right from crest (a), mining 30 m left from toe (b). ....	193
<b>Figure 5.25.</b>	Initial, pre-mining, principal stresses in slope. Maximum value 1.2 MPa. ....	194
<b>Figure 5.26.</b>	Distinct element models used to investigate the influence of panel location on slope instability and deformation. ....	197
<b>Figure 5.27.</b>	Slope geometry and three different positions of mined panel centerline relative to the analyzed slope. Panel dimensions are 100 m x 2.5 m. 1,2,3 - refer to different positions of mined panel centerline to the slope (1-under the slope toe, 2-under the mid-height of slope, 3-under the slope crest) ....	198
<b>Figure 5.28.</b>	Schematic illustration of numerical modelling procedure	

	for Model 1. ....	201
<b>Figure 5.29.</b>	Deformation associated with subsidence of the ground surface for model with 60 m overburden .....	203
<b>Figure 5.30.</b>	Opening of joints and bedding plane separation over edge of the panel for model with 60 m overburden .....	203
<b>Figure 5.31.</b>	Subsidence profiles for 100 m overburden (a) and 60 m overburden (b) for models with different block size, friction and joint stiffness. ....	205
<b>Figure 5.32.</b>	Location of points for displacement monitoring. ....	207
<b>Figure 5.33.</b>	Vertical and horizontal displacements for along the slope profile resulting from panel extraction in different positions to slope. ....	208
<b>Figure 5.34.</b>	Horizontal displacements resulting from panel extraction with centerline under the slope toe. ....	209
<b>Figure 5.35.</b>	Shear displacement on joints resulting from panel extraction with centerline under the slope toe. ....	209
<b>Figure 5.36.</b>	Horizontal displacements resulting from panel extraction with centerline under the mid-height of slope. ....	210
<b>Figure 5.37.</b>	Shear displacement on joints resulting from panel extraction with centerline under the mid-height of slope. ....	210
<b>Figure 5.38.</b>	Horizontal displacements resulting from panel extraction with centerline under the slope crest. ....	211
<b>Figure 5.39.</b>	Shear displacement on joints resulting from panel extraction with centerline under the slope crest. ....	211
<b>Figure 5.40.</b>	Shear displacements on joints for model with a fault daylighting in slope face and panel with centerline located under the slope toe. ....	216
<b>Figure 5.41.</b>	Displacement vectors for upper part of unstable wedge outlined by the ground surface and fault. ....	216
<b>Figure 5.42.</b>	Shear displacements on joints for model with a fault	

	daylighting in slope face. Increased shear strength on fault assumed (friction=30°, initial cohesion=0.05 MPa). .....	217
<b>Figure 5.43.</b>	Shear displacements on joints for model with bedding planes daylighting in slope face and panel with centerline located under the slope toe. ....	218
<b>Figure 5.44.</b>	Displacement vectors in slope developed as a consequence of panel extraction with centerline located under the slope toe. ....	219
<b>Figure 5.45.</b>	Slope deformation (magnified 4x) with panel centerline under the slope toe. ....	219
<b>Figure 5.46.</b>	Displacement vectors in slope with bedding planes dipping into the slope developed as a consequence of undermining. ....	220
<b>Figure 5.47.</b>	Slope deformation (magnified 4x) with panel centerline under the slope toe. Toppling mode of failure. ....	221
<b>Figure 6.1.</b>	Location of Frank Slide. ....	226
<b>Figure 6.2.</b>	Turtle Mountain before the Frank Slide (from Cost of Coal, 1995). ....	228
<b>Figure 6.3.</b>	The Frank Slide as seen today.....	228
<b>Figure 6.4.</b>	Cross-section through the north peak of Turtle Mountain (after Daly, 1912). ....	229
<b>Figure 6.5.</b>	View of the Frank Slide debris from the top of the Turtle Mountain .....	231
<b>Figure 6.6.</b>	The Stratigraphy of the Turtle Mountain (modified after Norris, 1955 and Cruden and Krahn, 1978). ....	232
<b>Figure 6.7.</b>	Plan view of the Turtle Mountain geological structure. ....	233
<b>Figure 6.8</b>	Tension cracks at the top of the Turtle Mountain, looking south. ....	233
<b>Figure 6.9.</b>	Cross-section through the central part of the Frank Slide (modified after Krahn, 1974). ....	234
<b>Figure 6.10.</b>	Flow chart of analytical procedure applied in the Frank Slide stability investigation. ....	241



<b>Figure 6.11.</b>	Geometry and boundary conditions for the continuum analysis of the Frank Slide .....	243
<b>Figure 6.1.</b>	Finite difference mesh in the central part of the Frank Slide model .....	243
<b>Figure 6.13.</b>	Modelled ground stress trajectories in the top central part of model (initial K ratio equal to 0.5). .....	245
<b>Figure 6.14.</b>	Assumed dip of implicit joints for the ubiquitous constitutive criteria .....	246
<b>Figure 6.15.</b>	Failed part of Turtle Mountain (magnified grid plot, 30x) .....	247
<b>Figure 6.16.</b>	Plasticity indicators for the top part of Turtle Mountain. ....	248
<b>Figure 6.17.</b>	Total displacement vectors developed in the model. ....	248
<b>Figure 6.18.</b>	Record of vertical displacement for a point at top of the Turtle Mountain with progressively decreased cohesion. ....	249
<b>Figure 6.19.</b>	Frank Slide analysis with an assumed groundwater table. ....	250
<b>Figure 6.20.</b>	Total displacement vectors for the application of ubiquitous constitutive criterion. ....	251
<b>Figure 6.21.</b>	The development of vertical displacement for point A (figure 6.11) located at the top of “pre-failure” Turtle Mountain. ....	252
<b>Figure 6.22.</b>	Failed part of Turtle Mountain after mine opening reached 70 x 5 m (magnified grid plot, 90x). ....	253
<b>Figure 6.23.</b>	Distinct Element model for Frank Slide analysis. Only bedding plane discontinuities are represented. ....	255
<b>Figure 6.24.</b>	Orthogonal jointing pattern in the top part of Turtle Mountain. ....	255
<b>Figure 6.25.</b>	Shear displacement along discontinuities for “elastic isotropic blocks” model simulating bedding planes. ....	258
<b>Figure 6.26.</b>	Shear displacement along discontinuities for “ elastic isotropic blocks” - model simulating orthogonal jointing. ....	258
<b>Figure 6.27.</b>	Shear displacement along discontinuities for “elastic isotropic blocks” resulting from the mine opening - model	

	simulating bedding planes. ....	259
<b>Figure 6.28.</b>	Shear displacement along discontinuities for “elastic isotropic blocks” resulting from the mine opening - model representing orthogonal jointing. ....	259
<b>Figure 6.29.</b>	Shear displacement along bedding planes for model with block cohesion equal to 550 kPa. ....	261
<b>Figure 6.30.</b>	Total displacement vectors in model. Maximum displacement 10.2 m. ....	261
<b>Figure 6.31.</b>	History of vertical displacement for three points in the model.	262
<b>Figure 6.32.</b>	Shear displacement along bedding planes developed in slope as a consequence of mine opening. ....	263
<b>Figure 6.33.</b>	Plasticity indicators for the top part of Turtle Mountain developed in model as a result of mining. ....	263
<b>Figure 6.34.</b>	Shear displacement along joints for the orthogonal discontinuity structure and block cohesion of 550 kPa. ....	264
<b>Figure 7.1.</b>	Concepts to be considered in the numerical modelling applications to complex slope deformations analysis. ....	276

## **CHAPTER 1**

### **INTRODUCTION**

#### **1.1 Background.**

The stability of slopes, either existing or man-made, is an important factor in many aspects of engineering. The accelerated economic development of mountainous regions, construction of transportation facilities, water supply, mineral resources, forestry, agriculture and recreational activities all require slopes that are both safe and economically feasible. Evaluation of slope failure potential is often very difficult as the factors promoting the instability may be unique not only from site to site but also often within the same slope. There are no standard procedures and routines that provide an “exact” solution. Only the combination of thorough site investigation, analytical techniques and a large portion of good engineering judgement can provide acceptable solutions.

The analytical part of a slope stability investigation has been traditionally performed using limit equilibrium methods. In this approach the slope is assumed to fail along a known surface or the surface is found by trial and error search techniques. In the last decade, numerical modelling techniques have developed into powerful analytical tools. Increased computing power allows the inclusion of more geological detail and the consideration of various environmental factors in the construction of models. The ability to represent the slope-forming material more realistically with improved constitutive criteria, the success of numerical modelling in other branches of mechanics, and the

availability of versatile and powerful computer programs has had a significant influence on the progress and confidence in numerical modelling application. Modelling enables the analysis of increasingly complex problems which have been previously approached mainly from an empirical point of view.

## **1.2 Objectives**

The main objective of this work is the characterization of varied complex slope deformations through the applications of numerical modelling techniques. The following investigations are undertaken:

- 1) Investigation of the deformation mechanisms and failure extent of block type slope movements involving relatively rigid, joint-bounded rock blocks overlying a weak base including a case study of deformations at the Spis Castle in Slovakia.
- 2) Investigation of toppling slope-failure mechanisms at the Luscar Mine in Alberta.
- 3) Investigation of the relationships between underground mining and slope stability.
- 4) Re-examination of the Frank Slide failure-mechanism in southwestern Alberta, emphasizing the possible influence of underground coal mining at the base of Turtle Mountain on the final failure.

The results of each phase of analyses are critically discussed, highlighting the advantages and/or disadvantages of the numerical modelling techniques as compared to more conventional analytical tools. New results, knowledge and understanding of deformation and failure mechanisms are generated. Hypothetical cases are analyzed to improve our understanding of the mechanisms of deformation operative in such complex slope failures.

### **1.3 Research Procedure and Thesis Structure**

An extensive literature survey on the various types and processes of slope deformation, and the selection of suitable analytical methods, was undertaken. Two numerical modelling programs, FLAC and UDEC, that are based on the finite difference and distinct element methods were used in the analyses. Field work and site visits were undertaken during 1992, 1993 and 1994 to obtain the input data for numerical analysis. The data collection and the numerical modelling itself were focused on understanding the failure mechanisms, rather than on the back-analysis of displacement rates or precise understanding of the stress-strain characteristics of materials involved. Collaborative research was undertaken with the Department of Geotechnics, Slovak Technical University, in the investigation of the deformation mechanism at the Spis castle. An overview of the research program is shown in figure 1.1.

Chapter 1 contains a statement of the research objectives and the research procedure adopted.

Chapter 2 presents the elements of classification, investigation, mitigation and analysis of landslides based on literature review and discusses the available analytical tools. The numerical modelling approach is discussed with emphasis on the methods used in this research. The principles of the modelling programs used in the research are outlined.

Chapter 3 presents an analysis of block-type slope movements of rigid, joint-bounded blocks overlying relatively weak, soft strata. The analysis of hypothetical slope geometries and a case study are undertaken with the distinct element method, allowing for the continuum representation of the soft base, as well as explicit modelling of the overlying jointed rock blocks. Hypothetical structures with variable jointing in the rigid rock cap and shear strength of the weak base layers are investigated. The main emphasis is given to the resulting deformation pattern allowing conclusions on the

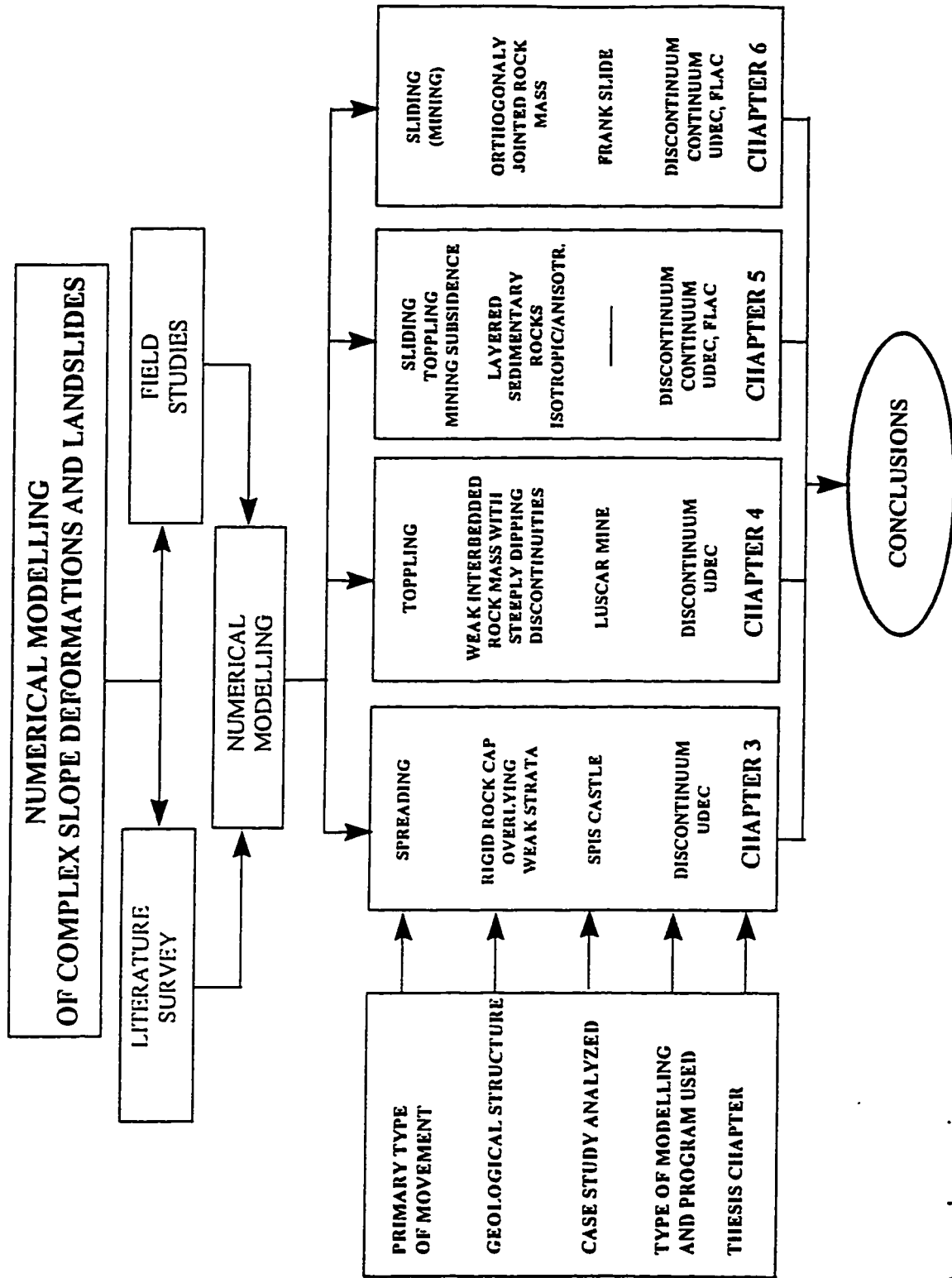


Figure 1.1. Research overview.

various mechanisms typical for this type of instability. As a case study, the deformation of travertine blocks forming the foundation of the Spis castle in Slovakia are investigated. The study is based on field work between 1992-94, which took place in collaboration with the Department of Geotechnics, Slovak Technical University. Detailed structural data as well as results from testholes were available for the numerical modelling analysis.

Chapter 4 analyzes toppling deformation with emphasis on slope failures experienced at the Luscar Coal Mine in Alberta. A review of toppling and the methods available for analysis is given. The slope failures at the Luscar Mine took place in rock slopes susceptible to flexural toppling deformation and were accentuated by the presence of weak rock, intense jointing and folding. The mechanism of failure in one of the open pits is investigated. Based on this analysis a preliminary conclusion is given regarding slope behavior in a planned pit extension in the same mine section.

Chapter 5 analyzes the influence of underground mining on slope instability mechanisms. Various types of slope movements were studied, including sliding and toppling deformation. The influence of underground mining was confined to mining under the base of the slope. Both continuum and discontinuum methods were applied.

Chapter 6 analyzes the Frank slide in southwestern Alberta, Canada. The mechanism of this 1903 failure is investigated, especially in terms of the possible influence of underground mining on the instability of the Turtle Mountain slope. The continuum finite difference method and the discontinuum distinct element method of numerical modelling were used in the study. This work presents the first detailed application of elasto-plastic numerical modelling to the analysis of this case study.

Chapter 7 summarizes the results of previous sections, highlighting the advantages and disadvantages of the numerical modelling methods as applied to complex slope deformations and makes recommendations for future work.

## CHAPTER 2

### LANDSLIDE MECHANISMS AND ANALYSES

#### 2.1 Definition and Classification of Landslides

The term landslide as proposed by the Working Party on World Landslide Inventory is a “ *movement of a mass of rock, earth or debris down a slope* ” (Cruden, 1991). It is possible to divide and classify landslides according to numerous factors including type and speed of movement, resulting failures, type of material involved, resulting deposits, age, state of activity, genesis and geometry of movement.

**Table 2.1.** Classification of landslides (after Varnes, 1978).

TYPE OF MOVEMENT	TYPE OF MATERIAL		
	BEDROCK	ENGINEERING SOILS	
		PREDOMINANTLY	
		COARSE	FINE
FALL	ROCK FALL	DEBRIS FALL	EARTH FALL
TOPPLE	ROCK TOPPLE	DEBRIS TOPPLE	EARTH TOPPLE
SLIDE	ROCK SLIDE	DEBRIS SLIDE	EARTH SLIDE
SPREAD	ROCK SPREAD	DEBRIS SPREAD	EARTH SPREAD
FLOW	ROCK FLOW	DEBRIS FLOW	EARTH FLOW



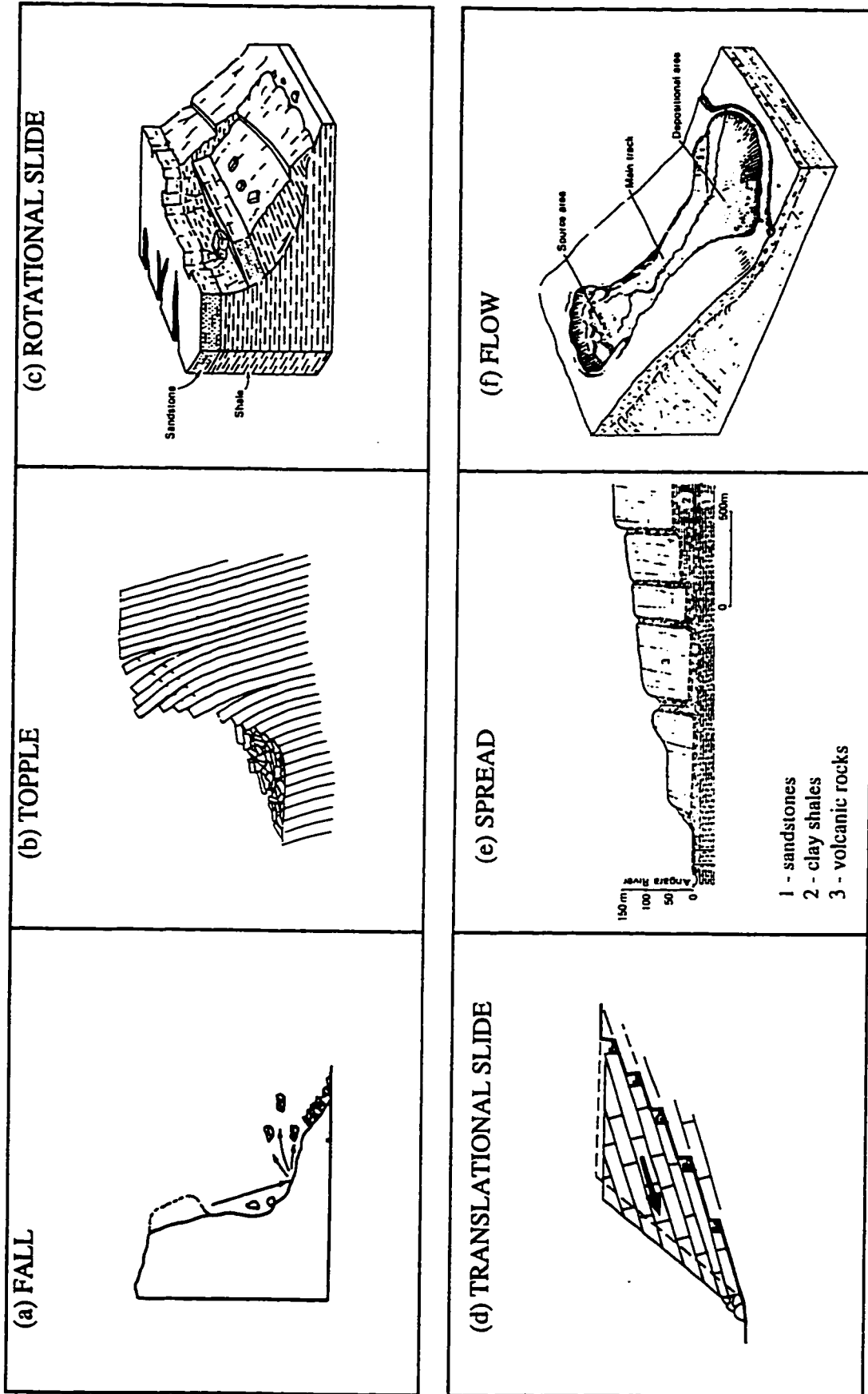


Figure 2.1 Examples of the main types of landslide mechanisms (based on Turner and Schuster, 1996).

A number of attempts have been made to classify landslides, each having its usefulness: e.g., Heim (1882), Howe (1909), Almagia (1910), Ladd (1935), Sharpe (1938), Emelyanova (1952), Varnes (1958 and 1978), Hutchinson (1969), Zaruba and Mencil (1969), Nemcok, Pasek and Rybar (1974). In the English speaking world the two most common classifications encountered are by Hutchinson (1969) and Varnes (1978). Varnes' classification is shown in table 2.1.

- **Falls** - a very rapid to extremely rapid gravitational movement of masses and single fragments on steep slopes. Part of the detached mass may fall freely through the air, followed by bouncing, rolling and/or a combination of these two types of movements depending on the slope angle below the unstable section (Hungr and Evans, 1988). The masses involved in falling can be moved a relatively great distance compared to its original position, due to the high kinetic energy. These rapid movements may be preceded by other types of movement, such as toppling and sliding. Cruden and Varnes (1996) consider *sturzstroms*, the extremely rapid flows of dry debris created by large falls and slides, as a type of complex fall. An example of a fall is shown in figure 2.1(a).
- **Topples** - a distinct type of slope movement characterized by downslope overturning, through rotation or flexure, of interacting blocks of rock under the forces of gravity, or the forces exerted by adjacent units or fluids within discontinuities. Slopes where well-developed discontinuities or pervasive foliation dip steeply into the slope, and trend parallel or sub-parallel to the slope face are especially susceptible to toppling. There are three main groups of toppling: flexural, block and block-flexural (Goodman and Bray, 1976). Toppling may lead to development of slides and falls dependent on the plane of separation, the geometry of the unstable part of the slope, and the orientation of discontinuities. Secondary toppling is generally initiated by undercutting of the slope toe by natural events such as erosion or weathering, or by human activity. The different modes of secondary toppling are discussed in chapter 4. An example of toppling is shown in figure 2.1(b).

- **Slides** - a movement of the soil or rock mass along one or several surfaces of rupture which separate the moving masses from the underlying material. The sliding type of movement is, according to Cruden and Varnes (1996), further divided into rotational, translational, compound, and complex and composite slides. In the rotational type of movement the main displacement takes place along a failure surface that is curved and concave with little internal deformation in the displaced mass. This type of failure is most typical for homogeneous materials. Translational slides follow a planar or undulating failure surface, being generally shallower than rotational slides. They commonly follow discontinuities, contacts between rock types, weak layers or weathering interfaces. Compound slides usually have steep main scarps, flattening with depth. Due to the curved failure surface, the failed part of slope undergoes internal deformation and shear along surfaces within the displaced material. Complex and composite slides include a variety of movement including, for example, both sliding and flow of fine sands and other cohesionless materials. Cruden and Varnes (1996) suggest the term *complex slide flows* for this kind of movement rather than *flowslide*. An example of rotational and translational sliding is shown in figures 2.1(c) and 2.1(d), respectively.
- **Spreads** - a movement characterized by “*extension of a cohesive soil or rock mass combined with a general subsidence of the fractured mass of cohesive material into softer underlying material.*” (Cruden and Varnes, 1996). This group includes block, liquefaction and complex spreads. Block spreading is characterized by a layer of rock overlying softer material. Yielding of the soft base causes fracturing and separation of the overlying rock, which typically takes place at an extremely slow rate. This type of deformation is analyzed in more detail in chapter 3. The liquefaction spread is typical for sensitive clays and silts with translational, retrogressive movement. Complex spreads include movements and deformations generally known as cambering and valley bulging, well described in England (Hutchinson, 1988). An example of spreading is shown in figure 2.1(e).

- **Flows** - a spatially continuous movement, where the surfaces of shear are short-lived, closely spaced and usually not preserved. The bottom boundary of the unstable mass may be a distinct surface or a relatively thick zone. Flows may develop from slides where there is an increased water content, loss of structural integrity, or steepening of slope gradient (Cruden and Varnes, 1996). Debris slides may, for example, develop into debris flows or debris avalanches. Skin flows may develop in permafrost regions, as referred to by McRoberts and Morgenstern (1974), into rapid movement of a thin thawed soil and vegetation. A special category within this type of movement is represented by the slow flow in bedrock, known also as “*sackung*” or deep-seated creep. In this type of movement large-scale gravitational deformation takes place without the formation of a pervasive failure surface. An example of a debris flow is shown in figure 2.1(f).

## 2.2 Stability Investigation

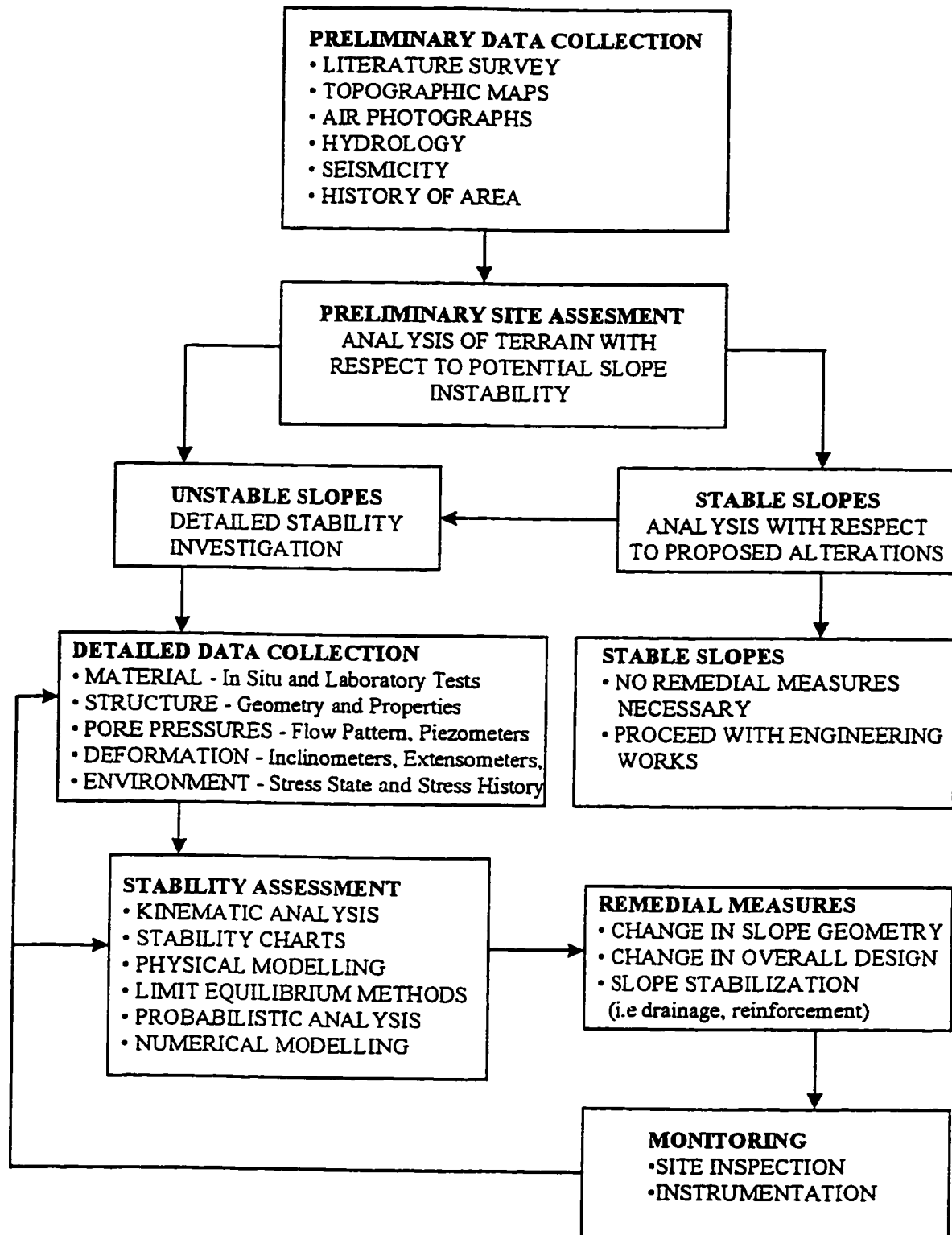
Over the years numerous methods and methodologies in slope stability investigation have been developed and used in research and routine engineering practice. Slopes, either natural, excavated or deposited, are subjected to investigation for various reasons. Slope stability investigations are conducted for urban development, planning construction and maintenance of transportation routes, energy development, extraction of natural resources, recreation and others.

The primary purpose, regardless of the objective of the investigation, is to ensure that slopes are both safe and economically sustainable. This goal is not always easy to achieve as the material behind every slope face is unique, precluding a standard, rigorous procedure that provides the “right answers” in every case. When dealing with slope stability concerns a proper understanding of four interrelated groups of topics is required (Skempton and Hutchinson, 1968):

- Recognition and classification of the various types of slope movements that can occur on slopes, their characteristic morphological features, geological setting, rates of displacement and the causes of failure.
- Classification and description of the material involved in slope movement and the quantitative measurement of their relevant properties.
- Methods of calculating the stability of a slope in terms of the type of failure, real or anticipated, and material properties.
- Correlation between field observations and the results of stability calculations based on the measured properties and deformation of the material involved in a slope movement.

Figure 2.2 presents the basic steps in an analytical procedure for slope stability investigation. The first step in a comprehensive slope stability investigation should be the collection of all relevant information about the site from aerial photographs, available maps and inventories, previous reports and field work. It is important to know the intended development of the site, as different levels of investigation are needed for various construction purposes.

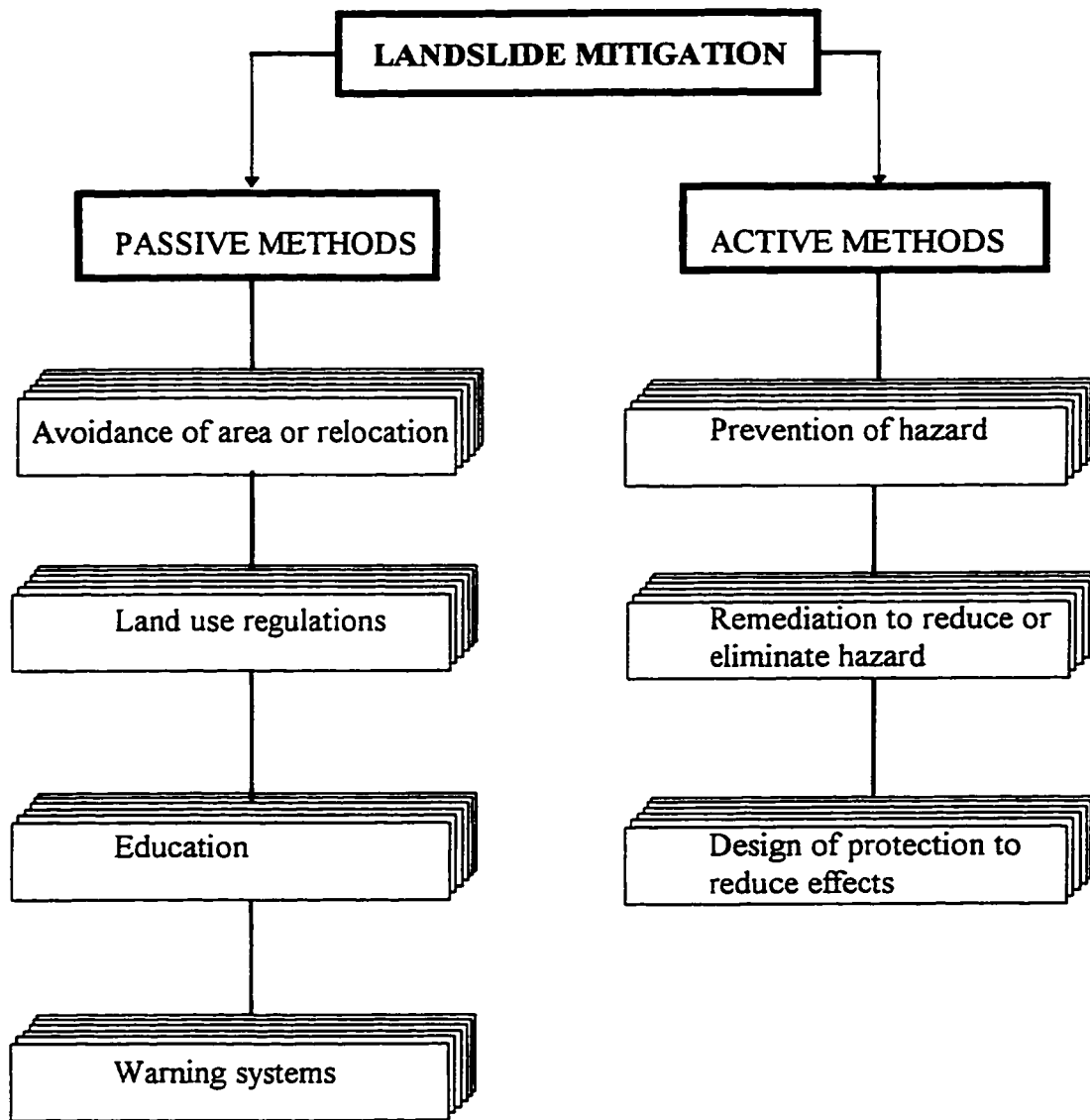
Once all available data is collected one should proceed to a preliminary stability assessment. This may require some form of laboratory or field testing, to acquire or at least approximate the input parameters for slope stability analysis. Areas that are presently stable and do not show evidence of previous instability should be assessed in terms of the planned development. If concern is expressed that the proposed works will contribute to slope destabilization, a detailed stability analysis should be undertaken. If the future loading will not decrease the stability to an unacceptable level, development can proceed as planned. For areas that are presently unstable or indicate previous instability, a detailed data collection program should be initiated. Information on the



**Figure 2.2.** General analytical procedure for slope stability investigation.

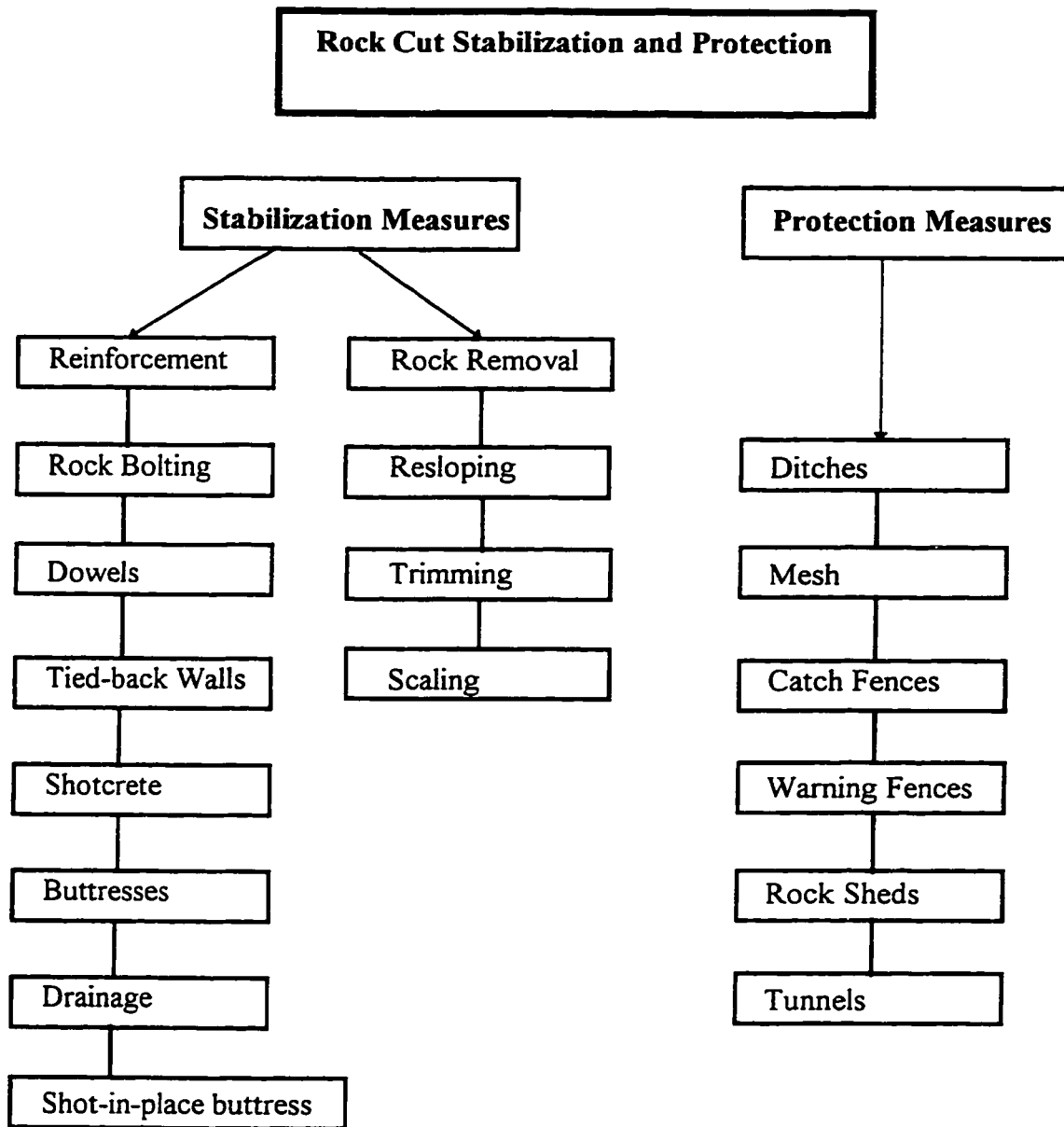
material properties, rock/soil mass structure, groundwater regime and overall environment should be obtained for a subsequent stability analysis. The currently available analytical methods are briefly reviewed in the following section. The analytical results will either confirm or disagree with the suspected slope-instability problems as determined from preliminary site assessment. Even if the analytical methods point to stable conditions one must use engineering judgment and common sense, based on previous experience, in the decision making process. Therefore, analytical methods should not be considered the solution to a problem but only a useful tool in the stability assessment procedure. In cases where the analysis confirms the presence of unstable conditions a decision must be made with respect to further action. This can result either in an improvement of existing site conditions or a change in the planned site use.

Figure 2.3 presents a general division of mitigative methods into two groups, passive and active, based on a classification used by VanDine (1996) for channelized debris flows. No direct engineering is involved in passive methods, because no attempt is made to prevent, modify or control the failure. Active methods on the other hand will require some degree of engineering once the potential hazard has been identified and assessed. These methods can involve some form of prevention of the hazard, remediation to reduce or eliminate the potential of failure, or the design and construction of some form of protection to reduce the effects. More specific examples of the application of remedial measures to rock and soil slope stabilization are shown in figures 2.4 and 2.5, respectively.

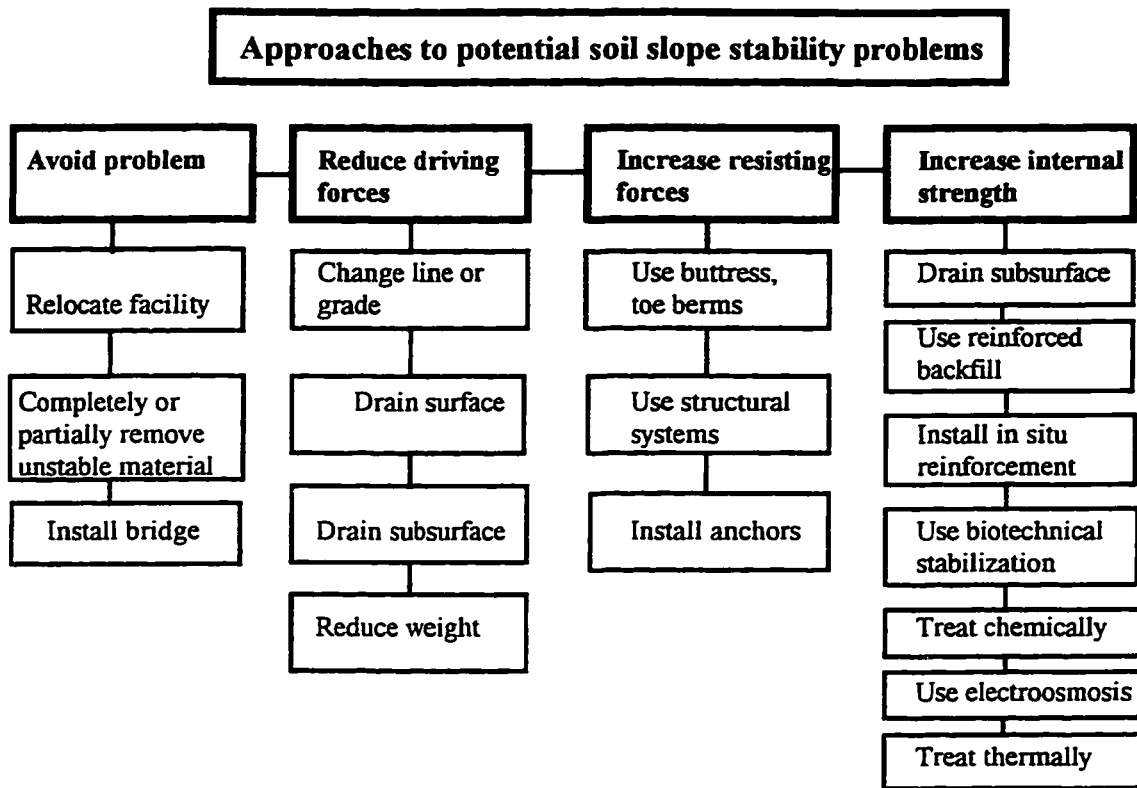


**Figure 2.3.** Example of landslide mitigation methods (modified from VanDine, 1996).





**Figure 2.4.** Categories of rock slope stabilization measures (after Wyllie and Norrish, 1996).



**Figure 2.5.** Approaches to potential slope stability problems (after Holtz and Schuster, 1996).

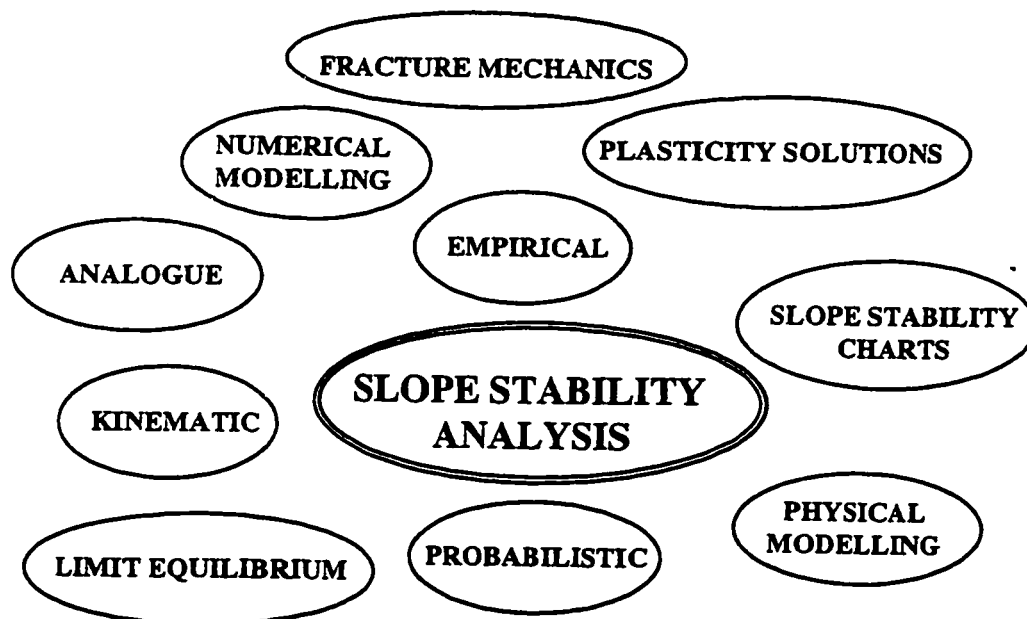
### 2.3 Methods of Analysis

Many different analytical methods have been developed and used in the assessment of slope stability. The primary objective of an analysis is to assist in the design of safe, functional and economic soil and rock slopes. The choice of a proper analytical technique should be dependent on the in situ conditions, scale, availability, reliability and understanding of relevant data, as well as the purpose of analysis. Different approaches will be used in a soil slope or a competent rock slope, in cases where the failure mechanism is well understood as opposed to cases in which a limited knowledge about the cause and mode of failure exists. Similarly a different approach may be used in cases where the stability of the slope along a well-defined failure surface is of interest, or where

the magnitude of the potential instability and the overall extent of deformations are important.

A comprehensive slope stability analysis will allow for the evaluation of various design parameters such as slope angle, slope height, construction and/or excavation sequencing, parametric studies and requirements for remedial measures. Figure 2.6 presents some of the more common analytical methods used in the assessment of slope stability.

It is beyond the scope of this study to discuss in detail all these individual approaches. Therefore, only a brief summary of the principles of those used most often in engineering practice is presented. The numerical modelling techniques, especially those used in this thesis, are then discussed in more detail.



**Figure 2.6.** Commonly used approaches to slope stability analysis.

### **2.3.1 Empirical and Analogue Approach**

Empirical and analogue approaches are based on previous experience dealing with particular geological structures, material types, groundwater regimes and slope problems. Although the experience factor may often be the key component, the decision making process usually must be supported by analytical procedures such as slope stability charts, kinematic analyses or limit equilibrium methods, as explained in the next sections.

The analogue approach extrapolates problems encountered in certain areas to new places of the same or similar geological and geomorphological structure, material type and human activity. It is closely related to the empirical approach in that one must have enough experience, confidence and sound engineering judgment from previous work in the particular area of interest. The analogue approach was used with success for example in a large project dealing with the prediction of slope instability due to undermining in the Vtacnik Mountains in the Slovak Republic (Malgot et al., 1986).

Slope mass rating (SMR) classification is potentially a very useful tool in the preliminary assessment of slope stability, providing information about instability modes and required support measures. This technique is an application and extension of the rock mass rating (RMR) system (Bieniawski, 1989). More information on this technique can be found, for example, in Romana (1995). It has found little use to date, however, in routine engineering practice. The rock-interaction matrix approach proposed by Hudson (1992) may allow further development in the empirical approaches. The application of GIS (Geographic Information Systems) to slope stability problems has seen a very rapid expansion in the last decade. GIS allows for the storage and manipulation of information concerning the different terrain factors as distinct data layers, and thus provides an excellent tool for slope stability hazard zonation (Soeters and VanWesten, 1996).

### **2.3.2 Kinematic Methods**

Kinematic analyses of slope stability are characteristic of rock slopes containing well developed discontinuities. This analysis is based on the orientation of discontinuities defined usually in terms of dip and dip direction. The interpretation of the data uses stereographic projections, allowing for a two dimensional representation of the three dimensional data. Kinematic analysis evaluates the freedom of the discontinuity bound blocks to displace. The analysis of the discontinuities data can be done either manually using a stereonet or by computer (Hoek and Diederichs, 1995). More sophisticated kinematic analyses based on topological block theory have been developed by Goodman and Shi (1985). They may be used to determine the keyblocks within a slope. Computer programs are available to allow routine block-theory analysis (Windsor, 1991).

More detailed explanation of the stereographic techniques and/or their application to slope stability analysis can be found in Goodman (1976), Hoek and Bray (1981), Priest (1985) or Goodman (1989).

### **2.3.3 Slope Stability Charts**

Slope stability charts provide a fast and useful tool for slope stability assessment. The charts are developed for a simple homogeneous slope. Therefore, in order to apply them to field conditions, it is necessary to approximate the real slope with an equivalent geometry and material. As suggested by Duncan (1996), the most effective method of developing a simple slope profile for chart analysis is to begin with cross-section of the slope drawn to scale. On this cross section, using judgment, the professional draws a geometrically simple slope that approximates the real slope as closely as possible. In the next step the shear strength for chart analysis needs to be averaged. Various charts have been developed (Bishop and Morgenstern, 1960; Janbu, 1968; Hunter and Schuster,

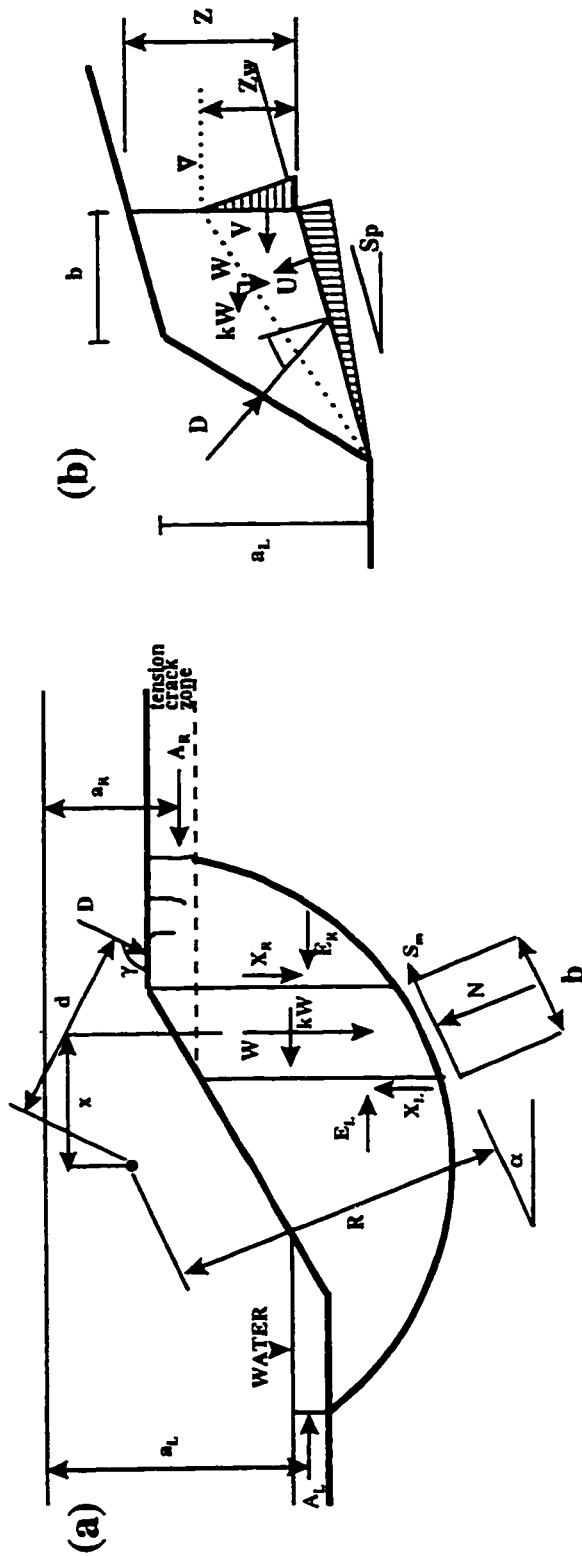
1968; Hoek and Bray, 1981; Duncan et al., 1987; and others) each taking into account different strength and slope geometry parameters.

### **2.3.4 Limit Equilibrium Methods**

The two-dimensional limit equilibrium method remains the most commonly used technique for slope stability analysis in routine engineering practice. This popularity can be attributed to its relative simplicity and ease of use, as well as the many decades of experience in its application. The stability of both soil and rock slopes can be assessed.

In limit equilibrium methods of analysis a condition of incipient failure is postulated along a continuous slip surface of a known or assumed shape. The slope stability, usually with respect to shear strength, is then defined using a factor of safety. The factor of safety can generally be defined as the ratio of the total force available to resist failure to the total force tending to induce failure (Hoek and Bray, 1981). Figure 2.7(a) shows a simple case of a circular slip surface, forces applied on a typical slice, and figure 2.7(b) a discontinuity controlled failure.

Circular failure plane is representative for homogeneous soils, waste rock and heavily fractured rock with no identifiable structural pattern. Composite failure surfaces are most common in field conditions. For hard rock and low stress conditions the failure surface would be predetermined by the existing discontinuities, as shown in figure 2.7(b). Limit equilibrium methods have been further developed for more complicated failure mechanisms, such as toppling, as demonstrated in chapter 4 (figure 4.4), or wedge and stepped-path failures. In an attempt to represent the actual field conditions more realistically, three-dimensional limit equilibrium methods have been developed, as for example by Hungr (1987). Comparisons between these two types of limit equilibrium methods (Cavounidis, 1987) show that factors of safety, calculated using three-dimensional methods, are larger than those calculated by two-dimensional



- W** - The total weight of the slices of width  $b$  and height  $h$   
**N** - The total normal force on the base of the slice  
 **$S_m$**  - The shear force mobilized on the base of each slice  
**E** - The horizontal interslice normal forces; L-left, R-right  
**X** - The vertical interslice shear forces; L-left, R-right  
**D** - An external seismic load  
 **$kW$**  - The horizontal seismic load applied through the centroid of each slice  
**R** - The radius for a circular slip surface or the moment arm associated with the mobilized shear force  $S_m$  for any shape of slip surface  
 **$x$**  - The horizontal distance from the centerline of each slice to the center of rotation or to the center of moments  
 **$d$**  - The perpendicular distance from a line load to the center of rotation or to the center of moments
- a** - The perpendicular distance from the resultant external water force to the center of rotation or to the center of moments; L-left, R-right  
**A** - The resultant external water forces; L-left, R-right  
 $\alpha$  - The angle between the tangent to the center of the base of each slice and the horizontal  
 $\gamma$  - The angle of the line load from horizontal  
**U** - Uplift water force  
**V** - Driving water force  
**Sp** - Inclination of failure plane  
**Z** - Depth of tension crack  
 **$Z_w$**  - Height of water in tension crack  
**b** - Distance of tension crack from slope face

**Figure 2.7.** Forces acting in and on slope considered in a limit equilibrium analysis for a circular failure surface (a) and a failure surface confined to pre-existing discontinuities (b). Based on Fredlund (1992) and Wyllie and Norrish (1996)

methods other things being equal. Limit equilibrium methods also allow for evaluation of various aspects, such as the dynamic loading by introducing a force representing horizontal acceleration, the role of progressive failure in the landslide mechanism (Chowdhury, 1978), or the unsaturated conditions (Fredlund and Rahardjo, 1993) and others.

Misfeldt et al. (1991) coupled the limit equilibrium methods with the seepage analysis to simulate a progressive valley deepening in order to understand the historical development of an unstable river bank. In a similar way, limit equilibrium methods can be used to assess the stability of a particular slope failure surface developed in a numerical modelling analysis.

Limit equilibrium methods provide reasonably good results for situations in which the failure mode is readily identifiable and involves translation or rotation. The advantages of limit equilibrium methods are in their simplicity of use and minimal requirements on computational power. The analysis can be performed relatively quickly using a commercially available slope stability program or even a standard spreadsheet program. Furthermore, this analysis method has a long tradition in use and a good understanding of the principles involved, providing quick and simple results in the form of a factor of safety.

Limit equilibrium methods have several disadvantages. The confining stresses are difficult to incorporate, no consideration is given to the stress/strain behavior of the slope material and the time factor. Furthermore, limit equilibrium methods are difficult to apply to complex geological conditions; they assume that failure occurs along a failure surface according to a perfectly plastic shear force law (i.e. shear force is independent of displacement) and no consideration is given to the displacement in the soil and rock mass.



### **2.3.5 Fracture Mechanics**

The application of fracture mechanics to rock slope stability takes into account the importance of crack-tip stress concentration and considers that the rock failure occurs as a result of crack initiation and propagation. This method is based on the principle that jointed rock slope stability is governed by the stress intensity factors at the joint tips rather than by the frictional resistance along joint surfaces (Whittaker et al., 1992).

Fracture mechanics makes it possible to predict the formation of failure surfaces in jointed rock masses and to explain how stepped-path failure occurs. This method has had little application in engineering practice. More information on this technique of slope stability analysis can be found in Whittaker (1992) or Tharp and Coffin (1985).

### **2.3.6 Probabilistic Analyses**

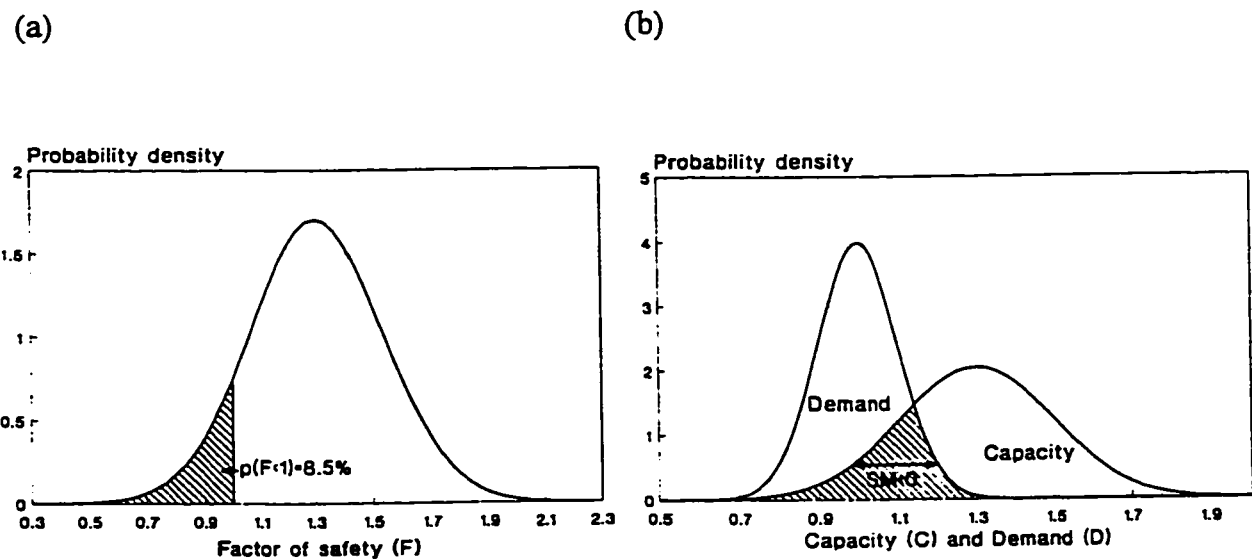
The development and application of probabilistic risk analysis in slope stability analysis have increased significantly in the last two decades, providing a powerful tool for solving problems, implementing design and decision making. Limited or uncertain data can be utilized in analysis and judgments can be quantified (Whittlestone et al., 1995). Probabilistic risk analysis is used in an effort to overcome the subjective judgment of slope stability parameters and resultant, single value, factor of safety. The subjectivity and uncertainties are due to the spatial variability of the material properties and their measurements, as well as uncertainties in reliability of the hypothesis carried out to approximate the mechanical behavior of the rock and soil mass.

In this method each variable used in the analysis is given a probability distribution function instead of a single design value. Typically a Monte Carlo or Latin Hypercube (Hoek et al., 1995) simulation are used to generate random numbers from which each of the variable values is assigned, using spreadsheet add-in programs, such as @RISK

(Palisade Corp., 1988). They both require that the distribution of all the input variables is either known or assumed.

The factor of safety, safety margin, reliability and reliability index can be assessed to determine the probability of failure. Figure 2.8 shows an example of a factor of safety probability distribution, and capacity and demand probability distribution. Considering, C is the capacity (or strength or resisting force) and D is the demand (or stress or disturbing force) the factor of safety is defined as  $C/D$  and failure is indicated when  $C/D$  is less than one (Pine, 1992). The probability of  $C/D$  being less than one can be used as a measure of stability. An alternative is the safety margin, defined as  $C - D$ , indicating failure when equal to zero.

Although probabilistic analysis was treated separately in this chapter, it is not a method in itself, but is linked and used in conjunction with other methods (limit equilibrium, block theory, numerical modelling, etc.). The reason for “highlighting” this approach in



**Figure 2.8.** Factor of safety (a) and capacity and demand (b) probability distributions (after Pine, 1992).

slope stability analysis was to point to its gaining importance in the decision making process, considering the uncertainty of input parameters, which very often are based on limited information and testing of the rock mass or soil material. More information and explanation of these methods can found in Priest and Brown (1983), Pine (1992), Whittlestone et al. (1995), and Hoek et al. (1995).

### **2.3.7 Physical Modelling**

Physical modelling has been used with success in all areas of geomechanics. It was a popular analytical tool especially two to three decades ago. Presently the use of centrifuge modelling provides very good results. A wide range of materials has been used ranging from mixtures of sand, oil, plaster and water to brick models. The problem of scaling from field to the laboratory has been recognized. Hencher et al. (1996) point out that it is not possible to scale all aspects of a model consistently with the prototype at the same time, and it is necessary, therefore, to concentrate on scaling particular relevant parameters according to some similar performance criterion that has been selected on the basis of the nature of the problem that is being modelled.

Centrifuge models are very capable of simulating the modes of deformation and failure in slopes to be expected under field conditions as the models can be constructed so that they simulate the geometry and stresses in a prototype slope. Their limitations appear to be the relatively high cost and specialized equipment needed, as well as the problem of deriving reliable quantitative results from the experiments. The principles and relevant scaling laws relating to centrifuge model testing have been discussed in detail by Schofield (1978, 1980) and a recent application of constraining numerical modelling results of slope stability with centrifuge modelling has been presented by Steward et al. (1996).

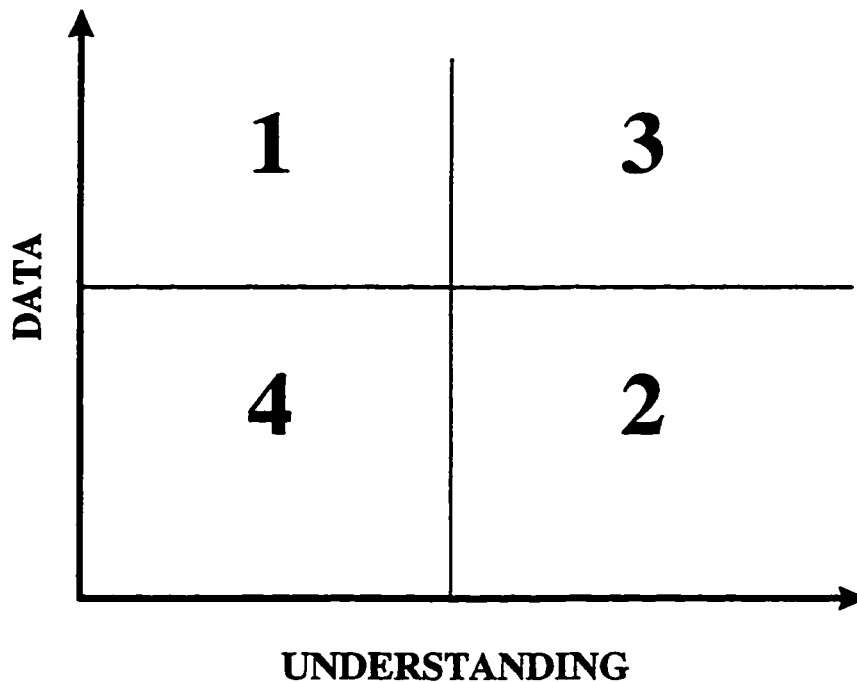
Good results with respect to slope stability have been obtained using the base friction model. The model is constructed from a weak material, placed on a flat base from frictional material such as sandpaper and the base moved to simulate the effects of gravity. More details on this technique are given, for example, in Bray and Goodman (1981).

### **2.3.8 Numerical Modelling**

In the last two decades, there has been a great expansion in the application of numerical methods in the field of geomechanics. Their application has gradually changed from predominantly experimental research to practical engineering design. Presently many engineering consulting offices fully utilize and incorporate the results of numerical modelling techniques in the decision making process. The main reason for this change can be found, according to Starfield and Cundall (1988), in:

- the ease of access to versatile and powerful computer programs
- the dramatic increase in the ability to include geological detail in the construction of a model
- the manifest success of modelling in other branches of mechanics

A new era has opened in analysis and design for a wide range of geomechanical problems. Numerical methods allow the analysis of complex factors such as nonlinear behavior, inclusion of complex discontinuity patterns, dynamic loading, inhomogeneity, anisotropy, coupling of the fluid flow and mechanical behavior, material softening, time dependent behavior and others. The adequate understanding of the behavior of geological materials and environmental factors is vital to a successful application of numerical modelling techniques. Geomechanical problems are “data-limited” as one seldom has enough data about the rock and soil mass. Holling (1978) introduced a schematic measure of the relationship between data and understanding as



**Figure 2.9.** Relationship between data and understanding (after Holling, 1978).

shown in figure 2.9. In region 1, where there is available data and little understanding, probabilistic techniques, as discussed in section 2.4.5, would be the most appropriate analytical/modelling tool. In region 3, with enough data and understanding, modelling can be used as a practical design method. Only in special cases has the slope stability analysis sufficient data or data and understanding.

Geomechanical problems fall in most cases in region 4 or 2, with little reliable data in most situations. As pointed by Hoek et al. (1991), in region 2, much of the understanding is in the form of practical experience and is difficult to quantify for incorporation into models. Slope stability problems belong, in most cases, in region 4 where there is a low level of data and understanding. Wittke (1993) pointed out that, although there is always a “desire to have as much data as possible,” it has to be also realized that complexity of the numerical model increases with the increase of input data, and the clarity and general utility is reduced correspondingly.

From the above it is quite clear that an approach to numerical modelling in geomechanics has to have a special methodology. The initial steps in this direction were taken by Starfield and Cundall (1988), Wittke (1993) and more specifically for underground excavations, by Hoek et al. (1991).

Coetzee et al. (1993) discuss the problem of data availability and the approach to numerical modelling in geomechanics. They stress that both qualitative and quantitative results can be obtained, as shown in table 2.2. The various numerical programs may be used either in a fully predictive mode or as a “numerical laboratory” to test various ideas and hypothesis. Therefore, it is the field situations and budget that determine the type of use of numerical methods. Practically all modern textbooks in the broad field of geomechanics include, to a certain extent, the basic principles of the application of numerical modeling techniques with summaries of their particular advantages and disadvantages. The basic guidelines in the numerical modelling application, as suggested by Starfield and Cundall (1988), are shown in table 2.3. Wittke (1993) discussed the upper and lower limits of complexity in numerical modelling in geomechanics. The upper limit is determined by the input data from site investigation, field and laboratory tests, as well as by the expense of the analysis including input data preparation, CPU time, memory and representation of results. The lower limit is given by the usefulness of the results that are to be achieved with the aid of the model.

**Table 2.2.** Spectrum of modelling situations (after Coetzee et al., 1993).

Typical Situation	Complicated Geology; Inaccessible; No testing budget	←————→	Simple geology; \$\$\$ spent on site: Investigation
Data	NONE	←————→	COMPLETE
Approach	Investigation of mechanism	← Bracket field behavior by parameter studies →	Predictive (direct use in design)

**Table 2.3.** Set of guidelines in modelling of geomechanical problems (after Starfield and Cundall, 1988).

1. *Be sure, before you start, that you are quite clear about why you are building a model and what questions you are trying to answer.*
2. *Use a model at the earliest possible stage in a project to generate both data and understanding. Do not delay while waiting for field data. You need a conceptual model in place as soon as possible.*
3. *Look at the mechanics of the problem. Try to identify important mechanisms, modes of deformation and likely modes of failure.*
4. *Think of experiments one would like to perform on the model and try to visualize, quantitatively, what the answers might be.*
5. *Design or borrow the simplest model that will allow the important mechanisms to occur, and could serve as a laboratory for the experiments you have in mind.*
6. *Implement the model, choose your simplest experiments, and run it. If the model ties in with your expectations, proceed to more complex experiments; if not identify the weakness in your thinking and remedy them before continuing.*
7. *If the only available model has weaknesses that you cannot remedy, make a series of simulations that will bracket the true case.*
8. *Once you have learned all you can from simple model or models, you may want to run more complex models to explore those neglected aspects of the geology that are most likely to affect the behavior of the simple model.*

Chowdhury (1978) presented the following observations in stress analysis for slope stability problems:

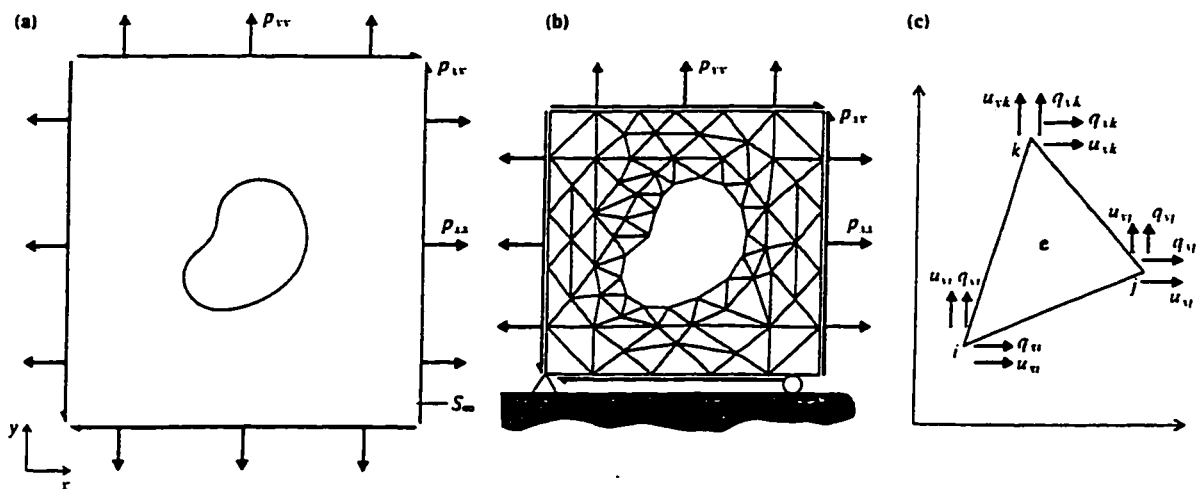
- Importance of the stress state within the slope-forming material, both before and after the formation of slope.
- Knowledge of localized overstressed zone and failure are important in relation to a possible progressive failure, slope alterations and remedial measures.
- Results of stress state enable a proper selection of laboratory testing methods.
- Determination of strains and deformations, important in particular from the strain-softening behavior point of view.
- The extent of deformation is very often a better indication of stability and slope performance than a factor of safety resulting from limit equilibrium methods.

- The incremental nature of excavation and deposition involved in slope creation can be simulated, and has a significant influence on the final stress distribution.
- The stress analysis is essential for the knowledge of pore pressures.
- Advantages of stress analysis over full scale test and/or physical models.
- Shear failure is not always the primary cause of slope failure. In the analysis of failures due to subsidence, spreading, toppling or piping, the knowledge of stress state is of paramount importance.

### 2.3.8.1 Numerical Modelling Techniques

The variety of numerical modelling methods can be generally divided into two distinct categories, domain and boundary methods (Hoek et al., 1991).

- In domain methods, the continuum or discontinuum interior of the rock mass is divided into geometrically simple zones, each with assumed properties (figure 2.10). The finite difference method, finite element method and distinct element method are examples of this approach. More information on these methods is provided in



**Figure 2.10.** Development of a finite-element model of a continuum problem (after Brady and Brown, 1993).



sections 2.4.7.2 and 2.4.7.3. Domain methods are used more frequently in the analysis of slopes than the boundary methods. In this study the finite difference methods (FLAC program; Itasca, 1992), representing a continuum interior, and distinct element method (UDEC program; Itasca, 1993), representing a discontinuum interior of the rock or soil mass, were applied.

- In boundary methods only the surface or excavation of the rock mass to be analyzed needs to be divided into smaller elements (discretized), and the rest of the rock mass is treated as a continuum. The boundary-element method (BEM), including the displacement-discontinuity method is based on this principle. The data preparation for this method is relatively simple. This method is very efficient for homogeneous, linear elastic problems, particularly in three dimensions (Pande et al., 1990). A particular advantages of the BEM is the correct modelling of the far-field boundary conditions and minimization of errors related to the discretization of problem geometry. BEM methods are used much more extensively in the analysis of underground excavations than for slope stability problems. The programs EXAMINE<sup>2D</sup> (Curran and Corkum, 1988) and EXAMINE<sup>3D</sup> (Curran and Corkum, 1993) are examples of BEM programs. More information on BEM can be found for example, in Crouch and Starfield (1983), Pande et al. (1990), Hoek et al. (1991), Manolis and Davies (1993), and Watson (1993).

As a response to the certain advantages and disadvantages of the domain and boundary methods, hybrid codes with a combination of these two methods have been developed. For example, certain areas in a model can be discretized using domain methods, especially in areas close to an excavation, whereas for remote areas the discretization used in boundary methods can be applied.

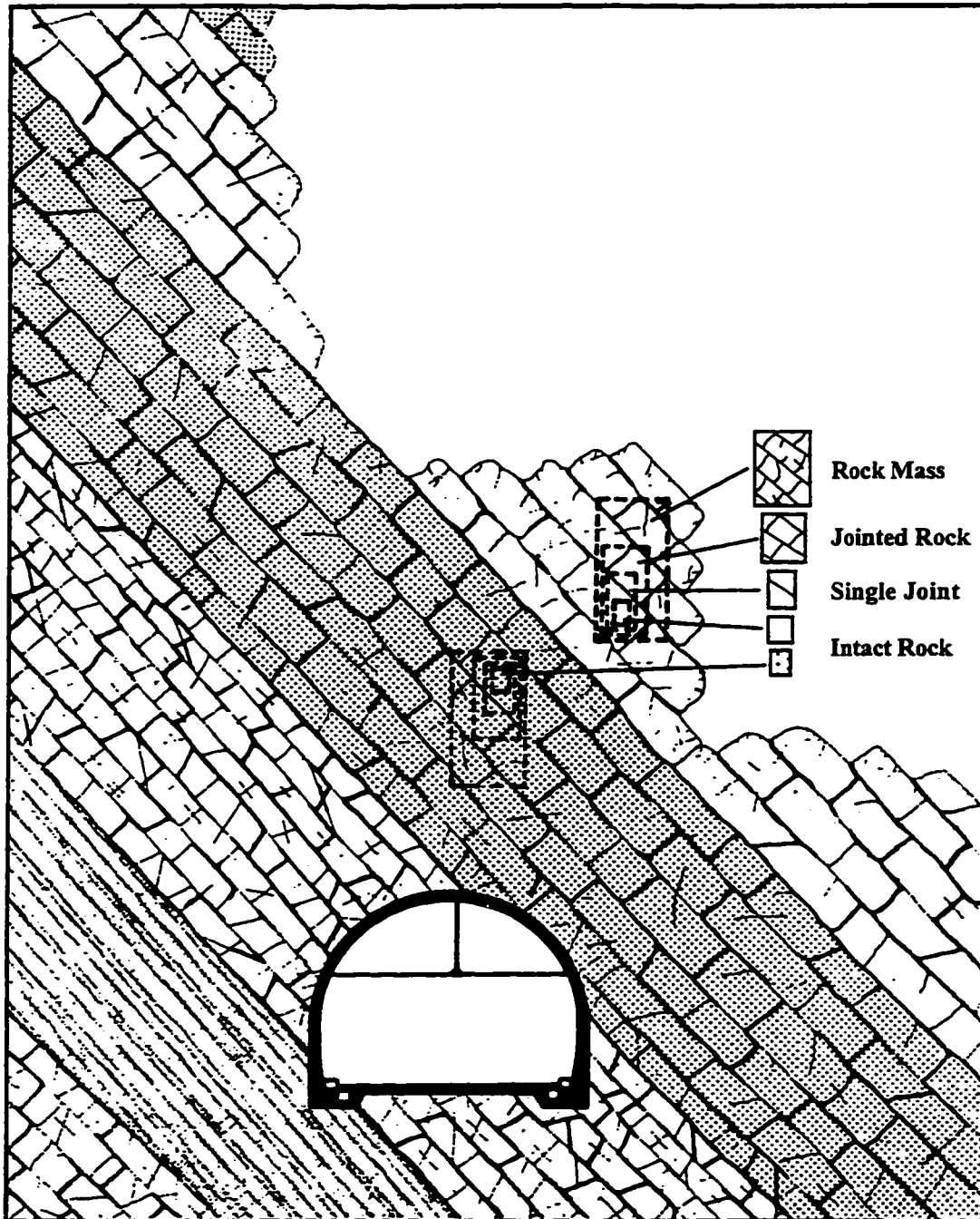
### **2.3.8.2 Continuum and Discontinuum**

There are generally two approaches when designing or analyzing a geomechanical problem: the rock or soil mass can be treated either as a continuum or a discontinuum. The approach adopted depends on the scale of the problem, the type and structure of the material and the purpose of the analysis.

Due to the nature of the soil material, soil mechanics problems are predominantly analyzed using the continuum approach. Although soil is composed of small particles, present limitations in computer technology (computational speed and memory), and understanding of particle behavior on a microscopic scale, do not allow for a practical analysis, where the function of each grain in the overall behavior could be determined. Rather, a holistic approach is used to evaluate the behavior of the soil mass. Recent advances in software development, such as the two and three-dimensional Particle Flow Codes (Itasca, 1995), represent new possibilities for the analysis of small sized, granular materials. The discontinuum approach in soil mechanics may be well justified when dealing for example with stiff jointed clays or in the analysis of a landslide with well developed block-type structure, where the mechanisms and rate of movement are of primary interest.

In rock mechanics problems, all excavation and loading usually occur in a discontinuous rock mass, consisting of a mosaic of joint-bounded blocks. There appear to be two different approaches to the problem of understanding and analyzing the effects of discontinuities on the behavior and properties of rock masses (Cook, 1992). The first approach considers the cumulative effects of discontinuities on the properties of rock masses, hitherto, analyzing the problem as a continuum. The second approach treats the discontinuities, especially the dominant set, statistically or as discrete entities.

The scale factor will play a major role, as illustrated in figure 2.11 (after Cunha, 1990). In laboratory testing, the determination of the physical properties of a certain rock type



**Figure 2.11.** Diagrammatic representation of scale effects (modified after Cunha, 1990).

uses samples varying from approximately 40 mm to 150 mm in diameter by 80 mm to 300 mm in length (Eberhardt, 1995). When the specimen size is increased certain anisotropic features may be incorporated, such as a single fracture or discontinuity in a larger core sample, multiple discontinuities in a block sample, or faults and multiple joint sets in a rock mass. The scale and presence of discontinuities will, therefore, determine the selection of either a continuum or discontinuum approach. When a sample contains no discontinuities or is highly fractured without a predominant discontinuity set, the continuum approach will be the most appropriate. For problems involving relatively few discontinuity sets or structures, where one set has the main influence on the overall behavior, the discontinuum approach will present the best analytical concept.

On a field scale, if for example the overall stability of an open pit mining operation is being investigated, including the layout of mine infrastructure, the surrounding rock mass, the general displacement directions, the overall stress changes and the groundwater flow, a continuum approach may be the most suitable, assuming that no major discontinuity (e.g. fault zone) is present. On the other hand, when a more localized instability is of concern, such as the stability of an individual or several benches that are usually controlled by joints or bedding planes, the discontinuum approach seems to be more appropriate. A comprehensive review and the fundamentals of continuum and discontinuum modelling can be found in Hudson and Fairhurst (1993).

Two acronyms, CHILE (Continuous, Homogeneous, Isotropic and Linearly Elastic) and DIANE (Discontinuous, Inhomogeneous, Anisotropic and Non-Elastic), have been described by Hudson (1993) when discussing the different approaches in rock mechanics analysis. He points out that even if a rock mass is not likely to be “CHILE”, there is often value in conducting analyses for such a material, if only to consider what the deviation from these ideal conditions might be in the practical case.

### **2.3.8.3 Finite Difference Method and the FLAC Program**

The finite difference method is perhaps the oldest numerical technique used for the solution of differential equations, given initial values and/or boundary values (Itasca, 1995). The finite difference method is based on the division of the problem domain into an assembly of discrete interacting nodes to which governing equations are applied. These equations include the differential equations of equilibrium, the strain-displacement relationship and the stress-strain equations.

The Fast Lagrangian Analysis of Continua (FLAC) program (Itasca, 1995) utilizes the explicit finite difference scheme and is a two-dimensional program for geotechnical and mining engineering applications. FLAC simulates the behavior of the rock/soil mass or structures built in, at or from them, as well as other materials which may undergo plastic flow when their yield limit is reached. Materials are represented by zones which form a grid that is adjusted by the user to fit the shape of the object to be modeled (figure 2.12).

Each zone behaves according to a prescribed linear or non-linear stress/strain law in response to the applied forces or boundary restraints. If the stresses are high enough to cause the material to yield, the grid will deform and move (in the large strain option). The power of FLAC is that it can analyze complicated geometries and various geological structures. Discontinuity planes can be incorporated in the form of interfaces. If, however, a highly jointed structure is analyzed the UDEC program described in section 2.4.7.4 must be used. The general calculation sequence embodied in FLAC is illustrated in figure 2.13. The equations of motion are first invoked to derive velocities and displacements from stresses and forces. Then, strain rates are derived from the velocities, and new stresses from the strain rates (Coetzee et al, 1993). Each box in figure 2.13 updates all of its grid variables from known values that remain fixed while control is within the box.

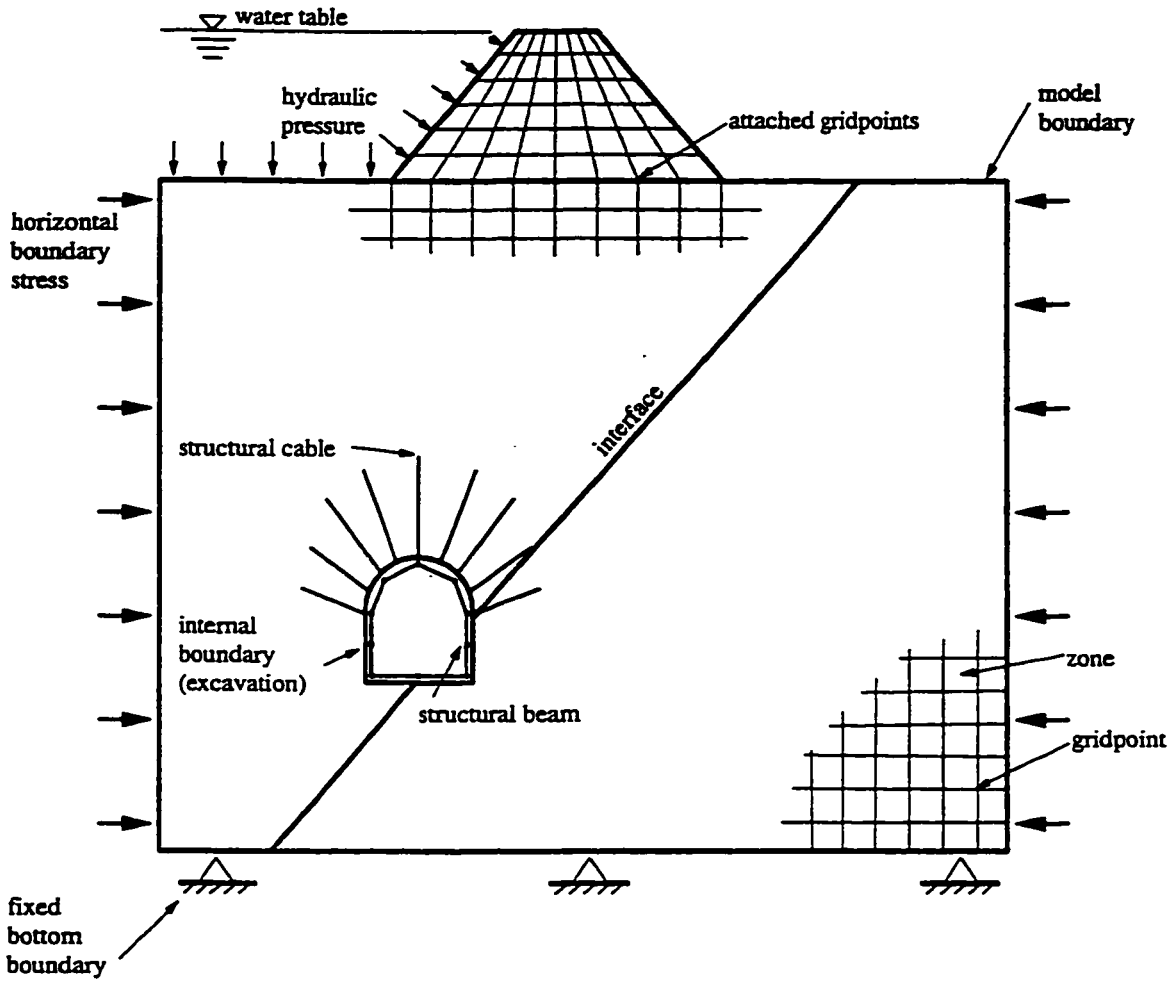


Figure 2.12. Various elements of a FLAC model (after Itasca, 1992)

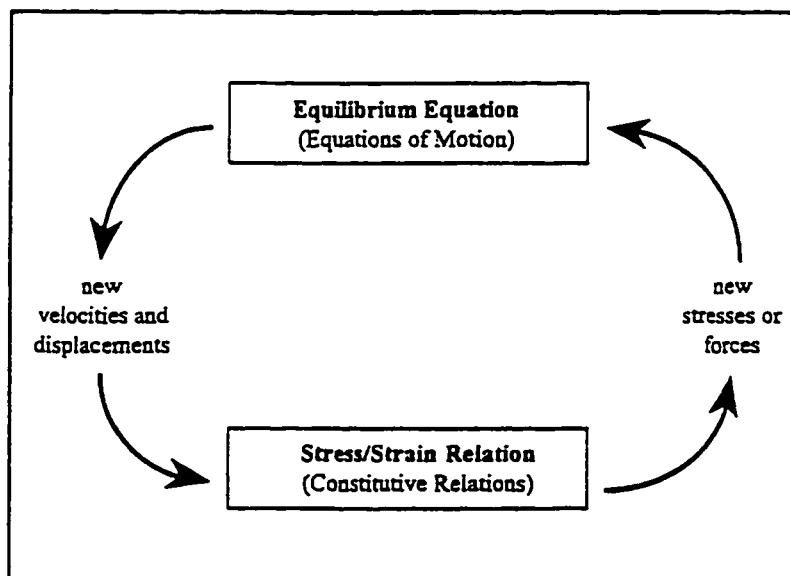
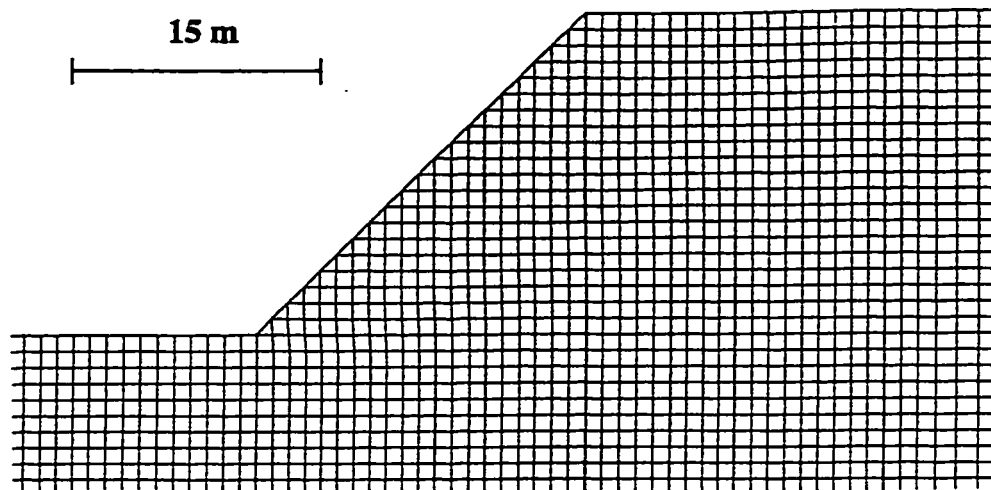


Figure 2.13. The basic explicit calculation cycle (after Coetzee et al., 1993).

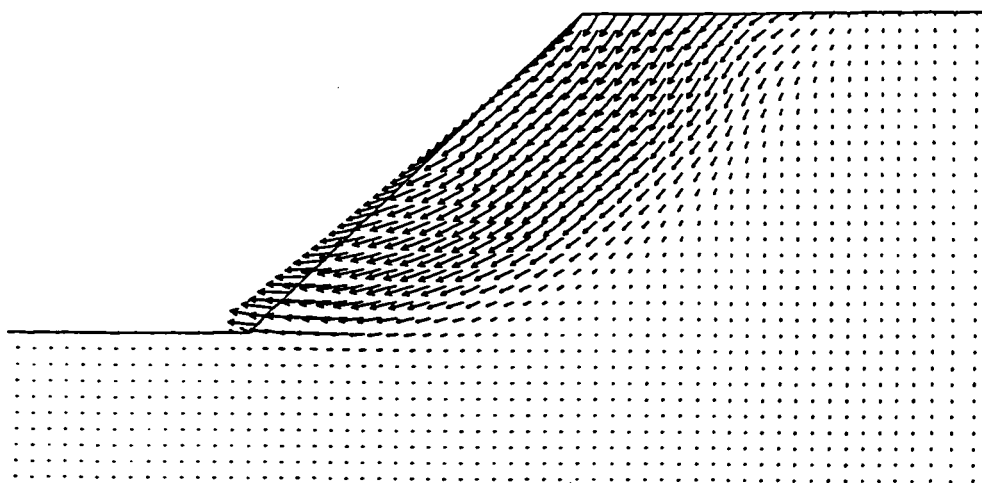
A simplified example of a finite difference analysis of slope stability is shown in figure 2.14. Figure 2.14 (a) shows the central part of a finite difference grid, for a 45° slope, 20 m high. Figure 2.14 (b) shows the displacement vectors at an advanced computational stage showing a failure of the slope and, in particular, indicating the location of the failure (slip) plane.

The program is primarily intended for geotechnical, mining and petroleum engineering application; the code embodies special numerical representation for the mechanical response of geologic materials (Itasca, 1993). The basic version of FLAC has nine built-in material models (table 2.4), and more recent versions enable the user to customize constitutive models by using a built-in programming language (“FISH” - stands for FLACish). Table 2.4 presents the input parameters for each material model commonly used in geomechanical applications.

(a)



(b)



**Figure 2.14.** Example of numerical modelling analysis of slope stability using FLAC; (a) finite difference grid, (b) displacement vectors and ground surface boundary.



Table 2.4. Material models and input parameters commonly used in geomechanical analyses using FLAC and UDEC (Itasca, 1992).

TYPE OF MODEL	REPRESENTATIVE MATERIAL	INPUT PARAMETERS
NULL	Void - excavation	-----
ELASTIC, ISOTROPIC	Homogeneous, isotropic continuum; linear stress-strain behavior	mass density ( $\rho$ ), elastic shear modulus ( $G$ ), elastic bulk modulus ( $K$ )
ELASTIC TRANSVERSELY ISOTROPIC*	Thinly laminated material exhibiting elastic anisotropy (e.g., wood)	angle of anisotropy ( $\alpha$ ), mass density ( $\rho$ ), Poisson's ratio in plane of isotropy due to uniaxial stress in perpendicular plane ( $\nu_{xz}$ ), Poisson's ratio in plane of isotropy due to uniaxial stress in plane of isotropy ( $\nu_{yz}$ ), elastic shear modulus ( $G_{xy}$ ), elastic Young's modulus in the plane of isotropy ( $E_x$ ), elastic Young's modulus in the plane perpendicular to the plane of isotropy ( $E_y$ )
MOHR-COULOMB PLASTICITY	Loose and cemented granular materials; soils, rock, concrete	mass density ( $\rho$ ), elastic shear modulus ( $G$ ), elastic bulk modulus ( $K$ ), cohesion ( $C$ ), friction angle ( $\phi$ ), dilation angle ( $\psi$ ), tension limit ( $\sigma'$ )
UBIQUITOUS JOINT	Thinly laminated material exhibiting strength anisotropy (e.g., slate)	mass density ( $\rho$ ), elastic shear modulus ( $G$ ), elastic bulk modulus ( $K$ ), cohesion ( $C$ ), friction angle ( $\phi$ ), dilation angle ( $\psi$ ), tension limit ( $\sigma'$ ), joint angle ( $\theta$ ), joint cohesion ( $C_j$ ), joint friction angle ( $\phi_j$ ), joint dilation angle ( $\psi_j$ ), tension limit ( $\sigma'$ )
STRAIN-HARDENING OR SOFTENING	Granular materials which exhibit non-linear material hardening or softening	mass density ( $\rho$ ), elastic shear modulus ( $G$ ), elastic bulk modulus ( $K$ ), cohesion ( $C$ ), c-table - table relating cohesion to plastic shear strain, friction angle ( $\phi$ ), f-table - table relating friction angle to plastic shear strain, dilation angle ( $\psi$ ), d-table - table relating dilation angle to plastic shear strain, tension limit ( $\sigma'$ ), t-table - table relating tensile limit to plastic tensile strain

\* Not available in UDEC

#### **2.3.8.4. Distinct Element Methods and the UDEC Program**

The distinct element method is a type of discrete element method simulating the complete behavior of systems of discrete, interacting bodies. Cundall and Hart (1992) suggest that the term discrete element method should be applied only to a program if it “...*(a) allows finite displacements and rotations of discrete bodies, including complete detachment, and (b) recognizes new contacts automatically as the calculation progresses.*” As further discussed by Cundall and Hart (1992), there are four main classes of computer programs that conform to this proposed definition:

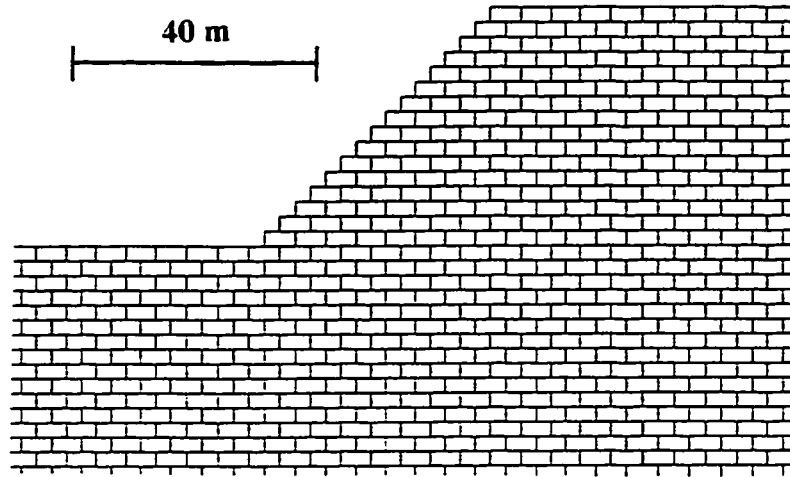
1. Distinct element programs
2. Modal Methods
3. Discontinuum Deformation Analysis
4. Momentum-exchange methods

The term distinct element method was introduced by Cundall and Strack (1979) and refers to a particular discrete element scheme that uses deformable contacts and explicit, time-domain solution of the original equations of motion.

The **Universal Distinct Element Code (UDEC)** is a two-dimensional numerical program based on the distinct element method for discontinuum modelling. It was designed to analyze the response of discontinuous media represented as an assemblage of distinct blocks, figure 2.15 (a), subjected to either static or dynamic loading. It is primarily intended for the analysis of rock engineering problems, ranging from studies of the progressive failure of rock slopes to evaluation of the influence of rock joints, faults and bedding planes on surface and underground excavations and rock foundations (Itasca, 1993).

A wide variety of joint patterns can be generated and analyzed. Blocks can undergo large displacements and rotations, and behave either as rigid or deformable material.

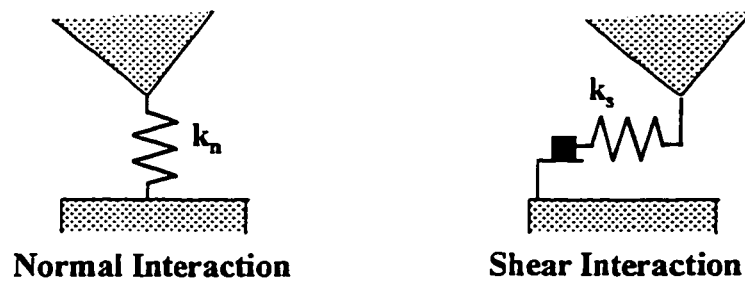
(a)



(b)



(c)



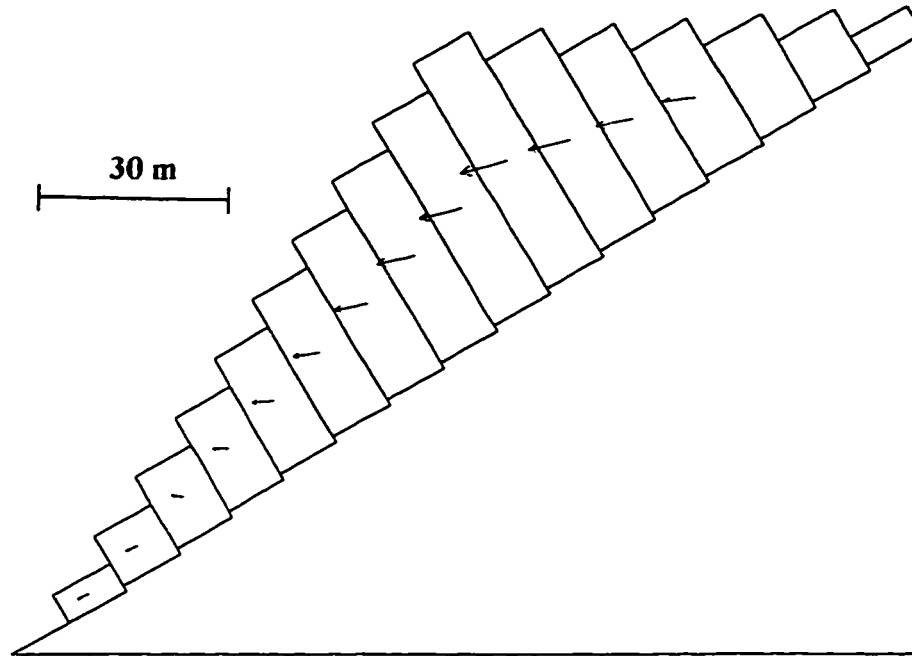
**Figure 2.15.** Principles of UDEC - (a) rock slope in orthogonal-jointed strata, (b) rigid or deformable blocks, (c) spring-slider elements for joint representation.

Deformable blocks are subdivided into a mesh of finite difference elements (figure 2.15 b), with a linear or non-linear stress-strain law. Fully deformable blocks are discretized into a mesh of triangular finite-difference zones, as in standard continuum modelling. The block deformability enables representation of problems with high stresses relative to block strength, and situations where a mixed continuum and discontinuum representation of the structure is required (as presented in chapter 3). Displacements on discontinuities are controlled by linear or non-linear force-displacement relations, in both the normal and shear directions, making use of spring-slider elements (figure 2.15 c; Itasca, 1993).

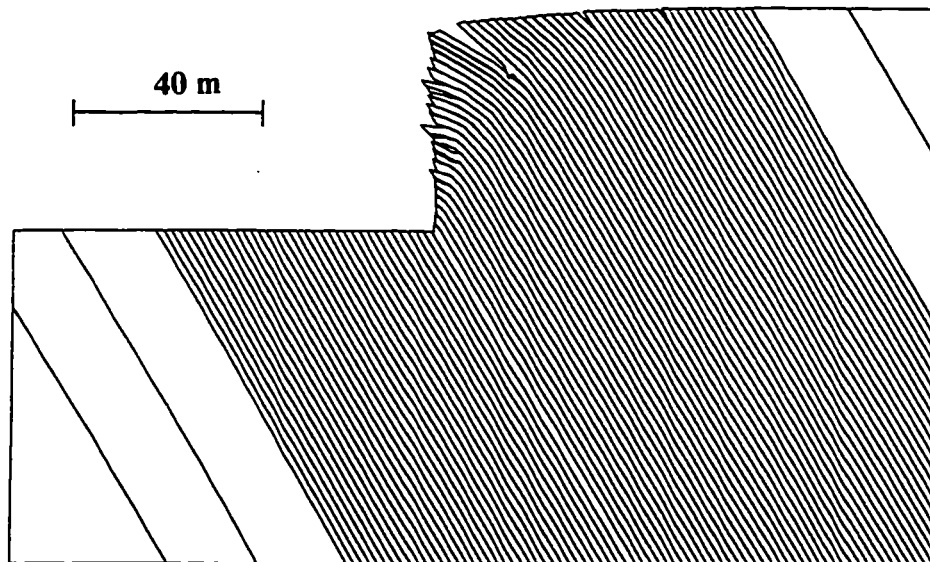
A two-dimensional plane-strain state is assumed, which is ideally associated with long structures or excavations with a constant cross-section, and with loads acting in the plane of the cross-section. All discontinuities are considered as planar features oriented normal to the plane of analysis. Stress or fixed displacement boundary conditions can be applied. Different types of reinforcement and support can be used, including point-anchored and fully-grouted cables and bolts, shotcrete and concrete linings. A thermal option enables simulation of the transient flux of heat in materials and development of thermally-induced stresses. A three-dimensional version (3-DEC) was developed by the Itasca Consulting Group. This version, however, was not available for this study.

Figures 2.16 (a) and (b) show two typical examples of slope failures using UDEC. The toppling of rigid blocks on an inclined, stepped base is demonstrated in case (a). Displacement vectors indicate the instability mode for each individual block. Case (b) presents results from a toppling analysis where fully deformable blocks were used for toppling analysis of thinly bedded strata in steep slopes (Pasloske, 1996). Figure 2.16 shows the advantage of UDEC, which is capable of analyzing not only the slope failure but also the associated deformations. In general, UDEC can account for various displacements associated with jointed media, such as sliding, separation and rotation of the joint-bounded blocks, as well as failure of the intact rock. The general solution procedure applicable to both, FLAC and UDEC and used in this work is presented in figure 2.17.

(a)



(b)



**Figure 2.16.** UDEC application to slope stability (toppling) analysis; (a) toppling of rigid (non-deformable) blocks on an inclined base, (b) flexural toppling of deformable blocks (magnified 10x).

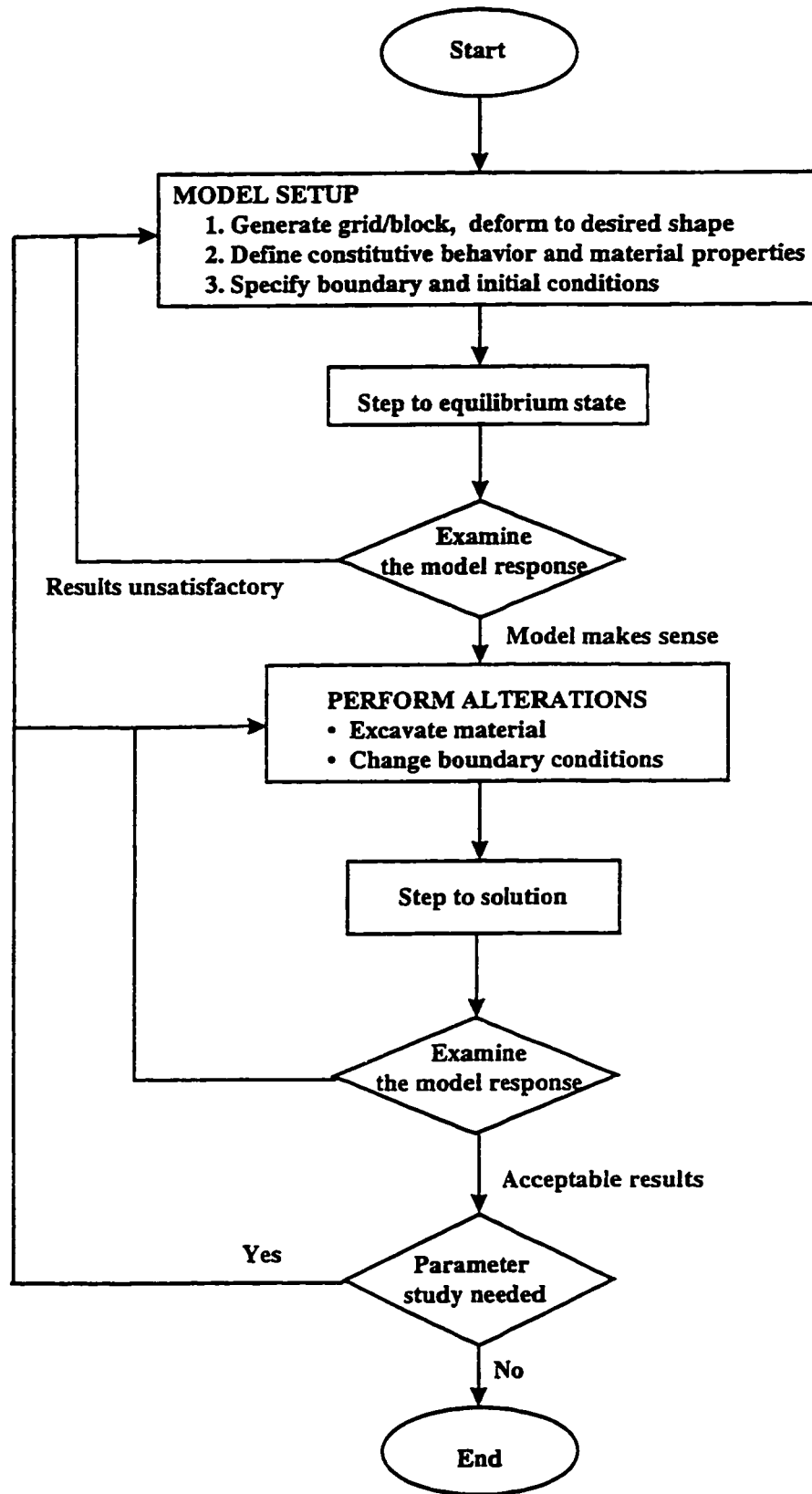


Figure 2.17. General solution procedure in FLAC and UDEC (based on Itasca, 1993).

## CHAPTER 3

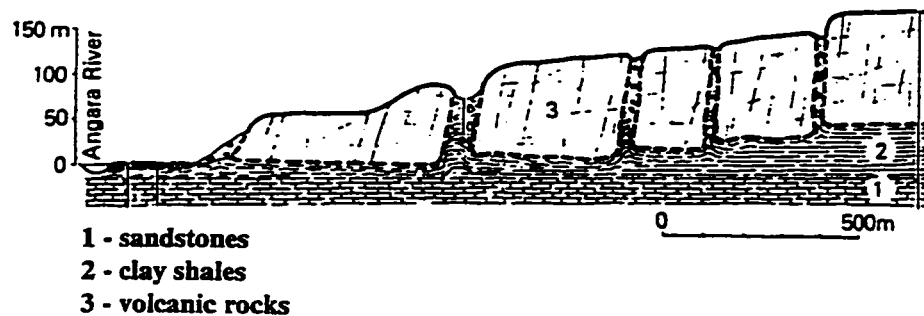
### BLOCK-TYPE MOVEMENTS OF RIGID JOINTED ROCK MASSES OVERLYING WEAK LAYERS

#### 3.1 Introduction

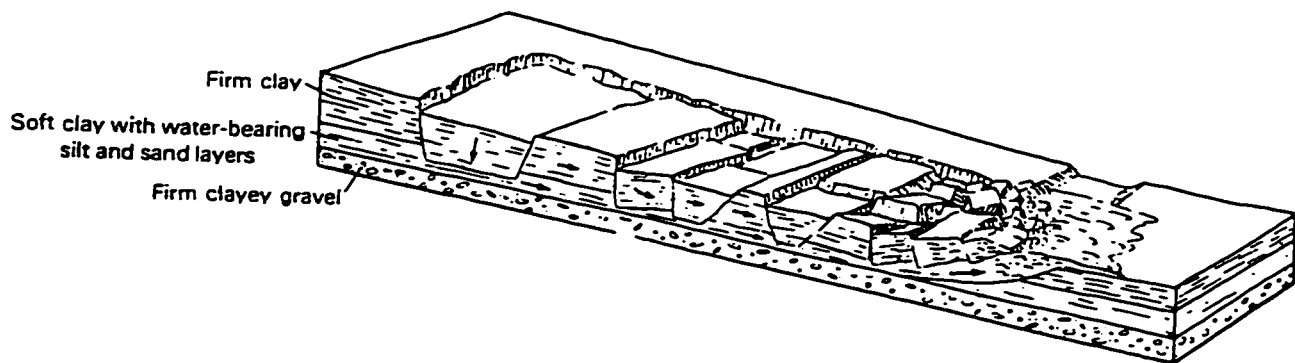
Block-type slope movements are generally associated with rigid, jointed rocks overlying relatively weak, low shear strength strata. Overlying rigid rocks, either horizontal or dipping down slope, displace on or into a relatively plastic substratum. The movements can range from microscopic to continental in scale. Analyses of block-controlled movements are important not only in slope instability studies, but also in foundation and mining engineering. Although such a geological structure is not unusual, this type of movement has received little attention from a numerical modelling perspective. The distinct element method is applied to the analysis and characterization of block-type slope movements in the discussion which follows.

Cruden and Varnes (1996) use the term *block spreads* to describe a movement where a thick layer of rock overlies softer materials. Two examples of block spreading are shown in figure 3.1. The rate of movement in its initial stage is usually very slow except where liquefaction may be a factor. The strong upper layer may fracture or separate along pre-existing discontinuities. The softer underlying material is squeezed from beneath the base of the stronger upper layer either into the cracks between the overlying rock blocks or outside their perimeter. Geological structure provides a controlling influence on the failure mechanism. The movement takes place usually in connection with other types of

(a)



(b)

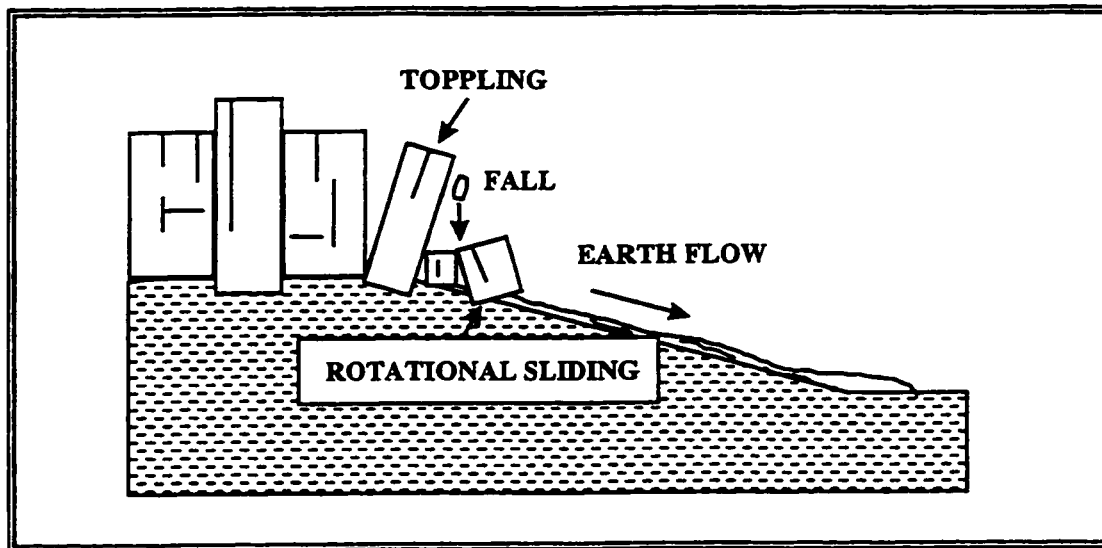


**Figure 3.1.** Two examples of block-type movement (after Cruden and Varnes, 1996).

movement mechanisms. The block spread, for example, may lead to toppling of the rigid blocks and/or falling of rock fragments into the cracks between the blocks. Blocks on the perimeter of the rigid layer may undergo rotational or translational sliding. Similarly, the material squeezed from underneath the upper layer may slide or form an earthflow. Figure 3.2 shows some of associated landslide mechanisms.

Cambering and valley bulging, although belonging generally to block-type deformation, were not considered in this study. This type of movement is characteristic of valleys incised into near-horizontal strata that comprise a rigid, jointed cap-rock overlying a thick layer of stiff, fissured clay or clay shale which, in turn, overlies a more competent substratum. They are believed to be relict periglacial features, of late Pleistocene Age,





**Figure 3.2.** Various secondary landslide mechanisms associated with block-type movements.

and are currently stable (Hutchinson, 1988). The competent blocks have generally a valleyward dip. The mechanisms of cambering and valley bulging were reviewed by Parks (1991) and Hutchinson (1991). Preliminary numerical modelling by the author, not presented in this study, indicated that these processes can be modelled effectively using distinct element models.

Block-type failures are complex, involving components of deformation due to translational sliding along basal surfaces, sliding along subvertical discontinuities, rotation and vertical subsidence movements. In the past, various attempts to analyze block failures have made use of simplified limit equilibrium techniques. Although these methods have been of considerable benefit in approximate design, they do not allow much insight into the mechanisms involved. The availability of numerical modelling techniques that allow both continuum and discontinuum materials to be analyzed, has particular advantages with respect to block-type slope failures. Distinct element models are able to simulate the blocks as discontinuum materials, either rigid or deformable, and the weaker underlying

layers as elasto-plastic continuum materials. This chapter explores the application of 2D distinct element models to block-type slope movements, examining the influence of different joint spacings and presenting a case history from Slovakia where block deformations are threatening the stability of an historical castle. The use of distinct element models allows a deeper insight into the factors effecting block-related deformations. This approach, combined with keyblock theory methods (Goodman and Shi, 1985; Tyler and Trueman, 1993), may be of considerable future benefit to the design of remedial measures for block-related failures.

Although the main emphasis in this work is on rigid jointed rocks overlying a soft substratum, the main condition in the development of this type of movement is the relative difference in strength between these two layers. Two soil layers where the upper layer is formed by a firm stiff clay and the lower one by a soft clay, may develop the same kind of block-type movement, as shown in figure 3.1(b).

### **3.2 Literature Review**

Ter-Stepanian (1977) summarizes the research on block-type slope movements up to 1977 with emphasis on description of this phenomena in the former Czechoslovakia, Soviet Union and Bulgaria. Ter-Stepanian (1977) refers to work by Trzhtsinsky (1974), who studied the large block-type slope movements on the banks of the Ilim River and middle Angara River valley (Russia). Rigid blocks, consisting mostly of sandstones, limestones and diabases, overlie soft clays. The rate of movement was reported between 0.2 mm/year to 1-3 mm/year. Kamenov et al. (1977) describe the necessary conditions for, and the mechanism of, block-type slope movements in Bulgaria. The variety of deformation is discussed with respect to the thickness of the layers and their mechanical properties.

Malgot (1977) described deep-seated gravitational slope deformation in the neovolcanic mountain ranges in Slovakia, where brittle volcanic rocks, mostly andesites, basalts and pyroclastic material, overlie softer plastic strata. Typical morphological features associated with such geological structures were identified. Pasek et al. (1979) describes the instability of plateau-edge rocks overlying soft substratum in the former Czechoslovakia. Yielding of the weak base dislodges the cap-rock along the joints, and due to subsequent sinking and downslope-sliding, numerous distinct blocks are displaced on the upper part of slopes. The extensive research on this topic in the former Czechoslovakia was summarized and published in classic works by Zaruba and Mencil (1976, 1982), Nemcok (1982) and Rybar and Novosad (1989).

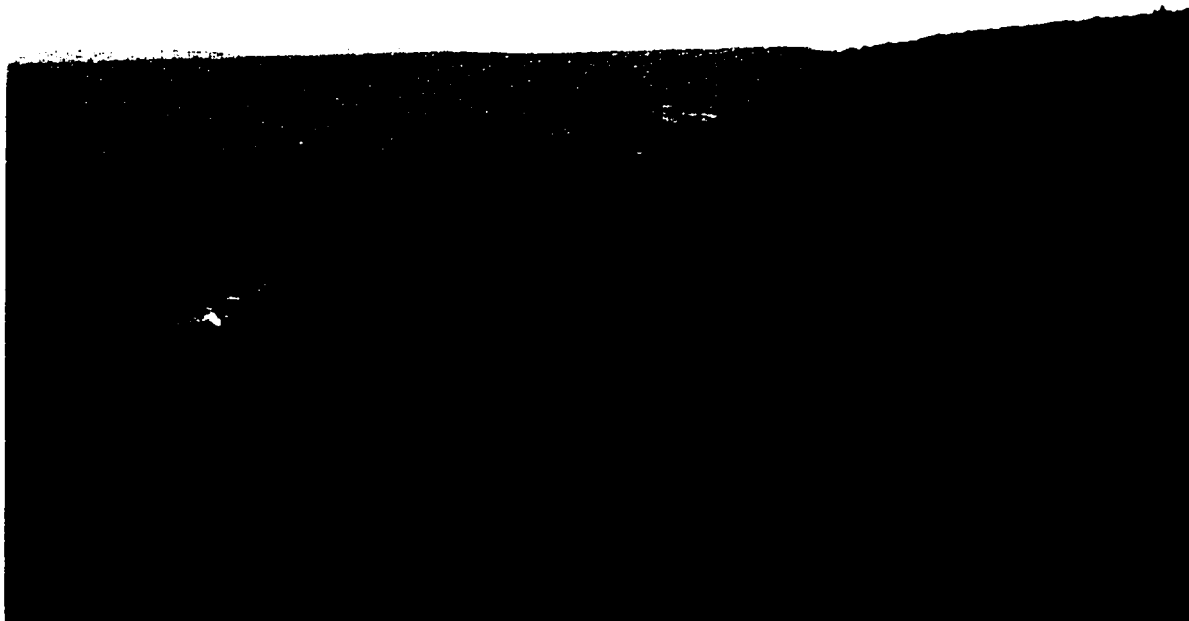
Caine (1982) describes large cliff failures by toppling taking place on the edges of a dolerite plateau in Tasmania. Topographic evidence and joint survey data suggested that failure was taking place by toppling of joint-bounded slabs, which in some places are triggered by failure in the underlying sediments.

Evans (1983) analyzed landslides in layered volcanic successions with a particular reference to the Tertiary rocks of south-central British Columbia. He presented a comprehensive literature survey of various landslide types in volcanic terrain. He concluded that:

- The studied landslides were commonly related to the presence of a weak layer beneath a rigid capping of lavas and breccias.
- The geological structure controls the lateral and headscarp geometries.
- The movement takes place along bedding planes at some angle to the true dip, along other low angle discontinuities which were not detected, or by the rupture of intact material within the weak layer.
- Movement direction was governed by the orientation of release surfaces in the cap rocks rather than the orientation of the weak layer or discontinuities within it.

- Initial movements are block-type movements, with complex variety of successive movements.
- Both sliding and spreading types of instability take place.
- Landslides in the British Columbia's volcanic successions are generally limited to displacements in pre-existing landslides, indicating that conditions for initiation of first-time-movements existed at some time in the past.

A typical example, of block-type slope failure involving volcanic rocks is the Chasm area in the Fraser Plateau, British Columbia, Canada (figure 3.3), where Evans (1983) identified several landslide complexes. The Chasm creek cuts through the basalts and interflow breccias forming a steep-walled valley about 290 m deep. The basaltic rocks overlie the relatively weak rocks of the Deadman River Formation, formed by tuffs, breccias, diatomites, diatomaceous siltstones - soft, poorly consolidated sediments (Campbell and Tipper, 1971).



**Figure 3.3.** View of landslide topography in the Chasm area.

Caldera et al., (1988) and Guerricchio et al., (1988) present an example of landslide-induced morphology in northern Italy in the Adda and Maratea Valleys. Relatively rigid conglomerate and carbonate units overlying softer clay and flyschoid strata underwent a series of dislocations estimated to be up to 100 m along sub-vertical cracks, parallel to the general trend of the valley.

Numerous case studies where the block-type movements presented a major geomechanical challenge in restoration and remedial works of historical monuments, sites and ancient works, were described in Marinos and Koukis (1988). In towns with ancient origins, castles and other historical monuments were, for reasons of defense and control, commonly located on the tops of hills. Such hills, which from the geological point of view, often represent erosional remnants where more competent rock overlies a weak substratum.

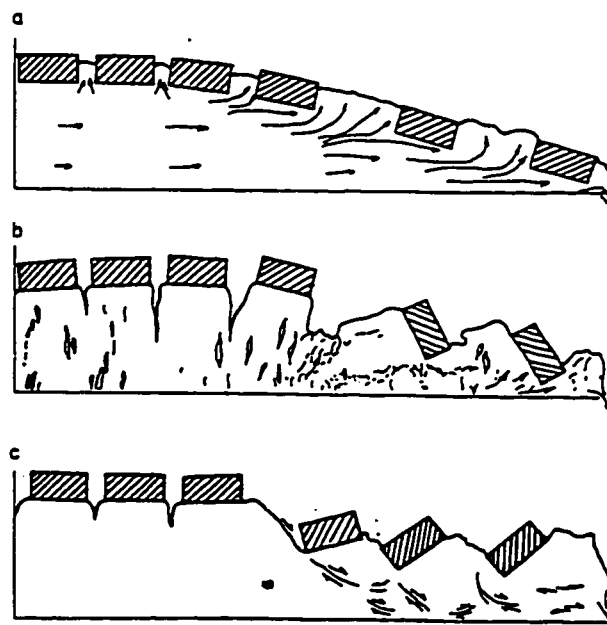
Garzonio (1990) described and analyzed deep-seated lateral spreading involving competent carbonate rocks overlying clay formation in Italy. He utilized limit equilibrium methods and block theory in his analysis. Kostak (1993) refers to an instability of a sandstone unit with rock walls up to 100 m high underlain by more plastic claystones. Most attention was given to interpretation of deformation monitoring data that indicated different failure mechanisms. Conti and Tosatti (1993) describe deformation and instability of more competent rock (limestone) overlying argillaceous and clay substrata. The high erodibility and deformability of the underlying substrata is identified as the main cause of slope instability.

Crescenti et al. (1994) refer to numerous case studies in sedimentary sequences where more competent rocks (conglomerates, breccias, sandstones and dolomites) overlie more plastic argillaceous rocks. The more competent rocks are usually fractured by a series of vertical or sub-vertical discontinuities, forming a prismatic structure. The most important movement appears to be the lateral spreading of the blocks. Depending on the block geometry and the strength of the substratum, blocks on the edges may undergo either a

toppling or back-tilting type of movement. The lateral spreading is believed to be a consequence of a long-term viscous deformation in the substratum, with squeezing and extrusion of the ductile material from underneath the blocks in response to the release of the high *in situ* horizontal stress induced by the tectonics. The occurrence of slow squeezing-out phenomena was confirmed by the presence of bulging zones around the rock slabs (Canuti et al., 1994). Slides and earthflows are frequent on the outer edges of the more competent rock units. Canuti et al. (1994) refer to the fundamental role played by the *in situ* stress state. Large horizontal displacements with the opening of gullies and trenches required the presence of a high *in situ* horizontal stress. This condition was believed to be reasonable as the areas were in an environment of intense compressive tectonics and strong erosion.

### 3.2.1 Physical Modelling

Kostak (1977) presents results from a physical modelling study on block-type slope deformation, where the weak underlying material was assumed to have various properties. Results of three such tests are shown in figure 3.4, demonstrating blocks



**Figure 3.4.** Different block-type deformations on various types of soft base - (a) - Viscous, (b) - Viscoplastic-brittle, (c) - Viscoplastic-ductile (after Kostak, 1977).

resting on a viscous (a), viscoplastic brittle (b) and viscoplastic ductile (c) layer.

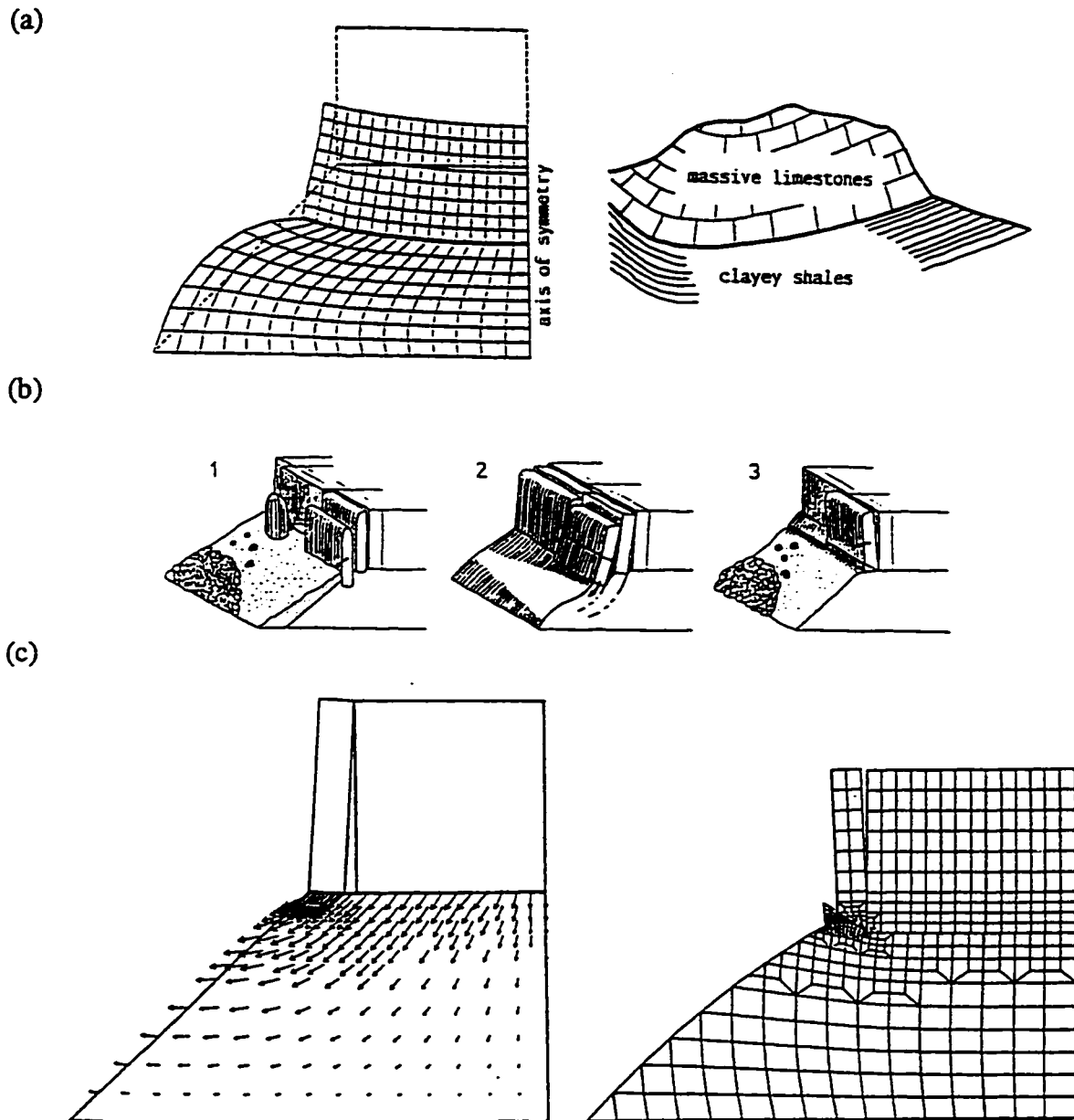
Silberbauer et al. (1988) performed physical modelling of a hard rock slab resting on a soft base. The models confirmed that a syncline typically develops as a consequence of the slab sinking and the squeezing-out of the soft underlying material. The slab showed vertical bending cracks, most of which are parallel to the long axis of the model. This fracture pattern was compared with the fracturing of the limestone forming the Acropolis hill in Athens. They further demonstrated that fractional parts of hard rock slabs with a small base sink more quickly into viscous base material than fractional parts with a bigger base, if all other conditions remained the same.

Physical modelling in connection with numerical modelling analysis was performed by Poisel and Eppensteiner (1988), Poisel et al. (1989), Steger and Unterberger (1990), Poisel (1990) and Poisel et al. (1991). More details of their results are given in the following section.

### **3.2.2 Numerical Modelling Studies of Block-Type Slope Deformations**

Radbruch-Hall et al. (1976) used the finite element method in the deformation analysis of a porphyry laccolith resting on shale. Large tensile stresses were observed at the base of the relatively strong laccolith as a result of the lateral ductile flow of the relatively weak shale. Stability analysis of large rock towers formed on the edge of a competent rock plateau was performed by Evans (1981) and Evans et al. (1981). Toppling appeared to be the main failure mechanism and was simulated by the finite element method. Weathering in the underlying claystone, and the progressive decrease in weathering inwards from the free face, were considered to be the main factors in this type of instability.

Poisel and Eppensteiner (1988), Poisel et al. (1989, 1991), Steger and Unterberger (1990), and Poisel (1990), at the Technical University of Vienna in Austria,



**Figure 3.5.** Deformation and instability of rigid joint-bounded rock overlying soft base; studied at the Technical University of Vienna, (a) finite element simulation of syncline development, (b) three different modes of instability for “tower shaped blocks, (c) rotational failure and toppling of blocks as simulated with the finite element method (Poisel et al., 1991).

performed a series of numerical modelling studies, supplemented by physical modelling, analyzing the deformation of hard, competent rock masses overlying a soft base. Some of their results are shown in figure 3.5. Figure 3.5 (a) shows a finite element simulation of a



continuous slab resting on soft substratum and a typical geological structure of a limestone overlying clay shales. The deformation shows a typical synclinal structure developing as a consequence of the slab sinking and squeezing-out of the soft material. As a consequence, the central part of the slab exhibited vertical bending cracks. Concentration of tensile stresses close to the free surface was observed in the numerical modelling, explaining in part the large vertical discontinuities that extend over the full height of the slope observed in the field. The vertical discontinuities at the edge of the competent rock promote the development of three distinct types of block movement (figure 3.5 b):

1. Translational and upright sliding.
2. Rotation resulting in the formation of an “A-shaped” structure between the block and the rest of the competent rock mass, followed by a rotational failure in the base or breaking of the block due to bending.
3. Rotation resulting in the formation of a “V-shaped” structure between the block and the rest of the competent rock mass, followed by toppling.

A finite element method incorporating gap-friction elements to represent discontinuities in the hard cap rock, was subsequently utilized for more detailed studies, as shown in figure 3.5 (c). The incorporation of the small fracture at the base of the block, promoting toppling type of movement, was based on the physical modelling studies.

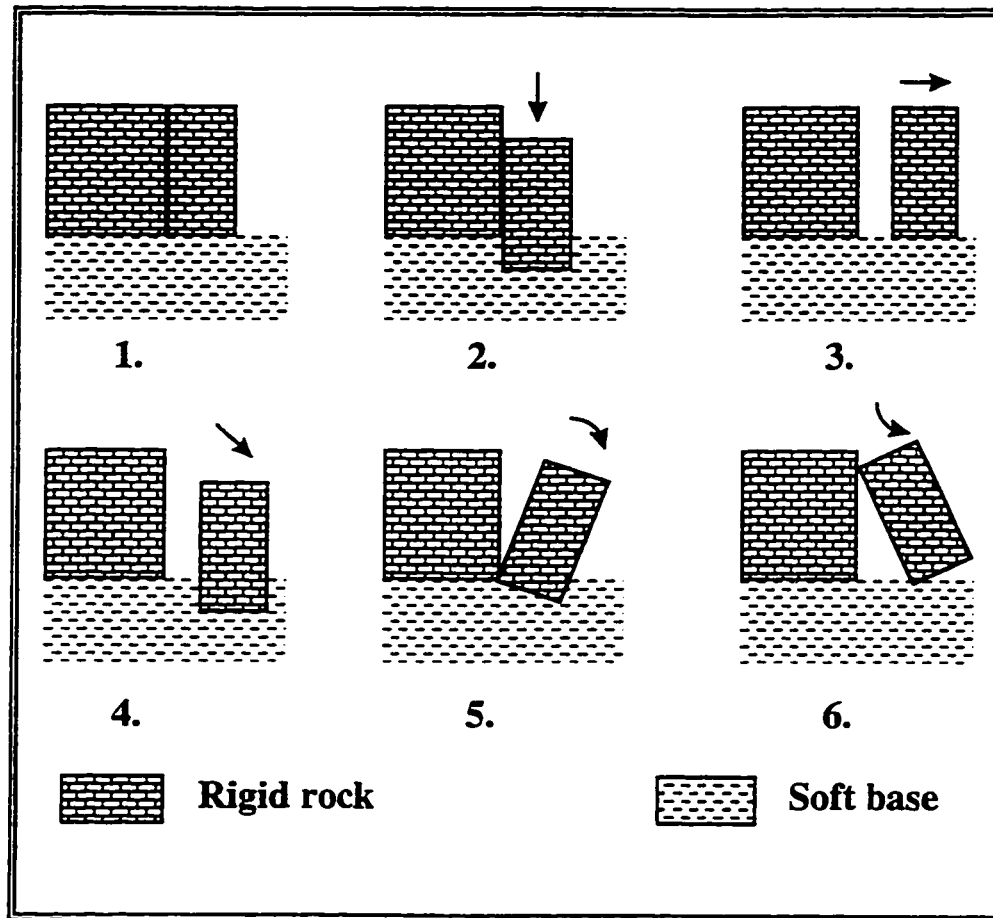
Benko et al. (1994) analyzed block-type slope movements of rigid, jointed rocks overlying relatively weak, low strength strata using the distinct element method. Rigid cap rocks with different jointing geometry were analyzed and the deformation mechanism investigated. Preliminary results on the deformation of the Spis castle foundation were presented. The distinct element method proved to be a powerful analytical method, allowing for discontinuum representation of the jointed rigid rock as well as continuum representation of the soft underlying strata.

### **3.3 Types of Block Movements**

The geological structure and lithology may influence block-related failures in numerous ways. The nature of block movement may be controlled by the joint orientation, joint spacing and persistence. Massive blocks may simply translate or rotate with little internal deformation. This may present more kinematic restraints to movement and demand both weaker and thicker underlying strata. Where blocks are more closely jointed, the translational and/or rotational movements will tend to be distributed within the block. Numerous sub-parallel zones of movement on varying scales may be involved. The nature of the discontinuity surfaces, forming the basal surface and within the block, will dictate the shear strength characteristics of the surface involved in deformation. As such, infill, roughness and weathering will all be important factors. The deformational characteristics of the block will also be controlled by the lithology, rock mass structure and the in-situ stress field.

Slope movements contribute significantly to the resulting topography, especially on the peripheral parts of volcanic mountain ranges, or where river erosion cuts through the volcanic rocks into a weaker base. Where erosion is quite localized, the deformation is less widespread and generally follows the valley or chasm closely. In some localities, however, the deformation process affects entire mountain ranges, especially in areas of tectonic uplift. An interesting example is the Vtacnik mountain in Slovakia where the deformation process is enhanced by anthropogenic undermining activity (Malgot et al., 1986).

Based on the movement mechanisms, the block-type deformations involving competent joint bounded blocks overlying low strength strata can be subdivided into five groups as shown in figure 3.6.



**Figure 3.6.** Types of block movements over plastic substratum

**1. Vertical subsidence without rotation (fig. 3.6-2).**

This type of deformation is more typical for the central parts of the competent rock layer than for the peripheral parts due to the lack of release surface. The vertical subsidence movement may be the result of a local change in underlying material type and/or its strength, localized groundwater seepage resulting in softening and erosion, block geometry, ground subsidence resulting from underground mining, and ground collapse. Apart from the factors causing the subsidence, the magnitude of movement will be dependent on the joint properties.

## **2. Translational (sub)horizontal sliding (fig. 3.6-3).**

This type of deformation, without a significant subsidence and/or block inclination, is characteristic for areas with a small thickness of the underlying soft base and a near level contact between the rigid and soft material. The driving forces for the deformation are represented by the lateral loss of support for the rigid block and lateral extension of the soft base. Both causes can be either natural (erosion, liquefaction, seismic loading, glacial retreat) or human-induced (excavation, blasting, change in groundwater regime). Voight (1973) presented an analysis of the mechanics of retrogressive block-gliding of the Turnagain Heights landslide in the Anchorage area, Alaska, that was triggered by an earthquake. Blocks of clay were displaced in a horizontal direction, preserving their original structure.

## **3. Translational downward sliding (fig. 3.6-4)**

This type of deformation is more typical for rigid blocks with a length to width ratio close to unity. In cases where the height of the block significantly exceeds the width, some degree of tilting and rotation is expected, if it is kinematically possible. When the height of the block is larger than its base this type of movement may be characteristic for slopes that have already been intensively covered by debris (Silbauer et al., 1988). In such cases, a significant part of the rigid block is under the surface, decreasing the exposed height of the block and the above-surface length-to-width block ratio.

## **4. Forward rotation and toppling (fig. 3.6-5)**

This type of deformation is typical when the strength of the underlying soft substratum is decreased by softening or weathering, or when the material is removed from underneath the base of the rigid block. In order for this type of deformation to develop, the strength must be decreased or material removed, progressively from the free face into the slope. Similarly, the rigid rock block may develop toppling if the underlying soft material fails along some planes of weakness daylighting on the slope. Poisel (1990) attributed the toppling of high rock blocks to the existing, inclined fractures at the base of the block. Such fractures were observed to develop in his physical modelling analysis.

### **5. Backward rotation and sliding (fig. 3.6-6)**

The backward rotation of a rigid block typically occurs when the bearing capacity of the underlying soft material is exceeded. This happens usually on the outer edges of the rigid overlying layer. The rotation may be then followed by a slow “creeping” movement of the block down the slope gradient and a retrogressive structure of unstable blocks may develop. If the length-to-width ratio of the rigid block is quite high, the block may undergo significant deformation mainly due to pre-existing discontinuities. This type of displacement can be most readily analyzed by the limit equilibrium method, assuming loading of the top part of slope.

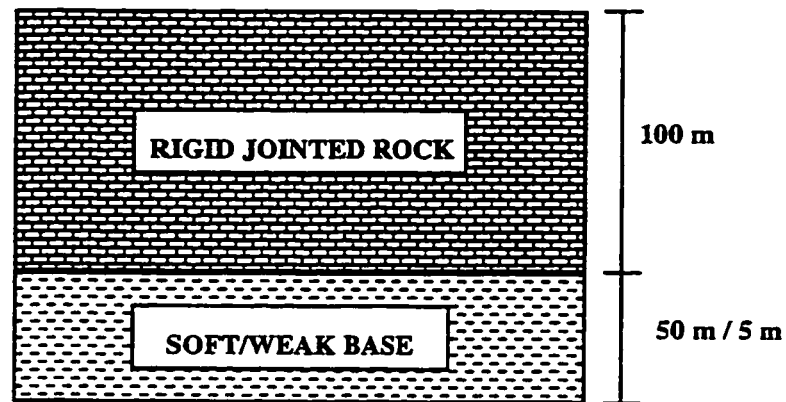
Most previous analysis of block movements have assumed rigid blocks. In high slopes composed of weathered, closely jointed low modulus rocks this may represent an oversimplification. Groundwater undoubtedly plays an important role in many block type failures. This may include both the effect of high water pressures acting on failure surfaces, and the decrease in material strength due to water present within the weaker underlying substrata. A literature review of block-type slope movement reveals the prevailing qualitative approach to analysis. Failures have been described in detail and, where possible, simplified static analyses attempted. A more quantitative approach is required to provide further insights into the complex deformation mechanisms that may be active. Such an approach, requiring a continuum mechanical formulation for the underlying plastic rock and discontinuum mechanical formulation for the blocks themselves, was suggested by Poisel (1990). Limit equilibrium and geometrical methods applied to blocky media are based on simplifying assumptions about the origins of forces, without relating the forces to displacements through a constitutive law (Cundall, 1990). With the possibility to include more geological detail into available numerical modelling techniques, they provide a potentially valuable analytical tool. The distinct element method in particular, has proved to be a powerful method for analysis of discontinua.

### **3.4. Application of Distinct Element Method to the Analysis of Block-Type Slope Deformations**

A distinct element analysis was undertaken to examine selected aspects of block-type slope failure mechanisms involved in a rigid rock - weak base environment. The variable geological structure and jointing pattern in the overlying rigid rock provide for numerous structures and factors to be analyzed. In this particular analysis the influence of various jointing patterns and thickness of the weak base on the deformations and failure mechanisms was investigated. The term rigid rock is used to define the relatively hard rock as opposed to the underlying base and should not be confused with the term rigid blocks, as used in the UDEC program (Itasca, 1993), which represent non-deformable blocks. In all the following analyses in this chapter, the rigid joint-bounded blocks are assumed to deform according to the elastic, isotropic constitutive criteria.

A 100 m thick rigid rock layer was assumed to overlie a 50 m and 5 m thick layer of a weak, low shear strength/elastic modulus material, as shown in figure 3.7. The rigid rock cap was assumed to be jointed in the vertical and/or horizontal direction. Various combinations of jointing geometry were investigated. No joints were assumed in the weak base, which was being modelled as one large deformable (elasto-plastic) block. Two examples of the models, one assuming a single block being separated from the rock cap and the other with a more complicated discontinuity pattern, are shown in figure 3.8.

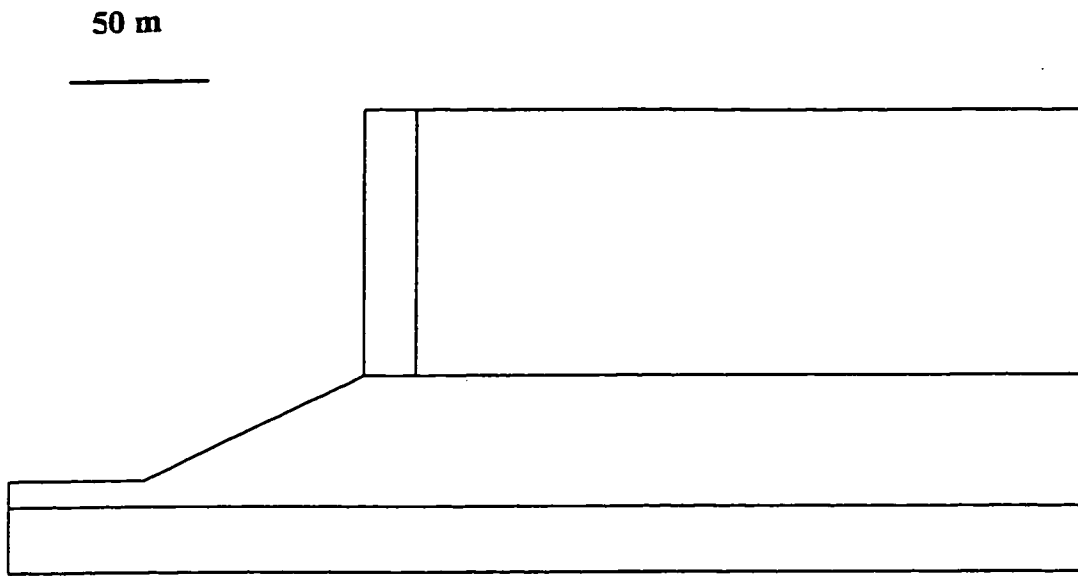
The general model, regardless of the jointing pattern used, had dimensions of 400 m x 175 m for the 50 m thick soft layer, and 400 m x 130 m for the 5 m thick soft layer. The boundaries were determined from preliminary model runs which investigated the sensitivity and dependence of induced deformations on boundary conditions. It was found that for smaller models, for example 300 m x 130 m, the deformations extended to the right boundary. The base of the model, underneath the weak base, was assumed to be an elastic isotropic rock.



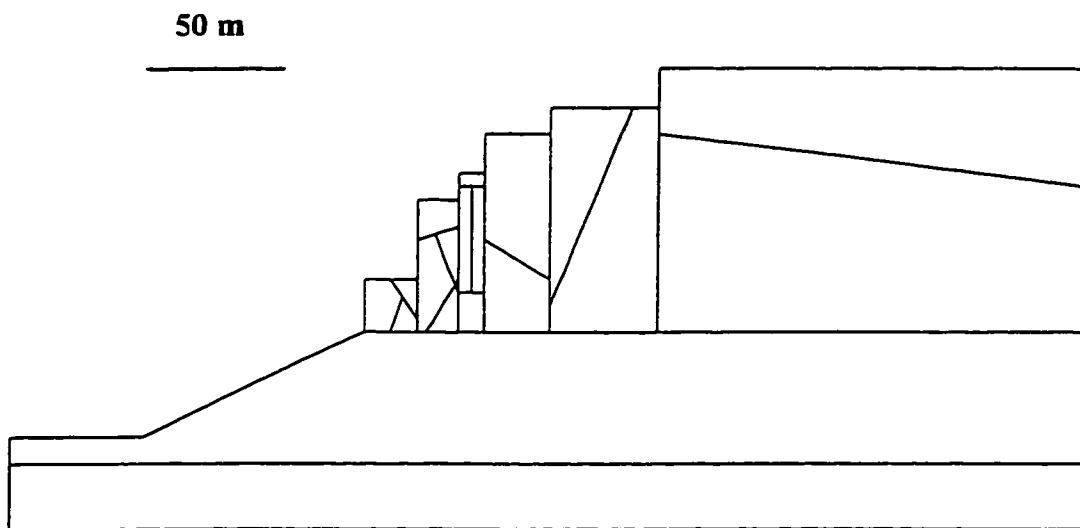
**Figure 3.7.** Sketch of geological structure analyzed using distinct element method

An elasto-plastic behavior, with the Mohr-Coulomb constitutive criteria, was adopted for the soft base material represented by one block only. The block was discretized into finite difference zones, allowing for a continuous representation of this part of model. No cohesion, tension or dilation was assumed for the joints in the rigid rock, for which the elastic isotropic constitutive criterion was assumed. The frictional resistance was assumed to be  $30^\circ$ . The basic input properties are summarized in table 3.1.

(a)



(b)



**Figure 3.8.** Examples of distinct element models with simulation of (a) single block (b) multiple blocks used in the analysis.



**Table 3.1.** Input properties for numerical model.

<b>Properties</b>	<b>Rigid Rock</b>	<b>Soft Base</b>
density (kg/m <sup>3</sup> )	2600.0	1900.0
bulk modulus (MPa)	20800.0	37.0
shear modulus (MPa)	27800.0	111.0
friction (°)	---	25.0
cohesion (MPa)	---	(0.0 - 0.2)
joint normal stiffness (MPa/m)	10000.0	---
joint shear stiffness (MPa/m)	1000.0	---
joint friction (°)	30.0	---

Various strength properties were initially applied to the weak base in order to investigate the deformation mechanisms. The final results presented in this chapter, summarize the induced deformations for the rigid rock cap and a “relatively strong” and “relatively weak” base properties. This material weakness was controlled only by the friction and cohesion in the weak layer. The values for these two properties have been changed to investigate the type of failure on the rigid block deformations. The elastic properties were assumed to be constant throughout the analysis. It is emphasized that the shear strength properties represent only arbitrary values for the weak base material and not properties from a particular case study. Only a contrast in strength properties was required (weak-strong) in order to investigate the different deformation mechanisms.

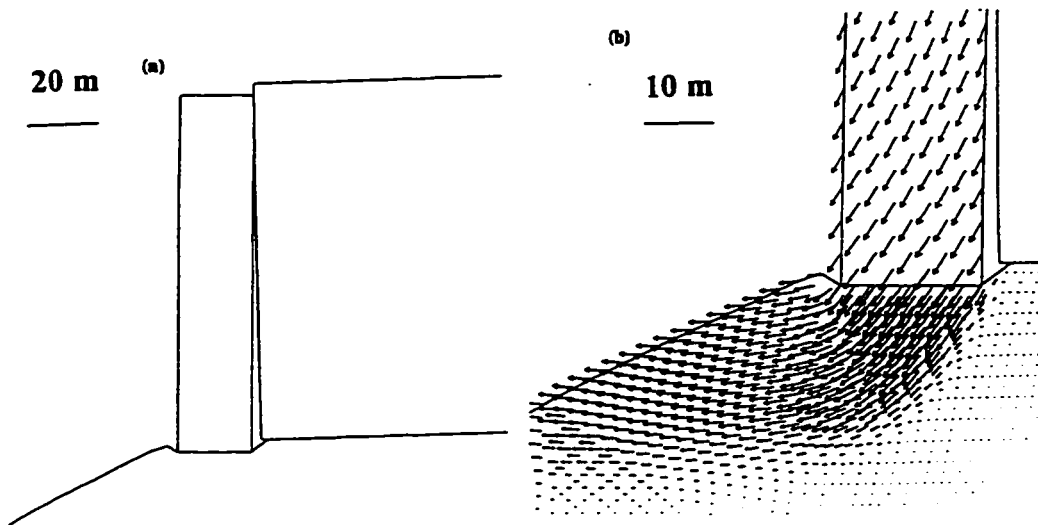
In the case of the relatively strong base, the material was assumed to have a friction of 25° and the cohesion value was decreased until failure in the underlying material occurred. It was not the main objective to back-calculate the cohesion at failure, but rather to have a situation where the cohesion of the weak base is progressively decreased until failure occurs. Therefore, a rather large interval in the increments by which the cohesion was decreased was selected. The relatively weak base was represented with

material where the assumption was made that the cohesive strength decreased significantly and/or reached residual shear strength. The same friction angle ( $25^\circ$ ) was assumed.

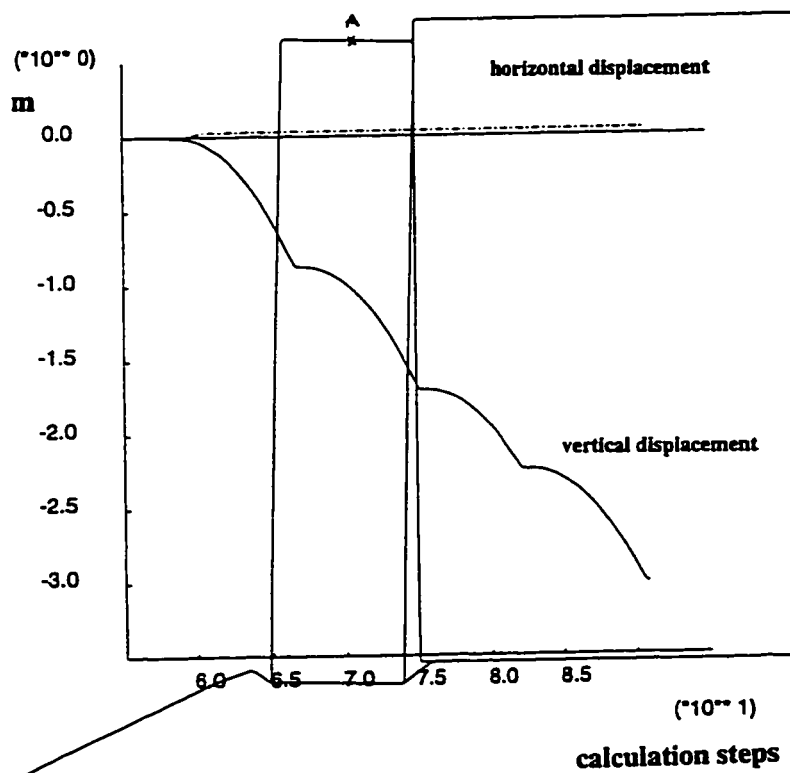
The modelling started with an initial level ground surface. A vertical cliff in the rigid rock cap and a 1:2 slope in the soft underlying material were excavated in several steps. Each step consisted of the removal of a block from the model with a 25 m thickness. The model was allowed to equilibrate after every excavation step under the new stress conditions. This initial excavation was done with high shear strength values for the materials, to prevent any plastic yielding at this stage of modelling. Only an initial ground stress state with a  $K = 1$  was investigated, and applied to the rectangular model before any excavation took place. No groundwater pressures were assumed to be acting in the model. Once the final geometry was reached, the displacement in the model that resulted from the initial excavation, was reset to zero and the model saved for the subsequent analyses.

Initially only a single, joint bounded block, was assumed to be isolated from the remaining rock mass at the edge of the structure. The block was 20 m wide and 100 m long. A block with dimensions of 10 m x 100 m was also investigated. The soft base was assumed to be both strong and soft, as explained in the two previous sections as well as 50 m and 5 m thick, respectively. The cohesion was progressively decreased until failure occurred. Models with cohesion values of 200, 150, 100, 50 and 0 kPa were investigated. The failure for the 20 m wide block, 50 m thick weak base and a cohesion of 50 kPa is shown in figure 3.9 (a) and (b) and figure 3.10.

Figure 3.9(a) shows that the rigid block subsided and rotated. An “A-shaped” joint, as referred to by Poisel (1990), opened and calculations resulted in a rotational failure in the base. The block became separated from the rest of the rock slab and, depending on its strength and internal jointing will be subjected to further deformations. A close-up view of the rotational failure in the base of block is shown in figure 3.9(b), presenting



**Figure 3.9.** Displacement of a single joint bounded block on a 50 m weak base (only part of the weak base shown in figure).

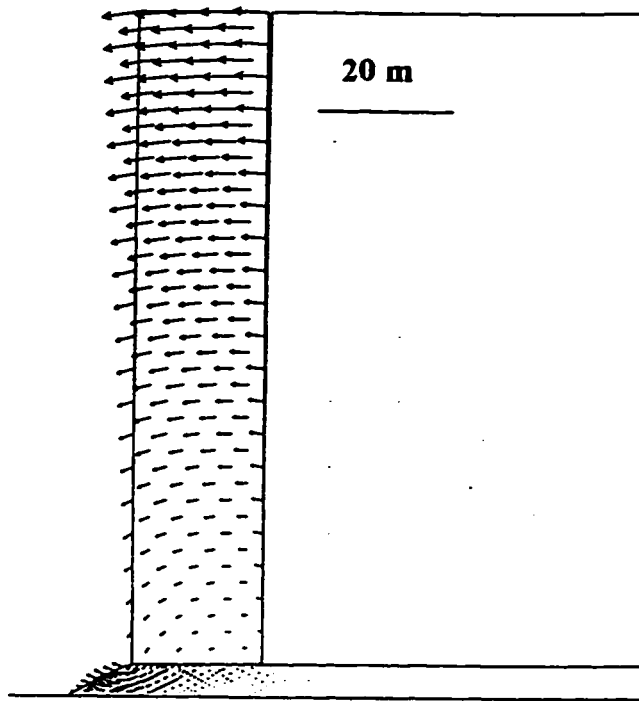


**Figure 3.10.** Record of horizontal and vertical displacement for a point on top of the joint separated rock block and 50 m thick weak base.

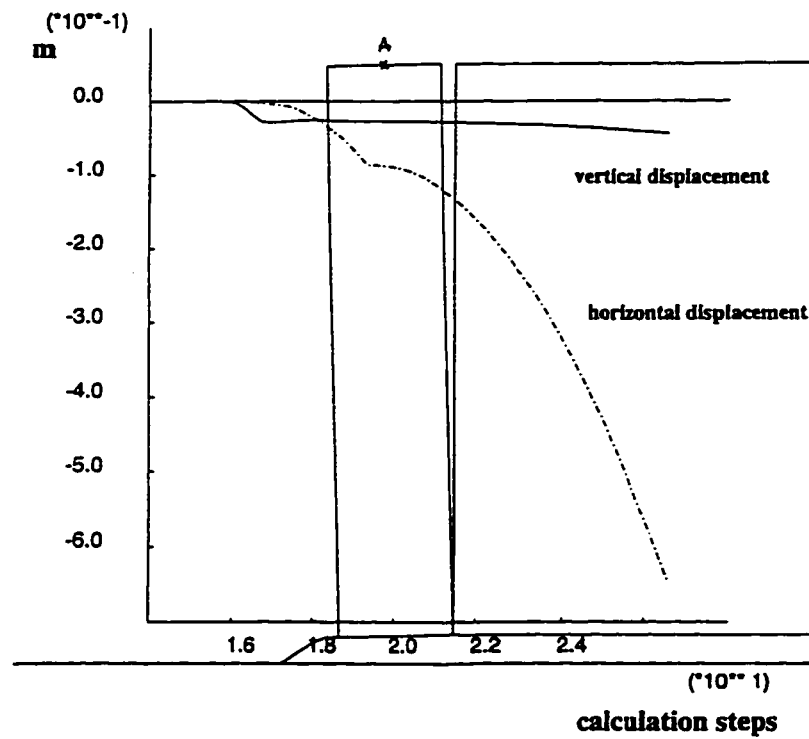
the total displacement vectors up to this calculation step. The maximum displacement shown in this figure is 3.8 m. Prolonged calculation will result in more displacement as the failure is accelerating as shown in the figure 3.10. This figure shows the plot of vertical and horizontal displacement for a point located at the top of the joint separated block (point A). The vertical displacement is by far the predominant one, with only minor horizontal displacement. Up to this calculation stage, the vertical displacement was 3 m and the horizontal 0.04 m.

In the second step, the thickness of the underlying base was changed to 5 m, resulting in a case where the weak base was constrained between the two rigid layers. The results of this analysis are shown in figure 3.11 and 3.12. Unlike the previous case, yielding in the weak base was constrained to an area of approximately 5-10 m inside the slope in the weak layer. This resulted in toppling of the overlying rock slab. Figure 3.11 shows the displacement vectors in the rock block and weak base. Figure 3.12 shows the plot for horizontal and vertical displacements for point A, located on top of the block. The total horizontal displacement up to this calculation stage was 0.65 m as compared to 0.04 m of vertical displacement.

These results are of particular interest because previous analyses required either a distinct joint in the lower part of the block (Poisel et al., 1991) or progressive erosion of the underlying material (Evans et al., 1981) to produce the block toppling. It seems that there is a certain limiting thickness of the soft base when the movement is changed from the toppling to the rotation of the tower-like block, assuming the same block dimensions.



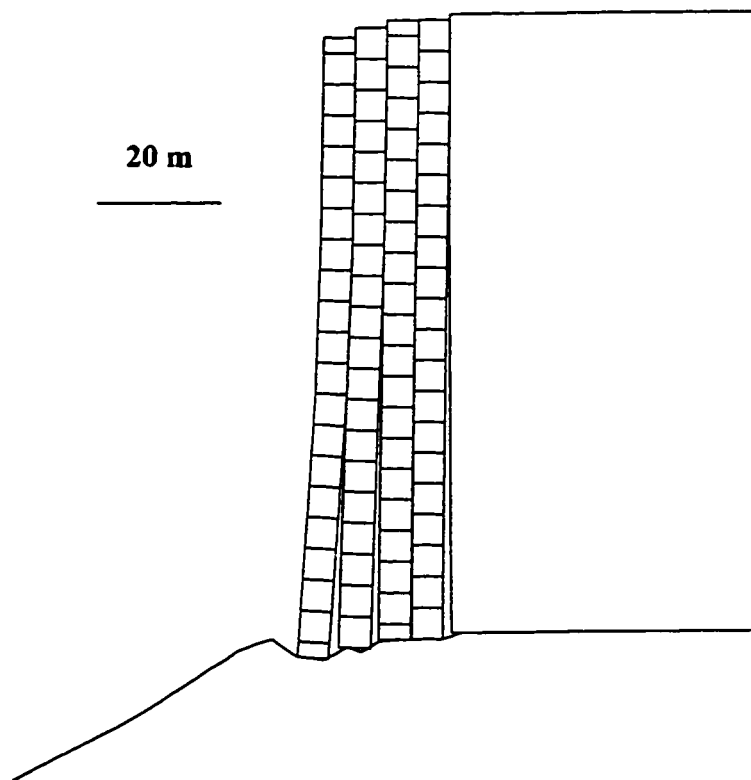
**Figure 3.11.** Displacement of a single joint bounded block on a 5 m weak base



**Figure 3.12.** Record of horizontal and vertical displacement for a point on top of the joint separated rock block and 5 m thick weak base.

Furthermore, rotational movement would be produced in the case of the 5 m thick, weak layer if the block width is the same or less than the zone which yields under its base. The weak base could also include several layers of different strength and deformation parameters, rather than be composed of a homogeneous isotropic material, as in this case. Therefore, each analysis of this type of instability should be based on comprehensive field investigation and will depend and vary most probably with each particular site.

In the next step of analysis the deformation of the rock block was investigated, by assuming an idealized orthogonal jointing pattern. The resulting deformations are shown in figure 3.13. Vertical, persistent discontinuities with a spacing of 5 m and cross joints with a spacing of 5 m were assumed.

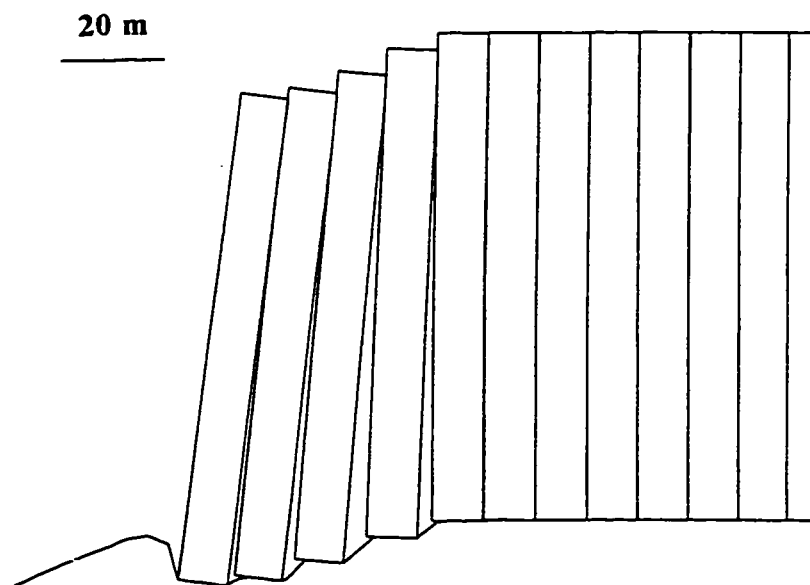


**Figure 3.13.** Deformation of an orthogonal-jointed block on a 50 m weak base.

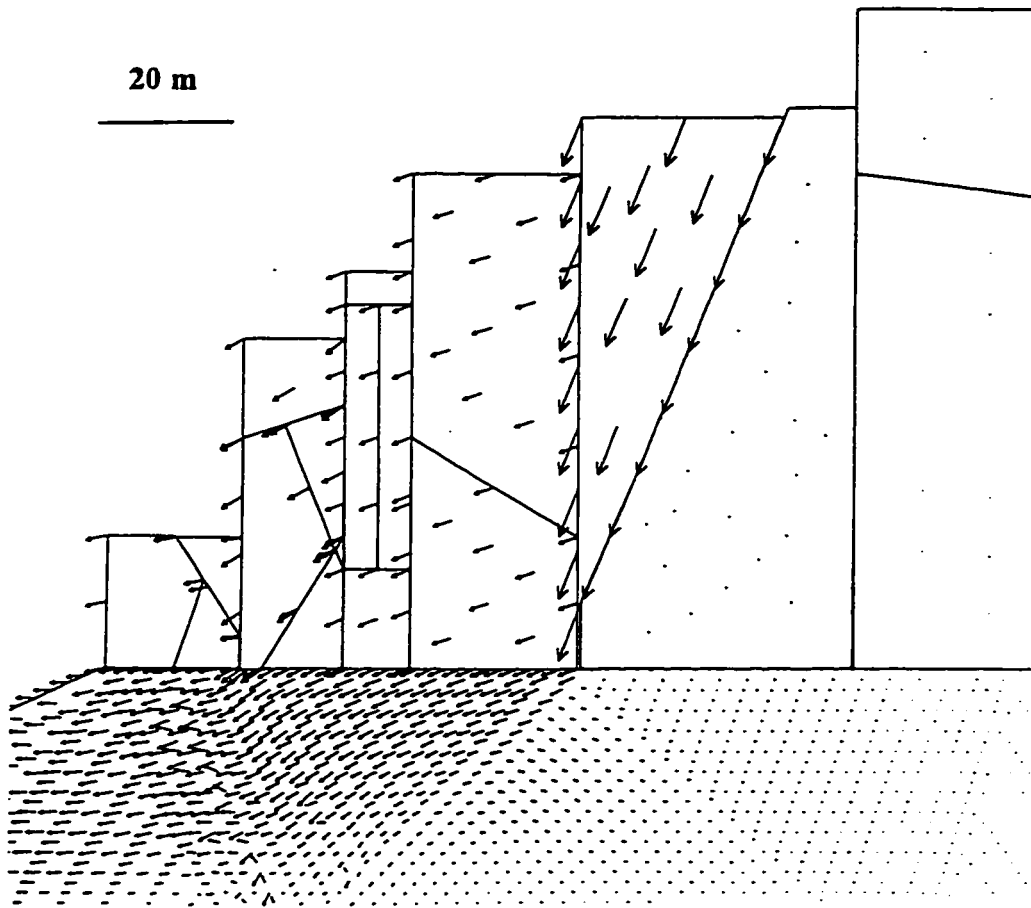
The deformations are presented for cohesion of 50 kPa and friction  $25^\circ$  for the weak base. Separation occurred along the vertical discontinuities with bending of individual columns made possible by the presence of cross joints.

Models with jointing of all of the rigid rock cap were assumed in the next stage of analysis. Figure 3.14. shows results of a simulation where 10 m spacing of the vertical discontinuity set was assumed. The blocks tend to subside into the plastic substratum and rotate backwards with a predominant vertical component of movement. A step-like topography results at the ground surface. The deformations in this particular case tend to be limited to the rigid rock edge.

Figure 3.15. shows the results of a model simulation with various joint orientation in the rigid rock. The displacements of the blocks are in this case controlled by both the extent of failure in the weak base and the discontinuity orientation in the rigid rock. Blocks with a smaller base showed more vertical displacement than blocks with a wider base.



**Figure 3.14.** Deformations in model assuming vertical jointing of the rigid rock.



**Figure 3.15.** Deformations in model assuming various joint direction in the rigid rock.



### 3.5 Gravitational Deformations at the Spis Castle

The Spis castle, founded in 1120, is one of the largest castles in central Europe (figure 3.16). The site represents a geologically favorable structure for the development of block-type slope deformation. Relatively rigid travertine blocks were deposited on top of flyschoid strata composed predominantly of clay shale. The castle was severely damaged by a fire in 1778 and subsequently abandoned. A plan for remedial measures was proposed in 1984 without a detailed geotechnical investigation of the castle structures and the foundation. Problems encountered during the work resulted in disruption of the remedial measures and a requirement for detailed mapping and analysis of the rock mass conditions. Most attention was concentrated on the geometry of the travertine blocks, their interaction with the relatively soft substratum, deformation mechanisms, and the identification of future problems. The author was involved in the engineering geological mapping program of the site in the summer of 1992 and 1993. Discontinuum modelling analysis was undertaken to investigate and confirm the assumed failure mechanism experienced at the site



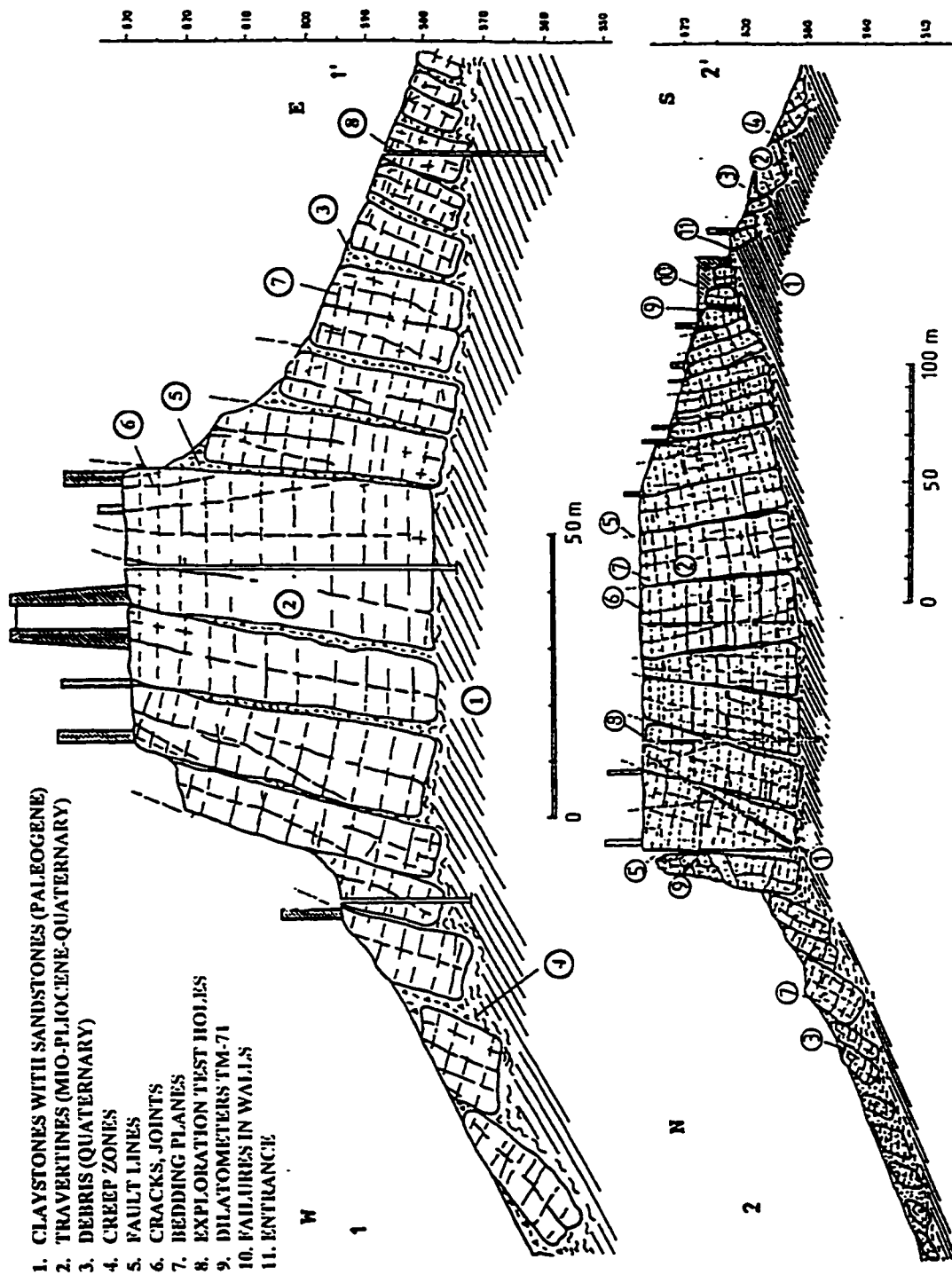
**Figure 3.16.** General view of the Spis castle looking north-west.

### 3.5.1 Geological Structure

The general geological structure is illustrated in figure 3.17, showing two cross-sections through the castle hill.

Pre-Quaternary rock units in the immediate area of the Spis castle are represented only by the uppermost layers of the flyschoid *Podtatranska Group* (Paleogene). The whole flyschoid complex has a thickness of 1500 to 3500 m, and only the *Hutnianske Formation* is exposed in the area of Spis castle. The *Hutnianske Formation* is comprised of mostly clay shales, that are partly calcareous, and dark, brown-gray in color. Conglomerate beds with a maximum thickness of 2 m can be found in the predominantly clay shale rock. The total thickness of the *Hutnianske Formation* is approximately 300 - 550 m. The dip of the flyschoid complex in the castle area is sub-horizontal (5 to 10°). All units were affected by post-Paleogene tectonics. As a result, the originally compact Paleogene units were broken into series of blocks with vertical and horizontal displacements. Two systems of normal Paleogene faults can be found in the general area of interest, belonging to the *Hornadska basin* (figure 3.17). The oldest faults have generally a ESE-WNW orientation. The younger faults have NW-SE or N-S orientation (Malgot et al., 1992).

The geomorphological development of the area is closely related to the tectonic history. The dominant factor was tectonic activity accompanied by mineral and thermal water springs along the faults. During the Miocene and Pleistocene large amounts of travertine were deposited. The major influence on the travertine deposition was the younger NW-SE and N - S faults. Deposition of travertines can be still observed at the *Siva Brada* hill, located approximately 10 kilometers to the west of the Spis castle. The original hemispherical shape of the travertine deposits was largely disturbed during the Pleistocene. Only erosional remnants, in the form either of rock cliffs or flat plateaus with sharp, steep edges, are presently visible. This degradation was caused mainly due to gravitational movements of the rigid travertine blocks on the more plastic substratum, as



1. CLAYSTONES WITH SANDSTONES (PALEOGENE)
2. TRAVERTINES (MIO-PLIOCENE-QUATERNARY)
3. DEBRIS (QUATERNARY)
4. CREEP ZONES
5. FAULT LINES
6. CRACKS, JOINTS
7. BEDDING PLANES
8. EXPLORATION TEST HOLES
9. DILATOMETERS TM-71
10. FAILURES IN WALLS
11. ENTRANCE

Figure 3.17. Cross-sections through the Spis castle hill.

well as due to karstification, weathering and erosion. Some influence on the development of creep movement of the travertine blocks is also ascribed to the intense periglacial freezing, especially at their contact with the plastic flyschoid base.

The present thickness of the travertine deposit is 50 - 52 m. The colluvial sediments are mainly scree slopes consisting from a mixture of travertine blocks of various sizes and soil with a thickness of less than 5 m. Artificial fill is present in the immediate area of the Spis castle, with a thickness of 2 m to 7 m.

The travertine deposition can be divided into three groups (Malgot et al., 1992):

- "Crater facies", represented by oolitic travertine. These are blocks with an irregular and steeply inclined travertine deposition, with veins containing material from underlying layers. Towards the upper sections, this part changes to veins with compact aragonite, which is gold-yellow in color with dark bands. This type changes relatively sharply into the facies of "strong travertine".
- "Facies of strong travertine", are porous and represented by cascade benches with a thickness greater than 3 m.
- "Rim facies" are found in the highest sections and are characterized by thin beds and brecciated travertine.

### **3.5.2 Previous Investigations**

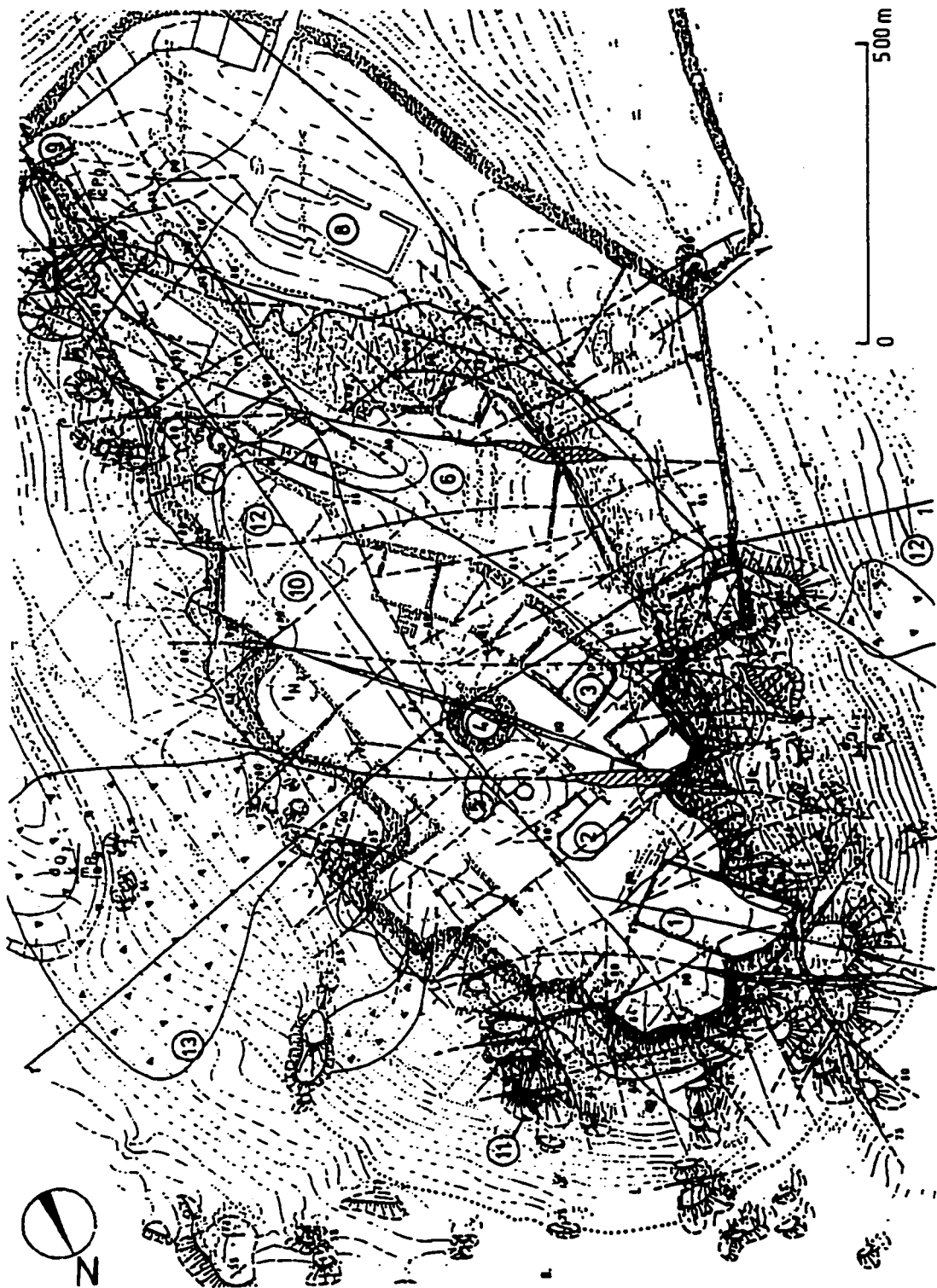
Chmelik (1959), based on paleobiological evidence, estimated a Pliocene age for the travertines. Similar considerations are presented by Lozek (1964, 1973). Chmelik (1963) presented a stratigraphical classification of the Quaternary and pre-Quaternary units in the general area of the Spis castle. Holec (1992), based on a find of mastodont teeth, states that at least part of the travertine was formed in the Upper Miocene. Several authors studied caves found in the travertines (Vitek, 1970; Cebecauer and Liska, 1972; Ivan, 1943). Most of these reports consider karstification, weathering and erosion as the

main cause of gradual deformation of the travertines. Slope movement was considered as the main destructive factor by Matula and Nemcok (1968) and Zaruba and Mencl (1987). Detailed descriptions of the gravitational deformation were presented by Nemcok and Svatos (1974), Nemcok (1982) and Malgot et al. (1992). Fussganger and Kostak (1983) and Fussganger (1985) studied the creep type movements of travertines, and based on measurements, proved that active deformation is still occurring.

The main geotechnical investigation of the immediate castle area was undertaken by Malgot et al. (1992) and summarized by Vlcko et al. (1993). The site investigation resulted in a detailed (1:500) engineering geological map, discontinuity measurements, clarification of geological structure and stability evaluation of castle walls. Twelve test holes extending under the base of the travertine blocks were drilled in the castle area to obtain information on the geometry of the travertines. Several extensometers (TM-71 type) were installed at the site to measure the long-term deformation.

### **3.5.3 The Rock Mass Structure of the Spis Castle Foundation**

Figure 3.18 presents the plan view of the Spis castle foundation illustrating the block-like structure. The travertine thickness in the area of the upper castle (eastern part), based on drilling and geophysical measurements, is approximately 50 - 53 m. The western part of the castle is characterized by a block field of travertines with the thickness of individual blocks estimated at 25 - 30 m. Somewhat more complicated is the area of the lower castle. Part of it is formed by a block field with a block thickness of 15 - 18 m. Towards the south and southeast, the block field gradually disappears and only isolated blocks of travertine are to be found, often covered by colluvial sediments. The absence of travertine blocks in this area can be explained by the uplift of a block of Paleogene clay shales along a tectonic line with a dip direction  $220^{\circ}$  -  $250^{\circ}$  and a dip of  $80^{\circ}$ . As a result, the original block field was destroyed with an intensification of creep movements, block separation, sinking and tilting of individual blocks.



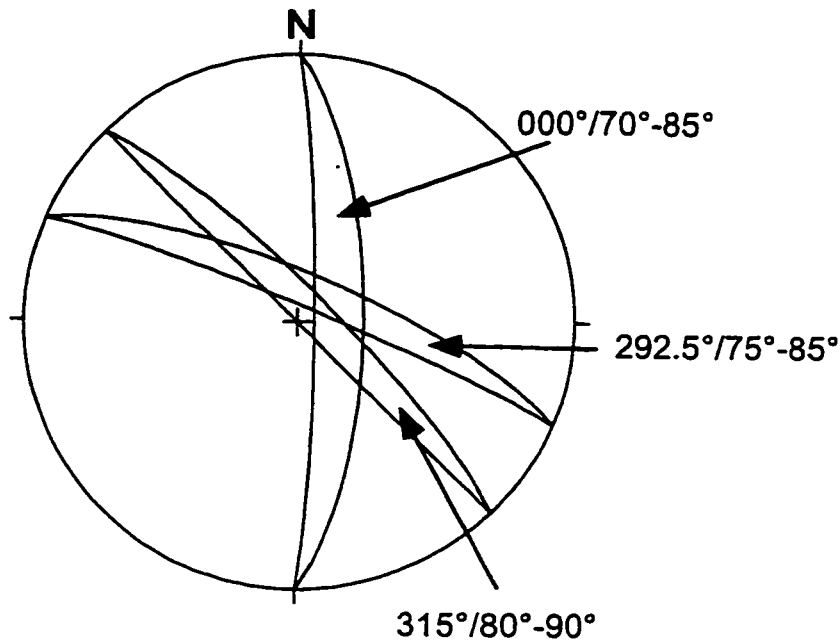
**Figure 3.18.** Plan view of the Spis castle (after Malgot et al., 1992). 1- Romanesque Palace, 2 - Chapell, 3 - Late Gothic Palace, 4 - Storage, 5 - Water Reservoir, 6 - 1<sup>st</sup> Romanesque Courtyard, 7 - 2<sup>nd</sup> Romanesque Courtyard, 8 - Lower Courtyard, 9 - Entrance, 10 - Main discontinuities, 11 - Separated travertine blocks, 12 - Cross-section lines, 13 - debris.

The direction of movement was predominately influenced by the gravitational forces. The shear movements in the dip direction of the underlying flyschoid rocks are believed to be only minor. Distinct blocks of varying size are displaced 150 - 300 m from the main mass of the travertine. Parts of these individual blocks were used in the early castle construction as a foundation of some of the structures, especially the outer castle wall.

The sides of the castle hill viewed from the NW, N, SE and SE, are represented by cliffs with a height of 15 - 22 m and an slope angle of 70° to 80°. Some parts are vertical, with local overhanging sections. The slope extending from the base of the rock cliffs ranges from 30° - 32°, with a gradual decrease to 22°. In the SW area the terrain inclination does not exceed 16°.

The travertine rock mass is disrupted by a series of tectonic lines and discontinuities with varying geometry and persistence. The most significant system of discontinuities is in the NW-SE direction, dipping 80° - 90° SW. Another discontinuity system is approximately N-S, dipping 70° - 85° W. A summary of the main discontinuity data is shown in figure 3.19. A significant discontinuity parallels the walls, separating two parts of the castle called "*Prve romanske predhradie*" and "*Dolne nadvorie*". Block displacement towards the west can be observed along this lineament. Apart from these main discontinuity systems there are several irregularly-oriented discontinuities producing a block structure in the travertine foundation.

The whole structure of the travertine hill can be divided into two parts; the central part and the outer part. The central part is represented by the thick deposit of travertine; the outer part by distinct blocks separated from the central part. The central part, considering the thickness and unit weight, exerts a normal stress of approximately 1.3 MPa, squeezing the plastic underlying material. Vertical displacement of the large central blocks is the main type of movement, whereas towards the outer boundaries the horizontal component



**Figure 3.19.** Orientation of main discontinuities at the Spis castle.

of displacement increases. Although several dilatometers of the TM-71 type were and are used for displacement, the measurements were interrupted for various reasons. Available results by Malgot et al. (1992) show a movement in northwest part of travertine hill of 1.13 mm/year.

#### **3.5.4 Rock Material Properties**

Paleogene rocks form the immediate base of the travertine. This complex comprises mostly clay shales, with only minor representation of sandstone layers and, in places, conglomerates. The clay shales, as observed in outcrop (figure 3.20), are highly weathered with only slight traces of original bedding. They are mainly sandy with a



calcareous cement. The presence of mica is distinct, especially in shales with a laminar texture. Local distinct concretions of iron oxide, 5 - 10 mm in diameter, are present. Laboratory testing results gave uniaxial compressive strengths ranging between 1.5 - 50 MPa (Malgot et al., 1992). The wide scatter in test results was assumed to be due to anisotropy, different degrees of lithification, lamination and mineralogical composition. The results showed a large strength variation even over a 1 m distance. Large differences in strength were also due to the varying size of test samples. The clay shales can be generally classified as a weak rock with a low uniaxial compressive strength. Unfortunately no other tests were performed on this rock type. The contact between the clay shales and the overlying travertine can be observed near the main castle entrance (figure 3.20). Travertine represents the major rock type in the area of interest.



**Figure 3.20.** Contact zone of travertines and underlying shales (black circular object in lower center of photographs is a camera lens).

The travertines are gray, white and yellow in color. They have micro- and macro porosity, with voids filled by calcite and aragonite. Their surface is usually weathered and karsted, especially along joints. Karstification is most significant in the vicinity of major discontinuities and their intersections. The unconfined compressive strength of the massive micro-porous travertines is 60 - 70 MPa, whereas that of the macro-porous and brecciated type is around 34 - 40 MPa (Malgot et al., 1992). Lower strength values were found in travertines near major tectonic lineaments and weathered zones (14 - 18 MPa).

An important material type occurs in the contact zone between the travertine blocks and clay shales. The material in this zone is very significant for the evolution of block-type movements. The zone is characterized by sandy clays and remolded clays, containing fragments of travertines and/or shales. The zone, as confirmed by test hole data, is 1 to 3 m thick. The laboratory testing program (shear box) performed at the Slovak Technical University in Bratislava, experienced problems due to the presence of rock fragments within the samples.

### **3.5.5 Landslide types and slope deformations at the site**

The geological structure formed favorable conditions for slope instability. Three types of landslides are typical for the site:

- **Block-type movements**

The block type structure of the castle site is best illustrated in cross-sections 1-1' and 2-2' in figure 3.17. The travertine blocks in cross-section 1-1' are sunken and rotated on the western side and have toppled on the eastern side. Blocks in cross-section 2-2' have rotated both on the northern and southern side. The thickness of the travertine blocks was determined by several test holes and is 50 m - 53 m in the central part, decreasing towards the south. The foundation of the upper castle is formed by travertine blocks of relatively uniform thickness from which individual blocks are separated towards the outer

boundaries. The movement of travertine blocks under the upper castle is mainly vertical. The individual blocks have irregular shape separated by major discontinuities as discussed in section 3.5.3.

- **Rock falls**

Rock falls are common on the steep, almost vertical, wall forming the rim of the travertine structure. Falls of travertine blocks originate due to slow creep movement of the larger outer blocks and mechanical weathering of travertines. Travertines are disrupted by a system of discontinuities with varying dip and dip direction, representing rear and lateral release surfaces for the blocks. Individual rock falls have resulted, in the past, in considerable damage to the castle walls and present an existing threat to the stability.

- **Slides**

Sliding types of movement probably took place in the past under different climatic conditions, on slopes formed by the Paleogene flyschoid rocks. The resulting forms of these slides are covered by more recent deposits.

### **3.5.6 Groundwater**

The geological structure of the castle foundations does not allow for groundwater inflow from the outside area. No water inflow was observed along the main fault lines. The groundwater table is influenced only by the infiltration in the immediate area of the castle structure. This catchment area totals 0.07 km<sup>2</sup>, having a good vertical permeability due to the existing fracture network. Although the amount of groundwater is relatively small it is affecting the overall stability, especially by altering (“softening”) the properties of clay shales in the contact area with overlying travertine blocks and increasing the pore pressures.

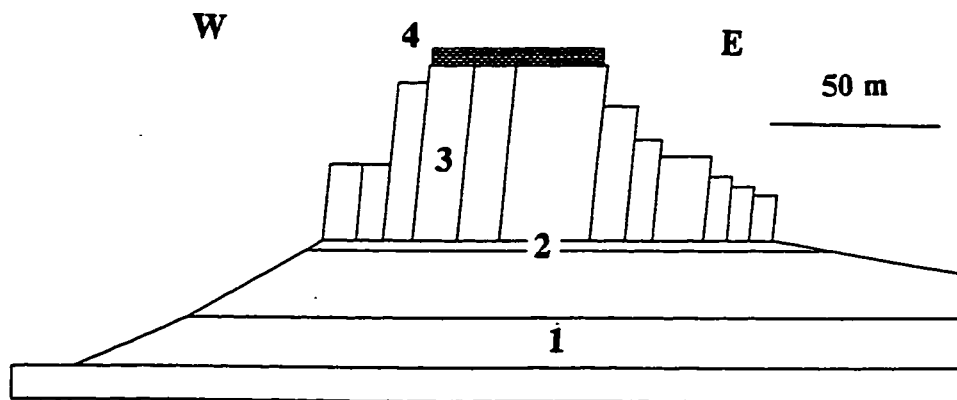
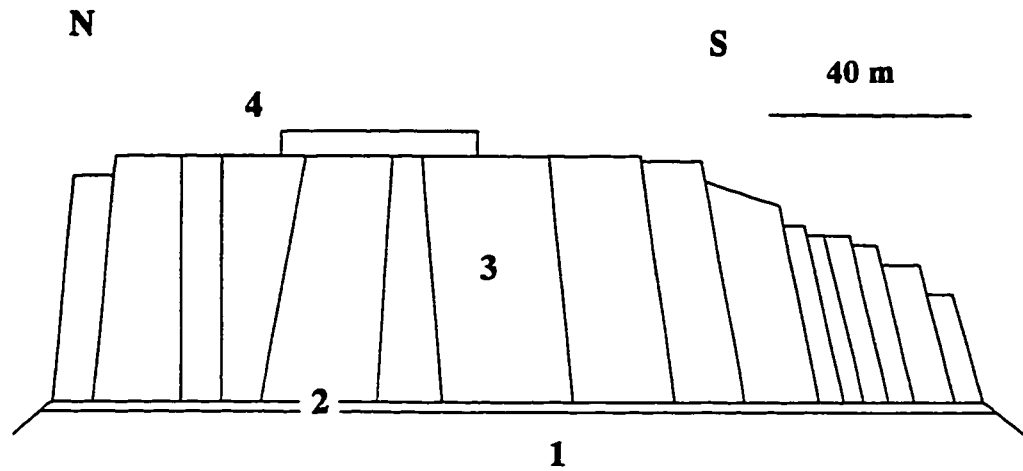
### **3.5.7 Numerical Analysis of Block Deformation in the Spis Castle Foundation**

Block deformations in the Spis castle foundation were analyzed using the distinct element method (UDEC). Simplified N-S and E-W cross-sections, based on figure 3.17 and field investigation, were used in the analysis. The analysis concentrated primarily on the investigation of the failure mechanism. The geometry of the cross-sections used in the numerical analysis is shown in figure 3.21 (a) and (b).

The base of the model was represented by the flysch complex. The upper section of the flysch complex comprises a 3 m thick clay shale eluvium, corresponding to the creep zone identified in the test holes. The upper blocks overlying the creep zone are formed by an approximately 50 m thick layer of travertine. A 5 m high structure was situated on the top of the travertine, to simulate a part of the castle wall structure. The castle structure has masonry walls, built predominantly from the local travertine blocks.

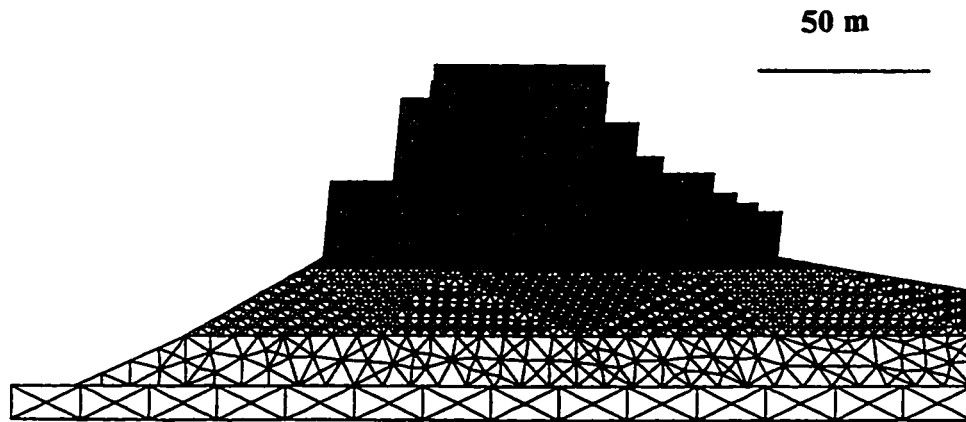
The upper travertine layer was divided into blocks based on the discontinuity survey. Only the main discontinuities, creating large columns in the travertine, were used in the analysis. As observed in the field survey, the primary type of instability results from the displacement of these large blocks. The remaining discontinuities - bedding planes and fractures - are the cause of predominantly localized, secondary instability, in the form of rock falls, sliding of small sized rock particles, and toppling.

The blocks in the model were discretized into a mesh of triangular finite difference zones, to allow for an analysis utilizing fully deformable blocks (figure 3.22). An elasto-plastic, Mohr-Coulomb constitutive criteria was used for the 3 m thick “creep zone”, as well as the castle wall structure placed on top of the travertine layer. The input parameters are summarized in table 3.2.



- 1. Flysch complex
- 2. Creep zone
- 3. Travertien blocks
- 4. Part of Castle structure

**Figure 3.21.** Geometry of distinct element models used for the analysis. Only central part of N-S cross-section is shown.



**Figure 3.22.** Discretization of blocks used for the analysis.

**Table 3.2.** Input properties for numerical model.

<b>Properties</b>	<b>Travertine</b>	<b>Creep zone</b>
density (kg/m <sup>3</sup> )	2530.0	2100.0
bulk modulus (MPa)	22000.0	100.0
shear modulus (MPa)	11000.0	30.0
friction (°)	---	(15.0 - 30.0)
cohesion (MPa)	---	(0 - 0.05)
joint normal stiffness (MPa/m)	10000.0	---
joint shear stiffness (MPa/m)	1000.0	---
joint friction (°)	30.0	---

The flyschoid zone and the part of the castle wall were assumed to have constant strength values throughout the analysis. Different values of cohesion and friction were assumed for the “creep zone”, representing the base of the travertine blocks.

An elastic isotropic constitutive criteria was adopted for the travertine blocks. The properties of the block discontinuities were defined in terms of their normal and shear stiffnesses and the angle of internal friction. The discontinuities were assumed to have no cohesion, tension and dilation. The input properties are summarized in table 3.1. The *in situ* stress ratio ( $K$ ), relating the horizontal and vertical stress components, was unknown. Ground stress ratios of  $K=1$ ,  $K=0.33$  and  $K=3$  were assumed for this analysis.

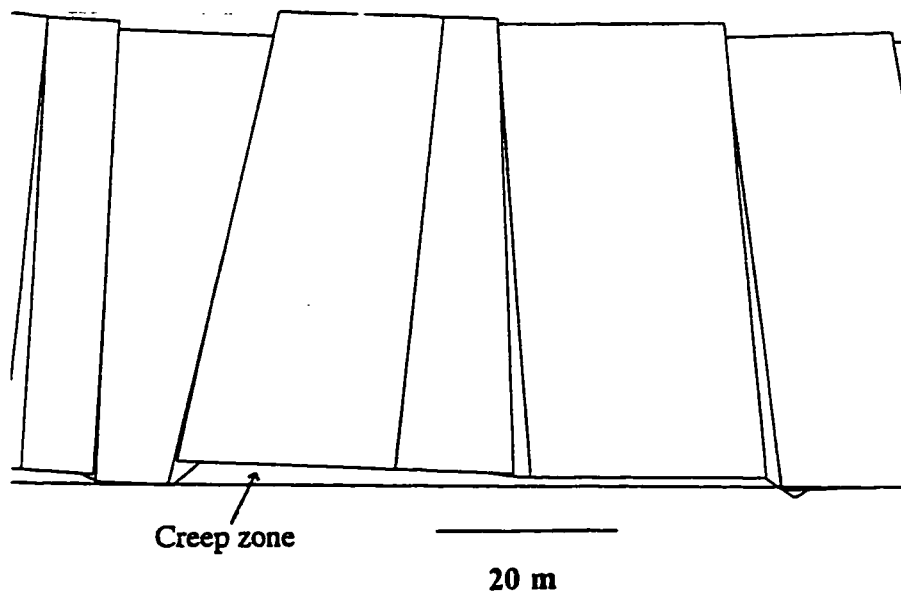
The initial numerical model was assumed to have a level topography. Blocks to the left and right of the castle foundation hill were removed step by step until the model geometry as shown in figure 3.21 was achieved. The model was allowed to equilibrate after each excavation step, under the new stress conditions. The assumed strength properties in this initial excavation were kept high, to prevent any yielding and non-elastic deformation in the model. After the final model geometry was achieved (figure 3.21), the model was saved and a series of sensitivity runs conducted to investigate the failure mechanism for both cross-sections. The sensitivity analysis consisted of varying the friction angle and cohesion for the creep zone forming the base of travertine blocks. Different values of friction angle, between  $15^\circ$  to  $30^\circ$ , and cohesion between 0 and 0.05 MPa were assumed.

### **3.5.7.1 Numerical Modelling Results**

Numerical results of the predicted deformation modes in the Spis castle foundation for the N - S cross-section are shown in figures 3.23 and 3.24. It is obviously impossible to know the precise initial conditions prior to movement of the travertine blocks. Different

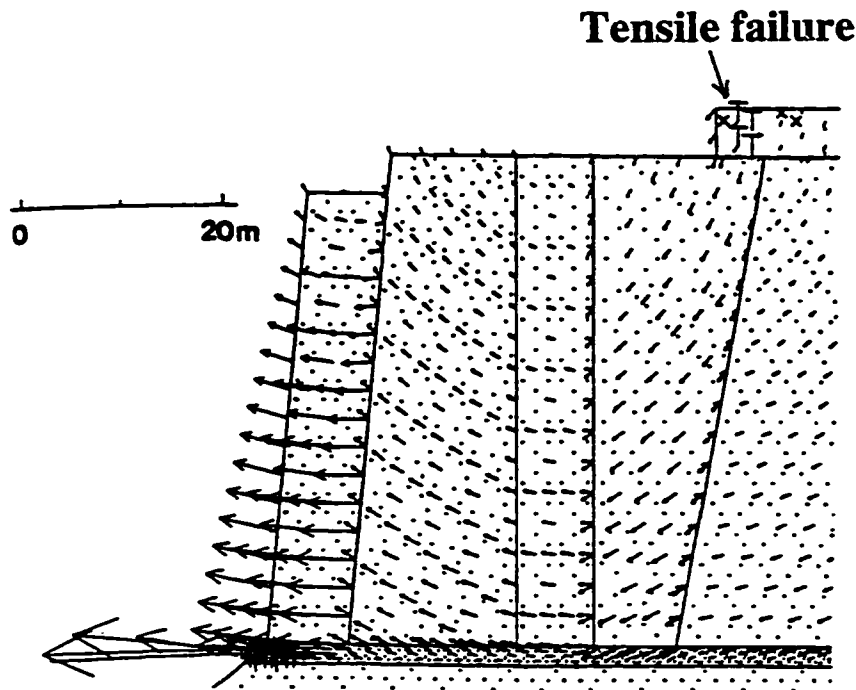
shear strength parameters (cohesion and angle of internal friction) were assigned to the "creep zone" and deformations recorded in form of displacements.

Figure 3.23 demonstrates the differential displacement between the blocks in the central part of the travertine structure. The displacement in this figure is magnified (10x) for illustration purpose. Blocks with a smaller base subside easier than blocks which have larger base. The amount of settlement is, in this case, controlled by the thickness of the creep zone under the travertine blocks. Figure 3.24 shows an enlarged view of the predicted deformation in the northern part of model (cross-section N - S). The displacement vectors infer a squeezing out or extrusion of the weak layer and displacement of the travertine blocks. The northernmost block is undergoing a significant displacement in a rotational mode, well in agreement with both field observations and reports from preliminary displacement measurements (Malgot et al., 1992). Plasticity indicators for the 5 m high structure show tension caused by differential displacement of the travertine blocks and are shown in detail in figure 3.24.



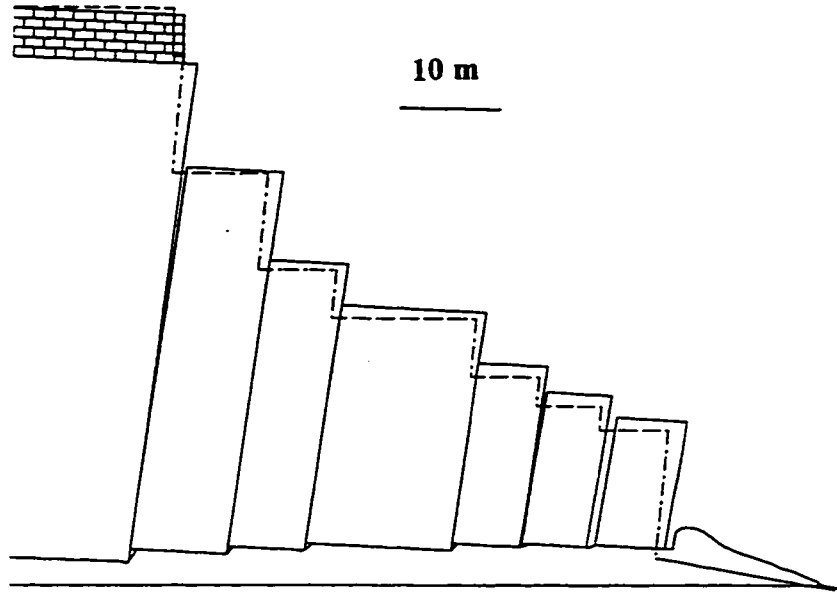
**Figure 3.23.** Differential settlement of travertine blocks in the central part of model.



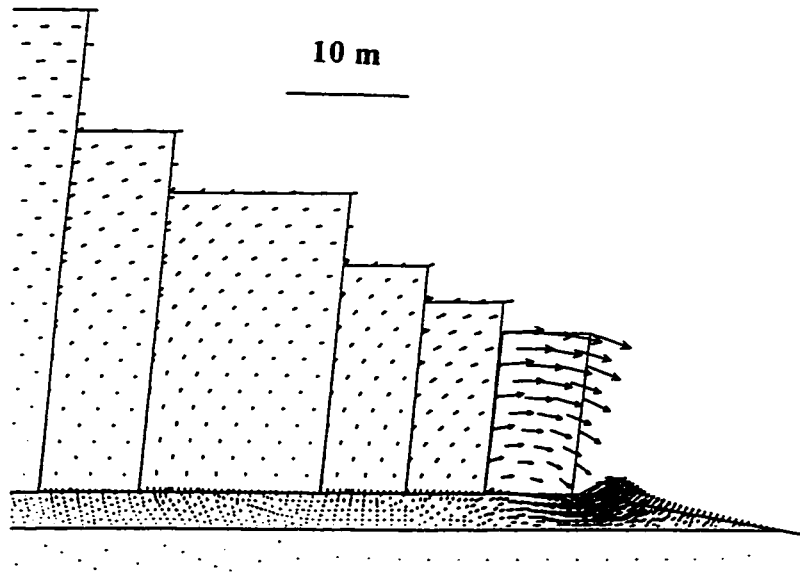


**Figure 3.24.** Displacement in the northern part of N - S cross section and tensile failure in the simulated castle wall.

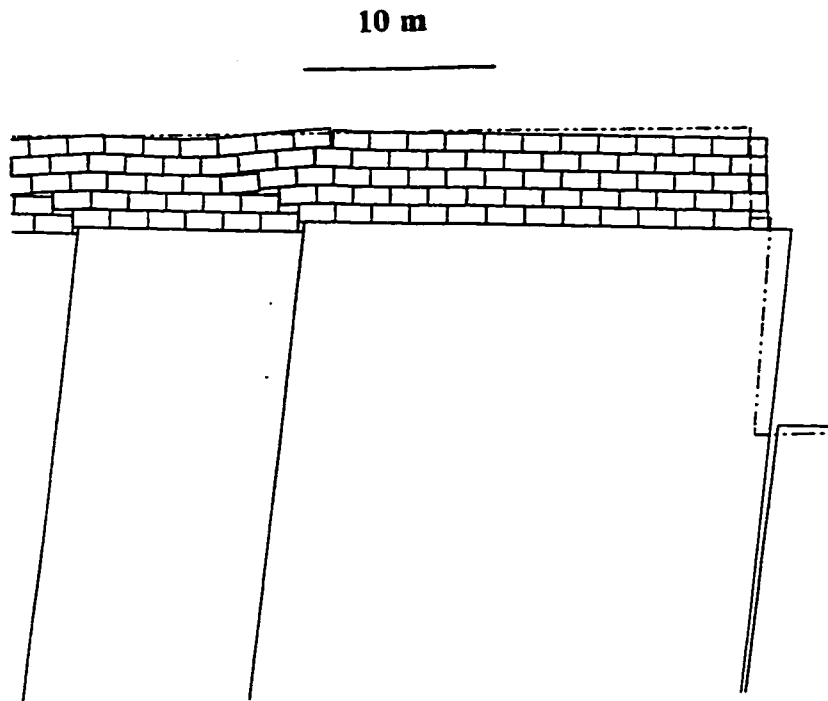
Figures 3.25 through 3.27 illustrate the predicted deformations for the E - W cross section. Figure 3.25 shows the deformations (magnified 50x) for the eastern part of model. The center blocks are subsiding and toppling, whereas the smaller blocks to the right appear to be displaced generally in an upward and outward direction. Given the assumption with regard to the material boundaries and properties (this particular model assumed a cohesion of 0.03 MPa and friction angle of  $25^\circ$ ), the larger, heavier central block appears to displace or "squeeze out" the more plastic underlying clay in an easterly direction. The variation in thickness of the clay horizon along the section is apparent. Figure 3.26 shows the displacement vectors for the same part of model, illustrating the squeezing of the weak base and toppling of the outermost travertine block. The maximum displacement vector at this calculation stage is 0.5 m. Figure 3.27 illustrates the deformation in the simulated castle wall, in the central part of model, due to the differential displacement of travertine blocks.



**Figure 3.25.** Displacement of travertine blocks for the eastern part of the E-W cross-section.



**Figure 3.26.** Displacement vectors in the creep zone and travertine blocks for the eastern part of E-W cross-section.



**Figure 3.27** Deformation of simulated castle wall.

### **3.6 Conclusions**

The block failures described and analyzed in this chapter consist of fairly massive joint-bounded blocks overlying soft layers. In practice, there is often a transition between such "conventional" block failures and other failure mode classifications. Wherever a soft layer underlies rock slopes comprising extensive blocks varying degrees of subsidence, sliding and rotation will be involved in failure. Slope deformation may involve sliding along joints, toppling of joint-bounded blocks, bearing capacity failure of the weak underlying strata and in large slopes composed of low modulus material, possible deformation and fracture of the blocks themselves. To analyze such a failure requires a detailed engineering geological knowledge of the slope and an appropriate modelling technique. The examples in this part of the study show the ability of distinct element

models to characterize block-type slope failure mechanisms and the potential use of this technique. This technique proved suitable for the analysis of a geological structure comprised by rigid joint bounded blocks overlying relatively weak layers assuming a mixed continuum - discontinuum approach. It is essential, however, that such analyses be constrained and calibrated wherever possible against slope instrumentation data. With the availability of such control, the model utilizing the distinct element method may provide a powerful method by which to analyze block-type slope failures.

The failure mechanism at Spis castle demonstrated in this study included toppling and rotational sliding of the rigid blocks. Hypothesis that the deformations at the Spis castle are governed primarily by the presence of a weak, plastic layer under the base of the travertine blocks, is in a good agreement with the presented numerical modelling results. The effect of differential block displacement on the fracturing of castle walls and objects was illustrated.

Several aspects of analysis would be of particular interest in future studies. The investigation of the effects of transitional material properties across the boundaries (between rigid blocks and soft base) would be of interest and probably more representative of the *in situ* conditions. In the case of the Spis castle, the effect and influence of jointing within the travertine itself should be investigated. It would be of interest to investigate the deformation at the Spis castle with the creep constitutive criterion. Unfortunately, this criterion was not available for the presented work. Little is known, quantitatively, about the strength and deformation properties of the rock and soil types. Additional material testing would provide interesting data, especially for the soils of the creep zone. It is not expected, however, that this would change in principle the results of the presented analysis. The rock mass structure of the Spis castle foundation, as well as the block displacements, are three-dimensional. The present analysis was confined to two-dimensions due to the lack of available software. The future application of a three-dimensional program capable of simulating the deformations would be of interest.

## **CHAPTER 4**

### **TOPPLING WITH EMPHASIS ON SLOPE DEFORMATION AT THE LUSCAR MINE, ALBERTA**

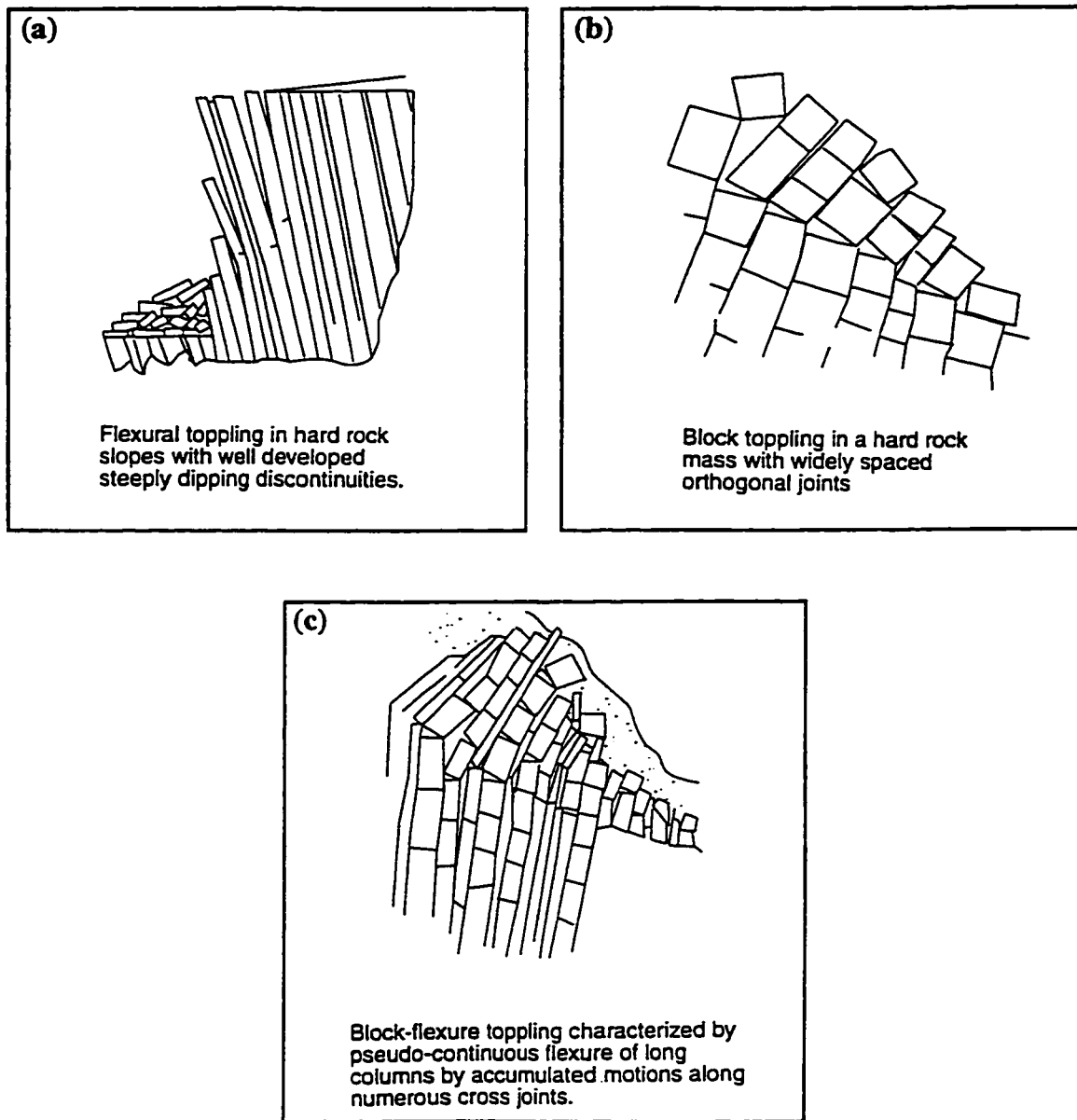
#### **4.1. Introduction**

Toppling is a distinct type of slope deformation characterized by downslope overturning, through rotation or flexure, of interacting blocks of rock under the forces of gravity or the forces exerted by adjacent units or fluids within discontinuities. This type of movement can occur at any scale and in all rock types. Rock mass structure, where well-developed discontinuities or pervasive foliation dip steeply into the slope and trend parallel or sub-parallel to the slope face, is especially susceptible to toppling.

Three general types of toppling described by Goodman and Bray (1976) are illustrated in figure 4.1:

- **Flexural Toppling**

This type of instability is most typical in rock slopes with one preferred discontinuity set forming semi-continuous cantilever beams that break in flexure as they bend out of the slope (figure 4.1a). Prior to beam fracture, displacement is accommodated by internal deformation of the rock columns and flexural slip along the discontinuities. The failure can be triggered by toe erosion, sliding or undermining. The progression of fracturing



**Figure 4.1.** Primary Toppling Modes (after Goodman and Bray, 1976).

and bending ends when the line of tension cracks intercepts the crest of the slope. The outward movement of each rock beam produces flexural slip and a portion of the upper surface of each bed is exposed in a series of back-facing/obsequent scarps. It is difficult to determine the base of the failure as the development of toppling is gradual. Numerical modelling techniques, especially methods capable of representing discontinuous media

with deformable blocks such as the distinct element method, prove to be very useful in the analysis of this type of toppling.

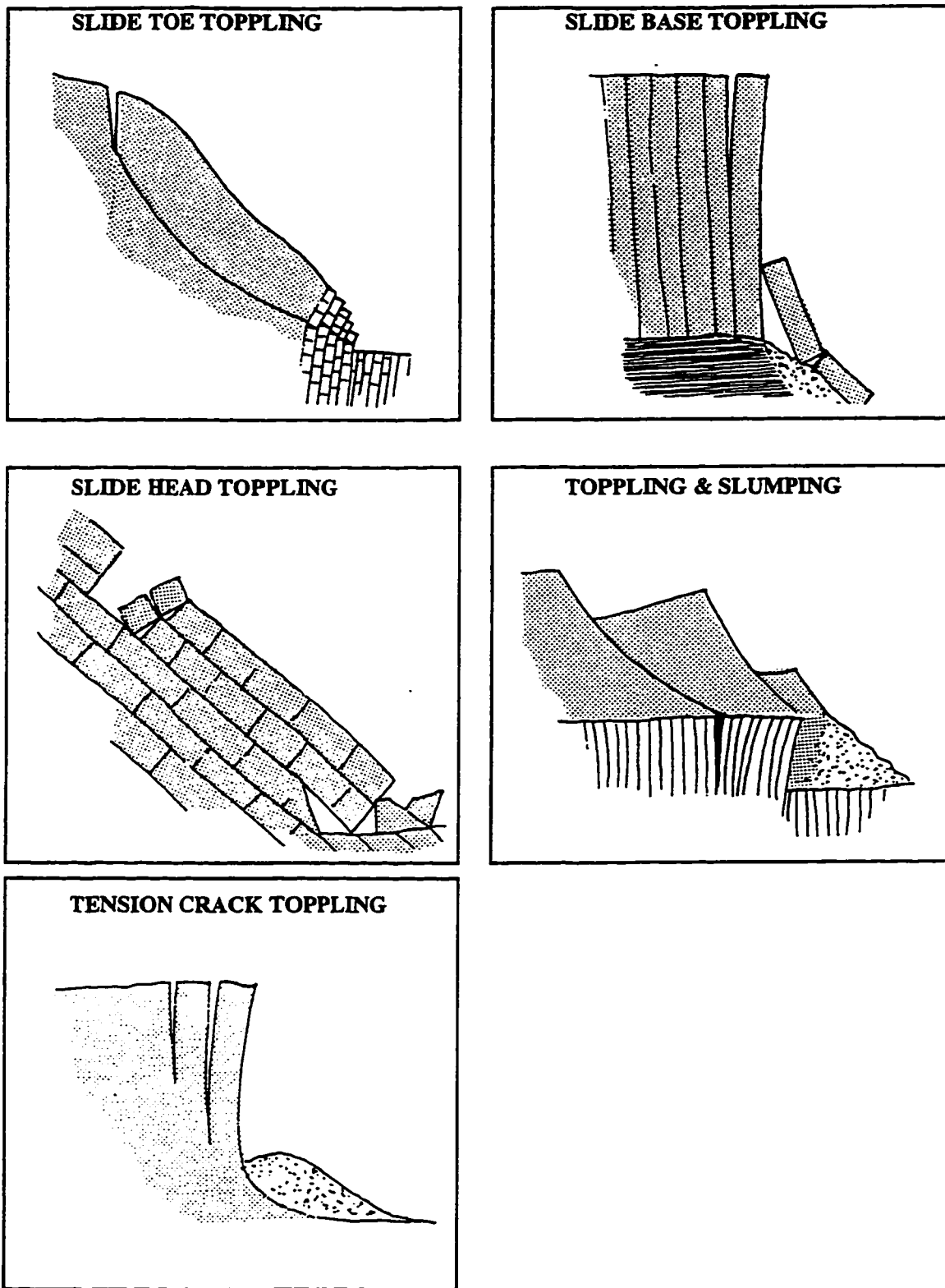
- **Block Toppling**

This type of toppling occurs where the individual columns are intersected by widely spaced cross joints, figure 4.1(b). Shorter columns in the toe zone receive the thrust from overturning of longer columns above. This thrusts the toe columns forward, enabling further toppling. The base of the disturbed rock slope is better defined than was the case for flexural toppling, consisting of a stairway generally rising from one layer to the next. These steps are formed by cross joints, which occupy the positions of primary flexural cracks in the flexural type of toppling. New rock breakage occurs to a much lesser degree than in flexural toppling. The limit equilibrium method of analysis may be appropriate if the stepped base is defined and the blocks do not undergo deformation.

- **Block-Flexural Toppling**

Pseudo-continuous flexure of long columns through accumulated deformation along numerous cross joints is characteristic of block-flexural toppling (figure 4.1c). Sliding is typical in the toe area whereas both, sliding and overturning occurs throughout the rest of the rock mass. The sliding movements result from steepening of the cross joints dip due to accumulated overturning. Because the movements involve many small incremental displacements, there are fewer tension cracks than in flexural toppling and fewer edge-to-face contacts and voids than in the block toppling.

Secondary toppling modes, shown in figure 4.2 and described in table 4.1, are generally initiated by undercutting of the slope toe, by natural events such as erosion or weathering, or by human activity. The primary failure mode involves the sliding or physical breakdown of the rock or soil and toppling is induced in some places as a consequence of this principal movement.



**Figure 4.2.** Secondary toppling mechanisms (after Hoek and Bray, 1981).



**Table 4.1.** Secondary toppling mechanisms (after Hoek and Bray, 1981)

<b>SLIDE HEAD TOPPLING</b>	Joint bounded blocks topple into voids created by downslope failure.
<b>SLIDE BASE TOPPLING</b>	Triggered by slide movement above a steeply dipping layered rock mass. The shear force from the slide is acting along the top of the rock mass.
<b>SLIDE TOE TOPPLING</b>	Consists of two types of movement: sliding in the upper formation induces toppling at the slope toe.
<b>TENSION CRACK TOPPLING</b>	Tension cracks developed above steep slopes. creates blocks susceptible to toppling.
<b>TOPPLING &amp; SLUMPING</b>	Occur where a rock slab rests on a soil/weak rock layer. Slumping in the underlying, weaker material, causes the overlying rock blocks to topple. This type of structure and failure mechanism are analyzed in more detail in chapter 3.

## 4.2 Literature Review

Perhaps the most significant and pivotal paper introducing toppling as a distinct type of slope movement was presented by de Frietas and Watters (1973). The authors describe in detail three field examples of toppling each in a different structural setting and involving different scales of movement. They concluded that toppling does not require unusual geological conditions in order to develop and that toppling can occur on a wide range of scales affecting a variety of rock types.

Muller (1968) proposed that block rotation or toppling may have been one of the contributory factors involved in the failure of the north face of the Vaiont slide in the Italian Alps. Bukovansky et al. (1974), describe a toppling failure of a cut slope in thinly bedded limestones, marls and sandstones dipping into the slope. Wide-open vertical tension cracks behind the cut crest were observed with a considerable movement along

the bedding planes. Heslop (1974) describes a toppling instability in the hanging wall during deepening of caving mines. Brawner and Stacey (1978) presented results from a monitoring program for assessment of highwall movements in the Steep Rock Mine in Ontario. Toppling was one of the failure mechanisms involved in the slope instability.

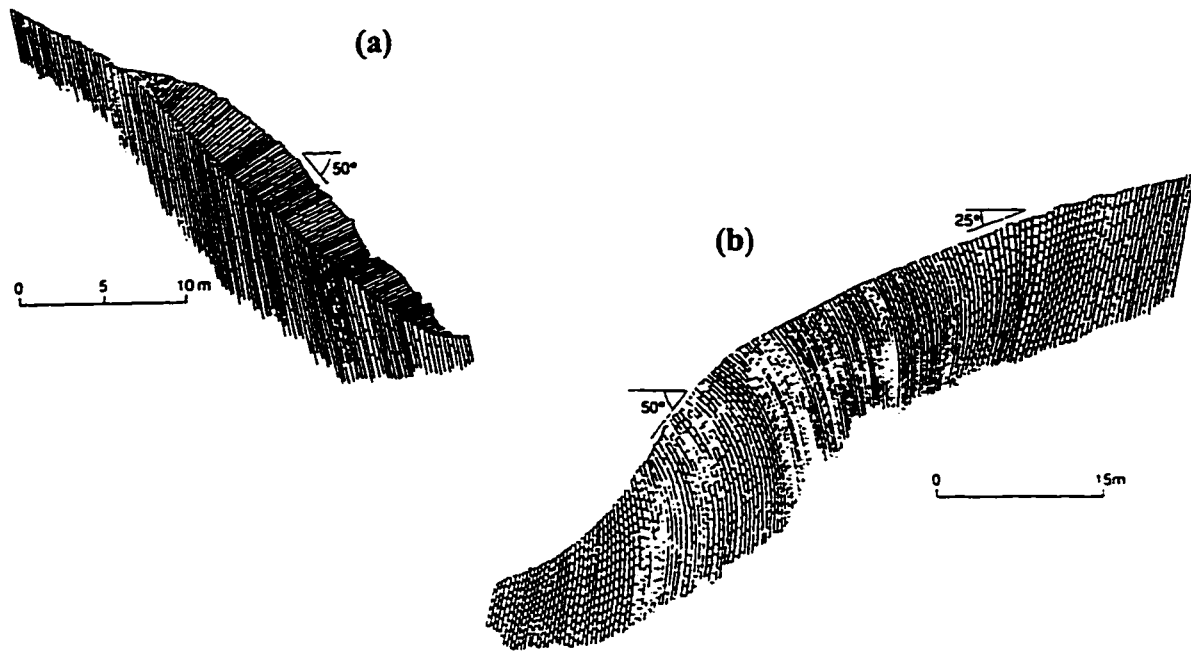
Piteau et al. (1978) analyzed the rock slope stability related to a Canadian highway road cut (Hell's Gate, British Columbia), where the toppling of steeply dipping tabular fault blocks presented a major geological hazard. An acceptable factor of safety was attained by the prevention of water pressure build-up, support and appropriate excavation design. Evans (1981) presents examples of secondary toppling failures due to bearing capacity failure or differential settlement due to weathering and creep in the softer underlying rocks.

Zaruba and Mencl (1982) describe an example of secondary toppling triggered by reactivation of sliding at the foot of a sandstone layer. Caine (1982) describes large cliff failures by toppling taking place on the edges of a dolerite plateau in Tasmania. Topographic evidence and joint survey suggested that failure was taking place by toppling of joint-bounded slabs that, in some places, are triggered by failure in the underlying sediments. Cruden (1994) refers to an early study by Lugeon who in 1933 suggested that toppling occurs on slopes where penetrative discontinuities dip more steeply than, but "in the same direction", as the slope. Reid and Stewart (1986) described toppling deformation at the Afton open pit mine in British Columbia. Crack formation and constant velocity movement preceded an acceleration phase and subsequent failure, which was successfully predicted by an extensive monitoring program.

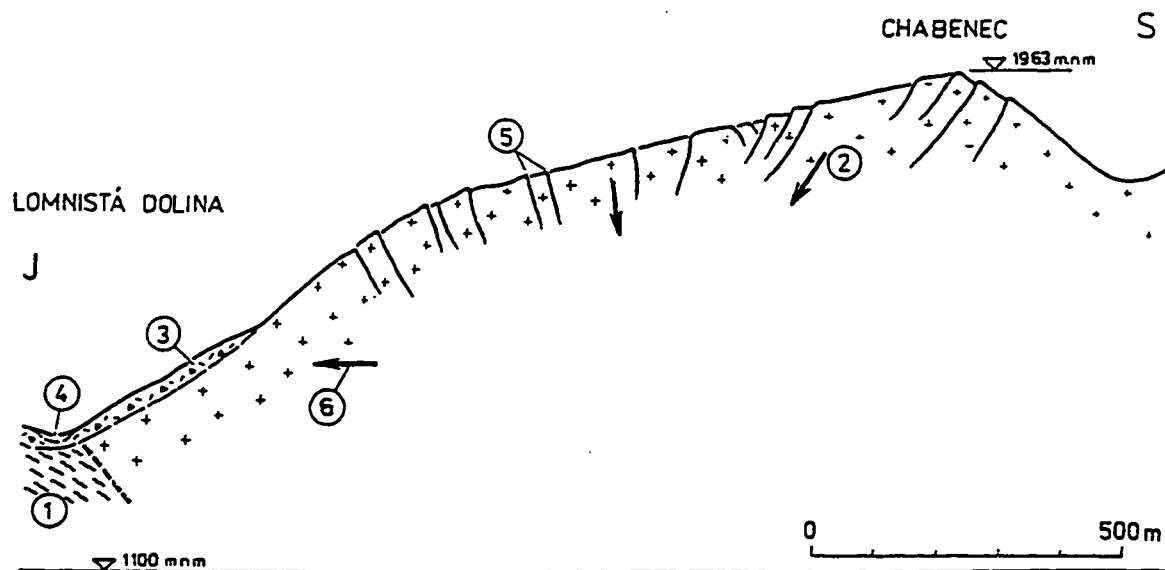
Brabb and Harrod (1989) published a worldwide review of landslide problems, indicating that toppling is a widespread phenomenon encountered in various geological environments. Giraud et al. (1990) describe several failures in metamorphic formations in the French Alps with toppling presenting one of the major instability mechanism. Richards (1993) refers to slope stability problems at the Jeffrey Mine in Canada. The

predominant geological structure and shear zones dip into the slope. The conclusion was reached that the slope response was too complex for prediction to be carried out by modelling, even when progressive failure mechanisms were considered. The historical performance data and intense monitoring were used as the primary basis for design. Glawe et al. (1993) presented results from long term monitoring of the kinematics of a toppling rock tower in Alps (Austria). A forecast of the time of failure was presented based on the mechanics of movement as well as stage of disintegration of the rock block. Hebil (1993) describes toppling failure at the Cardinal River Mine at Luscar, Alberta. This particular failure is analyzed in detail in the current chapter. Rapiman (1993) refers to the complex slope stability problems at the Chuquicamata mine in Chile. Toppling in the west sector appears to be the cause of tension crack development in the top of the wall and benches. Cruden and Hu (1994) described numerous toppling failures in the Highwood Pass, Alberta, on slopes where the penetrative discontinuities dip more steeply than, but in the same direction as the slope. Cruden (1989) calls slopes with such a discontinuity orientation, “underdip” slopes. Three basic toppling modes on such slopes were outlined by Cruden and Hu (1994): block flexure topple, multiple block topple, and chevron topple. An example of multiple block topple and block-flexure toppling on underdip slopes is shown in figure 4.3 (Cruden and Hu, 1994).

Several authors describe large scale toppling in natural slopes as one type of “sackung” or deep-seated creep deformation, where a large-scale gravitational deformation takes place without formation of a pervasive failure surface. Figure 4.4 shows an example of a large-scale toppling structure at the Chabenec ridge in the Nizke Tatry Mountains in the Slovak Republic. Cases where large scale toppling is, directly or indirectly, believed to be the main failure mechanism, were described by Zischinsky (1966), Tabor (1971), Mahr (1976), Radbruch-Hall et al (1976), Nemcok (1982), Holmes and Jarvis (1985), Evans (1987), Savage and Varnes (1987), Radbruch-Hall (1987), Riemer et al. (1988), Bovis (1982, 1990), Pritchard and Savigny (1991), Chigira (1992), Bovis and Evans (1995) and others.



**Figure 4.3.** Examples of multiple block (a) and block-flexure (b) toppling on “underdip” slopes (after Cruden and Hu, 1994).



**Figure 4.4.** Example of large scale toppling deformation at the Chabenec Ridge in Slovakia (after Nemcok, 1982). 1 - Gneiss, 2 - Granodiorite, 3 - Rockfall debris, 4 - Fluvial deposits, 5 - Shear planes, 6 - Direction of block movement.

#### **4.2.1. Methods of Analysis**

##### **4.2.1.1 Physical Modelling**

Physical modelling of toppling was a popular analytical tool especially in the seventies and early eighties, utilizing base friction models and tilt tables. Subsequently the use of the centrifuge in physical modelling provided a valuable insight into toppling mechanisms. All three types of toppling - flexural, block and block-flexural, were subjected to analyses. Ashby (1971), Erguvanli and Goodman (1972), Whyte (1973), Soto (1974), Byrne (1974), Hofmann (1974), Kuykendall (1975), Goodman (1976), Bray and Goodman (1981), and Niyom and Sakurai (1985), all applied physical modelling to the study of toppling deformation. Shimizu et al. (1992) used physical modelling to assess the dynamic response and stability of rock slopes during earthquakes with toppling being one of the failure modes analyzed. Adhikary et al. (1995) investigated flexural toppling in foliated rock slopes using centrifuge experiments and numerical simulations with the finite element method. The use of physical models was mostly replaced by more popular analytical tools such as limit equilibrium methods and especially numerical modelling techniques. Recent physical modelling research, (e.g., Aydan and Kawamoto, 1992; Jiang et al., 1995; Adhikary et al., 1995) is usually constrained to comparison and/or as a supplement to other analytical techniques.

##### **4.2.1.2 Kinematic Analysis**

Kinematic analysis was originally proposed by Goodman and Bray (1976) as a tool for the fast determination if toppling is kinematically feasible, utilizing a stereonet plot. The surface of the rock slope is in the direction of major principal stress. The shearing will occur along the discontinuities only if the direction of applied compression makes an angle greater than the angle of friction of the discontinuities to the normal to the layers (Goodman, 1989). As shown in figure 4.5, the poles to the discontinuity set dipping into

the slope must lie outside the great circle whose dip is the slope face angle plus the assumed friction angle of the discontinuity set. Goodman (1989) suggests that toppling can occur only if the rock layers strike nearly parallel to the strike of the slope within  $30^\circ$  ( $10^\circ$  more than shown in figure 4.5).

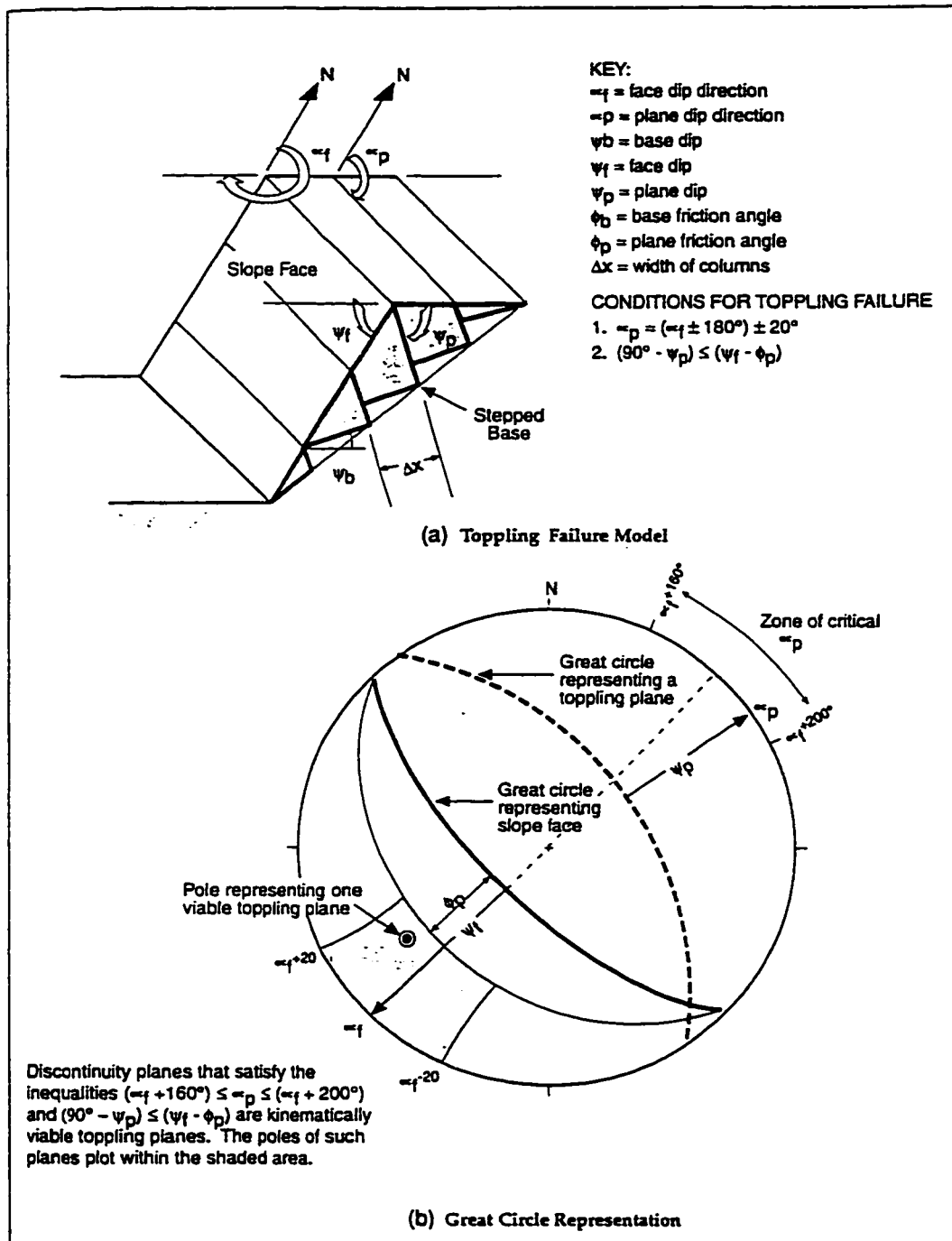


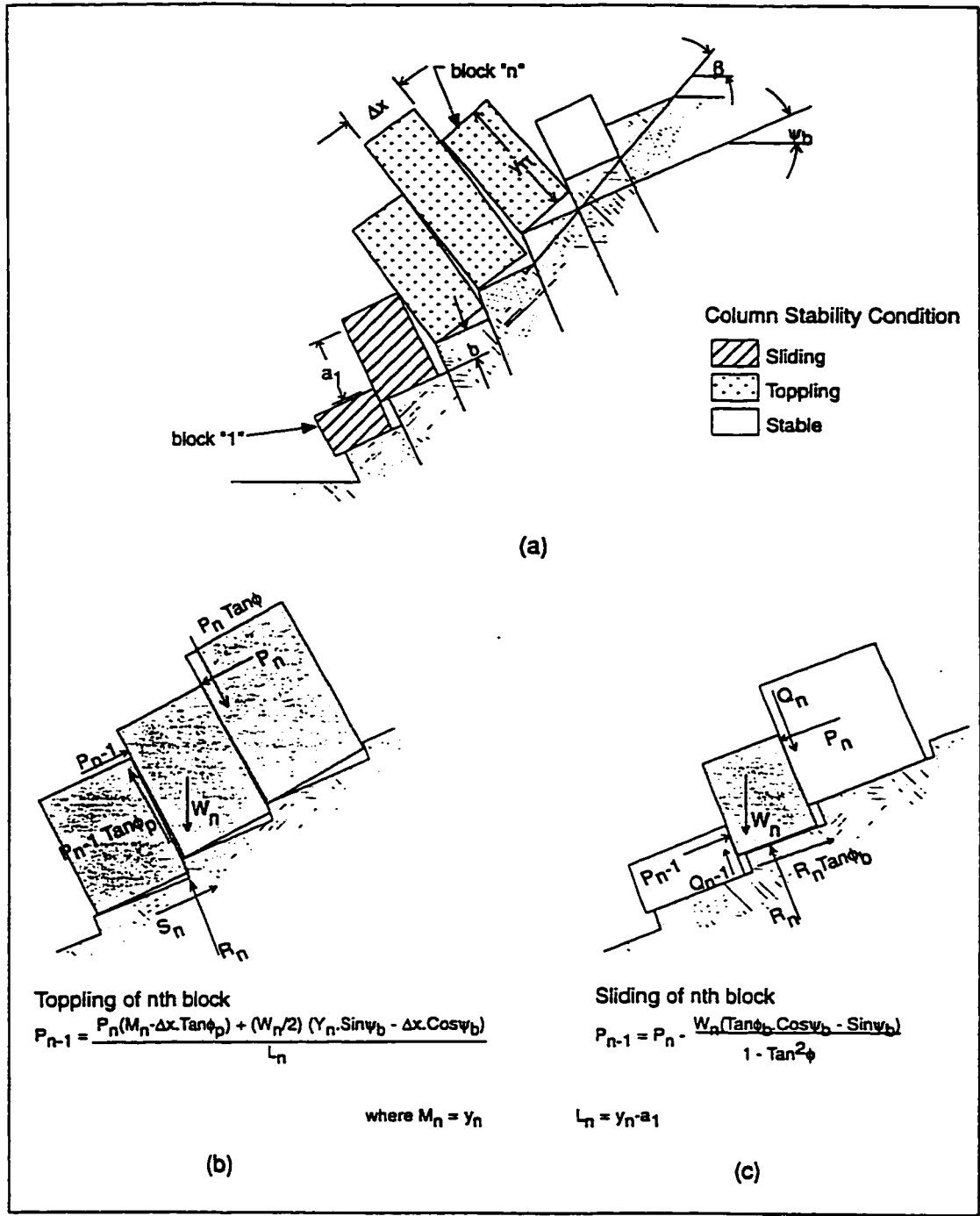
Figure 4.5. Kinematic analysis for toppling failure (after Norrish and Wyllie, 1996).

Cruden (1989) suggests that flexural toppling can also occur when the discontinuities dip in the same direction as the slope, but more steeply than the slope and the angle of friction on the discontinuities.

#### **4.2.1.3 Limit Equilibrium Analysis**

The limit equilibrium analysis of toppling was originally developed by Goodman and Bray (1976) and is used widely in engineering practice. The basic principles of this method are shown in figure 4.6. The slope is approximated as a series of blocks on a stepped base. The forces acting on the uppermost block are resolved into forces parallel and normal to its base. Two static problems are solved, one assuming block sliding and one block rotation, thereby determining the type of movement. The resultant parallel forces from each of these potential failure modes (sliding or rotation) are compared and the solution producing the largest resultant force indicates the type of block failure. The resultant parallel force is then applied to the neighboring block in the slope and the analysis is repeated, progressing from block to block down the slope towards the toe block. The final resultant force at the toe block is the force required to maintain the stability of the slope. A factor of safety can be calculated based on the friction angle of the last block. The program, "*Topple*", by the University of Toronto Rock Engineering Group is based on this approach to toppling analysis, and is outlined in Hoek and Bray (1981). The limitations of the limit equilibrium approach were summarized by Pritchard (1989):

- No block can be both toppling and sliding.
- Only continuous columns can be analyzed. Slip on joints or overturning of individual blocks defined by joints within a rock column is not allowed.
- Rock blocks can be only rigid (non-deformable).
- Location and dip of the basal failure plane must be assumed prior to analysis.
- The method does not account for non-linear stress displacement along joints.
- The slope geometry is restricted to a uniform step and block width.



**Figure 4.6.** Principle of Limit Equilibrium Method for Toppling Analysis (after Hoek and Bray, 1981).



All these limitations restrict the method to the analysis of small-scale block toppling where the process is limited to a planar failure surface with deformation by joint shear and separation (Pritchard and Savigny, 1990). Despite the limitations, the limit equilibrium method, with or without modifications, has proved to be useful in analyzing toppling of rock slopes in a number of engineering projects (Wyllie, 1980; Piteau et al., 1981; Piteau and Martin, 1981; Hoek and Bray, 1981; Teme and West, 1983; Zambak, 1983; Teme and West, 1983; Choquet and Tanon, 1985; Sagaseta, 1986; Scavia et al., 1990; Ke et al., 1994; Mongiovi et al., 1995).

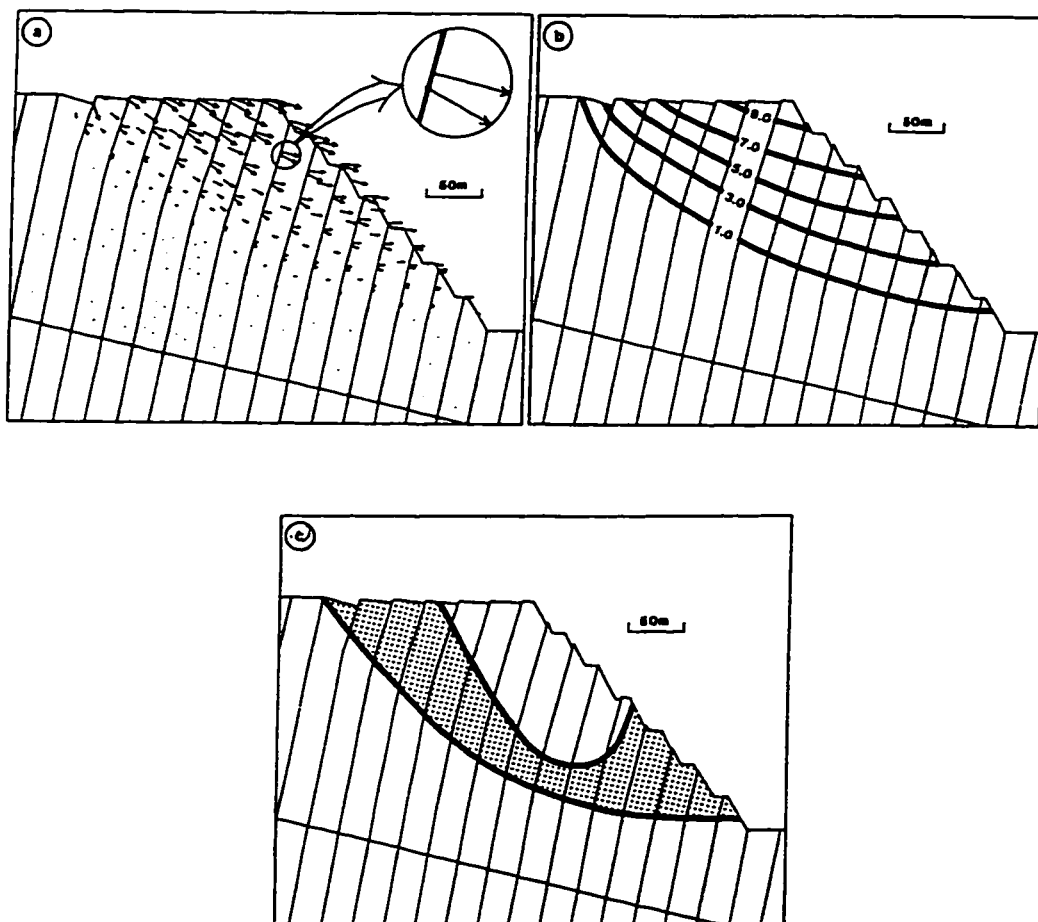
#### **4.2.1.4 Numerical Modelling of Toppling Instability**

Numerical modelling techniques have proven to be the most powerful analytical tools used in toppling analysis. Both continuum and discontinuum approaches have been applied to stability analysis, with the distinct element method being presently the most popular, numerical modelling technique.

Cundall (1971) developed the distinct element method for rock engineering. Initially the rock blocks were treated as rigid and non-deformable. Burman (1974), Hammett (1974) and Byrne (1974) analyzed toppling and block rotation using numerical modelling techniques and the influence of block rotation on planar failures. Hocking (1978) applied the distinct element method using rigid blocks only, to the analysis of toppling and sliding failures in hypothetical rock slopes.

The two-dimensional finite element method was utilized by Kalkani and Piteau (1976) when analyzing toppling at the Hell's Gate in British Columbia (Canada), Brown et al. (1980) in studying the Nevis Bluff rock slope failure in New Zealand, and Evans et al. (1981) in analyzing the mechanism of secondary toppling failure in New South Wales (Australia). Toppling analysis using numerical modelling methods was also discussed by Brown (1982) and Ishida et al. (1987).

Pritchard (1989), Pritchard and Savigny (1990,1991), and Pritchard et al. (1990) used the distinct element method to analyze toppling instability of the Heather Hill landslide in the Beaver Valley, Glacier National Park, British Columbia, Canada. The analyzed slope failed by flexural toppling was constrained by a curvilinear failure surface. Foliated pelitic rocks formed the lower part and stronger grits the upper part of slope. The authors compared the distinct element method to other types of toppling analysis (limit equilibrium and physical modelling) and concluded that it was suitable for modelling all types and scales of slopes susceptible to toppling. Figure 4.7 shows the results of toppling analysis after Pritchard and Savigny (1990) in the Brenda mine.



**Figure 4.7.** Distinct element model of toppling in Brenda mine, B.C., (a) grid point velocity vectors, (b) horizontal displacement contours in meters, (c.) area of failed nodes (after Pritchard and Savigny, 1990).

Adachi et al. (1991) analyzed a road cut toppling failure in layered sequences of tuff, tuffaceous sandstone and conglomerate. The distinct element method, UDEC (Itasca 1993), was utilized in the analysis, providing valuable input for the failure interpretation. Orr et al (1991) applied finite difference modelling to the analyses of flexural toppling failures in Australian gold mines. The failure surfaces were generally broadly-circular in shape, both in plan and section. Coulthard et al. (1992) presented a distinct element simulation of toppling in an open pit gold mine in Australia. Repeated hangingwall failures were experienced at the site leading to the mine closure. Geotechnical investigation studies carried out prior to the mine design were restricted to consideration of kinematic controls on stability without a more detailed computer-based stability simulation. Subsequent back-analysis with the distinct element method, confirmed the failure mechanism and instability that were experienced.

Martin and Mehr (1993) analyzed the hangingwall deformation mechanism at the Cassiar Mine in British Columbia. The instability involved the squeezing of soft deformable serpentinite rocks in the toe triggering planar sliding and graben toppling of stronger sedimentary rocks in the middle and upper sections of the slope. Bucek and Barron (1994) presented results from a numerical modelling program developed at the University of Alberta and applied to the toppling deformation at the Luscar mine, Alberta, Canada. The rock mass was approximated as a series of cantilevers breaking according to stress/strain conditions.

Hsu and Nelson (1995) analyzed the stability of rock slopes in weak rock using the distinct element method with discontinuities dipping into the slope. In addition to toppling, sliding and shearing through the rock blocks were observed. Board et al. (1996) applied both continuum (finite difference method) and discontinuum (distinct element method) methods of numerical modelling to the large toppling displacement experienced at the Chuquicamata pit in Chile. Both methods successfully reproduced the general features of the failure although in the continuum approach the ubiquitous joint constitutive criteria had to be used. The models were then used in a predictive fashion to

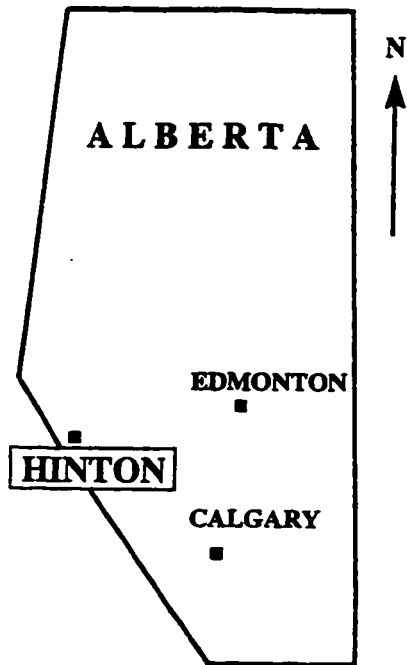
assess the stability of various design plans. Coggan and Pine (1996) analyzed the deformational behavior at the Delabola slate quarry in England, where deep-seated flexural toppling proved to be one of the failure modes. The numerical modelling provided insight into the instability mechanism and confirmed the influence of a raised water table on the slope stability. Hencher et al. (1996) presented various examples of slope design in complex geological conditions, including toppling, utilizing the distinct element method.

### **4.3 Toppling Instability at the Cardinal River Mine, Luscar, Alberta**

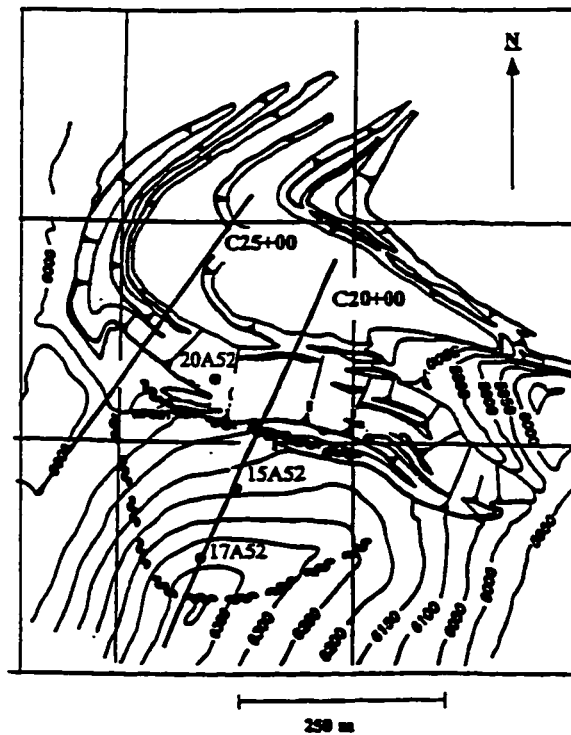
#### **4.3.1 Introduction**

The Luscar Mine of Cardinal River Coals Ltd., is situated in the foothills of the Rocky Mountains at Luscar Alberta, approximately 50 km southwest of the town of Hinton and 340 km west of Edmonton (figure 4.8). It is operated by Cardinal River Coals Ltd., a 50/50 joint venture between Luscar Ltd. and the Consolidation Coal Company of Canada Ltd. The 50-A-5 pit analyzed, is only one of several geologically-similar pits located along the side of a northwest trending ridge cut into a series of hills by several alpine valleys.

Mining began at Luscar in 1921 using underground methods to supply coal to the railways, and temporarily ceased in 1954 (Hebil, 1993). Mining resumed in 1968 with the development of an open pit, currently producing 2.6 million tonnes per annum of high quality, medium-volatile, metallurgical coal. The overburden is drilled and blasted using rotary blast hole drills and bulk slurry with waste material hauled to previously mined-out pits or external dumps. The Luscar Mine is an open pit coal operation where the rock mass structure is susceptible to toppling deformation along the south walls of the A-baseline pits (figure 4.9). The presence of weak rock material and daylighting cross joints results in a complex deformation mechanism involving both, sliding and toppling failure.



**Figure 4.8.** Sketch map showing the location of Luscar Mine near Hinton, Alberta.

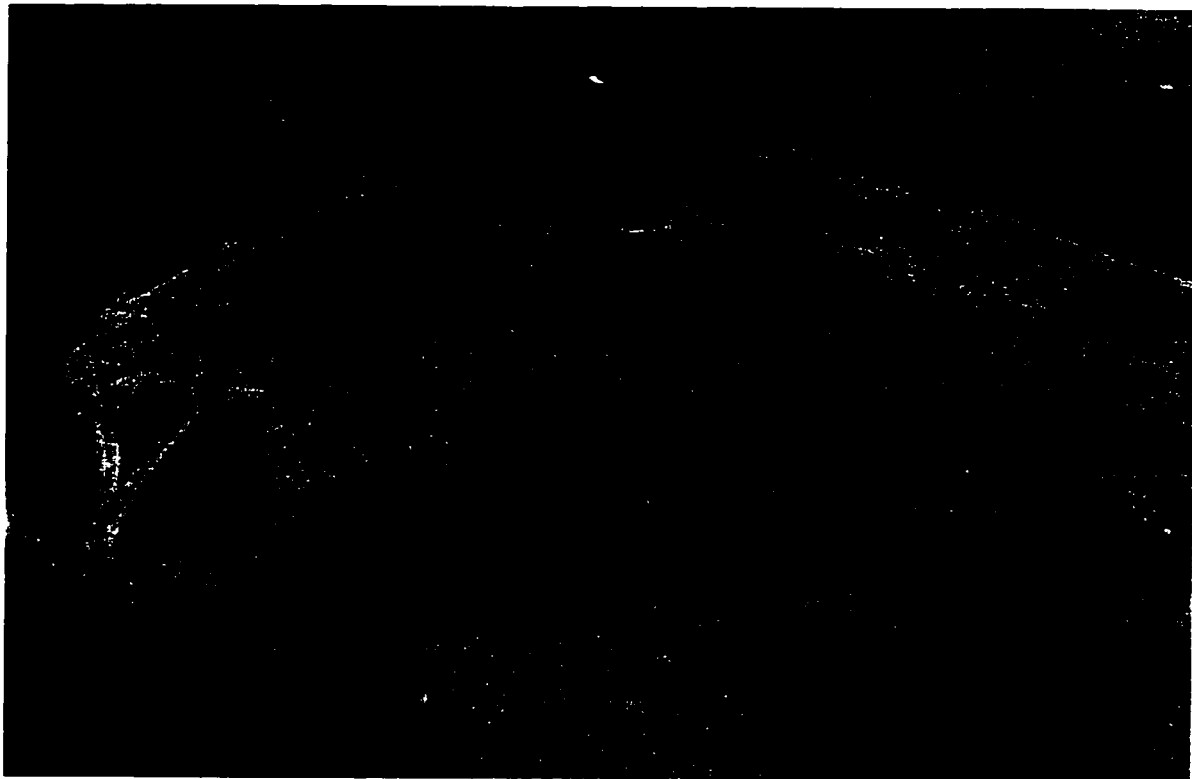


**Figure 4.9.** Schematic plan view of the 50-A-5-2 pit, location of cross sections C20+00 and C25+00 and location of monitoring points on the slope.

The Distinct Element Code, UDEC (Itasca, 1993), was used to analyze the slope instability experienced at the site. The 50-A-5-2 south wall, section C20+00 (figure 4.9), which experienced toppling during excavation of the upper benches, was first back-analyzed. Results were then applied to assessing the possibility of deepening the pit in a future phase, section C25+00 (figure 4.9). Input data used in the numerical analysis were obtained from previous published analyses and the mine management.

#### **4.3.2. Geology and Rock Mass Structure**

The mine is situated among the northwest trending ridges and steep-sided valleys of the Inner Foothills Belt of the Rocky Mountains. Tectonic activity has produced southwest dipping, overturned anticline/syncline folds and thrust folds. Coal bearing strata at



**Figure 4.10.** View of the 50-A-5 pit and surrounding area looking southwest.

Cardinal River belong to the Upper Cretaceous Luscar Formation. The 10 to 12 m thick Jewel Seam is the only economic seam in the area. The general stratigraphy at the mine site is shown in figure 4.11.

The 45° south wall of the 50-A-5 open pit (figure 4.12) was excavated entirely within members of the Luscar Formation. Member "D" is the uppermost sub-unit and occurs in the syncline at the bottom of the south wall. It consists of massive siltstones and sandstones with minor shale and coal beds. The Jewel coal seam defines the base of this sub-unit. The Torrens Member consists mostly of interbedded siltstones and sandstones. It is characterized by an 18 m thick sandstone which directly underlies the Jewel seam. Marine shales of the Moosebar Member are found in the upper part of the highwall underlain by the Gladstone Member, consisting of thinly interbedded siltstones and shales. The 11m thick Cadomin conglomerate separates the Luscar Formation from the thin-bedded shales and siltstones of the Nikanassin Formation which forms the top part of the hill.

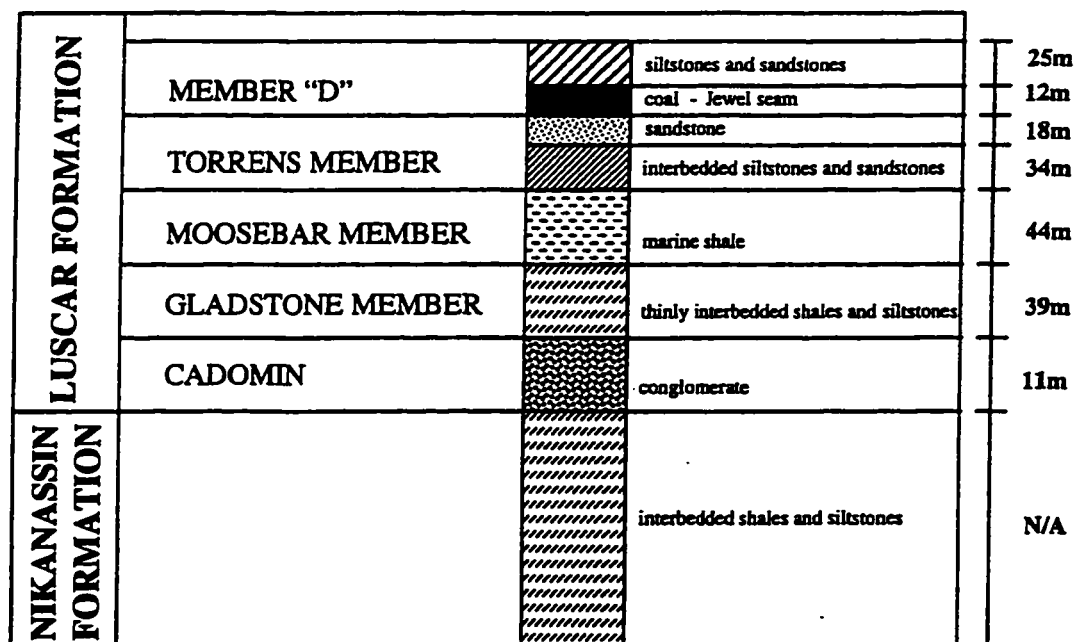
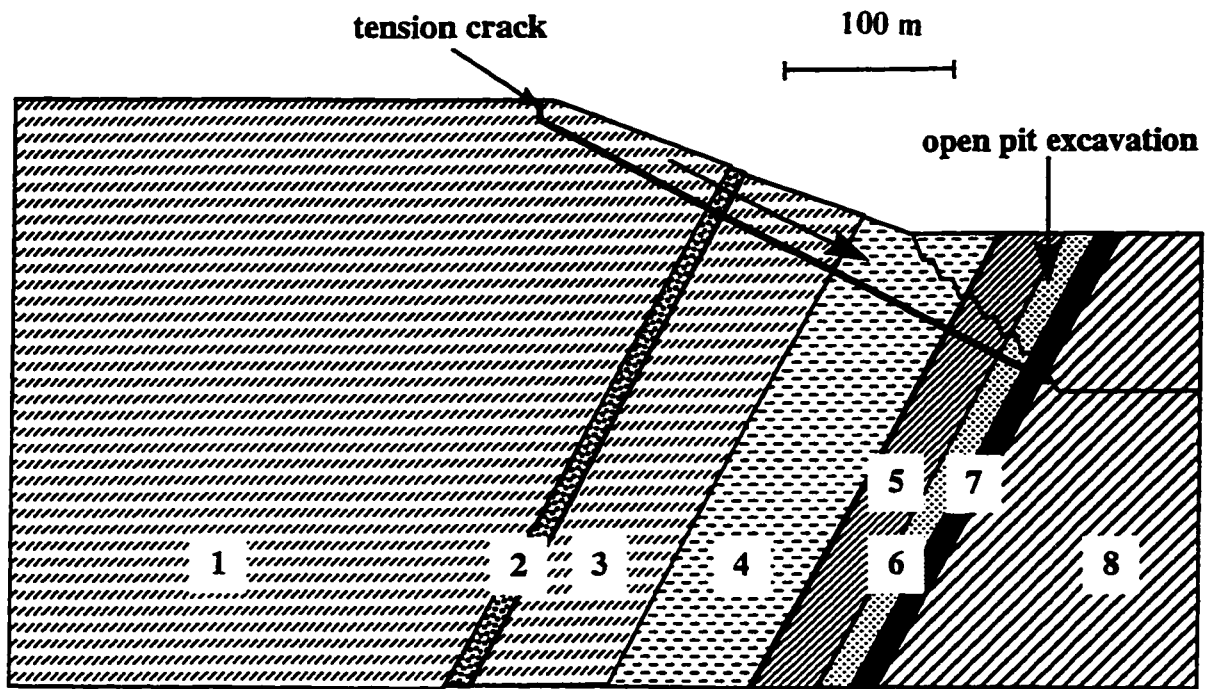


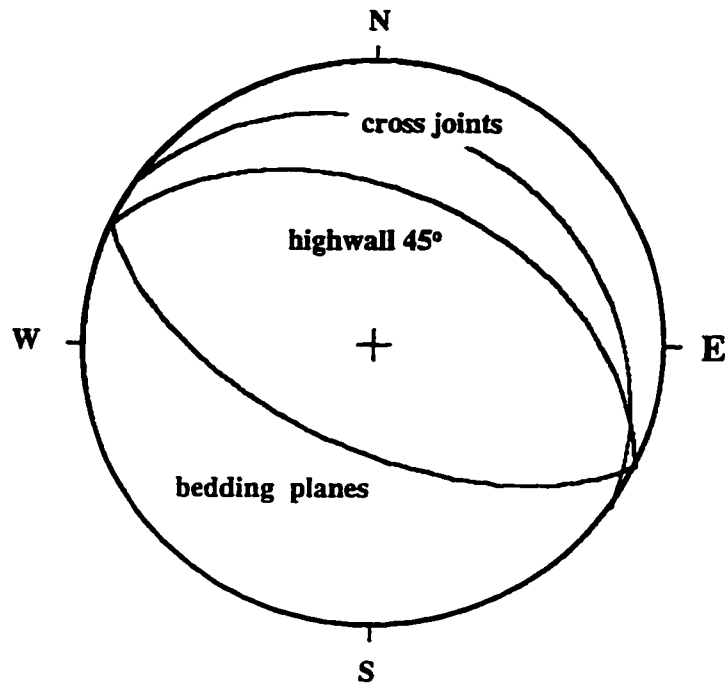
Figure 4.11. The general stratigraphy at the mine site.



**Figure 4.12.** Simplified geological structure, pit geometry and estimated failure plane in the 50-A-5-2 pit, section C20+00. 1 - Nikanassin formation, 2 - Cadomin conglomerate, 3 - Gladstone member, 4 - Moosebar member, 5 - Torrens member (interbedded siltstones and sandstones), 6 - Torrens member (sandstone), 7 - Jewel seam, Member "D"

The pit itself (section C20+00) was excavated into the southern limb of an overturned syncline/anticline fold pair which plunges to the northeast at  $24^\circ$ . The axial plane of the syncline dips to the southwest at about  $40^\circ$ . The hillside and highwall above the axial plane are susceptible to toppling because of overturned bedding which dips south at  $60^\circ$  to  $70^\circ$  into the slope. Bedding below the axial plane is upright and dips  $20^\circ$  to  $30^\circ$  south. The main discontinuity data in the slope above the axial plane of the syncline are summarized in figure 4.13 (Hebil, 1993). Several joint sets occur in the rock mass, but two dominant ones affect the slope stability. A sub-vertical set strikes northeast, approximately perpendicular to the trend of the highwall. A second joint set occurs orthogonal to bedding. This set dips between  $25^\circ$  to  $40^\circ$  north out of the south wall.

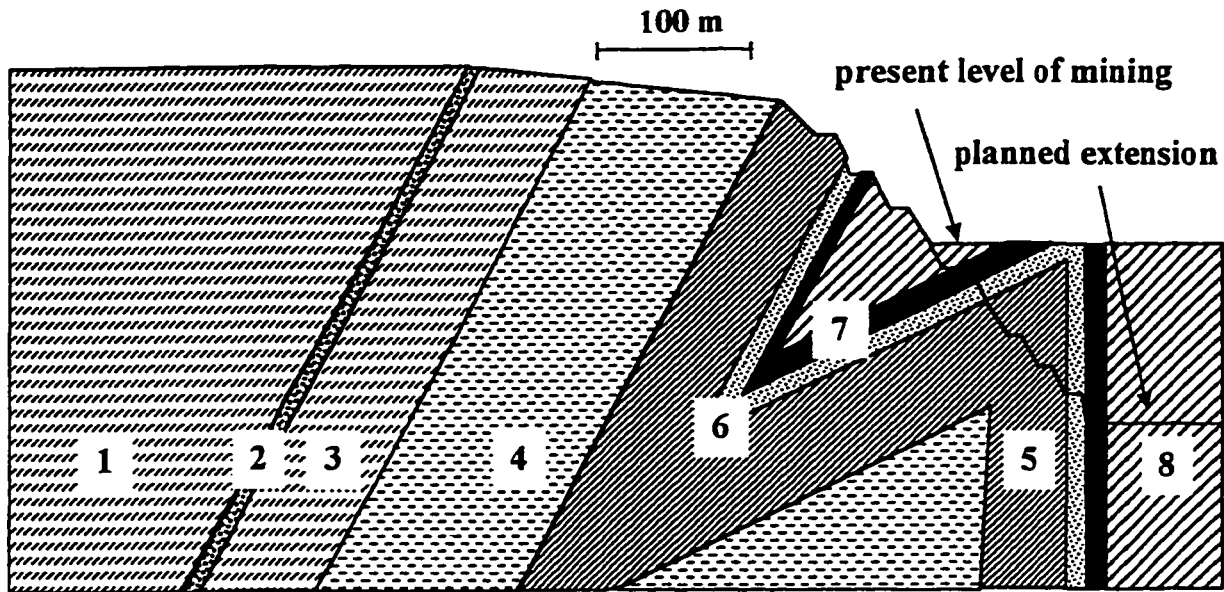




**Figure 4.13.** Summary of main discontinuity data (after Hebil, 1993).

Lineations formed by the line of intersection of these joint sets trend northeast at  $024^\circ$  and have an average plunge of about  $31^\circ$  out of the slope. The intersecting joint sets have weakened the rock mass along this direction and affected slope stability. Failure of the safety benches by bedding plane toppling and sliding along the cross-joints was expected to occur within a short period after excavation. This resulted in difficult operating conditions along the south wall.

The same stratigraphic units are present in the C25+00 section of the same pit, although the planed pit extension would intersect both, the syncline and anticline structures. Cross sections through the south wall of the 50-A-5-2 pit, C20+00 and C25+00, showing the geological structure and open pit excavation are given in figures 4.12 and 4.14. Cross sections shown in these figures were analyzed in the present numerical modelling study.



**Figure 4.14.** Simplified geological structure and pit geometry in the 50-A-5-2 pit, section C25+00. 1 - Nikanassin formation, 2 - Cadomin conglomerate, 3 - Gladstone member, 4 - Moosebar member, 5 - Torrens member (interbedded siltstones and sandstones), 6 - Torrens member (sandstone), 7 - Jewel seam, Member “D”

### 4.3.3. Rock Mass Properties

Only limited rock mass strength data on the individual rock types and discontinuities were available. This data was based on geological field survey, limit equilibrium back analysis performed by the mine personnel, as well as previous numerical analysis performed by Bucek and Barron (1994).

The unconfined compressive strength for rocks of the Luscar Formation ranges from 25-50 MPa for the Moosebar shales to 150 MPa for the Torrens sandstone. The interbedded sequences of sandstone, shale and siltstone have strengths that are intermediate between these values and average 25-70 MPa (Hebil, 1993). As the properties used in previous analyses were defined in the form of the Mohr-Coulomb failure criteria, and limited

quantitative data was available on the rock mass structure, it was decided to adopt the same criteria in this analysis. Assumed friction angle for bedding planes in carbonaceous shales and sheared coal surfaces average 18° and 20°, representing the weakest rock types. Discontinuities in sandstone were assumed to have a friction angle of 28°. The interbedded siltstones/sandstone/shale sequences and shales typically have a highly variable bedding plane spacing that ranges from 0.15 m up to 0.5 m.

The groundwater level was inferred from the development drilllogs, and was below the failure plane that developed in the slope (C20+00 section). The groundwater level in time of spring breakup will be much closer to the ground surface, and the infiltration into hillside would also be greater at an advanced mining stage due to the rock mass loosening caused by mine excavation. Two major periods of acceleration in slope movement were observed in the spring and early summer of 1990 and 1991 which were related to spring breakup. Therefore, a simplified case considering an assumed static groundwater table close to the surface was considered in one of the analyses. The planned deepening of the C25+00 section is expected to extend below the groundwater table, therefore, the influence of pore water pressures was considered by assuming a static groundwater table.

#### **4.3.4. Highwall Failure 50-A-5 Pit Section C20+00**

The slope excavation started at an elevation of 1864 m a.s.l. The bench height was 12 m, except the bench at the 1768 m level which was 24 m. The bench width was 6 m, creating an overall slope of 45°. Slope movement was first observed in mid-December 1989, when the upper two benches were excavated. Back-facing obsequent scarps developed in the crest and benches. Over the next several months, small obsequent scarps developed progressively upslope to the top of the hill, where eventually a 9 m wide tension crack,



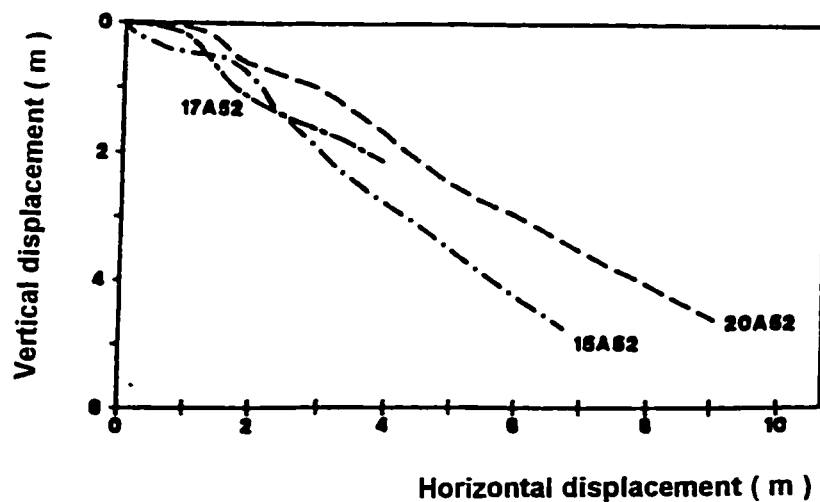
**Figure 4.15.** Tension crack at the top of the hillside defining the southern limit of failure.

shown in figure 4.15, defined the south limit of the failure. By the time the south wall was excavated to level 1768 m (maximum depth assessed in the back analysis), nearly all the benches in the slope had failed. The unbenced highwall caused operational difficulties with the remaining benches as they filled with debris, creating an 96 m high scree slope to the pit bottom. Most of the material entering the pit was due to the bench failure and sloughing of the pit crest. Rockfalls were controlled by flagging off areas near the toe and by placing windrow berms where required. The toppling in the hillside above the highwall did not directly affect the mining operations.

The total displacement in the crest area exceeded 25 m, but only small amounts of debris entered the pit. Extensive toppling, however, developed in the hillside. Tension cracks up to 9 m wide, and 6 m to 15 m deep, had developed at the top of the ridge. Two major periods of acceleration in slope movement were observed in the spring and early summer of 1990 and 1991 which were related to spring breakup. The south wall was regularly monitored using Electronic Distance Measurement (EDM) survey techniques. The

frequency of observations was increased according to slope performance, continuous monitoring of the slope being undertaken when conditions warranted (Hebil, 1993).

Figure 4.16, shows the horizontal versus vertical displacement plots for selected prisms located in the highest part of slope (Hebil, 1993). The location of monitoring prisms is shown in figure 4.9. The prism movement was nearly horizontal for the first 1 m to 2 m, with a relatively sudden steepening for the subsequent 2 m to 3 m. After about 4 m of movement, the dip direction tended to remain constant at 20° to 30°. This abrupt change in dip was interpreted to be a transition facilitating a planar component to the toppling movement. The first few meters of toppling resulted in sufficient displacement at the base of the rotating columns to produce a basal surface or surfaces on which sliding took place. This basal failure surface extended from the highwall above the fold axis to the base of the tension crack at the top of the ridge, with an estimated dip of 25°. Mining along the south wall was completed by summer 1991. Visual observation since then indicated that an equilibrium in the slope had been reached.

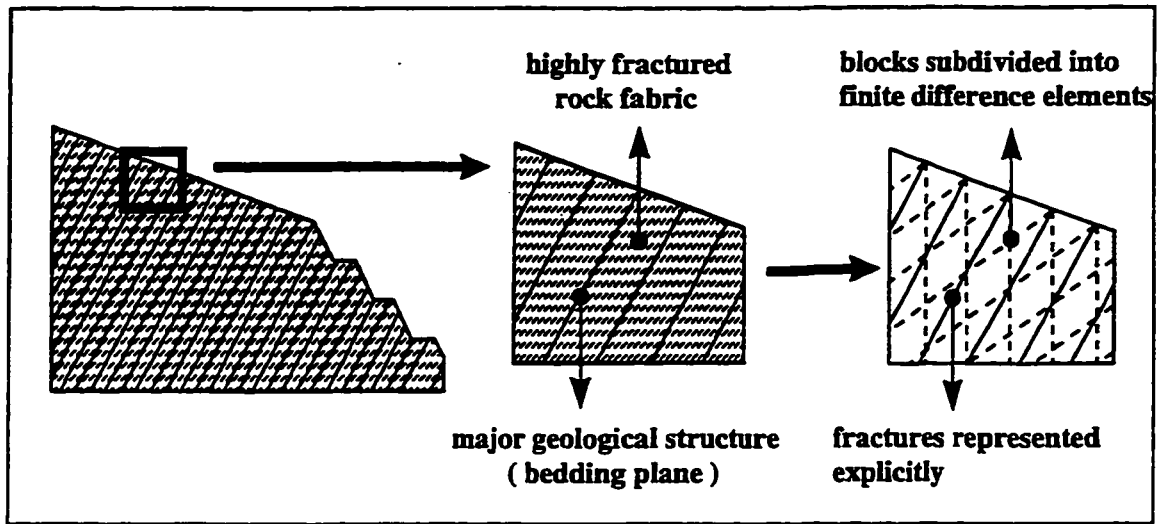


**Figure 4.16.** Displacement history for selected prisms on the open pit slope. Location of prisms shown in figure 4.9.

Toppling deformation developing a sliding surface(s) was described by Cruden and Hu (1994) on natural “*underdip*” slopes from the Highwood Pass, Alberta, in a similar lithology (interbedded sandstones, siltstones and shales). They describe this type of deformation as multiple block toppling, where sliding surfaces may develop through fracture of thin beds (figure 4.3). Several blocks may be present in a multiple block topple with different bedding orientation between the individual blocks, resulting from more than one episode of toppling. The driving mechanism for each toppling episode would be in case of the Luscar mine the progressive undermining of the slope. The distinct element method of numerical modelling was used to gain more insight into the failure mechanism.

#### **4.3.5. Numerical Modelling**

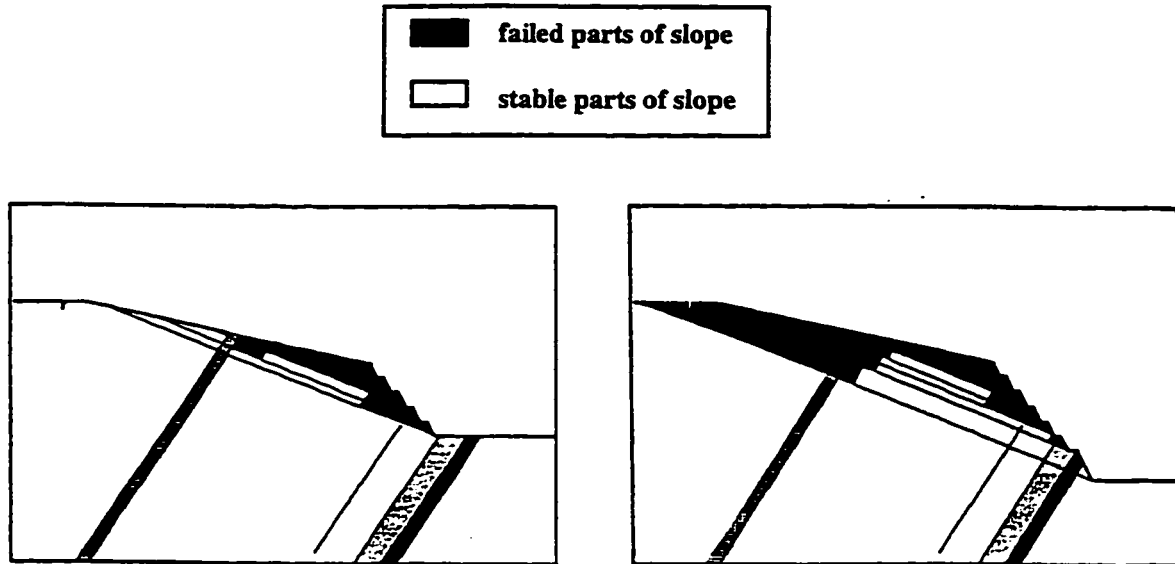
UDEC-Version 2.01 (Itasca, 1993) was used for the toppling analysis. A schematic illustration of the discontinuum method for geomechanical representation of jointed rock mass is shown in figure 4.17. The discontinuities, bedding planes in this case, are represented explicitly, and the rock mass between the joints is modelled as a continuum. It is important to realize that the UDEC blocks, especially in this analysis, with the presence of weak, thinly bedded, cross-jointed shales, do not represent intact rock material but rather a highly fractured rock fabric. It is practically impossible to incorporate into the model all the fractures and the small bedding plane spacing. Therefore, the material properties of the individual blocks, depending on the scale, are representative more of a rock mass than an intact rock.



**Figure 4.17.** Schematic illustration of discontinuum method for geomechanical representation of jointed rock masses.

#### 4.3.5.1 Previous Work

The toppling deformation of the 50-A-5-2 pit (section 20+00) had been previously analyzed by Bucek and Barron (1994) using a numerical modelling program developed at the University of Alberta. Their model represents the rock slope as a system of interacting cantilevers, and calculates the deformation of cantilevers utilizing the Mohr-Coulomb failure criterion to test the rock for failure. The cantilever thickness is defined by bedding plane spacing. The program first examines the bedding planes for minimum shear strength/shear stress ratio. The rock between these surfaces is initially considered to behave as a solid block and is subsequently examined with respect to bending. Their results proved the progressive failure extent with the increase of the open pit slope height. Figure 4.18 shows the extent of failure at the mining levels 1804 m and 1768 m. Solid black areas represent failed parts of slope. It is of interest that a stable block appeared to have formed in the middle of slope, between the base of highwall and the relatively strong conglomerate bed.

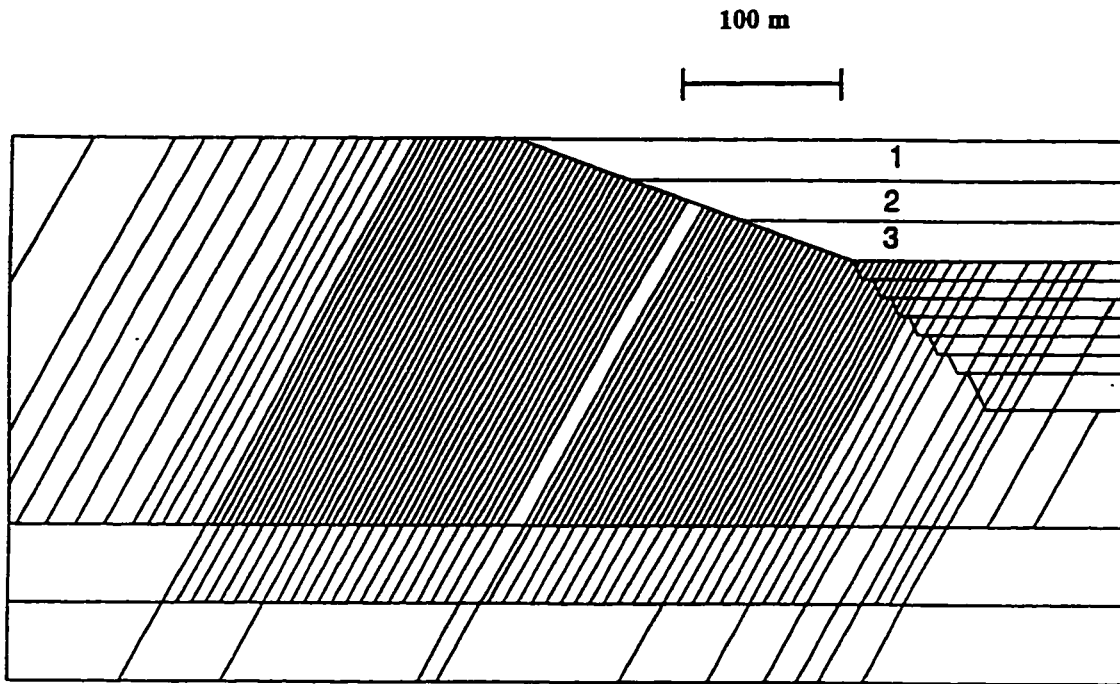


**Figure 4.18.** Failure extent in section C20+00 at mining elevation 1804 m and 1768 m, after Bucek and Barron (1994).

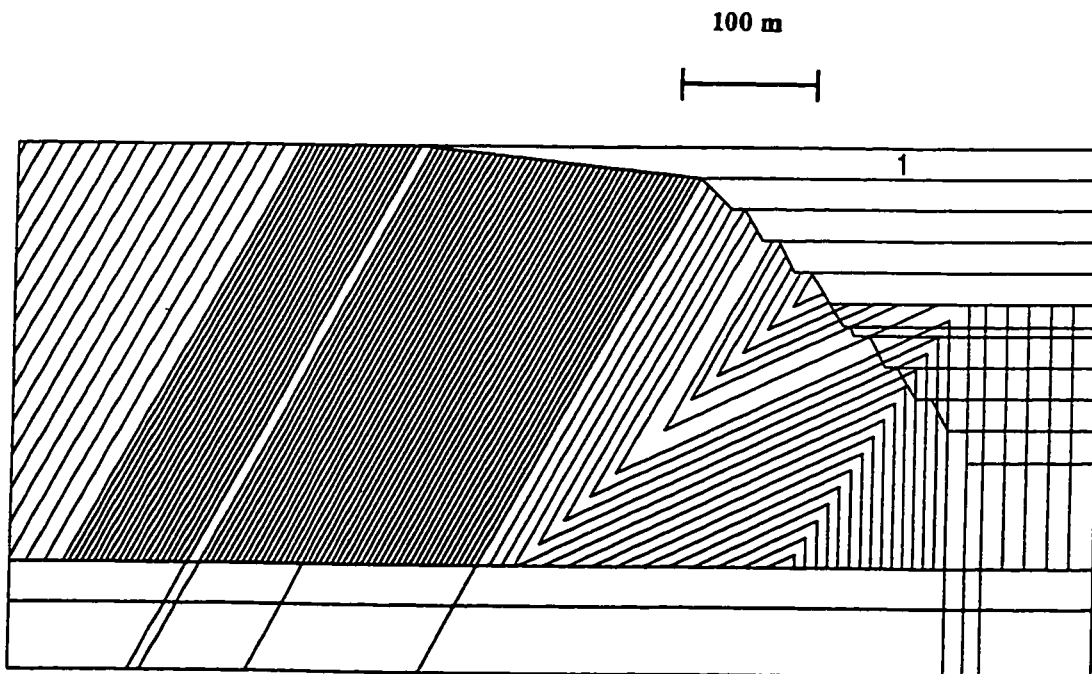
#### 4.3.5.2. Geometry

The slope geometry was based on a 1:1200 scale topographic map, cross-sections provided by Cardinal River Coals Ltd. and previous published analyses of toppling deformation at the site (Hebil, K.E., 1993; Bucek, R. and K. Barron, 1994). The numerical models adopted for the analysis are shown in figures 4.19 and 4.20. Numerical models with dimensions 700 m x 350 m (section C20+00) and 800m x 400 m (section C25+00) were used to ensure no model boundary effects. The dimensions of these models were determined from a preliminary modelling, that assumed 100 m larger or smaller distance of boundaries from the open pit slope to investigate the possible boundary interference. In section C20+00 (figure 4.19) the bedding planes dip  $62^\circ$  into the slope as determined from previous work (Bucek and Barron, 1994).





**Figure 4.19.** Distinct element model for 50-A-5-2 pit, section C20+00 at the Cardinal River mine.


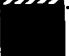
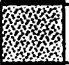

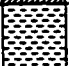


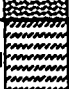


**Figure 4.20.** Distinct element model for 50-A-5-2 pit, section C25+00 at the Cardinal River mine.

Somewhat more complicated bedding orientation had to be modelled in section C25+00 (figure 4.20) as the present pit, as well as the intended pit extension, will intersect a syncline and an anticline structure. The same bedding plane thickness was assumed for both models. The bedding plane spacing was assumed to be 8 m in the Torrens member and 4 m in the Moosebar and Gladstone members, as well as in the Nikanassin Formation. This assumption represents up to an 8-fold increase in the actual bedding thickness, which are at maximum 1 m and 0.5 m, respectively. This approach was taken in order to optimize the numerical model in size, run time and memory requirements. The bedding plane joints were not represented in the bottom part of model. Blocks numbered 1 to 3 (section C20+00) and block 1 (section C25+00) were used only for the initial stage of modelling to obtain a pre-mining stress state.

#### **4.3.5.3. Rock and Discontinuity Strength**

The rock and discontinuity strength properties were based on a range of available properties provided by Cardinal River Coals Ltd. Owing to the lack of comprehensive test data, several runs with different properties were undertaken to back-analyze the failure and reproduce the observed slope failure development. The variable geological structure at the site results in numerous possibilities for the sensitivity analysis. Properties shown in figure 4.21 were found to “match” the *in situ* failure with reasonable accuracy for a model assuming the Mohr-Coulomb constitutive criterion and dry condition in slope. The shear and bulk modulus, as well as the rock density, were assumed to be constant throughout the analysis and were selected from typical values for sandstone, siltstone, shale, coal and conglomerate (Kulhawy, 1975; Hunt, 1986 and Goodman, 1989). The intact rock-block material comprising the joint bounded columns was represented as an elastoplastic, homogeneous, isotropic continuum with the Mohr-Coulomb yield criterion. In a later case the blocks were assumed to be anisotropic with the ubiquitous joint constitutive criterion. The discontinuities were represented with the area- contact Coulomb slip criteria (Itasca, 1993).

		density [kg/m <sup>3</sup> ]	shear modulus [ GPa ]	bulk modulus [ GPa]	friction [ ° ]	cohesion [ kPa]	joint friction [ ° ]	
LUSCAR FORMATION	MEMBER "D"	 siltstones and sandstones	2300	10	16.7	35	1000	25
		 coal - Jewel seam	1700	1.5	3.3	22	40	20
	TORRENS M.	 sandstone	2300	12	20	35	400	28
		 interbedded siltstones and sandstones	2300	10	16.7	30	90	25
	MOOSEBAR M.	 marine shale	2100	3.1	6.7	25	45	18
	GLADSTONE M.	 thinly interbedded shales and siltstones	2100	3.1	6.7	25	45	18
	CADOMIN	 conglomerate	2500	14	23.3	40	500	30
NIKANASSIN FORMATION		 interbedded shales and siltstones	2100	3.1	6.7	25	45	18

**Figure 4.21.** Summary of the initial input properties for numerical modelling analysis assuming dry conditions and Mohr-Coulomb constitutive criteria.

Sensitivity analyses were performed on the joint-stiffness characteristics (shear and normal stiffness), to assess the effects of this parameter. Values from the range 100 GPa/m to 1 GPa/m have been used for the normal stiffness, and the shear stiffness was assumed to be constant at 1/10 of the normal stiffness. As would be expected, larger movement occurred in the model for lower stiffness values, however, the extent of failed area in slope and the overall behavior of the model remained unchanged. It has to be stressed that insufficient data are presently available on the numerical value of joint stiffness properties as they are difficult to determine.

#### **4.3.5.4. Initial Stress Field**

No data was available with respect to the initial ground stress conditions at the mine site prior to mining. Measurements of horizontal stresses at civil and mining sites (Brown and Hoek, 1978; Herget, 1988) and theoretical considerations (Sheory, 1994) show that this stress component tends to be higher than the vertical stress at relatively shallow depths. Therefore, a K ratio (K - horizontal/vertical stress) of 1.5 was used in this numerical modelling study. The vertical stress component was assumed to be equal to the lithostatic weight of the overburden.

#### **4.3.5.5. Modelling Procedure**

Ground stress conditions were initiated in the model and the pre-mining topography was excavated by deleting blocks 1 to 3 (section C20+00, figure 4.16) and block 1 (section C25+00, figure 4.17). The model was allowed to equilibrate after each excavation step. Next the open pit slope itself was excavated bench by bench, by deleting the appropriate blocks from the model. After each excavation step the stresses were again allowed to equilibrate and the model stress state was saved for future analysis. This process resulted in six initial models representing the excavation of the 1840 m, 1828 m, 1816 m, 1804 m, 1792 m and 1768 m levels. Up to the excavation of the 1768 m level, the elastic isotropic constitutive criteria was used for the blocks as well as high properties for the joints to prevent any yielding in the model as a consequence of this initial excavation process.

The displacements (elastic) resulting from this initial excavation were then reset to zero, and the Mohr-Coulomb or Ubiquitous constitutive failure criteria with different sets of material properties applied for blocks and discontinuities. The model was run for a constant amount of calculation steps with several points selected for displacement and velocity monitoring. The failure and deformation at different excavation stages were saved and examined.

When the open pit excavation process was in a later stage of modelling, repeated with the “actual” rock mass properties and Mohr-Coulomb failure criteria as opposed to excavation in elastic regime and then switching to Mohr-Coulomb failure criteria, no difference was found in the location of failure plane and type of failure mechanism. The major difference was observed in the total accumulated displacement in the slope. The major problem with this approach was the large deformation in the upper benches during the progressive pit deepening.

#### **4.3.5.6. Results - Section C20+00**

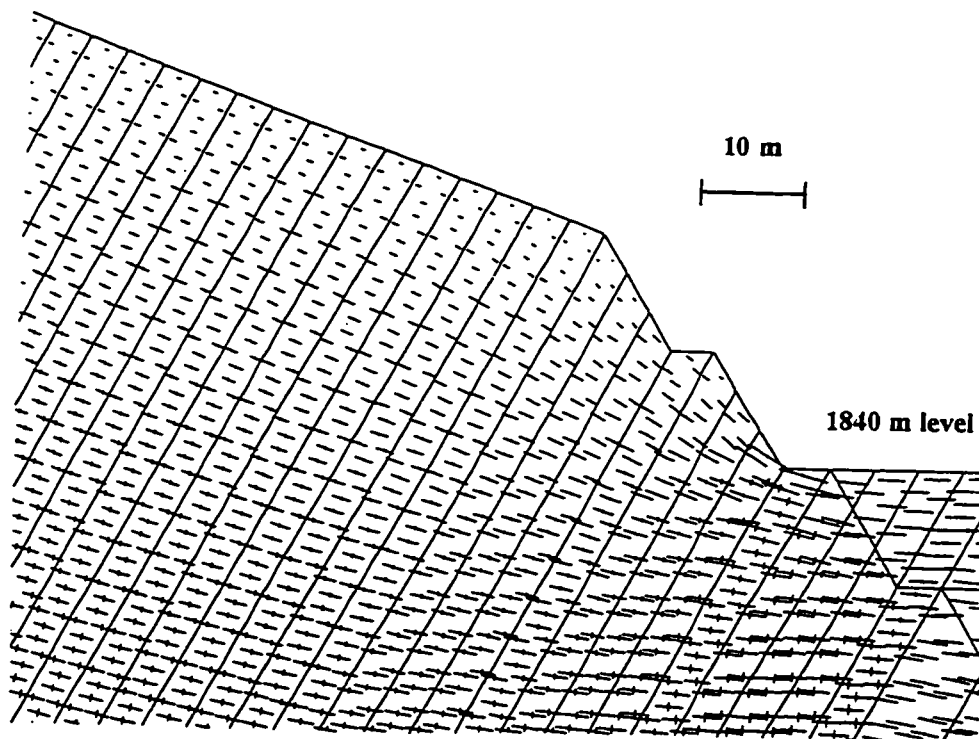
Information from the mine indicates that major instability failure development initiated with the excavation of the second bench (1840 m level). The pit deepening to this level of mining caused back-facing, obsequent scarps to develop in the crest and benches of the highwall, extending progressively to the top of the hillside over a period of several months. The analysis by Bucek and Barron (1994) indicates instability problems to start at this level, although limited only to a failure of the second bench and an area just under the relatively strong Cadomin conglomerate bed.

Therefore, as a first step, the rock mass strength that would produce such a failure was back-analyzed. The failure at this stage will be largely dependent on the strength of the Moosebar Member forming the slope material in which the upper three benches were excavated, and the Gladstone Member extending up to the Cadomin conglomerate bed. Hebil (1993) and Bucek and Barron (1994) assume the same properties for the Moosebar and Gladstone members, as well as for the Nikanassin formation above the Cadomin conglomerate. This assumption was also made in the present analysis. Additional modelling, where the strength of the Gladstone member and Nikanassin formation was assumed higher (due to the interbedded siltstones and shales as opposed to only shales in the Moosebar member), did not show a difference in the extent of the failed rock mass and/or depth of toppling. The in-situ stress trajectories before the application of Mohr-

Coulomb constitutive criterion for this bench elevation (1840 m) are shown in figure 4.22.

A friction angle of  $25^\circ$  was assumed for the blocks and  $18^\circ$  for the discontinuities representing the steeply inclined bedding planes in the Moosebar and Gladstone members and the Nikanassin Formation. The discontinuities were assumed to have zero cohesion, tension and dilation. The block cohesion in these three rock units was decreased in 5 kPa increments until the slope became destabilized and failure occurred.

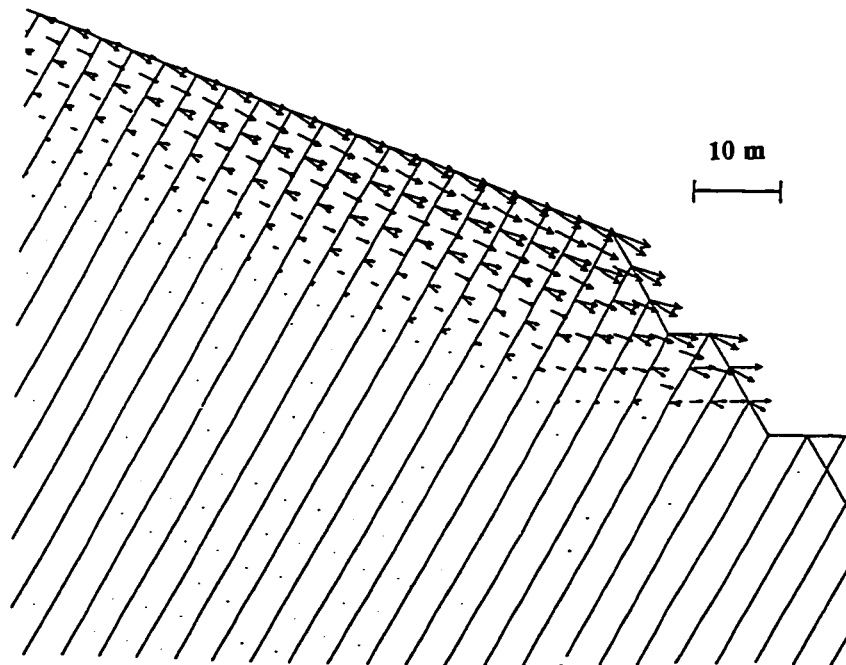
A cohesion of 45 kPa or less was found to be necessary for failure to develop after the excavation of the second bench (1840 m level), assuming dry conditions and Mohr-Coulomb constitutive criteria. The deformation in the model with cohesion value higher



**Figure 4.22.** Initial ground stress conditions after the excavation of 1840 m level.

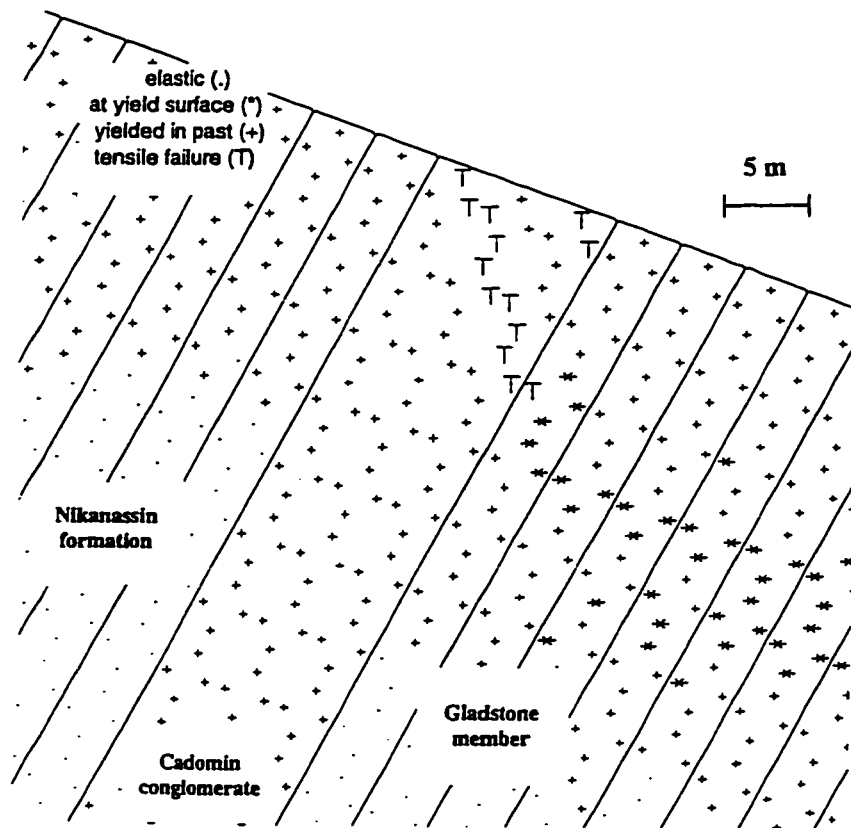
then 45 kPa, were in the elastic range, resulting from stress redistribution. Limited, non-progressive, shearing occurred along the joints in the temporary pit floor, benches and behind the crest of the open pit. Figure 4.23 shows the gridpoint velocity vectors developed in the model at this mining stage in the upper two benches and the slope behind the open pit. It has to be emphasized that the velocity as understood in UDEC is not with respect to real, but computational time. The different direction of velocity vectors on the opposite sides of blocks resulted from shearing along the bedding planes. This type of movement is typical for toppling and leads to the development of uphill facing scars.

Most of the deformation terminated against the relatively strong Cadomin conglomerate bed located in the middle of the hill, providing support for the upper portion of slope. The propagation of the failure surface through and beyond the conglomerate will be strongly dependent on its competence.



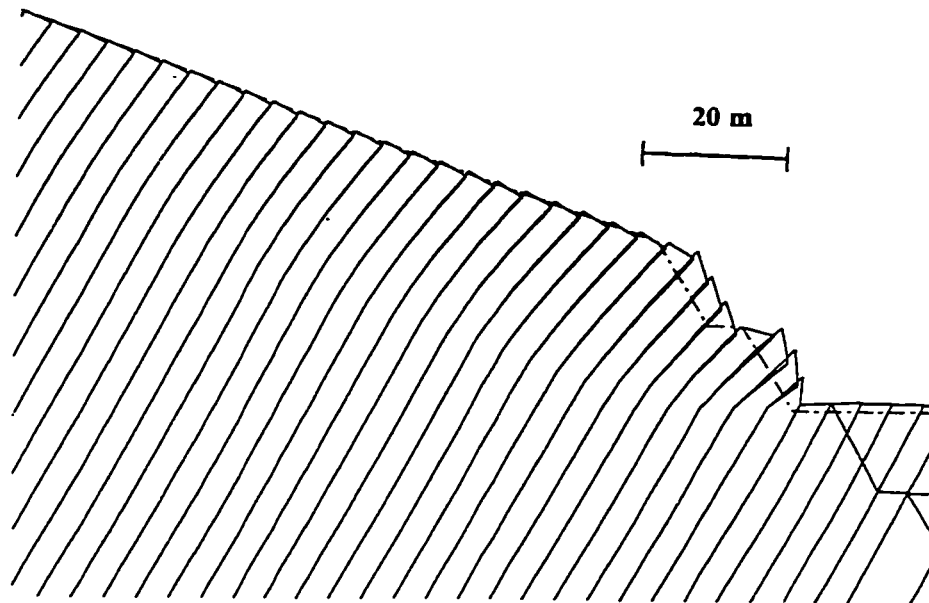
**Figure 4.23.** Velocity vectors in the upper two benches and slope above the pit crest after the excavation of 1840 m level.

Weathering, surface ravelling and increased fracturing, erosion, freezing and thawing cycles and dynamic loading, would all weaken the conglomerate bed and enable the failure to propagate easier through this unit. Tensile failure was predicted by the model in the right half of conglomerate bed, shown in figure 4.24, which is “undermined” by the downslope displacement of the Moosebar and Gladstone members.



**Figure 4.24.** Tensile failure in the Cadomin conglomerate and yielding in the Gladstone member after the excavation of the 1840 m level.





**Figure 4.25.** Magnified displacements (25x) in model after the excavation of the 1840 m level.

Figure 4.25 shows the magnified block plot (25x) with the original topography indicated by the dashed line.

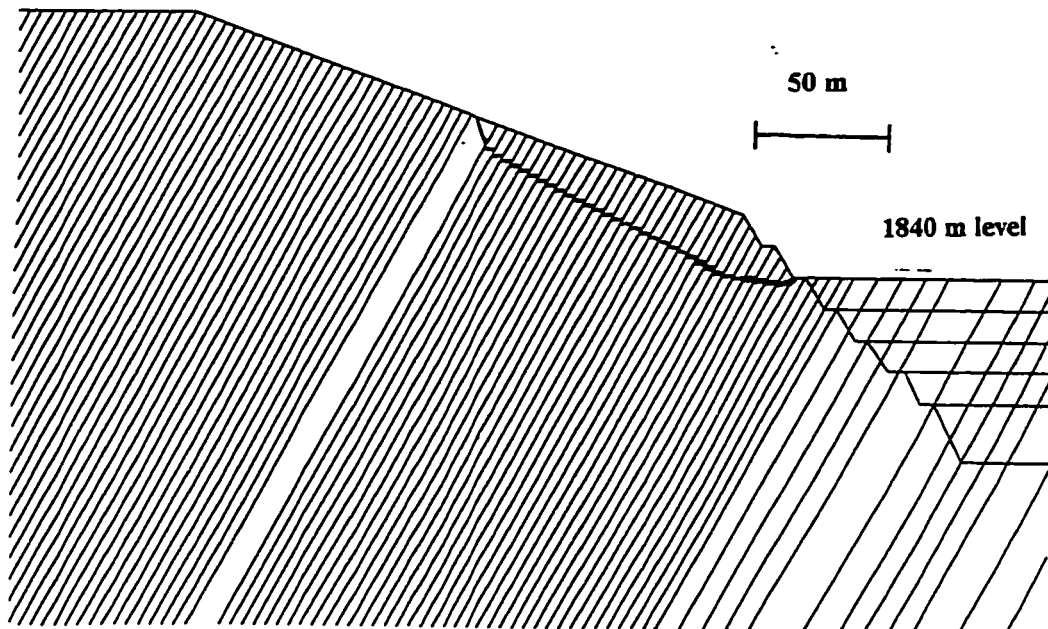
The location of the failure plane limiting the toppling deformation at this stage is shown in figure 4.26a. The cohesion of 45 kPa for Moosebar and Gladstone members and the Nikanassin formation was then used for the successive excavation stages - bench elevations 1828 to 1768. Properties for Cadomin conglomerate, Member "D" and coal were used as shown in figure 4.21. The basal surfaces limiting the toppling within the slope after each excavation step are shown in figure 4.26(a) to 4.26(f). Starting with the excavation of the 1828 m level, the failure propagates completely to the top of the hillside above the open pit. The final failure surface after the excavation of the 1768 m level is in good agreement with the actual failure surface as reported from the mine. The base of the toppled blocks extends from the slope toe, just above the contact between the member

“D” and the Jewel coal seam up to the crest of the hillside. It is interesting that the location of the failure plane at the top of the hillside does not change significantly after the excavation of 1828 m level.

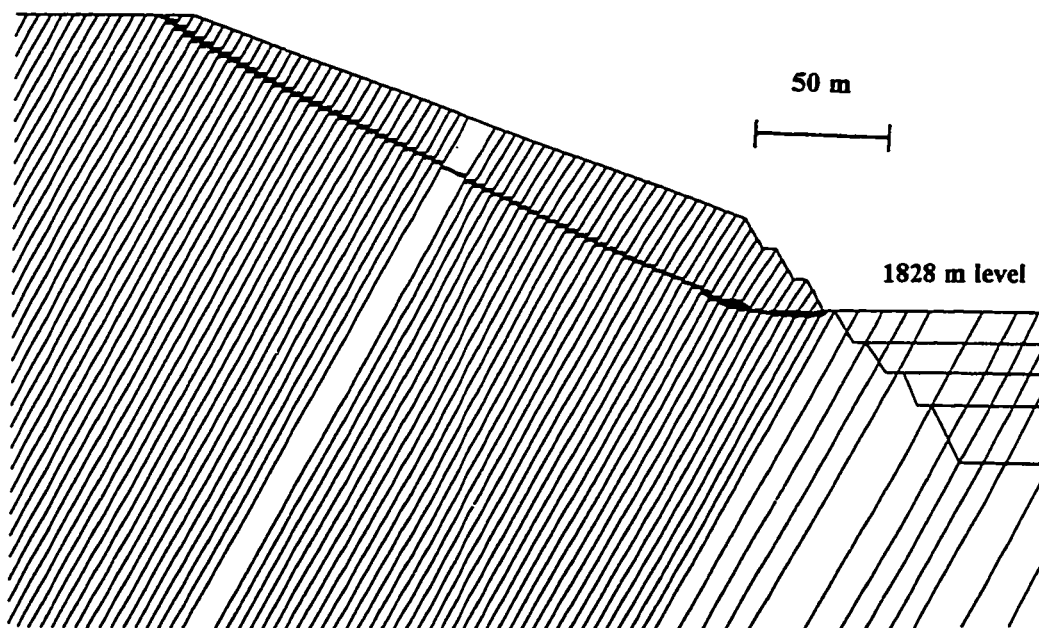
Figure 4.26(e) shows that the sandstone bed provides a temporary support of the slope toe at the 1792 m level, the failure plane daylights above the sandstone outcrop. This support, however, disappears, with the subsequent excavation of the final bench elevation (1768 m level), which includes the Jewel coal seam and part of the member “D”. Note that this bench has a twice the height as the previous benches.

The plasticity indicators after the excavation of the 1768 m level are shown in figure 4.27. Concentration of tensile failure can be seen in the relatively strong sandstone and conglomerate beds, at the outcrop of the failure plane at the top of the hillside and at the slope surface.

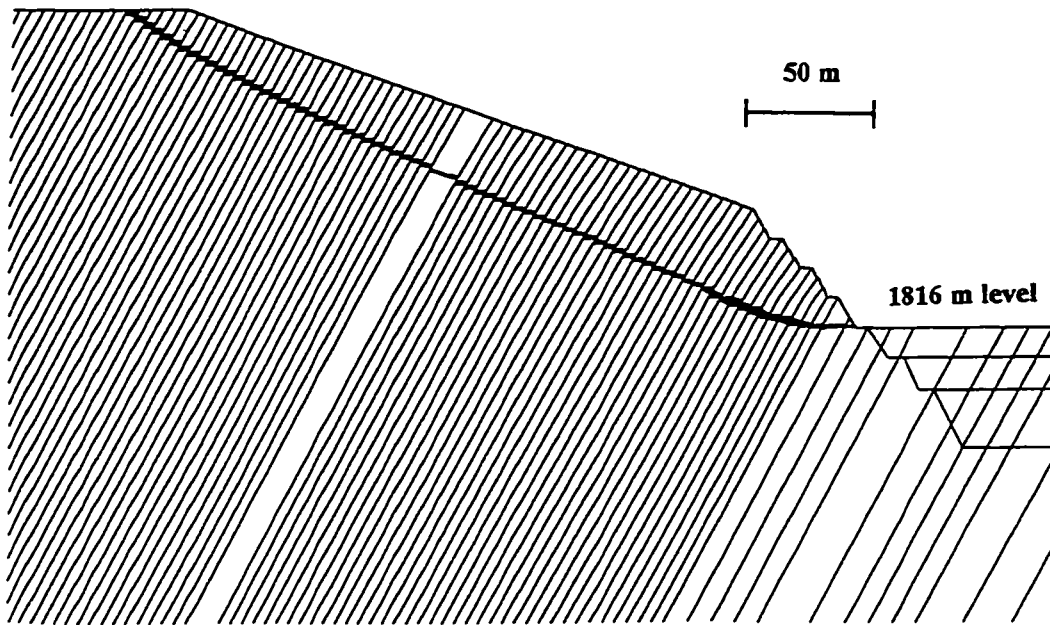
Figure 4.28 shows the flexural toppling in the lower part of the hillslope (Moosebar and Gladstone members) after the excavation of the 1768 m level. Figure 4.29 shows the displacement vectors for the lower part of slope after the excavation of the 1768 m level. The shear displacement along discontinuities are shown for the same stage of mining in figure 4.27. Failure propagation in the early stages of mining seems to be influenced by the relatively strong conglomerate layer located approximately in the middle of the slope. More information is needed to characterize with greater confidence the behavior of this unit.



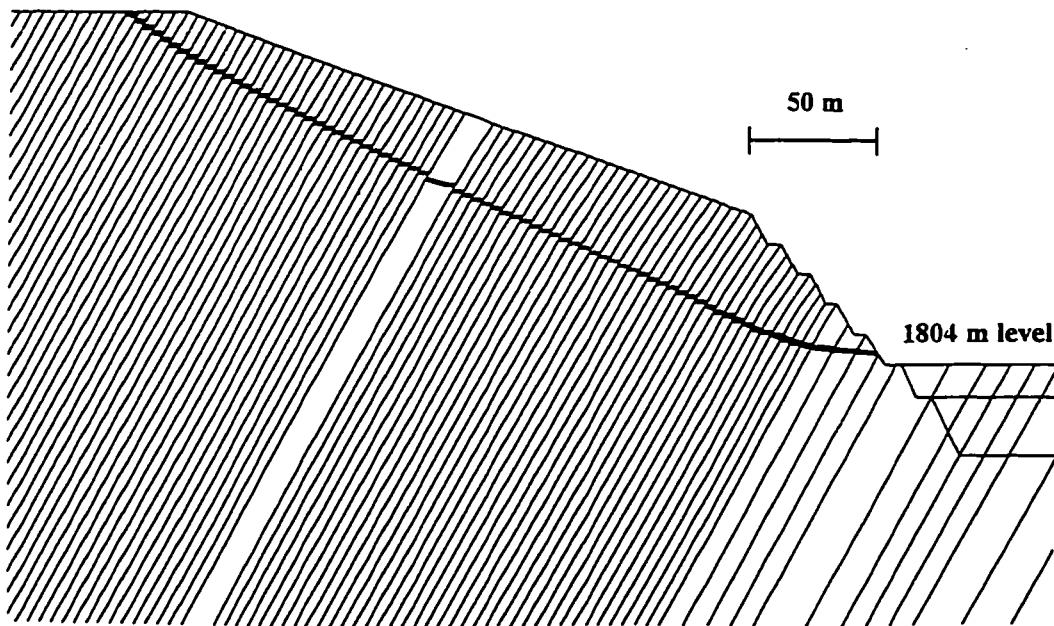
**Figure 4.26(a).** Zone limiting the toppling after excavation of the 1840 m level.



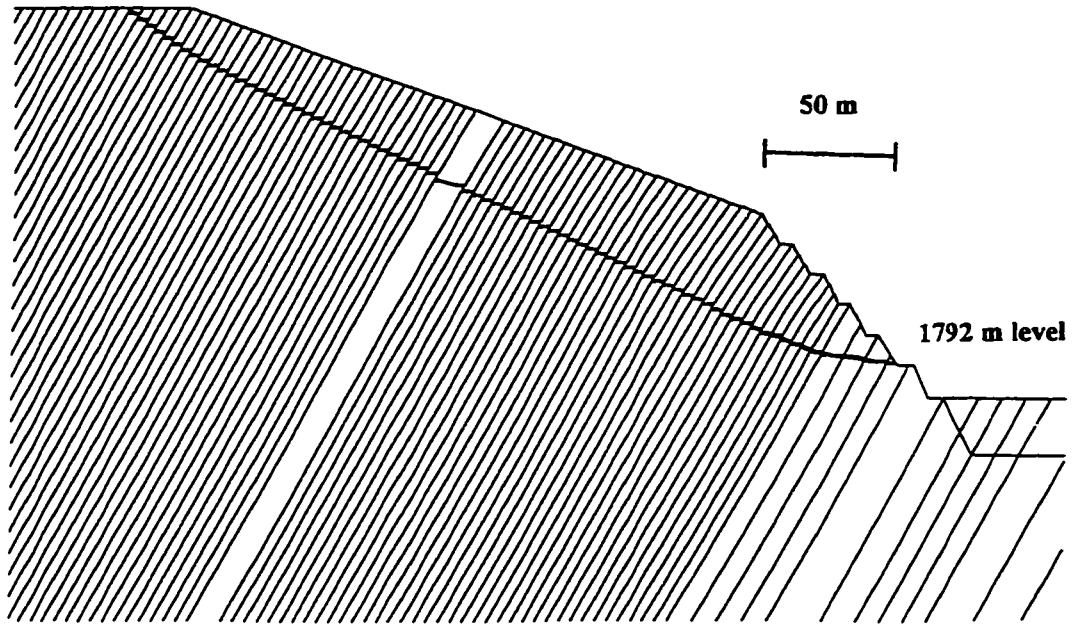
**Figure 4.26(b).** Zone limiting the toppling after excavation of the 1828 m level.



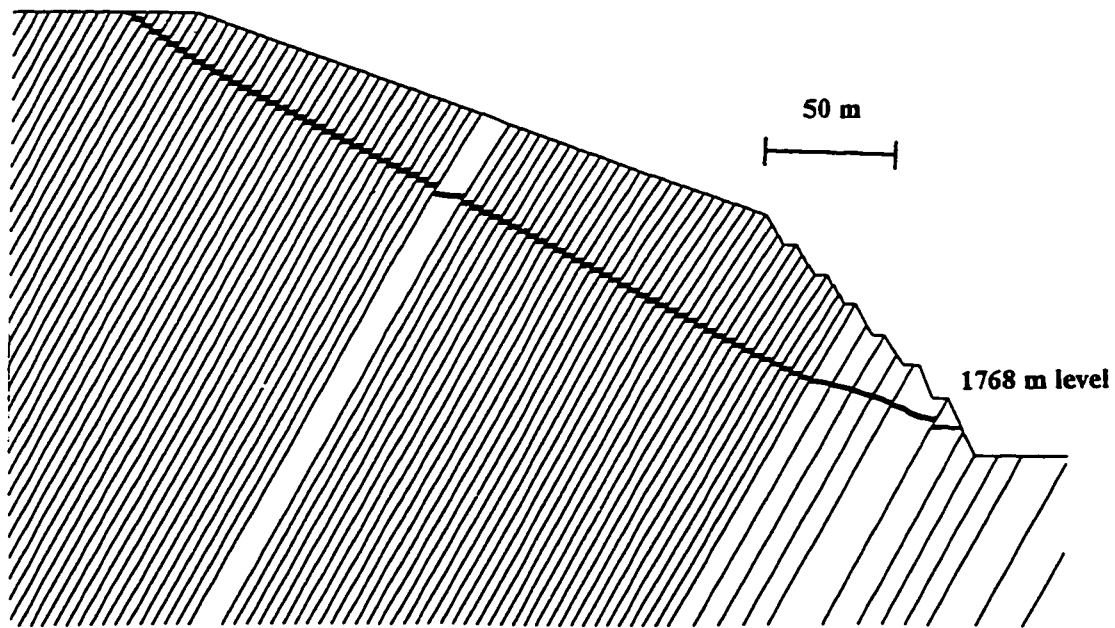
**Figure 4.26(c).** Zone limiting the toppling after excavation of the 1816 m level.



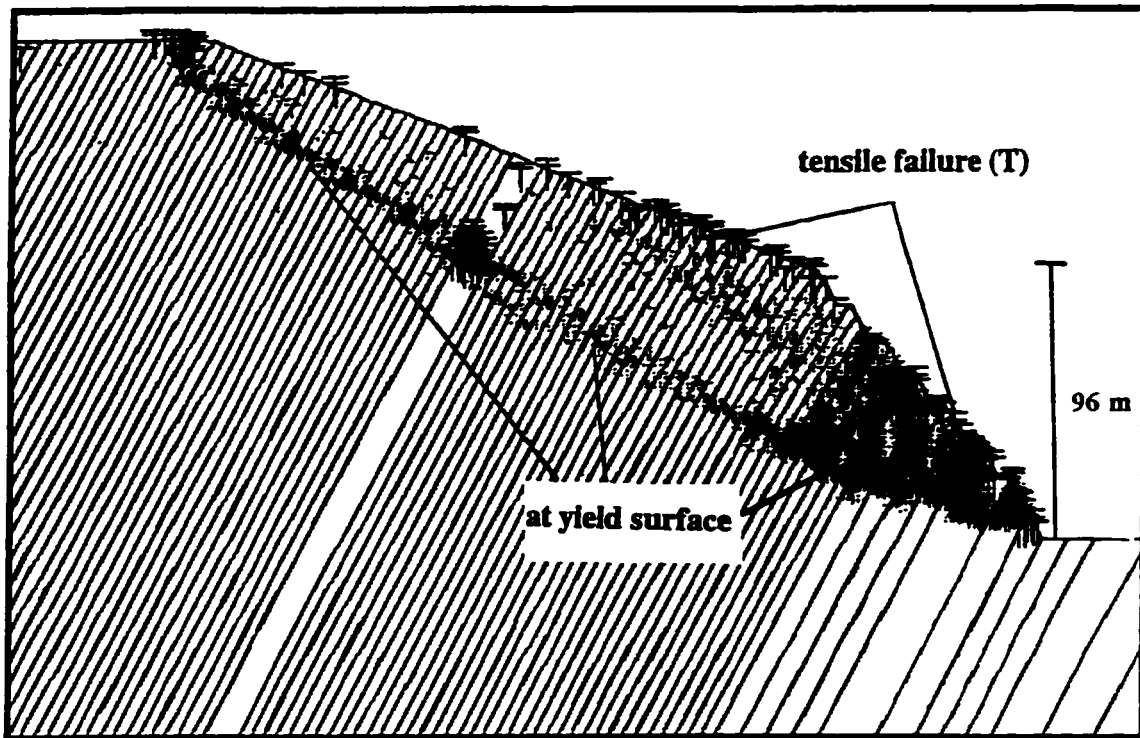
**Figure 4.26(d).** Zone limiting the toppling after excavation of the 1804 m level.



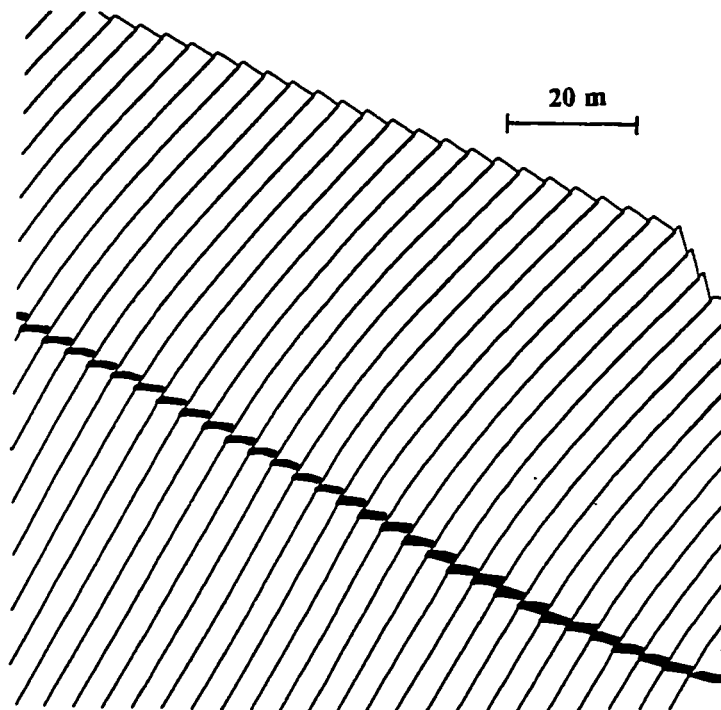
**Figure 4.26(e).** Zone limiting the toppling after excavation of the 1792 m level.



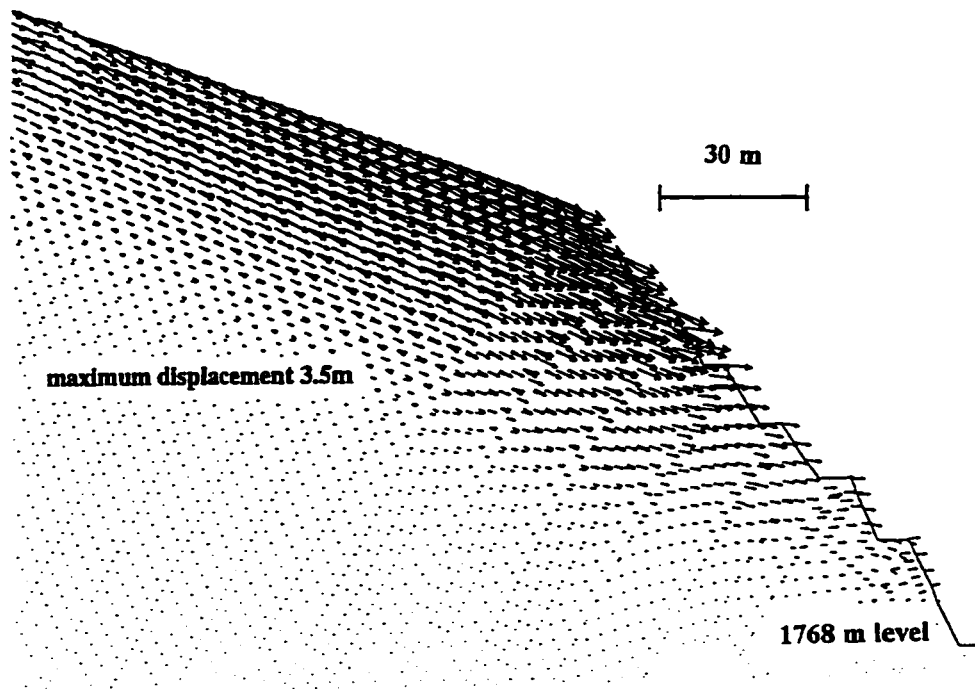
**Figure 4.26(f).** Zone limiting the toppling after excavation of the 1768 m level.



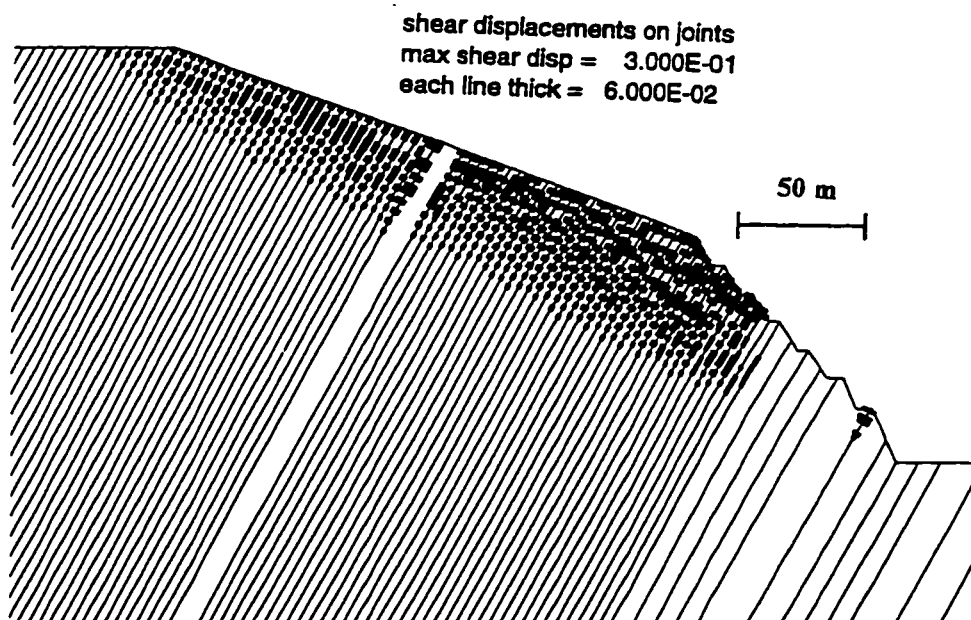
**Figure 4.27.** Plasticity indicators (yield and tension) after excavation of the 1768 m level.



**Figure 4.28.** Detail view of flexural toppling in the lower part of hillslope (Moosebar and Gladstone members) after excavation of the 1768 m level.



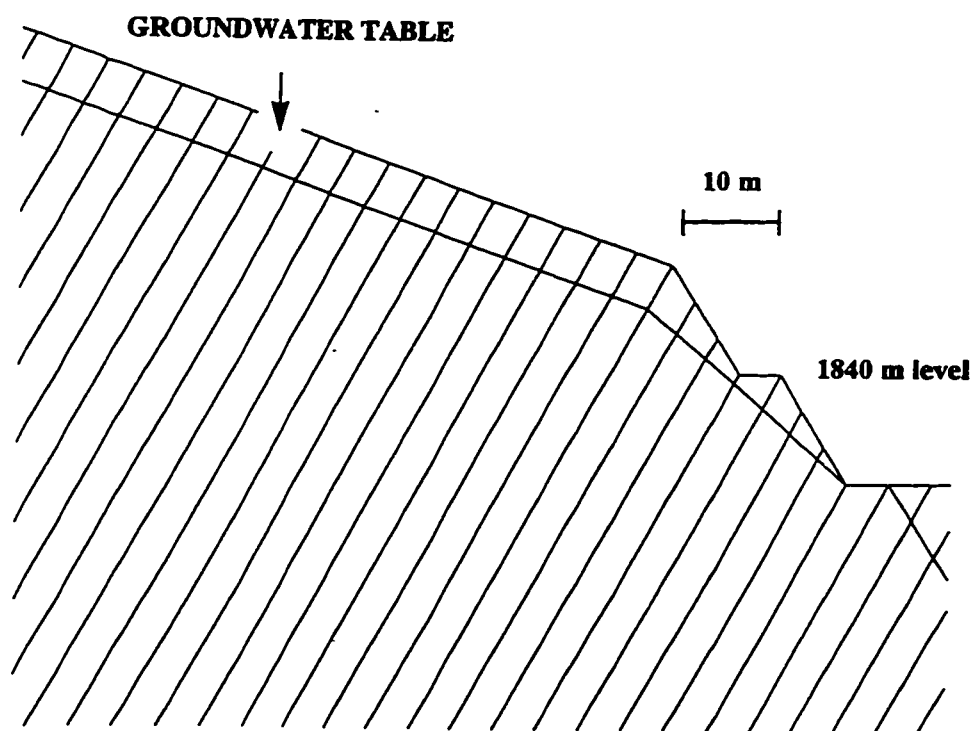
**Figure 4.29.** Displacement vectors in benches and the lower part of slope after the excavation of the 1868 m level.



**Figure 4.30.** Shear displacement on discontinuities after the excavation of the 1868 m level.

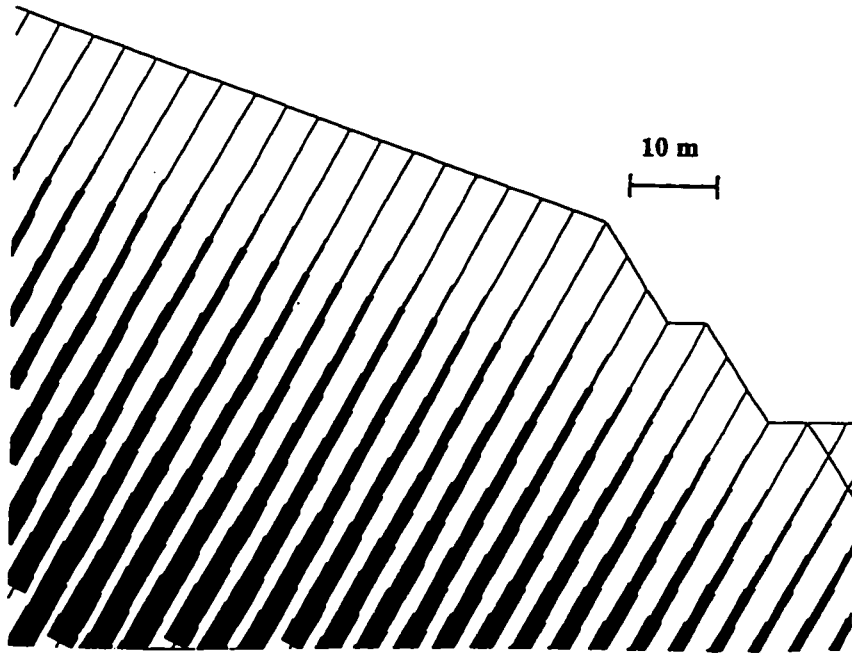
As mentioned earlier there is evidence for the influence of groundwater on the slope failure acceleration. Therefore, a model run with a groundwater table, as shown in figure 4.31, was included to investigate this influence. Only the slope stability after excavation of the 1840 m level was investigated. As seen from figure 4.31, a simplified case with a constant assumed groundwater table was investigated. The model was excavated in the elastic regime to the 1840 m level and the pore pressures based on the assumed position of groundwater table applied. The pore pressures mobilized in the model are shown, for the lower part of the slope, in figure 4.32.

The constitutive criterion was changed to Mohr-Coulomb elasto-plastic, with properties based on previous analyses. The stability of the model was examined for various values of cohesion, with all the other properties remaining the same, as in the dry case analysis. The failure initiated, as expected, for a higher cohesion. The cohesion value had to be decreased to 65 kPa in order to produce failure at this excavation stage. This value is 20 kPa higher than the dry case analysis. It is of interest, however, that the failure

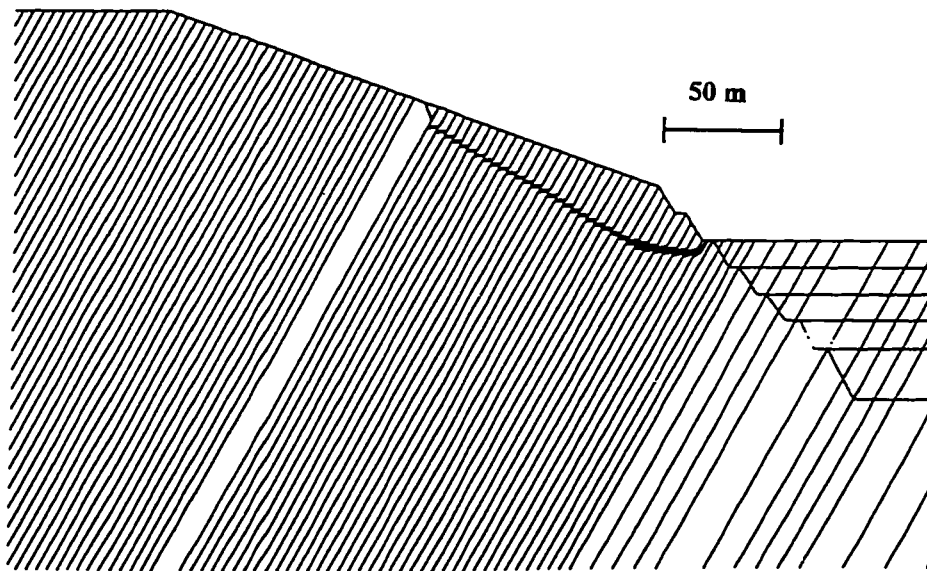


**Figure 4.31.** Model with assumed groundwater table - Section C20+00.





**Figure 4.32.** Domain pore pressures in the model with groundwater assumption - Section C20+00.



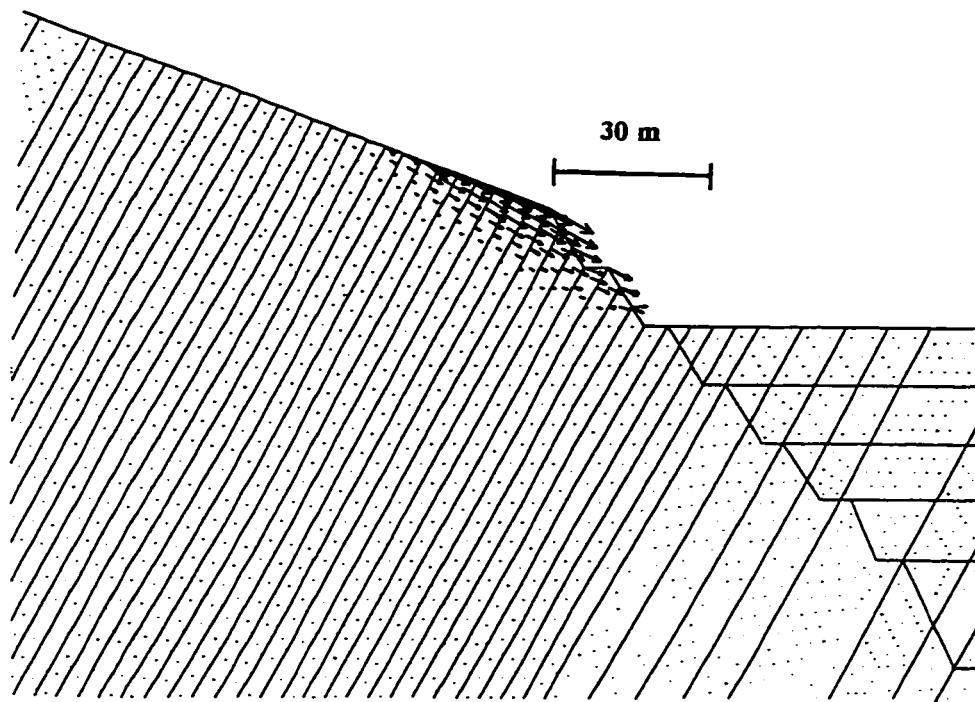
**Figure 4.33.** Zone limiting the toppling after excavation of the 1840 m level with assumed groundwater in model.

affected practically the same part of slope as in the dry case analysis, extending from the base of the 1840 m level to the Cadomin conglomerate layer located in the middle of the slope. The only change was in the deeper location of the failure surface in the toe area (compare figure 4.26(a) and 4.33).

Due to the anisotropy of the slope-forming rock types and the low bedding thickness in the Moosebar and Gladstone Member, as well as the Nikanassin Formation (maximum 0.5 m) and the Torrens Member (maximum 1 m), the “ubiquitous-joint” constitutive criterion was applied to the rock mass.

Ubiquitous constitutive criterion is an anisotropic plasticity model that includes weak planes of specific orientation embedded in a Mohr-Coulomb solid. Yield may occur on either the weak plane or solid, or both, depending on the stress state (Itasca, 1993).

Only the failure development at the 1840 m level, where the first signs of instability were reported from the mine, was investigated. The implicit joints were oriented parallel to and were given the same properties as the bedding plane joints. Other properties remained unchanged and dry conditions were assumed. The cohesion for the blocks was varied and the models’ response examined. The failure occurred for a block cohesion of 90 kPa. Different from the case with the Mohr-Coulomb constitutive criterion, the failure affected only the lower part of slope above the open pit mine as shown in figure 4.34. This figure represents the velocity vectors in the upper two benches, extending approximately 45 m behind the crest of the open pit slope. The shear displacement between the blocks decreased as compared to the model with Mohr-Coulomb constitutive criterion. A model where the ubiquitous constitutive criteria was applied to the final excavation stage (1768 m level) resulted in a failure similar to the one using Mohr-Coulomb criterion.

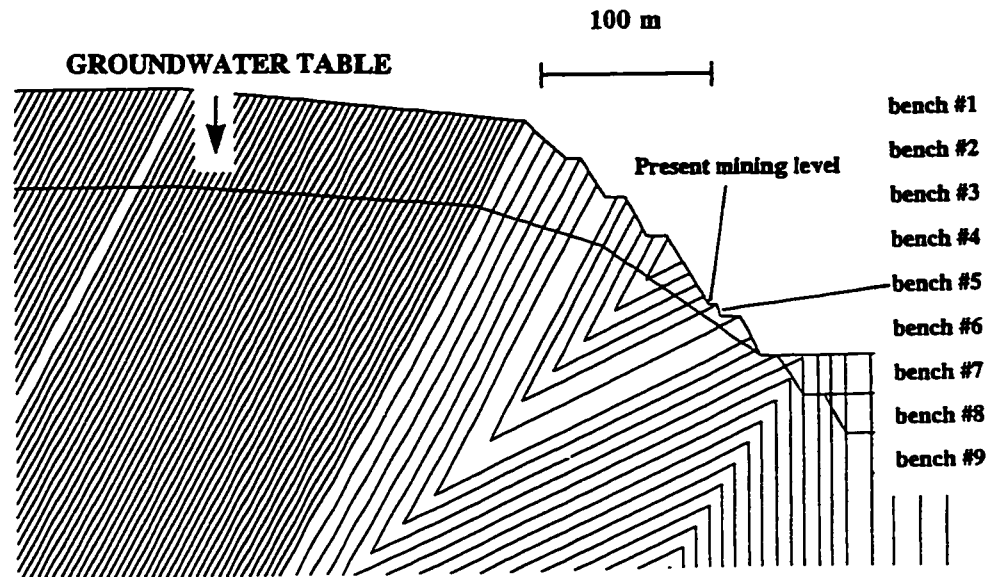


**Figure 4.34.** Velocity vectors in the upper two benches and slope above the pit crest after the excavation of 1840 m level and assumed ubiquitous constitutive criteria.

#### **4.3.5.7. Prediction of Slope Deformation in the C25+00 Section.**

The material properties from the analysis of section C20+00 were used for the stability assessment of the planned pit extension in section C25+00. The simplified geological cross-section and the distinct element model used, have been shown in figures 4.14 and 4.20, respectively, and figure 4.35 shows the area of the open pit slope excavation.

A similar modelling approach was used as in the previous analysis. The open pit slope was excavated using elastic isotropic constitutive criterion and high strength of discontinuities to allow only for elastic deformations. Only the upper four benches, representing the present mining level, were excavated and analyzed in the first step. The assumed groundwater table and bench numbers used for reference are shown in figure 4.35.

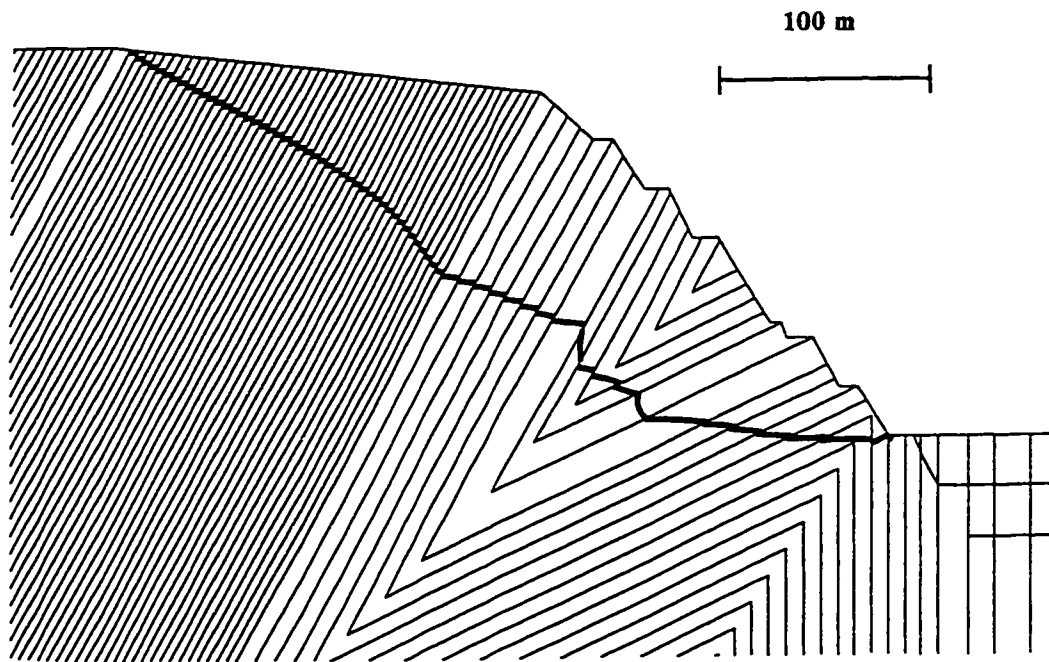


**Figure 4.35.** Model with assumed groundwater table and bench reference numbers in Section C25+00. This model shows the excavation of the upper six benches and the position of present mining level.

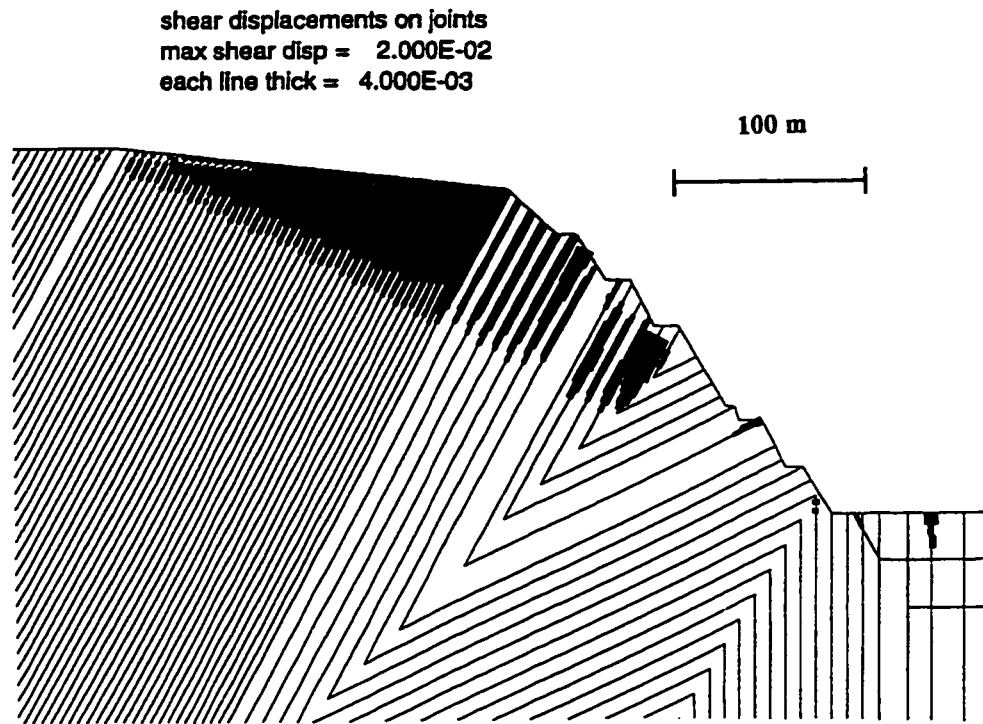
Once the pit was excavated to the present mining level (upper four benches), the constitutive criterion was changed to Mohr-Coulomb. The properties were based on the previous analysis for section C20+00, shown in figure 4.21. The slope with the four benches excavated (present mining level), caused only stable deformation with limited shearing along bedding planes due to the stress redistribution. This model prediction is in a good agreement with the mine reports (Hebil, 1995), indicating localized shearing along bedding planes with formation of obsequent, uphill facing, scarps, but no major slope failure.

The analysis indicates stable conditions upon further excavation of the next three benches. However, the excavation of the following bench (bench #7), initiated a failure in the model, propagating from the slope toe to the top of the hillside and terminating against

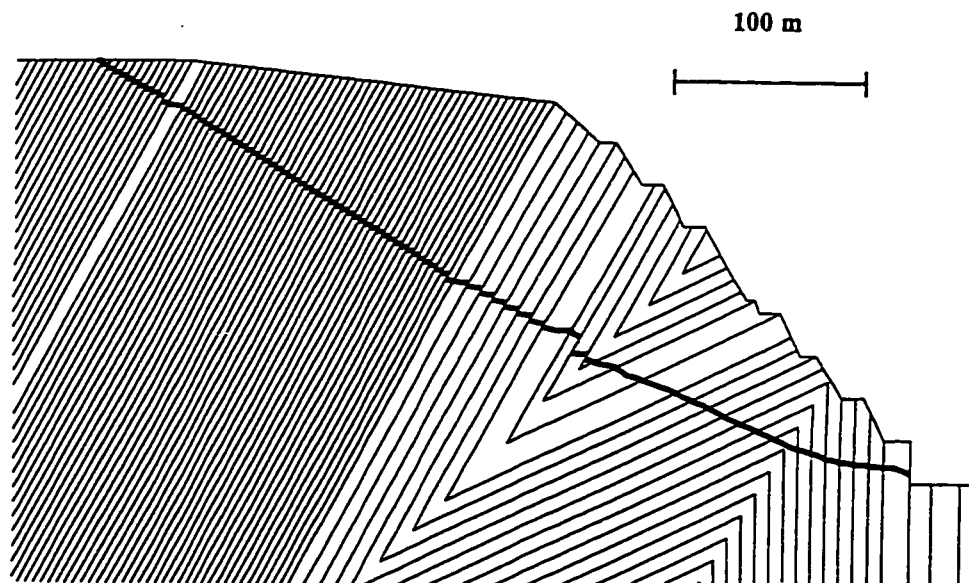
the relatively strong conglomerate bed as shown in figure 4.36. The failure plane is in parts irregular which may be due to the relatively strong “member D” unit. This unit is located in the middle of the slope, formed by the syncline structure. Because this unit was not involved in the slope failure in the section C20+00, no data on its strength were available from the mine management and were assumed as shown in figure 4.21. A future, more detailed analysis, will necessarily require testing of this unit as it appears to play a crucial role in the overall stability. The (in)competence could possibly determine the safe depth of the pit. Figure 4.37 shows the extent of shear displacement along the bedding planes at the same stage. To determine the location of failure surface at the final depth of planned mine extension, bench # 8 and # 9 were excavated and the result shown in figure 4.38. The failure surface extended approximately 50 m beyond the relatively strong Cadomin conglomerate unit.



**Figure 4.36.** Failure location in model after the excavation of the seventh bench - section C25+00.



**Figure 4.37.** Shear displacement on discontinuities after the excavation of the seventh bench.



**Figure 4.38.** Location of failure plane at the maximum planned deepening of pit in Section C25+00.

It is interesting that when the analysis was repeated for dry conditions, the same overall instability was observed. Although increased shearing and deformation took place with the assumed groundwater table, the model developed failure at the same excavation levels (after the excavation of bench #7). This, however, is only a preliminary observation based on the assumptions made in the analysis.

Using the back-calculated shear strength parameters for the C20+00 slope, a similar distinct element model of an observed stable slope at the Luscar Mine was analyzed by Douglas (1996). The model results indicated a stable condition, in agreement with the field observation. Analysis of another slope with more adverse toppling structures provided similar results to those presented in this thesis.

#### **4.3.6. Conclusions.**

Toppling confined by a quasi-linear basal failure surface, as shown in figure 26(a) to 26(f), proved to be the main failure mechanism. There is a large range in strength parameters that could result in slope failures as observed in the mine. The failure plane crosses seven stratigraphic units with lithology ranging from relatively strong conglomerate and sandstone to weak thinly bedded shales. Varied strength properties were used during the analysis, especially for the Moosebar and Gladstone members and the Nikanassin Formation. The failure after the excavation of the second bench required a cohesion value of 45 kPa or less, considering other parameters constant. Deformation with higher strength properties at this mining stage are only in the elastic range, ceasing with further computational steps. A certain amount of rock damage (fracturing, strain-softening) would occur, decreasing the competence of the rock mass.

A relatively low cohesion value of 45 kPa was obtained in back-calculation for failure after the excavation of the second bench. It is important to realize that the “rock blocks” used in the model for this type of rock mass are “an equivalent material” representing a

highly fractured rock fabric with cross joints rather than an intact rock material. This concept is shown in figure 4.17. *In situ* effects, such as lower rock mass competency of surficial layer due to weathering, freeze/thaw cycles, ravelling and erosion, would have an impact on the rock mass strength. The mine location is in an area of intense folding leading to a decrease in rock mass quality. Transient forces such as pore water pressure and blasting would allow for failure to originate with initially higher strength values.

The use of strain softening constitutive criteria is an available option in the present UDEC program and would seem to be the most appropriate. The use of such failure criteria should, however, be supported by sufficient data and understanding about the rock mass behavior. This was not the case in the presented study. Therefore, the less sophisticated Mohr-Coulomb and Ubiquitous-joint constitutive criteria have been applied. The use of Ubiquitous-Joint constitutive criteria, although more justified for this particular rock mass did not provide further insight into the failure mechanism than the more simple Mohr-Coulomb criteria. The failure was initiated for rock blocks with a higher cohesion and was initially confined to the immediate area behind the pit crest. Application of Ubiquitous criteria to the final pit geometry (1768 m level) showed, however, that the failure extended completely to the top of hillside as with the Mohr-Coulomb constitutive criteria. “Ubiquitous” models need approximately twice the time for the calculation procedure.

If the back-calculation is performed only for the final model geometry (Section C20+00) representing the excavation of all seven benches simultaneously, failure would occur at a higher cohesive strength value. The individual columns are longer at this stage and more susceptible to fracturing and failure due to bending. When a higher cohesion was applied to the model at the final excavation stage, the major difference observed was in less yielding in the slope above the failure plane. The resulting failure plane location was, however, the same as when the “bench by bench” excavation approach was used.



Good agreement with the observed failure surface was found without the presence of cross joints, although their influence was indirectly taken into account by the low cohesion value of the blocks in model. As observed in the field, cross joints in sedimentary formations are seldom continuous, being mostly limited to one or two layers of one lithological type. Therefore, the failure must involve fracturing of the rock material. UDEC does not allow for the intact rock blocks to fracture and thereby allow for an explicit development of the failure plane. The yielding zone, however, provides an excellent indicator of the failure geometry at depth. The cross-joints daylighting in the slope face seem to contribute more to the instability of individual benches and the weakening of the rock mass, whereas the pervasive bedding plane discontinuities control the overall instability. A preliminary, simplified model incorporating cross-joints was investigated. The main influence observed was that the failure surface followed more closely the orientation of cross-joints dipping at 28°.

When the strength of the Torrens Member (interbedded siltstones and sandstones) was increased a distinct failure surface developed only from the base of the 1828 bench (contact between the Moosebar and Torrens Member) to the Cadomin conglomerate, not representing the observed failure plane. Therefore, the strength of this unit must be “weak” enough if the failure is to propagate through this unit.

Bucek and Barron’s results (1994) indicated a stable block in the lower part of the slope, located between the Torrens sandstone and the Cadomin conglomerate bed. The presence of such a stable zone was not confirmed in the present numerical modelling nor by field observation. Therefore, UDEC appears to provide a more realistic indication of the failure mechanism and the overall slope deformation.

The stability analysis of the planned pit deepening in the C25+00 section provided only preliminary results for incorporation into the “decision making process”, as more information regarding the strength of the Member “D” is required. The results

nevertheless provided an important insight into the failure mechanism and were in agreement with mine experience.

It was found that the back-calculated strength properties are dependent on the discretization of blocks into finite difference triangles, block thickness as well as a combination of these two. Decreasing the bedding thickness enables toppling to develop at a higher block strength. Taking into account the actual average bedding plane spacing of 0.5 m and 1 m for the shales and interbedded siltstones and sandstones respectively, higher strength would be obtained in back-calculation. The discretization of blocks into finite difference triangles has also an effect on back-calculated values. The use of diagonally-opposed triangular zones with an aspect ratio close to unity is recommended if the numerical value of strength is of importance. It was found that a larger bedding spacing with diagonally opposed triangular zones with an aspect ratio close to unity provided better results than smaller bedding spacing with a coarse discretization of blocks into finite difference triangles. The failure mechanism and extent of the failure seemed to be insensitive to the discretization if the aspect ratio of finite difference triangles was kept reasonably low.

When pit excavation was simulated with Mohr-Coulomb constitutive criteria and properties as listed in figure 4.21, the same failure mechanism and failure extent resulted, as in the case when the pit excavation was performed in the elastic regime and the model changed subsequently to Mohr-Coulomb. The difference between these two approaches lies in the total accumulated displacement in the model. Using the first approach, large deformations may result in overlap problems, especially at later stages of modelling.

The modelling was performed only for one value of the initial ground stress condition. The higher horizontal stress component was considered justified based on the general location and available literature survey. It is realized that the complex geological structure at the mine site would have a much more complicated stress environment than the one assumed. Folding, faulting, cycles of loading and unloading, locked in stresses, sequences

of rock units with different deformation modulus would have contributed to a the stress field.

The results of the numerical modelling analysis demonstrated a good agreement with the observed instability. The main mode of failure proved to be flexural toppling which was constrained by a quasi-planar basal failure plane. The distinct element method offers considerable potential for the analysis of toppling failure in surface coal mine slopes. Although not providing a factor of safety against failure, it does indicate the possible failure mechanism, the extent of the failure behind the slope crest and the likely volume of the rock involved.

## **CHAPTER 5**

### **THE INFLUENCE OF UNDERGROUND MINING ON COMPLEX SLOPE DEFORMATION MECHANISMS**

#### **5.1 Introduction**

Considerable research has been undertaken throughout the world in an attempt to characterize the influence of underground mining on the stability of both natural and man-made slopes. The significance of this relationship becomes especially important when underground mining takes place in areas of:

- potentially unstable man-made or natural slopes
- steep, potentially unstable, mountainous terrain
- current surface mining
- previous underground or surface mining
- areas of urban development

The induced slope failures and ground deformations may exceed those observed in areas where mining takes place under flat or gently sloping topography by orders of magnitude. The analysis of this problem often becomes very complicated as factors of slope stability and underground mining, as well as their interaction, must be considered.

This chapter presents a literature review, examines the factors influencing the stability of slopes affected by underground mining, and applies numerical modelling techniques to

this analysis. The characteristics of such slope failures are presented, including their geometry and failure mechanisms. The methods of analysis which may be used to investigate the stability of slopes affected by underground mining are critically discussed. The use of numerical modelling techniques, both continuum and discontinuum, in analyzing the relationship between underground mining and slope stability, is presented. Numerical modelling is applied to hypothetical geometries. In chapter 6, the stability of Frank Slide in Alberta, Canada, is investigated with particular emphasis on the effect of underground coal mining at the foot of the mountain on stability of the Turtle Mountain.

## **5.2 Previous Work**

Significant work on this subject was undertaken in the United Kingdom following the disastrous event at Aberfan in October 1966, when a spoil heap failure caused the loss of 144 lives. Although the report on the failure concluded that mining subsidence was not the prime cause of disaster, certain effects of subsidence, such as the changes in hydrological regime and the stress field, may have contributed to the instability. The need for more knowledge regarding the effects of undermining spoil heaps appeared to be necessary (Report of the Tribunal, 1966).

The subsequent research initiated by National Coal Board Headquarters, Civil Engineering Branch, in 1971, investigated the effects of undermining spoil heaps, their behaviour and deformation mechanisms (Forrester and Whittaker, 1976; Forrester and Bacon, 1974; Subsidence Engineer's Handbook N.C.B., 1975). The principles of mining subsidence, the influence of site conditions, geology and time on mining subsidence were recognized. These workers reviewed several previous spoil-heap failures associated with mining subsidence and found that failures can be associated either with the transitional or travelling ground movements, or with the residual ground movements after mining has ceased. Several field investigations were undertaken in order to monitor spoil heap deformation during undermining. Comparison of observed data for each case with that

predicted using empirical methods (N.C.B., Subsidence Engineers' Handbook, 1975) showed that in all cases observed, subsidence in spoil heaps:

- was larger than predicted in both magnitude and extent
- was initially detected sooner than predicted
- continued to develop in most cases slower than predicted
- ceased later than predicted.
- occurred primarily in a downslope direction rather than in the predicted manner, relative to the position of the mine workings
- often caused extensive surface cracking when shallow mine workings were present

A draw angle value of  $45^\circ$  was found to be more representative for the spoil heaps than the average value for the U.K. of  $35^\circ$  for natural ground. As a result of the post-Aberfan studies it was found that mining subsidence can affect the stability of the tips by:

- altering the shear strength of the spoil
- altering the internal and surface drainage of both spoil heap and its foundation
- inducing pore pressure in both spoil heap and its foundation
- modifying the spoil-heap slope geometry
- motivating movement on old failure planes

Thomson and Yacyshyn (1976) and Thomson and Tiedemann (1982) refer to underground coal mining as a factor in slope instability in the city of Edmonton, Alberta. Instability is caused by the subsidence of old abandoned coal mines. Subsidence of the old shafts caused cracking of the ground allowing the ingress of water.

Walton and Taylor (1977) examined the potential modes of slope failures which can be induced in surface coal mines as a consequence of former underground mine workings. Old mine workings in England are mostly in the form of room and pillar mines, although ancient bell-pits and old shallow longwall workings are also encountered. They showed

that the extent of void migration, the degree of pillar collapse or pillar "robbing", failure of the roof and floor strata, and the bulking of failure debris must be considered. They divide the effect of underground mine workings on slopes into those:

- encountered within the slopes
- beneath the level of the slopes

Translational slides, toppling failures, span failures and slab sliding are the most common types of failure mode. They describe two near-horizontal sliding movements in Yorkshire and Staffordshire. In both cases the "critical tension" failures were practically coincident with extrapolated ribsides.

Gostelow (1977) analyzed slope stability problems in South Wales. Mining subsidence was believed to be one of the factors responsible for slope instability. A direct relationship between the dates of sliding and the onset and renewal of the mining activity was noted. The ground strains and the induced tilt at the ground surface as a result of the mining subsidence, increased the slope angle of the valley sides, caused fracturing and widespread changes in groundwater conditions. The development of mining-induced fractures was believed to be an important factor. The landslides in the South Wales coalfield area were analyzed also by Jones (1991) and Bentley and Siddle (1996).

Gentry and Abel (1978 a, b) presented results from a rock mechanics instrumentation program at the York Canyon mine in New Mexico (United States). The published results were only preliminary, with the mining still in progress at the time of publication. One of the project's purposes was to determine the magnitude and extent of surface subsidence resulting from mining a super-critical longwall panel beneath rugged mountainous topography. From these preliminary results, it appeared that the topography controlled the amount of horizontal movements on slopes. It appeared that when the direction of mining was in the downslope direction greater horizontal ground movements resulted than when mining was in the upslope direction. This conclusion is, however, based only

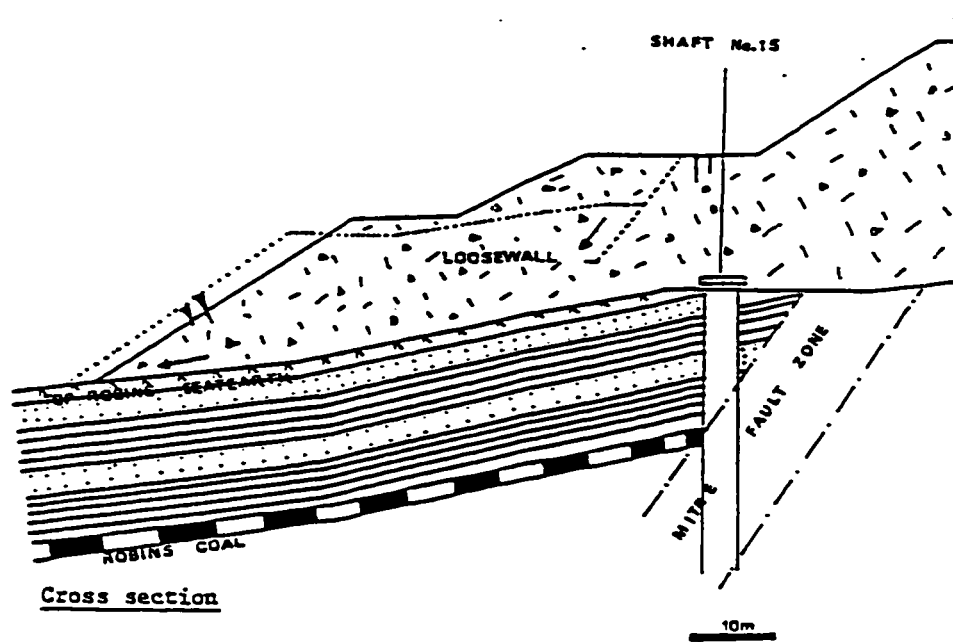
on the mining under gently dipping slopes. The angle of draw decreased in topographic lows and also where cross panel slopes face outwards from the panel centerline. The overburden material tended to be attracted towards the topographic lows.

Matula (1979) describes a 700 million m<sup>3</sup> landslide affecting an area of 8 km<sup>2</sup> near the town of Angren in Uzbekistan. The main cause of this catastrophic movement on a 15 to 20° slope was the collapse of relatively shallow underground space, created by underground gasification of coal. The movement was restricted by the construction of a 15 million m<sup>3</sup> berm at the toe of the slope.

Scoble (1981), Stead (1984, 1990) and Stead and Singh (1989) recorded data on over 240 slope failures at surface coal mines within the United Kingdom. Figure 5.1 shows an example of spoil instability involving translational failure along a weak seatearth-spoil interface. The failure had an volume of approximately 87,000 m<sup>3</sup> and took place in an area of previous underground mining activity. They indicated that underground workings were a possible contributory factor in over 25% of the instabilities. Several major failures were related to active longwall mining activity beneath the sites. The effect of underground workings on the slope stability in the British surface coal mines was emphasized also by Walton and Atkinson (1978) and Cobb (1981), who incorporated the effect of old mine workings in his stability index.

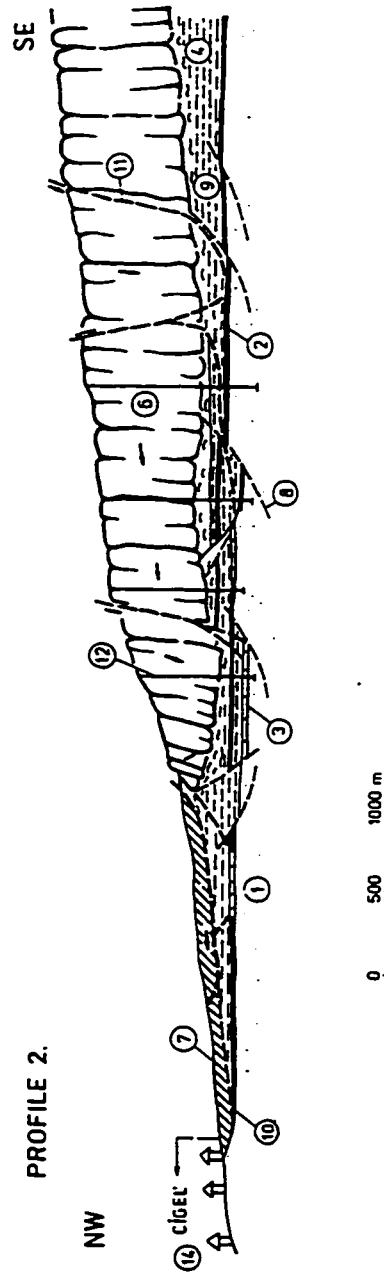
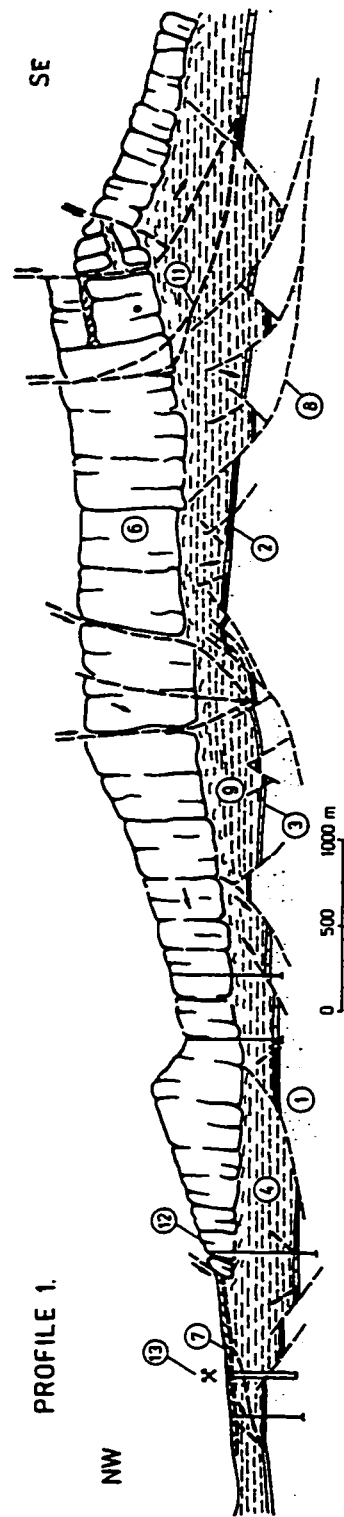
Extensive research on the influence of underground coal mining on slope stability was conducted in the Vtacnik Mountain, Slovak Republic (Fussganger et al., 1983; Malgot et al., 1986, 1991). The Vtacnik Mountain is a part of the Carpathian Mountain range, formed by volcanic rocks (andesites, agglomerate tuffs) overlying clays and coal seams as shown in figure 5.2. The underground coal mining in this area takes place under difficult geological engineering conditions, with the whole mountain range being





**Figure 5.1.** Spoil failure involving translational movement along a weak layer with Room and Pillar workings underneath (after Stead and Singh, 1989).

intensely deformed by deep gravitational movements. Slope movements of different types and mechanisms are represented in this area ranging from block-type movements of volcanic rocks on plastic substratum to translational and rotational failures in soil slopes. The longwall mining of 3 to 9 m thick coal seams without backfilling contributes significantly to the already unstable structure of the mountain slopes. The latter workers made a detailed engineering geological investigation of the unstable areas already undermined in the past. Based on this study a prognosis was made about the ground deformation and slope stability in areas of future undermining. The results were presented cartographically (1:10000 scale) and assisted in the protection of several endangered villages, in establishing protection zones around important objects, and optimizing the method of mining with respect to ground deformation. Detailed investigations were carried out in the village of Podhradie, where underground mining triggered a slope movement with severe damage to surface structures as shown in figure 5.3.



**Figure 5.2.** Underground Coal Mining in the Vtáčnik Mountains, Slovak Republic (after Malgot et al., 1986). 1-Tuffites, 2-Coal seam, 3-Mined-out Coal seam, 4-Clays, 6-Andesites, 7-Landslide debris, 8-Failure Surfaces in pre-volcanic sediments (gravitational tectonics), 9-Creep zones, 10-Failure of recent Landslides, 11-Failure of recent Landslides activated by underground Mining, 12-Boreholes, 13-Mine shaft, 14-Village



**Figure 5.3.** One of the damaged houses in the village of Podhradie (Slovak Republic), resulting from a landslide triggered by underground mining.

Iannacchione and Ackman (1984) remarked on the occurrence of landslides over longwall mining area in the Dunkard basin, Pennsylvania (United States). They noted that the gradual subsidence over panels can cause reactivation of older landslide deposits by decreasing the support to the landslide toe area. Examination of the area consisting of field investigations and examination of pre-mining aerial photographs. This led to the identification of several reactivated landslides, the largest of which ranges from 30 to 90 m in length and from 30 to 60 m in width.

Morris and Clough (1986) refer to anticipated slope stability problems associated with opencast mining in an area of old underground workings. They describe the modes of slope failure when underground workings are present and discuss analyses and the effects of the direction of mining on slope stability. The principal effect of underground mining

on slope instability is, according to these authors, the modification of existing structures and the development of new discontinuities which loosen the rock mass.

Matula and Pasek (1986) commented on the problem of undermining and slope instability in Czechoslovakia. They stated that subsidence of a terrain can lead to the development of slope movements if the mining approaches too close to the slope toe. They gave an example of such a case study where slope movement triggered by undermining damaged a forested area and a nearby road in the Czech Republic. Zaruba and Mencl (1987) discussed the relationship between underground mining and slope stability. The influence of the mining was, according to these authors, two-fold; both giving rise to slope instability problems:

- subsidence increases the surface slope angle
- rocks in the subsiding area are exposed to tensional strain

These authors also emphasized the problem of obtaining precise information regarding old mining activities, which causes problems for evaluating the groundwater regime as well as other important parameters necessary for slope stability assessment. The significance of altered hydrological conditions due to old mining activity was noted. They presented a case study of a slope movement in an area of previous mining activity where 900 l/min was discharging from an old mine adit.

Pells et al. (1987) analyzed rockfalls and landslides within eight areas in the Sydney Basin where coal and oil shale mining occurred beneath, or adjacent to a sandstone escarpment. The failures have ranged from minor rockfalls, to an approximately 30 million tones rockslide. Major failures appear to be associated with areas of full extraction immediately beneath or beyond the top edge of an escarpment. Extraction behind an escarpment causes surface cracking but not major rockfalls. They showed that there is some evidence of large rockfalls, resulting from a combination of full extraction and specific geological features such as faults or discrete continuous joints. The mechanism of the cliff failures

was not toppling, but comprised basal shear and crushing beneath massive slabs of sandstone which became separated from the cliff line as a result of mine subsidence movements.

Jeran and Adamek (1988) investigated subsidence due to the excavation of horizontal longwall panels beneath sloping terrain in Pennsylvania (United States). They used an empirical-based United States Bureau of Mines subsidence prediction model to compare numerically derived subsidence with measured data. It was noted that both the magnitude and the direction of subsidence movements were significantly affected by the topographic slope. Small horizontal adjustments were observed after the cessation of vertical movement which were believed to represent the reaction of the surface to changes in slope induced by subsidence.

Whittaker and Reddish (1989) analyzed the subsidence aspects of sloping ground surfaces. They presented subsidence profiles, strains and displacements above longwall extraction for ground surfaces with different inclination and summarized the subsidence effects on the ground stability of sloping terrain.

Liu and Xu (1989) refer to the Yangchihe slope failure induced by mining in 1980. The mining took place under high limestone and sandstone cliffs triggering a major slope failure killing 284 people. This slope failure is mentioned also by Xiaoning (1991) in his paper on geological properties of large-scale, high speed, landslides.

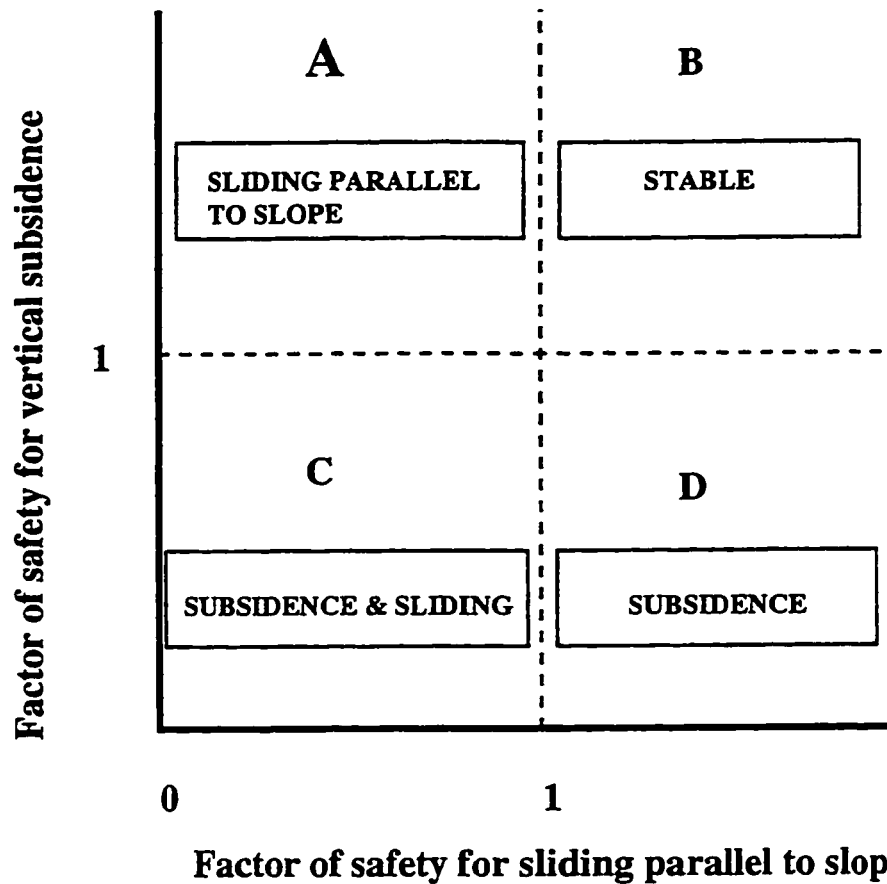
Barla and Jarre (1991) analyzed the subsidence caused by visco-elastic closure of underground cavities and dissolution of mine structures in a kyanite mine. A monitoring program was undertaken, inclinometers were installed in the slope to measure the horizontal displacements at depth. The results showed the whole slope rock mass sliding as a consequence of the subsidence of the rock salt.

Rybar et al. (1990) analyzed a deep-seated rockslide initiated by tin mining in the Czech Republic. The slope of an old open pit was moving continuously as a single unit separated from the solid beds along a existing plane. A monitoring of the slope deformations was suggested and alarming limits for recorded displacements determined.

Arcamone and Poirot (1983), Jennings et al. (1985), Graham (1989), Agljukov et al. (1990) and Swedzicki (1993) refer to and discuss problems with open pit mining in areas of previous or present underground mining activity. The overburden strength parameters are largely altered in such situations.

A special case in this category is the relation between natural subsidence phenomena and slope stability. Although not directly related to mining activity, the mechanism has the same principles, involving underground openings and their possible collapse as well as changes in groundwater regime. Reuter et al. (1977) refers to slope stability problems as a secondary process in subsidence areas of chloride karst in Germany. Natural subsidence and collapse of underground cavities caused the initiation of slope failures. Sassa et al. (1979 a, b, 1981) addressed vertical subsidence as a factor influencing slope stability. They recommend the use of two different analytical approaches to examine the slope stability: one for the stability parallel to slope and one for the vertical subsidence. Figure 5.4 shows their schematic classification of slope stability taking into account the vertical subsidence. The difficulty in distinguishing state A from state C was recognized. They supported their findings by presenting case studies of the influence of underground erosion on slope stability in sandy, as well as crystalline schist slopes.

Different types of underground construction have the same deformation effects as mining activity. Schenk (1994) referred to a case when the influence of tunnel construction on slope stability is addressed. Hoek and Moy (1993) presented an analysis of stresses around underground caverns near the toe of slopes employing an elastic boundary element program. They examined the zones of overstressed rock using three different cavern locations relative to the slope toe.



**Figure 5.4.** Schematic illustration of slope classification based on the type of instability, after Sassa et al. (1979).

### 5.2.1 Previous Analyses of the Influence of Underground Mining on Slope Instability

Analytical methods employed by previous researchers in analyzing the relationship between underground mining and slope stability include physical models, limit equilibrium methods and numerical modelling techniques.

Singh and Singh (1991, 1992) analyzed the slope stability of an open pit mine developed in an area of previous old underground and shallow surface workings in the Jharia coalfield, India. Using physical modelling they compared the deformation in the rise and dip side slopes (bedding planes inclined at  $8^\circ$  to the horizontal). They observed significant deformation in the form of secondary shear crack development and the opening of tension cracks on the rise side slope.

Physical modelling was used also by Jones et al. (1991) and Siddle et al. (1991) in their analysis of landslides in the South Wales Coalfields. They noted the disproportionately high frequency of occurrence of deep-seated landslides that involved substantial volumes of rocks over the last 130 years compared to the total number since deglaciation. This time period (the last 130 years) coincides with the industrial and mining development in that area. They investigated the interaction between slope stability and mining activity using not only physical modelling but also finite element numerical modelling and limit equilibrium stability analyses. They analyzed a situation where mining takes place close to the outcrop, and pillars of unworked coal are left within the workings. They found:

- a large increase in vertical compressive stresses over the pillars
- compressive strains in the floor rocks beneath the pillar and tensional strains above and below the worked areas, indicating "punching" of the pillar
- lateral displacement of the floor rocks towards the outcrop

The limit equilibrium approach to slope stability, was used both prior to and after mining. Two kinds of shear strength parameters were used based on previous results from the finite element analyses. The "undisturbed" parameters were used to represent strata where no potential fracture planes were predicted, as well as for the slope structure before mining. "Disturbed" parameters were used to represent the shear strength along the predicted fracture planes. The prediction of fracture planes was based on Mohr's theory of fracture, given the direction of the major principal stress and the effective angle of shearing resistance of the material. The factor of safety was reduced up to 66% when such mining effects were incorporated.

A limit equilibrium approach was used by Bowders and Lee (1988) who performed stability analyses for slopes affected by underground mining. They analyzed twenty slopes in three longwall mined areas, before and after subsidence had occurred due to undermining in both longitudinal and transverse direction. None of the analyzed slopes failed, with the most important change being the slope inclination.



A limit equilibrium approach was also employed in the analysis of a landslide reactivation due to undermining in the Vtacnik Mountain in Slovakia by Fussganger et al. (1983). The undermining caused a substantial decrease in the groundwater level (7 to 25 m) and undercutting of the slope toe, resulting in failure development. They back-calculated the individual stages in the landslide development in three steps:

- In the first step the uneven settlement was calculated;
- In the second step, the initiation of landslide, the undrained shear strength parameters were used in the analysis;
- In the third step, representing the complete development of landslide, the residual values of cohesion and friction were used.

A limit equilibrium approach (combined with finite difference modelling) was used by Watters et al. (1989), Watters et al. (1990) and Rehwoldt (1990) for an open pit slope stability assessment in an area containing old underground workings. The old workings, a network of drifts, stopes and adits were planned to be intersected by the Homestake open pit excavation, South Dakota. They utilized the limit equilibrium method to find a potential critical failure surface for various openings and fault zone distributions. Lower factors of safety were obtained with increasing numbers of underground openings within the slope. The failure path was influenced by the distribution of the openings. As their number increased the potential failure path was increasingly controlled by these features and became more complex. They concluded that the known distribution of abandoned workings would not contribute significantly to the overall instability of excavated slopes. Isolated bench failures, toppling and raveling of slopes, however, may be expected during excavation, producing a safety hazard, rather than overall instability. The instability of overall slopes was found to be controlled mainly by the fault geometry within the open pit walls.

Iannacchione and Vallejo (1995) analyzed factors affecting the slope stability of abandoned mine lands in Kentucky using the limit equilibrium approach. One of the two

major factors was the failure of natural soil slopes due to increased water saturation from mining-induced sources.

Hoek (1974) presented a limit equilibrium method of analysis of the progressive caving induced by mining an inclined orebody. This presents a special case of the relationship between underground mining and slope stability. The author presented approximate charts for estimation of the angle of break for various mining depths. Brown and Ferguson (1979) extended and applied this limit equilibrium method for the analysis of progressive hangingwall caving at Gath's mine in Zimbabwe.

Franks and Geddes (1984) presented results from a finite element analysis of movements on sloping ground due to longwall mining. The study was inspired by the geographical locations typical of the South Wales coalfield valleys. Slopes with gradients of 25° and 35°, and as high as 245 m were analyzed. They employed an homogeneous, transversely isotropic constitutive model to analyze the ground movements, strains and tilts produced by undermining of slopes. They demonstrated that the sloping ground affects the horizontal movements and the ground strains to a much greater degree than the vertical movements and tilts. The inter-relationships appeared to be complex, involving factors such as the direction and position of the mining edge relative to the toe of the slope and its dip direction, as well as the depth to and width of the extraction. Their results failed to confirm the National Coal Board's suggestion that maximum tensile and compressive ground strains are unaffected by surface slope, that mid-height of slope values can be used, and that it is only the distribution of ground strains on the slope that is modified.

Tang and Peng (1986) presented results of an investigation on surface fractures occurring above a West Virginia coal mine. They combined a finite element analysis with field observations. The topographic effect of the sloping terrain, together with the weak strength of the floor rocks and splitting of coal pillars, contributed to the origin of the surface fractures.

Siriwardane and Amanat (1984) analyzed numerically the subsidence in an hilly terrain using the finite element method. Their results indicated that plastic and tensile zones developed at the slope crest and hill sides. Problems were encountered in matching the elastic modulus to simulate the actually measured values of subsidence. Siriwardane and Moulton (1988) presented a case study and modelled numerically the damage to a building located at the toe of a hillside. It was concluded that the damage was a direct result of subsidence effects produced by nearby underground mining operation, generating large horizontal movements. The subsidence movements changed the groundwater flow pattern and caused the development of large tensile strains. As a consequence, a block glide type of slope failure originated with the failure surface following a weak clay layer, the strength properties of which decreased when in contact with water.

Cotton and Matheson (1989) pointed out that surface mining in an area of abandoned underground mines can be completed in a safe manner if the proper geotechnical constraints are understood. Using the finite difference numerical modelling technique, they analyzed the stress redistribution caused by stopes and open pit excavation.

Jones et al. (1990) and Ahola (1990) analyzed the stability of a sandstone escarpment over longwall mining operations using finite element, distinct element and a boundary element methods, respectively. Their results demonstrated that the natural yield zone at the base of an escarpment may be enlarged by the mining of longwall panels directly beneath the escarpment crest. They found it unlikely that block rotation could be a significant mechanism in escarpment failure, because of the relatively uniform outward and downward movement of the crest. The failure mechanisms may be caused by yielding of the "foundation" material at the base of the escarpment.

Stead and Benko (1993) analyzed the influence of underground workings on slope instability using a numerical modelling approach. They used finite difference and distinct element methods to analyze the slope instability generated by shallow as well as deeper

underground mines. Both longwall mining and room and pillar mining methods were examined. They show the distribution of tensile zones, displacements and the location of maximum shear strain in the slopes.

Clark et al. (1990) analyzed the stability of a combined open pit and underground mining operation. They used finite difference modelling to address the deformation mechanism. The main problems reported, appeared to be the development of tensile stresses in some toe areas of the slopes. This could lead to cracking normal to the direction of tension, allowing local block release from the toe areas.

Singh et al. (1993) analyzed a progressive failure development in a hangingwall and footwall with the increase in mining depth in sub-level caving. They used the finite difference code, FLAC, for analyzing the deformations. The results from numerical modelling were compared with two case studies from India and Sweden.

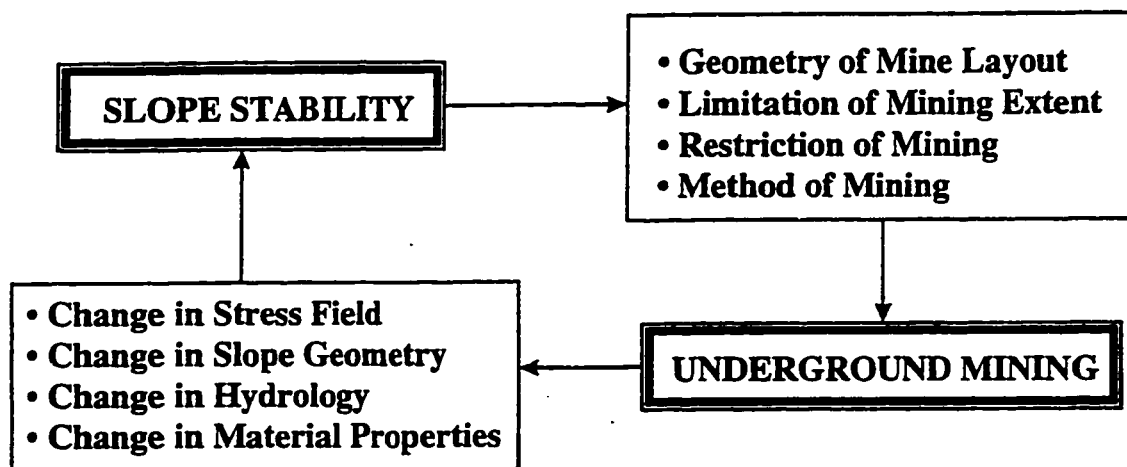
Stewart et al. (1996) performed both physical and numerical modelling, using centrifuge models and non-linear stress analysis. They reported reasonable agreement between these two techniques when strain-softening behavior was assumed in numerical modelling. The analysis was confined to workings within the slope, using both finite difference (FLAC program) and distinct element (UDEC program) techniques.

The literature survey shows a large number of cases where the underground mining and material extraction, as well as natural processes resulting in underground deformations, were considered the main factor or trigger of slope instability. The prevailing analytical approach in the past was based mainly on observations and measurements. In recent years, the focus has shifted more and more on the applications of more “sophisticated” analytical techniques such as centrifuge modelling and numerical analysis. The literature survey reveals, however, that most of the numerical modelling was applied mainly to isolated case studies rather than a comprehensive analysis of the main principles when slopes are undermined.

### 5.3 Factors Effecting Mining Induced Slope Deformation and Stability

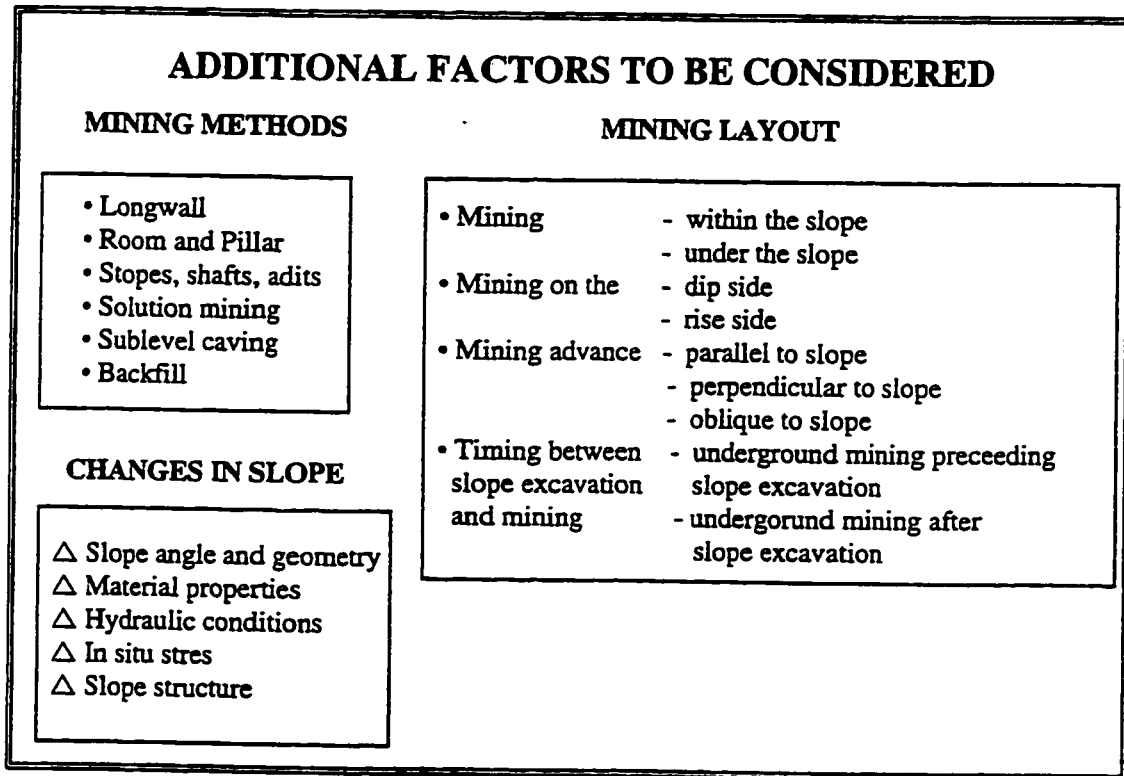
The relationship between underground mining and slope instability is mutual as the undermining influences the slope stability and vice versa. Unstable slopes or potentially unstable slopes may cause a change in the mine layout or mining method. This relationship is schematically illustrated in figure 5.5.

The factors effecting slope stability, underground mining, as well as factors resulting from their interaction, must be taken into account. Figure 5.6 presents the main points to be considered when concerned with the stability of slopes and underground excavations, as presented by Hudson (1992). These factors were slightly modified to include the soil slopes. New factors resulting from interaction of these two groups are shown in figure 5.6 and are discussed further in the text.



**Figure 5.5.** Relationship and factors of influence between slope stability and underground mining.

SLOPE STABILITY	UNDERGROUND EXCAVATIONS
<ul style="list-style-type: none"> <li>• OVERALL ENVIRONMENT</li> <li>• INTACT ROCK/SOIL QUALITY</li> <li>• DISCONTINUITY GEOMETRY</li> <li>• DISCONTINUITY PROPERTIES</li> <li>• ROCK/SOIL MASS PROPERTIES</li> <li>• IN SITU STRESS</li> <li>• HYDRAULIC CONDITIONS</li> <li>• SLOPE ORIENTATION</li> <li>• SLOPE DIMENSIONS</li> <li>• PROXIMATE ENGINEERING</li> <li>• SUPPORT/MAINTENANCE</li> <li>• CONSTRUCTION</li> </ul>	<ul style="list-style-type: none"> <li>• EXCAVATION DIMENSIONS</li> <li>• ROCK/SOIL SUPPORT</li> <li>• DEPTH OF EXCAVATION</li> <li>• EXCAVATION METHOD</li> <li>• ROCK/SOIL MASS QUALITY</li> <li>• DISCONTINUITY GEOMETRY</li> <li>• ROCK/SOIL MASS STRUCTURE</li> <li>• IN SITU STRESS</li> <li>• INTACT ROCK/SOIL QUALITY</li> <li>• ROCK/SOIL BEHAVIOR</li> <li>• DISCONTINUITY APERTURE</li> <li>• HYDRAULIC CONDITION</li> </ul>



**Figure 5.6.** Factors to be considered when analyzing the relationship between slope stability and underground mining.

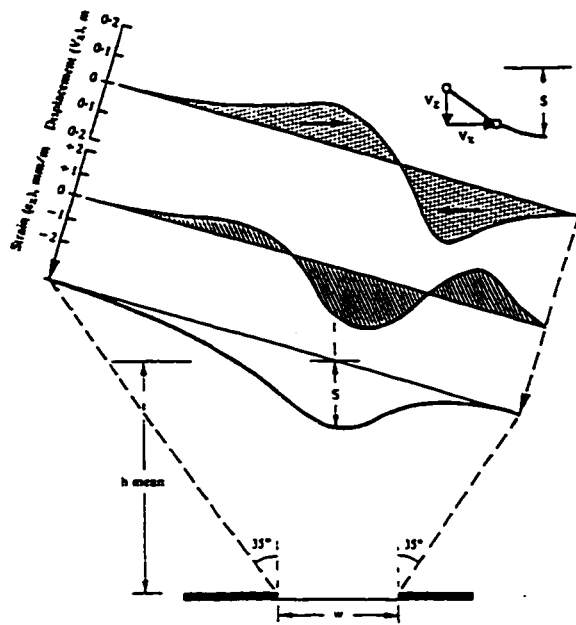
### **5.3.1 Longwall Mining**

Longwall mining is the most common method for underground coal mining where engineering has advanced technological capabilities (Jeremic, 1985). The effects of undermining, in the form of ground subsidence and deformation influencing slope stability, will depend largely on the longwall orientation relative to the slope. For simplicity only two limiting cases, where mining is either perpendicular or parallel to the plane of the slope face, will be considered in the following study. Mining perpendicular to slope face plane is referred to herein as panel extraction.

When panel extraction takes place under sloping terrain the deformation effects differ substantially from mining under a level topography. The usual way of determining the subsidence under a sloping terrain is the use of an empirical, graphical method as for example the one presented in the Subsidence Engineer's Handbook (1975). The accuracy, however, is dependent on the ratio between the width of the panel and the depth from the surface to the excavated panel ( $w/h$ ). With a decrease of the  $w/h$  ratio the accuracy of prediction increases (Whittaker and Reddish, 1989). Several other methods are used including the influence function method (Whittaker and Reddish, 1989), the rays projection method (Shu and Bhattacharyya, 1992) as well as different types of numerical and physical modelling techniques.

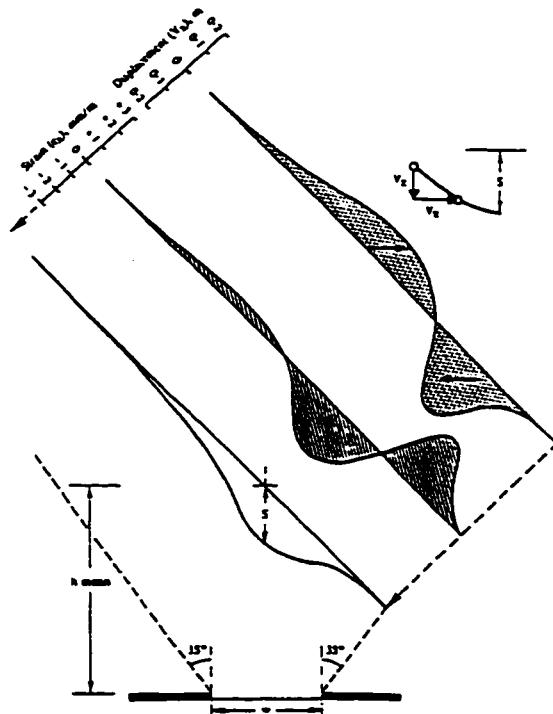
#### **5.3.1.1 Longwall Mining within the Slope**

Figures 5.7 and 5.8 shows the subsidence, strain and displacement profiles above a longwall panel extraction with the surface sloping  $15^\circ$  and  $45^\circ$ , respectively, using the influence function method (after Whittaker and Reddish, 1989). Several important features with respect to slope stability emerge from these figures:



Mining Data	
w	= 200 m
M	= 2 m
h <sub>MEAN</sub>	= 400 m
Surface	
slope	= 15°
S	= 1.15 m

**Figure 5.7.** Subsidence, Strain and Displacement above Longwall Extraction with a Surface Ground Slope of 15° (after Whittaker and Reddish, 1989).



Mining Data	
w	= 200 m
M	= 2 m
h <sub>MEAN</sub>	= 400 m
Surface	
slope	= 15°
S	= 1.15 m

**Figure 5.8.** Subsidence, Strain and Displacement above Longwall Extraction with a Surface Ground Slope of 45° (after Whittaker and Reddish, 1989).



- The horizontal component of displacement on the up-slope side indicates a significant movement down the slope. Although the maximum value on the up-slope side relative to the down-slope side decreases with increasing slope angle, the extent of the influenced zone becomes larger. The increased down-slope movement is reported from several field observations mentioned in the literature. The horizontal movement follows rather the direction of the surface slope than the direction towards the extracted panel.
- The extent of the tensile zone on the up-slope side increases with the increasing slope angle. This promotes the opening of existing discontinuities with kinematically favorable orientation. New fractures may originate as a result of the increased tensile forces and movement reactivation on existing failure planes (faults, shear zones, etc.) may result. The induced deformation may lead to a decrease in the overall slope integrity, changes in hydrological regime, and an increase in the slope angle and slope height. This can be of particular importance in landslide-prone areas where the slightest change in stability factors may trigger a substantial slope movement. The influence of underground mining on groundwater regime and hydraulic conductivity was examined recently in detail by Bai and Elsworth (1994) and Elsworth et al., (1995).

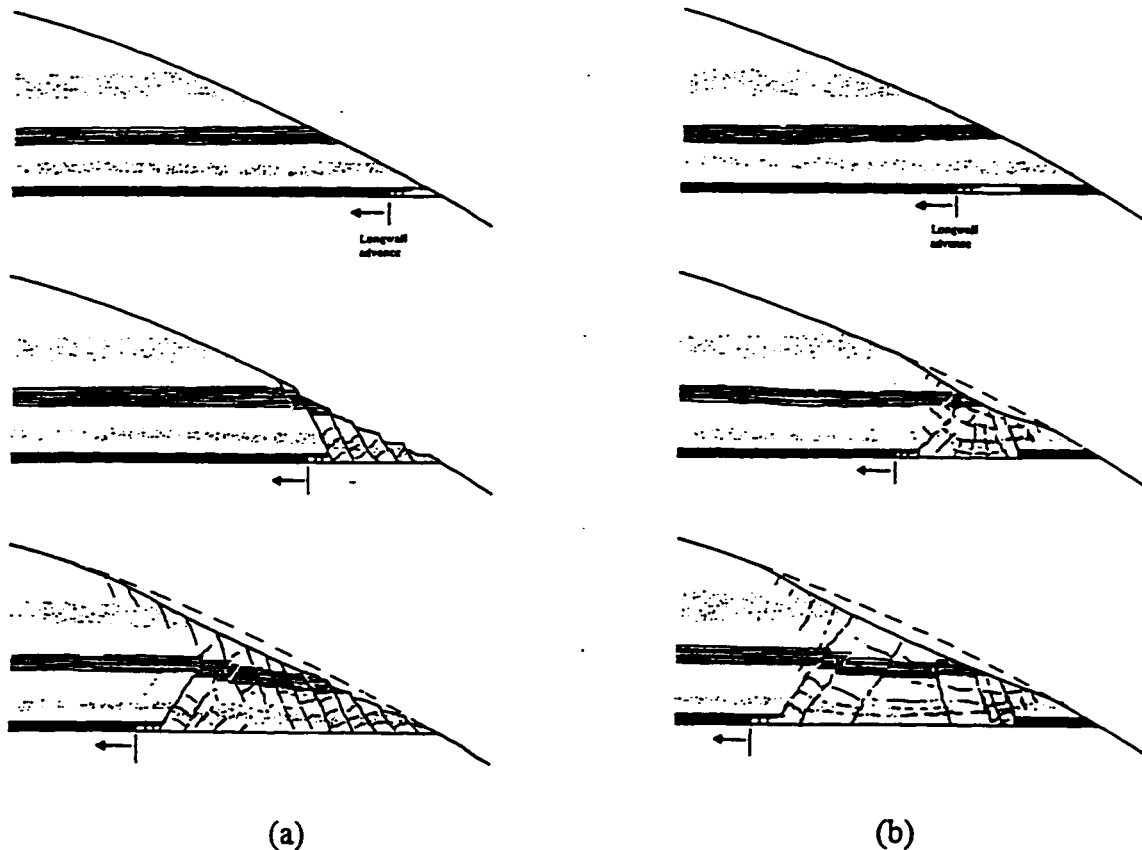
When mining takes place perpendicular to the slope face, its stability is affected by the transient displacement. The deformation depends largely on the depth of extraction and strength of the overburden. Figure 5.9 show the overburden deformation for extraction of a seam from the outcrop on a hillside (Whittaker and Reddish, 1989). A case with and without a supporting pillar at the outcrop is presented.

- Without a supporting pillar, undermining the slope toe arises, inducing slope instability and overburden collapse. The overburden rock/soil mass fails due to shearing followed by slumping down gradient. The frequency of shearing and size of sheared blocks will depend on the overburden competency. Further mining progress

results in less overburden fractures extending through to the surface. Large open cracks will form at the surface.

- Leaving a supporting pillar at the outcrop will substantially eliminate the initial sliding of the overburden. A passive wedge forms above the pillar restraining the out-of-slope deformations and potential slope failure. Formation of significant surface cracks above the pillar side is to be expected.

In both cases the induced deformations will, however, be largely influenced by the overburden structure, especially by the presence of pre-existing discontinuities. An important aspect is if the mining takes place with or without using backfill.



**Figure 5.9.** The initiation of subsidence and trough development with an increasing depth of overburden. A case without (a) and with (b) a supporting pillar at the outcrop is presented.

### **5.3.2 Room and Pillar Mining**

The ground deformation above room and pillar mines may be complex. In addition to subsidence troughs, crown-holes can develop, especially at shallow mining depths. Void migration presents another important factor (Gerrard and Taylor; 1984). These authors concentrated on the void migration and collapse of old shallow room and pillar coal workings at less than 75 m depth. They recorded over 60 variables on each working, providing more insight into the time factor of collapse mechanisms. Apart from the geological conditions and rock mass properties, the geometry of workings and mining dimensions are important factors.

Stead and Benko (1993) presented a simple example of void migration and the influence of room and pillar workings on slope instability employing the Universal Distinct Element Code (UDEC). Figures 5.10 and 5.11 show results from this analysis. An 8 m wide room was excavated in orthogonally jointed rock mass using the Mohr-Coulomb elasto-plastic constitutive model. Attempts have been made to simulate the process of void migration by deleting those fully deformable joint bounded blocks which show excessive movement into the excavation. As the model is stepped, the area of tension progresses towards the surface and if a weak soil cover were present might result in a surface crown hole collapse. It is interesting to note the tension zone extending to the surface as shown in figure 5.10. As would be expected, due to low overburden stresses, yield is restricted, unless highly weathered weak materials are present, and failure is mainly by roof migration rather than pillar collapse.

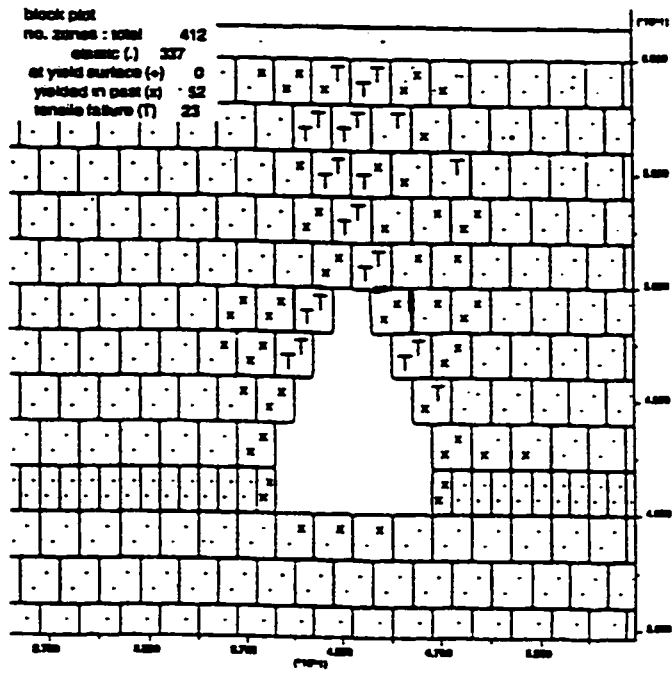


Figure 5.10. Tension zone above excavation with simulated void migration (after Stead and Benko, 1993).

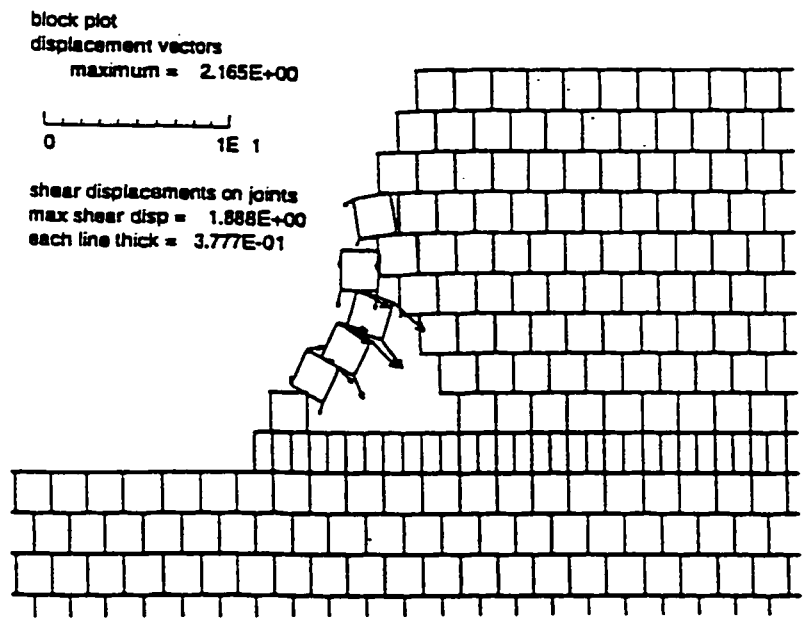


Figure 5.11. Slope face collapse due to advance of mine slope towards old workings (after Stead and Benko, 1993).

After simulation of void migration, a surface mine slope was progressively advanced towards the workings. As the distance between the slope face and the workings decreases, the tension zone increases, resulting in rockfall from the face and backward tilting of the rock blocks into the crown hole, as shown in figure 5.11. As the slope-ward side of the arch fails the vertical stress is transferred to the other side. It is at this stage that highly weathered "robbed" pillars could conceivably fail in practice, possibly leading to total failure of a bench slope.

Walton and Taylor (1977) analyzed the slope failure modes in surface coal mines as a result of former underground workings, mostly in form of room and pillar mines and ancient bell pits, as shown in figure 5.12. Based on their work, the slope failures can be classified as:

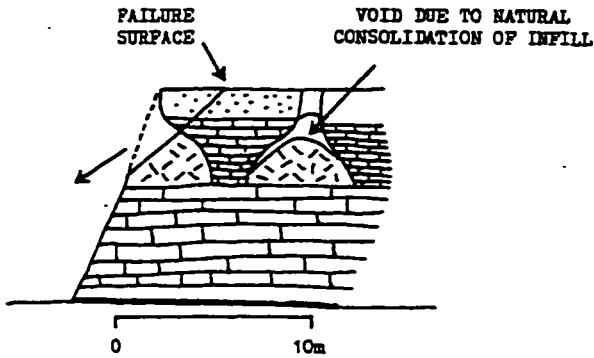
- Translational slides

These types of failure are usually connected with the ancient bell pits. Where the bell pits are located close to the ground surface, and especially where superficial deposits comprise part of the cover, undercutting of slopes can occur as shown in figure 5.12 (a). The failure surface is generally constrained to the contact between the rock and the infill. Translational slides may also result from movement along bedding planes which have been downwarped and tilted towards the apex of a migrated room void, shown in figure 5.12 (b). Some failures are plane or wedge-like in morphology as shown in figure 5.12 (c). The open-jointed overlying strata aggravate the failures, which are triggered primarily by the failure of the arch infill.

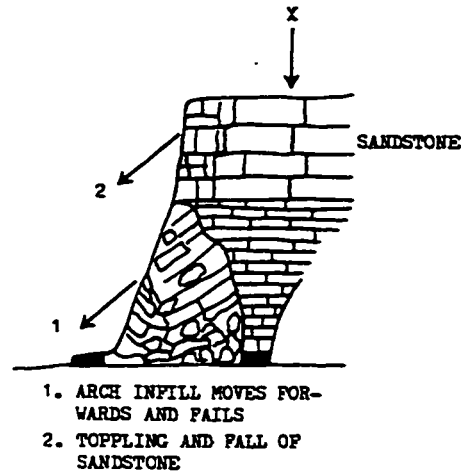
- Toppling failure

This type of failure may occur when a stronger bed overlies the arch infill that intersects a working face, as shown in figure 5.12 (d). The forward movement and collapse of infill leaves an unsupported, overhanging beam of layer in the upper part of the slope, failing in a toppling mode connected with rockfall.

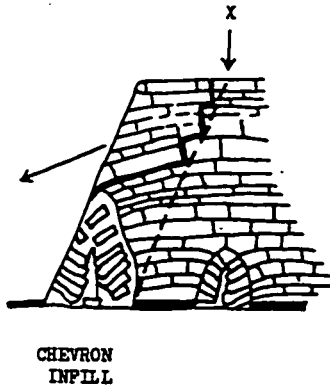
(a) SLOPE UNDERCUT BY BELL-PITS



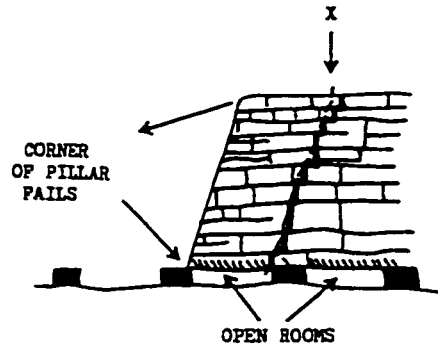
(d) TOPPLING FAILURE.



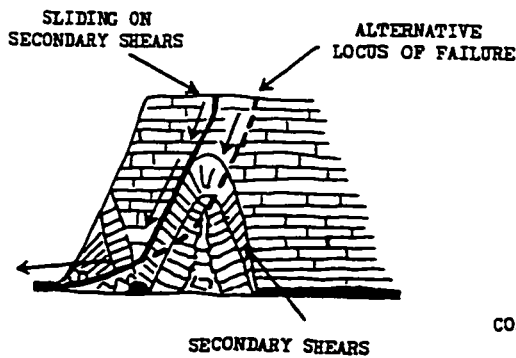
(b) SLIDING ON DOWNWARPED STRATA OVER VOID.



(e) SPAN FAILURE



(c) TRANSLATIONAL SLIDING ON SECONDARY SHEARS OR THROUGH ARCH INFILL



(f) CONTOURS OF DOWNWARDING

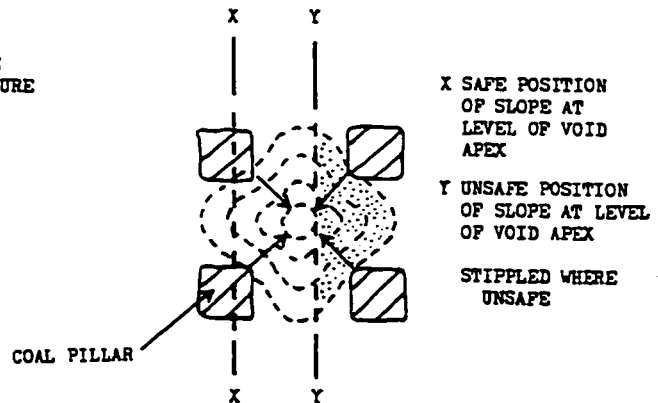


Figure 5.12. Modes of Failure of shallow Mine Workings (after Walton and Taylor, 1977).

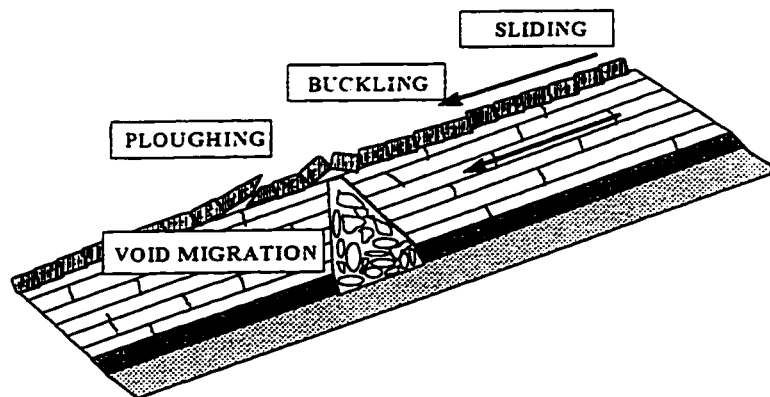
- Span failure.

This type of failure usually results from pillar collapse at the toe of the slope. The slope toe collapses into the void and the slope topples as shown in figure 5.12 (e). Raveling as well as rockfall occurs.

- Slab slides.

According to Walton and Taylor (1977) the interaction of room and pillar workings and the dip becomes important where the dips are in excess of  $18^\circ$  and the slope height greater than 25 m. Sliding on surfaces parallel to the general strata inclination is possible, accompanied with buckling or ploughing failure of the overlying layer, as shown in figure 5.13.

When the mine workings are located under the slope base there are according to Walton and Taylor (1977), generally two mechanisms of slope instability :



**Figure 5.13.** Sliding, buckling and ploughing instability due to void migration.

- Span/toppling failures.

The span/toppling failures due to room and pillar are possible if the void migration or the overbreak zone are situated beneath the slope toe. Such failures are rare in practice and result from overloading the slope toe. This type of failure may be possible also for shallow longwall mining.

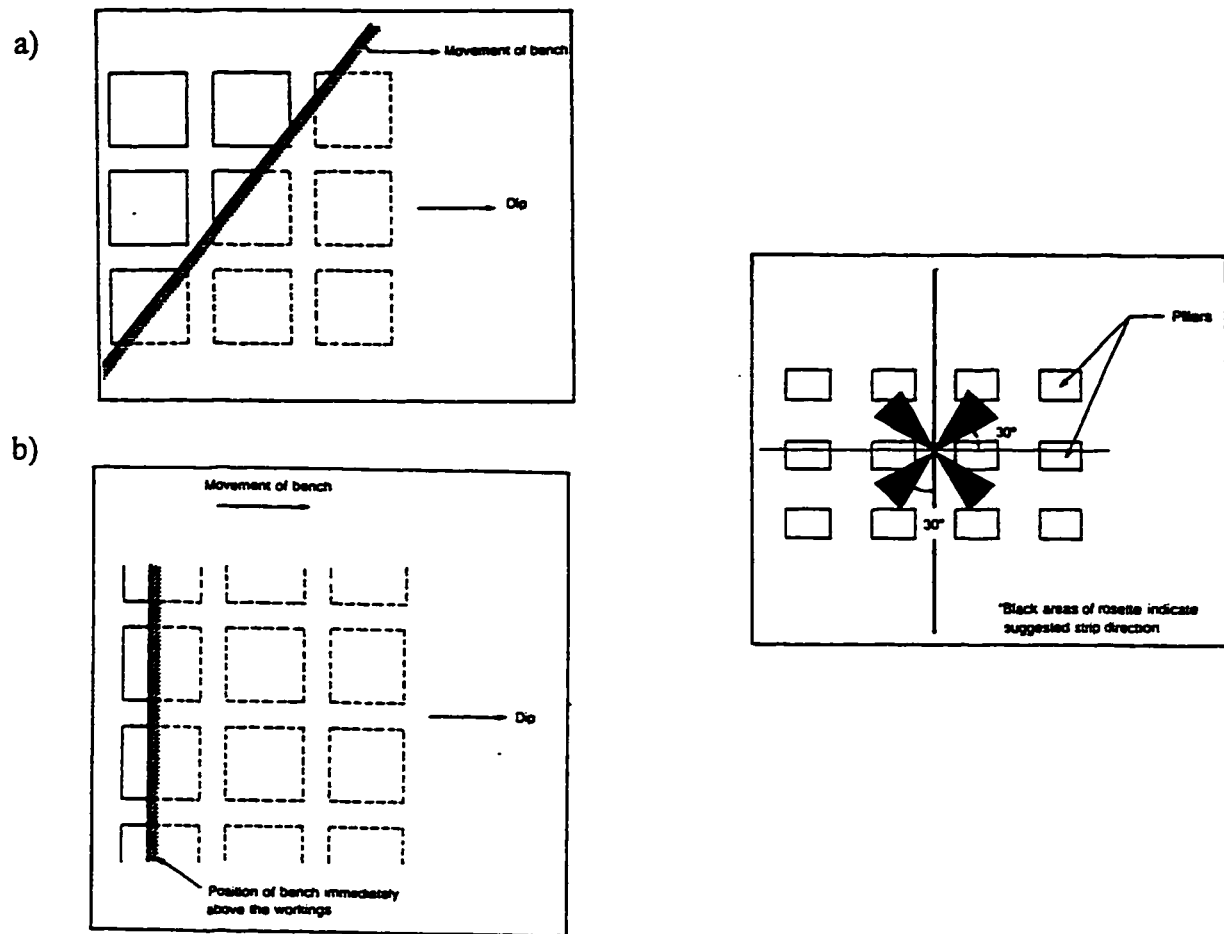
- Translation/rotational slides.

These are directly related to the subsidence effects (displacements and strains) generated by the underground mining.

The orientation of underground workings can be in its extreme position, be either normal or parallel to the slope. There can be an indefinite number of orientations between these two limits. Walton and Taylor (1977) and Morris and Clough (1986), referring to the work from Mozumdar and Atkinson, addressed the effects of the direction of mining on slope stability due to workings within the slopes.

Figure 5.14 shows the different alignments. Figure 5.14 (a) and 5.14 (b) presents the two cases addressed by Mozumdar (in Morris and Clough, 1986). Serious limitations on the continuous operation of heavy machinery were encountered when the mining method in figure 5.14 (a) was applied, due to ground caving above the workings. Therefore, the method in figure 5.14 (b) was suggested. Morris and Clough (1986) state that the principal geotechnical consideration in suggesting a particular mining direction is the nature of the underground workings. They advise that the direction should be at an angle of at least  $30^\circ$  to the direction of mining, as shown in figure 5.14 (c).

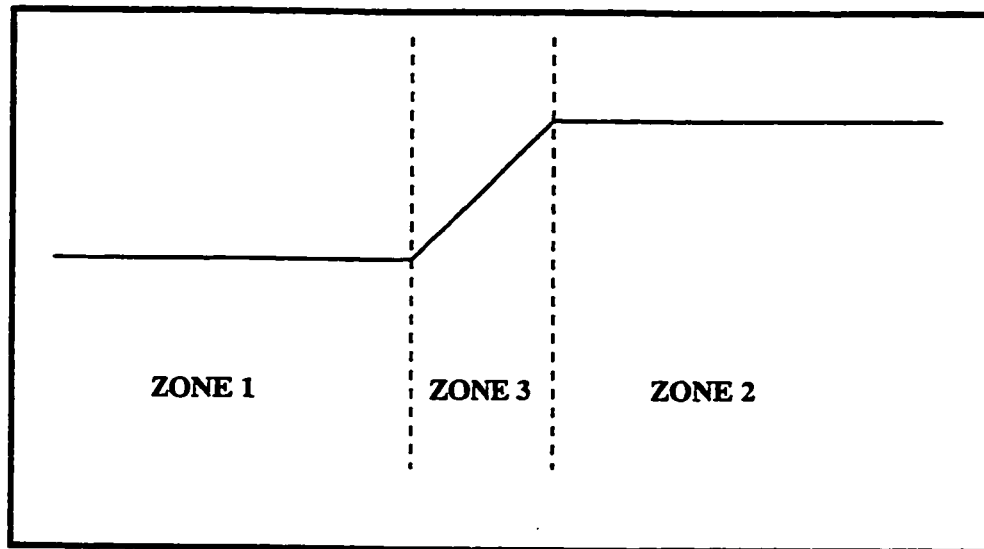




**Figure 5.14.** Relatively safe (a) and unsafe (b) direction of surface mining layout in an area of previous room and pillar mining.

### 5.3.3. Stopes, Shafts, Adits, Bell-Pits, Solution Mining and Sublevel Caving

All these mining excavations, excluding the sublevel caving, present generally localized deformation effects similar to room and pillar mining. Attention should be given to the position of the mining activity relative to the slope. Sublevel caving presents a transition between surface and underground mining, having its own characteristics. The main problem to address is the stability and the progressive development of fractures in the hanging-wall and footwall with increase in mining depth. More details are given in Hoek (1974) and Brown and Ferguson (1979).



**Figure 5.15.** Three different positions of the underground mining and slope.

#### **5.3.4. Workings on the Dip or Rise Side, Directly Underneath the Slope or in a Transient Position**

Depending on the position of the underground mining and the slope, four cases can occur, as shown in figure 5.15:

1. The underground mining is taking place a certain distance under the dip side (toe side) of the slope - Zone 1, in figure 5.15. This will involve a certain degree of movement towards the workings, depending on the distance between the slope and the workings. The geological conditions, properties of the rock/soil mass and distance to the slope will determine the nature of the deformation. The slope angle will increase, together with the tensile strain, and the local groundwater flow will be changed. Possible hydrodynamic effects must be considered. The mining will undercut the slope toe and generate a down-slope displacement. If the influenced

area is potentially unstable with a history of previous slope movements, slope failures may be reactivated. Very often the morphology of the resultant failure, however, will be not a typical for slope movement. It will lack the accumulation part, which has subsided. The resultant slope failure can have either the form of a fully developed slope movement or only the peripheral shear surfaces will be developed with very little deformation of the unstable main part. A typical example for the later case is the movement in Podhradie (Slovakia), where the main sliding mass displaced 2-3 metres with practically no damage to the houses. However, houses located on or near the peripheral shear planes experienced severe damage, as shown in figure 5.3.

2. The underground workings are taking place a certain distance under the rise side (crest side) of the slope - Zone 2, in figure 5.15. The subsidence trough will decrease the slope angle and there will be a significant change in the stress conditions. Decreasing the slope angle will generally result in an increase in slope stability. If the mining takes place too close to the slope the decrease in competence of the slope-forming material may contribute to the stability problems. Also, if the mining is too close to the slope, shear stresses in the slope will increase.
3. The underground workings are taking place directly underneath the slope - Zone 3, in figure 5.15. Deformation effects, depending on the depth to workings, will be significant. When the slope-forming material is strain-softening, as is common for the rock and soil mass, slopes in a close to limit equilibrium state may fail.
4. If the progressing underground workings are oriented normal to the slope, they will approach the slope either from the dip or rise side. Changing (transient) slope deformation will be characteristic for this type of mining. Most of the deformation will be similar to that associated with longwall mining.

### **5.3.5 Influence of Timing between Slope Excavation and Underground Workings**

From the time perspective, the slope can be either excavated in an area of previous mining activity or be undermined. Previous mining activity in an area of future slope excavation changes the stress conditions and the integrity of the rock mass. The rock mass properties in such areas will be highly altered due to the mining effects. If an existing slope is undermined the influence of the subsidence associated deformation into account. From the point of view of absolute time, Malgot et al. (1991) report that the most frequent origin of slope movements is 5 to 14 months after the mining, taking into consideration only the primary effects of undermining. This observation was derived from work in the Vtacnik Mountains in Slovakia, and is applicable therefore only to that particular regional structure.

The timing of underground mining can be harmonized so that the negative effects due to ground subsidence are minimized. The zones of tension and compression can be “superimposed” to reduce the induced strains.

### **5.3.6 Influence of Slope Angle on the Type of Deformation**

The slope angle will have an important role in determining the type of slope deformation and instability. Generally, steep slopes when undermined will show a tendency for falls and toppling modes of deformation. Steep rock slopes will be particularly sensitive to any change in ground tilt. These types of failure will be controlled by the discontinuities within the rock mass. Shallower slopes, on the other hand, will display a potential for sliding, flowing and spreading modes of failure.

### **5.3.7 Analysis of Slope Stability with Respect to the Factors generated by Underground Mining Activity**

Slope stability investigation may involve the assessment of slope instability due to mining induced deformations and stresses. One has to consider the:

- tensile stresses, the tensile strength of the rock and soil mass, and the opening of favorably oriented discontinuities
- shear stresses and the shear strength of the rock and soil mass
- changes in slope gradient
- changes in the hydrological regime, including pore pressures and hydrodynamic forces
- strain softening phenomena and decreasing shear strength
- degradation of rock mass quality
- presence of secondary slide surfaces

Using physical modelling one can directly characterize the deformation pattern and slope instability as the result of undermining. The effects and sequence of mining can be easily incorporated into the model by removing the appropriate parts of the rock mass. Although providing valuable results, a more complex analysis is required as for example that mentioned in previous section performed by Jones et al.,(1991) and Siddle et al., (1992). They combined physical modelling with numerical analysis (finite element method) and limit equilibrium method. Using the limit equilibrium approach, it becomes extremely difficult, if not unfeasible, to incorporate all the subsidence effects into the analysis.

Providing the data is available, the change in the slope angle due to undermining can be addressed quite easily. This approach can be sufficient in some areas, however, it becomes an oversimplification in others, by neglecting all the other effects caused by undermining.

## **5.4 Application of Numerical Modelling to Slope Stability Analysis Influenced by Underground Mining**

An investigation of slope deformation and instability mechanisms as a result of mining in horizontal strata at varying locations relative to a slope was investigated. A longwall mining situation was analyzed, both in the direction perpendicular and parallel to the slope. A case of longwall mining at shallow depth, as classified by Jeremic (1985), was simulated, representing an average working depth of 50 - 150 m, a length of longwall face up to 100 m and a face advance of about 500 m during its life.

The numerical modelling analysis was conducted for a 2.5 m thick seam at depth of 100 m and 60 m, with a longwall face of 100 m and a longwall advance 300 m. The rock mass was treated both, as a continuum and discontinuum.

### **5.4.1. Longwall Mining with Backfill under a Level and Slope Topography - Continuum Approach**

This section presents results of an analysis of the influence of longwall mining progressing perpendicular to the slope strike as shown in figure 5.16. The influence of mining direction relative to the slope, as well as the influence of changing overburden thickness in the slope area on the ground deformation, were investigated using a continuum method of numerical modelling. It was of particular interest to see if the direction of mining had a significant influence on slope instability, assuming all other factors constant. Therefore, the mine excavation was advanced towards the slope from both, the toe and crest side (figure 5.16). A typical longwall mining scenario with backfill was examined. The total modelled advance of the longwall was 300 m with a seam thickness of 2.5 m. The finite difference method was used for analysis, employing the FLAC code (Itasca, 1993).

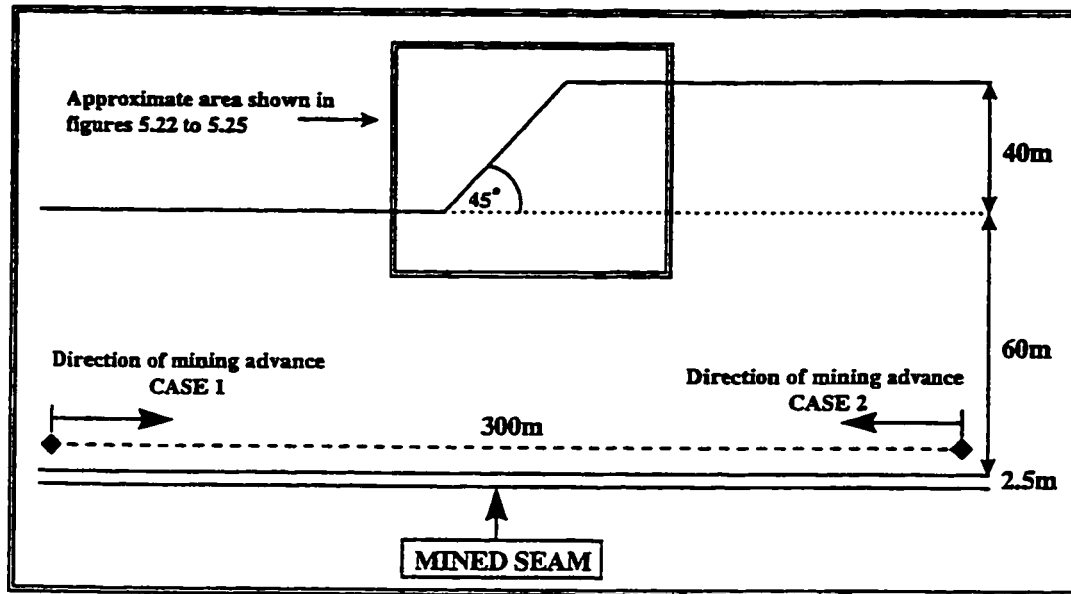
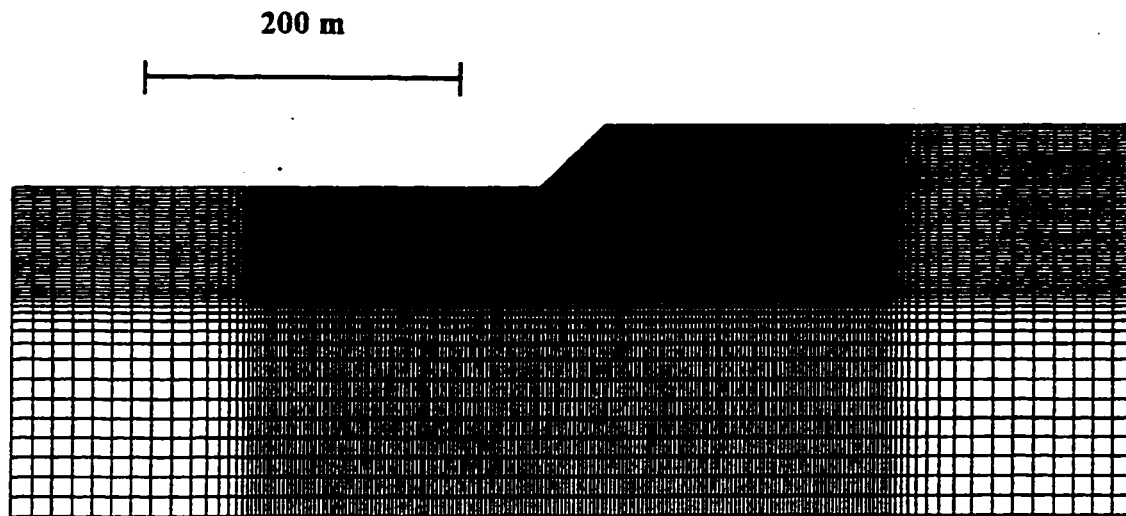


Figure 5.16. Investigation of the influence of mining direction on slope instability and deformation (sketch - not to scale).

Before the deformations for the model incorporating a slope were examined, an analysis of two models with level topography (overburden thicknesses of 100 m and 60 m) was undertaken.

#### 5.4.1.1 Geometry and Discretization of the Rock Mass

The model geometry and the finite difference grid used in the analysis are shown in figure 5.17. This particular finite difference mesh represented the case of a slope 40 m high with a 45° angle. The slope was created from an initial rectangular grid, representing the case with 100 m overburden, by removing part of the finite difference grid. The total dimensions of the model were 700 m x 250 m. For an overburden of 60 m, the upper 40 m section was removed from the model. The initial finite difference grid contained



**Figure 5.17.** Finite difference grid and geometry of model for continuum analysis of the influence of underground mining on slope stability.

11328 zones. A linearly graded numerical mesh was used with the zone aspect ratio limited to a maximum of 5:1 to avoid numerical artifacts. The largest aspect ratio was used along the outer boundaries of the model.

#### **5.4.1.2. Rock Mass Properties and Initial Stress Condition**

The elastic rock mass properties (density, shear and bulk modulus) were assumed to be uniform throughout the numerical model, and were based on typical published values for coal bearing rocks (Kulhawy, 1975; Hunt, 1986; Goodman, 1989). The middle section of the rock mass, 500 m × 150 m, was assumed to be elasto-plastic with an ubiquitous constitutive criterion. The rest of the model was linearly elastic because the failure in this part of model was not expected for the ground stresses adopted. To confirm this



decision, a model with boundaries extending an additional 150 m in each direction, as well as a case where the ubiquitous constitutive criterion was adopted for the whole model, were investigated in the initial stage of modelling.

The rock mass properties are summarized in table 5.1. The rock mass strength in the vertical direction was assumed to be higher than that in the horizontal direction, to represent the highly anisotropic character of sedimentary sequences usually encountered in coal-bearing strata.

The initial K ratio was assumed to be lithostatic ( $K=v/1-v$  or  $K=0.33$ , in this particular case). For the model incorporating a slope, excavation was performed in one step and the model allowed to come to equilibrium in the elastic deformation regime.

**Table 5.1.** Rock mass properties for continuum analysis.

DENSITY	2300 kg/m <sup>3</sup>
SHEAR MODULUS	31000 MPa
BULK MODULUS	67000 MPa
FRICTION	35°
UBIQUITOUS JOINT FRICTION	25°
COHESION	6.0 MPa
UBIQUITOUS JOINT COHESION	0.05 MPa
TENSION	0
JOINT TENSION	0
JOINT ANGLE	180° (horizontal)

### 5.4.1.3 Modelling Procedure

After the initial stress field was established, the constitutive criteria in the central part of the model (500 m × 150 m) were changed from elastic to elasto-plastic ubiquitous, with material properties as shown in table 5.1. The initial displacements in the model were reset to zero and the mining of the longwall panel simulated. The longwall excavation was performed in increments, each represented by the removal of a 5 m × 2.5 m section of the grid. The finite difference zones in the central part had dimensions of 2.5 m × 2.5 m. The void formed by the previous excavation was filled with a backfill, having properties as shown in table 5.2 (Itasca, 1993). The Mohr-Coulomb elasto-plastic constitutive criterion was assumed for the backfill.

After each excavation step, the model was cycled for a constant amount of numerical calculation steps (10000), allowing the model to reach a relative equilibrium of forces. The amount of calculations steps used was determined from previous trials, indicating that the unbalanced force dropped to a sufficiently low value (1%) from the initial model state immediately after the partial mine excavation. The drop to 1% in unbalanced forces is considered (Itasca, 1993) sufficient for indicating stabilized conditions.

**Table 5.2.** Properties for backfill

DENSITY	1800 kg/m <sup>3</sup>
SHEAR MODULUS	40 MPa
BULK MODULUS	100 MPa
FRICTION	30°
COHESION	0
TENSION	0

Histories of displacement were recorded at selected points in the model to capture the deformation development due to progressive mining. Several model stages during the excavation progress were saved and plots of the stress state, shear strain and plasticity state used, to assess the ground deformation at specific mining stages.

#### 5.4.1.4. Level Topography - 60 m Overburden

Before the investigation of potential slope instability due to undermining was undertaken, the deformations for a level topography were analyzed. Figure 5.18 shows the distribution of incremental shear strain after the completion of longwall panel excavation for the 300 m section under investigation. Only the central part of the model, is shown. The first 30 m of mining were characterized mostly by elastic deformation of the rock mass. Only a minor concentration of tensile stresses took place at the ground



**Figure 5.18.** Location of shear strain in the central part of model with level ground surface, overburden of 60 m after mining advance of 300 m.

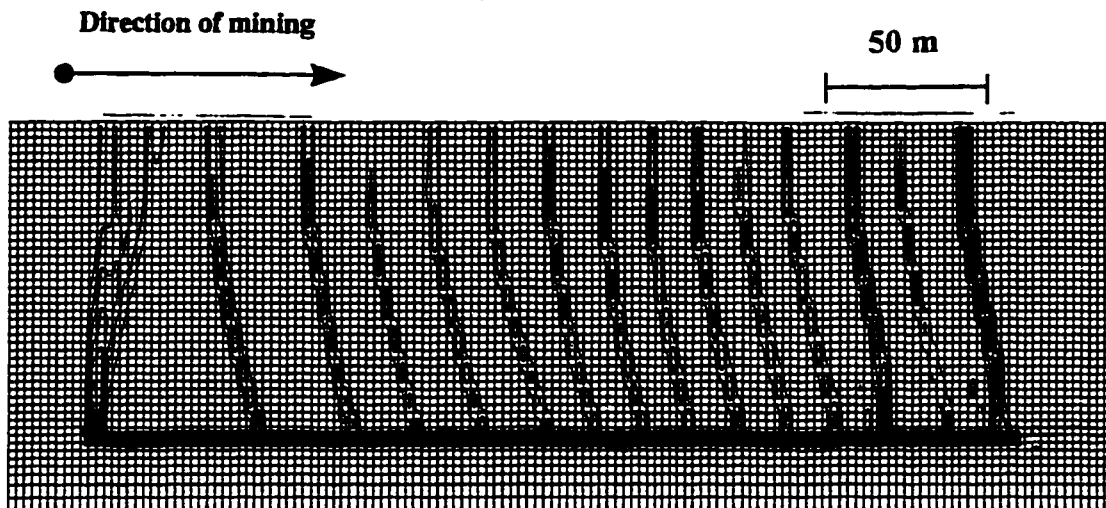
surface above the mine working. With further mining progress a fairly regular pattern of shear strain concentration (shear bands) formed in the mine overburden. The rock mass failed initially along these planes and displaced. It stabilized, however, with subsequent computational steps due to the support of the backfill material. The first apparent failure surface formed when the mining was 32.5 m from the start of the excavation. All the failure surfaces in the model were located at regular intervals, approximately 7.5 m apart, extending from the mined seam completely towards the surface.

It has to be stressed that the location of shear bands is dependent on the discretization of the rock mass and this distance (7.5 m), therefore, applies to this particular case with the assumed grid size, material properties and initial ground stresses. Nevertheless, when a model with smaller grid size was investigated for a smaller section of rock mass and changed material properties, the regularity in the shear band spacing remained.

The ground surface was affected by a major concentration of tensile failure above the place where mining started. Tension cracking could be expected to develop in this locality in the field.

#### **5.4.1.5. Level Topography - 100 m Overburden**

Figure 5.19 shows the shear strain increment at the end of mining with a 100 m overburden. Comparison with model representing a 60 m overburden (figure 5.18) demonstrates the effect of an increased overburden thickness on ground deformation for this particular mining situation. The ground behaved elastically for a longer mining distance from the start of panel excavation, and the spacing of places with incremental shear strain concentration increased. The first distinct failure surface (shear band) formed approximately 57.5 m from the place of mining start.

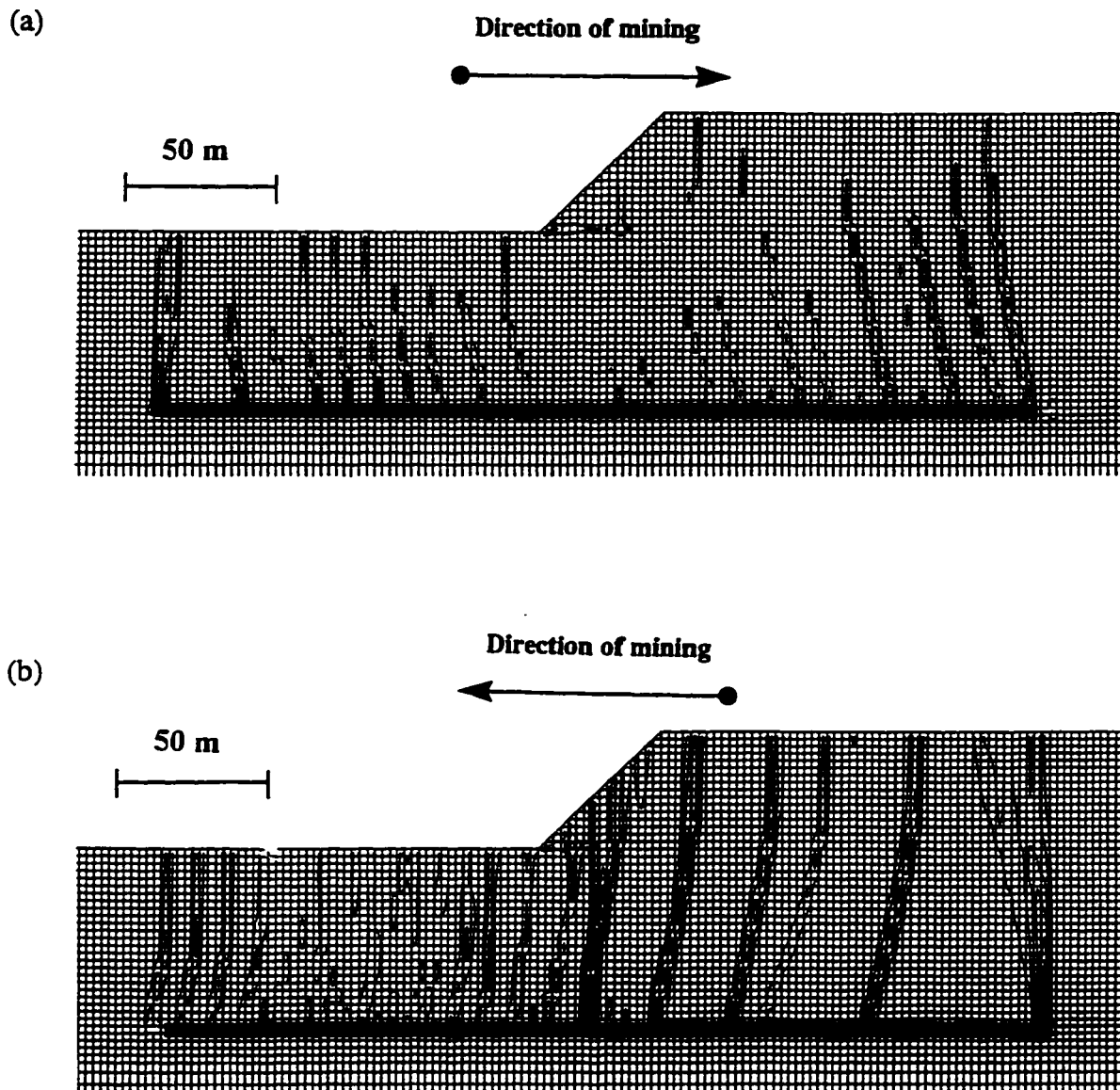


**Figure 5.19.** Location of shear strain in the central part of model with level ground surface, overburden of 100 m after mining advance of 300 m.

A relatively small total subsidence (a total of 0.035 m vertical and 0.02 m horizontal for 60 m overburden, and 0.06 m vertical and 0.02 m horizontal for the 100 m overburden) was achieved for both cases. The total displacement is, in this case, largely dependent on the backfill properties. Nevertheless, a pronounced change in the ground stresses, rock mass properties and groundwater conditions will result. This is of particular interest, because any surface excavation in such ground may experience unexpected stability problems.

#### 5.4.1.6. Slope Topography - Longwall Mining Approaching Slope from the Toe and Crest Side.

Simulation of the mining in the model took place from both sides of slope, as shown in figure 5.16. Figure 5.20 (a) and (b), shows the location of incremental shear strain after the mining simulation was completed.

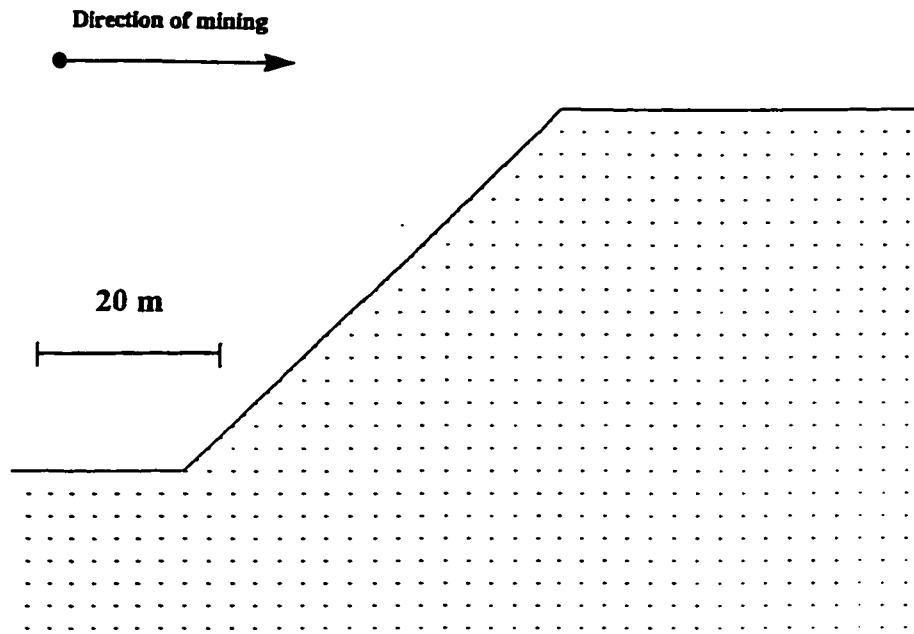


**Figure 5.20.** Location of shear strain concentration in the central part of model with slope after mining advance of 300 m, (a) mining approaching from the toe side, (b) mining approaching from the crest side.

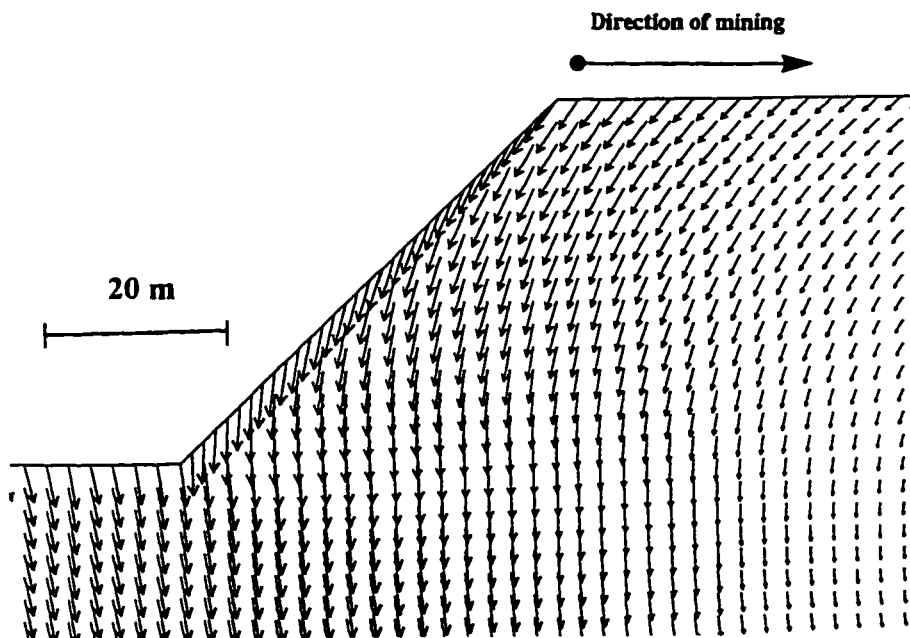
- For mining approaching slope from the toe side, the predicted deformations in the first approximately 150 m of longwall advance were practically identical to deformations with a level topography and 60 m overburden. Relatively regular concentration of incremental shear strain developed with an enlarged zone above the location where mining began. The excavation of the next section, approximately 80 m, showed the influence of the slope on the deformation pattern. No persistent shear strain concentration developed when mining took place under the slope. Shearing was observed in the slope toe along the horizontal joints (implicit) represented by the ubiquitous constitutive criterion. When mining was approximately 60 m from the slope crest another through-going shear band developed. The shear displacement in the slope gradually increased, forming a triangular shaped wedge in the lower part of slope. The shorter sides of this triangular wedge were approximately 25 m long. The development of such shearing surfaces presents lower and rear surfaces of weakness which may allow for slope failure initiation.
- The longwall mining approaching the slope from the crest side, shown in figure 5.20 (b), demonstrated the influence of mining direction on deformation within the slope. The first approximately 130 m of excavation were almost identical to a level topography and 100 m overburden thickness (figure 5.19). When the mining approached the slope in the next excavation stage, a gradual change in the deformation pattern was observed. Shearing occurred in the slope area predominantly in the vertical direction. The shearing occurred in a wider zone, indicating potential problems with a decrease in competency of the slope-forming material. The last 130 m of mining advance were characterized by deformations similar to those for a level ground surface and 60 m overburden thickness. The deformations in the slope area are more extensive in this case, as opposed to the model with mining advance from the toe.

The deformations induced in the slope area itself are shown in the form of displacement and stresses in figures 5.21 to 5.24. The area shown in these figures is outlined in figure 5.16. Initial principal stresses in the slope, before mining, are shown in figure 5.25.

(a)



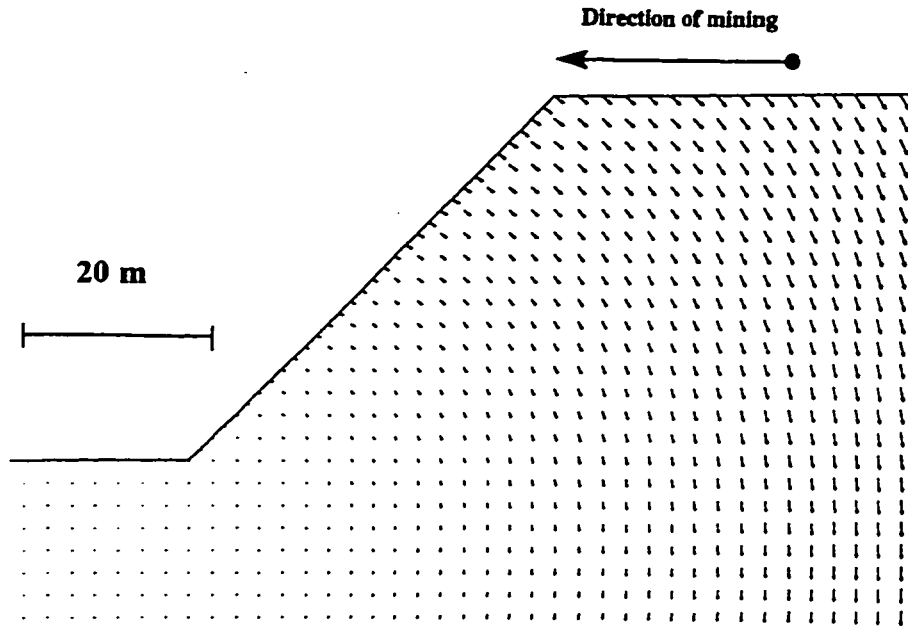
(b)



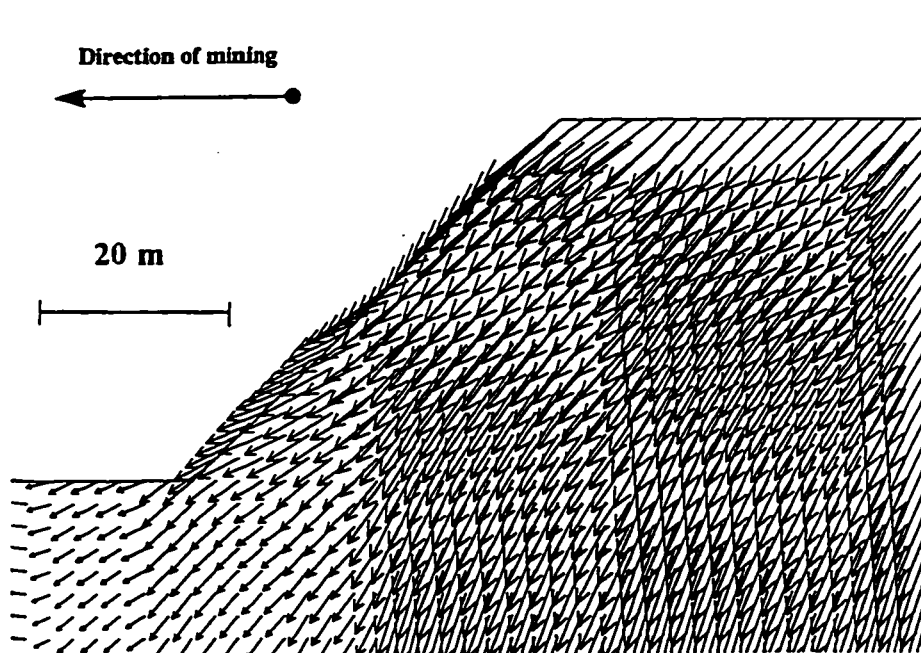
**Figure 5.21.** Displacement vectors in slope area for mining approaching and undergoing slope from the toe side. Mining 30 m left from toe (a), mining 30 m right from crest (b).



(a)

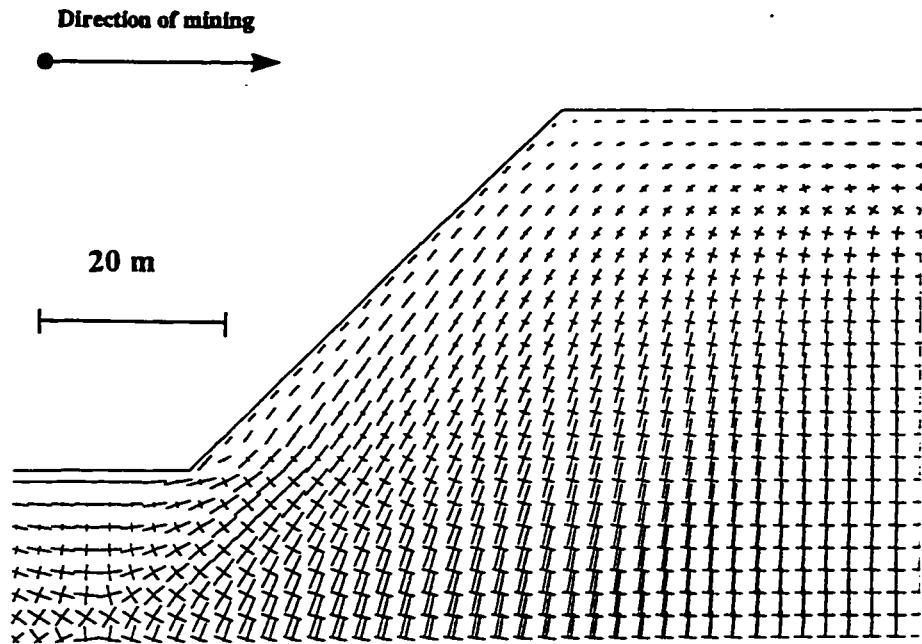


(b)

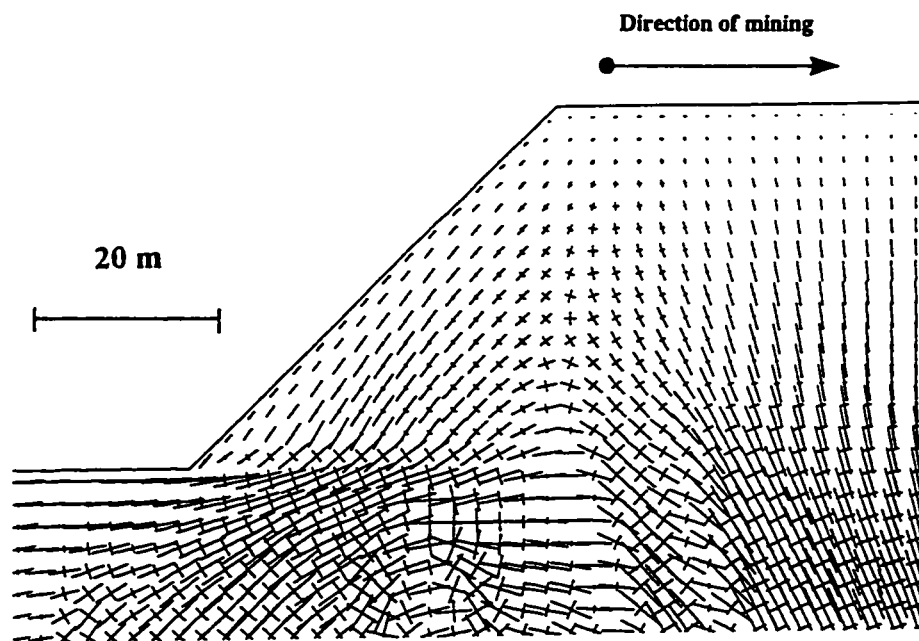


**Figure 5.22.** Displacement vectors in slope area for mining approaching and undergoing slope from the crest side. Mining 30 m right from crest (a), mining 30 m left from toe (b).

(a)

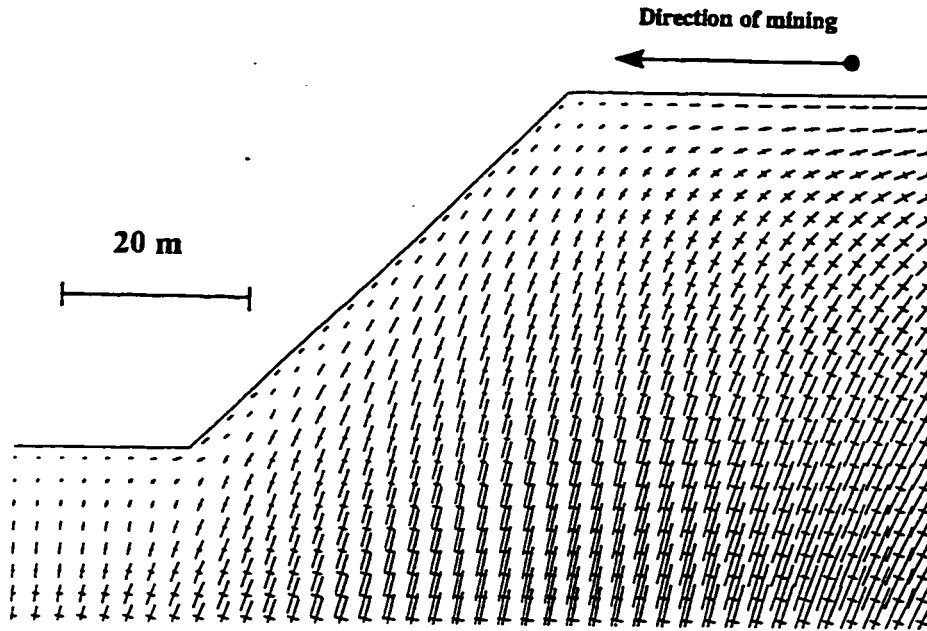


(b)

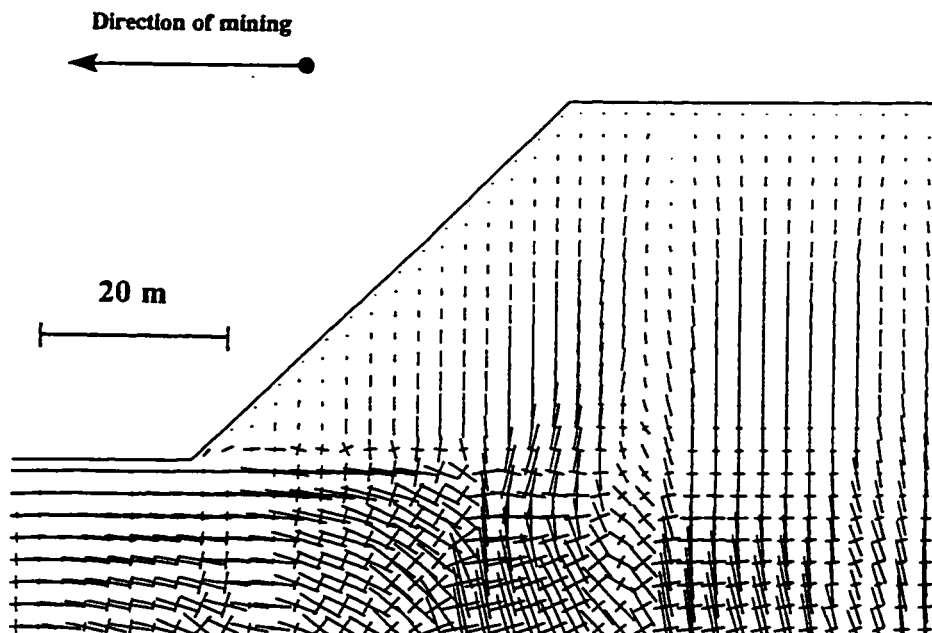


**Figure 5.23.** Principal stresses in slope area for mining approaching and undergoing slope from the toe side. Mining 30 m left from toe (a), mining 30 m right from crest (b).

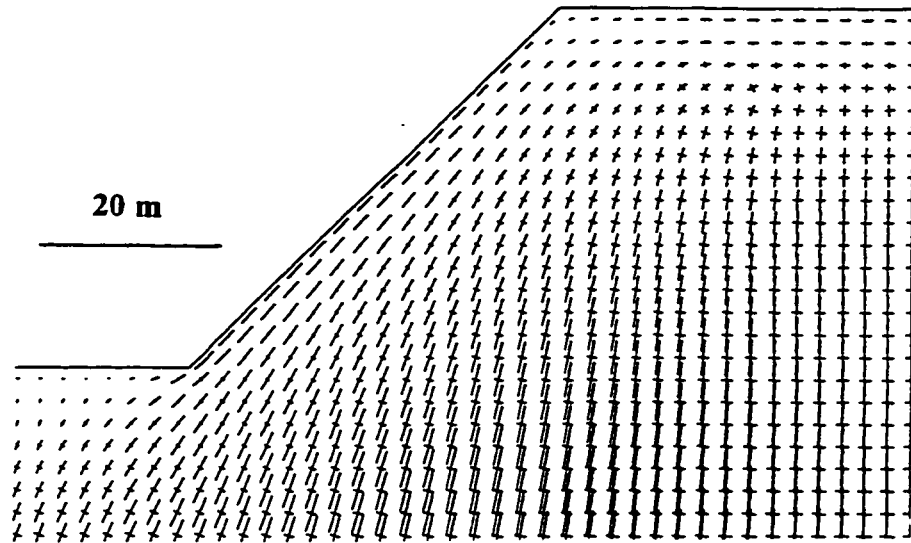
(a)



(b)



**Figure 5.24.** Principal stresses in slope area for mining approaching and undergoing slope from the crest side. Mining 30 m right from crest (a), mining 30 m left from toe (b).



**Figure 5.25.** Initial, pre-mining, principal stresses in slope. Maximum value 1.2 MPa.

- When mining approaches the slope from the toe side, and is 30 m left from the slope toe, no displacements are mobilized in the slope area itself (figure 5.21a). Minimal influence on the original stress field in slope is observed (figure 5.23a). Rotation of the principal stresses takes place approximately 15 m under the slope toe. It is of interest that after the slope was undermined (figure 5.21b), a horizontal component of displacement in the out-of-slope direction is present. Towards the base of slope, the displacement vectors gradually rotate and point either in the vertical direction or towards the present mine opening, located already 30 m behind the slope crest. The principal stresses in and under the slope become largely affected by undermining. Shearing takes place along the base of slope following the horizontally dipping joints (ubiquitous constitutive criterion).

- When mining approaches the slope from the crest side, and is 30 m right from the slope crest, displacements in the slope area are mobilized, they point, however, towards the approaching excavation (figure 5.22a). Once the mining passes the slope, relatively large (compared to other cases) displacements are present. The lower half of slope has a clear out-of-slope displacement component. Stresses for this stage are shown in figure 5.24 (a) and (b). Figure 5.24 (a) shows a rotation of principal stresses approximately 20 - 30 m inside the slope. The stress field shown in figure 5.24 (b) shows a large disturbance of the original stresses in slope.

It has to be emphasized, that the predicted deformations apply to this particular model with the assumed material properties for the host rock mass and backfill. Two different situations resulted. In the case when mining approached the slope from the toe side, the concentration of shear strain indicates a potential development of rear and bottom release surfaces in the model (figure 5.20a). If existing lateral release surfaces were present, or formed due to mining induced deformation, a relatively large slope failure could result. The cross-sectional area is approximately 312.5 m<sup>2</sup> with the total volume dependent on the lateral release surfaces. In the case when mining approached the slope from the crest side, large deformations in the slope area resulted with an out-of-slope direction of displacement. This would lead to an overall decrease in the rock mass quality of the slope-forming material and may result in an extensive failure.

### **5.4.2 Influence of Longwall Panel Location on Slope Deformation - Mining Parallel to Slope Strike - Discontinuum Approach**

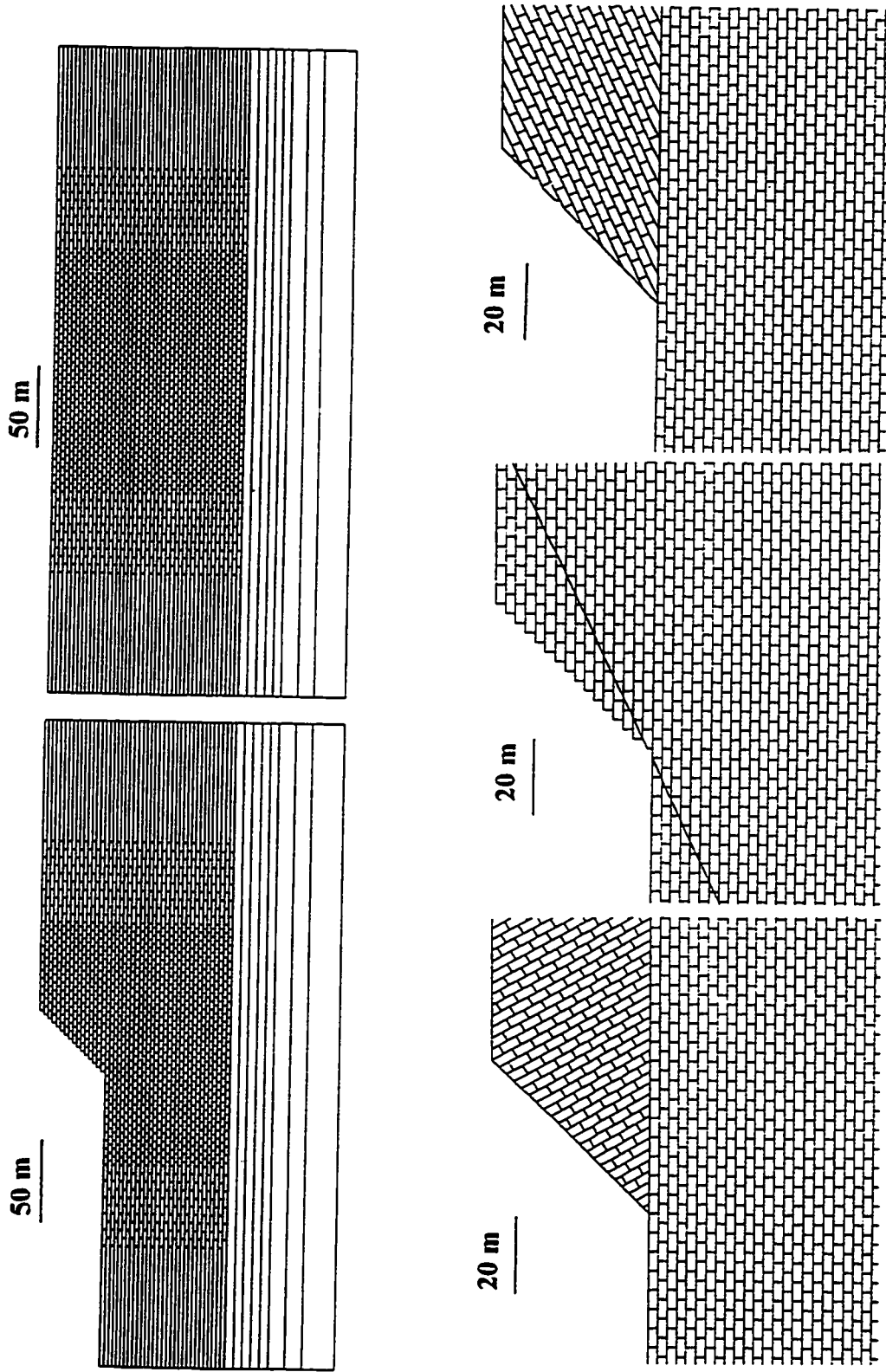
The influence of underground mining in the form of panel extraction on slope stability was investigated with the distinct element method (UDEC). A situation where mining takes place close to the slope and the panel centerline intersects the slope in three different locations was investigated. The analysis was performed using three models, as shown in figure 5.26. For Model 3 only the central part of the model is shown in this figure.

#### **Model 1 - Level Topography**

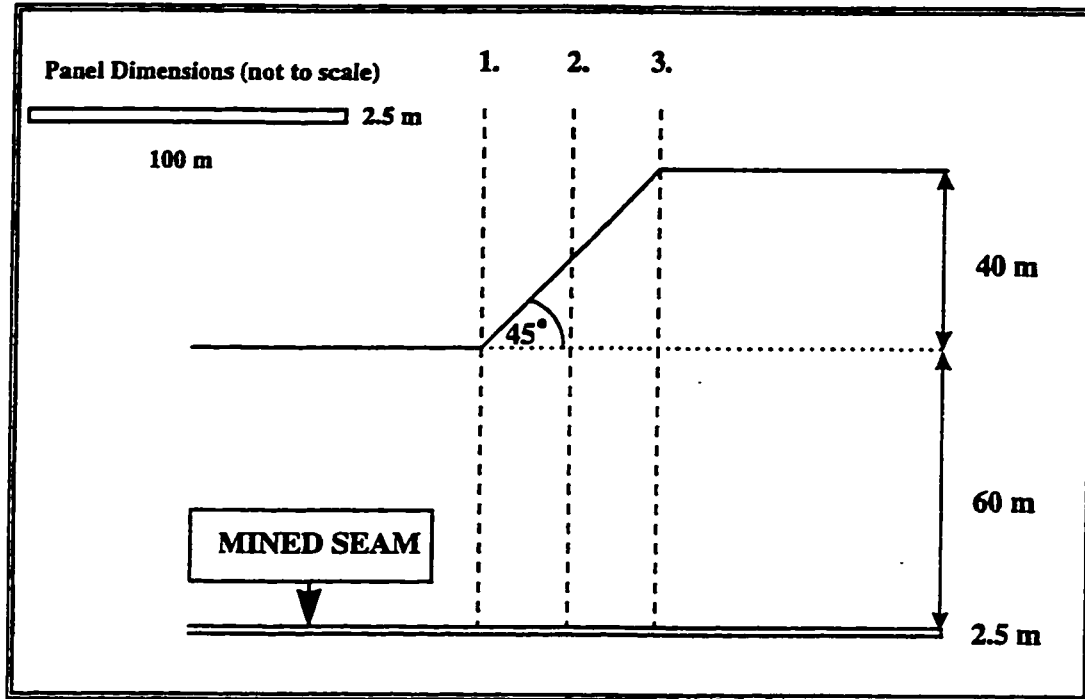
The influence of overburden thickness, rock mass properties, joint spacing and constitutive criterion was investigated, assuming level topography. Overburden thicknesses of 100 m and 60 m were analyzed. The influence of gravitational ( $K=v/1-v$ , where  $v$  is the Poisson ratio) and tectonic ( $K=3$ ) in-situ stress fields on rock mass deformation mechanisms were also studied. Model 1 also compares the qualitative and quantitative aspects of subsidence movement predicted from the numerical modelling with empirical results derived from the Subsidence Engineer's Handbook (1975). A single panel extraction is analyzed and the type and extent of deformation are investigated.

#### **Model 2 - 40 m high, 45° angle slope**

The influence of panel extraction beneath a 40 m high, 45° slope was analyzed. The location of the extracted panel under the slope was changed in order to examine the effect on slope deformation. The three positions of the panel assumed in the analysis are shown in figure 5.27. Analysis was performed for models with two different types of joint spacing, based on results from Model 1. The rock mass deformation, change in the ground stress, and the extent and type of influence of mining on slope deformation were examined.



**Figure 5.26.** Distinct element models used to investigate the influence of panel location on slope instability and deformation.



**Figure 5.27.** Slope geometry and three different positions of mined panel centerline relative to the analyzed slope. Panel dimensions are 100 m x 2.5 m. 1,2,3 - refer to different positions of mined panel centerline to the slope (1-under the slope toe, 2-under the mid-height of slope, 3-under the slope crest)

**Model 3 - 40 m high, 45° angle slope with variable geological structure**

This model investigates three different types of geological structure with respect to slope stability and longwall panel extraction. The joint orientation in the slope was changed to allow for a development of slope failure. Two basic modes of instability are investigated, planar sliding and toppling. The location of the excavated panel was changed, as in Model 2.



#### **5.4.2.1 Model 1 - Level Topography**

Although there have been numerous applications of numerical modelling to the analysis of panel extraction under a level topography, this case was analyzed first to provide a base case for comparison, before the analysis of a sloping topography was undertaken. The main objective was to have a model where the slope will be influenced by a subsidence magnitude corresponding to field situation. An overburden thickness of 100 m and 60 m was assumed, resulting in w/h ratios (w-panel width; h-depth of the panel) of 1.0 and 1.66, respectively. The 60 m and 100 m overburden thicknesses represent the toe and crest overburden after the excavation of a 40 m high slope in the subsequent analyses (Models 2 and 3). Empirical data compiled from numerous field observations (Subsidence Engineers' Handbook; 1975) allow predictions of the magnitude of the maximum subsidence movement. For the case w/h=1.0 the maximum subsidence totals 84% of the extracted seam height and for w/h=1.66 the amount is 90%. For the case under investigation with seam height of 2.5 m, this data result in 2.1 m and 2.25 m of subsidence movement, respectively. Coulthard and Dutton (1988), using the same numerical codes (UDEC and FLAC), emphasized the problem of achieving accurate quantitative results in numerical subsidence calculations. They demonstrated, however, satisfactory results in illustrating the qualitative character of subsidence profiles. Unrealistically low physical property values seemed to be necessary to achieve subsidence equivalent to field measurements.

The main controlling factor in mining-induced subsidence movement is the rock mass characteristics, including the deformation and strength of intact rock material and the slip and separation along discontinuity planes in the roof strata. The coal-bearing formations are usually orthogonally jointed, with horizontal bedding planes. Such a discontinuous rock mass was represented with the UDEC code. A "brick-type" pattern formed by continuous horizontal joints, the bedding planes, and two sets of discontinuous vertical joints was used, as shown in figure 5.26.

In the initial stage, a 2.5 m bedding thickness was assumed in the upper 115 m of model. The spacing of vertical joints in the central portion of the numerical model was set to twice the bedding thickness, resulting in blocks of 5 m x 2.5 m. The rock mass in the lower part of model and towards the outer model boundaries was represented using larger blocks because displacements in this part are of limited importance in predicting subsidence. The block rounding was assumed to be 1% of the block length. A rectangular part of rock mass 400 m x 180 m (400 m x 140 m for case with 60 m overburden) was analyzed. The right and left model boundaries were fixed in the horizontal direction and the base of the model was prevented from moving vertically. Fully deformable blocks with elastic isotropic constitutive criterion were used. The joints were assumed to have only frictional resistance. The initial input material and joint properties are summarized in table 5.3.

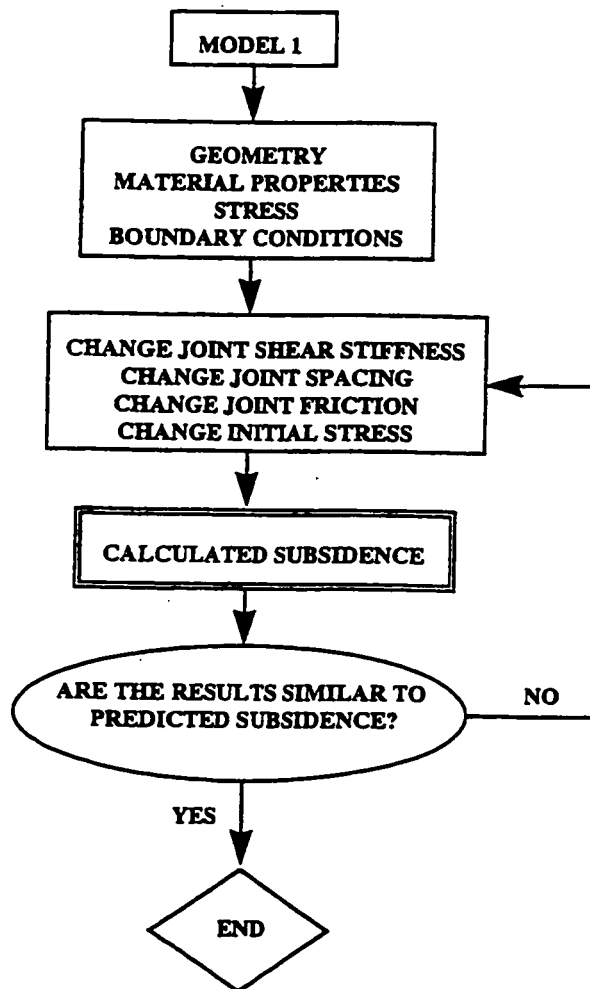
The numerical model set-up used was the same for both overburden thicknesses. The ground stresses were initiated with corresponding gravitational acceleration, boundary conditions and material properties assigned and the model examined for initial equilibrium. The panel was then excavated in one step and several history points for monitoring the vertical and horizontal displacement were placed on the surface at 5 m intervals. The results were analyzed and compared to the empirical subsidence data from the Subsidence Engineers' Handbook; (1975). If large differences were noticed, the material properties and/or joint spacing was changed until satisfactory results were obtained. The concept of the analytical procedure is shown in figure 5.29.

The results from the initial model run and the comparison with the empirical results from Subsidence Engineers Handbook (SEH) revealed that:

- Calculated maximum subsidence was in reasonable agreement with the predicted subsidence for overburden thickness of 60 m. Values in the interval of 75 -78% from the predicted were achieved

**Table 5.3.** Initial material properties for blocks and discontinuities

BLOCKS		DISCONTINUITIES	
Density	2300 kg/m <sup>3</sup>	Normal Stiffness	100 Gpa/m
Shear Modulus	3.1 Gpa	Shear Stiffness	10 GPa/m
Bulk Modulus	6.7 Gpa	Friction	25°
		Cohesion	0
		Tension	0
		Dilation	0

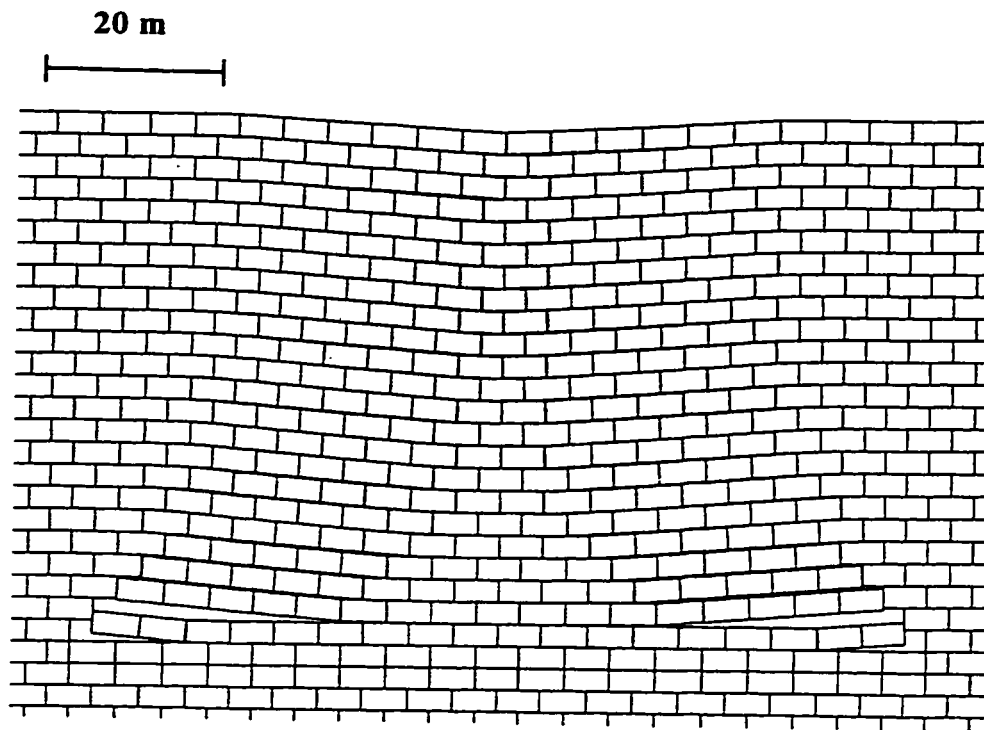


**Figure 5.28** Schematic illustration of numerical modelling procedure for Model 1. \*SEH - Subsidence Engineers Handbook (1975).

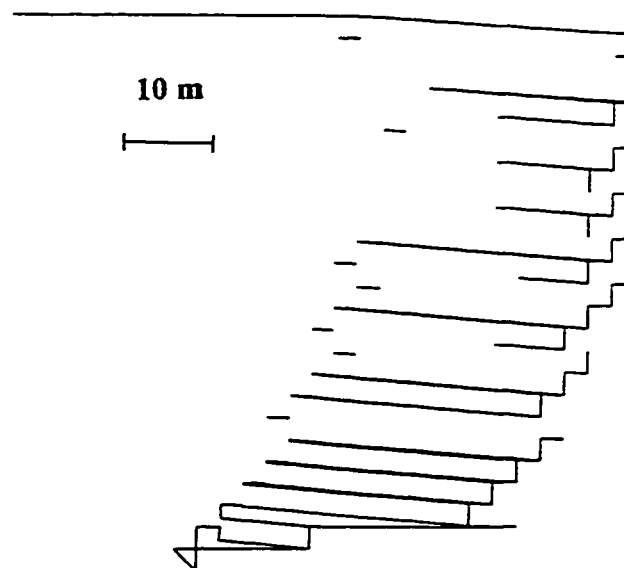
- Calculated maximum subsidence for overburden thickness of 100m was very low- only about 13% from the predicted subsidence;
- The different initial stress ( $K=0.33$  and  $K=3$ ) did not show a significant change in the calculated maximum subsidence; the SEH does not take into account different ratios of ground stresses;
- In both cases, 60 m and 100 m overburden, a complete closure of the excavation was achieved due to bedding plane separation and the slip on vertical cross joints;
- Comparisons between the present numerical modelling results and published results (Whittaker and Reddish, 1989) based on empirical and physical modelling, showed that UDEC duplicated the qualitative roof behavior with reasonable agreement;
- For the overburden of 60 m subsidence effects on ground were concentrated in an area of 30 m from the panel centre, and for 100 m overburden approximately 44 m from the centre;
- The maximum horizontal displacement at the ground surface resulting from subsidence was only 0.01 m for 100 m overburden and 0.06 m for 60 m overburden.

The deformation associated with subsidence of the ground surface for model with 60 m overburden is shown in figure 5.29. A subsidence trough developed above the panel, with maximum vertical displacement above the panel centre. Figure 5.30 demonstrates the opening of joints and bedding plane separation over edge of the panel for the same model.

After summarizing the results from this initial modelling, it was realized that the result for overburden of 100 m did not provide the subsidence equivalent to empirical results and, therefore, will not fully influence the slope analyzed in Model 2. A situation like this may, however, be representative for a ground with a more competent layer near the ground surface, largely influencing the ground deformations.



**Figure 5.29.** Deformation associated with subsidence of the ground surface for model with 60 m overburden



**Figure 5.30.** Opening of joints and bedding plane separation over edge of the panel for model with 60 m overburden

Considering previous published results on UDEC application to subsidence, for example Coulthard and Dutton (1988), the following approach was used:

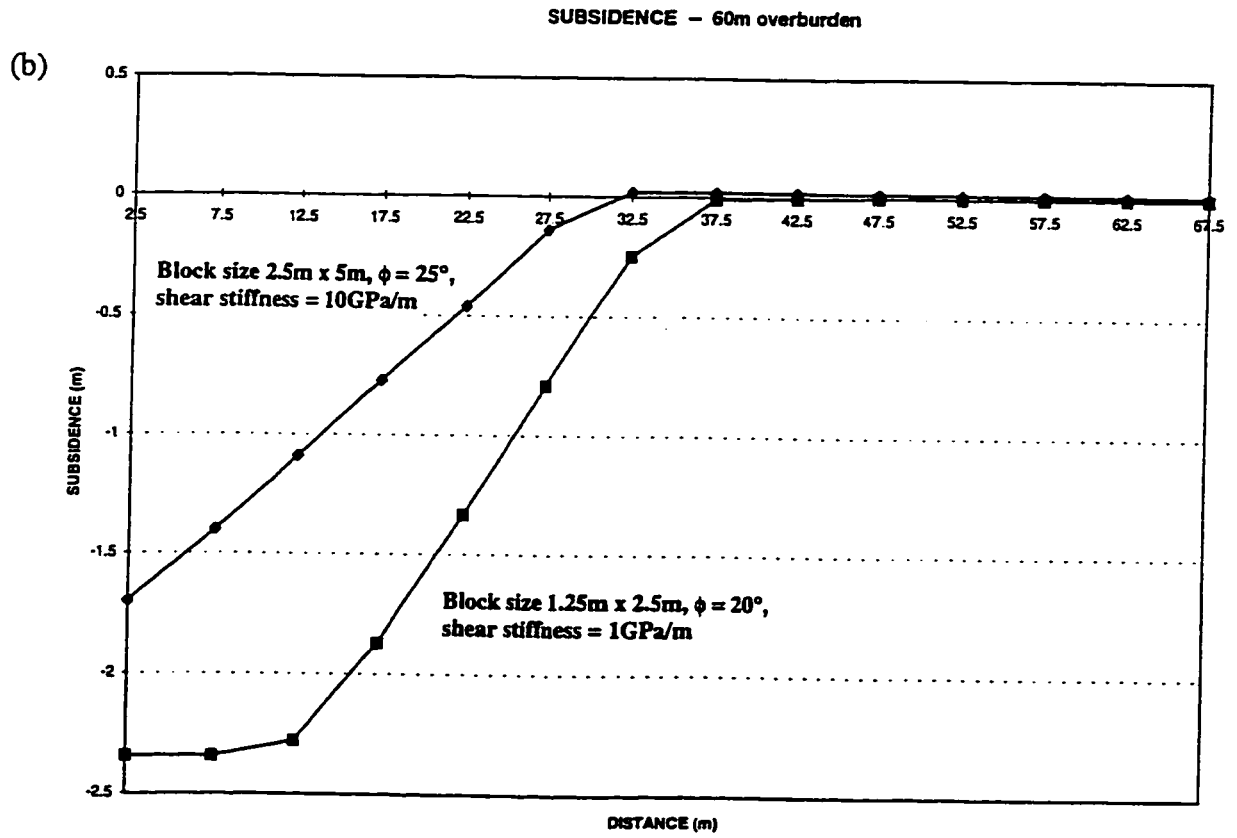
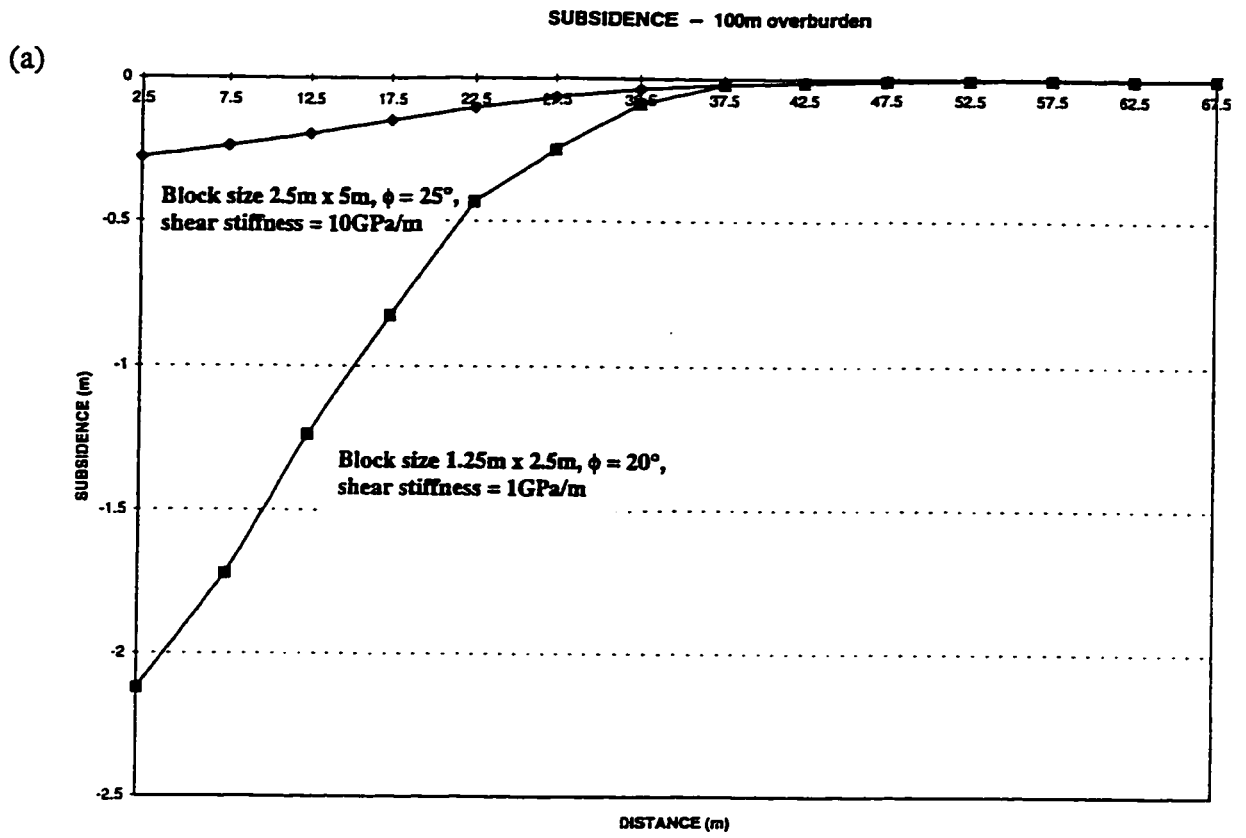
- A model with same block size was run again with a decreased joint shear stiffness to allow for more shear displacement along the joints
- A new model was constructed with blocks half the size (2.5 m x 1.25 m) of that in the initial model (5 m x 2.5 m), and the joint shear stiffness and joint friction changed to investigate the influence on subsidence magnitude. The influence of discretization of the fully deformable blocks was also investigated.

The modelling concentrated on the case with 100 m overburden and K ratio equal to  $\nu/1-\nu$ . The extent of these parametric studies for a model with block size 2.5 m x 1.25 m, was limited by the large size of the model. A total of 5136 deformable blocks had to be used, resulting in large requirements on data storage and processing speed. Considering the time that this model run required to converge, an Ultraspac 170E workstation was needed to obtain results in a reasonable time period. This was available only in the last month of the research. The results from these runs are summarized in table 5.4. The subsidence profiles for the results are shown in figure 5.31. Only results for half the panel are shown due to the model symmetry.

**Table 5.4.** Summary of results for mining subsidence with overburden thickness of 100 m and 60 m.

	OVERBURDEN 60m	OVERBURDEN 60m	OVERBURDEN 100m	OVERBURDEN 100m
Initial ground stress	K = 0.33	K = 3	K = 0.33	K = 3
Maximum predicted subsidence above panel centre (SEH)*	2.25m	2.25m	2.1m	2.1m
Maximum subsidence (block 2.5m x 5m, $\phi=25^\circ$ , $K_s=10$ GPa/m)	1.70m – 75.6%	1.75m – 77.8%	0.28m – 13.3%	0.27m – 12.9%
Maximum subsidence (block 2.5m x 5m, $\phi=25^\circ$ , $K_s=1$ GPa/m)	--	--	0.34m – 16.2%	--
Maximum subsidence (block 1.25m x 2.5m, $\phi=25^\circ$ , $K_s=10$ GPa/m)	--	--	0.80m – 38.1%	--
Maximum subsidence (block 1.25m x 2.5m, $\phi=20^\circ$ , $K_s=10$ GPa/m)	--	--	1.10m – 52.4%	--
Maximum subsidence (block 1.25m x 2.5m, $\phi=20^\circ$ , $K_s=1$ GPa/m)	2.34m – 104%	--	2.10m – 100%	1.80m – 86%

\* SEH - Subsidence Engineer's Handbook (1975).



**Figure 5.31.** Subsidence profiles for 100 m overburden (a) and 60 m overburden (b) for models with different block size, friction and joint stiffness.

The different initial ground stress conditions did not show a significant change in the maximum subsidence movement for the larger blocks (5 m x 2.5 m). For smaller blocks (2.5 m x 1.25 m) and smaller friction and shear stiffness, less subsidence for K=3 was achieved, as demonstrated in table 5.4. A more comprehensive analysis is required, however, before any conclusions can be drawn on the influence of horizontal stresses on the maximum subsidence. The shear displacement along the horizontal joints extended further into the rock mass for the higher horizontal stress level and became more limited on the vertical joints. Comparison with empirical data shows a better agreement for the lower overburden thickness (table 5.4).

#### **5.4.2.2 MODEL 2 - 40 m high, 45° angle slope**

This model investigates the interaction between the panel extraction and a single slope, 40 m high, inclined at 45°. The main purpose was to demonstrate the effect of underground mining on the induced slope deformation and to discuss the potential modes of slope instability. The influence of slope on the rock mass deformation as a consequence of coal seam extraction is generally due to the changing overburden thickness and altered stress conditions caused by slope formation.

Only the gravitational ground stress level was used in this analysis. The location of the panel relative to the slope was changed, to investigate the "worst case" situation. The panel was placed in three different positions, with its centerline intersecting the toe, crest and the mid-height of the slope.

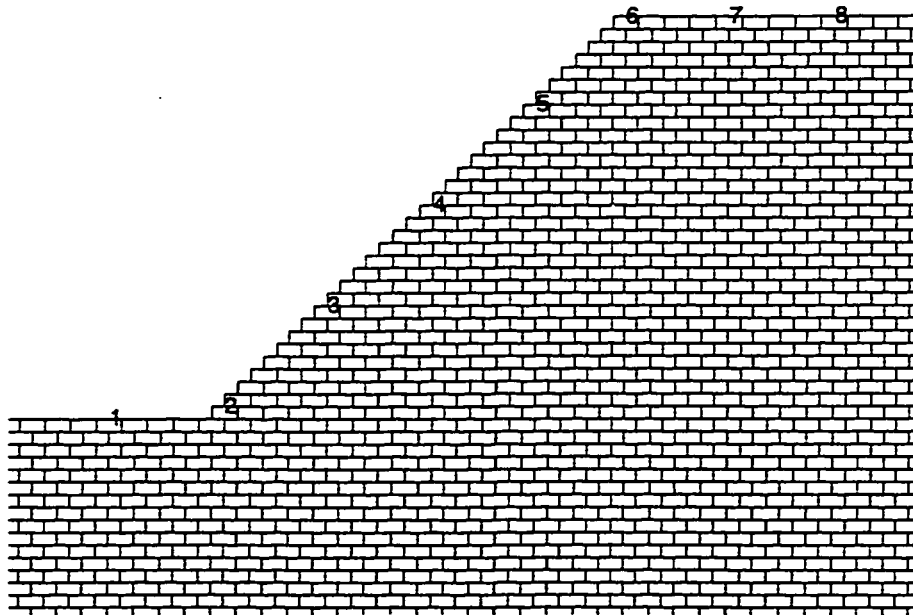
Based on the results from Model 1 analysis, a distinct element model with block size 2.5 m x 1.25 m was used. Initially, the same model as for the level topography assuming a 100 m overburden was used. The slope was excavated in four consecutive steps, each representing the removal of a 10 m thick layer of blocks. After each step, the model was allowed to deform only elastically. The final model geometry after the slope excavation is



shown in figure 5.26 (this figure shows the model when larger blocks were used - 5 m x 2.5 m). This state was saved as a "root model" and all further analysis was performed by simply restarting this model and excavating the panel.

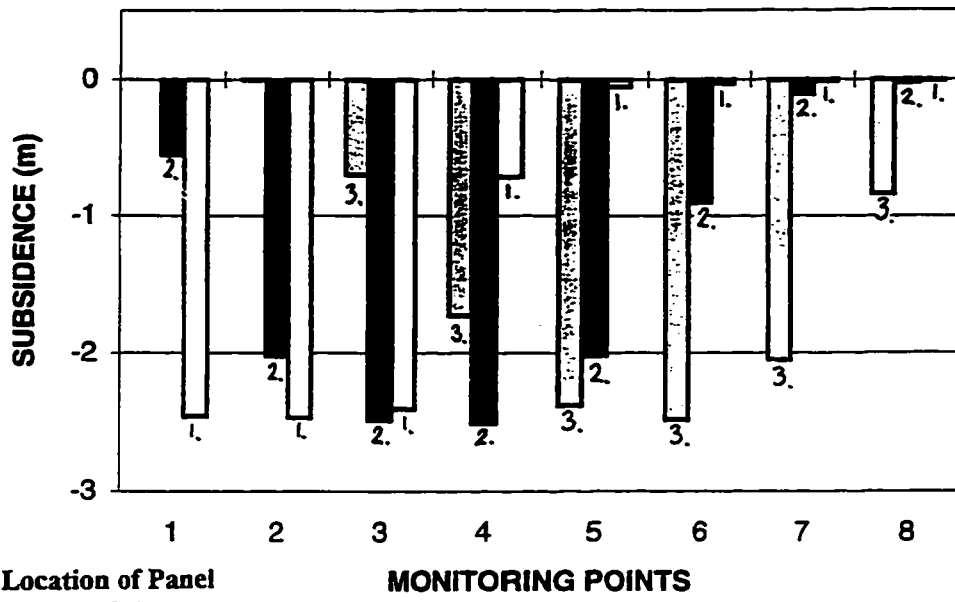
Figure 5.32 shows points at the ground surface that were selected for displacement monitoring. The displacement results are shown in graphical form in figure 5.33. Figures 5.34 to 5.39 present the contours of horizontal displacements and shear on joints in the slope area, resulting from panel extraction in different positions relative to slope.

The horizontal component of displacements increased significantly, both in extent and magnitude, when compared to case for level ground surface. The out-of-slope



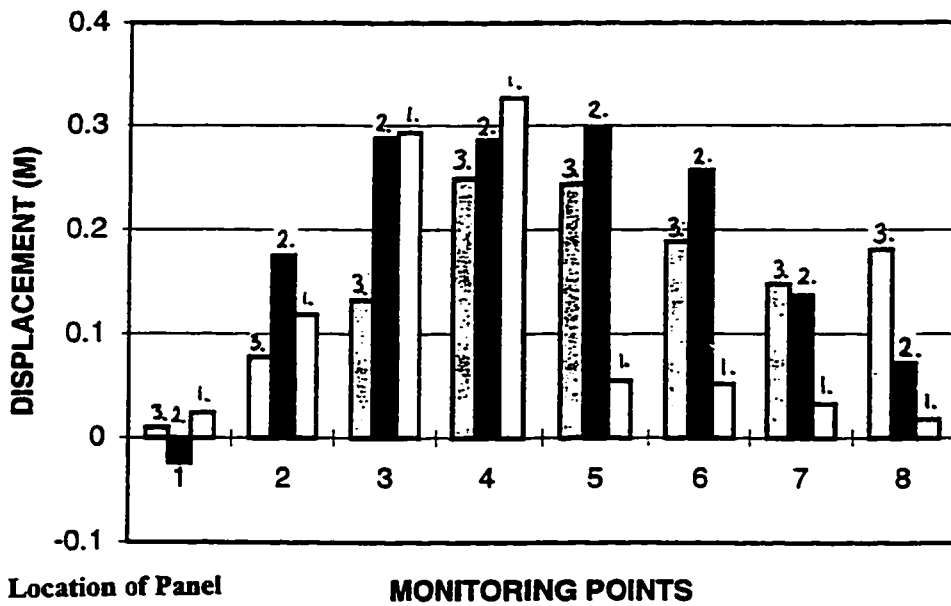
**Figure 5.32.** Location of points for displacement monitoring.

### VERTICAL DISPLACEMENT – Influence of slope



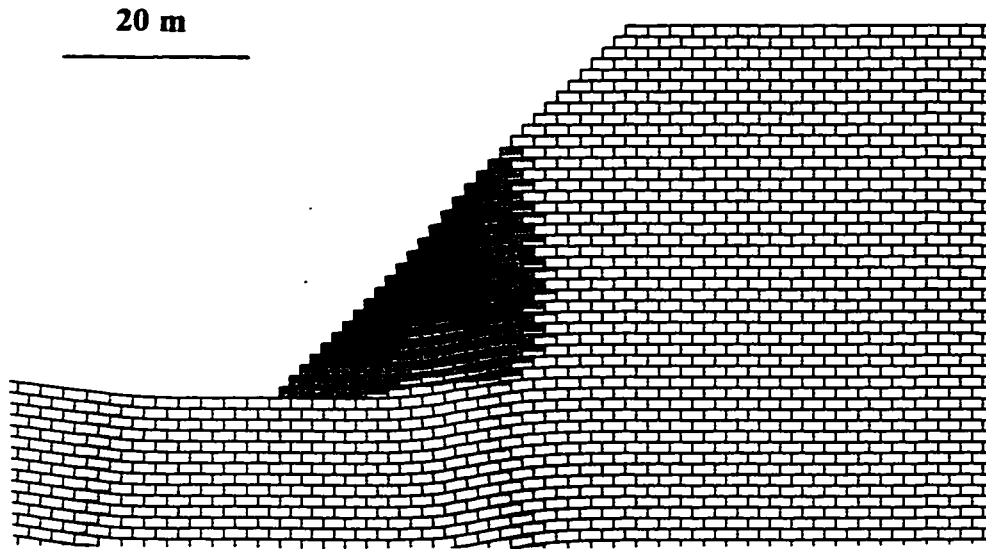
Location of Panel  
 1. Toe of slope  
 2. Mid-height of slope  
 3. Crest of slope

### HORIZONTAL DISPLACEMENT – Influence of slope

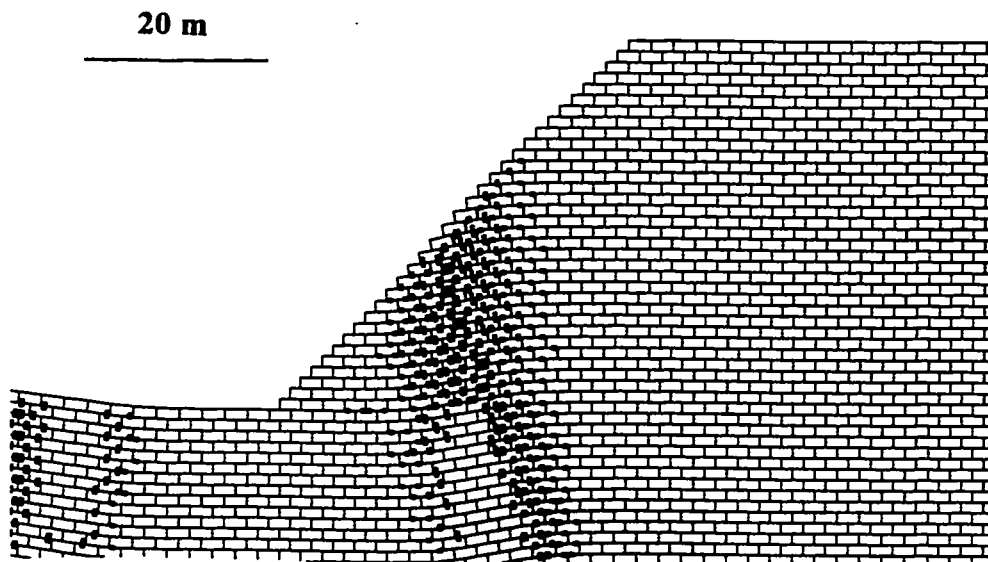


Location of Panel  
 1. Toe of slope  
 2. Mid-height of slope  
 3. Crest of slope

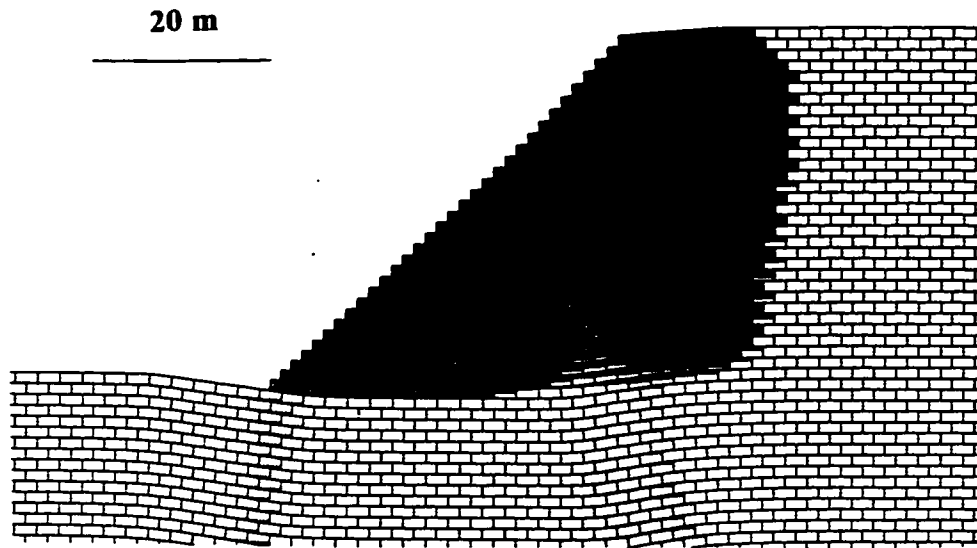
**Figure 5.33.** Vertical and horizontal displacements for along the slope profile resulting from panel extraction in different positions to slope. Location of monitoring points shown in figure 5.32.



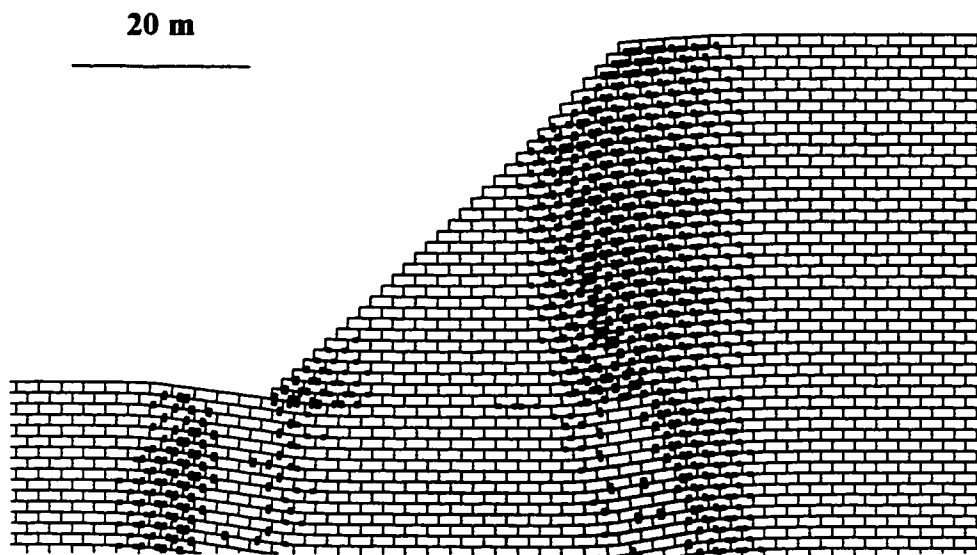
**Figure 5.34.** Horizontal displacements resulting from panel extraction with centerline under the slope toe.



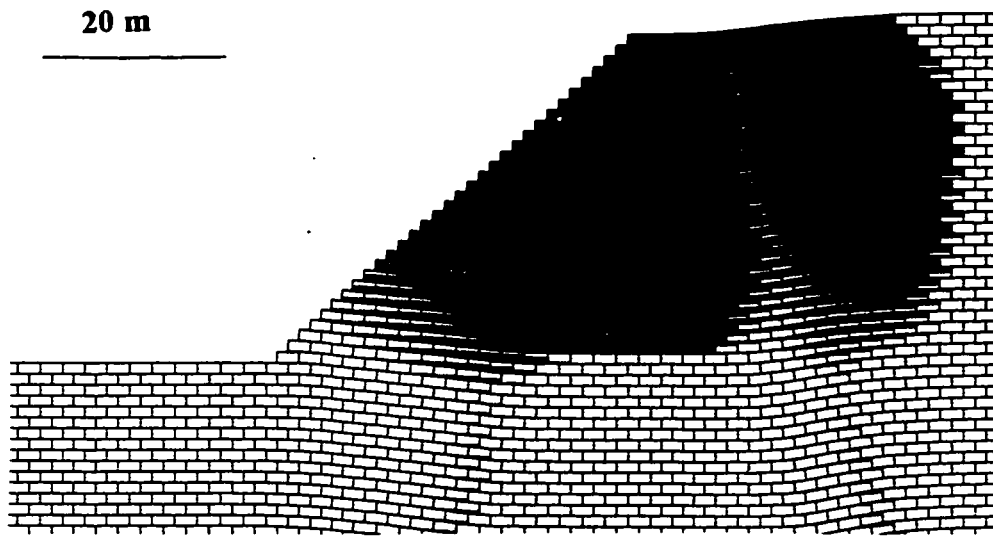
**Figure 5.35.** Shear displacement on joints resulting from panel extraction with centerline under the slope toe.



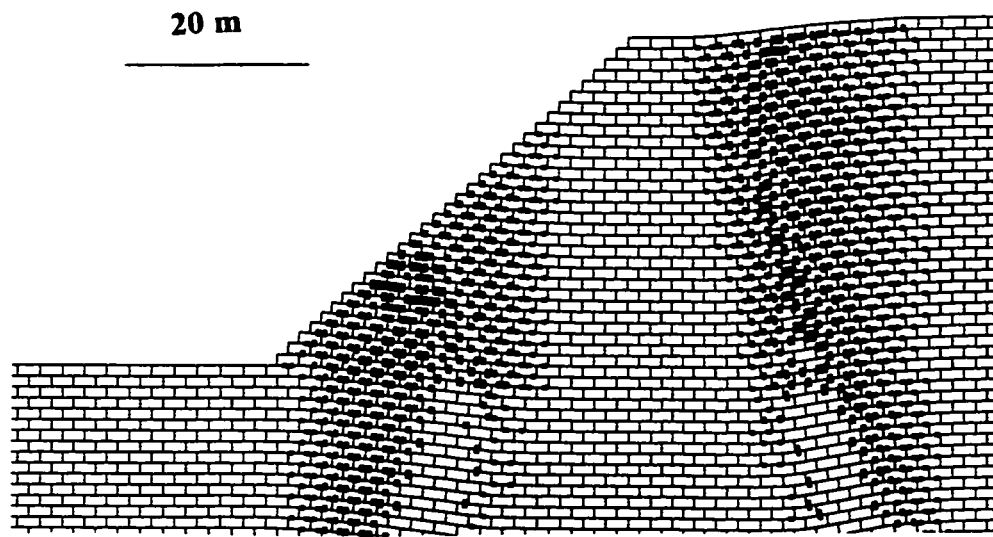
**Figure 5.36.** Horizontal displacements resulting from panel extraction with centerline under the mid-height of slope.



**Figure 5.37.** Shear displacement on joints resulting from panel extraction with centerline under the mid-height of slope.



**Figure 5.38.** Horizontal displacements resulting from panel extraction with centerline under the slope crest.



**Figure 5.39.** Shear displacement on joints resulting from panel extraction with centerline under the slope crest.

displacement and reached up to 0.6 m, depending on the panel location. All plots of displacement were taken for a model state where complete closure of panel occurred and no further displacements were observed.

- When the panel centerline was placed under the slope toe, figure 5.27, most of the deformations were constrained to the lower half of slope. This part of slope, subsided and displaced in the out-of-slope direction, with a maximum horizontal displacement of 0.6 m. Area in slope exhibiting the highest horizontal displacement, was located approximately 17.5 m above the slope base. Only limited deformations took place in the upper half of the slope as demonstrated in figures 5.33 and 5.34. The shear displacement on joints extended from the rib sides of panel, up to the ground surface. Increased shear displacement can be observed to take place above the slope base, figure 5.35. Generally, this location of mined panel, with the centerline under the slope toe will result in the loss of toe support for the slope. The slope angle in the lower half of slope will increase. The loss of toe support and increase in slope angle will both destabilize the slope. The potential initiation of a slope failure will depend on the “pre-mining” stability of slope. In case of weak rock mass or unfavorably oriented discontinuities the overall deformations may extend both, further up the slope and behind the slope crest, than demonstrated in this analysis.
- The movement of the panel center by 20 m inside the slope (panel centerline under the slope middle, figure 5.27), caused a decrease in the out-of-slope displacement magnitudes. The maximum horizontal displacement reached 0.4 m. Two areas of maximum horizontal displacement developed in the slope, figure 5.36. One was located in slope toe area, 5 m to 10 m above the slope base, the other 5 m to 17.5 m below the slope crest extending deeper inside the slope. It is of interest that the whole slope area developed a horizontal displacement in the out-of-slope direction as best demonstrated in figure 5.33. The area of increased horizontal displacement is limited by an approximately straight (vertical) line located 20 m behind the slope crest extending to the slope base. Inclination of bedding planes could be observed in

the upper part of slope. This deformations may lead to sliding of the top part of slope. This type of failure resembles the sliding on downwarped strata over void as described by Walton and Taylor (1977) and shown in figure 5.12 (b). Increased shear displacement on joints developed in the slope, figure 5.37, and was concentrated in a relatively wide zone, extending from the panel rib side to the slope crest.

- In the last case the panel centerline was located under the slope crest. The maximum out-of-slope displacement reached 0.3 m, figure 5.38, which was less than in the previous two cases. The maximum horizontal displacement was located in two areas. The first formed a continuous zone in the upper part of slope extending as much as 30 m inside the slope. The second area was located 20 m to 60 m inside the slope and was caused mainly due to the bedding plane slip as a consequence subsidence, similar as for case with level topography. The shear displacement on joints extended from the panel rib sides, influencing the area of slope toe and area 10 m to 30 m behind the slope crest. Figure 5.33 shows, that the displacement of all monitoring points on the slope was in the out-of-slope direction.

For all three cases the movement history of points for monitoring the displacement on the slope face was in the downslope direction, rather than towards the panel center as is the case for level topography, figure 5.33. The discontinuities orientation and the strength of joint bounded blocks (elastic constitutive criterion was assumed), did not allow for a full slope failure to develop in this particular case. Joint separation, shearing along bedding planes and cross joints and a decrease in the overall structural integrity of the slope resulted as a consequence of panel extraction in the model. Under field conditions, raveling of slopes, failure of any overhanging sections, opening of tension cracks, change in the hydrological regime and overall decrease in rock mass strength could be expected. Depending on the specific site conditions these effects could result in major slope failure, especially in the presence of a weak rock/soil material.

### **5.4.2.3 MODEL 3 - 40 m high, 45° angle slope with different discontinuity geometry in the slope part of model**

This model investigated three different slope structures with respect to slope stability and longwall panel extraction. Only models with block size 2.5 m x 5 m were analyzed. The main reason for this decision was the computer time requirements. As demonstrated in table 5.4, the 60 m overburden even for model with this block size, resulted in reasonably good agreement (75.6%) with the empirical subsidence values. Therefore, only the panel mining with the centerline under the slope toe, corresponding to a case with 60m overburden was investigated. This was believed to provide for reasonably good simulation of slope toe subsidence as a result of underground mining.

The models used in the analysis are shown in figure 5.26. As seen from this figure sliding and toppling types of instability were investigated. The sliding analysis was divided into two stages. In the first stage, a single discontinuity was assumed to daylight in the slope face, whereas in the second stage, several bedding planes above the slope base were daylighting in the slope face. The friction angle for the daylighting discontinuities was changed to examine the influence on the slope stability.

In all analyses the original ground stress (before the slope and panel excavation) was assumed to be gravitational only ( $K = \nu/1-\nu$ ). The blocks were represented as elastic isotropic only. The block and joint properties were the same as shown in table 5.1. The geological structure analyzed, includes:

- A slope excavated in an orthogonally jointed rock mass (horizontal bedding planes and two sets of discontinuous vertical joints), with a fault dipping at 25° daylighting in the slope face.
- A slope excavated above an unconformity, where in the top part the bedding planes are inclined at 25° and daylighting in the slope face.
- A similar situation as in previous model, except that the bedding planes are dipping 60° degrees into the slope. The potential for toppling instability is investigated.



#### **5.4.2.3.1 Fault Daylighting in the Slope Face**

In the case of a fault daylighting in the slope face, the major concern is the sliding instability of that part of the slope outlined by the ground surface and fault. The fault in this model had initially a friction angle of  $25^\circ$  - equal to its inclination. This placed the slope in a marginal stability case. This approach was used to examine development of the slope failure in response to mining-induced deformation. In the second stage the friction angle along the fault was increased to  $30^\circ$  and an initial cohesion of 0.05 MPa was assumed. Joint constitutive criterion, where the cohesion is set to zero once the shear strength is exceeded was assumed. This would case simulated a situation for a slope with higher pre-mining stability state. The influence of panel mining with a centerline under the slope toe, on deformation and instability development is shown in figure 5.40, 5.41 and 5.42.

- If the center of the mined panel was located under the slope toe then the main joint shear displacement took place on almost the entire length of fault and on bedding planes in the lower third of the slope, figure 5.40. The rock wedge formed by the fault and the ground surface was divided into two parts. The lower part, around the slope toe, was subjected to maximum vertical displacement due to the subsidence. The upper part of the wedge, became destabilized by the loss of toe support and subsequently slid along the fault (figure 5.41). The initially stable slope (only marginally stable due to low friction angle) was destabilized and a major failure of the rock wedge outlined by fault and ground surface took place. Under field conditions the presence of lateral release surfaces would be required for a full development of failure. The shear displacement for the model, where a fault with higher strength properties (friction= $30^\circ$ , initial cohesion=0.05 MPa) was assumed, decreased. The shearing, however, still took place over the entire length of fault as shown in figure 5.42. When the fault strength was progressively increased in additional analyses, its influence on slope deformation gradually decreased and no shearing was observed.

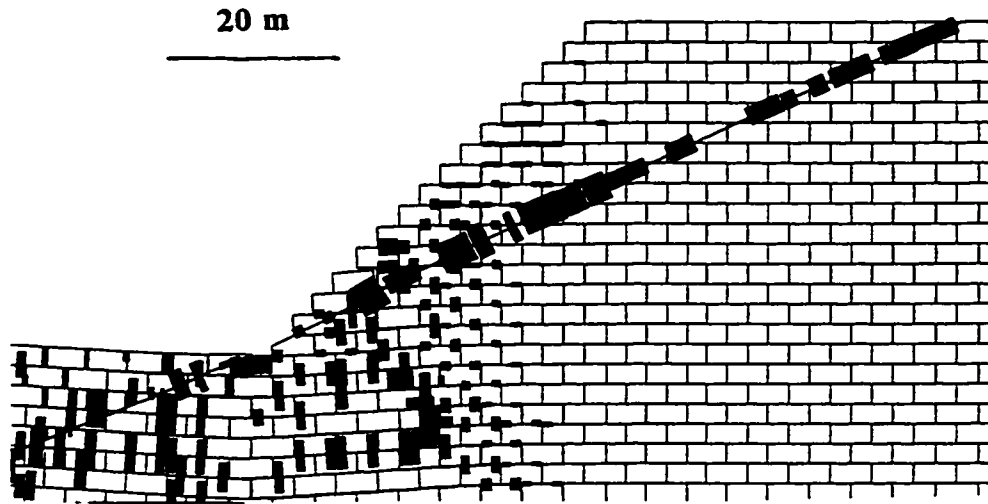


Figure 5.40. Shear displacements on joints for model with a fault daylighting in slope face and panel with centerline located under the slope toe.

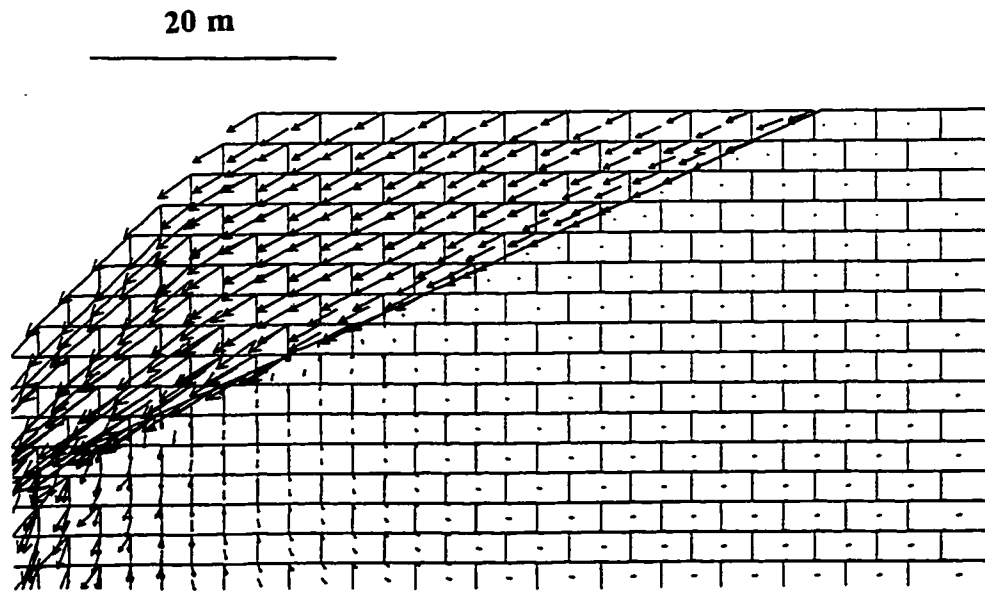
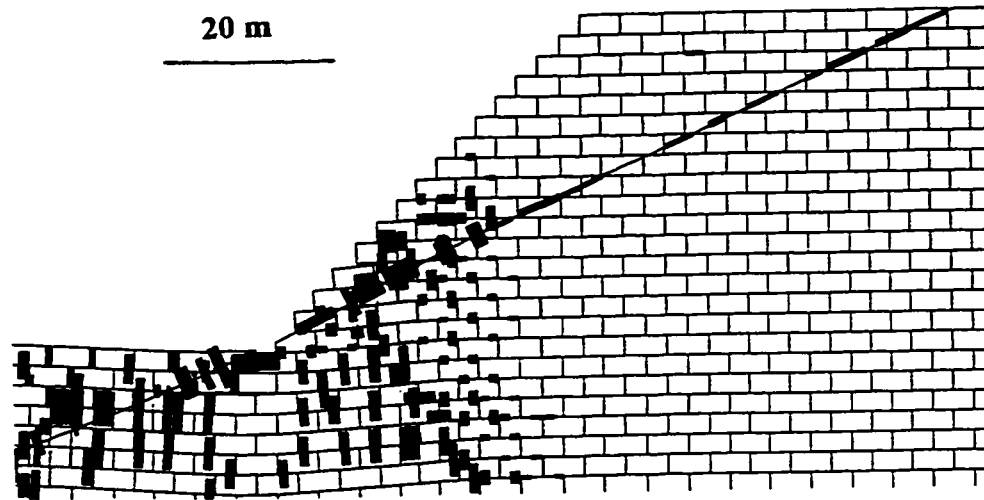


Figure 5.41. Displacement vectors for upper part of unstable wedge outlined by the ground surface and fault.



**Figure 5.42.** Shear displacements on joints for model with a fault daylighting in slope face. Increased shear strength on fault assumed (friction=30°, initial cohesion=0.05 MPa). Compare with figure 5.40.

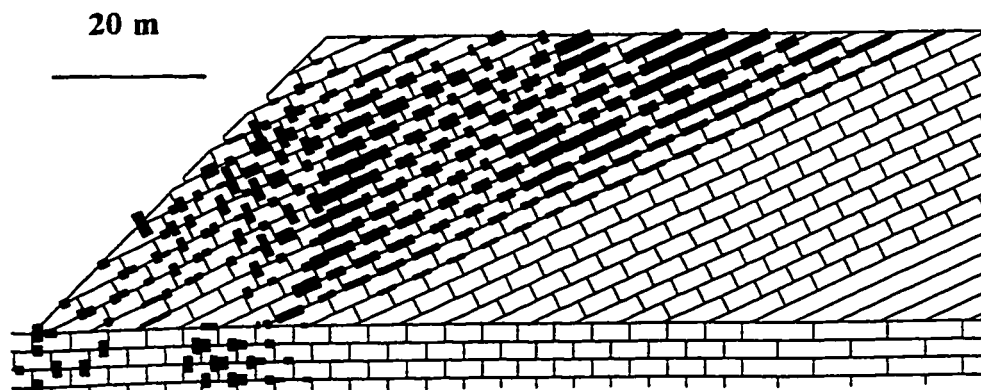
#### 5.4.1.3.2 Bedding Planes Daylighting in the Slope Face

The bedding planes in this model were inclined at 25° and daylighting in the slope face. Their initial shear strength, same as in the previous model with fault, was assumed to be only frictional and set equal to their dip. This resulted in a slope in a marginal stability state. In subsequent analysis the strength of the bedding planes was set higher (friction=30°, initial cohesion=0.05 MPa) to investigate deformations in a initially more stable slope. The deformations resulting from panel extraction with centerline under the slope toe are presented in figure 5.43, 5.44 and 5.45.

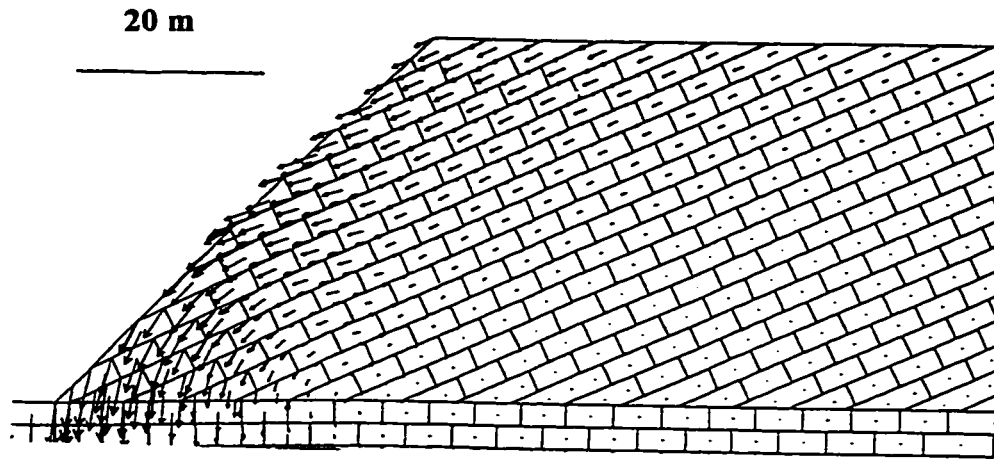
- The maximum out-of-slope displacement for the panel centerline located under the slope toe took place in the middle part of slope as shown in figure 5.43. The

displacement vectors in this part of slope have orientation identical with the dip of the bedding planes. The displacements in the slope were influenced as much as 80 m behind the slope crest. This is well demonstrated in figure 5.44, presenting shear displacement on joints developed after the panel extraction. Continuous shearing along the bedding planes resulted. It is interesting, that the shearing is concentrated on bedding planes originating within 35 m from the slope toe or center of panel. The subsidence movement increased the dip angle of the bedding planes especially in the toe area of slope. These became greater than their frictional resistance and sliding of joint bounded blocks resulted. In this particular case sliding of blocks especially from the slope face can be expected. The jointing pattern favors opening of existing joints caused by the toe subsidence as shown in figure 5.45. This figure shows a magnified plot (4 x) of the rock mass deformation in the slope area.

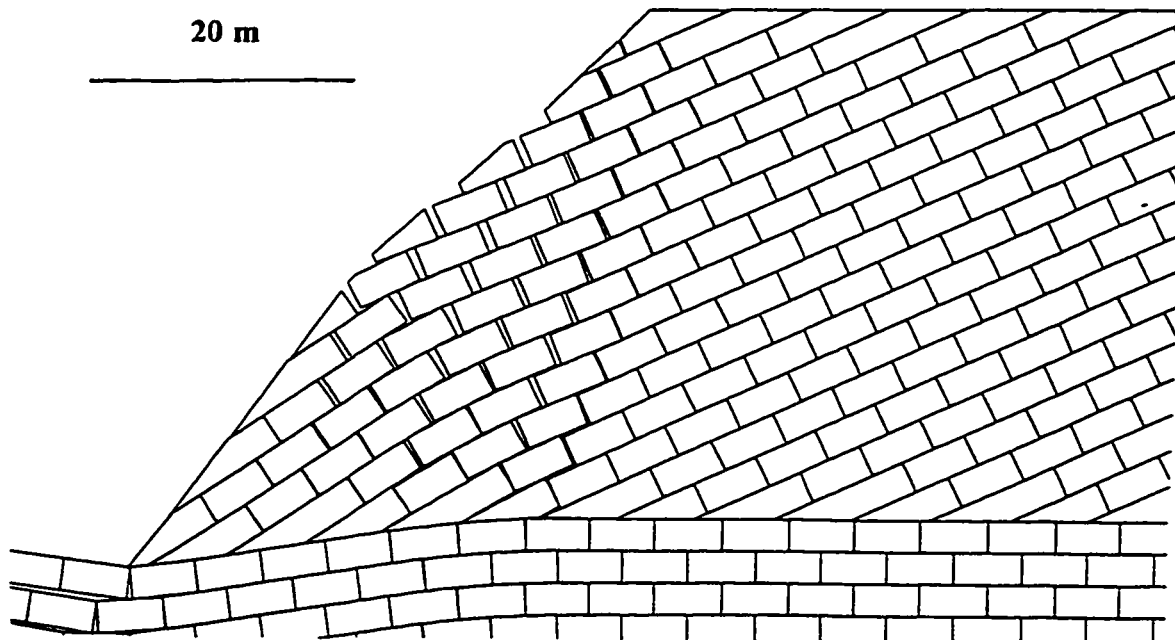
Due to the jointing pattern in slope the deformations can propagate far behind the slope crest. This can be critical for determining “safe limits” or set-backs for any



**Figure 5.43.** Shear displacements on joints for model with bedding planes daylighting in slope face and panel with centerline located under the slope toe.



**Figure 5.44.** Displacement vectors in slope developed as a consequence of panel extraction with centerline located under the slope toe.

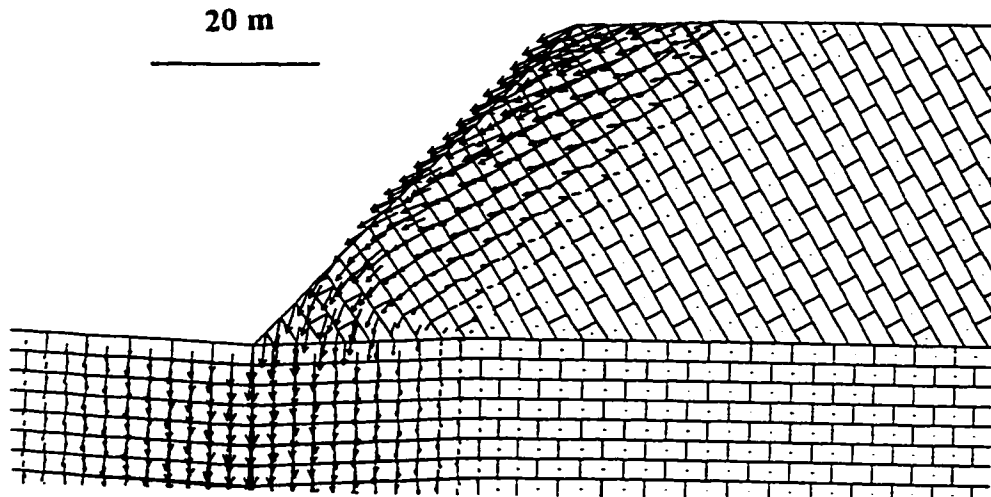


**Figure 5.45.** Slope deformation (magnified 4x) with panel centerline under the slope toe.

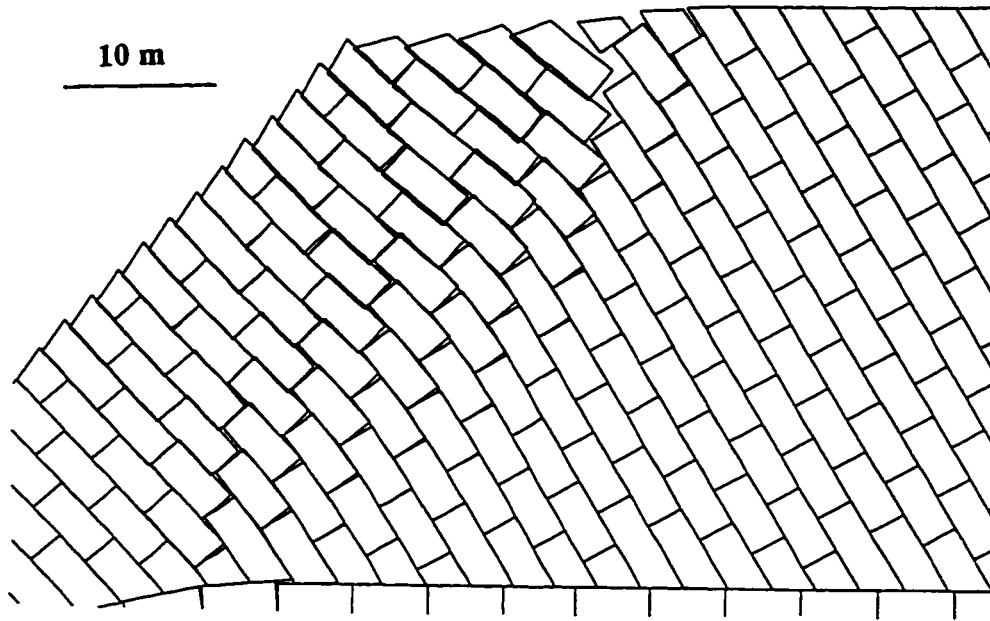
type of structures located in this area. Significant failure of the whole slope can be expected in field situation.

#### 5.4.1.3.3 Bedding Planes Dipping into the Slope

When the bedding planes are dipping into the slope at an assumed angle of  $60^\circ$ , toppling modes of slope deformation are the main concern. The response of a slope with such a jointing pattern to undermining, was investigated in this part of work. In addition to bedding plane joints the strata was assumed to be cross-jointed. This type of jointing pattern is susceptible to the block-flexural toppling mode of failure.



**Figure 5.46.** Displacement vectors in slope with bedding planes dipping into the slope developed as a consequence of undermining.



**Figure 5.47.** Slope deformation (magnified 4x) with panel centerline under the slope toe. Toppling mode of failure.

- When the panel with centerline located under the slope toe was excavated, major toppling was generated in the slope as shown in figures 5.45 and 5.46. Figure 5.45 shows the displacement vectors developed in the slope area. The slope toe shows a predominantly vertical displacement due to undermining, whereas the upper part has a strong horizontal component of displacement. Intense shearing took place along the bedding planes. The displacement are extending approximately 20 m behind the slope crest, where a formation of a major bedding plane separation was observed. A plot of magnified block deformations (4 x), of a more detailed area of slope, is shown in figure 5.46. The toppling extended approximately 15 - 20 m deep inside the slope. The analysis of the extent of deformations behind the slope crest is important for establishing set-back distance for location of structures. When compared to the case with bedding planes daylighting in the slope face the unstable part of slope decreased by 60 m.

## **5.5 Conclusions and Recommendations for Future Work**

This chapter analyzed the influence of underground mining on slope stability. The potential for application of the numerical modelling techniques was demonstrated, utilizing both, continuum and discontinuum approaches. It was shown that the undermining can lead a significant de-stabilization of slopes and be a triggering factor for large failures.

The potential for slope instability arising from underground mining subsidence can be summarized as following:

- Underground mining can result in large deformations in overburden leading to a decrease in the structural integrity of slopes.
- Undermining changes the shear strength of slope-forming material. As most rock and soil masses exhibit strain-softening behavior, a decrease of shear strength will result.
- Slope-forming material is exposed to increased tensional strain, resulting in fracturing or opening of existing weakness planes favorably oriented relative to the direction of undermining
- The internal and surface drainage is altered, leading to increase in pore pressures or rapid draw-dawn situation.
- The geometry of the slope is altered. Subsidence can increase the angle of slope, resulting in failure. Steep faces and rock scarps are particularly susceptible to even small changes in tilt leading to toppling, sliding and falling. In mountainous terrain, talus slopes which are often only marginally stable also vulnerable to changes in tilt.



- If an stabilized or dormant landslide is undermined, the subsidence can lead to re-activation of movement utilizing old failure planes
- The resultant movement down-slope can accentuate any natural creep taking place.
- The area effected by mining induced deformations in mountainous terrain can extend several times the deformations experienced when mining takes place under a level ground surface
- The distinct element and finite difference models proved the capability of analyzing and enhancing the understanding of the influence of underground mining on the slope stability.

Future work should concentrate on the:

- Examination of the influence of panel location on slope deformation in more than the three locations analyzed in this work. The estimation of “influence limits” or distances of panel influence on slope stability and deformations would have important practical applications. It is realized, however, that such a determination of the safe mining distance to a slope is very site dependent and must be constrained by field observations.
- Investigation on various slope geometry (slope height and slope angle) and different jointing pattern allowing for analysis of more types of slope failures.
- Examination of various other mining scenarios including mining inside the slope, multi-seam mining, or undermining of old workings
- Influence of mining an inclined seam in different positions with respect to the slope

- Analysis of deformations in weak material overlying more competent rock mass - representing the scenario where a loose spoil pile is placed on a more competent ground
- Numerical analysis of a case study based on field work, deformation monitoring and material testing would allow for a more comprehensive investigation and contribute to more understanding of the failure mechanisms. The use of more "sophisticated" constitutive criteria would be justified in such a case.
- Possible application of strain-softening criterion, allowing for a progressive decrease in strength with induced deformations. This criteria has a valuable potential application for future, representing most "realistically" the in-situ material properties. The use of such a criteria should again, be constrained by at least preliminary data from material testing or field estimates.
- Application of a three-dimensional analysis. Such an analysis would provide more information on the induced deformations and simulate the field situation more closely.

## CHAPTER 6

### THE FRANK SLIDE: A RE-EXAMINATION OF THE FAILURE MECHANISM

#### 6.1. Introduction

At 4:10 am on April 29, 1903 a major landslide, the Frank Slide, involving an estimated 30 million m<sup>3</sup> of rock occurred on the east face of Turtle Mountain in southwestern Alberta, Canada, resulting in the loss of approximately 70 lives (Kerr, 1990). The debris from the landslide covered an estimated area of 2.67 km<sup>2</sup>. Since the failure, several reinterpretations of the geological structure of the mountain have been published. The precise mechanisms involved in the landslide, however, still remain a subject of some controversy. The prime cause of the landslide has generally been recognized to be the geological structure, with the adverse anticlinal dip of the bedding planes within the mountain slope. Figure 6.1 shows the location of the landslide, which occurred on the east face of Turtle Mountain in the Crowsnest Pass, south-west Alberta, Canada. A photograph of the Turtle Mountain before the failure is shown in figure 6.2 and of the landslide as seen today in figure 6.3. This failure has been the subject of numerous investigations commencing with post-failure mapping by McConnell and Brock (1904) and including recent accounts of present day monitoring, such as Kostak and Cruden (1990).

The possible mechanism of the Frank Slide, using both finite difference (continuum) and distinct element (discontinuum) techniques of numerical modelling, is investigated in this chapter.



**Figure 6.1.** Location of the Frank Slide.

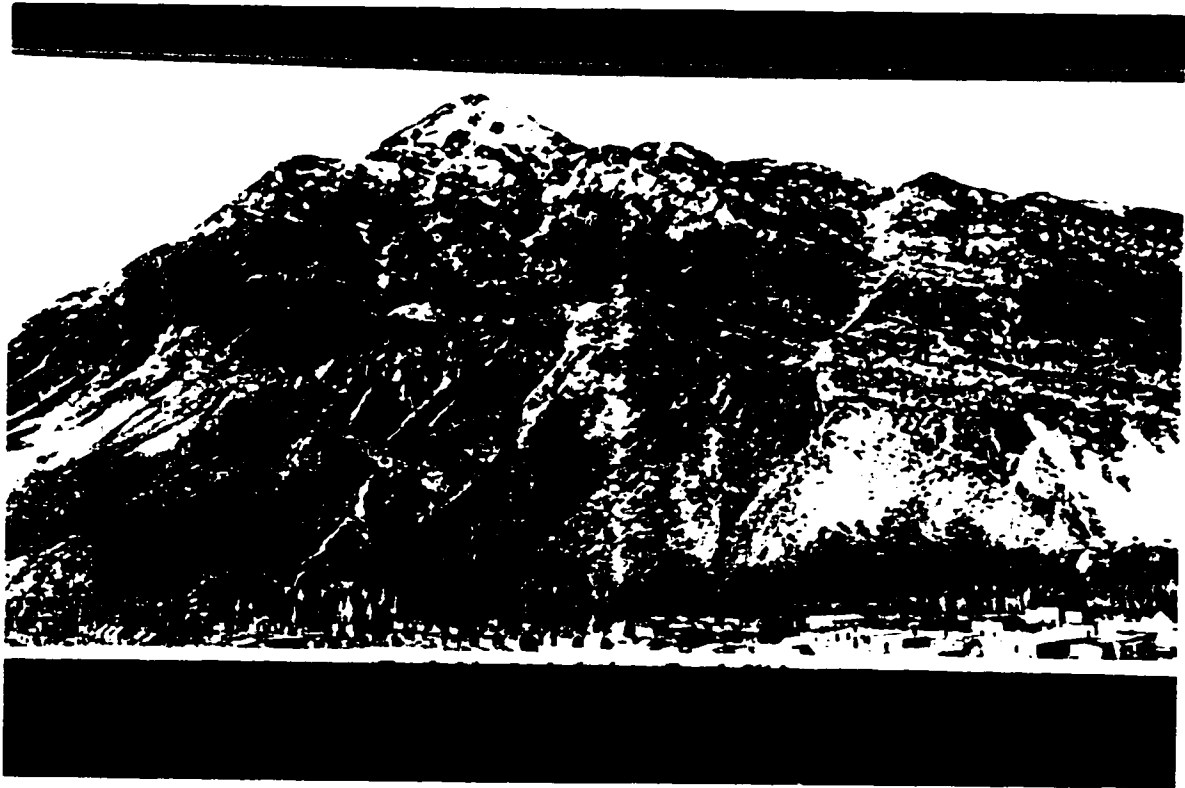
The main objective is to further our understanding of the failure mechanism in its initiation stage and to examine the possible effect of underground coal mining at the foot of the mountain as a trigger for the final failure. In terms of the suggested classification of landslide types, the Frank Slide is a complex, extremely rapid, dry rock fall-debris flow (Cruden and Varnes, 1996). In this chapter, the landslide is referred to as the *Frank Slide*.

## **6.2 History of Investigation**

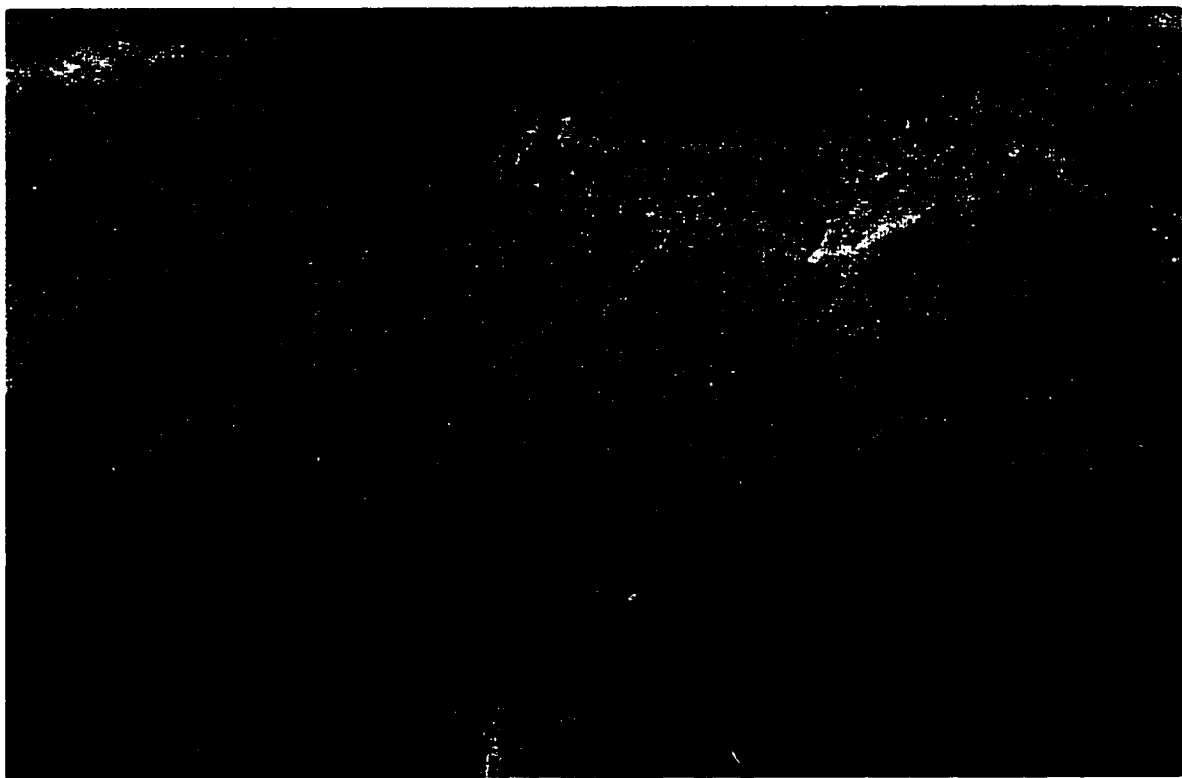
An outline of contributions made by various authors since 1903 is presented in Table 6.1. Dowlen (1903) produced one of the first published accounts on the Frank Slide failure in the *Engineering and Mining Journal*. In 1903, McConnell and Brock (1904) of the Geological Survey of Canada conducted a post-failure investigation of Turtle Mountain, producing a general geological appraisal. They believed that the Frank Slide had occurred across bedding planes which dipped steeply into the slope. The failure surface that they

**Table 6.1.** Summary of main contribution to investigations of the Frank Slide stability.

McConnell and Brock (1904, 1910, 1911)	<ul style="list-style-type: none"> <li>- First post-failure investigations.</li> <li>- Geological structure incorrectly identified as a monocline with movement believed to have taken place along steeply dipping cross-joints.</li> <li>- Indication of possible relationship between coal mining and landslide.</li> <li>- Concern about another failure from the north peak.</li> </ul>
Daly, Miller and Rice (1912)	<ul style="list-style-type: none"> <li>- Review of the Turtle Mountain stability with increased concern about stability of the north peak.</li> <li>- Recommendation to coal mining company to use “more caution” in mining.</li> </ul>
Allan (1931)	<ul style="list-style-type: none"> <li>- Recognized the implication of the anticlinal structure on the Frank Slide.</li> <li>- Suggested that further instability is more probable from the south peak which has the same structure as the failed part of Turtle Mountain.</li> </ul>
Cruden and Krahn (1973, 1978) Krahn (1974) Krahn and Morgenstern (1976)	<ul style="list-style-type: none"> <li>- Re-examination of the geology in the Frank Slide area.</li> <li>- Identification of a minor “flat lying” thrust fault “believed” to represent the lower release surface of the failed slope.</li> <li>- Shear testing of discontinuities.</li> <li>- Limit equilibrium analyses (Morgenstern-Price method).</li> <li>- Finite element analysis (elastic, isotropic).</li> </ul>
Cruden and Hungr (1985)	<ul style="list-style-type: none"> <li>- Investigation of the Frank Slide debris deposits.</li> <li>- Inversely graded debris deposits, possible mechanisms of the debris motion.</li> </ul>
Kostak and Cruden (1990)	<ul style="list-style-type: none"> <li>- Displacement monitoring (TM71 Crack Monitors) in the present crown of the Frank Slide.</li> </ul>
Kennard (1992) (unpublished)	<ul style="list-style-type: none"> <li>- First known application of an elasto-plastic numerical modelling analysis of the Frank Slide.</li> </ul>
Present analysis	<ul style="list-style-type: none"> <li>- Continuum and discontinuum numerical modelling of the Frank Slide.</li> </ul>



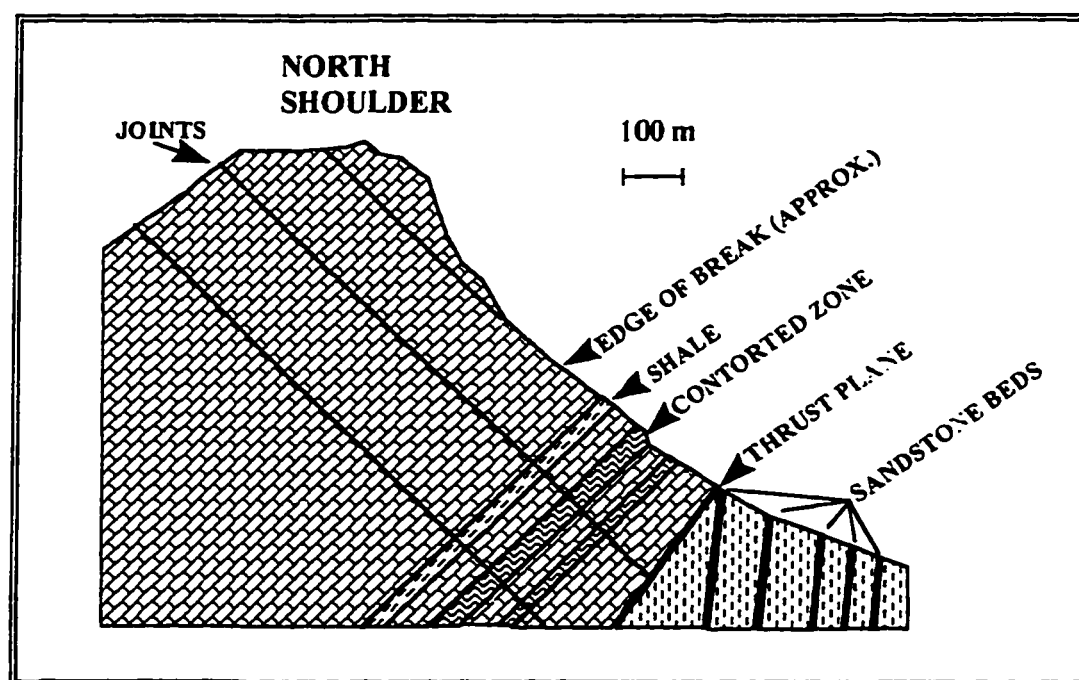
**Figure 6.2.** Turtle Mountain before the Frank Slide (from Cost of Coal, 1995).



**Figure 6.3.** The Frank Slide as seen today.

envisaged was predominantly along steeply dipping cross-joints, as shown in figure 6.4 (after Daly et al., 1912). This erroneous interpretation persisted in the literature for several decades. Brock (1910, 1911) expressed a concern that further movement from the north peak might occur. In 1910, a commission was appointed to analyze the stability of the Turtle Mountain, and again, the concern over the possibility of another failure affecting the north peak was emphasized (Daly et al., 1912).

Although the Turtle Mountain anticline was first recognized by Leach (1904), it was not until 1931, in an unpublished report by Allan (in Cruden and Krahn, 1978) that the implications of the anticlinal structure on the stability of Turtle Mountain and the Frank Slide were fully realized. Allan's work took place after concerns about the stability of the South Peak were expressed by McKay (in Cruden; 1986) which was “... *completely surrounded by fissures*”.



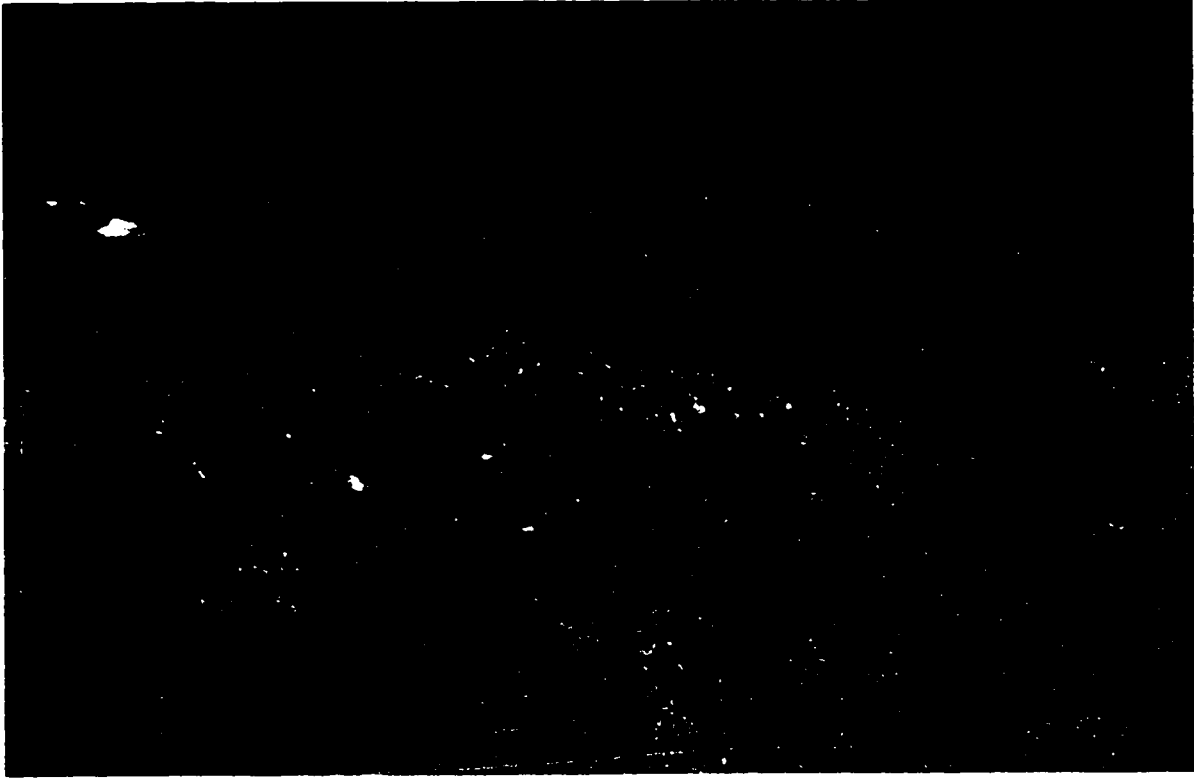
**Figure 6.4.** Cross-section through the North Peak of Turtle Mountain (after Daly et al., 1912).

Allan, from the re-mapping of Turtle Mountain, concluded that if any danger of another failure existed it was probably from the South Peak, where adverse bedding planes dipping to the east daylight into the valley. In subsequent geological mapping reports in the Turtle Mountain area, both MacKay (1932) and Norris (1955) identified the Turtle Mountain anticline.

Krahn (1974) described a detailed geological mapping of the Turtle Mountain area which he subsequently used in the most comprehensive analysis of the Frank Slide to date. In addition to limit equilibrium analysis, a simple two-dimensional finite element modelling study was performed (Cruden and Krahn, 1973; Krahn and Morganstern, 1976; and Cruden and Krahn, 1978).

In 1980, improvements to the monitoring network originally installed by Allan were made. The network was extended to all accessible sites at the margins of a  $5 \times 10^6 \text{ m}^3$  rock wedge that may potentially move eastward from the South Peak of the Turtle Mountain (Cruden, 1986). TM 71 crack monitoring instruments (Kostak and Cruden, 1990) and tape extensometers were installed, but have detected no hazardous movements to date. Fraser and Gruendig (1985) developed a high-precision photogrammetric deformation monitoring system for the detection of deformations on the south peak of Turtle Mountain. In addition, a seismograph is installed at the Turtle Mountain visitor center to record microseismic activity that may occur within the mountain. A subject of some controversy which is not addressed in the present study, is the mechanisms involved in the flow of the Frank Slide debris. Cruden and Hungr (1985) studied the debris deposit of the Frank Slide and examined the theories of rock slide-avalanche mobility. A view of the landslide debris from the summit of the Turtle Mountain is shown in figure 6.5. Kennard (1992) presented a preliminary, simplified numerical modelling analysis of the Frank slide using the finite difference method (FLAC). The results demonstrated the potential of this method in analyzing the failure mechanism, especially with respect to the possible influence of coal mining at the foot of the mountain.





**Figure 6.5.** View of the Frank Slide debris from the top of the Turtle Mountain.

### **6.3 Geology and Stratigraphy**

The Turtle mountain is composed of rocks varying in age from Mississippian (Banff Formation) to Jurassic (Fermie Group). Figure 6.6 shows the stratigraphic sequence of Turtle Mountain based on Norris (1955) and Cruden and Krahn (1978). Figure 6.7 presents a plan view of the Turtle Mountain geological structure with the area affected by the rock slide outlined (Krahn, 1974). The rocks involved in the Frank Slide consisted predominantly of Paleozoic limestone. The rock slide took place along the easterly dipping beds of the main geological structure, the Turtle Mountain anticline. The narrow hinge zone of the anticline outcrops less than 150 m below the mountain crest on the eastern face (Cruden and Krahn, 1978). The crown of the scarp contains a series of tension cracks parallel to the strike of the bedding, as shown in figure 6.8. Vertical displacement between blocks outlined by these cracks can be observed.

<b>MESOZOIC</b>	<b>LOWER CRETACEOUS</b>	<b>BLAIRMORE GROUP</b>		grey and greenish grey sandstone, red, green, and maroon mudstone; conglomerate; dark brown to black limestone
		<b>KOOTENAY FORMATION</b>		dark grey to black shale, carbonaceous shale, light to dark grey mudstone; coal
	<b>JURASSIC</b>	<b>FERNIE GROUP</b>		dark grey to black shale, silty shale, black and brown sandstone; thin black limestone; basal coquina and phosphate-pebble conglomerate
<b>PALEOZOIC</b>	<b>PENNSYLVANIAN AND PERMIAN (?)</b>	<b>ROCKY MNT. FORMATION</b>		grey sandstone, dark grey siltstone ( may include Triassic, Spray River Formation)
		<b>ROCKY MNT. FORMATION ETHERINGTON MEMBER</b>		light grey to variegated dolomite; limestone, dolomite and chert breccias, maroon and green shales
	<b>MISSISSIPPIAN</b>	<b>MOUNT HEAD FORMATION</b>		dark grey to black limestone; shaly, grey, cherty limestone; shaly, argillaceous, buff dolomite; limestone and dolomite breccias
		<b>LIVINGSTONE FORMATION</b>		massive, grey, fine to coarse crystalline limestone, grey crinoidal limestone; grey, crystalline dolomite
		<b>BANFF FORMATION</b>		shaly, grey, crystalline dolomite and limestone, chert-banded limestone

**Figure 6.6.** The Stratigraphy of the Turtle Mountain (modified after Norris, 1955 and Cruden and Krahn, 1978).

Numerous tension cracks extend far behind the failure scar. Three predominant discontinuity sets can be recognized, the bedding plane joints and two orthogonal joint sets perpendicular to bedding. Striations can be observed on the bedding surfaces which parallel the dip of the beds. Cruden and Krahn (1978) suggested that they were formed during flexural-slip folding. The dominant fault within the mountain is the Turtle Mountain thrust fault. A minor thrust fault located above the main Turtle Mountain fault was mapped by Cruden and Krahn (1978) and is shown in the figure 6.7. The significance of this minor fault in the Frank Slide failure has been noted by Cruden and Krahn (1978), who were able to trace this fault only on the northern margin of the landslide and assumed that it terminates against the main Turtle Mountain fault. The minor fault orientation was considered by the above mentioned authors to be "flat-lying".

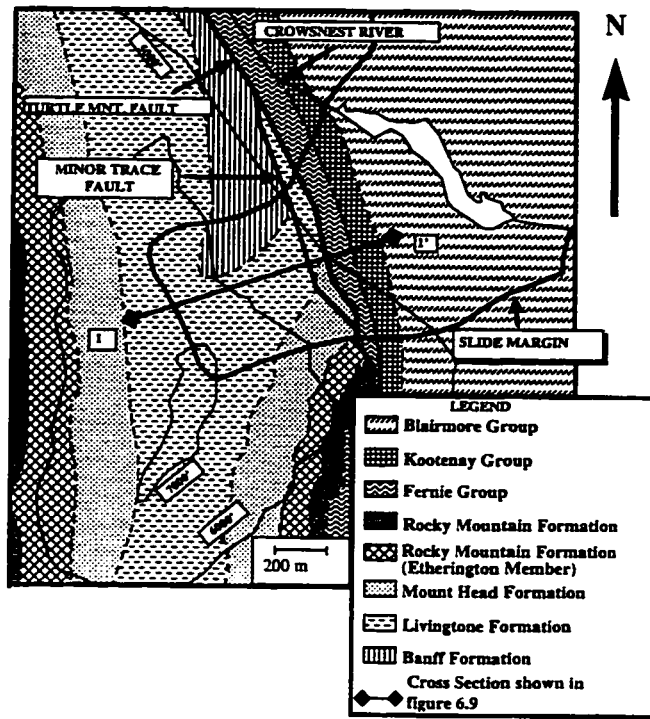


Figure 6.7. Plan view of the Turtle Mountain geological structure (after Cruden and Krahn, 1978).

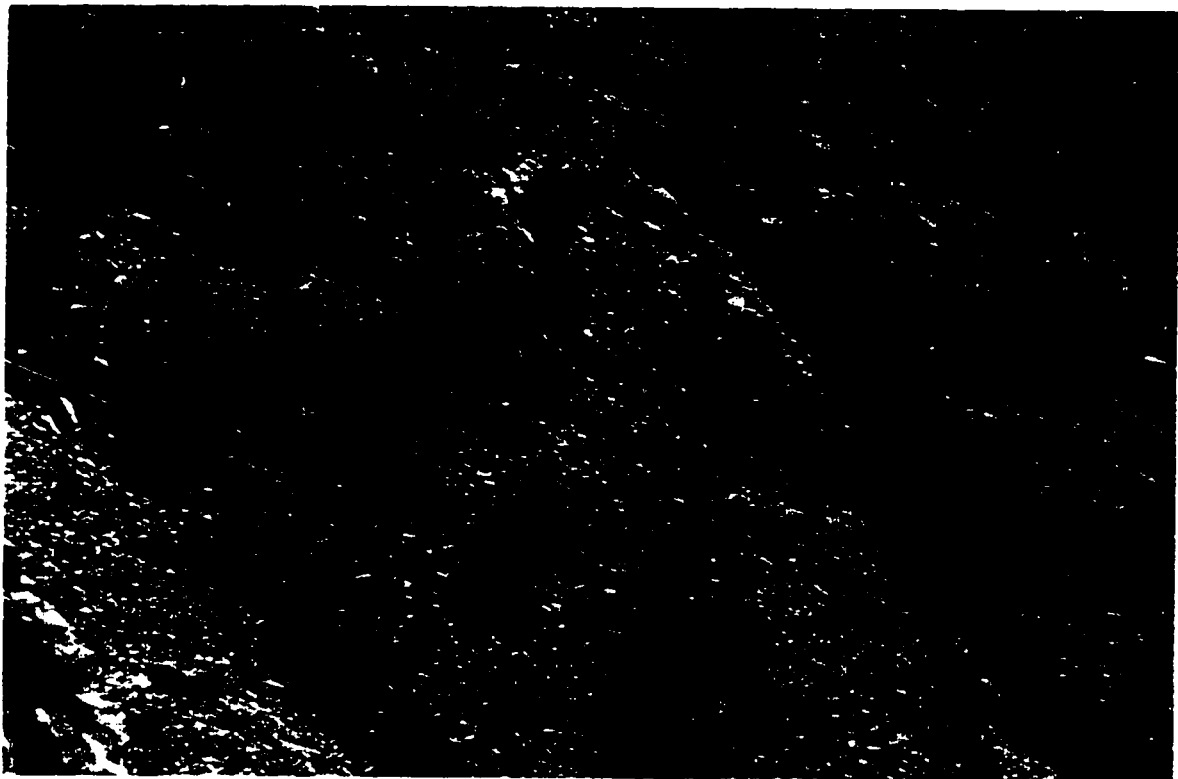
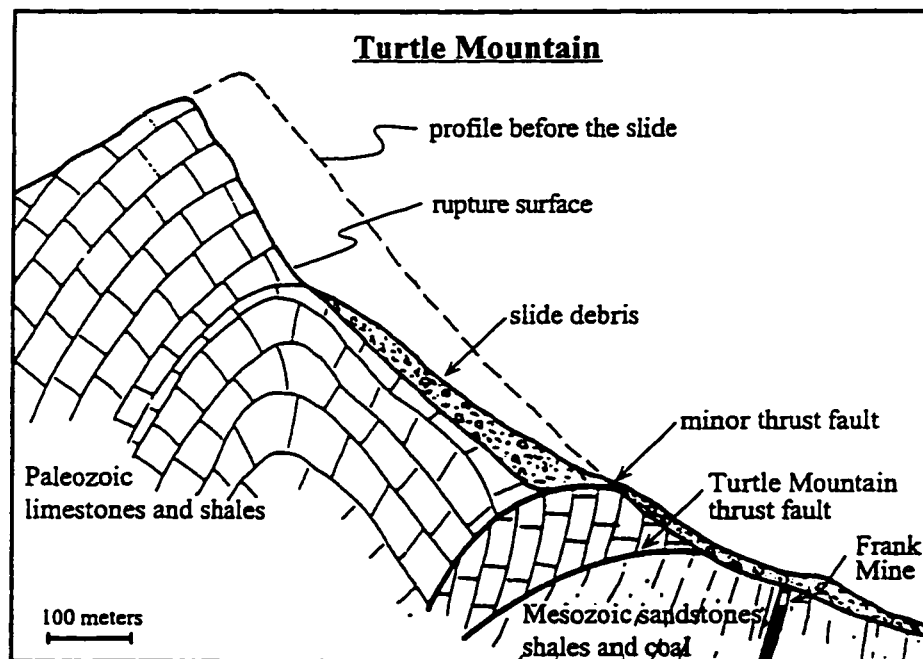


Figure 6.8. Tension cracks at the top of the Turtle Mountain, looking south.

## 6.4 Failure Mechanism

The first interpretations of the Frank Slide assumed movement to be across bedding planes, following a steeply dipping orthogonal joint set, as shown in figure 6.4 (Daly et al., 1912). The current, generally accepted opinion is that the failure surface followed bedding planes on the eastern limb of the Turtle Mountain anticline with rear release being provided by jointing within the anticlinal crest. The toe of the landslide is assumed to be controlled by the minor flat-lying thrust (Krahn, 1974). Figure 6.9 shows a cross-section through the central part of the landslide based on this assumption (Krahn, 1974). The failure mechanism appears to be complex involving components of both shear along, and separation of, discontinuities in addition to fracturing of the intact rock. The factors that may have exerted an influence on the instability and eventual failure of Turtle Mountain are diverse and preclude any “definitive” analysis of the failure mechanism. Table 6.2 lists these possible factors. The adverse geological structure within Turtle Mountain undoubtedly played the major role in promoting instability.



**Figure 6.9.** Cross-section through the central part of the Frank Slide (modified after Krahn, 1974).

**Table 6.2.** Summary of factors influencing the stability of Turtle Mountain.

• Creep of limestone units overlying interbedded sequence of shales, siltstones, sandstones and coal.
• Adverse jointing and faulting in the rock mass.
• Underground coal mining at the foot of the Turtle Mountain peak.
• Ice wedging in the discontinuities.
• Excessive rainfall over the four years preceding the slide.
• Seismic loading.

The jointed Paleozoic limestones that form the major part of the peak are thrust on a Mesozoic sequence of interbedded shales, siltstones, sandstones and coal. The folding and faulting processes would, in places, have reduced the available shear strength along bedding surfaces, joints and shears to values approaching residual, and decreased the overall rock mass strength. The effects of a progressive reduction in stability have been suggested by Terzaghi (1950) who thought that creep of the softer rocks under the weight of the limestone overburden may have contributed to the sliding. Such a time-dependent process may well have brought the Turtle Mountain slopes to a state of near limiting equilibrium, in the years immediately preceding the Frank Slide. This is corroborated to some extent by the historic inferences of instability and rock fall from the native name of the mountain - "The Mountain that moves" (Kerr, 1990). Krahn (1974) and Cruden and Krahn (1978) describe a detailed limiting equilibrium stability analysis of three sections through the Frank Slide, based on strength data from laboratory testing of samples from the slide debris. Their results also indicate that the slopes were in a state of marginal stability.

What were the possible triggering mechanisms for the Frank Slide? As indicated in table 6.2 several suggestions have been made ranging from ice-wedging at the top of the mountain, earthquake tremors, water pressures and underground coal mining at the base

of the mountain. This work attempts to show the influence of geological structure and mining on the Frank Slide failure mechanism. Although the work of Cruden and Krahn (1978) indicates that the effect of high water pressures “need not” have been a prerequisite for failure, a brief investigation into this aspect is attempted. The influence of ice-wedging has been ignored as, although this may have been a minor contributory factor, it is unlikely to have played a major role. This phenomenon would have been equally active, if not more, long before the eventual failure.

### **6.5 Influence of Mining on the Stability of Turtle Mountain**

At the time of the Frank Slide, the Canadian American Coal Company was mining a coal seam at the base of Turtle Mountain. The influence of mining on initiating the slide was expressed shortly after the slide occurred. McConnell and Brock (1904) stated:

*"It is almost impossible to avoid the conclusion that these great chambers, 130 feet long, 250 to 400 feet high, and 15 feet wide, situated directly under the foot of the mountain must have weakened it. The loose coal, being less resistant than the unmined, would allow slips or readjustments in the hangingwall, and the jar produced by these may have been sufficient to snap some of the few remaining supports, which held the unbalanced mass in place. For in its state of unstable equilibrium, the slightest movement, a movement of even one inch, might have a profound effect upon Turtle Mountain. It is a significant fact that these edges of the break correspond very closely with the limits of the big chambers of mined coal."*

These were extremely perceptive observations and the modeling results presented in this thesis endorse their statements in several respects. McConnell and Brock (1904) further reported that slight movements had been observed by miners several months prior to the failure. The tremors were somewhat alarming to the miners, and some left the mine on account of them. The coal began to "mine itself" because of ground squeeze, and hangingwall breaks became more frequent (the coal seam dipped approximately 85° to the west, i.e. into the mountain). The gangways and manways had to be frequently retimbered and were even condemned due to the impossibility of keeping them timbered.

It is not precisely known how much movement occurred in the mine either prior to, or at the time of the slide. The miners' accounts at the time of the disaster did not indicate any sudden movement within the mine walls just before the failure. However, as already noted, a slight inward deformation in the hanging wall could have caused the final failure of an already unstable slope above the mine (McConnell and Brock, 1904). The coal was mined in chambers ranging in height from 76 m to 122 m. The chambers varied in length from 18 m to 46 m, with an average of approximately 40 m, and were 5 m wide. The rooms were separated by pillars normally 12 m in length, containing man-ways and cross-cuts. All the workings were in coal. Most of the coal stopped down in the chambers, remained in them, with just enough being drawn at the chutes to keep the surface of loose coal a convenient distance below the roof of unmined coal for men to work. It was reported (McConnell and Brock, 1904; Anderson, 1986) that unusually heavy shipments of coal were made " ... *a little before the slide*", emptying at least partly the loose coal from the chambers.

Mining may have influenced or initiated the failure in a number of ways without the mine openings being directly affected by the landslide movement itself. Numerous accounts in the mining literature have shown the effects of underground mining on slope instability. The adjustment of the host rock above and adjacent to the working level can have effects ranging from gradual subsidence to rapid propagation of crown holes, wide reaching lateral deformation, alteration of the pre-mining stress field and changes in groundwater regime. The effects of caving reduce the rock mass quality of the slope-forming material, increasing fracturing, opening joints, promoting shear and a reduction in the available shear strength. Rock mass permeability and hence drainage may also be affected.

It is the author's hypothesis that mining at the base of the Turtle Mountain may have resulted in such effects and provided the final impetus for the failure of a marginally stable slope. This hypothesis is tested in the presented work using numerical modelling techniques.

## 6.6 Previous Analyses of the Frank Slide

The most comprehensive analyses of the Frank Slide undertaken to date were reported by Krahn (1974), Krahn and Morgenstern (1976), and Cruden and Krahn (1978). Both the limit equilibrium method and numerical modelling (the finite element method) were used in these investigations. Their analyses were based on detailed field mapping and laboratory testing of the main discontinuities. Test samples were obtained from the landslide debris, formed mainly by the limestones of the Livingstone formation, due to the inaccessibility of the actual slide surface. Three types of discontinuities were identified in the unstable rock mass: intact undisturbed bedding planes, orthogonal cross-joints and bedding planes along which previous tectonic movements had occurred, and referred to as flexural-slip surfaces. The test samples had dimensions 15 x 15 cm and 5 x 5 cm. A summary of the test results is shown in table 6.3. A need for a reassessment of this data and additional testing to provide data for the numerical models are indicated during this study. This, however, was beyond the scope of the present thesis.

**Table 6.3.** Summary of test results of main discontinuities, after Cruden and Krahn (1978).

Type of sample	Peak friction (°)	cohesion (kPa)	Residual friction (°)	cohesion (kPa)
Bedding plane	51.7	262	32.3	55
Cross-joints	32.0	172	14.0	83
Flexural-slip	28.0	221	15.6	124

**Table 6.4.** Results of stability analysis, after Cruden and Krahn (1978).

Friction required for safety factor equal to unity (c = 0)	Factor of safety for $\phi = 28^\circ$ c = 221 kPa	Factor of safety for $\phi = 28^\circ$ ; c = 221 kPa along bedding $\phi = 32^\circ$ ; c = 172 kPa across bedding
35.2°	0.89	0.90



The limit equilibrium analyses were carried out using the Morgenstern-Price method with no water pressure acting on the failure surface. The results for the section through the central part of the mountain (cross-section analyzed in the presented numerical modelling study) are shown in table 6.4. Three cases were analyzed:

1. The friction angle required for a safety factor of unity assuming zero cohesion was calculated.
2. Peak friction and cohesion parameters were assumed to act over the entire failure surface.
3. As for the second case, except where the failure surface crossed the bedding planes, the peak shear strength determined from the joints was used.

The factors of safety below unity were accounted for by the latter authors, as being due to not taking into consideration the surface roughness along the failure plane, the dip of the minor thrust fault representing the lower part of failure surface, and the possibility of failure involving fracturing of intact rock material. The two-dimensional limit equilibrium analysis, although excluding the effect of mining, remains the most comprehensive analysis of the slide to date.

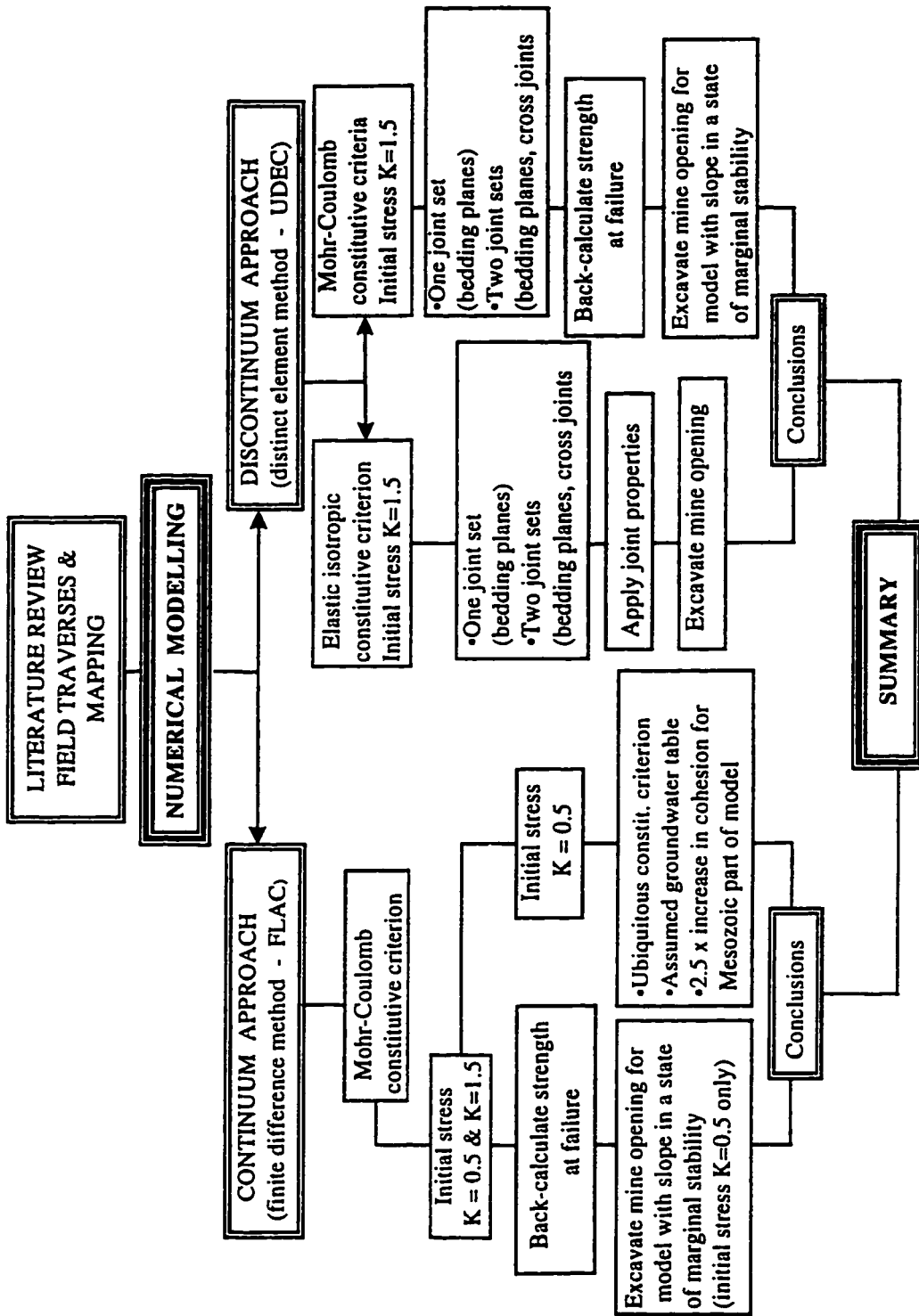
Finite element modeling was undertaken by Krahn (1974), reported also in Krahn and Morgenstern (1976), to investigate the possible effect that the mine could have had on the Frank Slide. A pseudo-factor of safety was defined, using the stress changes resulting from the mine opening. The factor of safety after the mine opening decreased by about one percent as compared to the "pre-mining" state. A limitation of the analysis conducted at that time was the use of an elastic-isotropic constitutive criterion for the rock mass and the necessary assumption of continuum behavior. The Turtle Mountain rock mass is neither elastic, continuous nor isotropic. Slope displacements predicted by the assumption of a continuous, elastic rock mass are relatively small compared with the use of an elasto-plastic discontinuum approach.

The rapid advance in numerical techniques, as applied to geomechanical problems, enables a re-examination of this failure and the use of a wide range of constitutive criteria in addition to the consideration of joint-block deformation.

### **6.7 Numerical Modelling of the Frank Slide**

The work in the previous chapter has shown that numerical modelling techniques are a powerful analytical tool when examining the influence of underground mining on slope instability. This observation and numerous visits to the Crowsnest Pass area, prompted the author to investigate the effects of underground coal mining on the Frank Slide. It was decided to apply both continuum and discontinuum methods of analysis. A schematic illustration of the analytical procedure is shown in figure 6.10. In the first stage of the analysis, Turtle Mountain was treated as a continuous rock mass and an elasto-plastic constitutive criterion adopted. The finite difference code, FLAC (Itasca, 1995), was used in the slope stability analysis, where the main objectives were to determine the location of the failure surface as it might have developed under the given topography and rock mass properties, and to investigate the influence of progressive mine excavation on the slope stability. Clearly this analysis is a simplistic first approximation - an attempt to see where the critical failure surface would occur regardless of geological structure. Variations in strength, elastic properties, ground stress, pore fluid pressures and the influence of mining were all investigated. In addition, the ubiquitous joint constitutive criterion was adopted in an effort to represent indirectly the Turtle Mountain anticlinal structure in a continuum analysis.

In the second stage of the analysis the discontinuous rock mass of the Turtle Mountain was addressed explicitly using the distinct element code, UDEC (Itasca, 1993). This allowed the consideration of fully-deformable joint bounded blocks and a more realistic representation of the geological structure. Models representing the bedding plane discontinuities alone, as well as assuming cross joints perpendicular to bedding planes,



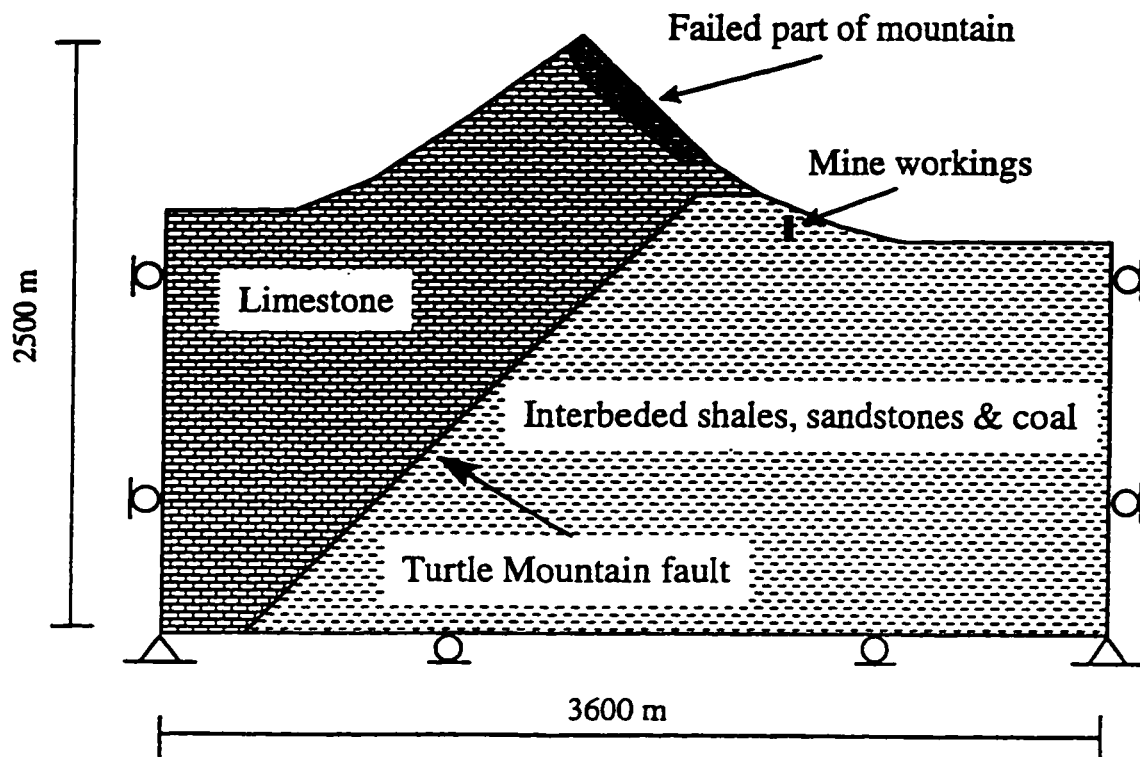
**Figure 6.10.** Flow chart of analytical procedure applied in the Frank slide stability investigation.

were analyzed. Both linear elastic and Mohr-Coulomb elasto-plastic constitutive criteria, were adopted to represent deformation of the intact blocks. The movement along discontinuities was controlled by the shear strength parameters. A constitutive model with joint area contact, elasto-plastic with Coulomb slip failure (where the joint cohesion is set to zero when its shear strength is exceeded) was used for the discontinuities (Itasca, 1993).

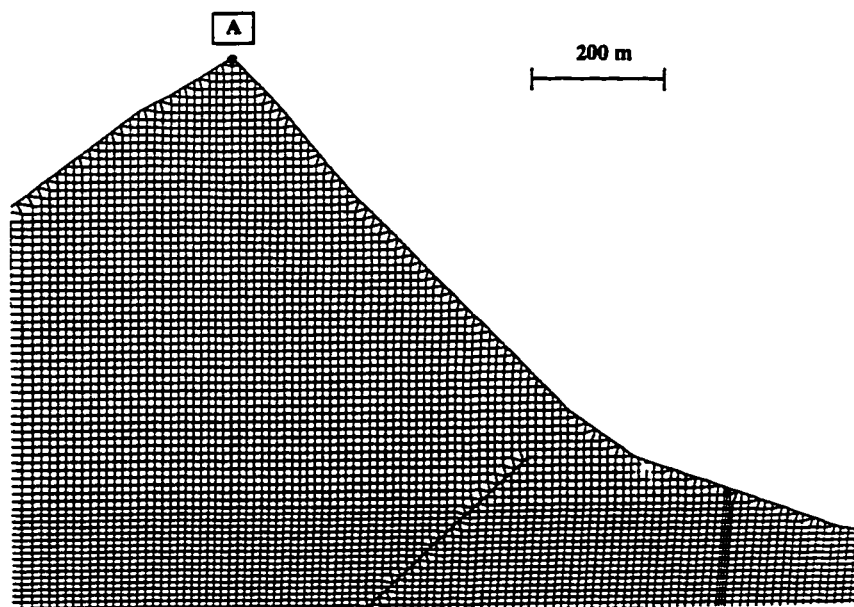
### **6.7.1 Continuum Approach**

The geometry of the model and the finite difference grid in the central part of the model are shown in figures 6.11 and 6.12, respectively. The pre-landslide topography of the Turtle Mountain was estimated from published cross sections in Krahn (1974) and Cruden and Krahn (1978). Only the cross section through the middle part of the slope was analyzed. This section corresponds to cross section, B-B', in Cruden and Krahn (1978), (figure 6.9). It is stressed that no exact pre-failure topographical map exists for Turtle Mountain.

The initial FLAC mesh contained 18480 finite difference zones representing a 3600 m by 2500 m section of rock mass. A linearly graded grid was used with a maximum zone aspect ratio of 5:1 to avoid numerical artifacts. In addition, a model with larger dimensions was examined to investigate the influence of boundary conditions on deformation and failure mechanisms. As no significant differences were found, only the results from the smaller section are reported. Two types of rock mass properties were assumed - one for the Paleozoic limestones above the Turtle Mountain fault, and one for the Mesozoic sequences of interbedded shales, siltstones, sandstones and coal. The rock slope was assumed to be elasto-plastic with either a Mohr-Coulomb or a Ubiquitous Mohr-Coulomb constitutive criterion. Table 6.5 summarizes the rock mass properties adapted for the continuum modelling. These properties were selected based on the published literature on the Frank Slide and similar rock types.



**Figure 6.11.** Geometry and boundary conditions for the continuum analysis of Frank Slide.



**Figure 6.12.** Finite difference grid in the central part of Frank Slide model.

**Table 6.5.** Rock mass properties for the numerical modelling of the Frank Slide

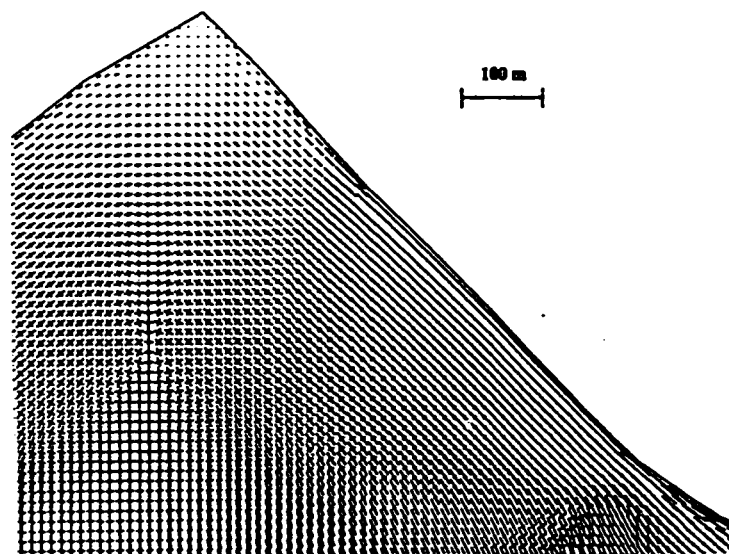
	<b>MESOZOIC FORMATIONS</b> (Shales, sandstones, siltstones and coal)	<b>PALEOZOIC FORMATIONS</b> (limestones and dolomites)
<b>density (kg/m<sup>3</sup>)</b>	2250	2600
<b>bulk modulus (MPa)</b>	2500	6670
<b>shear modulus (MPa)</b>	1150	4000
<b>friction (°)</b>	27	30
<b>cohesion (MPa)</b>	2.0	back-calculated

Elastic properties (Young's modulus and Poisson ratio) were estimated from Hoek et al. (1995) and are for blocky seamy rock mass of good (limestones and dolomites) and poor (shales, siltstones, sandstones and coal) quality, respectively.

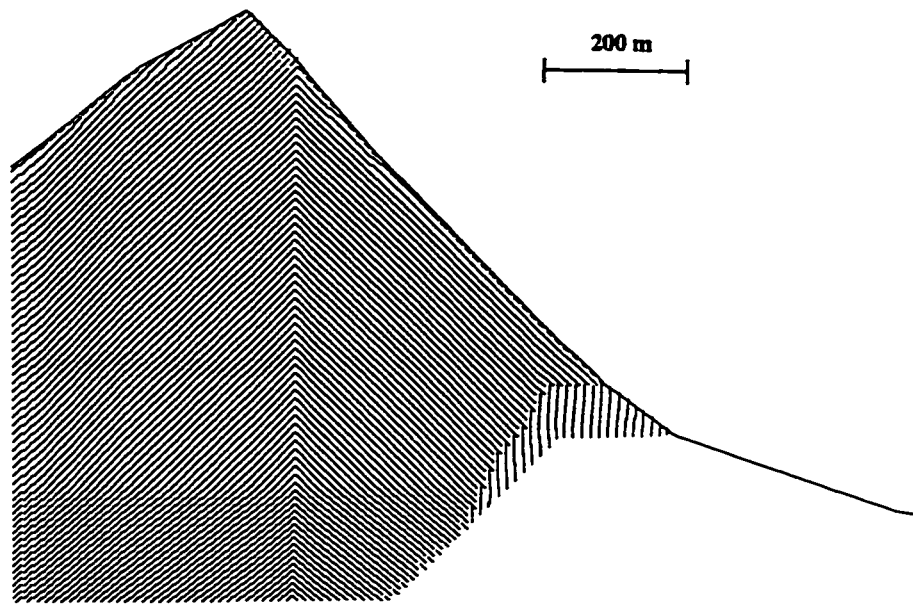
Having assumed an angle of internal friction of 30° for the Paleozoic limestones of Turtle Mountain, the magnitude of the cohesion was varied until failure occurred. The assumed "average" friction angle of 30° was based on the friction angle of flexural slip surfaces and cross joints, as determined by Cruden and Krahn (1978). Zero tensile strength was assumed for the model, owing to the jointed nature of the rock mass. In order to observe the effect of the initial *in situ* ground stresses, two conditions were modeled with initial horizontal to vertical *in situ* stress ratios of 0.5 and 1.5. These two values of ground stresses refer to a model with an initial level topography. The rock material to the left and right of the present Turtle Mountain peak was removed to represent erosion until the final topography was achieved as shown in figure 6.11. The formation of the final geometry of Turtle Mountain was performed in 6 steps, each representing an excavation approximately 160 m deep. After each excavation step the model was allowed to deform under the new stress regime in the elastic range, before excavation of the subsequent part

was performed. The trajectories of ground stresses after the final excavation step for the top central part of the grid and the initial K ratio equal to 0.5 is shown in figure 6.13. After the initial stresses had been established, the displacements resulting from the excavation were reset and the elasto-plastic model was run with decreasing values of cohesion until a clear failure surface developed. Plots of velocity and displacement vectors, stresses, plasticity state and shear strain rate were made to determine the (in)stability of model.

When a value of cohesion for the Turtle Mountain rock mass was reached that indicated unstable conditions, plots of the predicted failure surface were made. Further analysis was undertaken with a cohesion value of 15 kPa higher than that at failure. This placed the Turtle Mountain in a state of marginal stability, presumably similar to that which occurred in the period immediately preceding the Frank Slide as confirmed by earlier investigators. A 120 m x 5 m part of the model, in the locality where the mining took place, was excavated in 10m x 5 m increments. The mine excavation started from the top, representing the coal release through the chutes at the bottom of chambers.



**Figure 6.13.** Modelled ground stress trajectories in the top central part of model (initial K ratio equal to 0.5).



**Figure 6.14.** Assumed dip of implicit joints for the ubiquitous constitutive criterion.

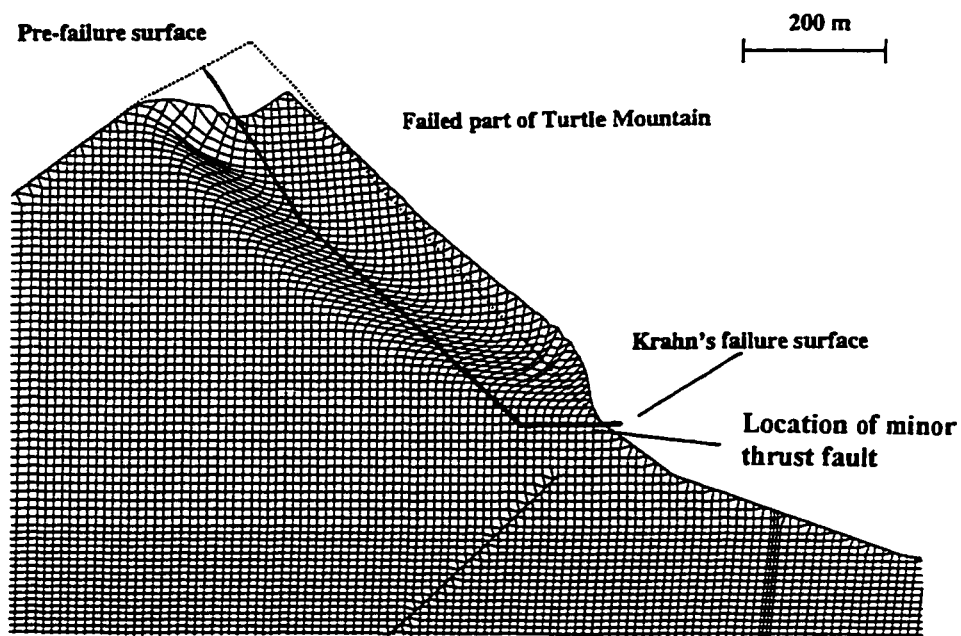
The dimension of the mine opening was progressively increased and the effects on the slope stability examined after each excavation step. In an attempt to represent the main bedding plane discontinuities more realistically and to examine their influence on the failure surface an ubiquitous constitutive criterion was applied to the model. The assumed bedding-joint dip is shown in figure 6.14. The strength of the bedding joints was assumed to be that of the flexural slip surfaces as determined from laboratory shear box testing, with cohesion equal 221 kPa and friction angle of  $28^\circ$  (Cruden and Krahn, 1978).

Various shear strength properties in terms of cohesion were assumed for the rock material. The influence of pore water pressures was not considered in previous analyses of the Frank Slide stability. The groundwater condition before the slide was not known. A model with a constant assumed groundwater table was analyzed. More detailed analyses that include groundwater were not considered justified due to the lack of information on the flow regime.

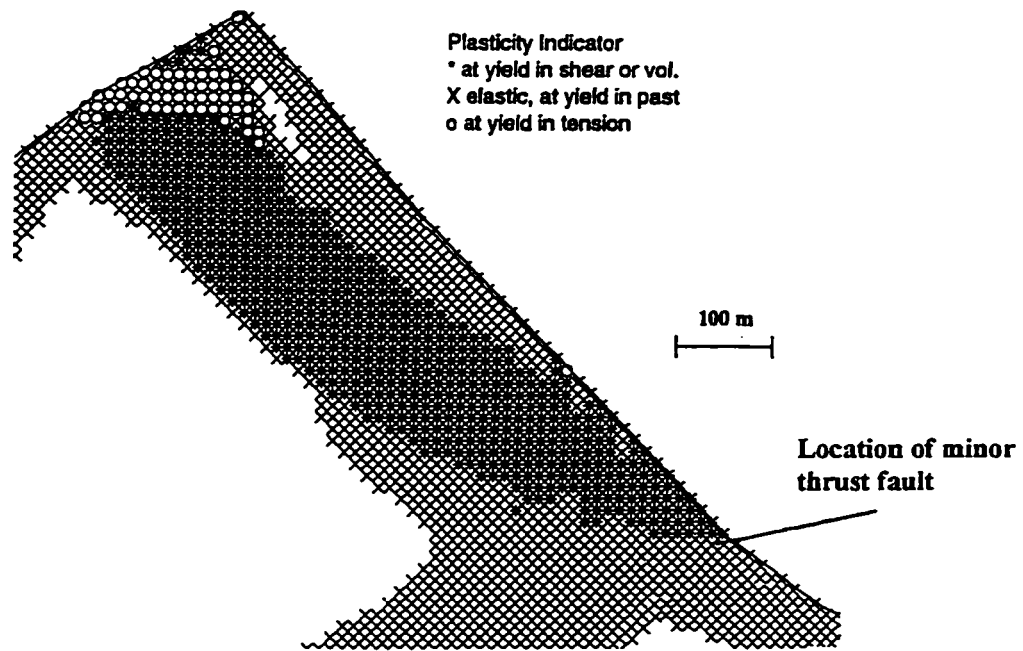


### 6.7.1.1 Location of the Failure Surface

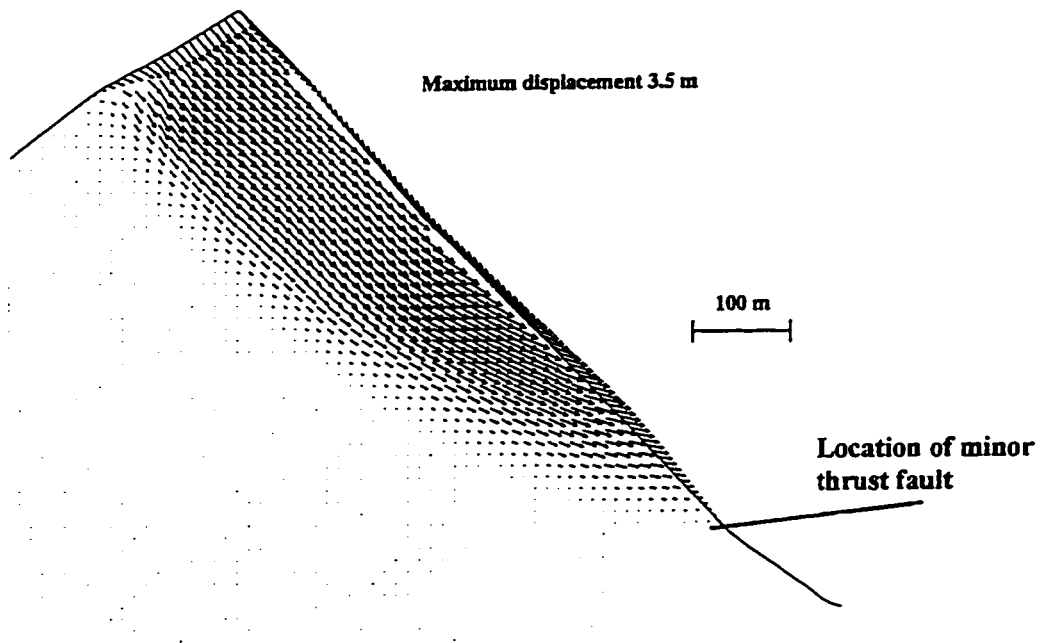
From preliminary analyses it was found that the slope became unstable with a cohesion magnitude of less than 600 kPa for the Turtle Mountain rock mass, assuming Mohr-Coulomb constitutive criterion and dry conditions. A sensitivity analysis based on varying the cohesion (in 15 kPa intervals) showed that the lowest value at which the model converged and remained stable was for a cohesion of 550 kPa (initial stress ratio  $K=0.5$ ). A decrease in the cohesion value from 550 kPa to 535 kPa causes the Turtle Mountain slope to fail along a distinct failure surface, as shown in figures 6.15, 6.16 and 6.17. The unstable part of the slope is shown in figure 6.15, presenting a magnified grid plot (30x) for the top central part of Turtle Mountain. The failure surface according to Cruden and Krahn (1978) is included for comparison. Figure 6.16 shows the plasticity indicators at the same stage for a more detailed portion of the grid. A clear band of yielding developed in the Turtle Mountain model with tensile failure behind the crest.



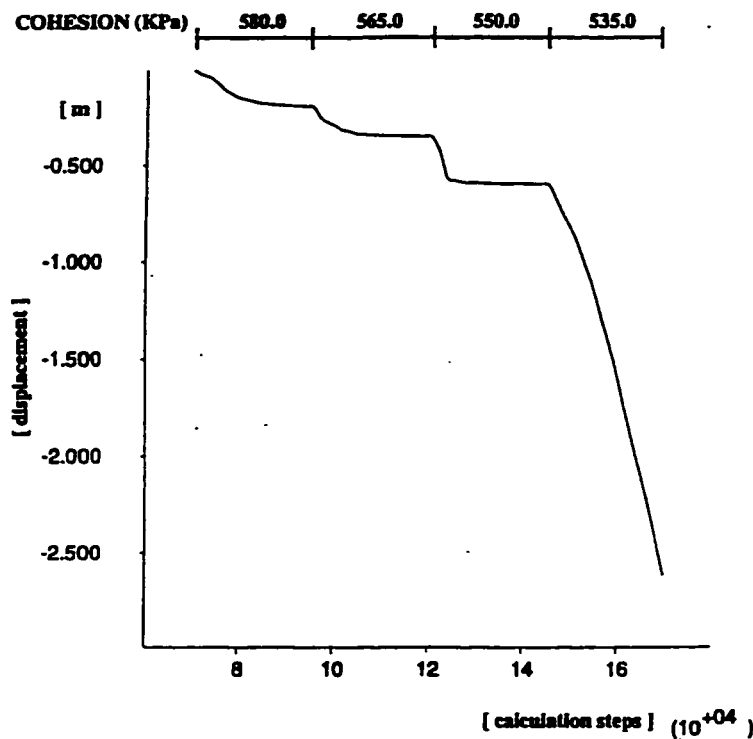
**Figure 6.15.** Failed Part of Turtle Mountain (magnified grid plot, 30x).



**Figure 6.16.** Plasticity indicators for the top part of the Turtle Mountain.



**Figure 6.17.** Total displacement vectors developed in the model.



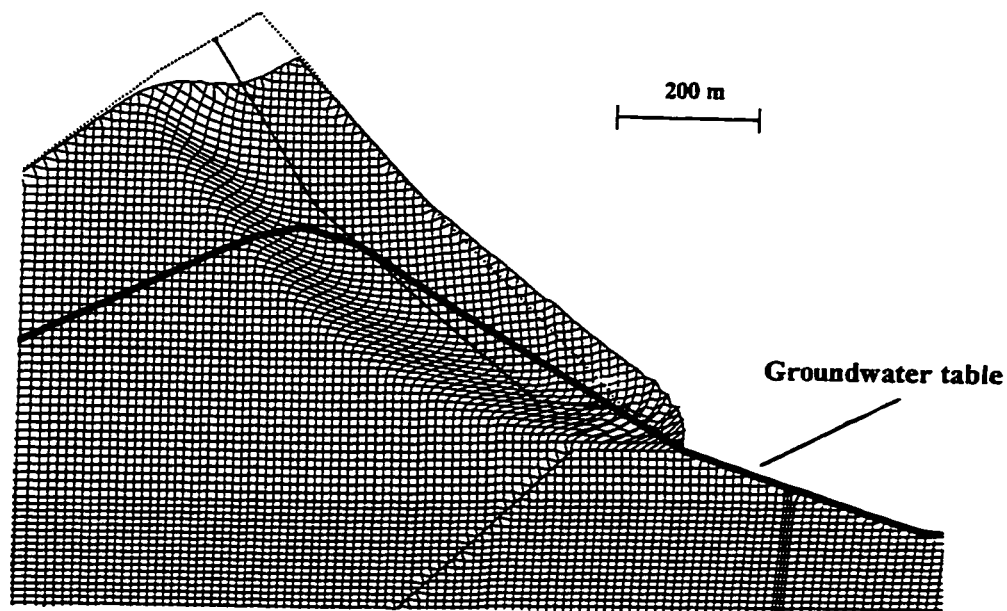
**Figure 6.18.** Record of vertical displacement for a point at top of the Turtle Mountain (point A, figure 6.13) with progressively decreasing cohesion.

Figure 6.17 shows the total displacement vectors developed in the model, and figure 6.18 the record of vertical displacement for a point located at the top of the Turtle Mountain (point A, figure 6.11) as the cohesion was progressively decreased.

Active failure is observed at the fourth solution (figure 6.18), corresponding to a cohesion value of 535 kPa. The predicted failure surface, assuming a continuum, elastoplastic isotropic model, appears to extend deeper into the mountain than suggested by Cruden and Krahn (1978), following a spoon-shaped failure plane typical for homogeneous, isotropic material. The Turtle Mountain rock mass is neither isotropic nor homogeneous, and the failure plane location was predetermined by the geological structure. It is, however, of interest that the failure toed out at the location of the minor thrust fault even in this idealized homogeneous model.

Figure 6.19 shows the result of a stability analysis with assumed groundwater table. A similar analysis procedure as for the “dry” slope was chosen, i.e. decreasing the cohesion value until failure occurred. The lowest value of cohesion for which the slope remained stable was 865 kPa. The decrease to 850 kPa caused a failure to develop as shown in figure 6.19. It is of interest that the failure extended deeper into the slope and toed out lower than was the case for a dry slope. This analysis represents, however, only one possible scenario as no information was available on the groundwater regime existing in the slope prior to failure. Mining would presumably have lowered the original groundwater table elevation.

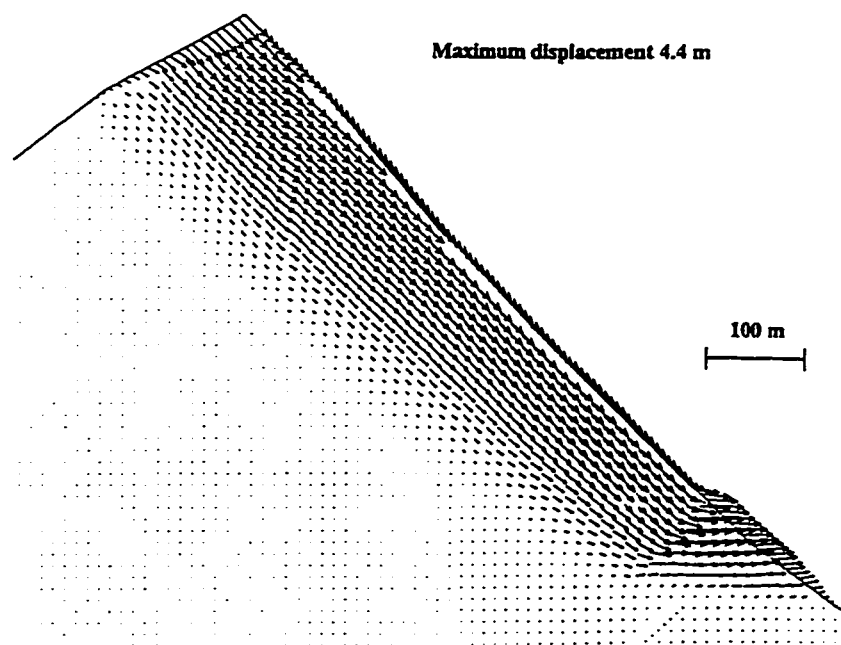
The analysis of a dry slope with a higher initial K-ratio ( $K=1.5$ ) did not show an influence on the location of the failure zone. The major change was that when the cohesion value was decreased to 550 kPa, the displacement in model did not converge and the slope failed, whereas the model with lower horizontal stresses indicated stable conditions at this cohesion value.



**Figure 6.19.** Frank slide analysis with an assumed groundwater table (magnified 50x).

Analysis using the ubiquitous elasto-plastic constitutive criterion with a directional weakness parallel to bedding simulated the probable over-riding structural control on stability. The failure surface became increasingly planar, following closely the dip of the discontinuities. The main break-out zone in the toe area corresponded to the change in dip at the location of the minor thrust fault. Figure 6.20 shows the vectors of total displacement for a model with ubiquitous joints. The cohesion for the rock material was 550 kPa and the friction 30°. The joints have the properties of the flexural slip surfaces, as shown in table 6.3.

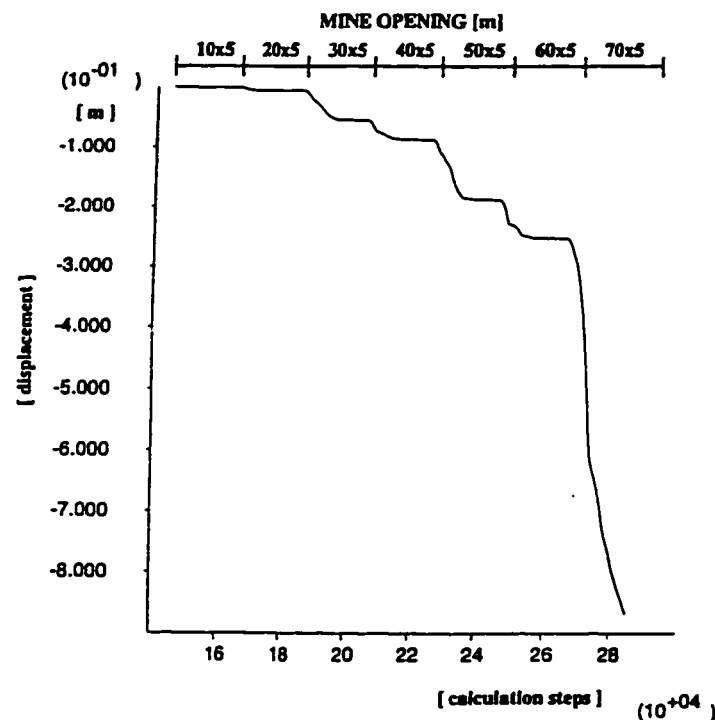
A contrast between the failure surface predicted by continuum modelling and that assumed by Krahn and co-workers is evident at the slope crest where the observed failure tended to follow a joint controlled path within the crest of the anticline as shown in figure 6.15. It is clear that to achieve a more realistic simulation of the joint-controlled upper section of the failure a discontinuum modelling approach is needed.



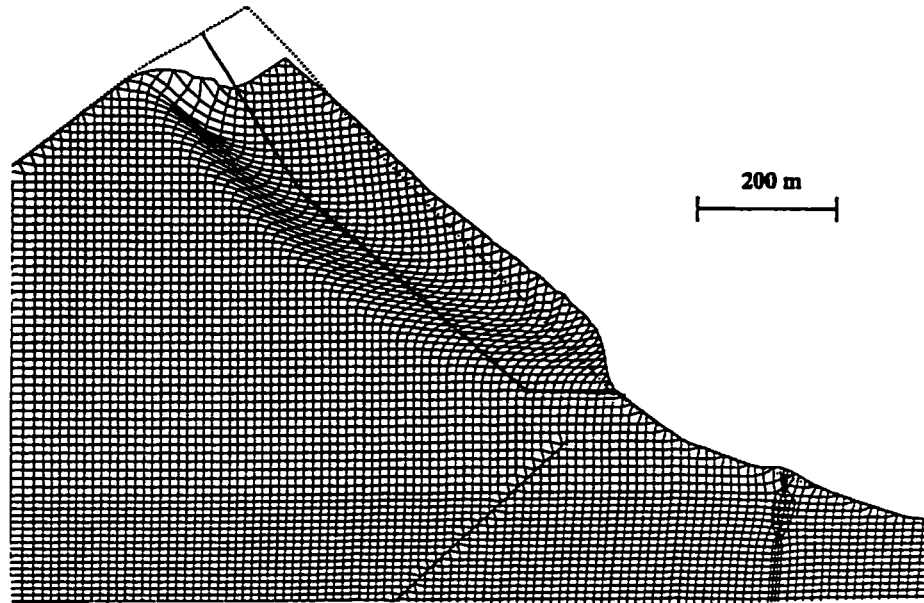
**Figure 6.20.** Total displacement vectors for the application of Ubiquitous constitutive criteria.

### 6.7.1.2 Influence of Mining on Slope Failure Development - Continuum Model

The Turtle Mountain slope is observed to be marginally stable with an assumed cohesion of 550 kPa and an initial in-situ ground stress ratio of  $K=0.5$ . If mining is simulated by progressively deleting 10 x 5 m sections of the model up to 120 x 5 m (representing the dimensions of the maximum coal chamber) a clear failure surface is seen to develop in the slope when the chamber dimensions reach 70 x 5 m. At this excavation stage the displacements in the model no longer converge to equilibrium with further computational time steps. Figure 6.21 shows the development of the vertical displacement history for a point located at the top of the “pre-failure” Turtle Mountain (point A, figure 6.12). A mine opening with a dimension of 60 x 5 m was the last for which the deformation in the slope converged as indicated by the horizontal trace in vertical displacement record. The shape of the predicted failure surface at this stage is shown in figure 6.22.



**Figure 6.21.** The development of vertical displacement for point A (figure 6.11), located at the top of the “pre-failure” Turtle Mountain.



**Figure 6.22.** Failed part of Turtle Mountain after mine opening reached 70 m x 5 m (magnified grid plot, 90x).

This figure shows the magnified (90x) finite difference grid for a mine opening of 70 m x 5 m with the failing slope. Minor upward deformations above the mine are present resulting from the relatively high horizontal stress component after the excavation of the final Turtle Mountain topography. It is of particular interest that the mine walls are seen to deform but essentially remain stable (figure 6.22 shows a magnified grid). No mine opening closure is necessary to induce the slope instability. The maximum inward displacement at the stage shown in figure 6.22 is 0.24 m for the hangingwall and 0.20 m for the footwall. This magnitude is, however, influenced by the discretization of the rock mass. In this case the mine opening walls are represented by zones 10 m x 5 m.

When the cohesion of the Turtle Mountain slope was increased to 580 kPa, representing more stable slope conditions, and the mine opening excavated, the displacement acceleration shown in figure 6.21 after the mine opening reached 70 m x 5 m, was not

achieved. Even a further increase of mine opening up to 120 m x 5 m did not cause the unstable conditions. After each mine-excavation increment, deformation in the slope occurred but the slope stabilized with further computational steps. The displacements in the slope, however, reached a maximum of 1.7 m affecting the same part of the model as in the case with lower cohesion (figure 6.22). As the rock mass behavior is usually strain-softening, it is a reasonable assumption that the actual failure could be induced also for an initially higher cohesion.

### **6.7.2 Discontinuum Approach**

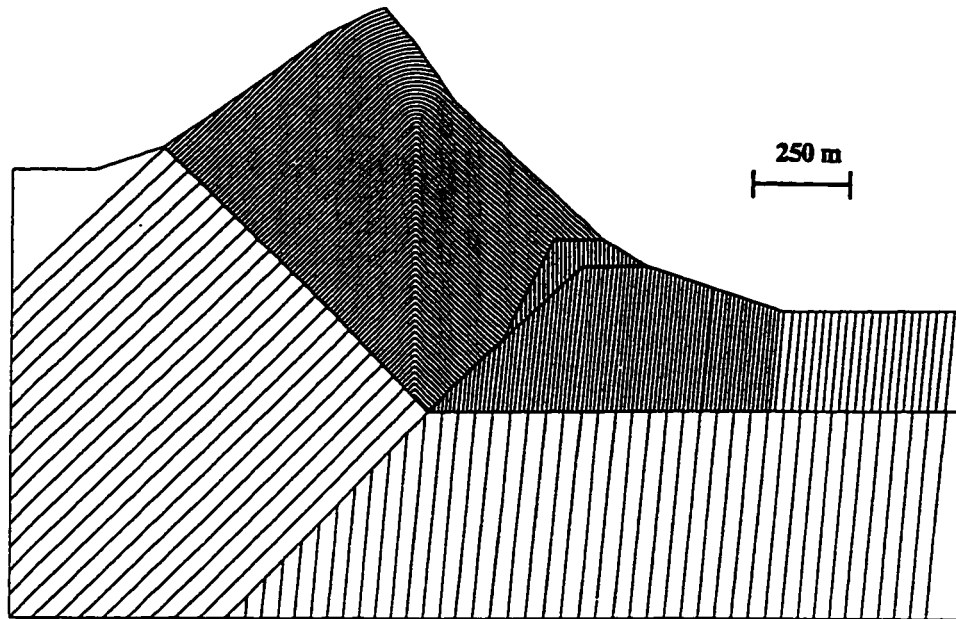
A discontinuum numerical modelling study was undertaken using the UDEC code, (Itasca, 1995) Two main models were analyzed:

- 1) A model assuming bedding discontinuities only (figure 6.23);
- 2) A model assuming both bedding and orthogonal discontinuities (figure 6.24).

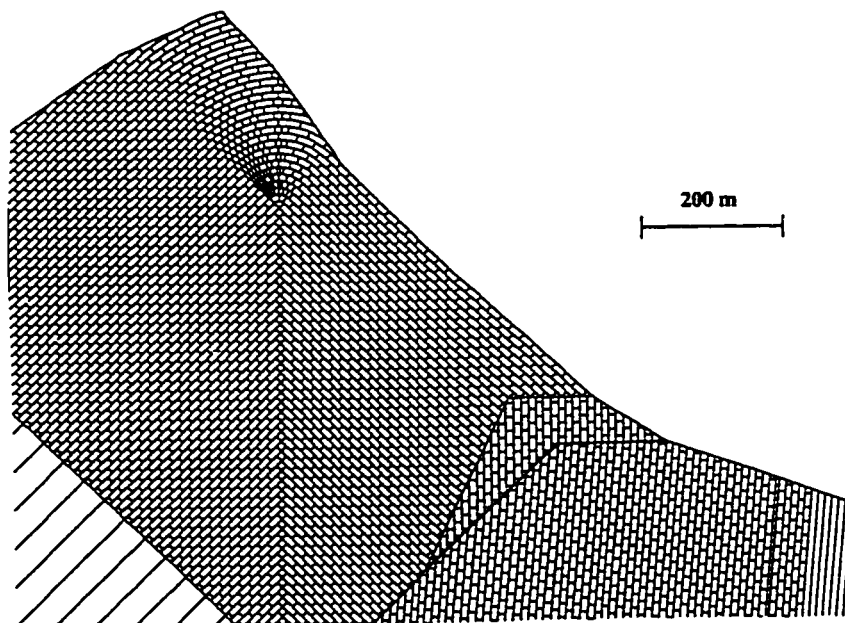
As an initial approximation a bedding plane spacing of 10 m and a spacing of 20 m for the orthogonal joint set was adopted. It is realized that in reality the bedding and jointing may have a spacing of a meter or less, but the modelling of such a geometry would involve a prohibitive number of joint-bounded blocks in terms of computer memory and computational time. A closer spacing for orthogonal jointing was used in the anticlinal crest as it was in this region that joint control on the tensile rear-release mechanism appears critical.

The effect of a minor fault within the slope was simulated as a change of dip in the bedding. The same properties for the intact rock were used as in the continuum analyses. The distinct element analysis also requires input of joint properties.





**Figure 6.23.** Distinct Element model for Frank Slide analysis. Only bedding plane discontinuities are represented.



**Figure 6.24.** Orthogonal jointing pattern in the top part of Turtle Mountain.

A frictional angle of 28° and a cohesion of 221 kPa were assumed to simulate flexural slip surfaces developed along the bedding, and a friction angle of 32° and a cohesion, of 172 kPa, were adopted for the orthogonal joints. Shear and normal joint stiffness values in the order of 20 and 200 GPa/m were assumed, respectively.

#### **6.7.2.1 Modelling Procedure**

Modelling with both types of jointing pattern started with an original rectangular model with dimensions of 2300 m by 1500 m. The material left and right of the Turtle Mountain peak was excavated in a series of 5 steps. The initial excavation was done for a model with high strength properties for blocks and joints to prevent any yielding at this point in the analysis. A value of  $K = 1.5$  was assumed for the in-situ ratio with zero pore water pressures. The modelling sequence was divided into two steps:

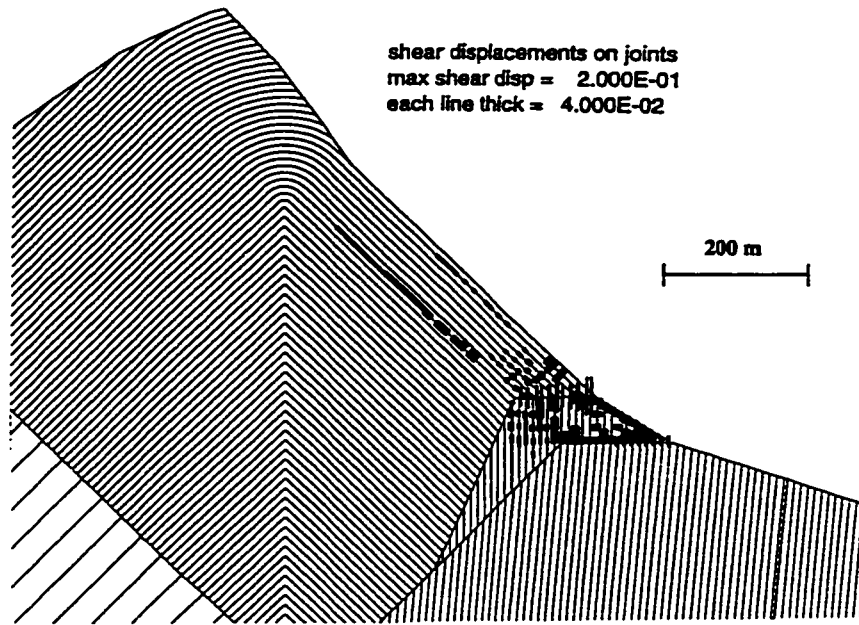
- In the first step the potential failure was confined to the discontinuity surfaces, by assuming a linear elastic behavior for the deformable joint bounded blocks. The discontinuity surfaces were given values from Cruden and Krahn (1978) as shown in table 6.3. The peak strength of flexural slip surfaces was used. The influence of mining was examined by assuming the maximum mine opening (120 m x 5 m).
- In the second step, failure of the joint bounded blocks was allowed in addition to failure along discontinuities, assuming a Mohr-Coulomb constitutive failure criterion. Varying strength parameters were applied, starting with properties as determined from the continuum modelling back-analysis (cohesion of 550 kPa, friction angle 30°). The influence of progressive mine opening was investigated in a similar way as in the continuum analysis.

### **6.7.2.2 Elastic Isotropic Model with Slip allowed on Discontinuities**

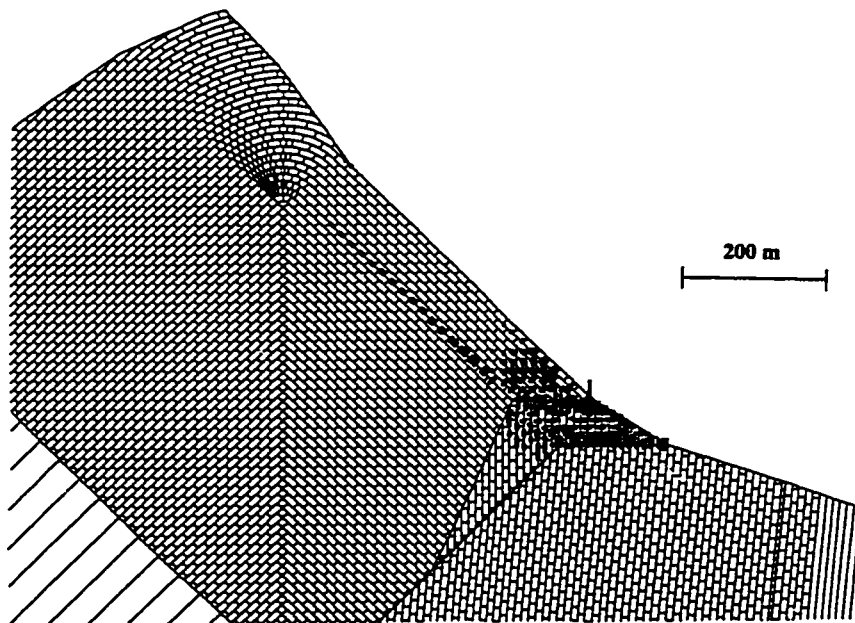
Analysis of the slope, with displacements confined mainly to the discontinuities due to the elastic joint bounded blocks, resulted in shear displacement mostly in the area between the two faults, as well as along the bedding surfaces within the slope as shown in figure 6.25. The main shearing movement was caused by the compression of the zone between the Turtle Mountain fault and the minor thrust fault. A fairly continuous shearing occurs along a bedding plane located 80 m inside the slope.

This shearing takes place on a length approximately 300 m long. Due to the absence of release surfaces and the elastic constitutive criteria used for blocks, the deformations in the model converge to zero with progressive computational steps. Similar results were obtained for a model with an orthogonal jointing pattern, as shown in figure 6.26. The location of shearing for both models seems to be influenced primarily by the geometry of the two faults.

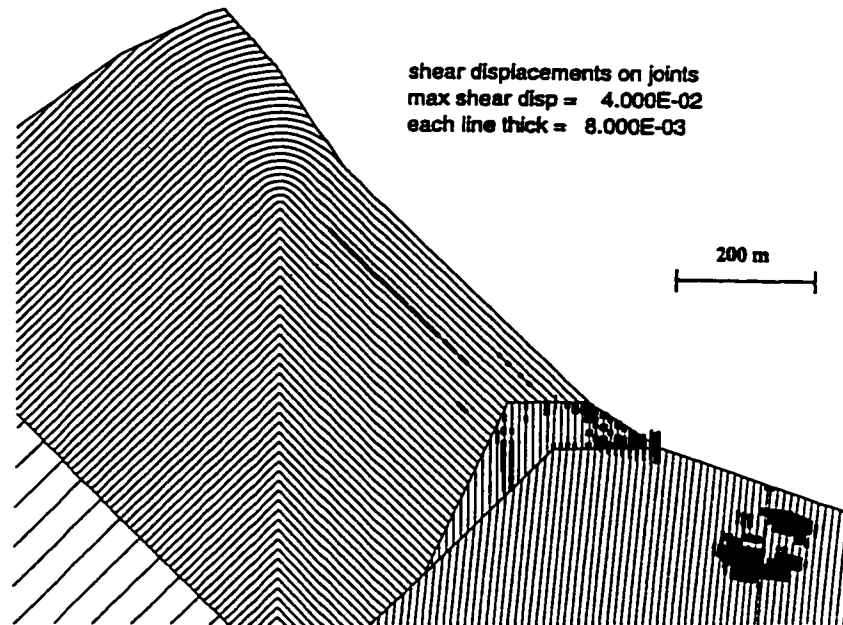
In the next step of the analysis, displacements in the model were reset to zero and the mine opening excavated. Only deformations for the maximum size of mine opening (120 m x 5 m) were investigated. Figure 6.27 shows the shear displacement for a model with bedding plane discontinuities. Most of the shear displacements in model resulting from mining are concentrated around the mine itself. It is of interest, however, that shearing is taking place also in the slope itself. The location of shearing above the Turtle Mountain fault is the same as the original shearing in the model without the mine opening. The orthogonal jointing geometry increased the shearing in model as shown in figure 6.28. Figures 6.27 and 6.28 have the same scale for the shear displacement with the maximum displacement of 0.2 m. The top part of the Turtle Mountain does not show major signs of movement due to the interlocking nature of blocks in this part of model and the absence of continuous release surfaces.



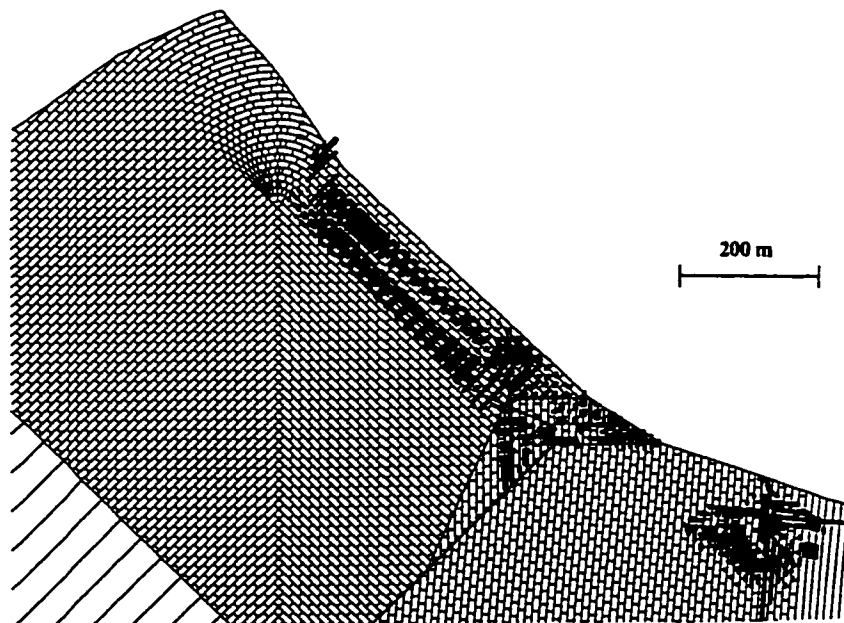
**Figure 6.25.** Shear Displacement along discontinuities for “elastic isotropic blocks”. Model simulating bedding planes.



**Figure 6.26.** Shear Displacement along discontinuities for “elastic isotropic blocks”. Model simulating orthogonal jointing. Shear displacement same scale as figure 6.25.



**Figure 6.27.** Shear displacement along discontinuities for “elastic isotropic blocks” resulting from the mine opening. Model simulating bedding planes.

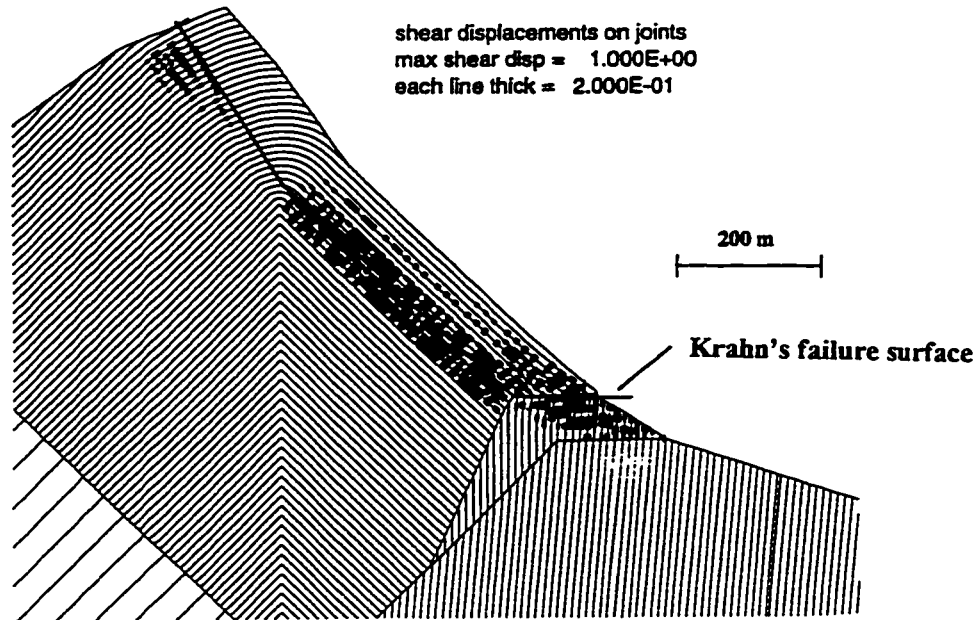


**Figure 6.28.** Shear displacement along discontinuities for “elastic isotropic blocks” resulting from the mine opening. Shear displacement same scale as figure 6.27. Model simulating orthogonal jointing.

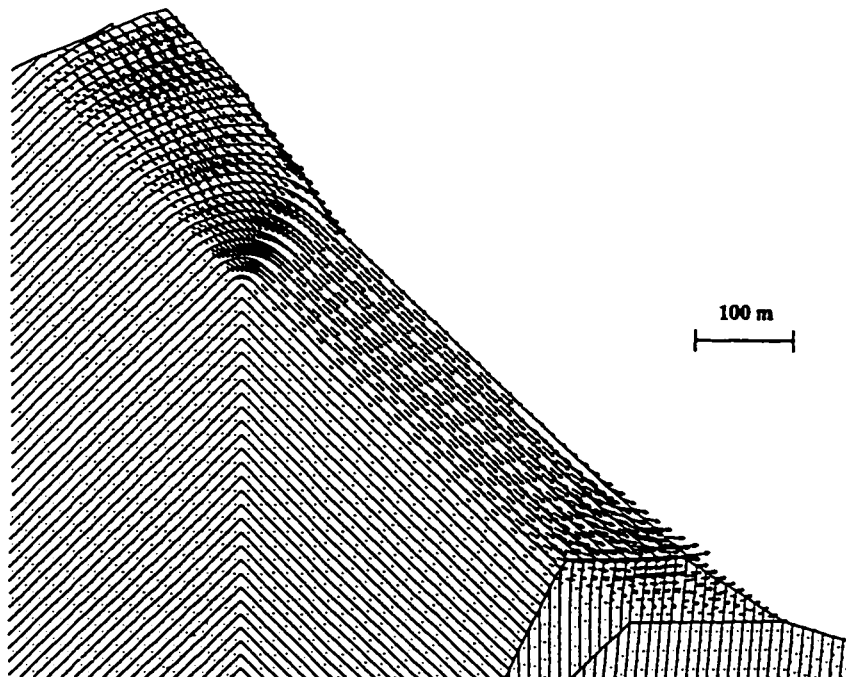
### **6.7.2.3 Elasto-Plastic Model**

In this model, Mohr-Coulomb constitutive criterion was assigned to the intact, joint bounded blocks to allow for a full development of the failure surface. The initial strength values were based on the results from the continuum modelling analysis and the cohesion of 550 kPa was assumed for the initial analysis. The model with this block strength proved to be unstable, with failure location as shown in figures 6.29 and 6.30. Figure 6.29 shows the shear displacement along bedding planes at an advanced computational stage with the failure surface after Cruden and Krahn (1978) included for comparison. The shearing corresponds closely to the location of in-situ failure surface. Figure 6.30 shows the displacement vectors at the same computational stage with the maximum displacement being 10.2 m. It has to be stressed, however, that the displacements are in this case for a failing slope and, therefore, a function of computational steps and not a actual field displacement.

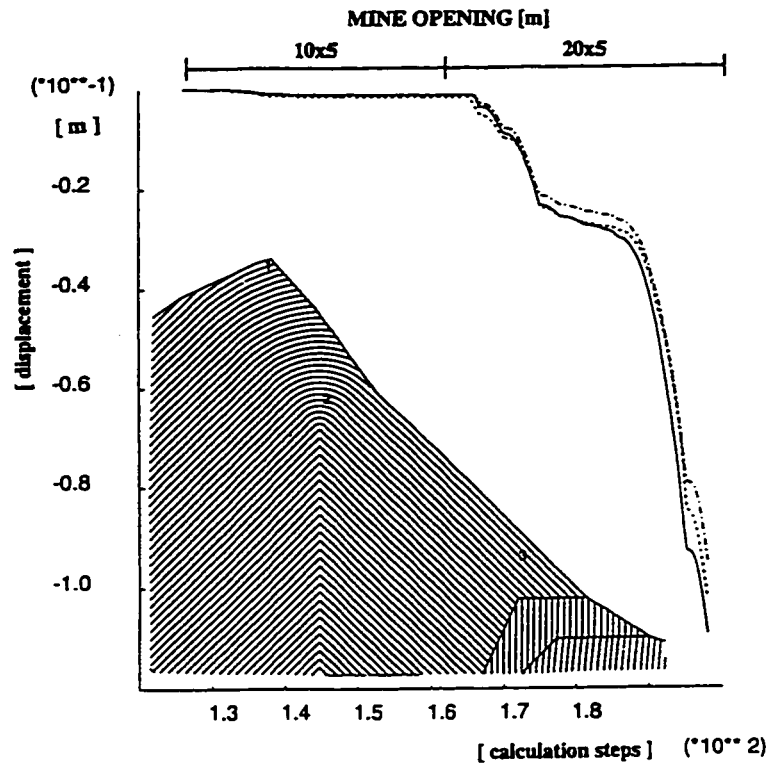
The cohesion of 550 kPa that resulted in stable conditions for the continuous model proved to be insufficient to prevent the failure development due to the inclusion of bedding planes in the discontinuous model. Therefore, as in the continuum modelling analysis, an attempt was made to determine a “marginal” stability state for the Turtle Mountain. To find this state, the cohesion of the joint bounded blocks was progressively increased until displacement in model did not show any acceleration. Three points in the slope, were selected for displacement monitoring as shown in figure 6.31. Points near the top of Turtle Mountain, in the hinge of the anticline, and near the minor trace fault were selected.



**Figure 6.29.** Shear displacement along bedding planes for model with block cohesion equal to 550 kPa.



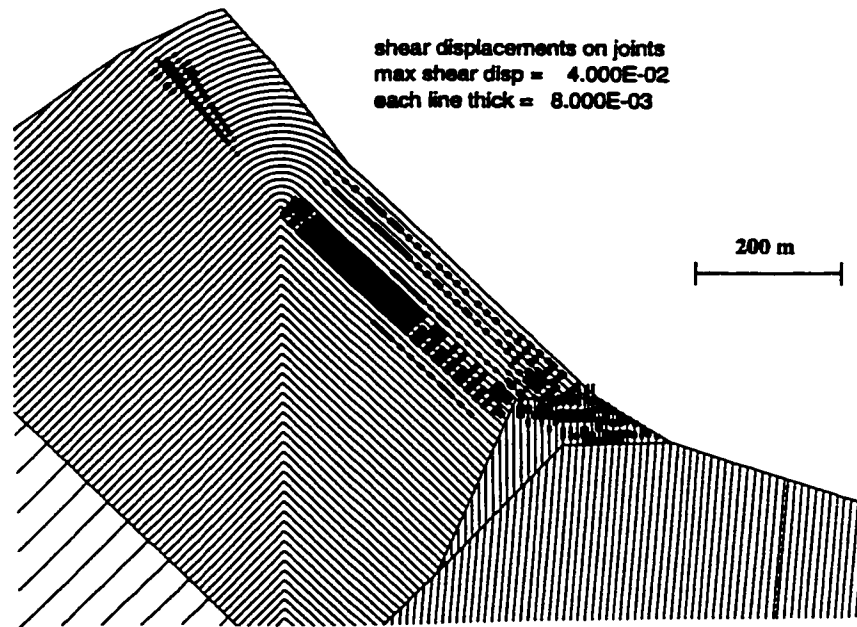
**Figure 6.30.** Total displacement vectors in model. Maximum displacement 10.2 m.



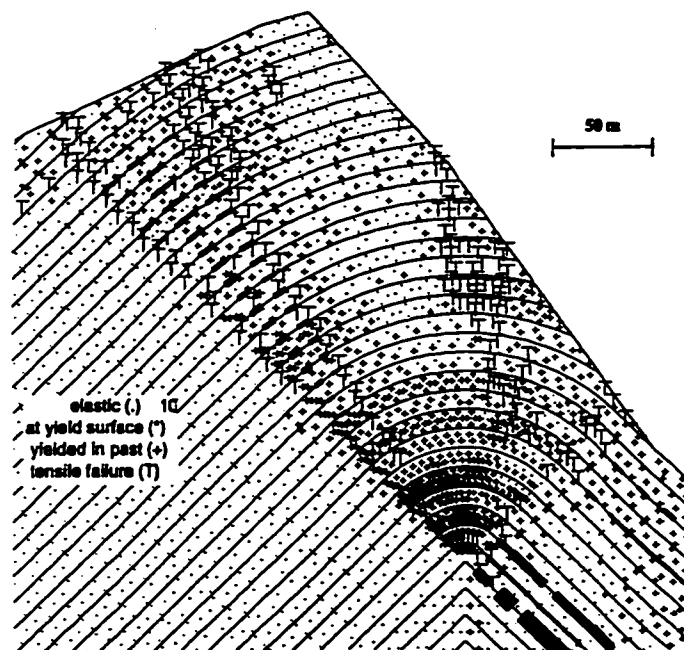
**Figure 6.31.** History of vertical displacement for three points in the model.

The required state of “marginal” stability was achieved when the cohesion for blocks was increased to 1050 kPa. The mine opening was then progressively excavated in 10 m x 5 m increments. Displacements in the model were monitored to record any changes in stability conditions. Overall instability was observed after the second stage, when the mine opening was 20 m x 5 m. Figure 6.31 shows the history of the vertical displacement at the three points selected for monitoring. Shear displacement along the bedding planes is shown in figure 6.32. Major shearing is concentrated at depth of approximately 80 m to 120 m within the slope, in the area between the Turtle Mountain and minor fault and behind in area at the top of Turtle Mountain. The shearing at the top of Turtle Mountain corresponds closely to the actual failure surface as determined by Cruden and Krahn (1978). Plasticity indicators and shear displacement for the top part of Turtle Mountain are shown in figure 6.33. Tensile failure and bedding plane shearing indicate the possible location of failure plane in this part of model.



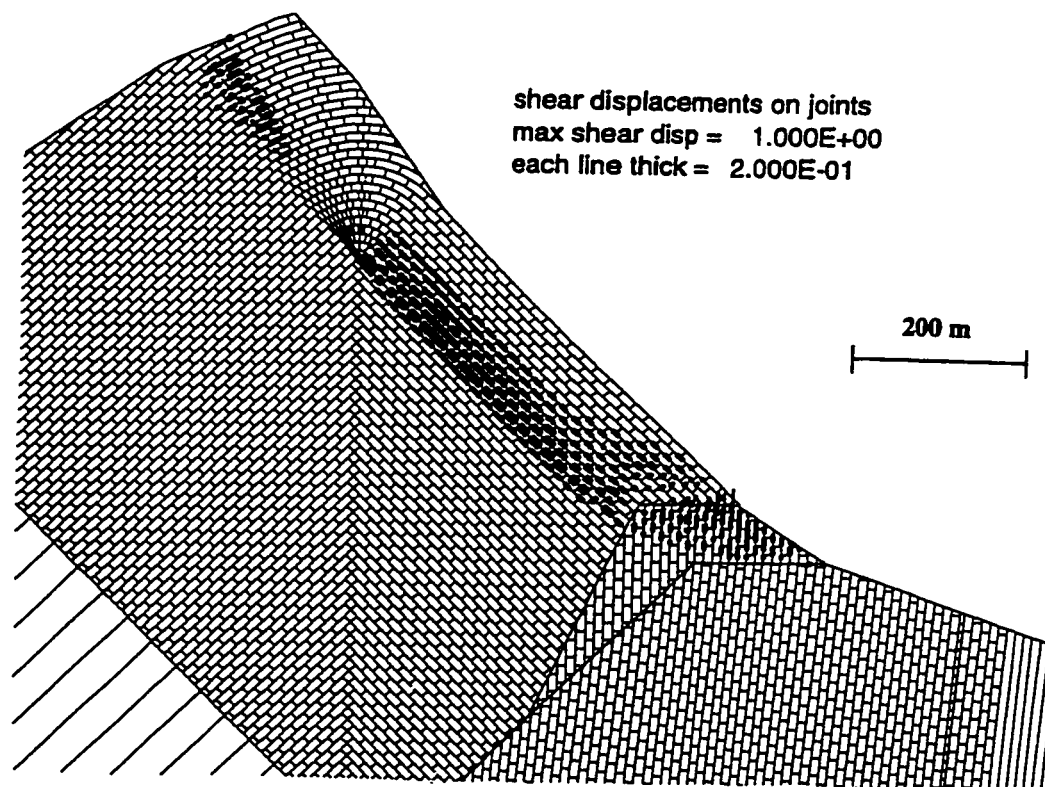


**Figure 6.32.** Shear displacement along bedding planes developed in slope as a consequence of mine opening.



**Figure 6.33.** Plasticity indicators for the top part of Turtle Mountain developed in model as a result of mining.

Figure 6.34 shows the shear displacement for the model with orthogonal jointing and intact cohesion of 550 kPa for the blocks. The deformation affected similar parts of slope, as in the case of the model with bedding planes only, and corresponded very closely with the actual failure surface. Attempts to increase the cohesion of the blocks and find a “marginally” stable slope were not successful as the blocks just above the minor fault were unstable for a wide range of strength parameters. An unrealistically high cohesion for the 10 m x 20 m blocks was necessary with results similar to the model with elastic isotropic constitutive criteria. A change in either the strength of the discontinuities or orientation of the minor thrust fault would have been required. These changes are, however, not supported by the available data.



**Figure 6.34.** Shear displacement along joints for orthogonal discontinuity structure and block cohesion of 550 kPa.

## 6.8 Conclusions

Both, continuum and discontinuum, numerical modelling techniques have been applied in the analysis of the Frank Slide. The use of a Mohr-Coulomb failure criterion for the rock mass as well as the explicit representation of discontinuities, provided new insights into the failure mechanism. The results demonstrate the presence of a structurally controlled failure surface and a high probability that underground mining acted as a trigger for the final movement. Similar general conclusions were obtained regardless of the numerical technique used in the analysis, although the distinct element method allowed for a more realistic representation of the jointed rock mass.

A relatively low cohesion value (535 kPa) is mobilized in the rock mass at failure using the continuum homogenous isotropic modelling approach. This value can to some extent, be justified by the highly jointed nature of the rock mass forming the Turtle Mountain. The use of Ubiquitous criterion allows for an increase in mobilized cohesive strength and results in a more realistic, failure surface orientation.

The varying initial ground stress conditions did not show a significant influence on the location of the failure surface. The difference between the back-calculated values of cohesion was only 15 kPa (550 kPa for  $K=0.5$  and 565 kPa for  $K=1.5$ ). It is realized that the two stress levels used in models are simplified assumptions. The pre-failure ground stress for the Turtle Mountain is not known and is rather very complicated, considering the intense folding, faulting and erosion processes.

The presence of an arbitrarily assumed groundwater table increased the cohesion necessary for stable condition by 57%. Again, the uncertainty in input data regarding the groundwater regime before and after the mining took place at the base of Turtle Mountain does not allow for wide reaching conclusions to be drawn. It can be assumed, however, that if the deformation developed in a model without the presence of groundwater its inclusion will only contribute to the overall instability.

With the slope at or near the limit equilibrium state the mining induced deformation proved to be an important factor in the stability of Turtle Mountain. Excessive mine deformation was not required to initiate the rock slide. This differs from previous findings that the mining could not have had an influence on the slide initiation because the mine did not suffer any damage and was reopened shortly after the slope failure. It was demonstrated that the deformations resulting from releasing the coal from the chambers accumulated until they reached a “critical threshold” overcoming the final resistance of the slope to failure.

Both continuum and discontinuum modelling indicate a close agreement between the critical predicted failure surface and the assumed surface in previous studies.

The primary cause of the Frank Slide is undoubtedly the adverse anticlinal structure that was present within Turtle Mountain. This, combined with the presence of thrust faults and a general reduction in available shear strength along discontinuity surfaces, would have resulted in a slope near to limiting equilibrium. Presented analyses attempt to clarify the failure mechanism involved in the Frank Slide. Results show that the observed failure surface, used in previous limiting equilibrium analyses, is indeed predicted by both continuum and discontinuum modelling. The importance of tensile failure and explicit jointing in the development of a rear release mechanism in the upper part of the slope is illustrated. A definitive analysis of the Frank Slide will probably never be attained as there will always remain too many unknowns, requiring assumptions based on engineering judgment. The presented modelling results, however, indicate that coal mining could have acted as a trigger for the final failure of the Turtle Mountain slope which may have been near limiting equilibrium. The Frank Slide is a complex failure, with numerous contributory causes. Analyses conducted in this thesis, although adding further insight into the failure mechanism, are nevertheless limited to two dimensions. To model the failure process more realistically, three dimensional continuum and/or distinct element models would be required. The amount of available

data with regard to structure, strength properties, mining and pre-failure groundwater conditions would probably not justify such an analysis.

## **6.9 Suggestion for Future Research**

Future analysis of the Frank Slide failure mechanism should include:

- A comprehensive rock mass characterization of both, the Paleozoic limestones and Mesozoic shales, siltstones, sandstones and coal as an input for numerical modelling.
- Additional laboratory testing to that by Krahn (1974) to enhance the understanding of the shear strength parameters.
- No data about groundwater regime are available. Presented numerical modelling analysis demonstrates this requirement. It would be of interest to conduct a sensitivity analysis assuming variable pore pressure distribution within the Turtle Mountain.
- A more detailed geomechanical assessment of the Turtle Mountain fault as well as the minor thrust fault is necessary due to their important role in Frank Slide stability.
- Although presently not justified by the lack of data, a simplified three-dimensional analysis could further enhance the understanding of the relationship between coal mining and stability of Turtle Mountain fault.
- The use of strain-softening constitutive criteria would allow failure to develop with a higher initial cohesion. The progressive “material softening” as a consequence of underground coal mining would be of particular interest.
- Analysis of various ground stress conditions to confirm the apparent insensitivity of failure mechanism to ground stresses.

## **CHAPTER 7**

### **Conclusions and Discussion**

The objective of this study was the analysis of complex slope deformations through the application of numerical modelling techniques. Complex slope deformations, in this thesis, included cases where the use of more conventional analytical tools such as limit equilibrium techniques or the use of empirical criteria were not readily applicable due to the adverse geological and environmental conditions or human activity. Both continuum and discontinuum numerical modelling techniques were applied to hypothetical slopes and selected case studies, concentrating primarily on the failure mode and deformation mechanisms. The main modes of failures included sliding, toppling, spreading as well as multi-component mechanisms. Modelling has been undertaken using a two dimensional finite difference code, FLAC (Itasca, 1992), and a distinct element code, UDEC (Itasca, 1993). Visits to sites with complex landslides were undertaken, including the Canadian Rocky Mountains, the Alps and the Western Carpathians. The study was motivated by the author's previous experience with various types of landslides in the Carpathian Mountain range.

#### **7.1 Summary of Results and Recommendation for Future Work**

The following main conclusions and recommendations with respect to research conducted on the following topics are presented:

### **7.1.1. Block-Type Deformations of Rigid Joint Rock Masses Overlying Weak Layers**

- I. The distinct element method proved suitable for the analysis of a geological structure comprising rigid joint-bounded blocks overlying relatively weak layers (assuming a mixed continuum - discontinuum approach).
- II. The failure mechanism at Spis castle included toppling and rotational sliding of the rigid blocks.
- III. The resultant deformations were dependent on the strength and thickness of the weak layer, as well as the jointing pattern in the rigid rock cap.
- IV. The relationship between the block width and the weak layer thickness proved to be a decisive factor in whether the block will topple or slide.
- V. The hypothesis that the deformations at the Spis castle are governed primarily by the presence of a weak, plastic layer under the base of the travertine blocks, was in good agreement with the numerical modelling results.
- VI. The different ground-stress ratios examined did not have an influence on the failure mechanisms. For higher horizontal stress, increased extrusion of the weak material from underneath the base of travertine blocks took place.
- VII. The effect of differential block displacement on the fracturing of castle walls and objects was illustrated.

### **Recommendations**

- I. The rock mass structure of the Spis castle foundation, as well as the block displacements, are three-dimensional. The present analysis was confined to two-dimensions due to the lack of available software. The future application of a three-dimensional program capable of simulating the deformations would be beneficial.
- II. Little is known, quantitatively, about the strength and deformation properties of the rock and soil types. Additional material testing would provide interesting data,

especially for the soils in the creep zone. It is not expected, however, that this would change in principle the results of the present analysis.

III. The creep constitutive criteria could be used in future studies once sufficient information from the displacement monitoring program is available.

### **7.1.2. Toppling with Emphasis on Slope Deformation at the Luscar Mine, Alberta**

- I. The mechanisms of instability in the initial phase were confirmed to be due to flexural toppling developed in thinly bedded strata comprising siltstones, sandstones and shales.
- II. The toppling was confined to a distinct quasi-linear failure surface developed through “fracture” of the thin beds. The average dip of the failure surface as predicted from modelling was  $28^\circ$ , providing a shear surface for the subsequent translation sliding movement inferred from monitoring data.
- III. UDEC proved suitable for simulating the complex failure mode and predicted behavior consistent with field observations.
- IV. Numerical modelling confirmed and provided increased understanding of the suspected failure mechanism.
- V. Simulation of a planned extension, using numerical modelling, predicted that problems with slope stability could be expected. This enabled the mine personal either to take a different direction in the mine layout, or to prepare for the instability problems, thereby minimizing the consequences of failure.

### **Recommendations**

- I. Modelling was performed only for one magnitude of initial ground stresses assuming a constant K ratio equal to 1.5. The intense folding in the area may justify further analyses to assess the influence of different ground stress conditions on the slope deformation.



- II. The present modelling analyses examined only one level of the groundwater table. The acceleration of failure during the spring breakup would justify a closer examination of the influence of groundwater on open pit slope stability at the mine site.
- III. The influence of cross-joints on the failure development could provide additional information on the failure mechanism.

### **7.1.3. The Influence of Underground Mining on Slope Instability**

- I. The horizontal component of displacement increases significantly when underground mining takes place under a slope.
- II. Numerical modelling confirmed field observations (from literature survey) that displacement of points located at the slope follow the slope gradient rather than the direction towards the panel centre.
- III. The degree and type of slope instability depends on both the location of underground mining relative to the slope as well as on the geological structure within the slope.
- IV. Underground mining can trigger slope failures controlled by both pre-existing discontinuities and fractures developed in the overburden as a consequence of ground subsidence.
- V. The deformations caused by underground mining may in the case of an unstable slope extend significantly beyond the expected or assumed “safe limits” of influence. This is especially important with respect to any structures located near the crest or toe of a slope.

### **Recommendations**

- I. The application of numerical modelling techniques presented involved the investigation of only a limited number of cases. Examination of other scenarios,

including mining inside the slope, multi-seam mining, or undermining of old workings, would be of significance.

- II. The analyses presented in this work using a continuum approach could be repeated with the incorporation of strain softening constitutive criteria to examine the “safe distance” from a slope for varying slope geometries and geology. Such analyses would require the use of more powerful computer hardware such as the Ultrasparc 170E.
- III. The influence of mining an inclined seam in different positions with respect to the slope would allow more insight into slope failure mechanisms.
- IV. Constraining of numerical modelling using subsidence measurements is necessary in future studies

#### **7.1.4. The Frank Slide: A Re-examination of the Failure Mechanism**

- I. The important influence of underground coal mining at the base of the Turtle mountain on the Frank Slide was suggested by the results of numerical modelling.
- II. Both continuum and discontinuum numerical modelling techniques predicted a slope failure with the progressive increase in mine opening.
- III. The failure surface developed in the model, especially utilizing UDEC, is in a good agreement with the failure surface observed in field.
- IV. Discontinuum analysis proved the influence of structural control on the resultant failure surface.

#### **Recommendations**

- I. A re-assessment of input parameters and rock mass characterizaton.
- II. The investigation of the influence of different ground stress conditions and groundwater table on the Frank slide stability should be considered.

- III. Three-dimensional modelling would allow for a more realistic simulation of the mine openings.
- IV. The orientation of the Turtle Mountain fault and the minor thrust, will have an influence on the deformations which should be investigated.
- V. Consideration of a strain softening constitutive criterion would allow for more deformation in the model.
- VI. The various factors influencing the stability of the Frank slide could be analyzed using a probabilistic approach.

## **7.2 Discussion**

Most of the analyses in this study have assumed that the rock and soil mass will behave as an elasto-plastic Mohr-Coulomb material with strength characteristics dependent on the friction angle and cohesion. More “sophisticated” material constitutive criteria can be incorporated into the models and used in analyses. The author’s experience with numerical modelling as well as the experience of other workers (i.e. Moss, 1994; Cundall, 1994), is that as increased attempts are made to use more complex models of rock and soil mass behavior to reflect more accurately the often complex material deformation, then the more modelling difficulties arise and the more tenuous the final results become.

This work has clearly demonstrated that numerical modelling methods allow for both qualitative and quantitative analysis of complex slope failures that were previously considered not to be readily subjected to an analysis. Sixteen years ago, Hoek and Bray (1981) indicated the importance of developing methods capable of analyzing the stability of slopes in which complex failures occur. They outlined several failure mechanisms in their classic book on Rock Slope Engineering, including sliding taking place simultaneously on two failure surfaces, buckling of thin rock slabs resting on low strength base plane, simultaneous sliding and toppling and deformation in horizontally

bedded slopes consisting of hard and soft materials. The present numerical modelling research has attempted to contribute to an increase in the understanding of failure mechanisms involving complex slope deformation. Analysis of both potential failures and back-calculation of existing ones, can be simulated.

Numerical modelling continues to evolve from qualitative investigation of the failure mechanism to a design tool in geomechanics. The literature survey conducted of publications during the past five years, shows a gradual shift in numerical modeling application away from applications assessing possible failure mechanisms and the development of overall instability, to a practical design tool used more and more in the routine engineering practice. This, in turn, necessitates a critical review of the mechanical properties of materials including scale effects. In most cases a scaling of input properties is necessary to simulate the observed field behavior. Physical properties that are not routinely determined, such as the joint normal and shear stiffnesses, are necessary input data when discontinuum analyses are conducted.

Various problems were encountered during the research program. A major difficulty was encountered with the length of individual model run times. For example, the UDEC program for subsidence prediction, more realistic displacement magnitudes for jointed media are obtained when blocks with smaller dimensions are used. This, in turn, requires models with a extremely large demands on computer speed and memory. Considering the different parametric studies which are necessary for model calibration, and the various models needed to evaluate or dismiss working theories throughout the research procedure, this presents a limiting factor with obtaining results in a practical time period. The execution time for individual models remains a limitation, although with the increase processing speed of new computers, this drawback is gradually decreasing.

An important aspect is also the availability of storage space for individual model runs. Large numerical models utilizing the FLAC and UDEC codes, can occupy as much as 15-20 Megabytes of memory. Multiplying this amount by numerous model runs when

investigating various parametric options, the data storage becomes significant. Numerical modelling for the present thesis work started in the fall 1991 with two SPARC2 workstations available for numerous projects. By the time of research conclusion their numbers increased several times and SPARC4, SPARC20 were added. In the final month of the research, an UltrasparcI workstation became available. From the research point of view, faster computers allow investigation of more models in the same time span and a more “realistic” representation of materials and structures. It is essential to realize that the model is always a simplification of reality rather than its imitation. Larger and “better” models will provide improved simulations but will not guarantee the “right answers”. The quality of input data will always control the model results and care must be taken to ensure that the final result does not lose sight of the often crude assumptions made at the outset. A state of constant re-analysis of results is an inherent factor in numerical modelling, involving the construction of bigger and better models, in an effort to understand and solve the problems. As Cundall and Starfield (1988) note “...as one includes more and more detail, one loses intellectual control of the model and so it becomes less instead of more effective.”

When analyzing the different types of complex slope deformations it is important to run numerical models several times, and to examine the influence of variations in applied stresses, excavation sequence, rock and soil mass properties and design of remedial measures. Each significant parameter should be varied systematically over its maximum credible range, in order to determine its influence on the overall slope behavior. This approach is becoming more and more popular with the growth of the large, high speed computers.

The validation/calibration of numerical modelling results with the actual deformation data should be always performed if warranted. However, as pointed out by Hoek et al. (1991) adequate validation can be often a difficult goal to achieve and, therefore, models should be used cautiously and thoughtfully at all times. They should never be run once

only. "...it is in the sensitivity of the results to changes in parameters and assumptions that the modelling is most informative."

Figure 7.1 presents several concepts which should be considered when applying numerical modelling techniques to slope analysis.

The importance of three-dimensional numerical modelling will increase in future. Three-dimensional numerical modelling programs are presently available, but these are either limited to an elastic assumption of the rock mass behavior or designed more for the analysis of underground excavations. Such three-dimensional models of slope failures have found, so far, very limited practical use due to the increased number of assumptions required, and the computing power needed.

In the future, the coupling of numerical modelling techniques with other types of analysis and investigations may offer particular advantages. For example, numerical

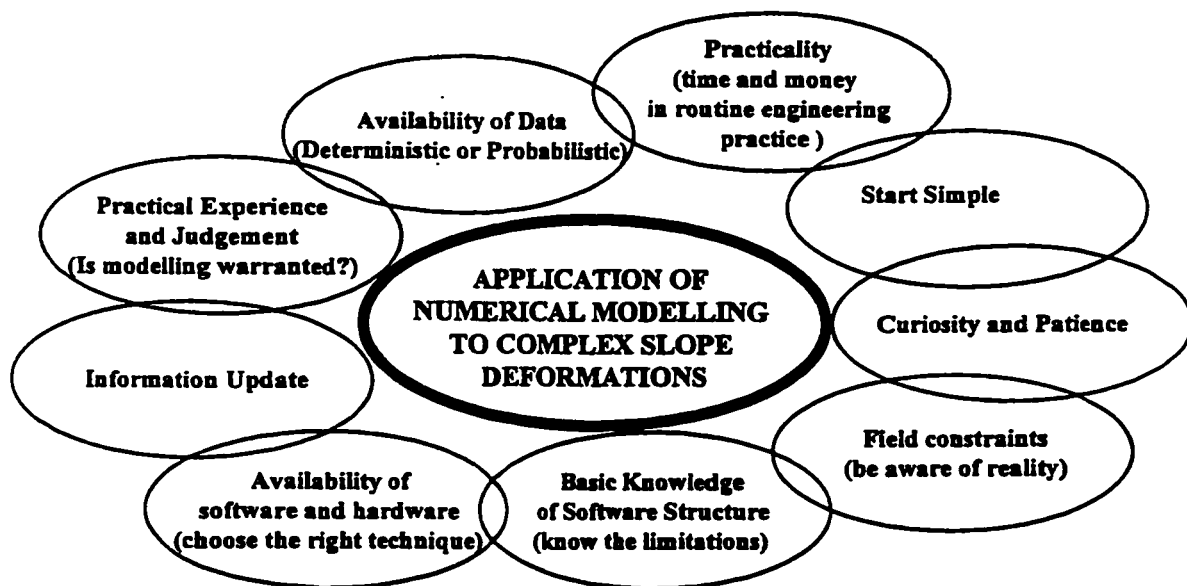


Figure 7.1. Concepts to be considered in the numerical modelling applications to complex slope deformation analysis.

modelling can be used to investigate the likely mode of failure and the location of failure surface and subsequently, limit equilibrium, and probabilistic methods can assess the factor of safety and likelihood of failure. The combination of numerical modelling and probabilistic techniques is a very useful approach. Eventually, the incorporation of probabilistic techniques will allow not only the risk of failure to be assessed but the probability of occurrence of various failure mechanisms, given specified material properties and geometry.

The question of time with respect to slope deformations should be addressed in the future. This will require both more information on the time-dependant behavior of rock and soil masses as well as developments in numerical codes.

This thesis has attempted to demonstrate that numerical modelling when fully integrated with field observations and experience is an invaluable tool in slope stability studies. It is believed that this work will be valuable to both research workers utilizing numerical modelling techniques as well as practical engineers.

## References

- Adachi, T., Ohnishi, Y. and K. Arai, (1991). Investigation of toppling slope failure at Route 305 in Japan. Proceedings International Congress of Rock Mechanics Aachen, Germany 1991, pp. 843-846.
- Adhikary, D.P., Dyskin, A.V. and R.J. Jewell, (1995). Analysis of fracture and deformation processes during flexural toppling in foliated rock slopes. Rossmannith (ed.), Proceedings Mechanics of Jointed and Faulted Rock, Vienna, pp. 611-616.
- Agljukov, C.I., Ivancov, L.M. and V.A. Bajkov, (1990). Effects of underground mining on mine slope deformation (in Russian). Gornyj Zhurnal. 7, pp. 21-23.
- Ahola, M.P., (1990). Geomechanical evaluation of escarpments subjected to mining induced subsidence. Hustrulid and Johnson (eds.) Rock Mechanics Contributions and Challenges. Proceedings 31st U.S. Rock Mechanics Symposium., pp. 129-136.
- Allan, J.A., (1933). Report on the stability of Turtle Mountain, Alberta. Department of Geology, University of Alberta, pp. (not available).
- Anderson, F.W., (1986). The saga of the Frank slide. Gopher book No.19, Publisher - Frank Anderson, P.O. Box 9055, Saskatoon, SK, S7K 7E7.
- Anguelov, K.A., Metchkarski, P.S., Iliev, T.A. and A.V. Lakov, (1983). Prognostication of the stability of slopes over underground works. Proceedings International Symposium on Engineering Geology and Underground Construction, Lisbon, Portugal, pp. 1135-144.
- Arcamone, J and R. Poirot, (1983). Open-pit mining over underground extraction - Interactive problems (in French). International Conference of Rock Mechanics, Melbourne, 2, pp. E115-118.
- Ashby, J., (1971). Sliding and toppling modes of failure in model and jointed rock slopes, M.Sc. Thesis, Imperial College, Royal School of Mines, London,
- Aydan, Ö. and T. Kawamoto, (1992). The stability of slopes and underground openings against flexural toppling and their stabilization. Rock Mechanics and Rock Engineering, 25, pp. 143-165.
- Bai, M. and D. Elsworth, (1994). Modeling of subsidence and stress-dependent hydraulic conductivity for intact rock and fractured porous media, Rock Mechanics and Rock Engineering, 31, pp. 879-886.



- Barla, G and P. Jarre, (1991). Subsidence over an abandoned dissolving salt mine. Rogiers (ed) Rock Mechanics as a Multidisciplinary Science. Proceedings 32nd U.S. Rock Mechanics Symposium, pp. 871-880.
- Benko, B. and D. Stead, (1993). The characterization and prediction of landslide movements using numerical modelling techniques. Proceedings 7<sup>th</sup> International Congress and Field Trip on Landslides, Rotterdam: Balkema, pp. 131-137.
- Benko, B., Stead, D. and J. Malgot, (1994). Numerical analysis of block movements as a slope failure mechanism. Oliveira, Rodrigues, Coelho and Cunha (eds), Proceedings 7<sup>th</sup> International Congress of the IAEG, Lisbon, Portugal, 6, pp. 4729-4735.
- Bentley, S.P., and H.J. Siddle, (1996). Landslide research in the South Wales coalfields. Engineering Geology, 43, pp. 65-80.
- Bieniawski, Z.T., (1989). Engineering rock mass classifications. J. Wiley & Sons, New York, 1989. 251 pp.
- Bishop, A.W., (1955). The use of the slip circle in the stability analysis of slopes. Geotechnique, 5, pp. 7-17.
- Bishop, A.W. and N.R. Morgenstern, (1960). Stability coefficients for earth slopes. Geotechnique, 10, pp. 29-150.
- Board, M., Chacon, E., Varona, P. and L. Lorig, (1996). Comparative analysis of toppling behavior at Chuquicamata open-pit mine, Chile. Trans. Inst. Min. Metall (Sect.A: Mining Industry), 105, pp. A11-21.
- Bovis, M.J., (1982). Uphill-facing (antislope) scarps in the Coast Mountains, southwest British Columbia. Geological Society of America Bulletin, 93, pp. 804-812.
- Bovis, M.J., (1990). Rockslope deformation at Affliction Creek, Southern Coast Mountains, British Columbia. Canadian Journal of Earth Sciences, 27, pp. 243-254.
- Bovis, M.J. and S.G. Evans, (1995). Rock slope movements along the Mount Currie "fault scarp", southern Coast Mountains, British Columbia. Canadian Journal of Earth Sciences, 32, pp. 2015-2020.
- Bowders, J.J. and S.C. Lee, (1988). Effect of longwall mining subsidence on the stability of surface slopes. 7th International Conference on Ground Control in Mining, W. Virginia Univ., Morgantown, W. Virginia, pp. 314-320.

- Brabb, E.E. and B.L. Harrod, (1989). Landslides: Extent and Economic Significance. Balkema: Rotterdam/Brookfield. 385 pp.
- Brady, B.H., and E.T. Brown, (1993). Rock mechanics for underground mining. Chapman & Hall, New York, 571 pp.
- Bray, J.W. and R.E. Goodman, (1981). The theory of base friction models. *International Journal of Rock Mechanics and Mining Sciences & Geomechanical Abstracts.*, **18**, pp. 453-468.
- Brawner, C.O. and P.F. Stacey, (1978). Hogarth pit slope failure, Ontario, Canada. B.Voight (ed.) *Rockslides and Avalanches*, **2**, Elsevier, Amsterdam, pp. 691-707.
- Brock, R.W. (1910). Turtle Mountain. *Summ.Rep.Geol.Surv.,Can.*, 1909, 29pp.
- Brock, R.W. (1911). Turtle Mountain, Frank, Alberta. Summary Report, Geological Survey of Canada, 1910, 13 pp.
- Brown, A. (1982). Toppling induced movements in large relatively flat rock slopes. *Proceedings 23<sup>rd</sup> U.S. Symposium on Rock Mechanics*, Berkeley, California, pp. 1035-1040.
- Brown, E.T. and E. Hoek, (1978). Trends in relationship between measured rock in situ stresses and depth. *International Journal of Rock Mechanics and Mining Sciences & Geomechanical Abstracts.*, **15**, pp. 211-215.
- Brown, E.T. and G.A. Ferguson, (1979). Prediction of progressive hanging-wall caving, Gath's mine, Rhodesia. *Trans. Instn Min. Metall.(Sect. A: Mining Industry)*, **83**, pp. A92-105.
- Brown, I., Hittinger, M. and R.E. Goodman, (1980). Finite element study of the Nevis Bluff (New Zealand) rock slope failure. *Rock Mechanics*, **12**, pp. 231-245.
- Bucek, R. and K. Barron, (1994). Flexural toppling failure at the Luscar Mine, Cardinal River Coals Ltd., Alberta. *Proceedings. Rock Mechanics and Ground Control in the Soft Rocks and Coal Industries. C.I.M. Workshop Saskatoon, SK October 21, 1994*, pp. 1-11.
- Bukovansky, M., Rodriguez, M.A. and G. Cedrun, (1974). Three rock slides in stratified and jointed rocks. *Proceedings 3<sup>rd</sup> International Congress Rock Mechanics Society. Denver, U.S.A.* **2B**, pp. 854-858.
- Burman, B.C., (1974). Developments of a numerical model for discontinua. *Australian Geomechanics Journal*, 1974, pp. 1-10.

- Byrne, R.J., (1974). Physical and numerical models in rock and soil slope stability. Ph.D. thesis, James Cook University, North Queensland, Australia.
- Caine, N., (1982). Toppling failures from Alpine cliffs on Ben Lomond, Tasmania. *Earth Surface Processes and Landforms*, 7, pp. 133-152.
- Caldara, M., Cancelli, A. and A. Giussani, (1988). The Adda Canyon, south of Lecco: An example of landslide induced morphology. Bonnard (ed.) *Proceedings 5<sup>th</sup> International Symposium on Landslides, Lausanne*, 1, pp. 89-94.
- Cebecauer, I., and M. Liska, (1972). Contribution to knowledge of karsting of the Spis travertines and their block slides (In Slovak). *Slovensky kras*, X, pp. 12-23.
- Campbell, R.B. and H.W. Tipper, (1971). Geology of the Bonaparte Lake map-area, British Columbia. Geological Survey of Canada, Memoir 363, 100 pp.
- Canuti, P., Casagli, N. and C.A. Garzonio, (1994). Deep-seated gravitational slope deformations in Toscana. In Crescenti, Dramis, Prestininzi and Sorriso-Valvo (eds). *Deep-seated gravitational slope deformations and large scale landslides in Italy*. Special volume for the International Congress IAEG, Lisbon, 1994, 71pp.
- Cavounidis, S., (1987). On the ratio of factors of safety in slope stability analyses. *Geotechnique*, 37, pp. 207-210.
- Chigira, M., (1992). Long-term gravitational deformation of rocks by mass rock creep. *Engineering Geology*, 32, pp. 157-184.
- Chmelik, F., (1959). Report on geological investigations of the central Carpathian Paleogene in area of Low and High Tatra, Spisska Magura and Levecske Vrchy Mountains (in Czech). Central Institute of Geology (UUG) Prague.
- Chmelik, F., (1963). Legend to the geological map of Czechoslovakia 1:200,000, Map sheet High Tatras (in Czech). Geofond Bratislava.
- Choquet, P. and D.D.B. Tanon, (1985). Nomograms for the assessment of toppling failure in rock slopes. *Proceedings 26<sup>th</sup> U.S. Symposium on Rock Mechanics*, Rapid City, pp. 19-30.
- Chowdhury, R.N., (1978). *Slope analysis*. Elsevier: Amsterdam, New York, 423 pp.
- Chrzanowski, A. and A.S. Chrzanowski, (1984). A comparison of empirical and deterministic prediction of mining subsidence. Johnson, Carbognin and Ubertini (eds.). *Proceedings 3<sup>rd</sup> International Symposium on Land Subsidence, Venice*, pp. 137-146.

- Clark, I.H., Fuller, P.G. and D. McLean, (1990). Numerical stress analysis to assess the stability of a combined open pit and underground mining operation in central Australia. In Brummer (ed.) *Static and Dynamic Considerations in Rock Engineering*, Balkema: Rotterdam, pp. 103-112.
- Cobb, Q. (1981). Slope stability in British surface coal mines. Ph.D. Thesis.(unpubl.) Dept. of Mining Engineering, University of Nottingham, England.
- Coetzee, M.J., Hart, R.D., Varona, P.M. and P.A. Cundall, (1993). *FLAC Basics*. Itasca Consulting Group Inc., Minneapolis, Minnesota, 68 pp.
- Coggan, J.S. and R.J. Pine, (1996). Application of distinct-element modelling to assess slope stability at Delabole slate quarry, Cornwall, England. *Trans. Inst. Min. Metall (Sect.A: Mining Industry)*, **105**, pp. A22-30.
- Conti, S. and G. Tosatti, (1993). Landslides affecting tabular rocks in complex geological situations: The case of Sasso di Simone and Simoncello (Northern Apennines, Italy). *Proceedings 7<sup>th</sup> International Conference and Field trip on Landslides*, Rotterdam:Balkema, pp. 305-312
- Cook, N.G.W., (1992). Natural joints in rock: Mechanical, hydraulic and seismic behavior and properties under normal stress, *International Journal of Rock Mechanics and Mining Sciences & Geomechanical Abstracts*. **29**, pp. 198-225.
- Cost of Coal, (1995). Publication of the Frank Slide Visitor Center, 11 figures, Frank, Alberta, 8 pp.
- Cotton, E.N. and G.M. Matheson, (1989). Geotechnical considerations in the design of open pit gold mines in areas of abandoned underground mines. Watters (ed.) *Engineering Geology and Geotechnical Engineering*, Balkema, Rotterdam, pp. 57-64.
- Coulthard, M.A., Journet, N.C. and C.F. Swindells, (1992). Integration of stress analysis into mine excavation design. In *Rock Mechanics, Proceedings 33<sup>rd</sup> U.S. Symposium*, Santa Fe, New Mexico, U.S.A., Tileron and Wawersik (eds) Balkema: Rotterdam, pp. 451-460.
- Crescenti, U., Dramis, F., Prestininzi, A. and M. Sorriso-Valvo, (1994). Deep-seated gravitational slope deformations and large scale landslides in Italy. Special volume for the International Congress IAEG, Lisbon, 1994, 71 pp.
- Crouch, S.L. and A.M. Starfield, (1983). *Boundary element methods in solid mechanics*. London: Allen and Unwin, 322 pp.

- Cruden, D.M. and J. Krahn; (1973). A re-examination of the geology of the Frank Slide. *Canadian Geotechnical Journal*, **10**, pp. 581-591.
- Cruden, D.M. and J.Krahn; (1978). Frank Rockslide, Alberta, Canada. In *Rockslides and Avalanches*, Voight (ed), Elsevier, Amsterdam, 1978, pp. 97-112
- Cruden, D.M. and O. Hungr; (1985). The debris of the Frank Slide and theories of rockslide-avalanche mobility. *Canadian Journal of Earth Sciences*, **23**, pp. 425-432.
- Cruden, D. M., (1986). Monitoring the south peak of Turtle Mountain, 1980 to 1985. Prep. for Alberta Environment, Research Management Division and Earth Sciences Division by Department of Civil Engineering, University of Alberta. RMD Report 86/37. 70 pp.
- Cruden, D.M., (1989). Limits to common toppling. *Canadian Geotechnical Journal*, **26**, pp. 737-742.
- Cruden, D. M., (1991). A simple definition of a landslide. *Bulletin of the International Association of Engineering Geology*, **43**, pp. 27-29.
- Cruden, D.M., and X.Q. Hu, (1994). Topples on underdip slopes in the Highwood Pass, Alberta, Canada. *Quarterly Journal of Engineering Geology*, **27**, pp. 57-68.
- Cruden, D.M. and D.J. Varnes, (1996). Landslide types and processes. In *Landslides, Investigation and Mitigation*, Special Report 247. Turner and Schuster (eds.), National Academy Press, Washington, D.C., pp. 36-75.
- Cundall, P.A., (1971). A computer model for simulating progressive large scale movements in blocky rock systems. *Rock Fracture. Proceedings International Symposium, Nancy, Paper 2-8.*
- Cundall, P.A., and O.D.L. Strack, (1979). The distinct element method as a tool for research in granular media, Part II. Report NFS Grant ENG76—20771, Department of Civil & Mineral Engineering, University of Minnesota, 1979. (unpublished).
- Cundall, P. (1990). Numerical modelling of jointed and faulted rock. In Rossmanith (ed): *Mechanics of Jointed and Faulted Rock*. Rotterdam:Balkema, pp. 11-18.
- Cundall, P.A., and R.D. Hart, (1992). Numerical modelling of discontinua. *Engineering Computations*, **9**, pp. 101-113.
- Cundall, P. and M.J. Coetzee, (1994). Notes - Itasca short-course on numerical modelling in geomechanics. Austin, Texas, May 1994.

- Cunha, A.P., (1990). Scale effects in rock mechanics. In Cunha (ed.) Scale Effects in Rock mechanics, Rotterdam:Balkema, pp. 3-27.
- Curran, J.H. and B.T. Corkum, (1988). EXAMINE<sup>2d</sup> Version 3.1 users manual. A 2D boundary element program for calculating stresses around underground excavations in rock. Data Visualization Laboratory, Department of Civil Engineering, University of Toronto, 60 pp.
- Curran, J.H. and B.T. Corkum, (1988). EXAMINE<sup>3d</sup> Version 2.0 users manual. Three-dimensional excavation analysis for mines. Data Visualization Laboratory, Department of Civil Engineering, University of Toronto, 181 pp.
- Daly, R.A., Miller, W.G. and G. S. Rice, (1912). Report of the Commission appointed to investigate Turtle Mountain, Frank, Alberta. Canadian Geological Survey. Mem. 27, 34 pp.
- De Frietas, M.H. and R.J. Watters, (1973). Some field examples of toppling failure. *Geotechnique*, **23**, pp. 495-514
- Douglas, L., 1996. Distinct element analysis of toppling at the Luscar Mine. Design Project Report. Department of Geological Sciences, University of Saskatchewan, Saskatoon, 44 pp.
- Dowlen, W.E., (1903). The Turtle Mountain rock slide. *Engineering and Mining Journal*, **77**, pp. 10-12.
- Drumm, E.C., Kane, W.F. and A.C. Orlowski, (1993). Subsidence effects on embankments: Combined empirical-FEM approach. *Journal of Geotechnical Engineering, ASCE*, **119**, pp. 173-178.
- Duncan, J.M., Buchignani, A.L. and M. DeWet, (1987). An engineering manual for slope stability. Virginia Polytechnic Institute and state University, Blacksburg, 80 pp.
- Duncan, J.M., (1996). Soil slope stability analysis. In Landslides, Investigation and Mitigation, Special Report 247. Turner and Schuster (eds.), National Academy Press, Washington, D.C., pp. 337-371.
- Elsworth, D., Liu, J., Entov, L. and S. Zhao, (1995). Determining the influence of longwall mining on groundwater resources. Daemen and Schultz (eds.), *Proceedings 35<sup>th</sup> U.S. Symposium on Rock Mecahnics*, Reno, pp. 605-610.
- Erguvanli, K. and R.E. Goodman, (1972). Applications of models to engineering geology for rock excavations, *Bulletin Association of Engineering Geologists*, **9**, pp. 128-137.

- Evans, R., Valliappan, S., McGuckin, D. and H.L. Raja Sekar, (1981). Stability analysis of a rock slope against toppling failure. Proceedings 3<sup>rd</sup> International Symposium on Weak Rock, Tokyo, pp. 665-670.
- Evans, R.S., (1981). An analysis of secondary toppling rock failures - the stress redistribution method. Quarterly Journal of Engineering Geology, 14., pp. 77-86.
- Evans, S.G., (1983). Landslides in layered volcanic successions with particular reference to the Tertiary rocks of south central British Columbia. PhD thesis (unpubl), University of Alberta, 350 pp.
- Evans, S.G., (1987). Surface displacement and massive toppling on the northeast ridge of Mount Currie, British Columbia. Geological Survey of Canada, Paper 87-1A, pp. 181-189.
- Fellenius, W., (1927). Erdstatische berechnungen mit reibung und kohasion (in German). Ernst, Berlin.
- Forrester, D.J. and B.N. Whittaker, (1976). Effects of mining subsidence on colliery spoil heaps - I.& II. International Journal of Rock Mechanics and Mining Sciences & Geomechanical Abstracts, 13, pp. 113-133.
- Forrester, D.J. and A.R. Bacon, (1985). The effects of mining subsidence on colliery spoil heaps. In Wright and Hoffman (eds.) Measurement and control of mining subsidence - A handbook for western Canada. The coal mining research company, Alberta, Canada, pp. 159-179.
- Franks, C.A.M. and J.D. Geddes, (1984). A comparative study by numerical modelling of movements on sloping ground due to longwall mining. Geddes (ed.) Ground movements and structures. Proceedings 3rd International Conference, Cardiff, Wales.
- Fraser, C.S. and L. Gruendig; (1985). The analysis of photogrammetric deformation measurements on Turtle Mountain. Photogrammetric Engineering and Remote Sensing, 51, pp. 207-216.
- Fredlund, D.G., and H. Rahardjo, (1993). Soil mechanics for unsaturated soils. John Wiley & Sons, New York, 517 pp.
- Fredlund, D.G., (1992). The analysis of slopes. Class notes for the Advanced Geotechnical Engineering course, Department of Civil Engineering, University of Saskatchewan, 522 pp.

- Fussganger, E., Oslac, J., Banský, M., Matejčeková, E., Novotný, P., Malgót, J., Mahr, T. and F. Baliak, (1983). Slope failures on the northwestern slopes of the Vtáčnik Mountain (in Slovak). Report for the Slovak Geological Institute, Bratislava, part A and B.
- Fussganger, E., and B. Kostak, (1983). Investigation of creep-type deformations of rock blocks on plastic substratum (in Slovak). Internal report - IGHP Zilina (unpublished), 1983, 145 pp.
- Fussganger, E., (1985). Knowledge from investigations of creep slope movements of travertine blocks in Spišský hrad castle. Scientific publications. IGHP Zilina (unpublished), 1985. 76 pp.
- Garzonio, C.A., (1990). Block theory and stability analysis of a slope subject to lateral spread; The example of 'Chiuse della Verna' mountain. In Rossmannith (ed.): Mechanics of Jointed and Faulted Rock. Rotterdam: Balkema, pp. 913-918.
- Gentry, D.W. and J.F. Abel, (1978a). Surface response to longwall coal mining in mountainous terrain. Bulletin Association of Engineering Geology, **XV**, pp. 191-220.
- Gentry, D.W. and J.F. Abel (1978b). Rock mass response to mining longwall Panel 4N, York Canyon Mine. Mining Engineering, **30**, pp. 273-280.
- Gerrard, G.F.G. and R.K. Taylor, (1988). Collapse mechanisms of shallow coal-mine workings from field measurements. In "Engineering Geology of Underground Movements", Bell, Culshaw, Cripps and Lovell (eds.), Society of Engineering Geology, Special Publication No. 5, pp. 181-192.
- Giani, G.P., (1992). Rock slope stability analysis. A.A. Balkema: Rotterdam. 361 pp.
- Giraud, A., Rochet, L., and P. Antoine, (1990). Processes of slope failure in crystallophyllian formations. Engineering Geology, **29**, pp. 241-253.
- Glawe, U., Zika, P., Zvelebil, J., Moser, M., and J. Rybar, (1993). Time prediction of a rock fall in the Carnic Alps. Quarterly Journal of Engineering Geology, **26**, pp. 185-192.
- Goodman, R.E., (1976). Methods in Geological Engineering in Discontinuous Rocks. West Publishing Co., St. Paul, Minnesota, 1976, 472 pp.
- Goodman, R.E. and J.W. Bray, (1976). Toppling of rock slopes. Proceedings of ASCE Specialty Conference, Rock Engineering for Foundations and Slopes, Boulder, CO, **2**, pp. 201-234.



- Goodman, R.E. and G.H. Shi, (1985). Block theory and its application to rock engineering. New Jersey: Prentice-Hall. 150 pp.
- Goodman, R.E., (1989). Introduction to Rock Mechanics. J. Wiley & Sons, 2nd edition, 562 pp.
- Gostelow, T.P. (1977). The development of complex landslides in the upper coal measures at Blaina, South Wales. The geotechnics of structurally complex formations, Capri, pp. 255-268.
- Graham, H.L. (1989). Description of a slope failure in the Vanderbijl pit, Thabazimbi, caused by underground mining activities. Proceedings of .SANGORM Symposium on Rock Slope Stability, Indaba Sun, pp. 22-27.
- Gu Xun, (1988). A case of slope slide induced by underground coal mining: Analysis for landslide genesis in Hancheng power plant(in Chinese). Scientia-Geologica Sinica—Ti-chih-ko-hsueh, 1, pp. 81-91.
- Hamett, R.D., (1974). A study of the behavior of discontinuous rock masses. Ph.D. thesis. James Cook University, North Queensland, Australia.
- Hebil, K.E., (1993). Stability and mining of slopes prone to toppling failure at the Cardinal River Mine, Luscar, Alberta. 95th Annual General Meeting, C.I.M. Calgary, pp. 75-86.
- Hebil, K.E., (1995, 1996). Personal Communication.
- Hencher, S.R., Liao, Q.H. and B.G. Monaghan, (1996). Modelling slope behaviour for open pits. Trans. Inst. Min. Metall (Sect.A: Mining Industry), 105, pp. A37-47.
- Herget, G., (1988). Stresses in rock. Rotterdam: Balkema. 179 pp.
- Heslop, F.G., (1974). Failure by overturning in ground adjacent to cave mining, Havelock Mine, Swaziland. Proceedings 3<sup>rd</sup> International Congress Society Rock Mechanics, Denver, 2B, pp. 1085-1089.
- H.M.S.O. Report of the tribunal appointed to inquire into the disaster at Aberfan on 21 October, 1966. London, 1967, 151 pp.
- Hocking, G., (1978). Analysis of toppling-sliding mechanism for rock slopes. Proceedings, 19<sup>th</sup> U.S. Symposium on Rock Mechanics, pp. 288-295.
- Holec, P., (1992). The imprints of mastodont teeth type Mammot borsoni in travertines in Spiske Podhradie (In Slovak). Mineralia Slovaca, 24, pp.5-6

- Holling, C.S. - editor, (1978). Adaptive environmental assessment and management. J.Wiley & Sons, Chichester, 1978.
- Hoek, E., (1974). Progressive caving induced by mining an inclined orebody. Trans. Instn Min. Metall.(Sect.A: Mining Industry), **83**, pp. A133-139
- Hoek, E. and J. Bray, (1981). Rock slope engineering (3<sup>rd</sup> edition). The Institute of Mining and Metallurgy, London. 358 pp.
- Hoek, E., and M. Diederichs, (1995). Dips - A program for plotting, analysis and presentation of structural geology data using spherical projection techniques. Rock Engineering Group, 12 Selwood Ave., Toronto, Ontario, 138 pp.
- Hoek, E., Grabinski, M.W., and M.S. Diederichs, (1991). Numerical modelling of underground excavations design. Trans. Instn Min. Metall.(Sect.A: Mining Industry), **100**, pp. A22-30.
- Hoek, E and D. Moy, (1993). Design of large powerhouse caverns in weak rock. In Hudson (Ed.) Comprehensive Rock Engineering. **5**, Pergamon Press Ltd., pp. 85-110.
- Hoek, E., Kaiser, P.K. and W.F. Baldwin, (1995). Support of Underground Excavations in Hard Rock. Balkema: Rotterdam, 215 pp.
- Hofmann, H., (1974). Zum Verformungs und Bruchverhalten regelmässig geklüfteter Felsböschungen. Rock Mechanics Supplement, **3**, pp. 31-34.
- Holmes, G. and J.J. Jarvis, (1985). Large scale toppling within a sackung type deformation at Ben Attow, Scotland. Quarterly Journal of Engineering Geology, **18**, pp. 287-289.
- Holtz, R.D. and R.L. Schuster, (1996). Stabilization of Soil Slopes. In Landslides, Investigation and Mitigation, Special Report 247. Turner and Schuster (eds. ), National Academy Press, Washington, D.C., pp. 439-473.
- Homand-Etienne, F. and N. Rode, (1990). Block modelling of jointed cliffs. In Rossmannith(ed): Mechanics of Jointed and Faulted Rock. Rotterdam: Balkema, pp. 819-825.
- Hudson, J.A., (1991). Rock Mechanics in Engineering Practice. CIRIA London, Butterworths, 72 pp.
- Hudson, J.A. (1992). Rock Engineering Systems; theory and practice. Ellis Horwood Limited, England, 185 pp.

- Hudson, J.A. and C. Fairhurst, (1993). *Comprehensive rock engineering, Volume 2*, Pergamon Press Ltd., pp. 575-600.
- Hudson, J.A., (1993). *Rock properties, testing methods and site characterization*. In Hudson (ed.) *Comprehensive rock engineering, Volume 3*, Pergamon Press Ltd., pp. 1-39.
- Hungr, O., (1987). *An extension of Bishop's Simplified method of slope stability analysis to three dimensions*. *Geotechnique*, **37**, pp. 113-117.
- Hungr, O. and S.G. Evans, (1988). *Engineering evaluation of fragmental rockfall Hazards*. In *Proceedings, Fifth International Symposium on Landslides*. C. Bonnard (ed.), Balkema: Rotterdam, **1**, pp. 685-690.
- Hunt, R.E., (1986). *Geotechnical engineering analysis and evaluation*. McGraw Hill Inc., New York, 134 pp.
- Hunter, J.H. and R.L. Schuster, (1968). *Stability of simple cuttings in normally consolidated clays*. *Geotechnique*, **18**, pp. 372-378.
- Hutchinson, J.N., (1988). *General Report: Morphological and geotechnical parameters of landslides in relation to geology and hydrogeology*. Bonnard (ed.) *Proceedings 5<sup>th</sup> International Symposium on Landslides, Lausanne*, **1**, pp. 3-35.
- Hutchinson, J.N., (1991). *Periglacial and slope processes*. Forster, Culshaw, Cripps, Little and Moon (eds.), *Quaternary Engineering Geology*, Geological Society Engineering Geology Special Publication No.7, pp. 283-331.
- Hsu, S.C., and P.P. Nelson, (1995). *Analyses of slopes in jointed weak rock masses using distinct element method*. Rossmanith (ed.), *Proceedings, Mechanics of Jointed and Faulted Rock*, Vienna, pp. 589-594.
- Iannacchione, A.T. and T.E. Ackman, (1984). *Reactivation of landslides by surface subsidence from longwall mining*. *Abstract, AAPG Bulletin*, **68**, pp. 1921.
- Iannacchione, A.T. and L.E. Vallejo, (1995). *Factors affecting the slope stability of Kentucky's abandoned mine lands*. Daemen and Schults (eds), *Proceedings of the 35<sup>th</sup> U.S. Symposium on Rock Mechanics*, Reno, pp. 837-842.
- Ishida, T., Chigara, M. and S. Hibino, (1987). *Application of the distinct element method for analysis of toppling observed on a fissured rock slope*. *Rock Mechanics and Rock Engineering*, **20**, pp. 277-283.
- Itasca Consulting Group, Inc. (1992). *FLAC Version 3.22*. Itasca Consulting Group Inc., Minneapolis.

- Itasca Consulting Group, Inc. (1993). UDEC Version 2.01. Itasca Consulting Group Inc., Minneapolis.
- Itasca Consulting Group, Inc. (1995). PFC<sup>2D</sup> Version 1.1. Itasca Consulting Group Inc., Minneapolis.
- Ivan, L., (1943). The occurrence of travertine in Slovakia (in Slovak). Praca SFU Bratislava, Geofond, Bratislava, 1943.
- Janbu, N., (1968). Slope stability computations. Soil Mechanics and Foundation Engineering Report. Technical University of Norway, Trondheim.
- Jennings, D.N., Bracegirdle, A. and G. Ramsay, (1985). Highwall design for a New Zealand opencast coal mine. Engineering Geology, **22**, pp. 23-33.
- Jeran, P.W. and V. Adamek (1988). Subsidence due to undermining of sloping terrain: A case study. U.S. Bureau of Mines, Report of Investigations, 9205, 10 pp.
- Jeremic, M.L. (1985). Strata Mechanics in Coal Mining. Balkema: Rotterdam, 566 pp.
- Jiang, Y., Esaki, T., Nagatomi, M., and T. Okada, (1995). Studies on toppling failure mechanism of slope in discontinuous rock mass. Rossmannith (ed.), Proceedings, Mechanics of Jointed and Faulted Rock, Vienna, pp. 605-610.
- Jones, D.B., Siddle, H.J., Reddish, D.J. and B.N. Whittaker, (1991). Landslides and undermining: Slope stability interaction with mining subsidence behaviour. 7<sup>th</sup> International Society Rock Mechanics Congress, Aachen, **2**, Balkema: Rotterdam, pp. 893-898.
- Jones, D.B., (1991). Slope stabilisation experience in South Wales, UK. In Chandler(ed) Slope stability engineering - developments and applications. Proceedings International Conference, Isle of Wight, April 15-18, 1991. Thomas Telford: 1991.
- Jones, R.E., Pariseau, W.G., Payne, V. and G. Takenaka, (1990). Sandstone escarpment stability in vicinity of longwall mining operations. Hustrulid and Johnson (eds.) Rock Mechanics Contributions and Challenges. Proc. 31<sup>st</sup> U.S. Symp., pp. 555-562.
- Kalkani, E.C., and D.R. Piteau, (1976). Finite element analysis of toppling failure at Hell's Gate Bluffs, British Columbia. Bulletin International Association Engineering Geology, **13**, pp. 315-327.

- Kamenov, B., Iliev, I., and E. Avramova, (1977). Conditions for the origin, mechanism and dynamics of block landslides in Bulgaria. *Bulletin International Association Engineering Geology*, **16**, pp. 98-101.
- Ke, T.C., Thapa, B., and R.E. Goodman, (1994). Stability analysis of a penstock slope. Nelson and Laubach (eds.), *Proceedings 1<sup>st</sup> North American Rock Mechanics Symposium*, Austin, Texas, pp. 1109-1116.
- Kerr, J.W., (1990). *Frank Slide*. Barker Publishing Ltd. Calgary, Alberta. 48 pp.
- Kennard, D., (1992). Numerical modelling of the Frank slide. Special Report for the Rock Mechanics Design Course, Department of Geological Sciences, University of Saskatchewan, Saskatoon, 32 pp.
- Kostak, B., (1977). Photoplastic slope deformation models. *Bulletin International Association Engineering Geology*, **16**, pp. 221-223.
- Kostak, B. and D.M. Cruden; (1990). The moire crack gauges on the crown of the Frank Slide. *Canadian Geotechnical Journal*, **27**, pp. 835-840.
- Kostak, B., (1993). Deformation effects on cracks in massifs and their interpretation. *Proceedings, 7<sup>th</sup> International Conference and Field Trip on Landslides*, Rotterdam: Balkema, pp. 305-312
- Krahn, J. and N.R. Morgenstern; (1976). Mechanics of the Frank Slide. *Rock Engineering*, **2**, pp. 309-332.
- Krahn, J., (1974). *Rock Slope Stability with Emphasis on the Frank Slide*. Ph.D. Thesis, University of Alberta, Edmonton, Alta.
- Kratzsch, H. (1983). *Mining Subsidence Engineering*. Springer-Verlag: Berlin, 543 pp.
- Kulhawy, F.H., (1975). Stress deformation properties of rock and rock discontinuities. *Engineering Geology*, **9**, pp. 327-350.
- Kuykendall, L., (1975). Kinematic Study of Toppling Failure Mode and Practical Aspects of Using the Base Friction Modelling Machine. Internal Report, University of California, Berkeley, Department of Civil Engineering.
- Lambe, T.W. (1967). The stress path method. *Journal of the Soil Mechanics and Foundations Division, ASCE*, **93**, pp. 309-331.
- Lambe, T.W. and W.A. Marr, (1979). Stress path method: Second edition. *Journal of the Soil Mechanics and Foundations Division, ASCE*, **105**, pp. 727-738.

- Leach, W.W., (1904). The Blairmore-Frank coal-fields. Summary Report, Geol. Survey of Canada, 1902-1903, pp. 169-185.
- Liu, G. and K. Xu, (1989). Environmental geologic investigation on rockfall and landslide hazards induced by mining in mountainous area of Western Hubei. Abstracts, 28<sup>th</sup> International Geological Congress, Washington, D.C., USA, 1989, 2, pp. 311-312.
- Lorig, L.J., Hart, R.D., and P.A. Cundall, (1991). Slope stability analysis of jointed rock using distinct element method. Transportation Research Record. 1339, Soils, Geology, and Foundations (Behavior of jointed rock masses and reinforced soil structures), pp. 1-9.
- Lowe, J. and L. Karafiath, (1960). Stability of earth dams upon drawdown. In Proc. 1<sup>st</sup> Pan-American Conference on Soil mechanics and Foundation Engineering, Mexico City, 2, pp. 537-552
- Lozek, V., (1964). Genesis and age of Spis travertines (in Slovak). Works of eastern Slovak Museum, Series A-Natural Sciences, Kosice, pp. 7-39.
- Lozek, V., (1973). The nature in Quaternary, Academia Prague, 235pp.
- MacKay, R.B., (1932). Geology and coal deposits of Crowsnest Pass area, Alberta. Summary Report, Geological Survey of Canada, 338 pp.
- McConnell, R.G. and R.W. Brock, (1904). Report on the great landslide at Frank, Alberta, Canada. Canadian Department of Interior, Annual Report, 1902-1903, Part 8, 17 pp.
- Mahr, T., (1976). Slope deformation in high mountain ranges in the Slovak Carpathians. (in Slovak) Ph.D. Thesis, Slovak Technical University, Department of Geotechnics, Bratislava. 152 pp.
- Malgot, J., (1977). Deep-seated gravitational slope deformations in neovolcanic mountain ranges of Slovakia. Bulletin of the International Association Engineering Geology, Symposium on Landslides and other Mass Movements, Prague, pp. 106-109.
- Malgot, J., Baliak, F. and T. Mahr, (1986). Prediction of the influence of underground coal mining on slope stability in the Vtacnik mountains. Bulletin International Association Engineering Geology, 33, pp. 57-65.

- Malgot, J., F. Baliak and J. Sikora, (1988). Engineering geological causes of failure of the middleage castles in Slovakia and the methods of their geotechnical stabilization. In Marinos and Koukis (eds.): The Engineering Geology of Ancient Works, Monuments and Historical Sites, 1, Rotterdam: Balkema, pp. 83-92.
- Malgot, J., Baliak, F. and M. Krippel, (1991). Prognosis of the slope stability influenced by coal mining in the Handlova deposit (in Slovak). Zapadne Karpaty, Series Hydrogeology and Engineering Geology 11., Geological Institute of D.Stur, pp. 201-233.
- Malgot, J., Baliak, F., Gregor, V., Bartos, P., Bartok, J., Satina, J., Kusy, P., Cabala, D. and J. Vlcko, (1992). Spis Castle: Engineering geological investigation and remedial measures (in Slovak). Research report for Ministry of Environment, 107 pp.
- Malgot, J., (1992). Gravitational disintegration of the Spis castle hill. Excursion guide book. International symposium in geomorphology. Tatranska Lomnica - Stara Lesna, 1992, pp.34.
- Manolis, G.D., and T.G. Davies - eds. (1993). Boundary element techniques in geomechanics. Computational Mechanics Publications, Southampton & Elsevier, Essex, 533 pp.
- Marinos, P.G. and G.C. Koukis, (1988). The engineering geology of ancient works, monuments and historical sites. Proceedings of an International Symposium. IAEG, 4 Volumes Rotterdam: Balkema
- Martin, D.C., and E.F. Mehr, (1993). Assesment of slope deformation and deep seated instability in the Cassiar open pit. Trans. Inst. Min. Metall (Sect.A: Mining Industry), 86, pp. A58-67.
- Matula, M and A. Nemcok, (1968). Guide to Excursion of the 28<sup>th</sup> International Geological Congress, Session XXIII, Prague 1968.
- Matula, M., (1979). Geology and Environment.(In Slovak) Obzor Bratislava, 291 pp.
- Matula, M and J. Pasek, (1986). Regional engineering geology of Czechoslovakia.(In Slovak) Alfa Bratislava and SNTL Praha, 295 pp.
- McRoberts, E.C. and N.R. Morgenstern, (1974). Stability of slopes in frozen soil, Mackenzie Valley, North West Territories. Canadian Geotechnical Journal, 11, pp. 554-573.

- Misfeld, G.A., Sauer, E.K., and E.A. Christiansen, (1991). The Hepburn landslide: An interactive slope-stability and seepage analysis, *Canadian Geotechnical Journal*, **28**, pp. 556-573.
- Mongioli, L., Bosco, G., and V. DeGennaro, (1995). Analysis of complex rotational and translational failure mechanisms in jointed rock slopes. Rossmannith (ed.), *Proceedings, Mechanics of Jointed and Faulted Rock*, Vienna, pp. 605-610.
- Morgenstern, N.R., and V.E. Price, (1965). The analysis of the stability of general slip surfaces. *Geotechnique*, **15**, pp. 79-93.
- Morris, R. and W.D. Clough, (1986). Effects of underground workings on the slope stability of an opencast mine. Deetlefs (ed.) *The planning and operation of open pit and strip mines*. Johannesburg, SAIMM, pp. 55-61.
- Moss, A.E., (1994). Numerical modelling review of the Cigar Lake Mine project. Report for the Cigar Lake Mining Corporation, Saskatoon, Saskatchewan. Golders Associates Ltd., Burnaby B.C., 4 pp.
- Muller, L., (1968). New consideration of the Vaiont slide. *Felsmechanik und Ingenieurgeologie*, **6**, pp. 29-91.
- Nemcok, A., J. Pasek and J. Rybar, (1972). Classification of landslides and other mass movements. *Rock Mechanics*, **4**, pp. 71-78.
- Nemcok, A., and A. Svatos, (1974). Gravitational disintegration of Drevenik (in Slovak). *Geograficky casopis, rad XXVI*, **3**, pp. 258-266.
- Nemcok, A., (1982). *Zosuvy v Slovenskych Karpatoch*. (In Slovak), Veda, Bratislava, 319 pp.
- Norris, D.K., (1955). Blairmore, Alberta. Geological Survey of Canada., Paper, 55-18.
- Norrish, I.N., and D.C. Wyllie, (1996). Rock slope stability analysis. In *Landslides, Investigation and Mitigation*, Special Report 247. Turner and Schuster (eds.), National Academy Press, Washington, D.C., pp. 36-75.
- Niyom, D, and S. Sakurai, (1985). Study on rock slope protection of toppling failure by physical modelings. *Proceedings 26<sup>th</sup> U.S. Symposium on Rock Mechanics*. Rapid City, pp. 11-30.
- Orr, M.Ch., Swindells, Ch.F., and Ch.R. Windsor, (1991). Open pit toppling failures: Experience versus analysis. Beer, Bookerand and Carter(eds.) *Computer Methods and Advances in geomechanics*, pp. 505-510.



- Palisade Corporation, (1988), @RISK - risk analysis and simulation add-in for LOTUS 1-2-3.
- Pande, G.N., Beer, G., and J.R. Williams, (1990). Numerical methods in rock mechanics. John Wiley & Sons Ltd., Toronto, 327 pp.
- Parks, C.D., (1991). A review of the mechanisms of cambering and valley bulging. Forster, Culshaw, Cripps, Little and Moon (eds.), Quarternary Engineering Geology, Geological Society Engineering Geology Special Publication No.7, pp. 373-380.
- Pasek, J., Malgot, J., and B. Kostak, (1979). Block-type slope movements (in Slovak). Matula (ed.) Inziniersko-geologicke studium horninoveho prostredia a geodynamickych procesov,. Bratislava: Veda, pp. 147-159.
- Pasloske, J., 1996. Investigating the influence of joint spacing and slope angle on toppling using UDEC. Design Project Report. Department of Geological Sciences, University of Saskatchewan, Saskatoon, 44 pp.
- Pells, P.J.N., Braybrooke, J.C., Kotze, G.P. and J. Mong, (1987). Cliff line collapse associated with mining activities. Walker and Fell (eds.) Soil slope instability and stabilisation. Proceedings. soil inst. and stab., Sydney, Balkema: Rotterdam, pp. 359-385.
- Pine, R.J., (1992). Risk analysis design applications in mining geomechanics. Trans. Instn. Min. Metall.(Sect.A: Mining Industry), 101, pp. A149-158.
- Piteau, D.R., McLeod, B.C., Parkes, D.R., and J.K. Lou, (1978). Rock slope failure at Hell's gate, British Columbia, Canada. B.Voight(ed.) Rockslides and Avalanches, 2, Elsevier, Amsterdam, pp. 691-707.
- Piteau, D.R., and D.C. Martin, (1981). Mechanics of rock slope failure. Proceedings 3<sup>rd</sup> International Conference on Stability in Surface Mining, Brawner (ed.), 113 pp.
- Piteau, D.R., Stewart, A.F., and D.C. Martin, (1981). Design examples of open pit slopes susceptible to toppling. Proceedings 3<sup>rd</sup> International Conference on Stability in Surface Mining, Soc. of Min. Eng. Of AIME, Vancouver, pp. 679-712.
- Poisel, R. and W. Eppensteiner, (1988). A contribution to the systematics of rock mass movements. Bonnard (ed.) Proceedings 5<sup>th</sup> International Symposium on Landslides, Lausanne, 1, pp. 1353-1357.

- Poisel, R., Steger, W., and W. Unterberger, (1989). 2D and 3D FE - Analyses of discrete rock blocks using gap-friction elements. Mustoe, Henriksen and Huttelmaier (eds.), Proceedings of the 1<sup>st</sup> U.S. Conference on Discrete Element Methods. Golden, Colorado.
- Poisel, R. (1990). The dualism discrete-continuum of jointed rock. In Rossmannith (ed.): Mechanics of Jointed and Faulted Rock. Rotterdam: Balkema, pp. 41-50.
- Poisel, R., Steger, W. and A. Zeitler, (1991). Standsicherheitsuntersuchungen spröder Felsmassen auf einem weichen Sockel (In German). Wittke (ed.), Proceedings 7<sup>th</sup> International Congress on Rock Mechanics, Aachen, 2, pp. 939-944.
- Priest, S.D., and E.T. Brown, (1983). Probability stability analysis of variable rock slopes. Trans. Instn. Min. Metall.(Sect.A: Mining Industry), 92, pp. A1-12.
- Priest, S.D. (1985). Hemispherical projections methods in rock mechanics. Allen & Unwin, London.
- Pritchard, M.A., (1989). Numerical modelling of large scale toppling. MSc. thesis. The University of British Columbia, Vancouver, B.C. 178 pp.
- Pritchard, M.A. and K.W. Savigny, (1990). Numerical modelling of toppling. Canadian Geotechnical Journal, 27, pp. 823-834.
- Pritchard, M.A., Savigny, K.W. and S.G. Evans, (1990). Toppling and deep-seated landslides in natural slopes. Rossmannith (ed.): Mechanics of Jointed and Faulted Rock. Rotterdam: Balkema, pp. 937-943.
- Pritchard, M.A. and K.W. Savigny, (1991). The Heather Hill Landslide, an example of a large scale toppling failure in a natural slope. Canadian Geotechnical Journal. 28, pp. 410-422.
- Radbruch-Hall, D.H., Varnes, D.J., and W.Z. Savage, (1976). Gravitational spreading of steep-sided ridges ("sackung") in western United States. Bulletin of the International Association Engineering Geology, 14, pp. 23-35.
- Radbruch-Hall, D.H., (1978). Gravitational creep of rock masses on slopes. B.Voight (ed.) Rockslides and Avalanches, 2, Elsevier, Amsterdam, pp. 607-657.
- Rapiman, M., (1993). Slope stability and rock mechanics analyses Chuquicamate mine, Codelco, Chile. Bawden and Archibald (eds.), Innovative mine design for the 21<sup>st</sup> century, Proceedings Congress on Mine Design, Kingston, pp. 35-44.
- Rehwoldt, E.B. (1990). Effects of abandoned underground workings on open pit slope stability. Master's Thesis (unpublished), University of Nevada, Reno, 173 pp.

- Reid, G., and D. Stewart., (1986). A large scale toppling at Afton. Proceedings International Symposium on Geotechnical Stability in Surface Mining. Calgary, pp. 215-223.
- Reynolds, R.T. (1991). Geotechnical field techniques used in monitoring slope stability at a landfill. Sorum (ed.): Field Measurements in geotechnics. Rotterdam: Balkema, pp. 883-891.
- Report of the tribunal appointed to inquire into the disaster at Aberfan on 21 October 1966. H.M.S.O., London, 1967, 157 pp.
- Reuter, F., Molek, H. and G. Bochmann, (1977). Slope sliding as secondary process in subsidence areas of chloride-karst. Bulletin International Association .Engineering Geology, 16, pp. 62-64, Krefeld.
- Richards,L., (1993). Case examples of rock mechanics principles used in rock engineering. Hudson (ed.) Comprehensive Rock Engineering, 1, Pergamon Press. pp. 691-718.
- Riemer, W., Locher, T. and I. Nunez, (1988). Mechanics of deep seated mass movements in metamorphic rocks of the Ecuadorian Andes. Bonnard (ed.) Proceedings 5<sup>th</sup> International Symposium on Landslides, Lausanne, 1, pp. 307-310.
- Romana, M.R., (1993). A geomechanical classification for slopes: Slope mass rating. In Hudson (ed.) Comprehensive Rock Engineering. 3, Pergamon Press Ltd., pp. 575-600.
- Rybar, J., and S. Novosad, (1989). Coping with landslide problems in Czechoslovakia. Brabb and Harrod (eds.) Landslides: Extent and Economic Significance. Balkema: Rotterdam., pp. 203-211.
- Rybar, J., Kostak, B. and M. Uher, (1990). Deep seated rockslide initiated by ore mining. Proc.6th International Congress Association Engineering Geology, Amsterdam, pp. 2681-2686.
- Sagaseta, C., (1986). On the modes of instability of a rigid block on an inclined plane. Rock Mechanics and Rock Engineering, 19, pp. 261-266.
- Sarma, S.K., (1973). Stability analysis of embankments and slopes. Geotechnique, 23, pp. 423-433.
- Sassa, K., Takei, A. and S. Kobashi, (1979a). Landslides triggered by vertical subsidences. Proceedings International Symposium on Landslides, New Delhi, India, I/11, pp. 49-54.

- Sassa, K., Takei, A. and S. Kobashi, (1979b). Consideration of vertical subsidence as a factor influencing slope instability. Proceedings International Symposium on Landslides, New Delhi, India, IV/10, pp. 293-296.
- Sassa, K., Takei, A. and H. Marui, (1981). Influences of "underground erosion" on instability of a crystalline schist slope. Proceedings International Symposium on weak Rock, Tokyo, pp. 543-548.
- Sauer, E.K., and E.A. Christiansen, (1983). The Denholm landslide, Saskatchewan, part I and II. Canadian Geotechnical Journal, **20**, pp. 208-220.
- Sauer, E.K., and E.A. Christiansen, (1987). The Denholm landslide, Saskatchewan, an update. Canadian Geotechnical Journal, **24**, pp. 163-168.
- Savage, W.Z., and D.J. Varnes, (1987). Mechanics of gravitational spreading of steep-sided ridges ("Sackung"). Bulletin of the International Association of Engineering Geology, **35**, pp. 31-36.
- Scavia, C., Barla, G., and V. Bernaudo, (1990). Probabilistic Stability Analysis of Block Toppling Failure in Rock Slopes. International Journal of Rock Mechanics and Mining Sciences & Geomechanical Abstracts. **27**, pp. 465-478.
- Schenk, V. 1994. Geotechnical approach for a road tunnel passing an old rock slide. 7<sup>th</sup> Congress International Association Engineering Geology, Lisbon, Portugal. Balkema: Rotterdam:1994.
- Scoble, M.J. 1981. Studies of ground deformation in British surface coal mines. Ph.D. Thesis. Dept. of Mining Engineering, University of Nottingham, England.
- Schofield, A.N., (1978). Use of centrifugal model testing to assess slope stability. Canadian Geotechnical Journal, **15**, pp. 14-31.
- Schofield, A.N., (1980). Cambridge geotechnical centrifuge operations. Geotechnique, **30**, pp. 227-268.
- Scott, G.A., 1995. Rock slopes: Some construction case histories. Daemen and Schultz (eds.). Proceedings 35<sup>th</sup> U.S. Symposium on Rock Mechanics, Reno, pp. 65-70.
- Sheory, P.R., (1994). A theory for in situ stresses in isotropic and transversely isotropic rock. International Journal of Rock Mechanics and Mining Sciences & Geomechanical Abstracts, **31**, pp. 23-34.

- Shimizu, Y., Aydan, Ö., and T. Kawamoto, (1992) The dynamic response and stability of rock slopes in discontinuous media. Bell (ed.) Proceedings of the 6<sup>th</sup> International Symposium on Landslides, Christchurch, New Zealand., pp. 1211-1217.
- Shu, D.M. and A.K. Bhattacharyya, (1992). Modification of subsidence parameters for sloping ground surfaces by the rays projection. *Geotechnical and Geological Engineering*, 10, pp. 223-248.
- Siddle, H.J., Jones, D.B., Whitakker, B.N. and D.J. Reddish, (1991). The influence of mining on hillslope stability. Bell (ed.) Proceedings of the 6<sup>th</sup> International Symposium on Landslides, Christchurch, New Zealand., pp. 1323-1328.
- Siekmeier, J.A., and K.M. O'Connor, (1993). Modelling overburden response to longwall mining. In Mitri (ed.) Proceedings 1<sup>st</sup> Canadian Symposium on Numerical Modelling Applications in Mining and Geomechanics, Montreal, pp. 110-118.
- Silberbauer, J., Poisel, R., and W. Eppensteiner, (1988). Geomechanical model tests concerning the gliding apart of hard rock on soft ground. In Marinou and Koukis (eds.): *The Engineering Geology of Ancient Works, Monuments and Historical Sites*, 1, Rotterdam: Balkema, pp. 123-128.
- Singh, T.N. and D.P. Singh, (1991). Slope behavior in an opencast mine over old underground voids. *International Journal of Surface Mining and Reclamation*, 5, pp. 195-201
- Singh, T.N. and D.P. Singh, (1992) Prediction of instability of slopes in an opencast mine over old surface and underground workings. *International Journal of Surface Mining and Reclamation*, 6, pp. 81-89.
- Singh, U.K., Stephansson, O.J. and A. Herdacia, (1993). Simulation of progressive failure in hanging-wall and footwall for mining with sub-level caving. *Trans. Instn. Min. Metall. (Sect. A: Mining Industry)*, 102, pp. A188-194.
- Siriwardane, H.J. and J. Amanat, (1984). Prediction of subsidence on hilly terrain using finite element method, in Proceedings of the 2nd International Conference on Stability in Underground Mining, Lexington, University of Kentucky, pp. 554-575.
- Siriwardane, H.J. and L.K. Moulton, (1988). Direct and indirect influence of mining related subsidence on structural damages - A case study. Proceedings 2<sup>nd</sup> International Conference on Case Histories in Geotechnical Engineering, St. Luis, 2, pp. 1443-1446.

- Skempton, A.W. and J. Hutchinson, (1969). Stability of natural slopes and embankments foundations - State-of-the-Art report. Proceedings 7<sup>th</sup> International Congress Soil Mechanics and Foundation Engineering, Mexico, pp. 291-335.
- Soto, C., (1974). A comparative study of slope modelling techniques for fractured ground, M.Sc. Thesis, Imperial College, Royal School of Mines, London.
- Spencer, E. (1967). A method of analysis of the stability of embankments assuming parallel interslice forces. *Geotechnique*, **17**, pp. 11-26
- Starfield, A.M. and P.A. Cundall, (1988). Towards a methodology for rock mechanics modelling. *International Journal of Rock Mechanics and Mining Sciences & Geomechanical Abstracts*, **25**, pp. 99-106.
- Stead, D. (1984). An evaluation of the factors governing the stability of surface coal mine slopes. Ph.D. Thesis. Dept. of Mining Engineering, University of Nottingham, England.
- Stead, D. and R. Singh, (1989). Loosewall stability in United Kingdom surface coal mines. *Canadian Geotechnical Journal*, **26**, pp. 235-245.
- Stead, D., (1990). The back analysis of rock slope failures in U.K. surface coal mining practice. In Singhal and Vaura (eds.) *Proceedings International Symposium on Mine Planning and Equipment Selection*, Calgary, Balkema: Rotterdam, pp. 343-352.
- Stead, D. and B. Benko, (1993). The influence of underground workings on slope instability: A numerical modelling approach. In Mitri (ed.) *Proceedings 1<sup>st</sup> Canadian Symposium on Numerical Modelling Applications in Mining and Geomechanics*, Montreal, pp. 207-216.
- Stead, D., Eberhardt, E., and B. Benko (1995). The influence of horizontal stresses on the stability of surface coal mine footwall slopes. In Singhal, Mehrotra, Hadjigeorgiou, and Poulin (eds.). *Mine Planning and Equipment Selection. Proceedings of the 4<sup>th</sup> International Symposium on Mine Planning and Equipment Selection*, Calgary, October 1995, pp. 1075 - 1080.
- Stead, D., (1996). Personal communication. Department of Geological Sciences, University of Saskatchewan, Saskatoon, Canada.
- Steger, W. and W. Unterberger, (1990). Rock slopes and dam abutments in jointed rock: FE-Analysis using gap-friction elements and contact procedures. In Rossmannith (ed.), *Mechanics of Jointed and Faulted Rock*. Rotterdam: Balkema, pp. 495-501.

- Subsidence Engineer's Handbook, National Coal Board, Production Department, London, 1975.
- Szwedzicki, T. - editor, (1993). Geotechnical instrumentation and monitoring in open pit and underground mining. Proceedings of the Australian conference, Kalgoorlie, Western Australia, June 21-23, 1993. 523 pp.
- Tabor, R.W., (1971). Origin of ridge-top depressions by large-scale creep in the Olympic Mountains, Washington. Geological Society of America Bulletin, **82**, pp. 1811-1822.
- Tang, D.H.Y. and S.S. Peng, (1986). Causes and mechanisms of surface fractures in a central West Virginia coal mine. Mining Science and Technology, **4**, pp. 41-48.
- Ter-Stepanian, G.I., (1977). Deep-reaching gravitational deformation of mountain slopes. Bulletin International Association Engineering Geology, **16**, Krefeld, pp. 87-94.
- Terzaghi, K., (1950). Mechanism of landslides. In: S.Paige (ed.), Application of Geology to Engineering Practice (Berkeley Volume). Geological Society of America, New York, N.Y., pp. 83-123.
- Terzaghi, K. and F.E. Richart, (1952). Stresses in rock about cavities. Geotechnique, **3**, pp. 57-90.
- Teme, S.C., and T.R. West, (1983). Some secondary toppling failure mechanisms in discontinuous rock slopes. 24<sup>th</sup> U.S. Symposium on Rock Mechanics, pp. 193-204.
- Tharp, T.M., and D.F. Coffin, (1985). Field applications of fracture mechanics analysis to small rock slopes. 26<sup>th</sup> U.S. Symposium on Rock Mechanics, pp. 667-674.
- Thomson, S. and C.E. Tiedemann, (1982). A review of factors affecting landslides in urban areas. Bulletin Association Engineering Geology, **XIX**, pp. 55-65.
- Thomson, S. and R. Yacyshyn, (1977). Slope instability in the city of Edmonton. Canadian Geotechnical Journal, **14**, pp. 1-15.
- Turner, A.K., and R.L. Schuster, (1996). Landslides - Investigation and mitigation. Special Report 247, Transportation Research Board, National Academy Press, Washington, D.C., 673 pp.
- Tyler, D.B. and R. Trueman, (1993). Probabilistic key-block analysis for support design and effects of mining-induced stress on key-block stability-a case study. Trans. Instn. Min. Metall.(Sect.A: Mining Industry), **102**, pp. A43-50.

- U.S. Army Corps of Engineers, (1970). Engineering and design - Stability of earth and rockfill dams. Engineer Manual EM 1110-2-1902. Department of the Army, Corps of Engineers, Office of the Chief of Engineers, Washington, D.C.
- VanDine, D.F., (1996). Debris flow control structures for forest engineering. Research Branch, B.C. Ministry of Forests, Victoria, B.C. Work Paper 22/1996.
- Vitek, J., (1970). From hell to paradise (in Czech). *Krasy Slovenska*, **47**, pp. 506-507.
- Vlcko, J., Baliak, F. and J. Malgot, (1993). The influence of slope movements on Spis Castle stability. Proceedings 7<sup>th</sup> International Congress and Field Trip on Landslides, Rotterdam: Balkema, pp. 305-312.
- Voight, B., (1973). The mechanics of retrogressive block-gliding, with emphasis on the evolution of the Turnagain Heights landslide, Anchorage, Alaska. In DeJong and Scholten (eds.), *Gravity and Tectonics*, J. Wiley & Sons, New York, pp. 97-121.
- Waltham, A.C. (1989). *Ground Subsidence*. Chapman and Hall: New York. 202 pp.
- Walton, G. and R.K. Taylor, (1978). Likely constraints on the stability of excavated slopes due to underground coal workings. Attewell, P.B. (ed.) *Proceedings Conference on Rock Engineering*. Newcastle, England.
- Walton, G. and T. Atkinson, (1978). Some geotechnical considerations in the planning of surface coal mines. *Trans. Instn Min. Metall. (Sect. A: Mining Industry)*, **87**, pp. A147-171.
- Wang, G.X., (1988). Landslides along the bank of the Yangtze Gorges Reservoir in China. Bonnard (ed.) *Proceedings 5<sup>th</sup> International Symposium on Landslides*, Lausanne, **1**, pp. 1259-1261.
- Watson, J.O., (1993). An overview of the boundary element methods. In Hudson (Ed.) *Comprehensive Rock Engineering*. **1**, Pergamon Press Ltd., pp. 469-490.
- Watters, R.J., Finn, D. and J. Coulthard, (1989). Pit slope instability problems induced by disused underground mine workings. Watters (ed.) *Engineering Geology and Geotechnical Engineering*, Balkema: Rotterdam, pp. 101-106.
- Watters, R.J., Rehwoldt, E. and J. Coulthard, (1990). Effects of abandoned underground workings on open pit slope design. Hustrulid and Johnson (eds.) *Rock Mechanics Contributions and Challenges*. Proc. 31<sup>st</sup> U.S. Rock Mechanics Symposium, pp. 721-728.



- Whittaker, B.N. and D.J. Reddish, (1989). Subsidence. Occurrence, Prediction and control. Elsevier, Amsterdam, 528 pp.
- Whittaker, B.N., Singh, R.N. and G. Sun, (1992). Rock Fracture Mechanics. Principles, Design and Applications. Elsevier, Amsterdam, 570 pp.
- Whittlestone, A.P., Johnson, J.D., Rogers, M.E., and R.J. Pine, (1995). Probabilistic risk analysis of slope stability. Trans. Instn. Min. Metall.(Sect.A: Mining Industry), **101**, pp. A149-158.
- Whyte, R.J., (1973). A study of Progressive Hanging Wall Caving at Chambishi Coppermine in Zambia Using the Base Friction Model Concept, M.Sc. thesis, Imperial College, London.
- Windsor, C.R., (1991). SAFEX - Stability assessment and reinforcement design package for surface rock excavations. Rock mechanics research center, CSIRO, Australia.
- Wittke, W., (1990). Rock Mechanics - Theory and Applications with Case Histories. Springer-Verlag, Berlin, Heidelberg, New York, Tokyo, 532 pp.
- Wittke, W., (1993). Remarks on the Practical Application of Rock Mechanics. International Society for Rock Mechanics - News Journal., **1**, pp. 20-42.
- Wyllie, D.C., (1980). Toppling Rock Slope Failures; Examples of Analysis and Stabilization. Rock Mechanics, **13**, pp. 89-98.
- Wyllie, D.C., and Norrish, I.N., (1996). Stabilization of Rock Slopes. In Landslides, Investigation and Mitigation, Special Report 247. Turner and Schuster (eds. ), National Academy Press, Washington, D.C., pp. 474-504.
- Xiaoning, W. (1991). Geological properties of large-scale high speed landslides and their mechanism models. Bulletin International Association Engineering Geology , **43**, pp. 93-99.
- Yu, Y.S. and D.F. Coates, (1978). Canadian experience in simulating pit slopes by the finite element method. In Voight (ed.) Rockslides and Avalanches, **2**, Elsevier, Amsterdam, pp. 709-758
- Zaruba, Q, and V.Mencl, (1987). Landslides and their control. 2<sup>nd</sup> edition. Elsevier, Amsterdam. 324 pp.
- Zischinsky, U., (1966). On the deformation of high slopes. Proceedings, 1<sup>st</sup> International Congress Society of Rock Mechanics, Lisbon, Portugal, **2**, 179-185.
- Zaruba, Q. and V. Mencl, (1976). Engineering Geology. Elsevier, Amstredam. 606 pp.

## **APPENDIX A**

### **Numerical Modelling Codes (FLAC and UDEC programs)**

\*\*\*\*\*

**NUMERICAL ANALYSIS OF GROUND DEFORMATIONS  
AT THE SPIS CASTLE (SLOVAKIA) - DISCONTINUUM MODELLING  
EAST - WEST CROSS - SECTION  
(CHAPTER 3)**

\*\*\*\*\*

- \* UDEC INPUT FILE
- \* UNIVERSITY OF SASKATCHEWAN
- \* DEPARTMENT OF GEOLOGICAL SCIENCES
- \* WRITTEN BY BORIS BENKO (UNIX Version - block addresses will differ if run on MSDOS Version of UDEC), Last revised fall 1996

new

\*Block rounding  
round 0.1

\*Initial block  
block 0,0 0,105 277.7128,105 277.7128,0

\*Jointing pattern

split 0,10	277.7128,10
split 0,25	277.7128,25
split 0,45	277.7128,45
split 0,48	277.7128,48
split 0,100	277.7128,100
crack 17.9952,10	50.1628,25
crack 50.1628,25	90,48
crack 221,48	277.7128,38
*85 degree lines	
crack 90,48	94.6,100
crack 100,48	104.6,100
crack 108,48	112.6,100
crack 116.5,48	121.1,100
crack 129.5,48	134.1,100
crack 141.5,48	146.1,100
crack 167.5,48	172.1,100
crack 177.5,48	182.1,100
crack 185.5,48	190.1,100
crack 200.5,48	205.1,100
crack 207.5,48	212.1,100

crack 214,48 218.6,100

crack 221,48 225.6,100

**\*Travertine blocks**

crack 90,70.5 104,70.5

crack 100,70.5 112,70.5

crack 108,95 120.5,95

crack 167.5,88 181.5,88

crack 177.5,78 189.5,78

crack 185.5,73 204.5,73

crack 200.5,67 211.5,67

crack 207.5,64 218,64

crack 214,61.5 225,61.5

jdelete

**\*Castle wall**

split 122,105 122,100

split 171,105 171,100

jreg 122,100 122,105 171,105 171,100

jset 180,0 50,0 0,0 1,0 122,100

jset 90,0 1,0 1,0 2,0 122,100

jset 90,0 1,0 1,0 2,0 123,101

**\*Joints for initial excavation**

crack 0,60 95,60

crack 277.7128,60 221,60

crack 0,80 112,80

crack 277.7128,80 177.5,80

jdelete

**\*Block discretization - finite difference triangles**

gen bl 1 quad 20

gen bl 86 edge 10

gen bl 237 edge 4

gen bl 388 edge 1

ge bl 2530 quad 3

ge bl 2853 quad 3

ge bl 3176 quad 3

ge bl 3499 quad 3

ge bl 3822 quad 3

ge bl 4145 quad 3

ge bl 4468 quad 3

ge bl 4791 quad 3

ge bl 5114 quad 3

ge bl 5437 quad 3

ge bl 5760 quad 3

ge bl 6083 quad 3

ge reg 122,100 122,105 171,105 171,100 quad 2.1

ge

edge 20

**\*Initial material properties - elastic constitutive criterion and high joint strength**

```
prop mat 1 dens 2530 shear 11e9 bulk 22e9
prop mat 2 dens 2370 shear 4e9 bulk 8e9
prop mat 3 dens 2100 shear 3e7 bulk 1e8
prop jmat 1 jkn 5e10 jks 5e9 jcoh 1e10 jten 1e10
chan 0 277.7128 0 45 mat 2
chan 0 277.7128 45 48 mat 3
chan 0 277.7128 48 105 mat 1
chan jmat 1
```

**\*Gravitational acceleration**

```
set grav 0 -9.81
```

**\*Automatic mass damping**

```
damp auto
```

**\*Initial stress ratio K=1**

```
in 0 277.7128 48 105 stress -2.61e6 0 -2.61e6 szz -2.61e6 &
      ygrad 24.8e3 0 24.8e3 zgrad 0 24.8e3
in 0 277.7128 45 48 stress -2.405e6 0 -2.405e6 szz -2.405e6 &
      ygrad 20.6e3 0 20.6e3 zgrad 0 20.6e3
in 0 277.7128 0 45 stress -2.52e6 0 -2.52e6 szz -2.52e6 &
      ygrad 23.25e3 0 23.25e3 zgrad 0 23.25e3
```

**\*Boundary conditions**

```
bou cor 50 63 xvel 0
bou cor 63 24 yvel 0
bou cor 24 37 xvel 0
```

**\*Initial equilibrium and unbalanced history**

```
history unbalance
cycle 200
```

**\* Progressive "excavation of travertine hill" with stress equilibration after each**

**\* excavation step**

```
del bl 690
del bl 9989
cycle 1500
save stav1
```

```
del bl 48121
del bl 48681
del bl 48358
```

del bl 7238  
del bl 7600  
del bl 8001  
del bl 8402  
del bl 8803  
del bl 9204  
del bl 9480  
del bl 539  
cycle 1500  
save stav2

del bl 6889  
del bl 6488  
del bl 47694  
del bl 49905  
del bl 49668  
del bl 49431  
del bl 49194  
del bl 48871  
del bl 50181  
cycle 1500  
save stav3

del bl 2250  
del bl 47970  
cycle 1500  
save stav4

del bl 1173  
del bl 1733  
cycle 1500  
save stav5

del bl 1496  
del bl 2056  
cycle 1500  
save stav6

del bl 841  
step 3000  
save bl\_elas.sav

**\*Change in constitutive criterion to Mohr-Coulomb with various assumed shear strength  
\*properties  
prop mat 4 dens 2530 shear 11e9 bulk 22e9**

```

prop mat 5 dens 2370 shear 4e9 bulk 8e9
prop mat 6 dens 2100 shear 3e7 bulk 1e8 coh =***!! fric =***!!
***!!Shear strength properties for mat 6 (cohesion and friction) - representing the "Creep
***!!zone" were varied to investigate the influence of various strength on deformations
prop mat 7 dens 2530 shear 11e9 bulk 22e9 fric=35 coh=5e6 ten=2e5
prop jmat 4 jkn 5e10 jks 5e9 jfric 25 jcoh 0 jten 0
prop jmat 5 jkn 5e10 jks 5e9 jfric 0 jcoh 1e20 jten 1e20
prop jmat 6 jkn 5e10 jks 5e9 jfric 20 jcoh 0 jten 0
prop jmat 7 jkn 5e10 jks 5e9 jcoh 50e3 jten 0 jfric 30
chan 0 277.7128 48 100 mat 4 jmat 4
chan 0 277.7128 0 44 mat 5 jmat 5
chan 0 277.7128 45 48 mat 6 cons 3
chan 0 277.7128 44 49 angle -10 10 jmat 6
chan 0 277.7128 100 105 mat 7
chan 0 277.7128 100 105 jmat 7

```

\*Displacement histories at selected points used for monitoring deformations in model

```

hist ydis 125,105
hist xdis 125,105
hist ydis 150,105
hist xdis 150,105
hist ydis 170,105
hist xdis 170,105
hist ydis 95,70.5
hist xdis 95,70.5
hist ydis 110,95
hist xdis 110,95
hist ydis 200,73
hist xdis 200,73
hist ydis 220,61.5
hist xdis 220,61.5

```

\*calculation cycle to be stopped at various stages to examine model response to used

\*material properties

```

step 1000
plot plas disp hold

```

```

step 1000
plot plas disp hold
step 3000
plot plas disp hold
plot block mag 20 hold
save kolf20c0.sav

```

```

quit

```

\*\*\*\*\*

**NUMERICAL ANALYSIS OF GROUND DEFORMATIONS  
AT THE SPIS CASTLE (SLOVAKIA) - DISCONTINUUM MODELLING  
NORTH - SOUTH CROSS - SECTION  
(CHAPTER 3)**

\*\*\*\*\*

- \* UDEC INPUT FILE
- \* UNIVERSITY OF SASKATCHEWAN
- \* DEPARTMENT OF GEOLOGICAL SCIENCES
- \* WRITTEN BY BORIS BENKO (UNIX Version - block addresses will differ if run on MSDOS Version of UDEC), Last revised fall 1996

new

\*Block rounding  
round 0.1

\*Initial block  
block 0,0 0,80 246,80 246,0

\*Jointing pattern

split 0,25	246,25
split 0,23	246,23
crack 30,25	0,0
crack 216,25	246,0
split 0,75	246,75

\*Travertine blocks

crack 30,25	34,71
crack 34,71	42,71
crack 42,71	38,25
crack 42,71	42,4,75
crack 68,75	52,25
crack 80,75	71,25
crack 98,75	92,25
crack 104,75	108,25
crack 129,75	134,25
crack 147,75	154,25
crack 147,74	159,74
crack 159,74	168,25
crack 159.5,70	175,65
crack 175,65	183,25



crack 175,61	180,61
crack 180,61	188,25
crack 180,59	184,59
crack 184,59	192,25
crack 184,59	189,59
crack 189,59	197,25
crack 189,57	194.5,57
crack 194.5,57	202.5,25
crack 195.5,53	203.5,53
crack 203.5,53	210.5,25
crack 205,47	210,47
crack 210,47	216,25

**\*Joints for excavation**

crack 0,35	32,35
crack 213,35	246,35
crack 0,45	32,45
crack 210,45	246,45
crack 0,55	33,55
crack 194,55	246,55
crack 0,65	35,65
crack 175,65	246,65
crack 0,15	18,15
crack 228,15	246,15

**\*Castle wall**

split 60,80	60,75
split 110,80	110,75
jreg 60,75 60,80 110,80 110,75	
jset 180,0 50,0 0,0 1,0 60,75	
jset 90,0 1,0 1,0 2,0 60,75	
jset 90,0 1,0 1,0 2,0 61,76	
jdelete	

**\*Block discretization - finite difference triangles**

gen bl 720	quad 4
gen bl 388	quad 1
gen bl 86	edge 5
gen bl 1621	edge 5
gen bl 2284	edge 5
gen bl 2607	edge 5
gen bl 2930	edge 5
gen bl 3253	edge 5
gen bl 3576	edge 5
gen bl 3899	edge 5
gen bl 4347	edge 5
gen bl 4821	edge 5

```

gen bl 5295                edge 5
gen bl 5769                edge 5
gen bl 6105                edge 5
gen bl 6579                edge 5
gen bl 7014                edge 5
ge reg 60,75 60,80 110,80 110,75  quad 2.1
ge                        edge 20

```

**\*Initial material properties - elastic constitutive criterion and high joint strength**

```

prop mat 1 dens 2530 shear 11e9 bulk 22e9
prop mat 2 dens 2370 shear 4e9 bulk 8e9
prop mat 3 dens 2000 shear 3e6 bulk 1e7
prop jmat 1 jkn 5e10 jks 5e9 jcoh 1e20 jten 1e20
chan 0 246 0 23  mat 2
chan 0 246 23 25  mat 3
chan 0 246 25 80  mat 1
chan jmat 1

```

**\*Gravitational acceleration**  
set grav 0 -9.81

**\*Automatic mass damping**  
damp auto

**\*Initial stress ratio K=1**

```

in 0 246 25 80 str -1985.54e3 0 -1985.54e3 szz -1985.54e3 &
      yg 248.2e2 0 248.2e2 zg 0 248.2e2
in 0 246 23 25 str -1855.56e3 0 -1855.56e3 szz -1855.56e3 &
      ygrad 196.2e2 0 196.2e2 zg 0 196.2e2
in 0 246 0 23 str -1939.05e3 0 -1939.05e3 szz -1939.05e3 &
      yg 232.5e2 0 232.5e2 zg 0 232.5e2

```

**\*Boundary conditions**

```

bou cor 50 63 xvel 0
bou cor 63 24 yvel 0
bou cor 24 37 xvel 0

```

**\*Histories for monitoring initial equilibrium state**

```

history unbalance
history ydis 50,75
history ydis 100,75
history ydis 150,75

```

**\*Steps to initial equilibrium**  
cycle 500

**\*Progressive “excavation of travertine hill” with stress equilibration after each excavation step**

**del bl 1405  
del bl 10497  
cycle 2500  
save step1.sav**

**del bl 9372  
del bl 9648  
cycle 2500  
save step2.sav**

**del bl 8820  
del bl 9096  
cycle 2500  
save step3.sav**

**del bl 8268  
del bl 8544  
cycle 2500  
save step4.sav**

**del bl 7716  
del bl 7992  
cycle 2500  
save step5.sav**

**del bl 2060  
del bl 7449  
cycle 2500  
save step6.sav**

**del bl 237  
del bl 1125  
cycle 2500  
save step7.sav**

**del bl 9786  
del bl 10023  
cycle 2500  
save step8.sav**

**del bl 1  
del bl 901  
cycle 6000**

save hrad.elas

\*Change in constitutive criterion to Mohr-Coulomb with various assumed shear strength

\*properties

prop mat 4 dens 2530 shear 11e9 bulk 22e9

prop mat 5 dens 2370 shear 4e9 bulk 8e9

prop mat 6 dens 2100 shear 3e7 bulk 1e8 coh =\*\*\*!! fric =\*\*\*!!

\*\*\*!! Properties for mat 6 - cohesion and friction - representing the "Creep zone" were

\*\*\*!! varied to investigate the influence of various strength

prop mat 7 dens 2530 shear 11e9 bulk 22e9 fric=35 coh=5e6 ten=2e5

prop jmat 4 jkn 5e10 jks 5e9 jfric 25 jcoh 0 jten 0

prop jmat 5 jkn 5e10 jks 5e9 jfric 0 jcoh 1e20 jten 1e20

prop jmat 6 jkn 5e10 jks 5e9 jfric 20 jcoh 0 jten 0

prop jmat 7 jkn 5e10 jks 5e9 jcoh 50e3 jten 0 jfric 30

chan 0 277.7128 48 100 mat 4 jmat 4

chan 0 277.7128 0 44 mat 5 jmat 5

chan 0 277.7128 45 48 mat 6 cons 3

chan 0 277.7128 44 49 angle -10 10 jmat 6

chan 0 277.7128 100 105 mat 7

chan 0 277.7128 100 105 jmat 7

\*Displacement histories at selected points used for monitoring deformations in model

history ydis 50,75

history xdis 50,75

history ydis 100,75

history xdis 100,75

history ydis 150,75

history xdis 150,75

\*Calculation cycle to be stopped at various stages to examine model response to used

\*material properties

step 1000

plot plas hold

step 1000

plot plas hold

step 3000

plot plas disp hold

plot block mag 20 hold

save kolf20c0.sav

quit

\*\*\*\*\*

**NUMERICAL ANALYSIS OF TOPPLING DEFORMATIONS AT LUSCAR  
MINE, LUSCAR, ALBERTA - DISCONTINUUM MODELLING  
CROSS - SECTION C20+00  
(CHAPTER 4)**

\*\*\*\*\*

- \* UDEC INPUT FILE
- \* UNIVERSITY OF SASKATCHEWAN
- \* DEPARTMENT OF GEOLOGICAL SCIENCES
- \* WRITTEN BY BORIS BENKO (UNIX Version - block addresses will differ if run on MSDOS Version of UDEC), Last revised fall 1996

new  
title  
LUSCAR MINE / PIT 50-A-52 / C20+00

\*Block rounding  
round 0.05

\*Initial block  
block 0,-350 0,0 700,0 700,-350

- \*Jointing pattern
- \*Original surface topography ~ angle 20 degr
- crack 318.9,0 530,-78
- crack 530,-78 700,-78
- \*Basic lithological boundaries - beds dipping 62 degrees into the slope
- \*MEMBER "D" (SILTSTONES & SANDSTONES)
- crack 537,-350 681.625,-78
- crack 509.8,-350 654.425,-78
- \*JEWEL SEAM (COAL)
- crack 496.2,-350 640.825,-78
- \*TORRENS MEMBER (MASSIVE SANDSTONE)
- crack 475.9,-350 620.525,-78
- \*TORRENS MEMBER (SILTSTONES & SANDSTONES)
- crack 439.7,-350 584.325,-78
- \*MOOSEBAR MEMBER (SHALES)
- crack 272.08,-350 435.3,-43.02
- \*GLADSTONE MEMBER (SILTSTONES & SHALES)
- crack 358.2,-350 507.25,-69.61
- \*CADOMIN CONGLOMERATE (11m thick)

crack 259.63,-350 424.9,-39.18

\*Artificial joint for zoning

split 0,-300 700,-300

split 0,-250 700,-250

jdelete

\*Bedding planes within formations

\*MEMBER "D" / SILTSTONES & SANDSTONES - 8m spacing

jreg 563,-250 654.425,-78 681.625,-78 590.2,-250

jset 62,0 300,0 0,0 8,0 563.6,-300

\*TORRENS MEMBER / SILTSTONES & SANDSTONES

\* Original 1m bedding spacing - scaled to 8m spacing

jreg 492.9,-250 584.325,-78 620.525,-78 529.1,-250

jset 62,0 300,0 0,0 8,0 475.9,-350

\*Lower part

jreg 466.3,-300 492.9,-250 529.1,-250 502.5,-300

jset 62,0 100,0 0,0 16,0 475.9,-350

jdelete

\*MOOSEBAR MEMBER / SHALES - 4M SPACING

\* Original 0.5m bedding spacing - scaled to 2m spacing

split 530,-78 385.375,-350

jreg 438.5,-250 530,-78 584.325,-78 492.9,-250

jset 62,0 300,0 0,0 4,0 530,-78

jreg 411.3,-250 507.2,-69.5 530,-78 438.5,-250

jset 62,0 300,0 0,0 4,0 530,-78

\*Lower part

jreg 298.7,-300 325.3,-250 492.9,-250 466.3,-300

jset 62,0 100,0 0,0 8,0 530,-78

jdelete

\*GLADSTONE MEMBERS / SILTSTONES & SHALES

jreg 325.3,-250 435.3,-43.02 507.2,-69.5 411.3,-250

jset 62,0 300,0 0,0 4,0 530,-78

jdelete

\*NIKANASSIN FORMATION / SHALES & SILTSTONES

\*Original 0.5m bedding spacing - scaled to 4m spacing

split 318.9,0 132.78,-350

jreg 185.96,-250 318.9,0 425,-39.19 313,-250

jset 62,0 300,0 0,0 4,0 318.9,0

jdelete

split 210.3,0 24.2,-350

jreg 77.37,-250 210.3,0 318.9,0 186,-250

jset 62,0 300,0 0,0 4,0 318.9,0

**\*Lower part**

jreg 50.8,-300 77.4,-250 312.8,-250 286.2,-300

jset 62,0 100,0 0,0 8,0 286.2,-300

**\*Back**

split 155.9,0 23,-250

jreg 23,-250 155.9,0 210.3,0 77.4,-250

jset 62,0 300,0 0,0 8,0 210.3,0

jreg 0,-250 0,0 155.9,0 23,-250

jset 62,0 300,0 0,0 35,0 155.9,0

jdelete

**\*New block rounding**

round 0.2

**\*Future mine excavation - 12m high benches**

**\*65 degr. face angle - 6.5m safety berm**

**\*45 degr. overall slope angle**

**\*bench #1**

crack 530,-78 537.2,-90

crack 537.2,-90 541.8,-90

**\*bench #2**

crack 541.8,-90 548.9,-102

crack 548.9,-102 553.5,-102

**\*bench #3**

crack 553.5,-102 560.7,-114

crack 560.7,-114 565.2,-114

**\*bench #4**

crack 565.2,-114 572.5,-126

crack 572.5,-126 576.9,-126

**\*bench #5**

crack 576.9,-126 584.6,-137.5

crack 584.6,-137.5 591.1,-137.5

**\*bench #6**

crack 591.1,-137.5 596.7,-150

crack 596.7,-150 602.5,-150

**\*bench #7 - double height + bottom of pit**

crack 602.5,-150 613.5,-172.2

crack 613.5,-172.2 700,-172.2

**\*Joints for mine excavation**

split 541.8,-90 700,-90

split 553.5,-102 700,-102

split 565.2,-114 700,-114

split 576.9,-126 700,-126

split 591.1,-137.5 700,-137.5

split 602.5,-150 700,-150

```

*Blocks under excavation bottom
jreg 590.2,-250 631.5,-172.2 690,-172.2 690,-250
jset 62,0 200,0 0,0 16,0 590.2,-250
jreg 563.6,-300 590.2,-250 690,-250 690,-300
jset 62,0 200,0 0,0 32,0 590.2,-250
*Artificial joints for initial slope excavation
split 389.3,-26      700,-26
split 459.6,-52     700,-52
jdelete

*Block discretization - finite difference zones
*Blocks at the far left side of model
ge reg 0,-250 0,0 155.9,0 23,-250      edge 35
*Blocks at the bottom
ge reg 0,-350 0,-300 700,-300 700,-350  quad 60
*Blocks above bottom
ge reg 0,-300 0,-250 700,-250 700,-300  quad 20
*Blocks in Nikanassin formation, Cadomin, Gladstone & Moosebar
ge reg 23,-250 155.9,0 210.3,0 77.4,-250  quad 16
ge reg 77.4,-250 210.3,0 530,-78 438.5,-250  quad 4.6
ge bl 51579      edge 5
ge bl 51487      edge 5
ge bl 51395      edge 5
ge reg 438.5,-250 530,-78 584.3,-78 492.9,-250  quad 4.6
*Blocks in Torrens Member
ge bl 51717      edge 5
ge bl 51671      edge 5
ge reg 492.9,-250 584.3,-78 620.5,-78 529.1,-250  quad 4.7
*Sandstone
ge reg 529.1,-250 620.525,-78 640.825,-78 549.3,-250  edge 5
*Coal
ge reg 549.3,-250 640.825,-78 654.425,-78 562.9,-250  edge 5
*Member "D"
ge reg 562.9,-250 654.425,-78 681.625,-78 590.1,-250  quad 5
*Rest of model - right part
ge reg 590.1,-250 681.625,-78 700,-78 700,-250  quad 15
*Part to be excavated
ge bl 68996      edge 25
ge bl 69233      edge 25
ge bl 125        edge 25

* "STRONG" COHESION AND TENSION FOR INITIAL EQUILIBRIUM
*jks=0.25jkn
*Member "D" + part of model to the right
ch reg 509.8,-350 654.425,-78 700,-78 700,-350  mat=1

```



prop mat=1 d=2300 bulk=16.66e9 shear=10e9  
prop jmat=1 jkn=4e9 jks=1e9 jfric=29 jcoh=1e20 jten=1e20  
\*Coal  
ch reg 496.2,-350 640.825,-78 654.425,-78 509.8,-350 mat=2  
prop mat=2 d=1700 bulk=3.33e9 shear=1.54e9  
prop jmat=2 jkn=4e9 jks=1e9 jfric=20 jcoh=1e20 jten=1e20  
\*Sandstone / Torrens member  
ch reg 475.9,-350 620.525,-78 640.825,-78 496.2,-350 mat=3  
prop mat=3 d=2300 bulk=20e9 shear=12e9  
prop jmat=3 jkn=4e9 jks=1e9 jfric=35 jcoh=1e20 jten=1e20  
\*Siltstone-sandstone / Torrens member  
ch reg 439.7,-350 584.3,-78 620.5,-78 475.9,-350 mat=4  
prop mat=4 d=2300 bulk=16.66e9 shear=10e9  
prop jmat=4 jkn=4e9 jks=1e9 jfric=29 jcoh=1e20 jten=1e20  
\*Shale / Moosebar & Gladstone members  
ch reg 272.08,-350 435.3,-43.02 584.3,-78 439.7,-350 mat=5  
prop mat=5 d=2100 bulk=6.66e9 shear=3.08e9  
prop jmat=5 jkn=4e9 jks=1e9 jfric=20 jcoh=1e20 jten=1e20  
\*Cadomin conglomerate  
ch reg 259.63,-350 424.9,-39.18 435.3,-43.02 272.08,-350 mat=7  
prop mat=7 d=2500 bulk=23.33e9 shear=14e9  
prop jmat=7 jkn=4e9 jks=1e9 jfric=35 jcoh=1e20 jten=1e20  
\*Shale / Nikanassin formation  
ch reg 132.78,-350 318.9,0 424.9,-39.18 259.63,-350 mat=8  
ch reg 0,-350 0,0 318.9,0 132.78,-350 mat=8  
prop mat=8 d=2100 bulk=6.66e9 shear=3.08e9  
prop jmat=8 jkn=4e9 jks=1e9 jfric=20 jcoh=1e20 jten=1e20  
\*Excavated blocks  
ch bl 68996 mat=8  
ch bl 69233 mat=8  
ch bl 125 mat=8  
prop mat=8 d=2100 bulk=6.66e9 shear=3.08e9  
prop jmat=8 jkn=4e9 jks=1e9 jfric=20 jcoh=1e20 jten=1e20  
  
\*ROLLER BOUNDARY CONDITIONS ALONG THE BASE & SIDES  
bou cor 50 63 xvel 0  
bou cor 63 24 yvel 0  
bou cor 24 37 xvel 0  
  
\*INITIAL STRESS STATE  
\*Kxy=1.5 Kzy=1.25 (sxx>szz>syy)  
\*based on "average density" - 2200 kg/m3  
in stress 0 0 0 szz 0 yg 323.73e2 0 215.82e2 zg 0 269.775e2  
  
\*Gravitational acceleration

```

set grav 0 -9.81

*Automatic mass damping
damp auto

*Histories for initial equilibrium monitoring
hist unbalance
hist ydis 150,-1
hist ydis 250,-1
hist ydis 318.9,-1
hist ydis 530,-79

*INITIAL EQUILIBRIUM
step 5000
save ini_0.sav
*INITIAL EXCAVATION TO PRE-MINING TOPOGRAPHY
del bl 68996
step 5000
save ini_1.sav
del bl 69233
step 5000
save ini_2.sav
del bl 125
step 5000
save ini.sav

*Excavation of benches
del reg 537.2,-90 530,-78 700,-78 700,-90
del reg 548.9,-102 542.7,-90 700,-90 700,-102
step 7500
save excav2.sav
del reg 560.7,-114 554.8,-102 700,-102 700,-114
step 7500
save excav3.sav
del reg 572.5,-126 566.9,-114 700,-114 700,-126
step 7500
save excav4.sav
del reg 584.6,-137.5 579,-126 700,-126 700,-137.5
step 7500
save excav5.sav
del reg 596.7,-150 591.1,-137.5 700,-137.5 700,-150
step 7500
save excav6.sav
del reg 614.4,-172.2 591.1,-138 700,-138 700,-172.2
step 7500

```

save excav7.sav

\*Change in material properties to analyze deformations  
\*Material properties were assigned various values throughout the study - only one set of  
\*properties for the Mohr-Coulomb constitutive criterion and "dry" slope is presented  
\*input for model state after the 2<sup>nd</sup> bench was excavated presented only

rest excav2.sav

reset disp

reset jdisp

reset history

\*MATERIAL PROPERTIES

\*Hebil jfr=18 shales jfr=20 coal jfr=28 sandstone

\*jks=0.25jkn

\*Member "D" + part of model to the right

ch reg 509.8,-350 654.425,-78 700,-78 700,-350 jmat=1 mat=1 cons=3

prop mat=1 d=2300 bulk=16.66e9 shear=10e9 fric=35 coh=1e6 ten=1e5

prop jmat=1 jkn=4e9 jks=1e9 jfric=25 jcoh=0 jten=0

\*Coal

ch reg 496.2,-350 640.825,-78 654.425,-78 509.8,-350 jmat=2 mat=2 cons=3

prop mat=2 d=1700 bulk=3.33e9 shear=1.54e9 fric=22 coh=40e3 ten=4e3

prop jmat=2 jkn=4e9 jks=1e9 jfric=20 jcoh=0 jten=0

\*Sandstone / Torrens member

ch reg 475.9,-350 620.525,-78 640.825,-78 496.2,-350 jmat=3 mat=3 cons=3

prop mat=3 d=2300 bulk=20e9 shear=12e9 fric=35 coh=400e3 ten=40e3

prop jmat=3 jkn=4e9 jks=1e9 jfric=28 jcoh=0 jten=0

\*Siltstone-sandstone / Torrens member

ch reg 439.7,-350 584.3,-78 620.5,-78 475.9,-350 jmat=4 mat=4 cons=3

prop mat=4 d=2300 bulk=16.66e9 shear=10e9 fric=30 coh=90e3 ten=9e3

prop jmat=4 jkn=4e9 jks=1e9 jfric=25 jcoh=0 jten=0

\*Shale / Moosebar Member

ch reg 358.2,-350 507.2,-69.5 584.3,-78 439.7,-350 mat=5 cons=3

ch reg 358.2,-350 507.2,-69.5 584.3,-78 439.7,-350 jmat=5

prop mat=5 d=2100 bulk=6.66e9 shear=3.08e9 fric=25 coh=45e3 ten=4.5e3

prop jmat=5 jkn=4e9 jks=1e9 jfric=18 jcoh=0 jten=0

\*Shale / Gladstone member

ch reg 272.08,-350 435.3,-43.02 507.2,-69.5 358.2,-350 mat=6 cons=3

ch reg 272.08,-350 435.3,-43.02 507.2,-69.5 358.2,-350 jmat=6

prop mat=6 d=2100 bulk=6.66e9 shear=3.08e9 fric=25 coh=45e3 ten=4.5e3

prop jmat=6 jkn=4e9 jks=1e9 jfric=18 jcoh=0 jten=0

\*Cadomin conglomerate

ch reg 259.63,-350 424.9,-39.18 435.3,-43.02 272.08,-350 jmat=7 mat=7 cons=3

prop mat=7 d=2500 bulk=23.33e9 shear=14e9 fric=40 coh=500e3 ten=50e3

prop jmat=7 jkn=4e9 jks=1e9 jfric=30 jcoh=0 jten=0

\*Shale / Nikanassin formation

ch reg 132,-350 318.9,0 424.9,-39.18 259.63,-350 jmat=8 mat=8 cons=3

```

ch reg 0,-350 0,0 318.9,0 132,-350          jmat=8 mat=8 cons=3
prop mat=8 d=2100 bulk=6.66e9 shear=3.08e9 fric=25 coh=45e3 ten=4.5e3
prop jmat=8 jkn=4e9 jks=1e9 jfric=18 jcoh=0 jten=0
*change contact weak/strong to weaker property
*coal/member"D"
ch reg 508.9,-350 653.425,-78 655.425,-78 510.8,-350  jmat=2
*sandstone/coal
ch reg 495.2,-350 639.825,-78 641.825,-78 497.2,-350  jmat=2
*sandstone/torrens
ch reg 474.9,-350 619.525,-78 621.525,-78 476.9,-350  jmat=4
*torrens/moosebar
ch reg 438.7,-350 583.325,-78 585.325,-78 440.7,-350  jmat=5
*moosebar/gladstone
ch reg 383.8,-300 506.2,-78 508.2,-78 385.8,-300      jmat=5
*cadomin/gladstone
ch reg 271.08,-350 434.3,-42.5 436.3,-42.5 273.08,-350 jmat=6
*cadomin/nikanassin
ch reg 258.63,-350 423.9,-39 425.9,-39 260.63,-350    jmat=8
*Artificial joints
ch angle -2 2  jmat=10
ch angle 100 130 jmat=10
prop jmat=10 jkn=4e9 jks=1e9 jfric=40 jcoh=1e20 jten=1e20

*Displacement history at selected points used for monitoring deformations in model
hist ydis 255,-1
hist xdis 255,-1
hist yvel 255,-1
hist xvel 255,-1
hist ydis 318.9,-1
hist xdis 318.9,-1
hist yvel 318.9,-1
hist xvel 318.9,-1
hist ydis 425,-40.2
hist xdis 425,-40.2
hist yvel 425,-40.2
hist xvel 425,-40.2
hist ydis 526,-80.5
hist xdis 526,-80.5
hist yvel 526,-80.5
hist xvel 526,-80.5

step 10000
save bench2.sav * Analysis procedure shown only for deformations after excavation of
*second bench
quit

```

\*\*\*\*\*

**NUMERICAL ANALYSIS OF TOPPLING DEFORMATIONS AT LUSCAR  
MINE, LUSCAR, ALBERTA - DISCONTINUUM MODELLING  
CROSS - SECTION C25+00  
(CHAPTER 4)**

\*\*\*\*\*

- \* UDEC INPUT FILE
- \* UNIVERSITY OF SASKATCHEWAN
- \* DEPARTMENT OF GEOLOGICAL SCIENCES
- \* WRITTEN BY BORIS BENKO (UNIX Version - block addresses will differ if run on MSDOS Version of UDEC), Last revised fall 1996

new  
title  
LUSCAR MINE / PIT 50-A-52 / C25+00/ PROGNOSIS

\*Block rounding  
round 0.1

\*Initial block  
block 0,-400 0,0 800,0 800,-400

\*Jointing pattern  
\*top topography (6.5 degrees) - present & future mining stage

crack 300,0	505,-23.4
crack 505,-23.4	528.8,-46.7
crack 537.9,-46.7	528.8,-46.7
crack 552.3,-70.7	537.9,-46.7
crack 564.3,-70.7	552.3,-70.7
crack 576.3,-94.7	564.3,-70.7
crack 588.3,-94.7	576.3,-94.7
crack 588.3,-94.7	613.2,-136.2
crack 613.2,-136.3	617.9,-136.3
crack 617.9,-136.3	620.3,-143.5
crack 620.3,-143.5	632.3,-143.5
crack 632.3,-143.5	644.3,-167.5
crack 644.3,-167.5	653.4,-167.5
crack 653.4,-167.5	668.3,-191.5
crack 668.3,-191.5	680.3,-191.5
crack 680.3,-191.5	692.3,-215.5
crack 692.3,-215.5	706.5,-215.5
crack 706.5,-215.5	706.5,-240.3

crack 706.5,-240.3 800,-240.3  
\*Present pit bottom  
crack 602.8,-118.7 800,-118.7  
\*Artificial joint for finite difference zoning  
split 0,-320 800,-320

**\*BASIC LITHOLOGY**

**\*CADOMIN CONGLOMERATE - 6m thick / 62 degrees**

crack 300,0 87.32,-400

crack 308.53,-0.97 96.36,-400

**\*GLADSTONE MEMBER**

crack 381.2,-9.25 173.44,-400

**\*MOOSEBAR MEMBER**

crack 505,-23.4 304.76,-400

**\*TORRENS MEMBER**

crack 548,-61.9 448.1,-249.9

**\*MASSIVE SANDSTONE - 14.4m thick**

crack 559.6,-70.7 481.9,-216.9

**\*JEWEL SEAM / COAL - 6m thick**

crack 481.9,-216.9 683.2,-118.7

crack 565.4,-72.9 501.5,-193.1

crack 501.5,-193.1 654,-118.7

**\*TORRENS MEMBER / MASSIVE SANDSTONE - 14.4m thick**

**\*26 degrees**

crack 692.3,-130.7 448.1,-249.9

crack 706.5,-400 706.5,-118.7

crack 692.3,-400 692.3,-130.7

**\*COAL / 12m**

crack 718.5,-400 718.5,-118.7

**\*BEDDING PLANE DISCONTINUITIES**

**\*syncline axis 44 degrees**

**\*anticline axis 58 degrees**

**\*Member"D" - SILTSTONES & SANDSTONES - 4M BEDDING**

jreg 565.4,-72.9 583,-75 593.2,-104.5 501.5,-193.1

jset 62,0 200,0 0,0 8,0 501.5,-193.1

jreg 501.5,-193.1 593.2,-104.5 625,-114 654,-118.7

jset 26,0 200,0 0,0 8,0 501.5,-193.1

jdelete

jreg 718.5,-320 718.5,-118.7 795,-118.7 795,-320

jset 90,0 250,0 0,0 16,0 718.5,-320

**\*TORRENS MEMBER / SILTSTONES & SANDSTONES / 56m thick**

**\* Original 1m bedding spacing - scaled to 4m spacing**

jreg 317.5,-376 505,-23.4 555,-50 448.1,-249.9

jset 62,0 300,0 0,0 8,0 505,-23.4

**\*TORRENS MEMBER / SILTSTONES & SANDSTONES / 26 degr.**

jreg 375.5,-320 448.1,-249.9 692.3,-130.7 574,-320

jset 26,0 300,0 0,0 8,0 692.3,-130.7

jreg 692.3,-320 574,-320 628.3,-233.2 692.3,-130.7

jset 90,0 300,0 0,0 8,0 692.3,-130.7

jdelete

**\*Moosebar Member**

jreg 216,-320 381.2,-9.27 505,-23.4 347.3,-320

jset 62,0 500,0 0,0 4,0 347.3,-320

**\*Gladstone Member**

jreg 138.9,-320 308.53,-0.97 381.2,-9.27 216,-320

jset 62,0 500,0 0,0 4,0 347.3,-320

**\*Nikanassin Formation**

split 209.4,0 39.2,-320

jreg 39.2,-320 209.4,0 300,0 129.8,-320

jset 62,0 500,0 0,0 4,0 300,0

jreg 0,-320 0,0 209.4,0 39.2,-320

jset 62,0 500,0 0,0 12,0 209.4,0

**\*Artificial joint for initial excavation**

crack 800,-23.4 505,-23.4

crack 800,-46.7 537.9,-46.7

crack 800,-70.7 564.3,-70.7

crack 800,-94.7 588.3,-94.7

**\*Artificial joint for zoning**

split 0,-350 800,-350

**\*Artificial joints for open pit deepening**

crack 800,-136.3 617.9,-136.3

crack 800,-143.5 620.3,-143.5

crack 800,-167.5 653.4,-167.5

crack 800,-191.5 680.3,-191.5

crack 800,-215.5 704.3,-215.5

jdelete

round 0.2

**\*Blocks discretization - finite difference zones**

ge reg 0,-400 0,-350 800,-350 800,-400

quad 60

ge reg 0,-350 0,-320 800,-320 800,-350

quad 20.1

ge bl 2276

edge 30

ge bl 45724

quad 30

ge bl 45862

quad 30

ge bl 46000

quad 30

ge bl 46138

quad 30

ge reg 613.2,-136.3 600.3,-118.7 800,-118.7 800,-136.3

edge 20

ge reg 620.3,-143.5 617.9,-136.3 800,-136.3 800,-143.5

edge 20

ge reg 656.3,-167.5 620.3,-143.5 800,-143.5 800,-167.5

edge 20

ge reg 668.3,-191.5 656.3,-167.5 800,-167.5 800,-191.5	edge 20
ge reg 692.3,-215.5 668.3,-191.5 800,-191.5 800,-211.5	edge 20
ge reg 706.5,-240.3 692.3,-215.5 800,-215.5 800,-240.3	edge 20
ge bl 45573	edge 20
ge bl 43524	edge 20
ge reg 0,-320 0,0 209.4,0 39.2,-320	quad 20
ge reg 39.2,-320 209.4,0 300,0 129.8,-320	quad 4.6
ge bl 2670	quad 4.6
ge reg 138.9,-320 308.53,-0.97 505,-23.4 347.3,-320	quad 4.6
ge bl 13925	quad 4.6
ge bl 13412	quad 4.6
ge bl 12899	quad 4.6
ge bl 10208	edge 5
ge bl 9859	edge 5
ge bl 9596	edge 5
ge bl 8687	edge 5
ge bl 5484	edge 5
ge bl 4657	edge 5
ge bl 4230	edge 5
ge bl 16783	quad 5
ge bl 16417	edge 5
ge bl 15857	quad 5
ge bl 18282	edge 5
ge bl 18760	quad 5
ge bl 19156	quad 5
ge bl 19552	quad 5
ge bl 19948	quad 5
ge bl 20344	quad 5
ge bl 20740	quad 5
ge bl 21050	quad 5
ge bl 21360	quad 5
ge bl 21670	quad 5
ge bl 21980	quad 5
ge bl 22290	edge 5
ge reg 706.5,-320 706.5,-240.3 800,-240.3 800,-320	quad 10
ge bl 18045	quad 5
ge bl 17145	quad 5
ge bl 7177	quad 5
ge bl 6087	quad 5

\* "STRONG" COHESION AND TENSION FOR INITIAL EQUILIBRIUM

\*jks=0.25jkn

\*Siltstone-sandstone / Torrens member

ch

mat=4

prop mat=4 d=2300 bulk=16.66e9 shear=10e9



```

prop jmat=4 jkn=4e9 jks=1e9 jfric=29 jcoh=1e20 jten=1e20
*Member "D" + part of model to the right
ch reg 718.5,-400 718.5,-118.7 800,-118.7 800,-400 mat=1
ch bl 10208 mat=1
ch bl 9859 mat=1
ch bl 9596 mat=1
ch bl 8687 mat=1
ch bl 5484 mat=1
ch bl 9273 mat=1
ch bl 8997 mat=1
ch bl 5260 mat=1
prop mat=1 d=2300 bulk=16.66e9 shear=10e9
prop jmat=1 jkn=4e9 jks=1e9 jfric=29 jcoh=1e20 jten=1e20
*Coal
ch bl 4657 mat=2
ch bl 50111 mat=2
ch bl 4911 mat=2
ch reg 706.5,-400 706.5,-118.7 718.5,-118.7 718.5,-400 mat=2
prop mat=2 d=1700 bulk=3.33e9 shear=1.54e9
prop jmat=2 jkn=4e9 jks=1e9 jfric=20 jcoh=1e20 jten=1e20
*Sandstone / Torrens member
ch bl 4230 mat=3
ch bl 50723 mat=3
ch bl 49831 mat=3
ch bl 6462 mat=3
ch reg 692.3,-400 692.3,-118.7 706.5,-118.7 706.5,-400 mat=3
prop mat=3 d=2300 bulk=20e9 shear=12e9
prop jmat=3 jkn=4e9 jks=1e9 jfric=35 jcoh=1e20 jten=1e20
*Cadomin conglomerate
ch reg 87.32,-400 300,0 308.53,-0.97 96.36,-400 mat=7
prop mat=7 d=2500 bulk=23.33e9 shear=14e9
prop jmat=7 jkn=4e9 jks=1e9 jfric=35 jcoh=1e20 jten=1e20
*Shale / Moosebar & Gladstone members
ch reg 96.36,-400 308.53,-0.97 505,-23.4 304.76,-400 mat=5
prop mat=5 d=2100 bulk=6.66e9 shear=3.08e9
prop jmat=5 jkn=4e9 jks=1e9 jfric=20 jcoh=1e20 jten=1e20
*Shale / Nikanassin formation
ch reg 0,-400 0,0 300,0 87.32,-400 mat=8
prop mat=8 d=2100 bulk=6.66e9 shear=3.08e9
prop jmat=8 jkn=4e9 jks=1e9 jfric=20 jcoh=1e20 jten=1e20

```

**\*ROLLER BOUNDARY CONDITIONS ALONG THE BASE & SIDES**

```

bou cor 50 63 xvel 0
bou cor 63 24 yvel 0
bou cor 24 37 xvel 0

```

**\*INITIAL STRESS STATE  $K_{xy}=1.5$   $K_{zy}=1.25$  ( $s_{xx}>s_{zz}>s_{yy}$ )**

**\*Based on "average density" - 2200 kg/m<sup>3</sup>**

**in stress 0 0 0 szz 0 yg 323.73e2 0 215.82e2 zg 0 269.775e2**

**\*Gravitational acceleration**

**set grav 0 -9.81**

**\*Automatic mass damping**

**damp auto**

**\*Histories for monitoring of initial equilibrium state**

**hist unbalance**

**hist ydis 300,-1**

**hist ydis 505,-24.4**

**hist ydis 559,-78**

**hist ydis 631,-155**

**hist ydis 672.5,-197**

**\*INITIAL EQUILIBRIUM**

**step 5000**

**save ini\_0.sav**

**\*INITIAL EXCAVATION TO PRE-MINING TOPOGRAPHY**

**del bl 2276**

**step 5000**

**save topo.sav**

**del bl 45724**

**step 5000**

**save ini\_1.sav**

**del bl 45862**

**step 5000**

**save ini\_2.sav**

**del bl 46000**

**step 5000**

**save ini\_3.sav**

**del bl 46138**

**step 7500**

**save present\_equilib.sav**

**\*This example is for the analysis of slope deformation with mining at present open pit**

**\*depth**

reset disp  
reset jdisp  
reset history

**\*MATERIAL PROPERTIES**

**\*Change in material properties to assumed**

**\*Material properties were assigned various values throughout the study - only one set of  
\*properties for the Mohr-Coulomb constitutive criterion and "dry" slope is presented**

**\*jks=0.25jkn**

**\*Siltstone-sandstone / Torrens member**

ch jmat=4 mat=4 cons=3

prop mat=4 d=2300 bulk=16.66e9 shear=10e9 fric=30 coh=90e3 ten=9e3

prop jmat=4 jkn=4e9 jks=1e9 jfric=25 jcoh=0 jten=0

**\*Member "D" + part of model to the right**

ch reg 718.5,-400 718.5,-118.7 800,-118.7 800,-400 jmat=1 mat=1 cons=3

ch bl 10208 jmat=1 mat=1 cons=3

ch bl 9859 jmat=1 mat=1 cons=3

ch bl 9596 jmat=1 mat=1 cons=3

ch bl 8687 jmat=1 mat=1 cons=3

ch bl 5484 jmat=1 mat=1 cons=3

ch bl 9273 jmat=1 mat=1 cons=3

ch bl 8997 jmat=1 mat=1 cons=3

ch bl 5260 jmat=1 mat=1 cons=3

prop mat=1 d=2300 bulk=16.66e9 shear=10e9 fric=35 coh=1e6 ten=1e5

prop jmat=1 jkn=4e9 jks=1e9 jfric=25 jcoh=0 jten=0

**\*Coal**

ch bl 4657 jmat=2 mat=2 cons=3

ch bl 50111 jmat=2 mat=2 cons=3

ch bl 4911 jmat=2 mat=2 cons=3

ch reg 706.5,-400 706.5,-118.7 718.5,-118.7 718.5,-400 jmat=2 mat=2 cons=3

prop mat=2 d=1700 bulk=3.33e9 shear=1.54e9 fric=22 coh=40e3 ten=4e3

prop jmat=2 jkn=4e9 jks=1e9 jfric=20 jcoh=0 jten=0

**\*Sandstone / Torrens member**

ch bl 4230 jmat=3 mat=3 cons=3

ch bl 50723 jmat=3 mat=3 cons=3

ch bl 49831 jmat=3 mat=3 cons=3

ch bl 6462 jmat=3 mat=3 cons=3

ch reg 692.3,-400 692.3,-118.7 706.5,-118.7 706.5,-400 jmat=3 mat=3 cons=3

prop mat=3 d=2300 bulk=20e9 shear=12e9 fric=35 coh=400e3 ten=40e3

prop jmat=3 jkn=4e9 jks=1e9 jfric=28 jcoh=0 jten=0

**\*Cadomin conglomerate**

ch reg 87.32,-400 300,0 308.53,-0.97 96.36,-400 jmat=7 mat=7 cons=3

prop mat=7 d=2500 bulk=23.33e9 shear=14e9 fric=40 coh=500e3 ten=50e3

prop jmat=7 jkn=4e9 jks=1e9 jfric=30 jcoh=0 jten=0

**\*Shale / Moosebar & Gladstone members**

ch reg 96.36,-400 308.53,-0.97 505,-23.4 304.76,-400 jmat=5 mat=5 cons=3  
prop mat=5 d=2100 bulk=6.66e9 shear=3.08e9 fric=25 coh=45e3 ten=4.5e3  
prop jmat=5 jkn=4e9 jks=1e9 jfric=18 jcoh=0 jten=0

**\*\*\*Shale / Nikanassin formation**

ch reg 0,-400 0,0 300.0 87.32,-400 jmat=8 mat=8 cons=3  
prop mat=8 d=2100 bulk=6.66e9 shear=3.08e9 fric=25 coh=45e3 ten=4.5e3  
prop jmat=8 jkn=4e9 jks=1e9 jfric=18 jcoh=0 jten=0

**\*\*\*Artificial joints**

ch angle -10 10 jmat=10  
ch angle 95 175 jmat=10  
ch 705 710 -241 -215 angle 85 95 jmat=10  
prop jmat=10 jkn=4e9 jks=1e9 jfric=40 jcoh=1e20 jten=1e20

**\*Displacement histories for selected points used for monitoring of deformation in model**

hist unbalance  
hist ydis 300,-1  
hist xdis 300,-1  
hist yvel 300,-1  
hist xvel 300,-1  
hist ydis 505,-24.4  
hist xdis 505,-24.4  
hist yvel 505,-24.4  
hist xvel 505,-24.4  
hist ydis 559,-78  
hist xdis 559,-78  
hist yvel 559,-78  
hist xvel 559,-78  
hist ydis 631,-155  
hist xdis 631,-155  
hist yvel 631,-155  
hist xvel 631,-155  
hist ydis 672.5,-197  
hist xdis 672.5,-197  
hist yvel 672.5,-197  
hist xvel 672.5,-197

step 10000  
save present\_state.sav

quit

**\*\*Similar procedure was used for other excavation states**

\*\*\*\*\*

**NUMERICAL MODELLING OF GROUND SUBSIDENCE  
DUE TO UNDERMINING - LEVEL SURFACE  
DISCONTINUUM MODELLING  
(CHAPTER 5)**

\*\*\*\*\*

- \* UDEC INPUT FILE
- \* UNIVERSITY OF SASKATCHEWAN
- \* DEPARTMENT OF GEOLOGICAL SCIENCES
- \* WRITTEN BY BORIS BENKO (UNIX Version), Last revised fall 1996
- \* This example only for model with Elastic constitutive criterion

new

title

LONGWALL MINING - SINGLE PANEL EXTRACTION / LEVEL SURFACE

;Rock mass 300 x 180 meters

;panel width = 100m

;panel height = 2.5m

;w/h ratio 1.0

;Memory requirements 15MB

\*Block edge rounding

round 0.1

\*Initial block

block 50,-180 50,0 350,0 350,-180

\*Jointing pattern

split 50,-115 350,-115

split 50,-140 350,-140

split 50,-150 350,-150

split 50,-160 350,-160

jreg 50,-140 50,-115 350,-115 350,-140

jset 180,0 301,0 0,0 5,0 50,-140

jreg 50,-115 50,-100 350,-100 350,-115

jset 180,0 301,0 0.0 2.5,0 50,-115

jreg 50,-100 50,0 350,0 350,-100

jset 180,0 301,0 0,0 1.25,0 50,-100

jreg 124,-100 124,0 276,0 276,-100

jset 90,0 1.25,0 1.25,0 2.5,0 123.75,-98.75

jset 90,0 1.25,0 1.25,0 2.5,0 122.5,-100

```
split 150,-100      150,-102.5
split 250,-100      250,-102.5
jdelete
```

**\*Block discretization - finite difference zones**

```
gen 50 350 -180 -160      quad 51 21
gen 50 350 -160 -140      quad 21 11
gen 50 350 -140 -115      quad 11 6
gen 50 350 -115 -100      quad 5 2.6
gen 125 275 -100 0        quad 5 2.6
gen 50 125 -100 0         quad 10.1 2.6
gen 275 350 -100 0        quad 10.1 2.6
```

**\*MATERIAL PROPERTIES**

**\*Elastic properties taken for blocky/seamy fair rock - Hoek et al. 1993**

**\*E=10GPa/m2 v=0.25 density=2300kg/m3**

**prop mat 1 d=2300 bulk=6.667e9 shear=4e9**

**prop jmat 1 jkn=100e9 jks=1e9 jfric=20 jcoh=0 jten=0**

**change mat=1 jmat=1**

**\*INITIAL STRESS STATE Kxy=0.33 Kzy=0.66 (sxx<szz<sy)**

**in stress 0 0 0 szz 0 yg 74.458e2 0 225.63e2 zg 0 148.916e2**

**\*ROLLER BOUNDARY CONDITIONS ALONG THE BASE & SIDES**

**bou cor 50 63 xvel 0**

**bou cor 63 24 yvel 0**

**bou cor 24 37 xvel 0**

**\*Gravitational acceleration**

**set grav 0 -9.81**

**\*Automatic mass damping**

**damp auto**

**\*Initial Equilibrium**

**hist ydis 222.5,-0.6**

**hist ydis 232.5,-0.6**

**hist ydis 132.5,-0.6**

**hist unbalance**

**step 500**

**reset disp**

**reset jdisp**

**reset history**

history unbalance

**\*\*History points at ground surface for displacement monitoring**

hist ydis 202.5,-0.6

hist xdis 202.5,-0.6

hist ydis 207.5,-0.6

hist xdis 207.5,-0.6

hist ydis 212.5,-0.6

hist xdis 212.5,-0.6

hist ydis 217.5,-0.6

hist xdis 217.5,-0.6

hist ydis 222.5,-0.6

hist xdis 222.5,-0.6

hist ydis 227.5,-0.6

hist xdis 227.5,-0.6

hist ydis 232.5,-0.6

hist xdis 232.5,-0.6

hist ydis 237.5,-0.6

hist xdis 237.5,-0.6

hist ydis 242.5,-0.6

hist xdis 242.5,-0.6

hist ydis 247.5,-0.6

hist xdis 247.5,-0.6

hist ydis 252.5,-0.6

hist xdis 252.5,-0.6

hist ydis 257.5,-0.6

hist xdis 257.5,-0.6

hist ydis 262.5,-0.6

hist xdis 262.5,-0.6

hist ydis 267.5,-0.6

hist xdis 267.5,-0.6

hist ydis 272.5,-0.6

hist xdis 272.5,-0.6

hist ydis 277.5,-0.6

hist xdis 277.5,-0.6

hist ydis 282.5,-0.6

hist xdis 282.5,-0.6

\*panel excavation

del 150 250 -102.5 -100

Step 20000

save step1.sav

step 20000

save step2.sav

quit

\*\*\*\*\*

**NUMERICAL MODELLING OF SLOPE DEFORMATIONS  
DUE TO UNDERMINING - SINGLE PANEL EXTRACTION  
DISCONTINUUM MODELLING**

\*\*\*\*\*

- \* UDEC INPUT FILE
- \* UNIVERSITY OF SASKATCHEWAN
- \* DEPARTMENT OF GEOLOGICAL SCIENCES
- \* WRITTEN BY BORIS BENKO (UNIX Version), Last revised fall 1996
- \* This example only for model with Elastic constitutive criterion

new

title

LONGWALL MINING / SINGLE PANEL EXTRACTION / SLOPE SURFACE

;Rock mass 300 x 180 meters

;panel width = 100m

;panel height = 2.5m

;w/h ratio 1.0

;Memory requirement 12MB

\* Block rounding

round 0.1

\*Initial block

block 50,-180 50,0 350,0 350,-180

\*Block jointing

split 50,-115 350,-115

split 50,-140 350,-140

split 50,-150 350,-150

split 50,-160 350,-160

jreg 50,-140 50,-115 350,-115 350,-140

jset 180,0 301,0 0,0 5,0 50,-140

jreg 50,-115 50,-100 350,-100 350,-115

jset 180,0 301,0 0,0 2.5,0 50,-115

jreg 50,-100 50,0 350,0 350,-100

jset 180,0 301,0 0,0 1.25,0 50,-100

jreg 124,-100 124,0 276,0 276,-100

jset 90,0 1.25,0 1.25,0 2.5,0 123.75,-98.75

jset 90,0 1.25,0 1.25,0 2.5,0 122.5,-100



```

split 130,-100      130,-102.5
split 230,-100      230,-102.5
split 150,-100      150,-102.5
split 250,-100      250,-102.5
split 170,-100      170,-102.5
split 270,-100      270,-102.5
jdelete

```

**\*Block discretization - finite difference zones**

```

gen 50 350 -180 -160      quad 51 21
gen 50 350 -160 -140      quad 21 11
gen 50 350 -140 -115      quad 11 6
gen 50 350 -115 -100      quad 5 2.6
gen 125 275 -100 0        quad 5 2.6
gen 50 125 -100 0         quad 10.1 2.6
gen 275 350 -100 0        quad 10.1 2.6

```

**\*\*\*\*\* MATERIAL PROPERTIES \*\*\*\*\***

**\*Elastic properties taken for blocky/seamy fair rock, Hoek et al., 1993**

**\*E=10GPa/m2 v=0.25 density=2300kg/m3**

**prop mat 1 d=2300 bulk=6.667e9 shear=4e9**

**prop jmat 1 jkn=100e9 jks=1e9 jfric=20 jcoh=1e20 jten=1e20**

**change mat=1 jmat=1**

**\*\*\*\*\* INITIAL STRESS STATE Kxy=0.33 Kzy=0.66 (sxx<szz<sy) \*\*\*\*\***

**in stress 0 0 0 szz 0 yg 74.458e2 0 225.63e2 zg 0 148.916e2**

**\* ROLLER BOUNDARY CONDITIONS ALONG THE BASE & SIDES \*\*\*\*\***

**bou cor 50 63 xvel 0**

**bou cor 63 24 yvel 0**

**bou cor 24 37 xvel 0**

**\*Gravitational acceleration**

**set grav 0 -9.81**

**\*Automatic mass damping**

**damp auto**

**\*Histories for block deformation monitoring**

**hist ydis 222.5,-0.6**

**hist ydis 232.5,-0.6**

**hist ydis 132.5,-0.6**

**hist unbalance**

**\*\*\*\*\* INITIAL CONSOLIDATION (equilibrium) \*\*\*\*\***

**step 500**

**\*\*\*\* SLOPE EXCAVATION & HISTORIES \*\*\*\***

reset disp  
reset jdisp  
reset history

hist ydis 222.5,-1.25  
hist xdis 222.5,-1.25  
hist ydis 227.5,-1.25  
hist xdis 227.5,-1.25  
hist ydis 232.5,-1.25  
hist xdis 232.5,-1.25

del reg 50,-10 50,0 220,0 210,-10  
step 5000  
save excav1.sav

del reg 50,-20 50,-10 210,-10 200,-20  
step 5000  
save excav2.sav

del reg 50,-30 50,-20 200,-20 190,-30  
step 5000  
save excav3.sav

del reg 50,-40 50,-30 190,-30 180,-40  
step 15000  
save slope\_el.sav

reset disp  
reset jdisp  
reset history

**\*\*\*\*\* MATERIAL PROPERTIES (change in joint properties) \*\*\*\*\***

\*Elastic properties taken for blocky/seamy fair rock  
\*E=10GPa/m2 v=0.25 density=2300kg/m3  
prop mat 1 d=2300 bulk=6.667e9 shear=4e9  
prop jmat 1 jkn=100e9 jks=1e9 jfric=20 jcoh=0 jten=0  
change mat=1 jmat=1

step 500  
save slope\_el.sav1  
reset disp  
reset jdisp  
reset history

**\*Monitoring points**

**\*Point 1**

**hist xdis 170.-40**

**hist ydis 170.-40**

**\*Point 2**

**hist xdis 181.-39.5**

**hist ydis 181.-39.5**

**\*Point 3**

**hist xdis 191.-29.5**

**hist ydis 191.-29.5**

**\*Point 4**

**hist xdis 201.-19.5**

**hist ydis 201.-19.5**

**\*Point 5**

**hist xdis 211.-9.5**

**hist ydis 211.-9.5**

**\*Point 6**

**hist xdis 220.-0.5**

**hist ydis 220.-0.5**

**\*Point 7**

**hist xdis 230.-0.5**

**hist ydis 230.-0.5**

**\*Point 8**

**hist xdis 240.-0.5**

**hist ydis 240.-0.5**

**\*Panel excavation**

**\*Case 1 - Panel centerline under the slope toe**

**del 130 230 -102.5 -100**

**\*Case 2 - Panel centerline under mid slope height**

**del 150 250 -102.5 -100**

**\*Case 1 - Panel centerline under the slope crest**

**del 170 270 -102.5 -100**

**step 20000**

**save kol-20.sav**

**step 20000**

**save kol-20.sav**

**step 20000**

**save kol-20.sav**

**quit**

\*\*\*\*\*

**NUMERICAL MODELLING OF SLOPE DEFORMATIONS  
DUE TO UNDERMINING - SINGLE PANEL EXTRACTION  
BEDDING PLANES DIPPING INTO THE SLOPE ABOVE UNCONFORMITY  
DISCONTINUUM MODELLING (TOPPLING)**

\*\*\*\*\*

- \* UDEC INPUT FILE
- \* UNIVERSITY OF SASKATCHEWAN
- \* DEPARTMENT OF GEOLOGICAL SCIENCES
- \* WRITTEN BY BORIS BENKO (UNIX Version), Last revised fall 1996
- \* This example only for model with Elastic constitutive criterion
- \* Only input for analysis of toppling deformation presented

new  
title  
LONGWALL MINING / PANEL EXTRACTION / SLOPE SURFACE / TOPPLING

;Block edge rounding  
round 0.1

\*Initial block  
block 0,-180 0,0 400,0 400,-180

\*Block jointing  
split 0,-115 400,-115  
split 0,-140 400,-140  
split 0,-150 400,-150  
split 0,-160 400,-160  
jreg 0,-140 0,-115 400,-115 400,-140  
jset 180,0 301,0 0,0 5,0 0,-140  
jreg 0,-115 0,-39 400,-39 400,-115  
jset 180,0 301,0 0,0 2.5,0 0,-115  
split 375.9,0 399,-40  
jreg 180,-40 220,0 375.9,0 399,-40  
jset 120,0 100,0 0,0 2.5,0 220,0  
crack 180,-40 220,0  
crack 0,-10 210,-10  
crack 0,-20 200,-20  
crack 0,-30 190,-30  
jdelete  
jreg 74,-115 74,-40 124,-40 124,-115  
jset 90,0 2.5,0 2.5,0 10,0 95,-107.5

```

jset 90,0 2.5,0 2.5,0 10,0 90,-110
jreg 276,-115 276,-40 326,-40 326,-115
jset 90,0 2.5,0 2.5,0 10,0 305,-107.5
jset 90,0 2.5,0 2.5,0 10,0 310,-110
jreg 124,-115 124,-40 276,-40 276,-115
jset 90,0 2.5,0 2.5,0 5,0 125,-107.5
jset 90,0 2.5,0 2.5,0 5,0 122.5,-110
jdelete
***** Part above unconformity - 60 degrees bedding
jreg 182,-39 222,-1 362,-1 276.2,-39
jset 30,0 2.5,0 2.5,0 5,0 182.5,-40
jset 30,0 2.5,0 2.5,0 5,0 187.7,-34.1
jdelete

```

**\*\*Discretization of model - finite difference zones**

```

gen 0 400 -180 -160 quad 51 21
gen 0 400 -160 -140 quad 21 11
gen 0 400 -140 -115 quad 11 6
gen 125 275 -115 -40 quad 5.1 2.6
gen 0 125 -115 -40 quad 10.1 2.6
gen 275 400 -115 -40 quad 10.1 2.6
gen r 0,-40 0.0 170.0 170,-40 quad 20
ge bl 24168 edge 5
ge reg 180,-40 220,0 400,0 400,-40 quad 5.1,5.1

```

**\*\*\*\*\* MATERIAL PROPERTIES \*\*\*\*\***

```

*Initially strong properties for joints
*Elastic properties taken for blocky/seamy fair rock
*E=10GPa/m2 v=0.25 density=2300kg/m3
prop mat 1 d=2300 bulk=6.667e9 shear=4e9
prop jmat 1 jkn=100e9 jks=10e9 jfric=25 jcoh=1e20 jten=1e20
change mat=1 jmat=1

```

```

***** INITIAL STRESS STATE Kxy=0.33 Kzy=0.66 (sxx<szz<sy) *****
in stress 0 0 0 szz 0 yg 74.458e2 0 225.63e2 zg 0 148.916e2

```

**\* ROLLER BOUNDARY CONDITIONS ALONG THE BASE & SIDES \*\*\*\*\***

```

bou cor 50 63 xvel 0
bou cor 63 24 yvel 0
bou cor 24 37 xvel 0

```

**\*Gravitational acceleration**

```
set grav 0 -9.81
```

**\*Automatic mass damping**

```
damp auto
```

**\* INITIAL CONSOLIDATION (equilibrium) \*\*\*\*\***

hist ydis 222.5,-1.25  
hist ydis 232.5,-1.25  
hist ydis 132.5,-1.25  
hist unbalance  
step 1500  
save ini.sav

**\*\*\*\* SLOPE EXCAVATION**

**\*\*\*\*\***

reset disp  
reset jdisp  
reset history

history unbalance  
hist ydis 222.5,-1.25  
hist xdis 222.5,-1.25  
hist ydis 227.5,-1.25  
hist xdis 227.5,-1.25  
hist ydis 232.5,-1.25  
hist xdis 232.5,-1.25

del bl 31685  
step 7500  
save excav1.sav  
del bl 31922  
step 7500  
save excav2.sav  
del bl 32060  
step 7500  
save excav3.sav  
del bl 31560  
step 15000  
save slope\_el.sav

reset disp  
reset jdisp  
reset history

**\*Change of material properties for joints and bedding planes**

change jmat=2  
change angle 110 130 jmat=4  
prop jmat 2 jkn=100e9 jks=10e9 jfric=25 jcoh=0 jten=0  
prop jmat 4 jkn=100e9 jks=10e9 jfric=25 jcoh=0 jten=0

```
hist unbalance
***** DISPLACEMENT HISTORIES AT THE SURFACE
hist ydis 222.5,-1.25
hist xdis 222.5,-1.25
hist ydis 232.5,-1.25
hist xdis 232.5,-1.25
hist ydis 242.5,-1.25
hist xdis 242.5,-1.25
hist ydis 252.5,-1.25
hist xdis 252.5,-1.25
hist ydis 262.5,-1.25
hist xdis 262.5,-1.25

step 1000
save slope.sav 1

step 1000
save slope.sav 2

step 1000
save slope.sav 3

step 1000
save slope.sav 4

quit
```

\*\*\*\*\*

**NUMERICAL MODELLING OF FRANK SLIDE**  
**CONTINUUM MODELLING**

\*\*\*\*\*

- \* FLAC INPUT FILE
- \* UNIVERSITY OF SASKATCHEWAN
- \* DEPARTMENT OF GEOLOGICAL SCIENCES
- \* WRITTEN BY BORIS BENKO (UNIX Version), Last revised fall 1996
- \* This example only for model with Mohr-Coulomb constitutive criterion and dry slope conditions

new

title

FRANK SLIDE / FLAC APPLICATION

;rock mass 3600\*2500

;18480 finite difference zones

;grid in central part 12.5 \* 12.5m

config extra 5

\*finite difference grid

g 165 112

mo mo

\*Geometry of model

ge -1600,-2500 -1600,-1500 -1100,-1500 -1100,-2500		i=1,11	j=1,17
ge s s -620,-1500 -620,-2500		i=11,21	j=1,17
ge s s -300,-1500 -300,-2500	rat .9,1	i=21,33	j=1,17
ge s s 757.77,-1500 757.77,-2500		i=33,120	j=1,17
ge s s 772.79,-1500 772.79,-2500		i=120,123	j=1,17
ge s s 1000,-1500 1000,-2500		i=123,141	j=1,17
ge s s 1400,-1500 1400,-2500	rat 1.1,1	i=141,154	j=1,17
ge s s 2000,-1500 2000,-2500		i=154,166	j=1,17
ge s -1600,-900 -1100,-900 s	rat 1,.93	i=1,11	j=17,38
ge s s -620,-900 s	rat 1,.93	i=11,21	j=17,38
ge s s -300,-900 s	rat .9,.93	i=21,33	j=17,38
ge s s 757.77,-900 s	rat 1,.93	i=33,120	j=17,38
ge s s 772.79,-900 s	rat 1,.93	i=120,123	j=17,38
ge s s 1000,-900 s	rat 1,.93	i=123,141	j=17,38
ge s s 1400,-900 s	rat 1.1,.93	i=141,154	j=17,38
ge s s 2000,-900 s	rat 1,0.93	i=154,166	j=17,38
ge s -1600,-729.4 -1100,-729.4 s		i=1,11	j=38,55
ge s s -620,-729.4 s		i=11,21	j=38,55



ge s s -300,-729.4 s	rat .9,1	i=21,33	j=38,55
ge s s 772.7,-729.4 s		i=33,120	j=38,55
ge s s 787.72,-729.4 s		i=120,123	j=38,55
ge s s 1015,-729.4 s		i=123,141	j=38,55
ge s s 1400,-729.4 s	rat 1.1,1	i=141,154	j=38,55
ge s s 2000,-729.4 s		i=154,166	j=38,55
ge s -1600,0 -1100,0 s		i=1,11	j=55,113
ge s s -620,0 s		i=11,21	j=55,113
ge s s -300,0 s	rat .9,1	i=21,33	j=55,113
ge s s 772.7,0 s		i=33,120	j=55,113
ge s s 787.72,0 s		i=120,123	j=55,113
ge s s 1015,0 s		i=123,141	j=55,113
ge s s 1400,0 s	rat 1.1,1	i=141,154	j=55,113
ge s s 2000,0 s		i=154,166	j=55,113

\*Turtle Mountain topography

ge line -1600,-653.9	-1160,-653.9
ge line -860,-578.5	-1160,-653.9
ge line -860,-578.5	-620,-452.7
ge line -152,-88.03	-620,-452.7
ge line -4.08,0	-152,-88.03
ge line -4.08,0	69.9,-75.46
ge line 69.9,-75.46	193.2,-226.4
ge line 193.2,-226.4	526.1,-578.5
ge line 526.1,-578.5	629.1,-653.9
ge line 629.1,-653.9	961,-769.5
ge line 961,-769.5	1210,-809.7
ge line 1210,-809.7	2000,-809.7

\*Turtle Mountain Fault

mark i=95,166 j=61  
ge line 464.5,-653.9 -1400,-2438  
mark i=5 j=1,2

\*Mark points for Turtle mountain excavation - 150m intervals

mark j=103	i=1,42
mark j=103	i=67,166
mark j=91	i=1,28
mark j=91	i=78,166
mark j=79	i=1,22
mark j=79	i=88,166
mark j=67	i=1,16
mark j=67	i=101,166
mark j=55	i=126,166

\*Mark future mine excavation  
mark i=121,122 j=42,54

\*\*\*\*\* MATERIAL PROPERTIES \*\*\*\*\*

\*Limestone - typical properties(E,v) from literature Hoek et al  
\* blocky seamy material good for limestone / poor for shale  
\* density from Cruden & Krahn (1978)  
\*Paleozoic Limestone: E=10000 MPa v=0.25 d=2600kg/m3  
\*Mesozoic interbedded series: E= 3000 MPa v=0.30 d=2250kg/m3  
\*High cohesion and tension for development of initial stress field  
prop d=2600 b=6666.67e6 s=4000.00e6 fr=30 coh=1e10 ten=1e10  
prop d=2250 b=2500.00e6 s=1153.85e6 fr=27 coh=1e10 ten=1e10 reg 20,1  
prop d=2250 b=2500.00e6 s=1153.85e6 fr=27 coh=1e10 ten=1e10 reg 150,50  
prop d=2250 b=2500.00e6 s=1153.85e6 fr=27 coh=1e10 ten=1e10 reg 150,57  
prop d=2600 b=6666.67e6 s=4000.00e6 fr=30 coh=1e10 ten=1e10 j=61 i=106,107

\*\*\*\*\* INITIAL STRESS CONDITIONS BEFORE EXCAVATION OF \*\*\*\*\*

\*\*\*\*\* TURTLE MOUNTAIN K=0.5 \*\*\*\*\*  
\*\*\*\*\* Initial stress based on "average" density = 2425kg/m3 \*\*\*\*\*  
\*\*\*\*\*  $s_{xx} = 0.5 * s_{yy}$  /  $s_{zz} = 0.75 * s_{yy}$  \*\*\*\*\*  
ini syy -5947.3125e4 var 0.5947.3125e4  
ini sxx -2973.6563e4 var 0,2973.6563e4  
ini szz -4460.4844e4 var 0.4460.4844e4

\*\*\*\*\* BOUNDARY CONDITIONS \*\*\*\*\*

;Roller left, right side & the base  
fix y j=1  
fix x i=1  
fix x i=166

\*\*\*\*\* GRAVITY ON \*\*\*\*\*

set grav 9.81

\*\*\*\*\* HISTORIES FOR DEFORMATION MONITROING \*\*\*\*\*

hist unbalance  
hist ydis i=57 j=113  
hist xdis i=57 j=113

\*\*\*\*\* INITIAL EQUILIBRIUM IN MODEL \*\*\*\*\*

step 5000  
save ini.sav

\*\*\*\*\* TURTLE MOUNTAIN EXCAVATION \*\*\*\*\*

m n reg 1,105  
m n reg 150,105

```
step 5000
save excav1.sav
```

```
m n reg 1,93
m n reg 150,93
step 5000
save excav2.sav
```

```
m n reg 1,81
m n reg 150,81
step 5000
save excav3.sav
```

```
m n reg 1,69
m n reg 150,69
step 5000
save excav4.sav
```

```
m n reg 1,62
m n reg 150,62
m n reg 150,57
m m i=106,107 j=61
prop d=2600 b=6666.67e6 s=4000.00e6 fr=30 coh=1e10 ten=1e10 i=106,107 j=61
step 5000
save excav5.sav
```

```
m n reg 150,50
step 20000
save slope_el.sav
```

```
ini xdis=0 ydis=0
```

```
history unbalance
hist ydis i=57 j=113
hist xdis i=57 j=113
hist yvel i=57 j=113
hist xvel i=57 j=113
```

```
hist ydis i=64 j=100
hist xdis i=64 j=100
hist yvel i=64 j=100
hist xvel i=64 j=100
```

```
hist ydis i=88 j=72
hist xdis i=88 j=72
```

hist yvel i=88 j=72  
hist xvel i=88 j=72

\*\*\*\*\* MATERIAL PROPERTIES \*\*\*\*\*

prop d=2600 b=6666.67e6 s=4000.00e6 fr=30 coh=0.58e6 ten=0  
prop d=2250 b=2500.00e6 s=1153.85e6 fr=27 coh=2e6 ten=0 reg 20,1  
prop d=2600 b=6666.67e6 s=4000.00e6 fr=30 coh=0.58e6 ten=0 i=106,107 j=61

set large  
step 25000  
save c580.sav

\*\*\*\*\* MATERIAL PROPERTIES \*\*\*\*\*

prop d=2600 b=6666.67e6 s=4000.00e6 fr=30 coh=0.565e6 ten=0  
prop d=2250 b=2500.00e6 s=1153.85e6 fr=27 coh=2e6 ten=0 reg 20,1  
prop d=2600 b=6666.67e6 s=4000.00e6 fr=30 coh=0.565e6 ten=0 i=106,107 j=61

set large  
step 25000  
save c565.sav

\*\*\*\*\* MATERIAL PROPERTIES \*\*\*\*\*

prop d=2600 b=6666.67e6 s=4000.00e6 fr=30 coh=0.55e6 ten=0  
prop d=2250 b=2500.00e6 s=1153.85e6 fr=27 coh=2e6 ten=0 reg 20,1  
prop d=2600 b=6666.67e6 s=4000.00e6 fr=30 coh=0.55e6 ten=0 i=106,107 j=61

set large  
step 25000  
save c550.sav

\*\*\*\*\* MATERIAL PROPERTIES \*\*\*\*\*

prop d=2600 b=6666.67e6 s=4000.00e6 fr=30 coh=0.535e6 ten=0  
prop d=2250 b=2500.00e6 s=1153.85e6 fr=27 coh=2e6 ten=0 reg 20,1  
prop d=2600 b=6666.67e6 s=4000.00e6 fr=30 coh=0.535e6 ten=0 i=106,107 j=61

set large  
step 25000  
save c535.sav

\*\*\* SIMULATION OF MINING\*\*\*\*\*

rest c550.sav  
ini xdis=0 ydis=0  
history reset

history unbalance

```
hist ydis i=57 j=113
hist xdis i=57 j=113
hist yvel i=57 j=113
hist xvel i=57 j=113
```

```
hist ydis i=64 j=100
hist xdis i=64 j=100
hist yvel i=64 j=100
hist xvel i=64 j=100
```

```
hist ydis i=88 j=72
hist xdis i=88 j=72
hist yvel i=88 j=72
hist xvel i=88 j=72
```

```
m n i=121 j=54
step 20000
save kol10.sav
```

```
m n i=121 j=53
step 20000
save kol20.sav
```

```
m n i=121 j=52
step 20000
save kol30.sav
```

```
m n i=121 j=51
step 20000
save kol40.sav
```

```
m n i=121 j=50
step 20000
save kol50.sav
```

```
m n i=121 j=49
step 20000
save kol60.sav
```

```
m n i=121 j=48
step 20000
save kol70.sav
```

```
quit
```

\*\*\*\*\*

**NUMERICAL MODELLING OF FRANK SLIDE  
DISCONTINUUM MODELLING  
MODEL WITH SIMULATION OF BEDDING PLANE JOINTS**

\*\*\*\*\*

- \* UDEC INPUT FILE
- \* UNIVERSITY OF SASKATCHEWAN
- \* DEPARTMENT OF GEOLOGICAL SCIENCES
- \* WRITTEN BY BORIS BENKO (UNIX Version - block addresses will differ if run on MSDOS Version of UDEC), Last revised fall 1996

new  
title  
FRANK SLIDE / UDEC APPLICATION

\*Block rounding  
round 0.5

\*Initial block  
bl 0,-1500 0,0 2300,0 2300,-1500

\*Jointing

\*Topography

crack 1850,-755	2300,-755
crack 1525,-641.7	1850,-755
crack 1421.7,-574.4	1525,-641.7
crack 1080.1,-232.8	1421.7,-574.4
crack 975,-83.3	1080.1,-232.8
crack 900,0	975,-83.3
crack 757,-65.4	900,0
crack 757,-65.4	361,-342.7
crack 361,-342.7	200,-400
crack 200,-400	0,-400

\*Artificial joint for zoning

crack 2300,-998.6	1017,-998.6
crack 1017,-998.6	361,-342.7

\*Turtle Mountain fault

crack 1525,-641.7	1374,-641.7
crack 1374,-641.7	515.7,-1500

\*Minor fault traced by Cruden (65 degr.)  
 crack 1421.7,-574.4            1309,-574.4  
 crack 1309,-574.4            1193.5,-822.3

\*\*\*\*\* PALEOZOIC FORMATIONS \*\*\*\*\*

\*Bedding planes in failure block  
 jreg 1308.5,-574.4 1004.5,-270.3 1065.3,-209.7 1421.7,-574.4  
 jset 135,0 600,0 0,0 10,0 1309,-574.4

\*Bedding planes under the failure block - 1  
 jreg 1193.5,-822.3 983.3,-612.1 983.3,-250 1309,-574.4  
 jset 135,0 600,0 0,0 10,0 1309,-574.4

\*Bedding planes under the failure block - 2  
 jreg 983.3,-965 983.3,-612.1 1193.5,-822.3 1017,-998.6  
 jset 135,0 600,0 0,0 10,0 1309,-574.4

\*Contorted zone - between faults  
 jreg 1195,-819 1308.5,-574.4 1421.7,-574.4 1525,-641.7  
 jset 90,0 150,0 0,0 10,0 1525,-641.7

\*Anticline crest / arc increment 2.5 degrees  
 arc 983.3,-291.6 757,-65.3            -90 18 ;1  
 arc 983.3,-291.6 764.1,-72.4        -90 18 ;2  
 arc 983.3,-291.6 771.2,-79.5        -90 18 ;3  
 arc 983.3,-291.6 778.2,-86.5        -90 18 ;4  
 arc 983.3,-291.6 785.3,-93.6        -90 18 ;5  
 arc 983.3,-291.6 792.4,-100.7       -90 18 ;6  
 arc 983.3,-291.6 799.4,-107.7       -90 18 ;7  
 arc 983.3,-291.6 806.5,-114.8       -90 18 ;8  
 arc 983.3,-291.6 813.6,-121.9       -90 18 ;9  
 arc 983.3,-291.6 820.7,-129         -90 18 ;10  
 arc 983.3,-291.6 827.7,-136         -90 18 ;11  
 arc 983.3,-291.6 834.8,-143.1       -90 18 ;12  
 arc 983.3,-291.6 841.9,-150.2       -90 18 ;13  
 arc 983.3,-291.6 848.9,-157.2       -90 18 ;14  
 arc 983.3,-291.6 856,-164.3         -90 18 ;15  
 arc 983.3,-291.6 863.1,-171.4       -90 18 ;16  
 arc 983.3,-291.6 870.2,-178.5       -90 18 ;17  
 arc 983.3,-291.6 877.2,-185.5       -90 18 ;18  
 arc 983.3,-291.6 884.3,-192.6       -90 18 ;19  
 arc 983.3,-291.6 891,-199.7         -90 18 ;20  
 arc 983.3,-291.6 898.4,-206.7       -90 18 ;21  
 arc 983.3,-291.6 905.5,-213.8       -90 18 ;22  
 arc 983.3,-291.6 912.6,-220.9       -90 18 ;23  
 arc 983.3,-291.6 919.7,-228         -90 18 ;24  
 arc 983.3,-291.6 926.7,-235         -90 18 ;25  
 arc 983.3,-291.6 933.9,-242         -90 18 ;26  
 arc 983.3,-291.6 941,-249.1         -90 18 ;27

arc 983.3,-291.6 948,-256.1           -90 18 ;28  
 arc 983.3,-291.6 955.1,-263.2       -90 18 ;29  
 arc 983.3,-291.6 962.1,-270.3       -90 9 ;30  
 arc 983.3,-291.6 969.2,-277.4       -90 9 ;31  
 arc 983.3,-291.6 976,-284.8          -120 12 ;32

**\*Behind crest**

jreg 361,-342.7 757,-65.4 983.3,-291.6 983.3,-965  
 jset 45,0 300,0 0,0 10,0 757,-65.4  
 jdelete

**\*Behind crest - large blocks**

jreg -800,-1500 361,-342.7 1017,-998.6 510,-1500  
 jset 45,0 500,0 0,0 40,0 757,-65.4  
 jdelete

**\*\*\*\*\* MESOZOIC FORMATIONS - 85 degrees dip \*\*\*\*\***

**\*Artificial joints**

crack 1689,-998.6                   1714.7,-708.2

**\*Mine**

crack 1654,-998.6                   1680.6,-696.4

crack 1659,-998.6                   1685.4,-698.1

**\*Coal chamber jointing 10m interval**

jreg 1654,-998.6 1670,-696.4 1686,-699 1659,-998.6

jset 180,0 10,0 0,0 10,0 1659,-998.6

jdelete

jreg 1659,-998.6 1685.4,-698.1 1714.7,-708.2 1689,-998.6

jset 85,0 500,0 0,0 10,0 1689,-998.6

jreg 1689,-998.6 1714.7,-708.2 1841.5,-752 1820,-998.6

jset 85,0 300,0 0,0 10,0 1689,-998.6

jreg 1493,-998.6 1524.5,-641.7 1680.6,-696.4 1654,-998.6

jset 85,0 500,0 0,0 10,0 1654,-998.6

jreg 1017,-998.6 1374,-641.7 1524.5,-641.7 1493,-998.6

jset 85,0 500,0 0,0 10,0 1654,-998.6

**\*Bottom part**

jreg 515.7,-1500 1017,-998.6 2290,-998.6 2290,-1500

jset 85,0 550,0 0,0 40,0 1654,-998.6

jdelete

**\*Right top part**

jreg 1820,-998.6 1841.5,-752 2290,-752 2290,-998.6

jset 85,0 850,0 0,0 20,0 2290,-1500

**\*Joints for slope excavation**

crack 0,-150                       637,-150

crack 0,-300                       422,-300



crack 1022,-150 2300,-150  
 crack 1145,-300 2300,-300  
 crack 1295.6,-450 2300,-450  
 crack 1522.2,-641.7 2300,-641.7  
 jdelete

\*\*\*\*\* DISCRETIZATION \*\*\*\*\*

\*finite difference triangles - fully deformable blocks

\*excavated blocks

ge bl 149466	edge 100
ge bl 149541	edge 100
ge bl 22911	edge 100
ge bl 149616	edge 100
ge bl 149928	edge 100
ge bl 150207	edge 100
ge bl 150381	edge 100
ge bl 229	edge 100

\*left bottom portion

ge bl 107962	edge 65
ge bl 106950	edge 65
ge reg -800,-1500 361,-342.7 1017,-998.6 515.7,-1500	quad 80

\*bottom part

ge bl 148580	edge 80
ge bl 144517	edge 80
ge reg 515.7,-1500 1017,-998.6 2300,-998.6 2300,-1500	quad 80

\*right side

ge bl 149352	edge 40
ge reg 1820,-998.6 1841.5,-752 2290,-752 2290,-998.6	quad 41

\*rest of Mesozoic

ge reg 1654,-998.6 1670,-696.4 1686,-699 1659,-998.6	quad 20
ge reg 1659,-998.6 1685.4,-698.1 1714.7,-708.2 1689,-998.6	quad 20
ge reg 1689,-998.6 1714.7,-708.2 1841.5,-752 1820,-998.6	quad 20
ge reg 1493,-998.6 1524,-642 1680.6,-696.4 1654,-998.6	quad 20
ge bl 136547	edge 20
ge reg 1017,-998.6 1374,-641.7 1525,-641.7 1493,-998.6	quad 20

\*central part

ge bl 18076	edge 20
ge bl 13650	edge 20
ge bl 106424	edge 20
ge bl 106101	edge 20
ge bl 105778	edge 20
ge bl 105468	edge 20
ge bl 105033	edge 20
ge bl 104598	edge 20
ge bl 104163	edge 20

ge bl 103728	edge 20
ge bl 103349	edge 20
ge bl 106424	edge 20
ge bl 102927	edge 20
ge bl 102247	edge 20
ge bl 101309	edge 20
ge bl 99433	edge 20
ge bl 98495	edge 20
ge bl 96533	edge 20
ge bl 94485	edge 20
ge bl 92265	edge 20
ge bl 91069	edge 20
ge bl 88591	edge 20
ge bl 85941	edge 20
ge bl 81235	edge 20
ge bl 79265	edge 20
ge bl 77209	edge 20
ge bl 73097	edge 20
ge bl 68985	edge 20
ge bl 66927	edge 20
ge bl 63657	edge 20
ge bl 61169	edge 20
ge bl 60661	edge 20
ge bl 49063	edge 20
ge bl 46096	edge 20
ge bl 24597	edge 20
ge bl 22416	edge 20
ge bl 1943	edge 20
ge reg 361,-342.7 900,0 1525,-641.7 1017,-998.6	quad 20

\*top of mountain

ge bl 1	edge 20
ge bl 23873	edge 20
ge bl 24959	edge 20

\*\*\*\*\* MATERIAL PROPERTIES \*\*\*\*\*

- \*Limestone - typical properties(E,v) from literature Hoek et al
- \*blocky seamy material good for limestone / poor for shale
- \*density from Cruden & Krahn (1978)
- \*Paleozoic Limestone: E=10000 MPa v=0.25 d=2600kg/m3
- \*Mesozoic interbedded series: E= 3000 MPa v=0.30 d=2250kg/m3
- \*jks=0.2jkn

prop mat 1 d=2600 bulk=6666.67e6 shear=4000.00e6  
prop jmat 1 jkn=20e9 jks=5e9 jfric=28 jcoh=1e20 jten=1e20

prop mat 2 d=2250 bulk=2500.00e6 shear=1153.85e6  
prop jmat 2 jkn=10e9 jks=2.5e9 jfric=25 jcoh=1e20 jten=1e20  
ch mat=1 jmat=1  
ch reg 515.7,-1500 1374,-641.7 2300,-641.7 2300,-1500 mat=2 jmat=2

\*Gravitational Acceleration  
set grav 0 -9.81

\*Automatic mass damping  
damp auto

\*\*\*\*\* INITIAL STRESS STATE \*\*\*\*\*  
\*\*\*\*\* Kxy=1.5 Kzy=1.25 (sxx > szz > syy) \*\*\*\*\*  
\*Gravitational stress field based on average density = 2425kg/m3  
in stress 0 0 0 szz 0 yg 356.8388e2 0 237.8925e2 zg 0 297.3656e2

\*\*\*\*\* ROLLER BOUNDARY CONDITIONS ALONG THE BASE & SIDES \*\*\*\*  
bou cor 50 63 xvel 0  
bou cor 63 24 yvel 0  
bou cor 24 37 xvel 0

\*\*\*\*\* HISTORIES \*\*\*\*\*  
hist unbalance  
hist ydis 895,-21.5  
hist xdis 895,-21.5  
hist xvel 895,-21.5  
hist yvel 895,-21.5

\*\*\*\*\* TURTLE MOUNTAIN EXCAVATION \*\*\*\*\*  
step 10000  
save ini0.sav

del bl 1  
del bl 23873  
del bl 24959  
del bl 24597  
del bl 149466  
del bl 149616  
step 10000  
save ini1.sav

del bl 149541  
del bl 149928  
step 10000

```
save ini2.sav
del bl 22911
del bl 150207
step 10000
save ini3.sav
```

```
del bl 150381
step 10000
save ini4.sav
```

```
del bl 229
step 10000
save topo.sav
```

```
*
reset disp
reset jdisp
reset history
```

```
***** MATERIAL PROPERTIES *****
```

```
***** Change in material properties to analyze deformations *****
```

```
*Material properties were assigned various values throughout the study - only one set of
*properties for the Mohr-Coulomb constitutive criterion, cohesion=1050KPa and "dry"
*slope is presented
```

```
prop mat 1 d=2600 bulk=6666.67e6 shear=4000.00e6 fric=30 coh=1.050e6
```

```
prop jmat 1 jkn=30e9 jks=5e9 jfric=28 jcoh=0.221e6 jten=0
```

```
prop mat 2 d=2250 bulk=2500.00e6 shear=1153.85e6 fric=27 coh=2e6
```

```
prop jmat 2 jkn=10e9 jks=2.5e9 jfric=25 jcoh=0 jten=0
```

```
ch mat=1 cons=3
```

```
ch jmat=1
```

```
ch reg 515.7,-1500 1374,-641.7 2300,-641.7 2300,-1500 mat=2 cons=3
```

```
ch reg 515.7,-1500 1374,-641.7 2300,-641.7 2300,-1500 jmat=2
```

```
*Artificial joints - glued
```

```
ch reg 1016,-1000 1016,-997 2300,-995 2300,-1005 angle -5 5 jmat=10
```

```
ch reg 1018,-1000 360,-343 361,-341 1018,-997 angle 130 140 jmat=10
```

```
*future coal chambers
```

```
ch reg 1650,-1000 1650,-690 1690,-690 1690,-1000 angle -5 5 jmat=10
```

```
prop jmat 10 jkn=50e9 jks=10e9 jfric=40 jcoh=1e20 jten=1e20
```

```
***** HISTORIES *****
```

```
hist unbalance
```

```
hist ydis 895,-21.5
```

```
hist xdis 895,-21.5
```

```
hist xvel 895,-21.5
```

```
hist yvel 895,-21.5
```

```
hist ydis 991,-246
hist xdis 991,-246
hist xvel 991,-246
hist yvel 991,-246
hist ydis 1308,-508
hist xdis 1308,-508
hist xvel 1308,-508
hist yvel 1308,-508
```

```
step 10000
save modelc1050.sav_1
```

```
step 10000
save modelc1050.sav_2
```

```
step 10000
save modelc1050.sav_3
```

```
step 10000
save modelc1050.sav_4
```

```
step 20000
save modelc1050.sav_5
```

```
step 20000
save modelc1050.sav_6
```

```
***** MODELLING OF UNDERGROUND MINING *****
```

```
reset disp
reset jdisp
reset history
```

```
***** HISTORIES FOR MONITORING DISPLACEMENTS *****
```

```
hist ydis 895,-21.5
hist xdis 895,-21.5
hist xvel 895,-21.5
hist yvel 895,-21.5
hist ydis 991,-246
hist xdis 991,-246
hist xvel 991,-246
hist yvel 991,-246
hist ydis 1308,-508
hist xdis 1308,-508
hist xvel 1308,-508
hist yvel 1308,-508
```

```
step 5000  
save kol0.sav
```

```
*excavate mine opening - maximum size 120x5m  
*10x5m increments  
del bl 108219  
step 30000  
save kol1.sav
```

```
del bl 108242  
step 30000  
save kol2.sav
```

```
quit
```

\*\*\*\*\*

**NUMERICAL MODELLING OF FRANK SLIDE  
DISCONTINUUM MODELLING**

**MODEL WITH SIMULATION OF ORTHOGONAL JOINTING PATTERN**

\*\*\*\*\*

- \* UDEC INPUT FILE
- \* UNIVERSITY OF SASKATCHEWAN
- \* DEPARTMENT OF GEOLOGICAL SCIENCES
- \* WRITTEN BY BORIS BENKO (UNIX Version - block addresses will differ if run on MSDOS Version of UDEC), Last revised fall 1996

new  
title  
FRANK SLIDE / UDEC APPLICATION

\*Block rounding  
round 0.5

\*Initial block  
bl 0,-1500 0,0 2300,0 2300,-1500

\*Jointing  
\*topography

crack 1850,-755	2300,-755
crack 1525,-641.7	1850,-755
crack 1421.7,-574.4	1525,-641.7
crack 1080.1,-232.8	1421.7,-574.4
crack 975,-83.3	1080.1,-232.8
crack 900,0	975,-83.3
crack 757,-65.4	900,0
crack 757,-65.4	361,-342.7
crack 361,-342.7	200,-400
crack 200,-400	0,-400

\*Artificial joint for zoning

crack 2300,-998.6	1017,-998.6
crack 1017,-998.6	361,-342.7

\*Turtle Mountain fault

crack 1525,-641.7	1374,-641.7
crack 1374,-641.7	515.7,-1500

\*Minor fault traced by Cruden (65 degr.)

crack 1421.7,-574.4	1309,-574.4
crack 1309,-574.4	1193.5,-822.3

\*\*\*\*\* PALEOZOIC FORMATIONS \*\*\*\*\*

\*Bedding planes in failure block

jreg 1308.5,-574.4 1004.5,-270.3 1065.3,-209.7 1421.7,-574.4

jset 135,0 600,0 0,0 10,0 1309,-574.4

\*Bedding planes under the failure block - 1

jreg 1193.5,-822.3 983.3,-612.1 983.3,-250 1309,-574.4

jset 135,0 600,0 0,0 10,0 1309,-574.4

\*Bedding planes under the failure block - 2

jreg 983.3,-965 983.3,-612.1 1193.5,-822.3 1017,-998.6

jset 135,0 600,0 0,0 10,0 1309,-574.4

\*Contorted zone - between faults

jreg 1195,-819 1308.5,-574.4 1421.7,-574.4 1525,-641.7

jset 90,0 150,0 0,0 10,0 1525,-641.7

\*Anticline crest / arc increment 2.5 degrees

arc 983.3,-291.6 757,-65.3 -90 18 ;1

arc 983.3,-291.6 764.1,-72.4 -90 18 ;2

arc 983.3,-291.6 771.2,-79.5 -90 18 ;3

arc 983.3,-291.6 778.2,-86.5 -90 18 ;4

arc 983.3,-291.6 785.3,-93.6 -90 18 ;5

arc 983.3,-291.6 792.4,-100.7 -90 18 ;6

arc 983.3,-291.6 799.4,-107.7 -90 18 ;7

arc 983.3,-291.6 806.5,-114.8 -90 18 ;8

arc 983.3,-291.6 813.6,-121.9 -90 18 ;9

arc 983.3,-291.6 820.7,-129 -90 18 ;10

arc 983.3,-291.6 827.7,-136 -90 18 ;11

arc 983.3,-291.6 834.8,-143.1 -90 18 ;12

arc 983.3,-291.6 841.9,-150.2 -90 18 ;13

arc 983.3,-291.6 848.9,-157.2 -90 18 ;14

arc 983.3,-291.6 856,-164.3 -90 18 ;15

arc 983.3,-291.6 863.1,-171.4 -90 18 ;16

arc 983.3,-291.6 870.2,-178.5 -90 18 ;17

arc 983.3,-291.6 877.2,-185.5 -90 18 ;18

arc 983.3,-291.6 884.3,-192.6 -90 18 ;19

arc 983.3,-291.6 891,-199.7 -90 18 ;20

arc 983.3,-291.6 898.4,-206.7 -90 18 ;21

arc 983.3,-291.6 905.5,-213.8 -90 18 ;22

arc 983.3,-291.6 912.6,-220.9 -90 18 ;23

arc 983.3,-291.6 919.7,-228 -90 18 ;24

arc 983.3,-291.6 926.7,-235 -90 18 ;25

arc 983.3,-291.6 933.9,-242 -90 18 ;26

arc 983.3,-291.6 941,-249.1 -90 18 ;27

arc 983.3,-291.6 948,-256.1 -90 18 ;28

arc 983.3,-291.6 955.1,-263.2 -90 18 ;29

arc 983.3,-291.6 962.1,-270.3 -90 9 ;30



arc 983.3,-291.6 969.2,-277.4-90 9 ;31  
arc 983.3,-291.6 976,-284.8 -120 12 ;32

\*Behind crest  
jreg 361,-342.7 757,-65.4 983.3,-291.6 983.3,-965  
jset 45,0 300,0 0,0 10,0 757,-65.4  
jdelete

\*Behind crest - large blocks  
jreg -800,-1500 361,-342.7 1017,-998.6 510,-1500  
jset 45,0 500,0 0,0 40,0 757,-65.4  
jdelete

\*\*\*\*\* MESOZOIC FORMATIONS - 85 degrees dip \*\*\*\*\*

\*Artificial joints  
crack 1689,-998.6 1714.7,-708.2

\*Mine  
crack 1654,-998.6 1680.6,-696.4  
crack 1659,-998.6 1685.4,-698.1

\*Coal chamber jointing 10m interval  
jreg 1654,-998.6 1670,-696.4 1686,-699 1659,-998.6  
jset 180,0 10,0 0,0 10,0 1659,-998.6  
jdelete

jreg 1659,-998.6 1685.4,-698.1 1714.7,-708.2 1689,-998.6  
jset 85,0 500,0 0,0 10,0 1689,-998.6  
jreg 1689,-998.6 1714.7,-708.2 1841.5,-752 1820,-998.6  
jset 85,0 300,0 0,0 10,0 1689,-998.6  
jreg 1493,-998.6 1524.5,-641.7 1680.6,-696.4 1654,-998.6  
jset 85,0 500,0 0,0 10,0 1654,-998.6  
jreg 1017,-998.6 1374,-641.7 1524.5,-641.7 1493,-998.6  
jset 85,0 500,0 0,0 10,0 1654,-998.6

\*Bottom part  
jreg 515.7,-1500 1017,-998.6 2290,-998.6 2290,-1500  
jset 85,0 550,0 0,0 40,0 1654,-998.6  
jdelete

\*Right top part  
jreg 1820,-998.6 1841.5,-752 2290,-752 2290,-998.6  
jset 85,0 850,0 0,0 20,0 2290,-1500

\*\*\*\* JOINTS NORMAL TO BEDDING PLANES \*\*\*\*\*

\*\*\*\* MESOZOIC FORMATIONS \*\*\*\*\*

jreg 1659,-990 1685.4,-700 1734,-716 1709,-990  
jset 175,0 10,0 10,0 20,0 1670.6,-866  
jset 175,0 10,0 10,0 20,0 1681.4,-857  
jreg 1493,-990 1524.5,-643 1680.6,-698 1654,-990

jset 175,0 10,0 10,0 20,0 1654,-998.6  
jset 175,0 10,0 10,0 20,0 1645,-987.7  
jreg 1017,-995 1374,-641.7 1524.5,-641.7 1493,-995  
jset 175,0 10,0 10,0 20,0 1654,-998.6  
jset 175,0 10,0 10,0 20,0 1645,-987.7  
jdelete

\*\*\*\* PALEOZOIC FORMATIONS \*\*\*\*\*

\*contorted zone  
jreg 1193.5,-822.3 1309,-574.4 1375,-574.4 1374,-641.8  
jset 180,0 10,0 10,0 20,0 1374,-641.7  
jset 180,0 10,0 10,0 20,0 1365,-631.7  
jreg 1374,-641.7 1375,-574.4 1421.7,-574.4 1525,-641.7  
jset 180,0 10,0 10,0 20,0 1374,-641.7  
jset 180,0 10,0 10,0 20,0 1365,-631.7  
jdelete

\*Turtle Mountain  
\*Bedding planes in failure block  
jreg 1308.5,-574.4 1004.5,-270.3 1065.3,-209.7 1421.7,-574.4  
jset 45,0 10,0 10,0 20,0 1309,-574.4  
jset 45,0 10,0 10,0 20,0 1309,-560.3  
jdelete

\*Bedding planes under the failure block - 1  
jreg 1192,-825 983.3,-616.5 983.3,-250 1309,-574.4  
jset 45,0 10,0 10,0 20,0 1309,-574.4  
jset 45,0 10,0 10,0 20,0 1295,-574.3  
jdelete

\*Bedding planes under the failure block - 2  
jreg 983.3,-965 983.3,-616.5 1192,-825 1017,-998.6  
jset 45,0 10,0 10,0 20,0 1309,-574.4  
jset 45,0 10,0 10,0 20,0 1295,-574.3  
jdelete

\*Behind crest  
jreg 361,-342.7 757,-65.4 983.3,-291.6 983.3,-965  
jset 135,0 10,0 10,0 20,0 757,-65.4  
jset 135,0 10,0 10,0 20,0 757,-79.5

\*Anticline jointing  
\*-42.5  
jreg 969.19,-277.4 755.7,-64.05 782.4,-52.22 970.49,-276.3  
jset 132.5,0 10,0 9.95,0 50,0 976.5,-284.2

\*-40  
jreg 969.8,-276.9 769.3,-58.1 795.2,-46.5 971.2,-275.8  
jset 130,0 10,0 10,0 50,0 983.3,-291.6  
\*-37.5

jreg 970.49,-276.3 782.4,-52.22 807.79,-40.95 971.87,-275.5  
jset 127.5,0 10,0 9.95,0 50,0 977.19,-283.6  
\*-35  
jreg 971.3,-275.5 795.2,-46.52 820.12,-35.48 972.6,-274.8  
jset 125,0 10,0 10,0 50,0 983.3,-291.6  
\*-32.5  
jreg 971.87,-275.5 807.79,-40.95 832.3,-30.07 973.35,-274.3  
jset 122.5,0 10,0 9.95,0 50,0 977.9,-283.1  
\*-30  
jreg 972.6,-274.8 820.12,-35.48 844.36,-24.71 974.1,-273.9  
jset 120,0 10,0 10,0 50,0 983.3,-291.6  
\*-27.5  
jreg 973.35,-274.3 832.3,-30.07 856.37,-19.38 974.89,-273.5  
jset 117.5,0 10,0 9.95,0 50,0 978.66,-282.7  
\*-25  
jreg 974.1,-273.9 844.36,-24.71 868.34,-14.06 975.7,-273.2  
jset 115,0 10,0 10,0 50,0 983.3,-291.6  
\*-22.5  
jreg 974.89,-273.5 856.37,-19.38 880.35,-8.73 976.5,-272.9  
jset 112.5,0 10,0 9.95,0 50,0 979.46,-282.3  
\*-17.5  
crack 893.1,-5.53 896.04,-15.05  
jreg 976.5,-272.9 880.35,-8.73 907.07,-7.05 978.17,-272.3  
jset 107.5,0 10,0 9.95,0 50,0 980.28,-282  
\*-15  
crack 910.64,-21.02 908.18,-11.51  
jreg 977.33,-272.6 892.42,-3.37 923.96,-23.96 979.02,-272.1  
jset 105,0 10,0 10,0 50,0 983.3,-291.6  
\*-12.5  
jreg 978.17,-272.3 907.07,-7.05 938.7,-38.7 979.87,-272  
jset 102.5,0 10,0 9.95,0 50,0 981.14,-281.8  
\*-7.5  
jreg 979.87,-272 938.7,-38.7 963.34,-63.32 981.61,-271.7  
jset 97.5,0 10,0 9.95,0 50,0 982,-291.6  
\*-2.5  
jreg 981.61,-271.7 963.34,-63.32 983.3,-83.3 983.34,-271.7  
jset 92.5,0 10,0 9.95,0 50,0 982.86 -281.6  
\*0  
jreg 982.46,-271.7 973.8,-73.8 991.88,-95.16 984.21,-271.7  
jset 90,0 10,0 9.9,0 50,0 983.3,-291.6  
\*2.5  
jreg 983.34,-271.7 983.3,-83.3 999.55,-105.8 985.07,-271.7  
jset 87.5,0 10,0 9.95,0 50,0 983.74,-281.6  
\*7.5  
jreg 985.07,-271.7 999.55,-105.8 1012.8,-124.2 986.81,-272

```

jset 82.5,0 10,0 9.95,0 50,0 984.6,-281.7
*15
jreg 987.66,-272.15 1018.68,-132.2 1029.5,-146.6 989.34,-272.6
jset 75,0 10,0 10,0 50,0 983.3,-291.6
*22.5
jreg 990.17,-272.9 1033.75,-153.1 1042.35,-165.1 991.78,-273.5
jset 67.5,0 10,0 9.95,0 50,0 987.14,-282.3
*30
jreg 992.56,-273.9 1046.3,-170.6 1053.8,-181 994.07,-274.8
jset 60,0 10,0 9.9,0 50,0 983.3,-291.6
*37.5
jreg 994.8,-275.3 1057.4,-185.9 1064.18,-195.3 996.17,-276.3
jset 52.5,0 10,0 9.95,0 50,0 989.42,-283.7

```

\*Middle of anticline jointing

```

crack 983.3,-281.6      983.3,-271.6
crack 970.4,-276      976,-285
crack 989.1,-282.8    995.3,-274.8
jdelete

```

\*Joints for slope excavation

```

crack 0,-150          637,-150
crack 0,-300          422,-300
crack 1022,-150       2300,-150
crack 1147,-300       2300,-300
crack 1295.6,-450     2300,-450
crack 1522.2,-641.7   2300,-641.7
jdelete

```

\*\*\*\*\*

\*finite difference triangles - fully deformable blocks

\*excavated blocks

```

ge bl 1271029          edge 100
ge bl 1271171          edge 100
ge bl 22911            edge 100
ge bl 1271356          edge 100
ge bl 1271498          edge 100
ge bl 1271769          edge 100
ge bl 1271911          edge 100
ge bl 229              edge 100

```

\*left bottom portion

```

ge bl 107962          edge 65
ge bl 106950          edge 65
ge reg -800,-1500 361,-342.7 1017,-998.6 515.7,-1500 quad 80

```

\*bottom part

ge bl 148580	edge 80
ge bl 144517	edge 80
ge reg 515.7,-1500 1017,-998.6 2300,-998.6 2300,-1500	quad 80
*Right side	
ge bl 149352	edge 40
ge reg 1820,-998.6 1841.5,-752 2290,-752 2290,-998.6	quad 41
*Rest of Mesozoic	
ge reg 1654,-998.6 1680,-696.4 1685,-698.1 1659,-998.6	quad 20
ge reg 1659,-998.6 1685,-698.1 1714.7,-708.2 1689,-998.6	quad 21
ge reg 1689,-998.6 1714.7,-708.2 1841.5,-752 1820,-998.6	quad 21
ge reg 1493,-998.6 1524,-642 1680.6,-696.4 1654,-998.6	quad 21
ge bl 136547	edge 20
ge bl 136224	edge 20
ge bl 135901	edge 20
ge bl 135578	edge 20
ge bl 135307	edge 20
ge bl 135036	edge 20
ge bl 134679	edge 20
ge bl 132623	edge 20
ge bl 132266	edge 20
ge bl 131909	edge 20
ge bl 131552	edge 20
ge bl 131195	edge 20
ge bl 130838	edge 20
ge bl 129053	edge 20
ge bl 128739	edge 20
ge bl 128382	edge 20
ge bl 128025	edge 20
ge bl 127668	edge 20
ge bl 127311	edge 20
ge reg 1017,-998.6 1374,-641.7 1525,-641.7 1493,-998.6	quad 21
*Contorted zone	
ge bl 457964	edge 20
ge bl 457641	edge 20
ge bl 456995	edge 20
ge bl 456435	edge 20
ge bl 455466	edge 20
ge bl 454497	edge 20
ge bl 453205	edge 20
ge bl 451633	edge 20
ge bl 450018	edge 20
ge bl 445539	edge 20
ge bl 444893	edge 20
ge bl 444247	edge 20
ge bl 443278	edge 20

ge bl 442309	edge 20
ge bl 441082	edge 20
ge bl 439998	edge 20
ge bl 438686	edge 20
ge bl 437460	edge 20
ge bl 22149	edge 20
ge bl 21705	edge 20
ge bl 21218	edge 20
ge bl 20851	edge 20
ge bl 20532	edge 20
ge bl 20170	edge 20
ge bl 19808	edge 20
ge bl 19498	edge 20
ge bl 19024	edge 20
ge bl 18550	edge 20
ge reg 1193.5,-822.3 1309,-574.4 1375,-574.4 1374,-641.8	quad 21
ge bl 13288	edge 20
ge bl 11478	edge 20
ge bl 11116	edge 20
ge bl 1943	edge 20
ge reg 1374,-641.7 1375,-574.4 1421.7,-574.4 1525,-641.7	quad 21
*Bedding planes in failure block	
ge bl 79265	edge 20
ge bl 77209	edge 20
ge bl 75153	edge 20
ge bl 73097	edge 20
ge bl 71041	edge 20
ge bl 68985	edge 20
ge bl 66927	edge 20
ge bl 64853	edge 20
ge bl 63657	edge 20
ge reg 1308.5,-574.4 1004.5,-270.3 1065.3,-209.7 1421.7,-574.4	quad 21
*Bedding planes under the failure block	
ge bl 686009	edge 5
ge bl 1270904	edge 20
ge bl 1264898	edge 20
ge bl 1267888	edge 20
ge bl 686233	edge 20
ge bl 1260043	edge 20
ge bl 1262632	edge 20
ge bl 59137	edge 20
ge bl 57613	edge 20
ge bl 56089	edge 20
ge bl 54565	edge 20
ge reg 1192,-825 983.3,-616.5 983.3,-250 1309,-574.4	quad 21

```

ge bl 132623 edge 20
ge reg 983.3,-965 983.3,-616.5 1192,-825 1017,-998.6 quad 21
*behind crest
ge bl 106424 edge 20
ge bl 106101 edge 20
ge bl 105778 edge 20
ge bl 105468 edge 20
ge bl 105033 edge 20
ge bl 104598 edge 20
ge bl 104163 edge 20
ge bl 103728 edge 20
ge bl 103349 edge 20
ge reg 361,-342.7 757,-65.4 983.3,-291.6 983.3,-965 quad 21
ge bl 102927 edge 20
ge bl 102247 edge 20
ge bl 92265 edge 20
ge bl 84487 edge 20
ge bl 82947 edge 20
ge bl 81235 edge 20
ge bl 24597 edge 20
ge bl 1 edge 20
ge bl 500391 edge 20
ge bl 1265911 edge 20
ge reg 983.3,-291.6 757,-65.4 900,50 1100,-200 quad 21

```

\*\*\*\*\* MATERIAL PROPERTIES \*\*\*\*\*

\*\*\*\*\* Strong for initial equilibrium \*\*\*\*\*

\*Limestone - typical properties(E,v) from literature Hoek et al

\* blocky seamy material good for limestone / poor for shale

\* density from Cruden & Krahn (1978)

\*Paleozoic Limestone: E=10000 MPa v=0.25 d=2600kg/m3

\*Mesozoic interbedded series: E= 3000 MPa v=0.30 d=2250kg/m3

\*jks=0.2jkn

```

prop mat 1 d=2600 bulk=6666.67e6 shear=4000.00e6
prop jmat 1 jkn=20e9 jks=5e9 jfric=28 jcoh=1e20 jten=1e20
prop mat 2 d=2250 bulk=2500.00e6 shear=1153.85e6
prop jmat 2 jkn=10e9 jks=2.5e9 jfric=25 jcoh=1e20 jten=1e20
ch mat=1 jmat=1
ch reg 515.7,-1500 1374,-641.7 2300,-641.7 2300,-1500 mat=2 jmat=2

```

\*Gravitational Acceleration

set grav 0 -9.81

\*Automatic mass damping

damp auto

\* INITIAL STRESS STATE  $K_{xy}=1.5$   $K_{zy}=1.25$  ( $s_{xx} > s_{zz} > s_{yy}$ ) \*\*\*\*\*

\*gravitational stress field based on average density = 2425kg/m<sup>3</sup>

in stress 0 0 0 szz 0 yg 356.8388e2 0 237.8925e2 zg 0 297.3656e2

\*\*\*\*\* ROLLER BOUNDARY CONDITIONS ALONG THE BASE & SIDES \*\*\*\*\*

bou cor 50 63 xvel 0

bou cor 63 24 yvel 0

bou cor 24 37 xvel 0

\*\*\*\*\* HISTORIES \*\*\*\*\*

hist unbalance

hist ydis 895,-21.5

hist xdis 895,-21.5

hist xvel 895,-21.5

hist yvel 895,-21.5

\*\*\*\*\* TURTLE MOUNTAIN "EXCAVATION" \*\*\*\*\*

step 10000

save ini.sav

del bl 1

del bl 23873

del bl 24959

del bl 24597

del bl 149466

del bl 149616

step 10000

save ini1.sav

del bl 149541

del bl 149928

step 10000

save ini2.sav

del bl 22911

del bl 150207

step 10000

save ini3.sav

del bl 150381

step 10000

save ini4.sav

del bl 229

step 10000

save topo.sav

(rest of modelling as for model with bedding plane joints only - change of material properties (cohesion and friction) to various values and examine deformation, progressive opening of coal mine)